

AD 671029

AD

USAAVLABS TECHNICAL REPORT 68-33

**FEASIBILITY STUDY OF ADVANCED V/STOL
PROPELLER TECHNOLOGY**

By

W.M. Adamson

June 1968

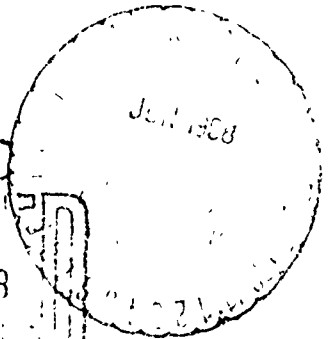
**U. S. ARMY AVIATION MATERIEL LABORATORIES
FORT EUSTIS, VIRGINIA**

**CONTRACT DAAJ02-67-C-0073
HAMILTON STANDARD DIVISION
UNITED AIRCRAFT CORPORATION
WINDSOR LOCKS, CONNECTICUT**

*This document has been approved
for public release and sale; its
distribution is unlimited.*



DDO
RECEIVED
JUL 1 1968



Reproduced by the
CLEARINGHOUSE
for Federal Scientific & Technical
Information Springfield Va 22151

Disclaimers

The findings in this report are not to be construed as an official Department of the Army position unless so designated by other authorized documents.

When Government drawings, specifications, or other data are used for any purpose other than in connection with a definitely related Government procurement operation, the United States Government thereby incurs no responsibility nor any obligation whatsoever; and the fact that the Government may have formulated, furnished, or in any way supplied the said drawings, specifications, or other data is not to be regarded by implication or otherwise as in any manner licensing the holder or any other person or corporation, or conveying any rights or permission, to manufacture, use, or sell any patented invention that may in any way be related thereto.

Disposition Instructions

Destroy this report when no longer needed. Do not return it to the originator.

ACCESSION FOR		
CFSTI	WHITE SECTION	<input checked="" type="checkbox"/>
DDC	BUFF SECTION	<input type="checkbox"/>
UNANNOUNCED		<input type="checkbox"/>
JUSTIFICATION		
.....		
.....		
Y		
DISTRIBUTION/AVAILABILITY CODES		
DIST.	AVAIL. and or	SPECIAL
/		



DEPARTMENT OF THE ARMY
U. S. ARMY AVIATION MATERIEL LABORATORIES
FORT EUSTIS, VIRGINIA 23604

This report was prepared by the Hamilton Standard Division of United Aircraft Corporation under the terms of Contract DAAJ02-67-C-0073. It consists of investigations of advanced propeller aerodynamics, structures, design concepts, and advanced materials. An optimum 1970-1975 state-of-the-art, 2000-shaft-horsepower V/STOL propeller system was defined.

The primary objective of this contractual effort was to investigate the application of advanced materials which would significantly reduce the overall weight of the propeller system compared to that of current V/STOL propellers.

Task 1G121401D14415
Contract DAAJ02-67-C-0073
USAAVLABS Technical Report 68-33
June 1968

FEASIBILITY STUDY OF ADVANCED V/STOL
PROPELLER TECHNOLOGY

Final Report

By
W. M. Adamson

Prepared by

Hamilton Standard Division
of United Aircraft Corporation
Windsor Locks, Connecticut

for

U.S. ARMY AVIATION MATERIEL LABORATORIES
FORT EUSTIS, VIRGINIA

This document has been approved
for public release and sale; its
distribution is unlimited.

ABSTRACT

A feasibility study of advanced V/STOL propeller systems for the 1970-1975 time period was conducted. The primary objective of the study was to investigate the application of new materials and new design concepts to define the maximum reductions in specific weight of the complete propeller system (including reduction gearbox) attainable in this time period. Preliminary designs of future propeller systems presented in the report are over 50 percent lighter than comparable present-day V/STOL systems. This is considerably more weight reduction than that targeted at the beginning of the study program.

The projected weight reductions were the culmination of the study program encompassing the following major trade-off studies:

Aerodynamic Studies —A parametric study to define the optimum propeller configuration by relating the trade-off of static thrust cruise efficiency and propeller weight.

Materials Study —An evaluation of advanced materials with improved strength-to-weight and stiffness-to-weight ratios and recommendations of those materials that would be most beneficial in achieving weight reductions.

Design Studies —An evaluation of new design concepts and application of advanced materials which will result in the optimum configurations for minimum weight.

Structural Parametric Studies —A parametric optimization of the blade, barrel, and retention.

Preliminary designs of three integral gearbox (IGB) propeller systems, with and without cyclic pitch and with and without a cross-shaft drive pad, were defined in this report using the advanced technology indicated as feasible by the study. Each major component of the IGB propeller system was optimized and then merged into complete system designs. A summary weight tabulation is presented showing the relative contributions of each major component of the IGB propeller system to the total indicated weight reductions.

A significant portion of the weight reductions is shown to be achievable by 1970, since the technology required is presently under development or is a natural extension of existing technology. Other significant weight reductions, such as those resulting from the use of boron blade spars and titanium gearing, are at an early phase of their technology development and are not considered attainable much before 1975, unless supported by a vigorous R&D effort.

Planning for propeller R&D programs should be conducted with the above factors in mind.

FOREWORD

The preparation of this final report concluded a seven-month feasibility study conducted by Hamilton Standard on advanced V/STOL propeller technology for the 1970-1975 time period. The study was initiated upon the award of U. S. Army Aviation Materiel Laboratories Contract DAAJ02-67-C-0073.

Grateful acknowledgement is made of USAAVLABS' demonstrated interest in advancing V/STOL propeller technology. Mr. James Gomez was the USAAVLABS technical representative and was helpful in providing technical coordination and assistance.

Various departments in the Hamilton Standard Engineering organization have contributed to the total study effort. The study program was directed by Mr. W. M. Adamson, Program Manager, under the supervision of Mr. A. H. Jackson, Chief of Advanced Systems, and Mr. George Rosen, Chief of Propeller R&D.

Significant contributions in specific areas of study were made by the following Hamilton Standard technical personnel:

Aerodynamic Studies:	Mr. C. Rohrbach, Chief Aerodynamicist Mr. R. Ladden, Senior Aerodynamicist
Materials Study:	Mr. T. Zajac, Chief of Materials Engineering Mr. P. Arnold, Metallurgist Mr. J. Cutler, Senior Metallurgist Mr. E. Delgrosso, Project Metallurgist
Design Studies:	Mr. R. Quenneville, Chief Design Engineer Mr. P. Barnes, Design Project Engineer Mr. H. Wiitanen, Supervisor Blade Design Mr. M. Mayo, Senior Design Engineer Mr. R. Gustafson, Design Engineer Mr. M. Hamilton, Senior Gear Analyst
Structural Parametric Studies:	Dr. R. Cornell, Chief of Applied Mechanics and Mathematics Mr. A. Seibert, Senior Analytical Engineer Mr. J. Marti, Analytical Engineer Mr. J. Kostoss, Analytical Engineer Dr. R. Mattox, Senior Analytical Engineer Mr. W. Westervelt, Senior Analytical Engineer

Acknowledgement is also made of the contributions of the following companies that provided data on present-day turboprop systems which are listed with Hamilton Standard data in Appendix I:

AiResearch Manufacturing Company
Curtiss-Wright Corporation
Dowty Rotol, Limited
General Electric Company
Harzell Propeller, Inc.
Hawker Siddeley Dynamics, Limited
Pratt & Whitney Aircraft
Rolls-Royce, Limited
United Aircraft of Canada, Limited

TABLE OF CONTENTS

	<u>Page</u>
ABSTRACT	iii
FOREWORD	v
LIST OF ILLUSTRATIONS	x
LIST OF TABLES	xviii
LIST OF SYMBOLS	xx
INTRODUCTION	1
AERODYNAMIC STUDIES	2
Aerodynamic Optimization Parametric Study	2
Aerodynamic State-of-the-Art Review	22
MATERIALS REVIEW	33
General Approach	33
Steels-Wrought	33
Low Alloy Steels	33
Ultrahigh Strength Steels	38
Experimental Steels	39
Titanium-Wrought	39
Titanium-Cast	41
Magnesium-Cast	41
Aluminum-Wrought	42
Aluminum-Cast	42
Beryllium-Wrought	43
Composites	44
Summary-Materials Selected	50
COMPONENT DESIGN STUDIES	53
Point Design Sizing Criteria	53
Gearbox	53

TABLE OF CONTENTS (Cont)

	<u>Page</u>
Gear Sizing Trade-Off Study	53
Gear Train Configurations	31
In-Line Star-Epicyclic	61
Gearing and Gear Tooth Shapes	76
Propeller Barrel Mounting	81
Bearings	85
Gearbox Housing	86
Overrunning Clutch	91
Cross-Shaft Decoupler	94
Lubrication System	97
Barrel and Retention	102
Blades	111
Collective Pitch Change Mechanism	119
Cyclic Pitch Change Mechanism	130
Control System	142
Hydromechanical Control	144
Electromechanical Control	151
Fluidic Control	155
Synchrophasing	155
Deicing System	155
SYSTEM DESIGN	160
Description	160
Integral Gearbox Assembly	160
Propeller Assembly	167
Control System	180
Maintainability and Reliability Assessment	186
Weight Summary	190
Performance Summary	193

TABLE OF CONTENTS (Cont)

	<u>Page</u>
Scaling Factors	211
CONCLUSIONS AND RECOMMENDATIONS	220
APPENDIX I. Present-Day Turboprop Systems	222
APPENDIX II. Derivation of Optimum Aerodynamics Trade-Off Criterion	240
APPENDIX III. Matching the Propeller and Engine for Optimum Flight Performance	245
APPENDIX IV. Feasibility Study of Novikov Gears	255
APPENDIX V. Study of Methods to Adjust the Dynamic Response of Involute Gears	261
APPENDIX VI. Parametric Study of the Propeller Barrel Structure	275
APPENDIX VII. Parametric Study of the Integral Ball Race Blade Retentions	288
APPENDIX VIII. Stability Analysis of the Cyclic Pitch Propeller Including 1XP Isolation Methods	300
APPENDIX IX. Parametric Optimization Study of Two-Piece Hollow Propeller Blades	314
REFERENCES	358
DISTRIBUTION	364

LIST OF ILLUSTRATIONS

<u>Figure</u>		<u>Page</u>
1	Typical Blade Characteristics	5
2	Static Propeller Performance - Parametric Study	6
3	Static Propeller Performance - Parametric Study	7
4	250-Knot Cruise Performance - Parametric Study	8
5	250-Knot Cruise Performance - Parametric Study	9
6	250-Knot Cruise Performance - Parametric Study	10
7	250-Knot Cruise Performance - Parametric Study	11
8	Propeller and Gearbox Weights - Parametric Study.....	12
9	Propeller and Gearbox Weights - Parametric Study.....	13
10	Propeller Optimum Criterion Plot	14
11	Cyclic Pitch Propeller Static Thrust Performance Comparison	19
12	Cyclic Pitch Propeller Static Control Moment Comparison	20
13	Concepts of Blades Incorporating Aerodynamic Devices	23
14	Slotted Airfoil Characteristics (11.8% Clark Y)	25
15	Effect of Lead-Edge Slots on Lift-to-Drag Ratio.....	26
16	Slotted Airfoil Correction Curve	27
17	Static Propeller Performance Comparison With and Without Slots	29
18	Gear Ratio Split-Weight Comparison	55
19	Effect of Number of Planet Gears	57

LIST OF ILLUSTRATIONS (Cont.)

<u>Figure</u>		<u>Page</u>
20	Effect of Gear Size on Weight	58
21	First-Stage Gear Train Weight Trend.....	59
22	Effect of Gear Ratio Split on Gear Size.....	60
23	In-Line (Star-Epicyclic) Gear Train	63
24	Offset (Pinion-Bull) - Epicyclic Gear Train.....	65
25	Differential Gear Train With Offset	67
26	Roller Gear Train	68
27	Roller Gear Train With Offset	69
28	Compound Star Gear Train	70
29	Compound Star Gear Train With Offset.....	71
30	Split-Power Gear Train	73
31	Split-Power Gear Train With Offset.....	74
32	Planetary System Meshing Sequence	82
33	Barrel Mounting Concepts	84
34	Cast Magnesium Housing	88
35	Back-to-Back Cone Housing Concept.....	89
36	Strut Housing Concept.....	90
37	Titanium Housing Concept	92
38	Overrunning Clutch Concepts.....	93
39	Jaw-Type Decoupler	95
40	Spring-Type Decoupler	96

LIST OF ILLUSTRATIONS (Cont.)

<u>Figure</u>		<u>Page</u>
41	Centrifugal Pump and Air-Oil Separator	98
42	Lubrication Schematic	100
43	Integral Oil Cooler and Fan.....	101
44	Heat Exchanger	103
45	Integral Ball Race Blade Retention	104
46	Tapered Roller Bearing Blade Retention	106
47	Ball Race Blade Retention With Inserts.....	107
48	Four-Point Bearing Retention.....	108
49	Barrel Concept.....	110
50	Crossed Cylinder Barrel	112
51	Shell Structure Barrel Concept	113
52	Lightweight Blade Design (Structural Spar-Fiberglass Cover).....	117
53	Blade Twisting Moment vs Blade Angle.....	120
54	Collective Pitch Actuator	121
55	Actuator Wet Weight Per Inch of Length.....	123
56	Actuator Stroke vs Actuator Weight.....	124
57	In-Place Pitchlock Concept	126
58	Ball Screw Actuator.....	129
59	Ball Joint Cyclic Pitch Actuator Concept	132
60	Cyclic Blade Twisting Moments	134

LIST OF ILLUSTRATIONS (Cont.)

<u>Figure</u>		<u>Page</u>
61	Summation of Cyclic Blade Twisting Moments	136
62	Nonrotating Cyclic Actuator	139
63	Cyclic Pitch Actuation With Linkage	140
64	Cyclic Pitch Actuation Using a Planetary Gear Train	141
65	Gimbaled Propeller Concept	143
66	Hydromechanical Propeller Control Schematic.....	145
67	Control Assembly.....	147
68	Valve Module	148
69	Electromechanical Control Concept.....	152
70	Synchrophasing Schematic	156
71	Blade and Spinner Deicing Zones	158
72	Collective Pitch IGB Propeller System With Cross-Shaft Drive	161
73	Preliminary Nacelle Layout.....	169
74	Cyclic Pitch IGB Propeller System With Cross-Shaft Drive	171
75	Collective Pitch IGB Propeller System Without Cross-Shaft Drive	175
76	Control Block Diagram	181
77	Electrical Wiring Schematic	187
78	Propeller Efficiency Map Based on Strip Analysis Calculations	195
79	Static Propeller Performance	196

LIST OF ILLUSTRATIONS (Cont.)

<u>Figure</u>		<u>Page</u>
80	Compressibility Correction Factors For The 4-Way/120 AF/0.40C _{L_i} Efficiency Map.....	197
81	Blade Characteristic Chart	199
82	Static Propeller Performance (Torque vs Blade Angle)	200
83	Static Propeller Performance (Horsepower vs Blade Angle)	201
84	Static Propeller Cyclic Pitch Performance	203
85	Noise Estimates for 14.8-Foot-Diameter Propeller	208
86	Noise Estimates for 12.8-Foot-Diameter Propeller	209
87	Variation of Horsepower With Propeller Diameter	212
88	Diameter - Weight Factor	213
89	Gear Ratio - Weight Factor	214
90	Torque Limit - Weight Factor	215
91	"g" Loading - Weight Factor	218
92	Activity Factor - Weight Factor	218
93	Present-Day Turboprop System Weights	239
94	Thrust Required for Various Aircraft Speeds	246
95	Variation of Propeller, Engine, and Total Efficiency With RPM-SLSD	247
96	Variation of Propeller, Engine, and Total Efficiency With RPM-15,000 Ft., Std Day	248
97	Engine Military Power Rating	249
98	Variation of Optimum Engine RPM With Optimum SHP	250

LIST OF ILLUSTRATIONS (Cont.)

<u>Figure</u>		<u>Page</u>
99	Horsepower Loss at Nonoptimum Engine Speeds	251
100	Optimum Flight Operating RPM - SLSD	253
101	Optimum Flight Operating RPM - 15,000 Feet, STD Day	254
102	Addendum-Dedendum Gear Teeth	258
103	All-Dedendum Gear Teeth	258
104	Free-Body Diagram for Mating Gears	262
105	Richardson's Dynamic Models for a Gear Pair	263
106	Dynamic Loads on Gear Teeth	265
107	Tooth Slot Damping and Flexibility	269
108	Rim Slot Damping and Flexibility	271
109	Examples of Using Coulomb Damping on Gears	273
110	Conventional Barrel, Analytical Model	276
111	Barrel Capacity Under Centrifugal Loading	278
112	Barrel Capacity Under Steady Out-of-Plane Bending Loads	279
113	Barrel Capacity Under Steady In-Plane Bending Loads	280
114	Barrel Capacity Under 1P In-Plane Bending Loads	281
115	Barrel Capacity Under 1P Out-of-Plane Bending Loads	282
116	Basic Load-Carrying Barrel Structures	284
117	Sketch of Monocoque Shell Barrel Concept	286

LIST OF ILLUSTRATIONS (Cont.)

<u>Figure</u>		<u>Page</u>
118	Design Parameters for the Single- and Multiple-Ball-Race Retentions	289
119	Effect of Number of Races on Moment Capacity/Weight	292
120	Effect of Number of Races on Axial Load Capacity/Weight	293
121	Effect of Number of Races on Retention Stiffness/Weight	294
122	Effect of Ball-Race Fit on Retention Stiffness/Weight	295
123	Effect of Retention Diameter-to-Ball Diameter Ratio	296
124	Effect of Number of Races on Axial Load Capacity	298
125	Coordinate System and Sign Convention	302
126	Blade Element Vector Diagram	302
127	Flutter Plot for Fully Gimbaled Propeller	309
128	Flutter Plot for Fully Gimbaled Propeller	310
129	Approximation of the Two-Piece Blade Section	315
130	Blade Design Chart (S-Glass Cover/Boron-Aluminum Spar)	318
131	S-Glass Cover/Boron-Aluminum Spar Blade Section Torsional Properties	319
132	Blade Section Geometry Limits Spar Width	320
133	Maximum Moment Capacity vs Shell Wall Thickness for Constant Weight	323
134	Properties of S-Glass/Boron-Aluminum Blade Section	333

LIST OF ILLUSTRATIONS (Cont.)

<u>Figure</u>		<u>Page</u>
135	S-Glass Cover/D6A Steel Spar Blade Section Properties	334
136	S-Glass Cover/Titanium Spar Blade Section Properties	335
137	Spar Material vs Moment Capacity	336
138	Spar Material vs Bending Stiffness	337
139	Boron-Aluminum Cover/Boron-Epoxy Spar	336
140	Properties of S-Glass Shell/Boron-Aluminum Blade Section	341
141	970 Glass Cover/Boron-Aluminum Spar Blade Section Properties	342
142	Blade Design Dimensions	345
143	Calculated Stress Distributions for Blade Design	346
144	Critical Speed Diagram	347
145	Frequency Influence Coefficients	349
146	Section Properties of Blade Design	352

LIST OF TABLES

<u>Table</u>		<u>Page</u>
I	Propeller Designs Listed in Order of Range	16
II	Design Allowable Mechanical Properties for Selected Materials as Compared to Steel (at Room Temperature).....	34
III	Typical Properties of Various Structural Materials (Room Temperature)	35
IV	Typical Properties of Reinforcing Materials (Room Temperature)	46
V	Data Summary of Gear Train Configurations	62
VI	Summary of Gear Train Configurations	75
VII	Gear Weight Comparison	79
VIII	Gearing Data	83
IX	Bearing Data	87
X	Blade Properties	115
XI	Blade Frequency Spectrum	116
XII	Collective Pitch Actuator Design Data	128
XIII	Cyclic Pitch Actuator Design Data	137
XIV	Deicing Power Requirements	159
XV	Weight Summary and Comparison	191
XVI	Weight Reduction 1975 Technology Vs 1965	192
XVII	Performance Summary ..	194
XVIII	Estimated Pressure Recovery	202
XIX	Operating Conditions for Noise Estimates	204

LIST OF TABLES (Cont.)

Table		Page
XX	Near-Field Noise Estimates	205
XXI	Far-Field Noise Estimates	207
XXII	Present-Day Turboprop Systems	223
XXIII	Comparison of Design Data and Stress for NIVIKOV and Involute Pinion Teeth for the USAAVLABS Propeller Gear Mesh.....	256
XXIV	USAAVLABS Retention Parameter Analysis.....	291
XXV	Relative Weights, A/D = 1.5	299
XXVI	Symbols Used in Appendix IX.....	301
XXVII	Shell Materials	325
XXVIII	Core Materials	326
XXIX	Bending Properties Based on Fatigue, 78-inch Radius.....	327
XXX	Bending Properties Based on Fatigue, 78-inch Radius.....	329
XXXI	Torsional Properties Based on Fatigue, 78-inch Radius...	330
XXXII	Bending Properties Based on Ultimate Stress, 24-in. Radius	331
XXXIII	Fixed Parameters of the Blade Design	340
XXXIV	Blade Design	343
XXXV	Symbols Used in Appendix X.....	355

LIST OF SYMBOLS

A	Area, FT ²
AF	Blade Activity Factor
Aq	Propeller Inflow Angle Times Dynamic Pressure, DEG-LB/FT ²
ATM	Aerodynamic Twisting Moment, IN-LB
b	Blade Section Widths
B	Number of Blades
C _B	Deformation Factor
C _D	Airfoil Drag Coefficient
C _L	Airfoil Lift Coefficient
C _{L_D}	Blade Section Design Lift Coefficient
C _{L_i}	Blade Integrated Design Lift Coefficient
C _P	Propeller Power Coefficient
C _T	Propeller Thrust Coefficient
CTM	Centrifugal Twisting Moment, IN-LB
D	Pitch Diameter, Gear, IN
D _p	Diametral Pitch
E	Modulus of Elasticity, LB/IN ²
E.F.	Excitation Factor (E.F. = Aq/409)
EL	Endurance Limit, LB/IN ²
F	Face Width, Gear (equation), IN

LIST OF SYMBOLS (Cont.)

FTM	Friction Twisting Moment, IN-LB
F.W.	Face Width, Gear (curves), IN
G.W.	Gross Weight, LB
h	Blade Section Maximum
HP	Horsepower
IGB	Integral Gearbox
I_p	Polar Moment of Inertia, LB-FT ²
J	Propeller Advance ratio
K	Constant
K_t	Stress Concentration Factor
L	Lift, LB
N	Propeller rpm
n	Propeller Speed, rps
Q	Torque, LB-IN
r	Radius to Blade Section
R	Gear Ratio
Rc	Rockwell C Hardness Number
R_p	Pitch Radius, Gear, IN
S_B	Bending Stress, LB/IN ²
S_c	Hertz Stress, LB/IN ²
SHP	Propeller Shaft Horsepower

LIST OF SYMBOLS (Cont.)

T	Thrust, LB
T.O.	Takeoff
UTS	Ultimate Tensile Strength, LB/IN ²
V_k	Aircraft Forward Velocity - KTAS
V_p	Pitch Line Velocity, FT/MIN
W_d	Dynamic Load Gear, LB
W_D	Propeller Diameter Weight Factor
W_g	g Loading Weight Factor
W_{GR}	Gear Ratio Weight Factor
W_t	Tangential Tooth Load, Gear, LB
W_{TL}	Torque Limit Weight Factor
W_x	Total Activity Factor Weight Factor
X	Tooth Form Factor, Gear
φ	Pressure Angle, DEG
μ	Poisson's Ratio
ρ, σ	Density, LB/IN ³ , LB-SEC ² /FT ⁴
σ	Stress, LB/IN ²
$\beta^{3/4}$	Blade Angle at 0.75 Radius - DEG
η	Propeller Efficiency

INTRODUCTION

This feasibility study of advanced V/STOL propeller systems encompasses investigations of applicable propeller aerodynamics, advanced materials, structures, and design concepts. Its primary overall focus is weight reduction. In addition, a survey of present-day turboprop systems was conducted, and the appropriate data are presented in Appendix I for reference.

The aerodynamic study involved a parametric evaluation to define the propeller size used in the design and structural studies. A separate evaluation was made of possible aerodynamic devices that could be applied to propeller blades for performance advantages.

The materials study consisted of a review of present and new materials and their feasibility for use in advanced propeller systems. A recommended list of materials and their properties was compiled, and this list formed the basis for the design studies.

In the design studies, each major component was examined to define the optimum combination of materials and design concepts to achieve minimum weight. Parametric studies were also used to aid in optimizing the blade, barrel, retention, and gearing.

The optimized components were then used in preliminary designs of three specific propeller systems, and the weight of each of the advanced systems was compared with present-day V/STOL systems.

AERODYNAMIC STUDIES

AERODYNAMIC OPTIMIZATION PARAMETRIC STUDY

The design of an optimum V/STOL propeller requires some definition of the V/STOL aircraft configuration and mission before a parametric study of propeller geometries and performance can be conducted. Furthermore, in order for the propeller optimization study to be meaningful, there must be some optimization criteria to relate the trade-offs between static and cruise performance and propeller weight. Since there was not a specific aircraft, powerplant, or mission defined for the subject advanced propeller system study, reasonable assumptions had to be made of a representative aircraft configuration with appropriate trade-off factors.

Aircraft Configuration and Mission

In consultation with USAAVLABS, the following criteria were jointly selected:

Aircraft type:	utility tilt-wing V/STOL
Propulsion:	2 engines, 2 propellers
Engine rating:	2000 shp @ S. L. , standard day
Hover design point:	1400 shp per propeller @ 6000 ft; 95°F (see "Engine Scaling" for consideration of other powers)
Cruise design point:	643 shp per propeller @ 250 kn, S. L. , standard day
T/G.W. @ hover:	1.07
Disk loading @ hover:	35.0 lb/sq ft
Tip speed @ T. O. :	900 ft/sec
Wing loading:	70 lb/sq ft
Wing aspect ratio:	8.0
Oswald efficiency factor:	0.8

Flat plate drag:	1.0 sq ft per ton gross weight. (This latter value is representative of both the XC-142 and the CL-84 V/STOL aircraft.)
Mission:	vertical takeoff with a fixed payload transition to forward flight, cruise @ 250 kn @ S.L., standard day transition to hover, vertical landing

A more detailed definition of the aircraft mission was not considered to be necessary for the purposes of this study. Aircraft range, gross weight, and propeller diameter were not specified, these having been selected as the primary dependent variables for the trade-off study. The aircraft V_{max} capability was not to be part of the optimization study but merely the end result of the selected aircraft and propeller configuration.

Hover and Cruise Design Points

The principal propeller sizing factor for this study was the specification of 35.0 lb/sq ft thrust disk loading, and 900-ft/sec tip speed at the design hover point of 1400 shp, 6000 ft, 95° F. The 900 ft/sec tip speed has been demonstrated as being near optimum at this disk loading. Over 50 propeller aerodynamic configurations were defined, each representing a specific combination of diameter, solidity, and camber selected to provide the 35.0/sq ft disk loading. It should be noted that fixing disk loading rather than a propeller static thrust requirement meant that, despite the same horsepower input, each propeller would produce a different thrust level. When coupled with the specified thrust-to-gross weight ratio of 1.07, this, in turn, resulted in a different aircraft gross weight corresponding to each propeller configuration.

For the determination of an appropriate value of shaft horsepower at the cruise design point of 250 kn, S. L., standard day, a representative value of 82% was assumed for propeller efficiency. When combined with the assumed aircraft drag listed above, this defined a cruise power requirement of 643 shp, and this value was not varied throughout the optimization study. Cruise tip speed was separately determined for each propeller configuration on the basis of best range.

All propeller performance determinations in this study were computed by the most advanced V/STOL propeller performance methods currently available, as defined in Appendix II. The considerations leading to the selection of four-bladed propellers for this study are also discussed in Appendix II.

Propeller Optimization Criterion

The optimum propeller is now defined as that propeller which will yield the greatest aircraft range for a given payload on the basis of the trade-off assessment of propeller static thrust, cruise efficiency, and propeller system weight for the assumed mission. Cost or mission effectiveness has not been a factor in this study. To evaluate various propeller designs more easily, a relation among static thrust, cruise efficiency, propeller weight, and aircraft range was derived. Briefly, the relationship shows that an increase in static thrust of 1%, or a decrease in propeller weight of 10%, is comparable to an increase in cruise efficiency of approximately 5%. The derivation and final relationship are given in Appendix II.

Optimum Propeller Performance

The optimum propeller was determined by varying the selected parameters, which were number of blades, blade activity factor, design lift coefficient, thickness ratio, cruise tip speed, twist and camber distribution, planform shape, and airfoil sections; and by observing the corresponding performance versus weight trade-offs. Typical blade characteristics are given in Figure 1 for a 105AF, 0.5 C_{L_i} blade. The b/D and C_{L_D} distributions of other propellers studied with different activity factors and integrated design lift coefficients can be calculated by using the b/D and C_{L_D} distributions given in this figure. (For example: a 100 AF propeller would have a similar distribution of b/D along the blade radius, but 100/105 lower in magnitude; similarly a propeller with an 0.4 C_{L_i} would have the same C_{L_D} distribution as shown in Figure 1, but 0.4/0.5 lower in magnitude.)

Representative results for a family of blades having the same twist, camber distribution, basic planform shape, and section airfoils are given in Figures 2 through 7. Figures 2 and 3 show hover performance, and Figures 4 through 7 give the 250-kn cruise performance. The propeller diameter for a disk loading of 35.0 lb/sq ft is superimposed on the figures. Propeller weights estimated from the equations in Appendix II are plotted in Figures 8 and 9. The data from Figures 2 through 9 were then used to generate points on the optimum criterion plot shown in Figure 10, which relates propeller cruise efficiency to static thrust and propeller weight. The relationship is derived by the simultaneous solution of a generalized aircraft component weight equation and the Breguet range equation (Appendix II), which yields the parameters that are plotted in Figure 10 along with lines of constant range. Each point plotted on the figure corresponds to a different propeller geometry. The optimum geometry would be the one farthest to the right in the direction of increasing range.

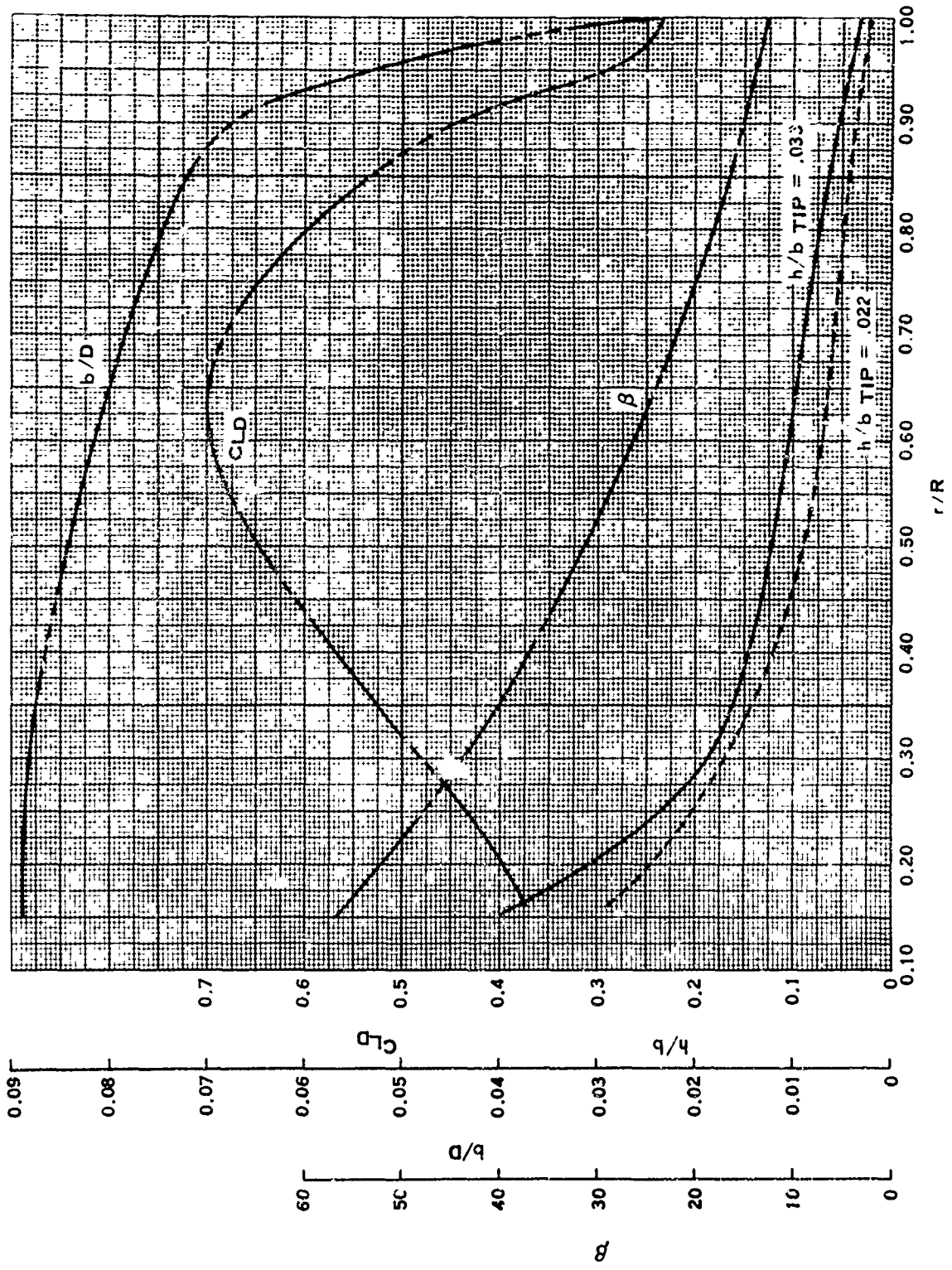


FIGURE 1. TYPICAL BLADE CHARACTERISTICS

$\frac{T}{A} = 35.0$ 1400 HP 6000FT 95° F $900\pi r D$

h/b TIP = .033

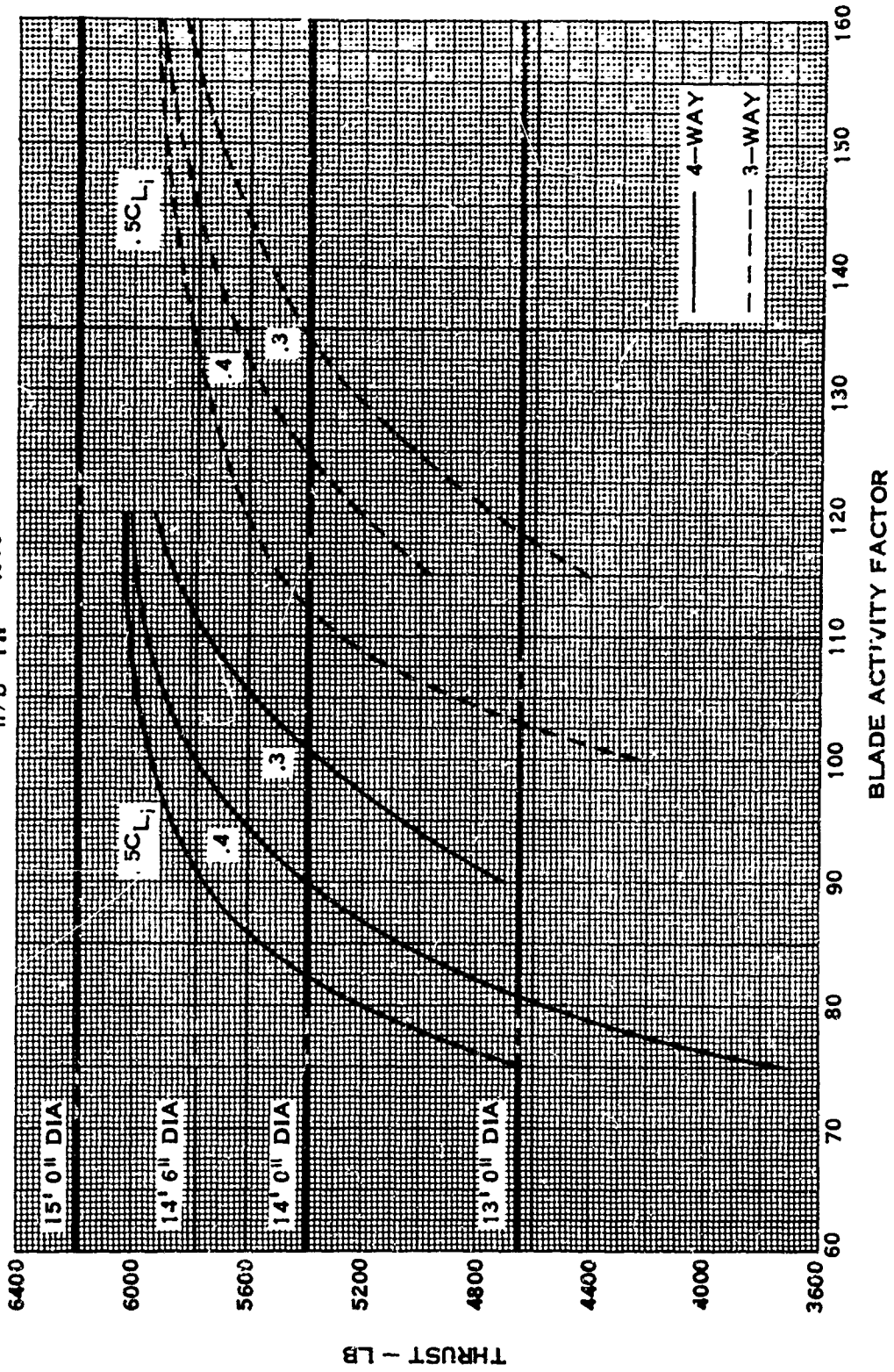


FIGURE 2. STATIC PROPELLER PERFORMANCE - PARAMETRIC STUDY

$\frac{T}{A} = 35.0$ 1400 HP 6000 FT 95° F 9007rD
 h/b TIP = .022

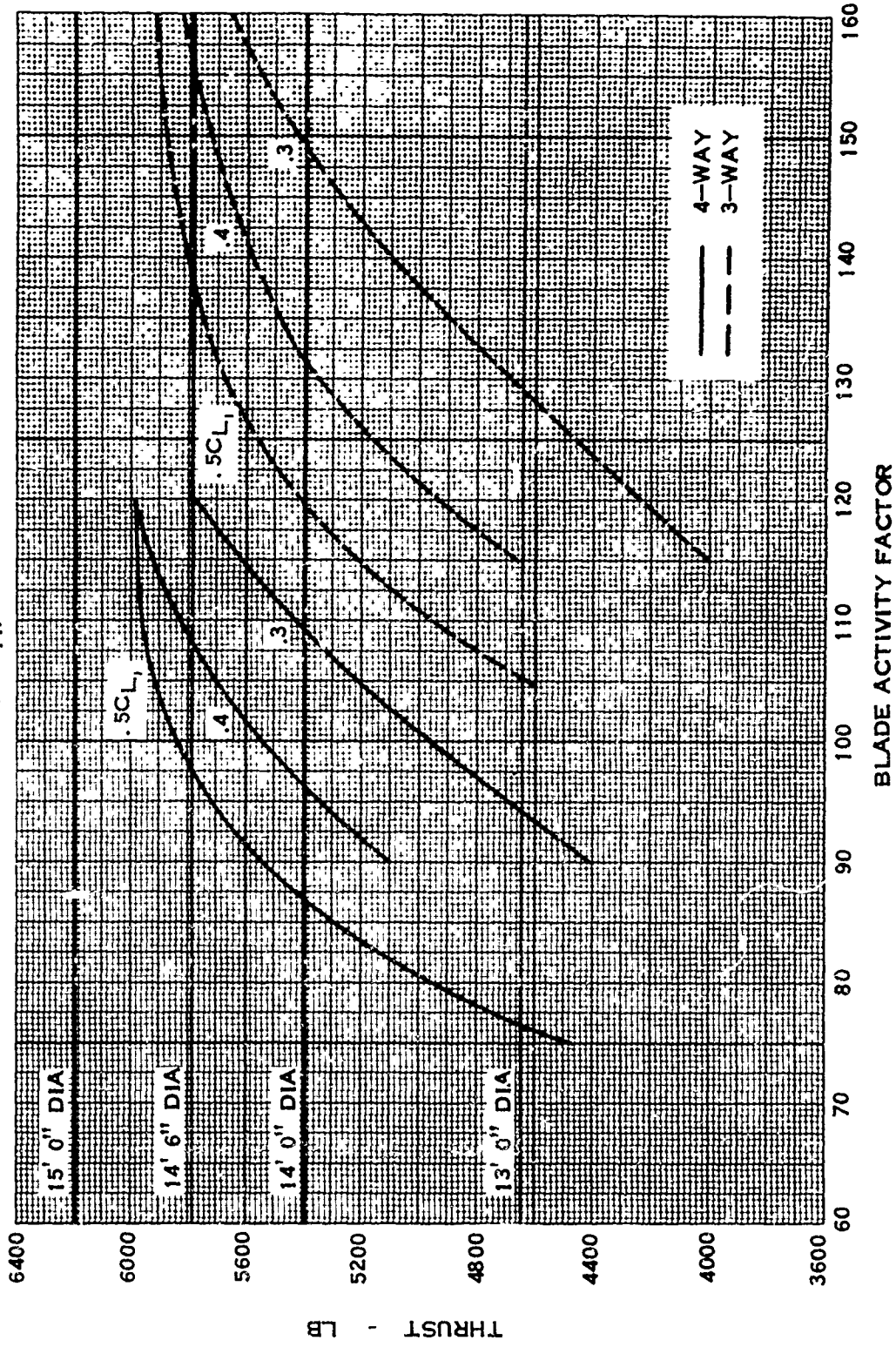
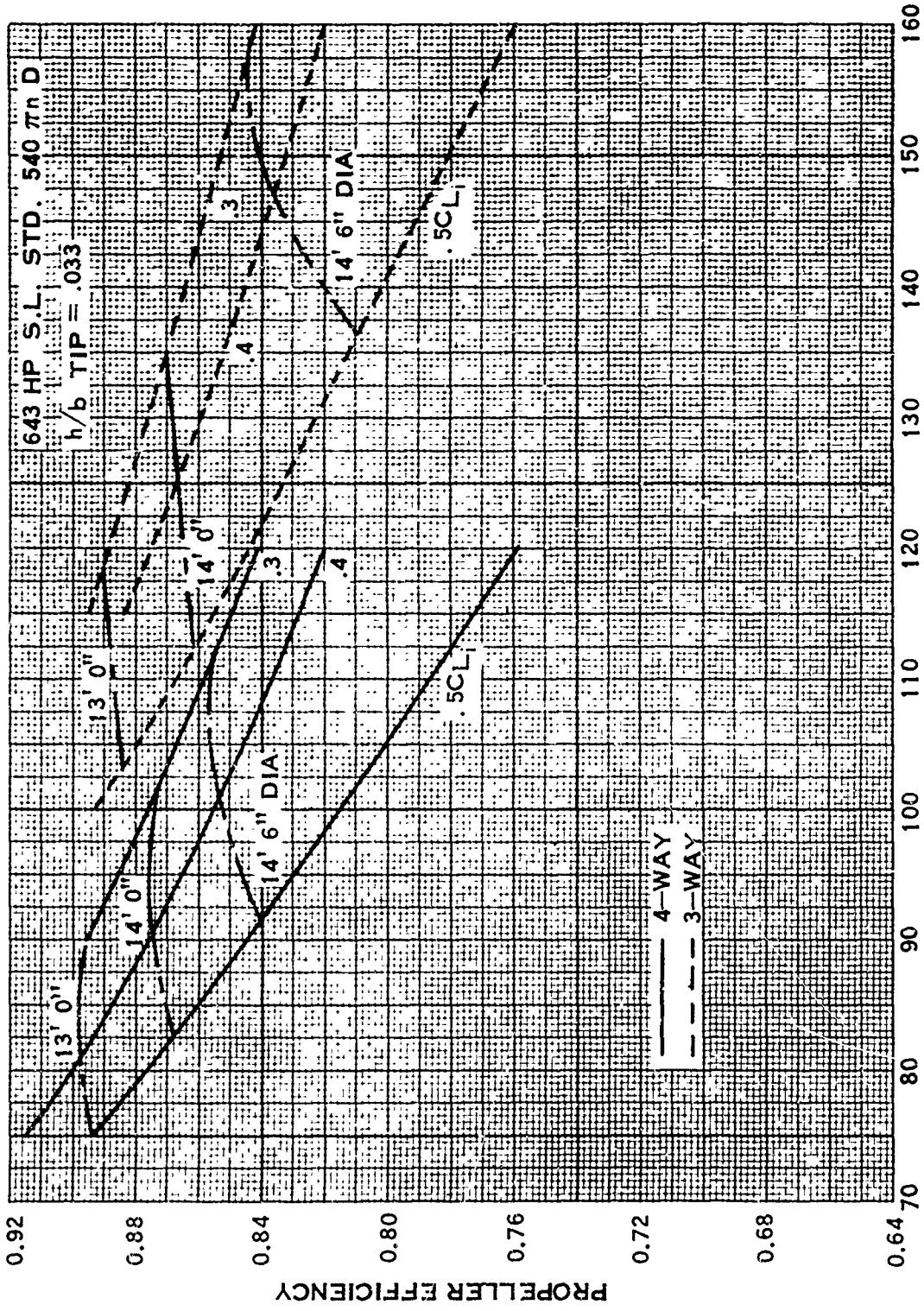


FIGURE 3. STATIC PROPELLER PERFORMANCE - PARAMETRIC STUDY



BLADE ACTIVITY FACTOR
 FIGURE 4. 250-KNOT CRUISE PERFORMANCE -- PARAMETRIC STUDY

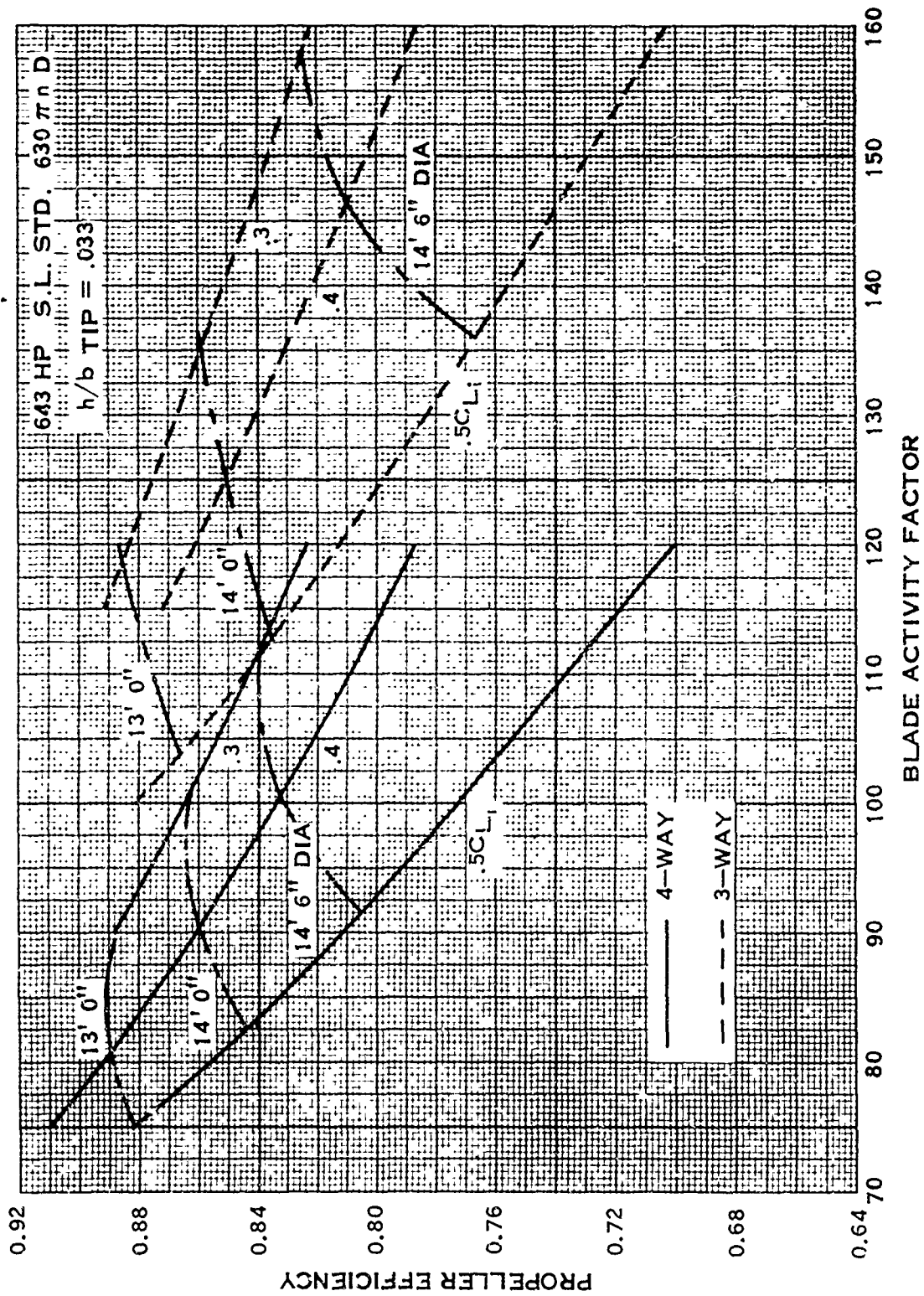


FIGURE 5. 250-KNOT CRUISE PERFORMANCE — PARAMETRIC STUDY

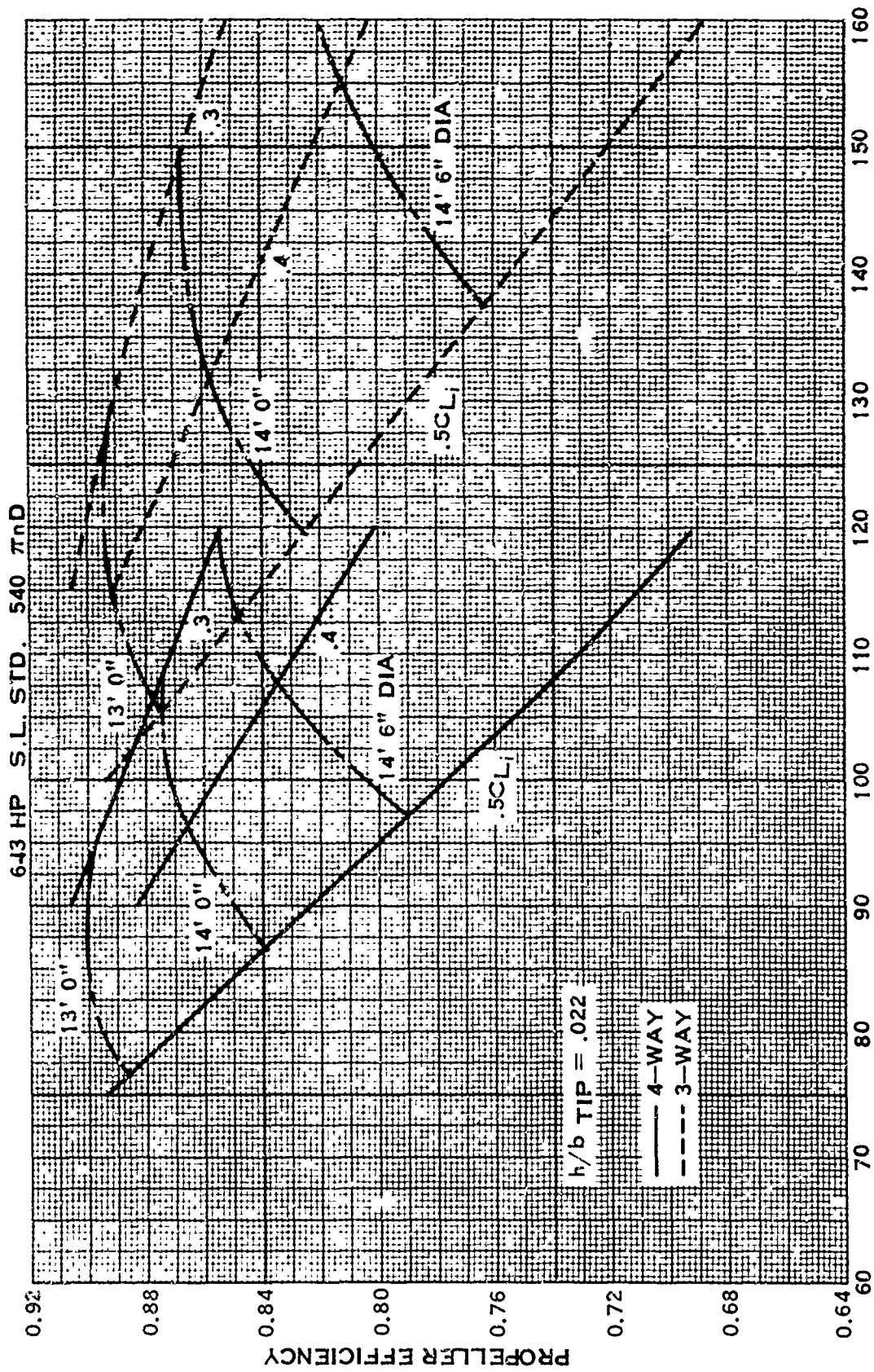


FIGURE 6. 250-KNOT CRUISE PERFORMANCE — PARAMETRIC STUDY

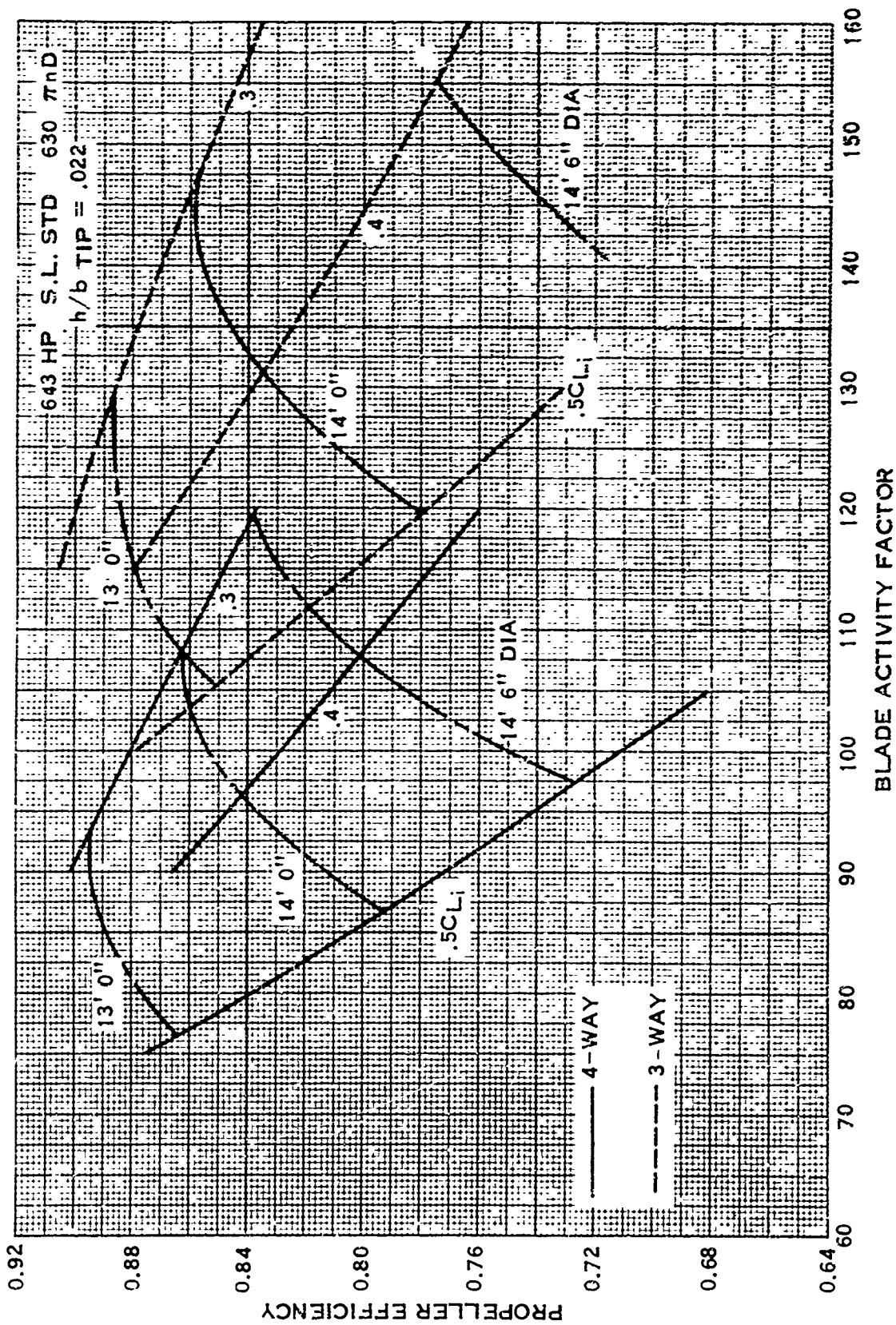


FIGURE 7. 250 KNOT CRUISE PERFORMANCE -- PARAMETRIC STUDY

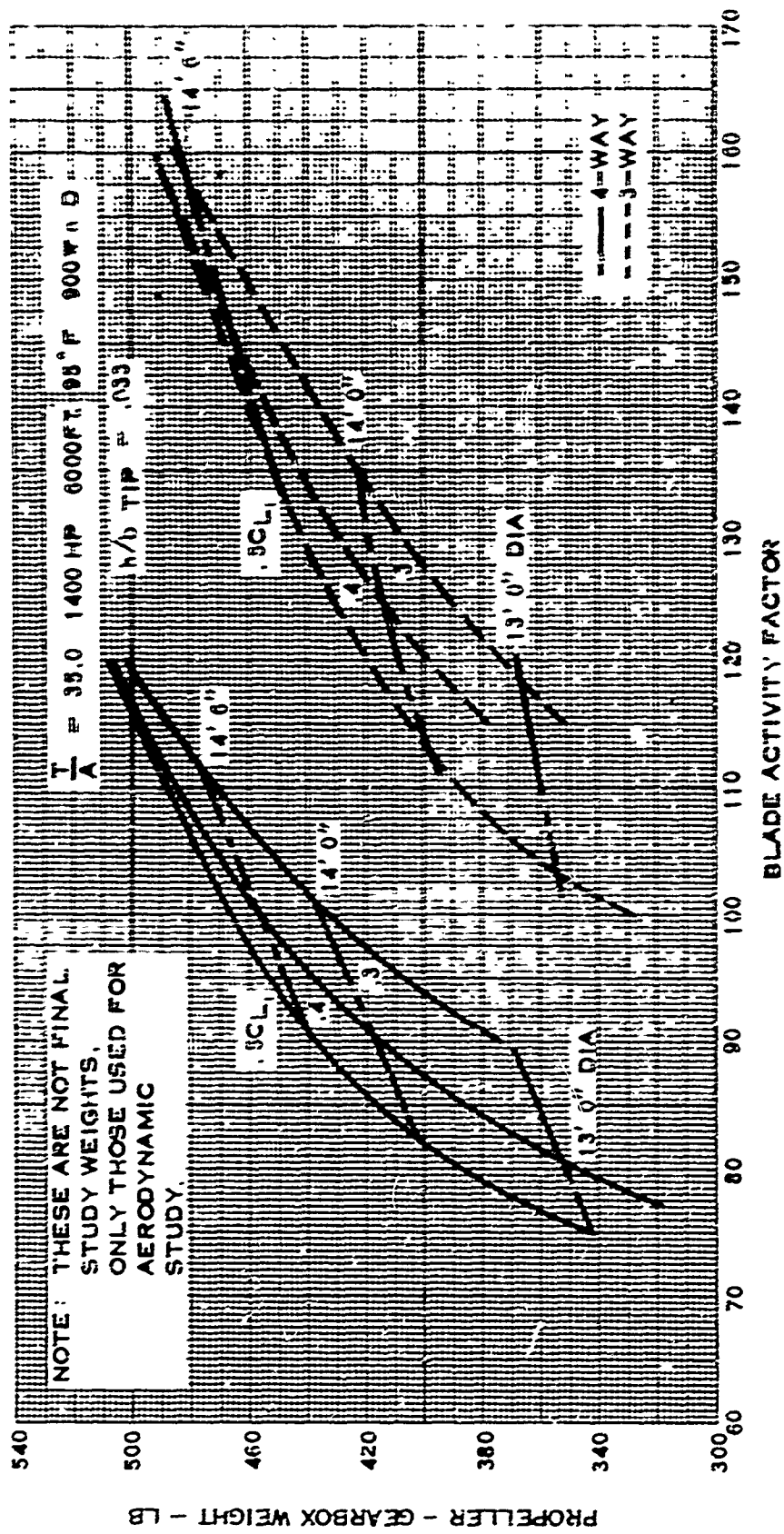


FIGURE 8. PROPELLER AND GEARBOX WEIGHTS--PARAMETRIC STUDY

$\frac{T}{A} = 35.0$ 1400 HP 0000 FT 95 F° 900 RPM

h/b Tip = .022

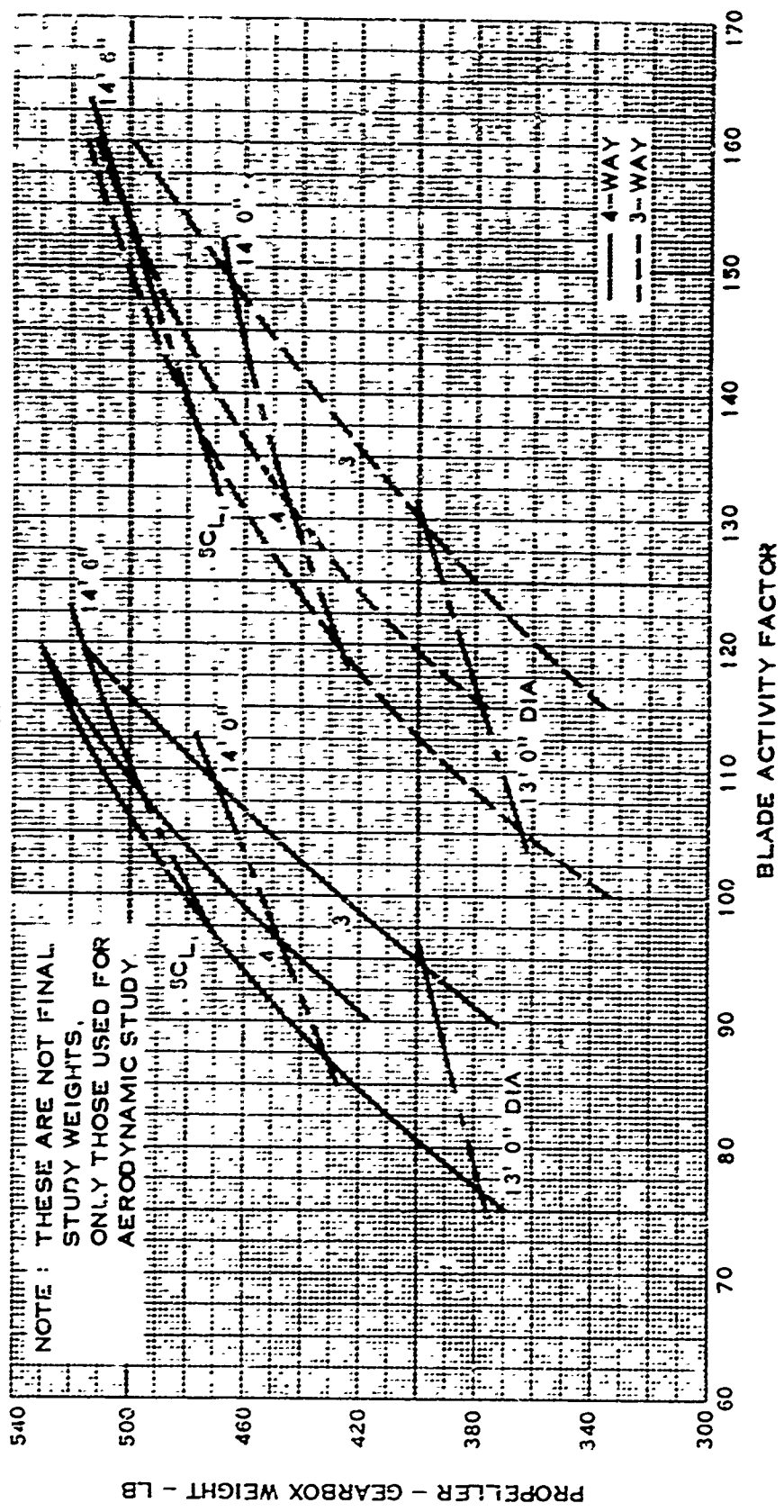


FIGURE 9. PROPELLER AND GEARBOX WEIGHTS—PARAMETRIC STUDY

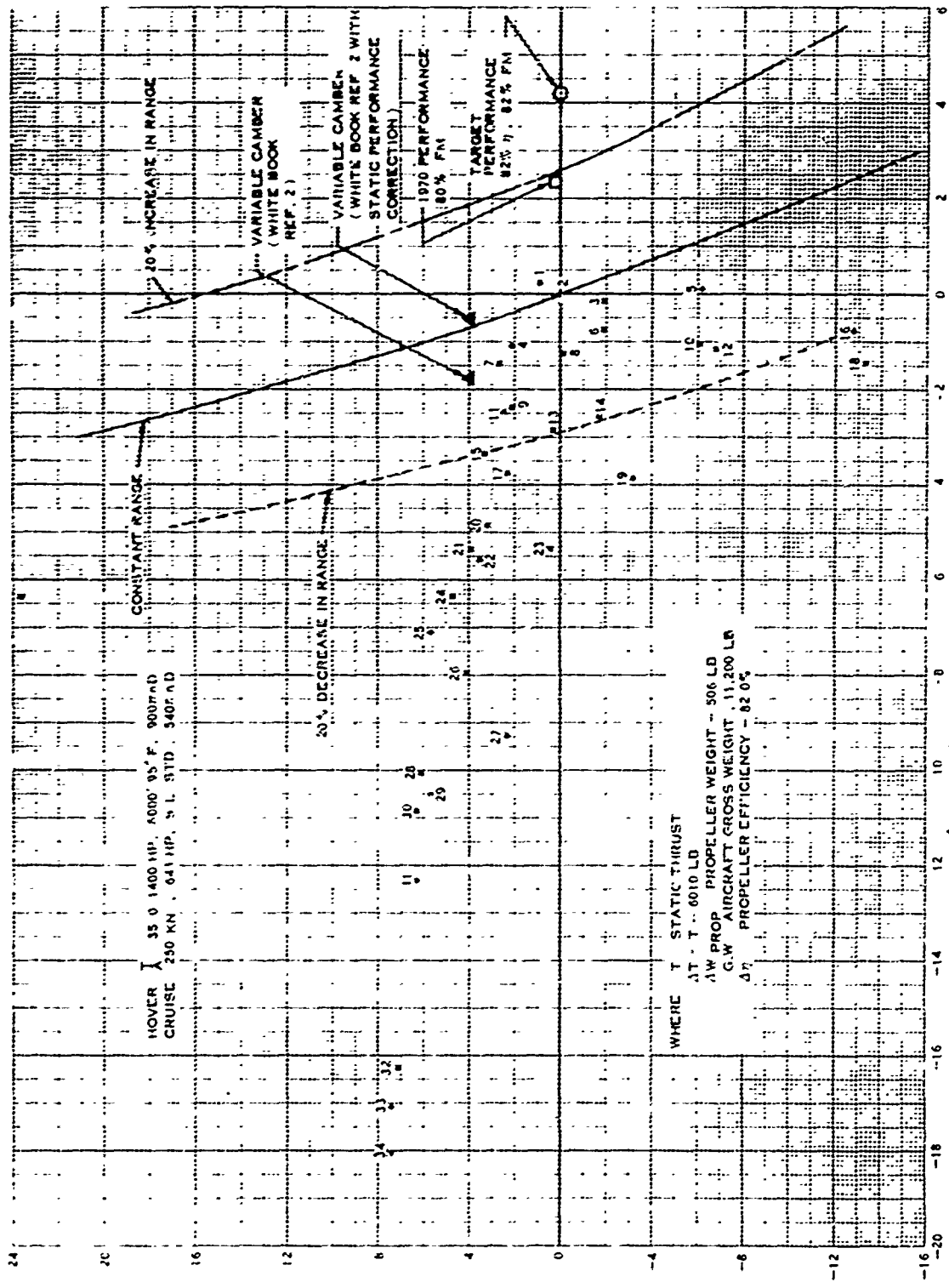


FIGURE 10. PROPELLER OPTIMUM CRITERION PLOT

All points have been referenced to an arbitrary propeller. The reference propeller selected was a four-bladed 120 activity factor, 0.400 design lift coefficient, 0.033 tip thickness ratio propeller. This propeller yielded 82% efficiency at the 250-kn, 540-fps tip speed cruise and a hover figure of merit of 0.773 (6010 lb of static thrust), with a propeller-plus-gearbox weight of 566 lb (preliminary assumed weight). Shown as Propeller #2 in Figure 10, it proved to be the best propeller of the basic family analyzed.

However, Propeller #1, shown slightly to the right of Propeller #2 (reference propeller) in the direction of increasing range, is the optimum design using present state-of-the-art technology. This propeller has the same geometry as the basic family but with a modified planform (slightly increased tip chord).

Changes in blade twist were also studied for this optimum propeller. Static performance gains of up to 1% were estimated to be possible by reducing the blade angle in the tip region. However, the twist change caused the 250-kn cruise performance to drop enough to more than offset the static thrust gain and, thus to reduce the range of the aircraft. Therefore, the twist change was not incorporated. Camber distribution changes are roughly equivalent to twist changes and are not considered to be beneficial. The selected camber distribution has been derived empirically from extensive full-scale propeller tests and was the one which yielded the highest static performance measured to date. NACA series 16 sections have been selected for the outer half of the blade because of their superior performance at high critical Mach numbers. Inboard, NACA series 64 sections have been utilized to yield high lift-to-drag ratios for the thicker sections. Static test experience has shown that this selection of section airfoils yields near-optimum static performance.

Table I identifies some of the propellers plotted in Figure 10. They are listed in the order of descending range. The blade characteristics and performance for the optimum design are listed in the "System Design" section in a performance summary.

1970 Propeller Performance

Also plotted in Figure 10 is the performance that is considered to be realistically obtainable by 1970 (80% figure of merit). It is important to note that this corresponds to an increase in range of nearly 20%. It was assumed in making the cruise performance estimates that this propeller has the same geometry as the present SOTA optimum but in a larger diameter (15'0"), which is needed to maintain 35.0 lb/sq ft disk loading. The target performance for this study (82% figure of merit and 82% cruise efficiency) is also shown in Figure 10.

TABLE I PROPELLER DESIGNS LISTED IN ORDER OF RANGE

DESIGN	B	AF	CL _i	$\frac{1}{6}$ TIP	REMARKS	% RANGE
1	4	120	0.4	0.033	REVISED PLANFORM	3.0 %
2	4	120	0.4	0.033	ORIGINAL PLANFORM	0.0 %
3	4	105	0.5	0.033	ORIGINAL PLANFORM	- 3.0 %
4	4	120	0.3	0.033	ORIGINAL PLANFORM	- 5.2 %
5	4	120	0.5	0.033	ORIGINAL PLANFORM	- 6.6 %
6	4	120	0.4	0.022	ORIGINAL PLANFORM	- 7.1 %
7	4	105	0.4	0.033	ORIGINAL PLANFORM	- 7.5 %
8	3	160	0.4	0.033	ORIGINAL PLANFORM	- 8.8 %
9	3	160	0.3	0.033	ORIGINAL PLANFORM	-14.3 %
10	3	160	0.5	0.033	ORIGINAL PLANFORM	-14.3 %
11	4	90	0.5	0.033	ORIGINAL PLANFORM	-14.3 %
12	4	105	0.5	0.022	ORIGINAL PLANFORM	-14.3 %
13	3	130	0.5	0.033	ORIGINAL PLANFORM	-14.3 %
14	3	130	0.4	0.022	ORIGINAL PLANFORM	-14.3 %
15	4	120	0.3	0.022	ORIGINAL PLANFORM	-20.0 %
16	4	120	0.5	0.022	ORIGINAL PLANFORM	GREATER THAN 20%LOSS
17	4	105	0.4	0.022	ORIGINAL PLANFORM	GREATER THAN 20%LOSS
18	3	160	0.5	0.022	ORIGINAL PLANFORM	GREATER THAN 20%LOSS
19	3	130	0.5	0.022	ORIGINAL PLANFORM	GREATER THAN 20%LOSS
20	3	160	0.3	0.022	ORIGINAL PLANFORM	GREATER THAN 20%LOSS
21	3	130	0.4	0.033	ORIGINAL PLANFORM	GREATER THAN 20%LOSS
22	3	115	0.5	0.033	ORIGINAL PLANFORM	GREATER THAN 20%LOSS
23	4	90	0.5	0.022	ORIGINAL PLANFORM	GREATER THAN 20%LOSS
24	4	105	0.3	0.033	ORIGINAL PLANFORM	GREATER THAN 20%LOSS
25	4	90	0.4	0.033	ORIGINAL PLANFORM	GREATER THAN 20%LOSS
26	3	130	0.4	0.022	ORIGINAL PLANFORM	GREATER THAN 20%LOSS
27	3	115	0.5	0.022	ORIGINAL PLANFORM	GREATER THAN 20%LOSS
28	4	105	0.3	0.022	ORIGINAL PLANFORM	GREATER THAN 20%LOSS
29	3	130	0.3	0.033	ORIGINAL PLANFORM	GREATER THAN 20%LOSS
30	4	90	0.4	0.022	ORIGINAL PLANFORM	GREATER THAN 20%LOSS
31	3	115	0.4	0.033	ORIGINAL PLANFORM	GREATER THAN 20%LOSS
32	3	115	0.4	0.022	ORIGINAL PLANFORM	GREATER THAN 20%LOSS
33	4	75	0.5	0.033	ORIGINAL PLANFORM	GREATER THAN 20%LOSS
34	3	115	0.3	0.033	ORIGINAL PLANFORM	GREATER THAN 20%LOSS

An 30 figure of merit propeller should be conservatively obtainable in the future through the combined attack of further experimental investigation and refinement of static thrust propeller theory. Previous testing at Wright Field on Propeller Static Test Rig #4 has yielded figures of merit slightly over 79% on propellers that have had blade tips retwisted. Calculations, however, have shown excessive cruise efficiency losses for retwists of this type. Other tests have shown that small detailed tip geometry changes have appreciably affected static performance, indicating that proper changes in twist, tip planform, and tip camber could yield significant increases in figure of merit without hurting cruise performance. Some tests of this type are planned in 1968. In addition, it is expected that new, rigorous static propeller theories and design methods will soon become available. (For example, Therm Advanced Research, Cornell Aeronautical Laboratory, and United Aircraft are each working on the derivation of advanced static propeller theory.) These theories should help to define the optimum static propeller configuration.

Variable Camber Propeller

An evaluation of the variable camber propeller performance for the hover and cruise design points based on Reference 2 "White Book" indicates that the propeller yields a lower range than the optimum fixed camber propeller. This is primarily because of the relatively low hover disk loading and the low 250-kn cruise speed requirement. This situation could possibly change in the future and is discussed below.

The geometric feasibility of the variable camber propeller had been established with the design, fabrication, and static whirl testing of two different full-scale propellers. Moreover, several wind tunnel tests had been previously performed on six different model variable camber propellers over a Mach number range from 0.02 to 0.85 in the United Aircraft Research Laboratories facility. The latest test, which provides data on four models, was completed in October 1967. A generalization of these test data indicates an envelope static performance level significantly above the envelope which was previously expected and outlined in Reference 2. This is probably attributable to a beneficial slotted-flap effect of the paired blades, which had not been considered in preparing the static thrust charts of Reference 2. Unfortunately, all but one of the variable camber test propellers mentioned above were designed for hover power loadings above the range of interest in this study. Thus, the static performance in the range of interest has not been solidly established.

The performance of a six-way, 100 activity factor propeller was estimated using both the method of the "White Book" (Reference 2) and this method with the static thrust corrected to represent the latest test experience more closely. These two points are also shown in Figure 10. It is apparent from the graph that, on the

basis of available test data, the variable camber propeller indicates promise for application to V/STOL aircraft. However, the greatest benefit would be for propellers sized at disk loading ranges higher than the range used in this study. In view of the limited test data in the low power loading range, more experimental data are needed, particularly static performance on large-scale models, to ascertain the performance potential of the variable camber propeller for V/STOL aircraft of the 1970's.

Cyclic Pitch Propeller

A computerized performance calculation method recently developed was used to determine the cyclic pitch propeller performance. The program is a variation of the normal propeller performance strip analysis method, in that it allows the propeller blade angle to vary with time in any prescribed manner. Checks of the cyclic pitch propeller method with test data have been difficult because of the small amount of reliable test data available. The most comprehensive data were found in the test of a 6-foot-diameter propeller which was accomplished under USAAVLABS sponsorship (Reference 4). However, these data also exhibited a large percentage of scatter.

A comparison of the cyclic pitch propeller performance method and test data is shown in Figures 11 and 12. Figure 11 shows a comparison of the thrust loss due to cycling blade angle at a fixed value of power coefficient (C_p). The C_p chosen was that giving the peak figure of merit. Although the calculation is within the band of scatter of the test data, it is believed that the use of unsteady airfoil data may improve the accuracy of the computation.

Figure 12 shows the comparison of cyclic pitch control moment for the same power coefficient condition of 0.07. The correlation of calculation and test is quite good.

The calculated cyclic pitch propeller performance (thrust loss, control moment, and thrust offset) of the optimum propeller is given in the performance summary of the "System Design" section. For the design studies, a maximum control moment requirement equivalent to a 25% offset of the thrust vector was assumed. This required a maximum cyclic blade angle of 9.6° , which could cause a thrust loss of 12.5%.

Engine Scaling

The propeller parametric study and the ensuing optimum propeller selection were based on the utilization of a 2000-hp (S. L., standard day) engine. It is of interest to see what effect scaling the engine to a different size and horsepower will have on the propeller aerodynamic design and performance. To take an example, assume

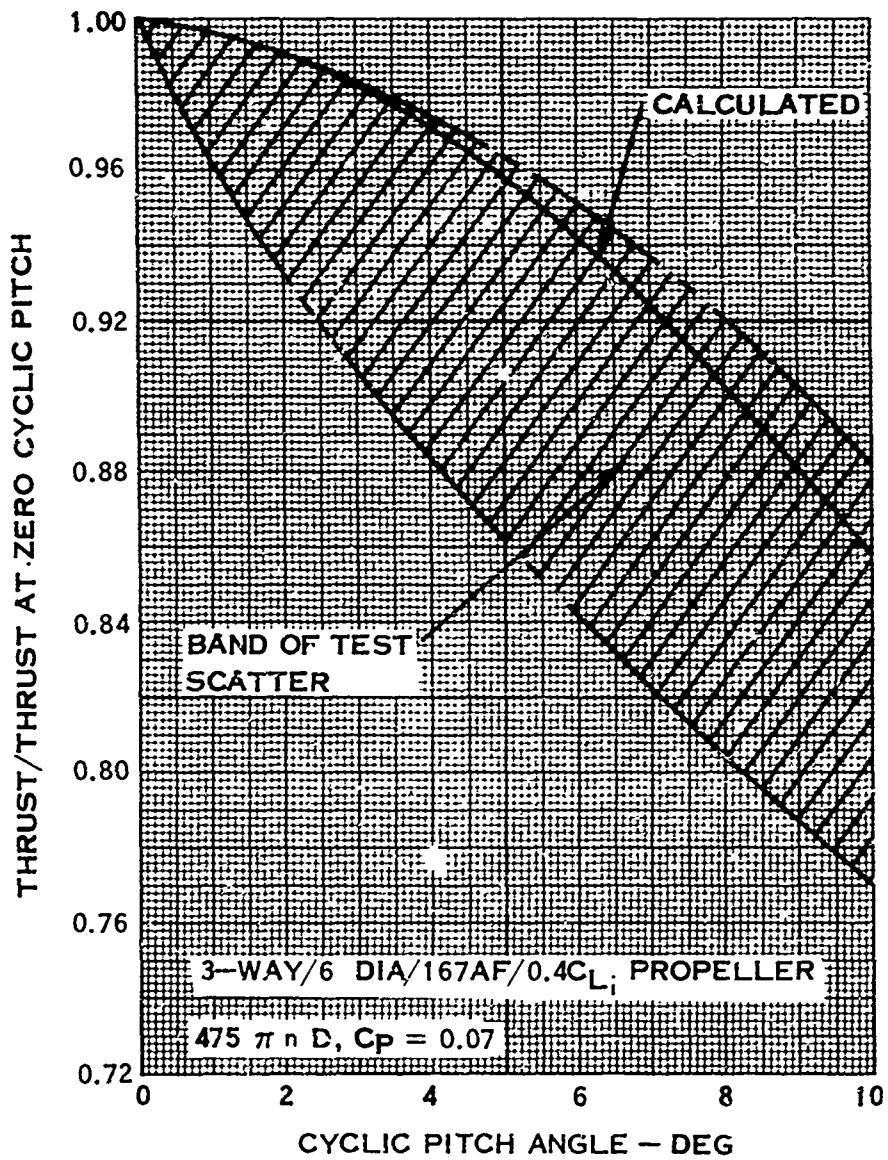


FIGURE 11. CYCLIC PITCH PROPELLER STATIC THRUST PERFORMANCE COMPARISON

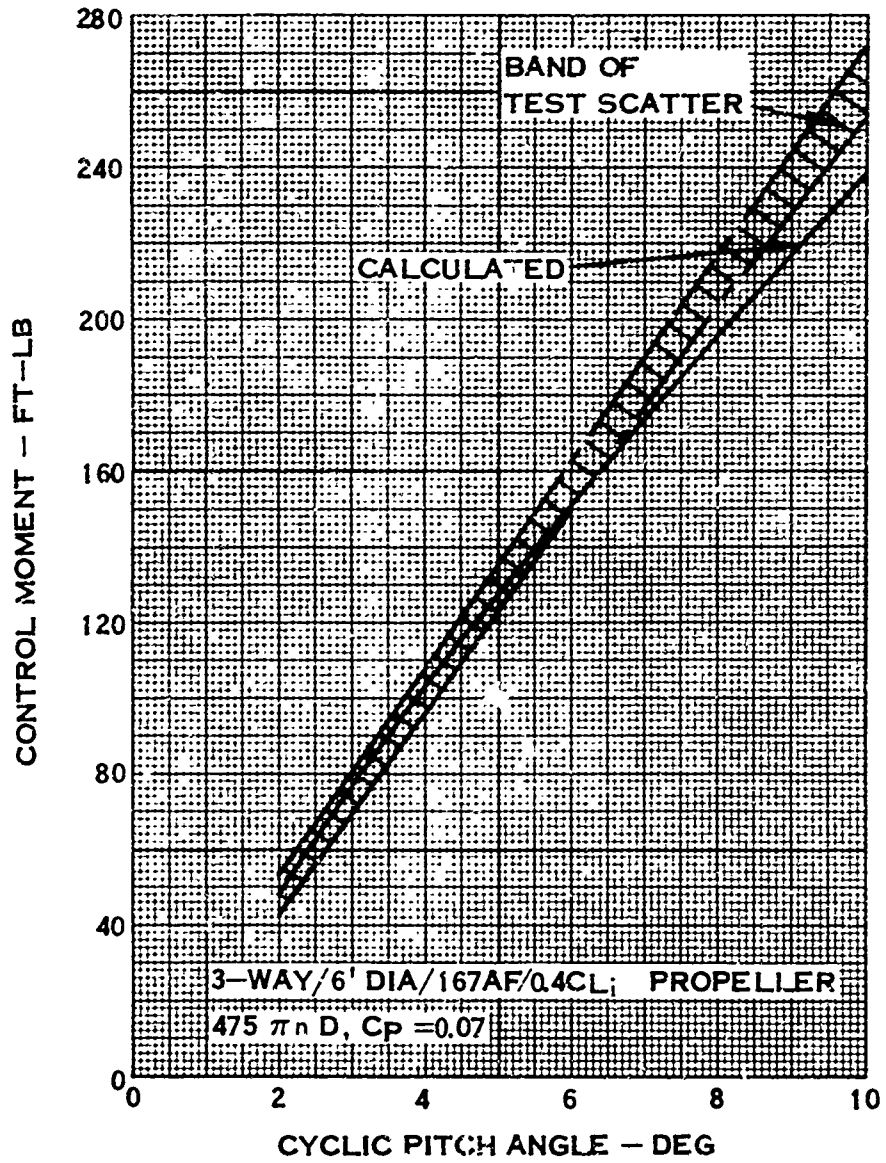


FIGURE 12. CYCLIC PITCH PROPELLER STATIC CONTROL MOMENT COMPARISON

that the 2000 hp is scaled down to 1500 hp. As before, the 6000 ft, 95° F power is reduced to 70%, which is 1050 hp. Since the disk loading is still 35 lb/sq ft, the optimum propeller geometry would not be changed except for diameter. This can be proved by showing that scaling the horsepower does not change the design power coefficient, C_p , at the hover and 250-kn cruise conditions if the diameter is adjusted to maintain the same disk loading. The optimum blade design is still completely defined on the basis of hover and 250-kn cruise performance and propeller weight. If the operating power coefficients at hover and cruise are unchanged, then the performance and the nondimensional blade geometry that yields the performance are also unchanged for the same tip speeds.

To show that the power coefficients are unchanged, look first at hover. Since the disk loading (T/A) is unchanged, so is the thrust coefficient (C_T). For a given geometry, the relation between C_T and C_p is fixed; therefore, the C_p must remain unchanged. Since C_p is proportional to HP/D^2 at a given propeller tip speed, the optimum propeller must be reduced in diameter to yield the same figure of merit. Since horsepower was reduced from 1400 to 1050 hp, the diameter must be reduced to 12.8 feet to maintain a constant HP/D^2 .

Lowering the horsepower by 25% also lowers the thrust by 25%. This reduces the airplane gross weight by the same amount. The assumption was also made in this study that the profile drag coefficient was a function only of wing loading which remains unchanged at 70 lb/sq ft. The induced drag coefficient and lift coefficient were also functions of wing loading. Therefore, the aircraft L/D is independent of gross weight. Thus, a lower gross weight yields a lower drag and therefore a lower thrust required in cruise. Since these changes are all directly proportional, the horsepower required at the 250-kn cruise is also lowered by 25%. This then keeps the C_p unchanged and keeps the cruise efficiency the same.

In summary, engine scaling affects the propeller diameter but not the blade design (i. e., AF , C_{Li}), the hover figure of merit, or the cruise efficiency. The term HP/D^2 remains a constant. Therefore, the following equation can be written for the required propeller diameter for some other size engine.

$$D = 14.8 \sqrt{\frac{HP}{1400}} \quad (1)$$

where HP is the horsepower available to the propeller on a 6000 ft, 95° F day.

AERODYNAMIC STATE-OF-THE-ART REVIEW

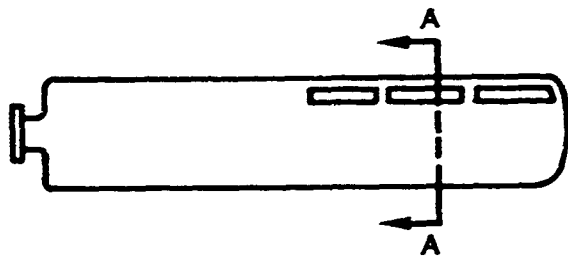
The aerodynamic blade optimization study discussed in detail in the previous section utilized present state-of-the-art techniques and experience. The optimization criterion developed as part of this study showed that for constant range, a 1-percent change in static thrust produces the same effect as a 5-percent change in 250-kn cruise efficiency. Within these ground rules, the optimum propeller that could be predicted using presently known technology yielded a figure of merit of 0.776 and a cruise efficiency of 0.829. It was also shown that figures of merit of 79% are now attainable but not without large cruise losses and therefore a reduction in available aircraft range.

The above, then, briefly summarizes today's V/STOL propeller performance technology. With this as a base point, consideration was directed to defining the 1970-1975 potential for improved static thrust and cruise efficiency. Projections, predicted on continuing active experimental and theoretical research, show potential gains of from 6 to 8% in 250-kn cruise efficiency and perhaps as much as 2 to 4% in static thrust. However, determining the exact potential gain in static thrust is difficult.

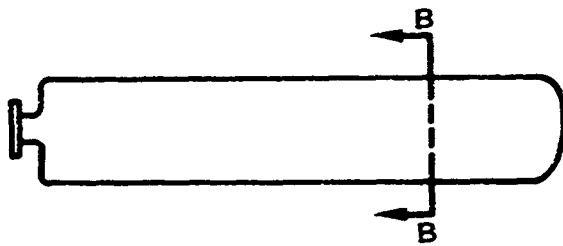
The problem arises because of both the lack of an adequate static propeller theoretical method to analytically relate geometry parameters to performance, and the lack of a sufficient amount of parametric static propeller test data from which to derive an empirical performance method. Therefore, even the ultimate attainable level of static performance is not yet definable. If an accurate theory or empirical method does become available, it will contribute greatly toward advancing V/STOL potential, because of the high leverage of static thrust on V/STOL mission effectiveness.

Programs aimed at accomplishing the derivation of a static propeller theory are being pursued. Moreover, experimental programs have been proposed and should be undertaken. However, there are other prospects for improving V/STOL propeller performance which can be generally classed as unconventional aerodynamic configurations. The purpose of this portion of the study is to initiate some of the groundwork for evaluating the potential for some of these unconventional aerodynamic configurations.

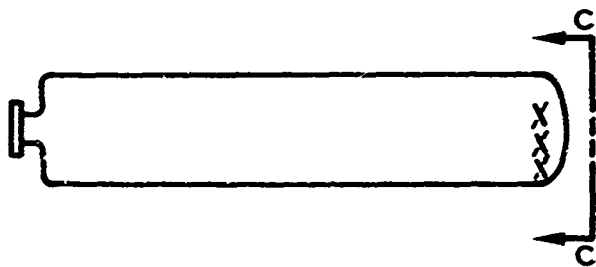
Because of the success wing designers have had with high lift devices, the aerodynamic feasibility of slots, flaps, slotted flaps, and vortex generators, as applied to the V/STOL propeller, was studied. In addition, devices that could improve the severe three-dimensional flow effects in the blade tip region were also given consideration. Some of these concepts are sketched in Figure 13. Each is discussed in the following sections; finally, the results of this phase of the study, as well as recommendations for further R&D, are outlined.



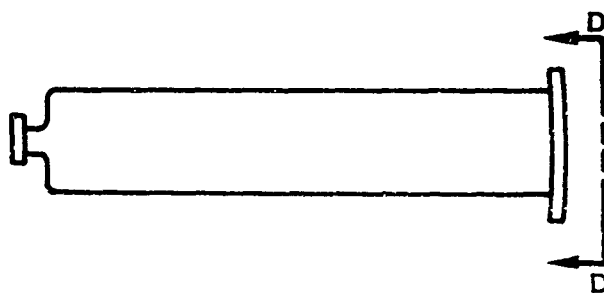
SLOTTED PROPELLER



FLAPPED PROPELLER



VANED PROPELLER



END-PLATED PROPELLER



FIGURE 13. CONCEPTS OF BLADES INCORPORATING AERODYNAMIC DEVICES

Slotted Propeller Blades

Traditionally, fixed slots on wings have been used to extend the linear portion of the lift curve to a higher stall angle of attack. Thus, much higher maximum lift coefficients can be obtained. Typical comparative performance of a wing with and without an optimum slot, taken from Reference 5, can be seen in Figure 14. It is noted that the slot improves the performance once stall takes place. Its effect on lift-to-drag ratio is given in Figure 15. Below stall, the data for the slotted airfoil predict a reduction in performance.

As applied to propeller blades, it would appear that slots could benefit a stalled portion of the blade. In order to gain some insight into the effect of slots on V/STOL propeller performance, some calculations were attempted. First an assumption was made that the change in airfoil performance shown in Figure 14 was typical of all slotted airfoils and relatively independent of series section, the thickness ratio, camber, and Mach number. (More will be said about this assumption later.) This fact yielded the slotted airfoil correction $C_{L,slot}$ which is shown in Figure 16. The Univac 1103 propeller performance strip analysis program was modified to accept these incremental airfoil changes. It was noted that the inboard sections of the optimum propeller were operating at high angles of attack at the design hover condition. The hover and 250-kn cruise performance of the optimum SOTA propeller was recalculated installing leading-edge slots in the stank region (out to 46% blade radius). The hover figure of merit was raised only from 0.776 to 0.778. The 250-kn performance was lowered from 0.829 to 0.805. The net effect was a reduction in aircraft range, indicating that, based on calculation, slots would not improve the performance of a propeller at its design condition. A propeller design different from the optimum selected was also analyzed. The performance of the optimum propeller with a lowered activity factor of 75 was calculated with slots in both the stank and the tip region. In hover, an increase in FM of 4.5% was predicted with a decrease in cruise efficiency of 5.5%, the total effect was a definite improvement.

Because of the known deficiencies of the strip analysis calculation method in predicting static performance, and because of the crude approximation made of the slotted airfoil data, it was felt desirable to check the calculation against a known quantity. Hamilton Standard has tested an XC-142 propeller with and without leading edge slots at Wright Field's Rig #1 during 1967. The original intention of the test was to install slots in the tip region to alleviate the undesirable three-dimensional effects caused by the strong tip vortex. Unfortunately, for structural reasons, the slots were not located beyond the 0.95 blade radius station. The leading edge slots extended inboard to about the 0.60 station. The slot geometry was selected on the basis of available test data, and no attempt was made to optimize the slot geometry further. Also, because of the unavailability of Rig #4 at Wright Field, testing had to be done on Rig #1, which, because of strong wall effects,

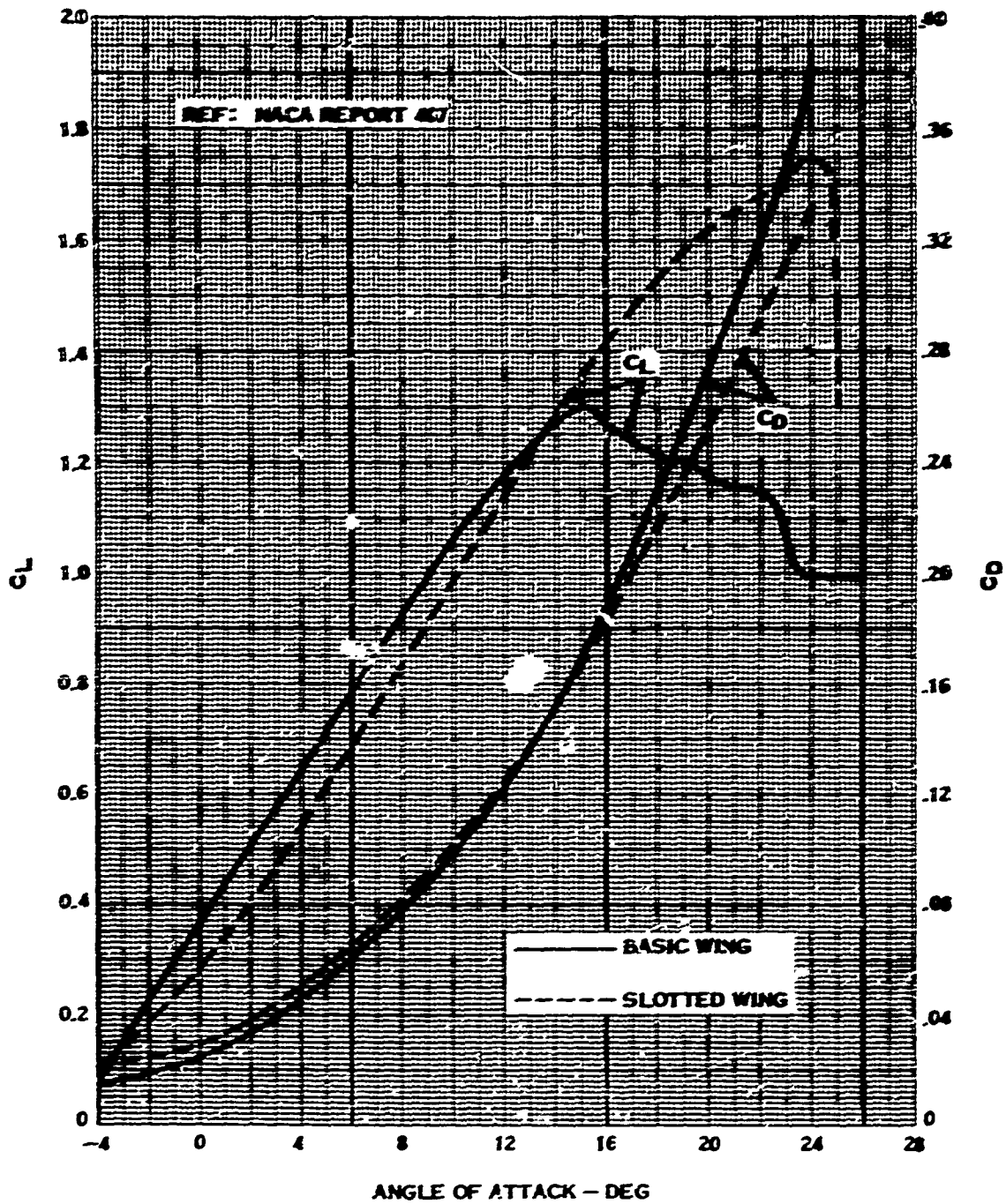


FIGURE 14. SLOTTED AIRFOIL CHARACTERISTICS (11.8% CLARK Y)

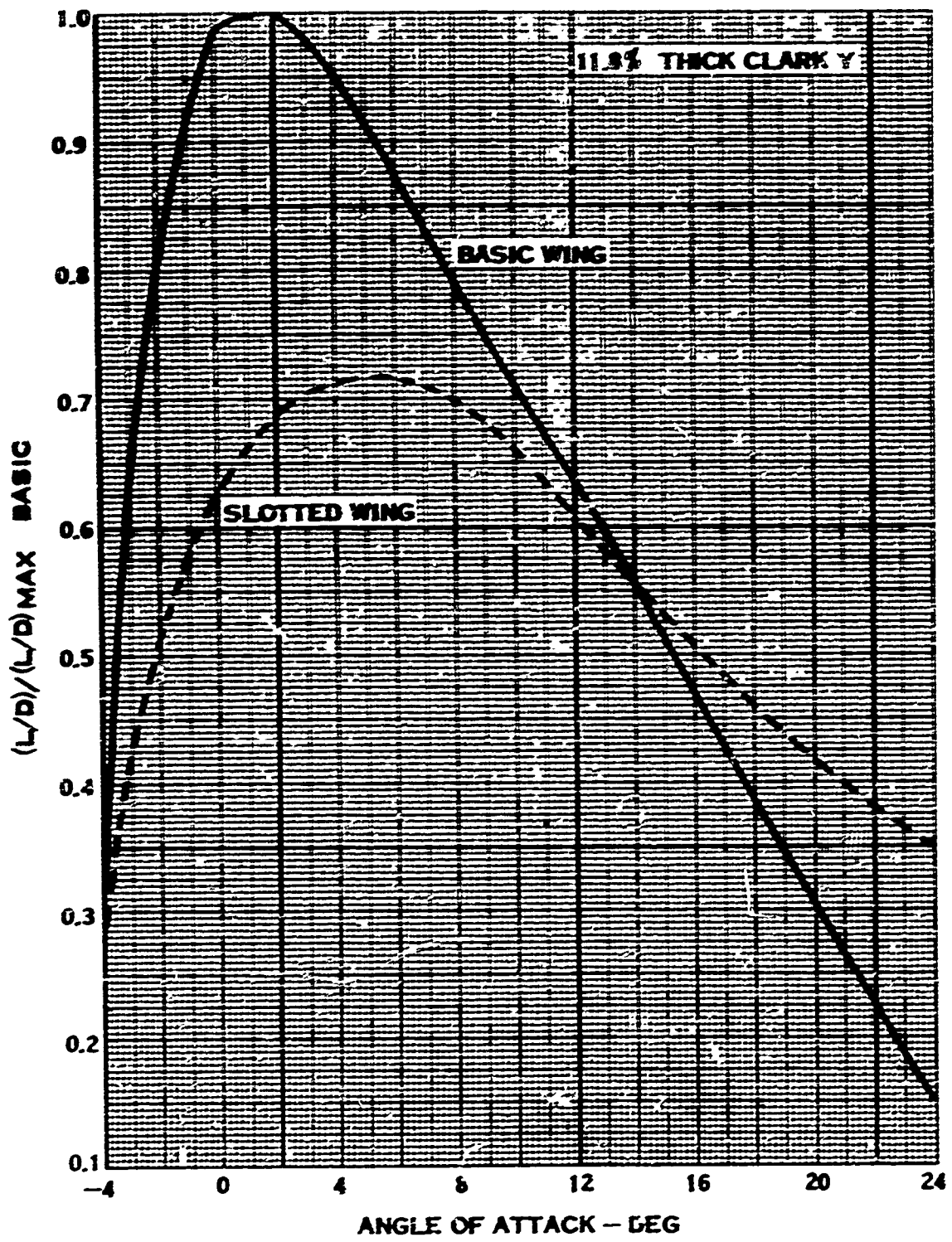


FIGURE 15. EFFECT OF LEAD-EDGE SLOTS ON LIFT-TO-DRAG RATIO

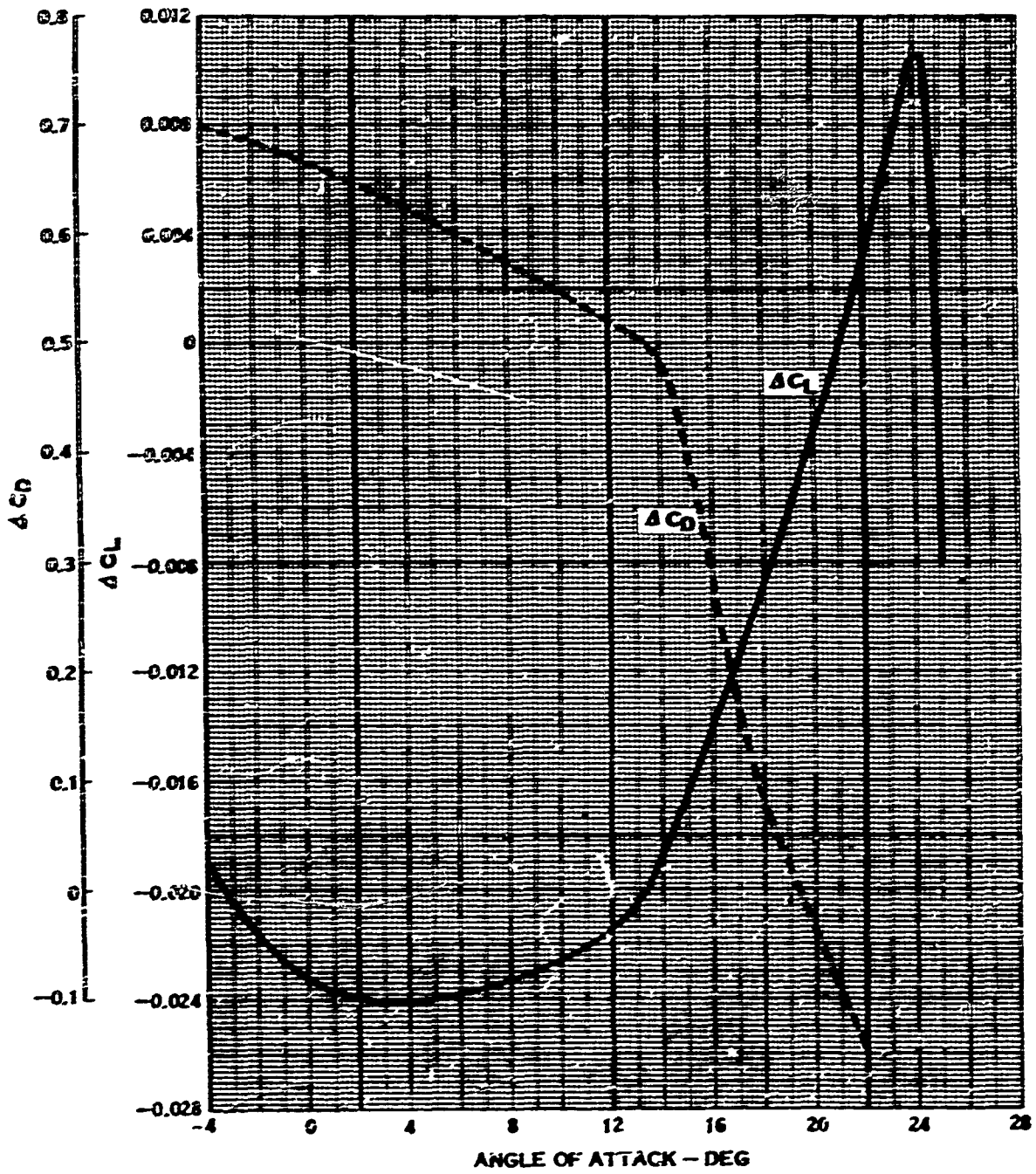


FIGURE 16. SLOTTED AIRFOIL CORRECTION CURVE

yields lower performance than the free propeller. However, it was believed that the comparative performance of the slotted and unslotted propellers was valid. Figure 17 shows the comparative performance on a figure of merit versus power coefficient plot. Note that the slotted propeller is lower only by 1% or less in figure of merit in the normal operating regime (C_p between 0.07 and 0.10) for a propeller of this solidity. A performance calculation was then run which predicted a larger reduction in slotted propeller performance of 6.5%. This indicates two possible sources of error in the calculation, both of which are interesting. The first is that the Goldstein inflow, upon which the strip analysis calculation is based and which neglects contraction as well as the strong tip vortex, predicts a much higher inflow in the tip region than actually exists. This means that the calculation would predict a lower angle of attack. In actuality, the tip stations may be stalled or near stall and in a region where the slots start to show benefits. Yet on Rig #4, this propeller without slots yielded a peak figure of merit of 78%. The geometry of the propeller tested is similar to the propeller geometry optimized for this study. A 78% figure of merit has been obtained, and if the blade tips are not operating efficiently, the possibility then exists to make important gains by systematic propeller testing to define the optimum tip configuration. The other possible error in the calculation deals with the use of the corrected slotted airfoil curve of Figure 15. It may be too pessimistic for this series 15 sections in a propeller flow field. If this were so, it could explain the high variable camber propeller static performance as discussed in the previous section. The variable camber design is very similar to that of a slotted flap. However, if two-dimensional slotted-flap data are studied (for example, Reference 6), the maximum lift-to-drag ratio is lower compared to the basic airfoil. Again, improvement is seen only after stall is reached. Variable camber static test data indicate an improvement in L/D near its maximum value.

In summary, the effect of slots on propeller performance has not been satisfactorily determined. Calculations appear to give pessimistic results compared to the more encouraging experimental results. There is also a possibility that the outboard sections of the optimum propeller are operating at too high an angle of attack, which is not predicted by the Goldstein inflow theory. There appears to be a potential for improvement in V/STOL propeller performance by the use of slotted blades, but this will have to be defined by further testing.

Flapped Propeller Blades

Putting fixed flaps on propeller blades is not a new concept. Many steel blades manufactured in the 1940's and 1950's were made with trailing edge extensions, which were generally used to increase activity factor or to resolve a structural problem. They were installed with a flap angle to simulate a desired camber level in accordance with the theory of Reference 7. On the basis of two-dimensional airfoil data, the indications are that higher L/D's are possible by adding camber

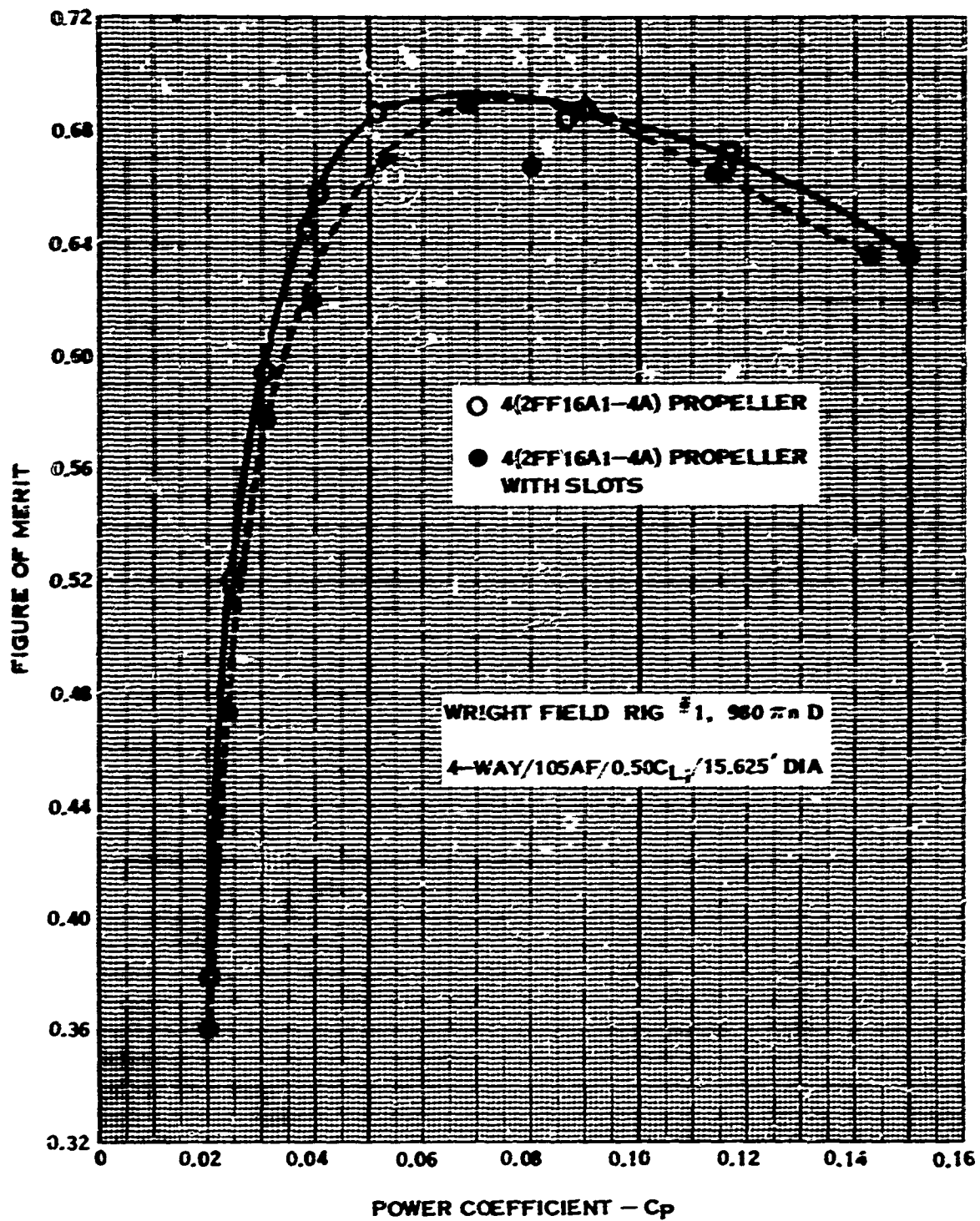


FIGURE 17. STATIC PROPELLER PERFORMANCE COMPARISON WITH AND WITHOUT SLOTS

rather than flap angle. There is now available Wright Field Rig #4 static test data of a propeller with fixed flaps (wedges were added to the blade trail edge to simulate split flaps) and a propeller with increased tip camber. Both tests showed about the same effect. There was no improvement in peak figure of merit; however, there was improvement at the higher C_p 's beyond the peak figure of merit of about 15% in figure of merit.

On the basis of limited test data, flapped propeller blades do not appear to show much potential of increasing static propeller performance capability and state of the art. Flaps do, however, improve off-design static performance and may have merit for certain installations other than V/STOL applications; for example, on aircraft having cruise speeds where high critical Mach numbers for the blade sections would increase cruise efficiency. The critical Mach number of a flapped airfoil is higher than that for an unflapped airfoil of the same equivalent camber.

Vortex Generators on Propeller Blades

Vortex generators have been successfully used on wings to extend the angle of attack range to a higher stall angle. The tip vortex tends to mix the high-energy air with the low-energy boundary layer. This mixing temporarily prevents flow separation. It was also discovered by NACA in Reference 8 that vortex generators were unsuccessful when utilized on thin airfoils which tend to separate near their leading edge. This indicates that installing vortex generators in the propeller blade tip region, where thin airfoils are used, would not be beneficial.

Utilizing vortex generators in a completely different manner, that of redirecting flow, theoretically has some merit. For example, situating vortex generators at a propeller blade tip, at the proper angle of attack, could redirect the tip flow opposite to the inherent tip vortex, thereby reducing the strength of the vortex. This could realign the blade circulation distribution to a more favorable one. It is now believed that the strong tip vortex shed from a statically operating propeller blade causes a locally high angle of attack and, therefore, a reduction in lift-to-drag ratio in the blade tip region. On this basis, any weakening of this tip vortex could be beneficial. Tests were performed adding vanes to a wing tip which simulated a rotor tip in Reference 9, in an attempt to weaken the tip vortex to reduce rotor noise. Unfortunately, the test did not include force measurements (since it was not a performance test) nor did it include the important rotational flow field. It would be of interest to obtain some static performance data with propellers having devices which change the induced flow in the blade tip region. Reference 9 also suggested devices such as porous tips, vanes, planform sweep and radial blowing (ejecting air radially outward).

End-Plated Propeller Blades

Another obvious device which could improve blade tip flow conditions is the addition of blade tip end plates which would effectively increase the aspect ratio of the blades and therefore lower the induced drag. If the induced drag were reduced more than the profile drag of the end plates, the total blade drag would be reduced, and the end plates would have a beneficial effect.

An analytical study was made to assess the advantages of adding end plates to the original XC-142 propeller blades. The results of this study showed an increase in static performance of a few percent as well as an increase in cruise performance at the low Mach numbers.

The study was encouraging enough to add end plates to the XC-142 propeller fiber glass blade tips to assess performance. The end plates were 4 x 6 in. with an air-foil cross section. The blade chord at the tip station was only 5 in. Unfortunately, thrust could not be measured. Horsepower measurements did not show any difference between the propellers with or without end plates. Thus, the test was inconclusive. The end plates did stay attached to the blade tips, so, at least from a structural standpoint, the concept appears feasible. Tests should be run to assess whether static performance gains can be obtained by adding end plates to a propeller blade.

Conclusions

On the basis of the above study, the following conclusions can be drawn:

There are probably potential gains of from 6 to 8% in 250-kn cruise efficiency and perhaps as much as 2 to 4% in static thrust over and above the present state of the art. But, because there is no static thrust theory or empirical prediction method that accurately relates all of the propeller geometry parameters, the upper limit of attainable static performance is not exactly known.

It is believed that probably the most immediate important gains in state of the art can be made by continued conventional propeller experimental research.

Certain unconventional propeller designs appear to be promising. A design for slotted propeller blades is one of these. On the basis of static variable camber propeller test data, indications are that high levels of static performance are obtained. The variable camber propeller is similar to a propeller blade with a slotted flap at the static condition.

It appears that devices which weaken the strong propeller tip vortex could have a beneficial effect on static performance. The most likely device is an

end plate. Calculations predicted an important gain in V/STOL propeller performance when applied to the original XC-142 propeller. Flow turning vanes could also be promising. Unfortunately, there is no experimental performance data available to assess these concepts properly.

Recommendations

Because of the importance of advancing V/STOL propeller performance for the aircraft mission requirements of the 1970's, it is of prime importance that a static propeller theory be developed.

Since there is a lack of a reliable static theory to use as a tool, the following experimental programs are needed and, therefore, are recommended.

Conventional Propellers - There are many gaps in the experimental information needed to fully optimize a V/STOL propeller. A systematic investigation is needed to assess, on an individual basis, the effect of varying activity factor, integrated design C_L , number of blades, tip planform, tip twist, and tip camber distribution on static performance. Propeller testing should be performed on a rig that is free of rig interference effects, so that the performance of the free propeller can be obtained.

Unconventional Propellers - A propeller such as the optimum propeller of this study should be built and tested. It will be desirable then to test two-dimensional slotted airfoils typical of the propeller shank and tip airfoil over a range of Mach numbers to obtain slotted airfoil data for analytical studies. Slots should then be added to the propeller. This same propeller should be tested with flow turning vanes and also with end plates to determine whether weakening the tip vortex will improve static performance.

MATERIALS REVIEW

GENERAL APPROACH

A portion of this feasibility study is the evaluation of existing and future materials. Because the primary focus of this study is weight reduction, the basic objective translates to a program that will evaluate advanced materials and fabrication techniques, as applied to design concepts which will potentially produce a significant reduction in propeller weight for the time period 1970-1975. The prime factors to be considered for the various areas evaluated are: (1) present state of the art, (2) projection of feasible technology advances, (3) degree of potential weight reduction, and (4) degree of technical jeopardy including required additional development. These factors, with regard to existing and future materials and their fabrication, will be discussed in this section. Design allowables of each of the various materials preferred for future application are compared with steel in Table II. Typical properties of all the materials evaluated are summarized in Table III.

STEELS - WROUGHT

Low Alloy Steels

The major components of a propeller system, specifically the barrel, blade spar, gears, and shafts, are presently made of low alloy steels. Therefore, low alloy steel may be considered as a convenient reference point from which potential weight savings may be measured. Vast amounts of service and test experience on steel alloy propeller components have been accumulated and, by relating this experience to material specimen data, it is possible to provide an accurate assessment of the materials' mechanical design properties for specific component applications. The majority of experience with steels has been with the air-melted alloy steels, such as AISI 4340 and HS 44 (a modified 0.50% carbon steel otherwise similar to AISI 4340).

A laboratory evaluation was conducted on a vacuum degassed, carbon-deoxidized heat of HS 44 to determine the effect of the vacuum treatment on composition, gas content, cleanliness, and mechanical properties. The conclusions drawn from this evaluation were that the vacuum degassed, carbon-deoxidized material exhibited significant improvements in tensile ductility, impact strength, and fatigue properties over the conventionally air-melted steel. However, because only one heat of steel was evaluated, design allowables were not increased over those previously used for air-melted steel; rather, it was assumed that a greater factor of safety was obtained.

TABLE II DESIGN ALLOWABLE MECHANICAL PROPERTIES FOR SELECTED MATERIALS AS COMPARED TO STEEL (AT ROOM TEMPERATURE)									
MATERIAL	CONDITION	ULTIMATE TENSILE STRENGTH		0.2% YIELD STRENGTH	10 ⁵ CYCLES	FATIGUE STRENGTH 10 ⁶ CYCLES			
D6A STEEL (AMS 643)	VACUUM MELTED, HEAT TREATED TO RC 40-44	1.0	1.0	1.0	1.0	1.0			
AFC-77 STEEL	HEAT TREATMENT 1800°F, OIL QUENCH SUBCOOL (-100°F), DOUBLE TEMPER 1050°F	1.27	1.12	1.12	1.0	0.92			
TITANIUM 6A1-6V-2SN	FORGING, SOLUTION TREATED AND AGED	0.97	1.0	1.0	0.86	0.67			
TITANIUM 6A1-4V	CAST, ANNEALED	0.45	0.44	0.44	0.37	0.27			
ZE63A MAGNESIUM	CAST, HYDRIDING HEAT TREATMENT	0.18	0.12	0.12	0.12	0.13			
BORON-EPOXY (60%-40% VOL) (EPON 828/EPON 1031)	UNIDIRECTIONAL	1 0.73 2 0.026 12 0.036	1 0.59 2 0.028 12 0.042*	1 1.2 2 1.2 12 1.2	1 0.48 2 0.029 12 0.040	1 1.2 2 1.2 12 1.2			
S-GLASS-EPOXY (50%-50% VOL) (EPON 828/EPON 1031)	WOVEN	1 0.46 2 0.27 12 0.46	1 0.27 2 0.24 12 0.37	1 0.24 2 0.24 12 0.24	1 0.24 2 0.24 12 0.24	1 0.23 2 0.15 12 0.11			
S-GLASS-EPOXY (50%-50% VOL) (EPON 828/EPON 1031)	UNIDIRECTIONAL	1 0.58 2 0.010 12 0.011	1 0.76 2 0.028 12 0.012*	1 1.2 2 1.2 12 1.2	1 0.34 2 0.029 12 0.023	1 1.2 2 1.2 12 1.2			
GRAPHITE-EPOXY (60%-40% VOL) (EPON 828/EPON 1031)	UNIDIRECTIONAL	1 0.58 2 0.010 12 0.013	1 0.47 2 0.011 12 0.014*	1 1.2 2 1.2 12 1.2	1 0.39 2 0.010 12 0.017	1 1.2 2 1.2 12 1.2			
BORON-ALUMINUM (50%-50% VOL) (BORSIC-6061)	UNIDIRECTIONAL	1 0.86 2 0.054 12 0.032	1 0.71 2 0.059 12 0.035	1 1.2 2 1.2 12 1.2	1 0.59 2 0.058 12 0.035	1 1.2 2 1.2 12 1.2			
NOTES	T - TENSION C - COMPRESSION	STRESSING OF COMPOSITES:							
* MATERIALS DO NOT EXHIBIT YIELD POINT, THESE VALUES ARE BASED ON MAXIMUM ALLOWABLE DESIGN STRESS.									

TABLE III
AVERAGE PROPERTIES OF VARIOUS STRUCTURAL MATERIALS (ROOM TEMPERATURE)

MATERIAL	CONDITION	DENSITY (p) (LB IN. ³)	MODULUS OF ELASTICITY (E) (10 ⁶ LB IN. ²)	E P (10 ⁶ IN.)	ULTIMATE TENSILE STRENGTH (σ _U) (10 ⁵ LB IN. ²)	0.2% YIELD STRENGTH (σ _{0.2}) (10 ⁵ LB IN. ²)	0.1% P (10 ⁵ IN.)	FL P (10 ⁵ LB IN. ²)	NOTCHED- UNTREATED UTR RATIO (RTS)	STRESS CORROSION SUSCEPTIBILITY	CURRENT STATUS OF TECHNOLOGY	
												(SEE NOTE 1)
STEELS (WROUGHT):												
AISI 4340	HEAT TREATED TO RC 40-44	0.283	30	106	200	180	640	340	1.4	SMALL	VERY HIGH PRODUCTION	
D-2A	VACUUM MELTED HEAT TREATED TO RC 40-44	0.284	30	105	210	170	670	161	1.3	SMALL	HIGH PRODUCTION	
18 NICKEL MARAGING (300)	VACUUM MELTED SOLUTION ANNEALED & AGED	0.289	28	97	290	270	938	122	1.5	SMALL	PRODUCTION	
CUSTOM 455	SOLUTION ANNEALED & AGED	0.282	29	123	265	240	920	110	1.1	VERY SMALL	PRODUCTION DEVELOPMENT	
ALMAR 36A	SOLUTION ANNEALED & AGED	0.281	29.5	103	140	135	810	97	1.35	VERY SMALL	PRODUCTION DEVELOPMENT	
APC 77	AUSTENITIZE, REFRIGERATE, DOUBLE TEMPER	APPROX 0.29	29.5	102	240	210	720	109	1.7	NO DATA	PRODUCTION DEVELOPMENT	
H-11	AUSFORMED 1060 F REDUCED NO. OIL QUENCH, DOUBLE TEMPER	0.280	29	104	367	330	1160	180	NO DATA	NO DATA	LAB R&D	
AISI 301	CRYOSHOCKED	0.280	13	52	210	200	690	NO DATA	NO DATA	NO DATA	LAB R&D	
MAGNESIUM ALLOYS (CAST):												
ZE51A	SAND CAST HYDRIDE HEAT TREATED	0.089	6.3	44	42	38	349	17	NO DATA	NO DATA	PRODUCTION DEVELOPMENT	
AZ 92A	SAND CAST SOLUTION TREAT. AGE	0.086	6.3	98	40	21	320	15	0.8	HIGH	HIGH PRODUCTION	
TITANIUM ALLOYS (WROUGHT):												
Ti-6Al-4V-2Sn	SOLUTION TREATED & AGED	0.164	16.3	100	180	170	1740	74	NO DATA	MODERATE HIGH	PRODUCTION	
Ti-6Al-4V-7Sn	ANNEALED	0.164	13.0	92	150	140	6 ¹	00	NO DATA	MODERATE	PRODUCTION	

TABLE II--CONTINUED

MATERIAL	COMBINATION	DENSITY (G/CM^3)	MODULUS OF ELASTICITY (10^{11} LB./IN. ²)	5% STRENGTH (10^5 LB./IN. ²)	ULTIMATE TENSILE STRENGTH (10^5 LB./IN. ²)	5% YIELD STRENGTH (10^5 LB./IN. ²)	2% STRENGTH (10^5 LB./IN. ²)	ELONGATION (%)	NOTCHED TENSILE STRENGTH (10^5 LB./IN. ²)	STRESS CORRUSSION RESISTANCE	CURRENT STATUS OF TECHNOLOGY	
TITANIUM ALLOYS (FROUNT) (CONT.)												
Ti-6Al-4V	ANNEALED	0.166	16.3	100	140	100	810	60	315	1.1	MODERATE	HIGH PRODUCTION
Ti-11Cr-3Al	SOLUTION TREATED & AGED	0.175	15.5	90	100	170	1000	30	210	0.0	HIGH	PRODUCTION
TITANIUM ALLOYS (CAST)												
Ti-6Al-4V	ANNEALED	0.166	16.3	100	130	100	781	60	605	NO DATA	MODERATE	LAB DEVELOPMENT
Ti-3Al-2.5Sn	ANNEALED	0.162	17.0	100	130	115	715	60	310	1.0	NO DATA	
ALUMINUM ALLOYS (FROUNT)												
AA 2014	SOLUTION TREATED & AGED TO T6	0.101	16.3	90	75	60	900	10	100	1.0	MODERATE	HIGH PRODUCTION
AA 7075	SOLUTION TREATED & AGED TO T6	0.101	16.3	90	63	75	700	20	310	1.1	HIGH	HIGH PRODUCTION
ALUMINUM ALLOYS (CAST)												
AA C355	PERMANENT MOLD CAST, SOLUTION TREATED & AGED TO T6	0.098	15.2	104	40	30	300	14	100	NO DATA	SMALL	PRODUCTION
AA A336	PERMANENT MOLD CAST, SOLUTION TREATED & AGED TO T6	0.097	16.3	100	41	30	310	10	100	NO DATA	SMALL	PRODUCTION
HO1	CAST, SOLUTION TREATED & AGED TO T6	NO DATA	NO DATA	-	65	60	-	0	-	NO DATA	SMALL	PRODUCTION DEVELOPMENT
BERYLLIUM ALLOYS												
BERYLLIUM	HOT PREPRESSED EXTRUSION (LARGE REDUCTION)	0.097	47	617	45	307	445	30	100	0.1	MODERATE- HIGH	LAB DEVELOPMENT
BE-30Al (LOCKALLOY)	HOT PREPRESSED, EXTRUSION	0.075	20	300	30	35	600	17	310	NO DATA	NO DATA	LAB DEVELOPMENT

Further improvement in mechanical properties is found in vacuum-melted steels. AMS 6431 (vacuum-melted D6 steel) has been used for several recent applications, the most notable of which is the AH-56 helicopter for the U. S. Army. This material provides excellent hardenability along with a good combination of mechanical properties. A substantial amount of mechanical property data has been generated for both specimens and hardware made of this alloy.

The maximum hardness level normally specified for alloy steels at Hamilton Standard is 40-44 Rc, since the fatigue strength does not appreciably increase at hardnesses above 44 Rc while the ductility and toughness decrease. Therefore, the optimum combination of mechanical properties occurs at 40-44 Rc.

Ultrahigh-Strength Steels

Considerable effort in the industry is being expended to upgrade the quality of the ultrahigh-strength alloy steels, such as the maraging steels, and to extend their application in both missile and airframe structures. Recent work has concentrated on the problems associated with environment, embrittlement, and fracture sensitivity, with the major effort focused on the areas of alloy composition and melting practice. By optimizing the steel composition and by using vacuum melting or degassing casting methods, it has been possible to increase the tensile strength without compromising the fracture toughness. In addition, the anisotropy encountered in air-melted steel in the short transverse forging direction has been eliminated.

A great amount of work also is being devoted to the development of families of high-strength steels that have "stainless steel" characteristics and/or significantly improved fracture properties. To date, the structural applications of the more highly alloyed and essentially more expensive steels have been limited. These steels have not been used at Hamilton Standard for two major reasons: (1) extensive application experience, as is available with the more common alloy steels, is lacking, and (2) maximum attainable hardness is below that of AMS 6415 or D6 material. Also, the design fatigue strength of these alloys is no better than that of the alloy steels presently used. However, their static tensile strengths are considerably higher than those of other steels, so that Goodman diagram calculations indicate a 20 to 25% increase in allowable cyclic stress in the regimes of stressing normally encountered in propeller barrels and blade spars.

The problem of maximum attainable hardness may eliminate the "stainless steel" family from consideration, because 50 Rc is essentially the highest hardness obtainable. This value is substantially lower than the minimum value now specified for induction or flame-hardened raceways for the ball-type blade retention system presently employed. The high-strength stainless steels have demonstrated a decrease in toughness when the carbon content goes above 0.45%. This would limit the maximum attainable hardness to approximately 54 Rc. These steels may be

suitable for retention purposes if the Hertzian contact stresses can be decreased or if a hardened steel insert can be used for the bearing race. Representative high-strength stainless steels, such as AM 352, Custom 455, and AFC-77, were considered in this evaluation.

Experimental Steels

The effects of novel combinations of thermal and mechanical treatments on the strength of steels have been studied only experimentally to date. These include several treatments both at elevated and at subzero temperatures, the oldest and best known of which is ausforming. Ausforming consists of mechanical deformation in the stable austenite bay of the time-temperature-transformation diagram. It has produced strength levels of 450 ksi in sheet material that has been drastically reduced in section thickness. Fatigue strengths obtained from such material are among the highest known strengths obtained from any material.

A treatment which has been investigated at Hamilton Standard is the cryokinetic processing of materials, primarily austenitic stainless steels. The process consists of deforming material a fraction of 1% at cryogenic temperatures (-100° F to -320° F) to promote a phase change to a martensitic structure and, hence, an increase in strength while maintaining the corrosion resistance of the stainless steel.

Several problem areas exist which will limit these treatments to laboratory and development work until the 1970's. Most of the experimental work has been restricted to sheet and bar stock; therefore, a great deal more development work is necessary to establish the feasibility of applying these new thermomechanical treatments to forged and extruded shapes. Uniform deformation throughout a complex shape must be achieved to ensure consistent properties, and either special techniques must be developed to permit machining or shapes must be produced to near-final dimensions.

TITANIUM - WROUGHT

The use of titanium alloys has been increasing in both airframe and missile structures and will further increase with the advent of the EST and other lightweight aircraft. The reasons for the increasing usage and application are obvious upon consideration of the favorable material properties relative to the stringent requirements of the aerospace industry. The density of titanium is about midway between that of steel and aluminum, justifiably classifying the material as a lightweight metal. This low density, in conjunction with the high strengths attainable, results in exceptionally high strength-to-weight ratios. The tensile modulus is about one half that of steel; however, again upon consideration of the low density, the stiffness-to-weight ratio is comparable to that of steel. The corrosion resistance of

titanium alloys is excellent, particularly at the lower temperatures encountered in subsonic aircraft.

Considerable effort is being expended to develop present alloys to their maximum capabilities by minor changes in alloying or by the adaptation of new processing methods in the areas of forgings and extrusions. The most promising alloy development work is being conducted by New York University, where modifications of production alloys of Ti-6Al-6V-2Sn, called the Margolin-Farrar alloys, have been produced with tensile yield strengths of 190 to 200 ksi and reasonably good ductility. Further work remains to evaluate and optimize these modifications with regard to fatigue, impact, and fracture toughness.

With respect to forgings, the most natural approach to explore is the possible use of higher forging temperatures. This means actually forging titanium in a high-temperature single-phase, rather than a lower temperature two-phase region, and producing microstructures not generally considered to be acceptable by today's standards. This allows the attainment of more complex forge shapes and closer forging practice. The static mechanical properties have been similar, but the effects on fatigue strength have yet to be determined. Also, most of the work has been with Ti-6Al-4V. Other alloys, such as the ones discussed in the following paragraphs, also need to be explored.

An evaluation of existing alloys and their potential application must discern between the alpha-beta and beta alloys. Ti-13V-11Cr-3Al is the only commercially available beta alloy. This alloy can be heat treated to the highest tensile strengths of any commercial titanium alloy. However, the beta alloy fatigue strength is 25% less than that of the high-strength alpha-beta alloys. Also, its fracture toughness is inferior. The one distinct advantage of the Ti-13V-11Cr-3Al is its ability to be heat treated in sections up to 10-in. thick while maintaining uniform properties throughout the entire section. The configurations of propeller components are such that thin-enough sections should be able to be forged and/or machined, prior to heat treatment, to enable the attainment of maximum strengths in the finished component. Therefore, the alpha-beta alloys appear to be the ones most likely to provide the required mechanical properties to effect a substantial weight savings.

Of the alpha-beta alloys, Ti-6Al-4V accounts for the large majority of stock currently being produced. However, the trend toward the use of the higher-strength titanium alloys is now evident with emphasis on Ti-6Al-6V-2Sn, which is heat treatable to higher strengths than are any other alpha-beta alloys. Therefore, Ti-6Al-6V-2Sn, or its possible modifications, has been selected as the titanium alloy possessing the greatest potential for future applications. This conclusion was also reached during two recent programs that structurally evaluated several forging alloys, and both programs recommended Ti-6Al-6V-2Sn as having the optimum combination of mechanical properties. Lockheed, in References 17 and 18,

evaluated Ti-6Al-4V; and Sikorsky, Reference 20, evaluated Ti-13V-11Cr-3Al and Ti-6Al-6V-Sn.

One of the major problems with titanium has been its affinity for galling and seizing in rubbing applications, a problem which, historically, has been averted by the use of steel sleeving or inserts. A substantial amount of development effort has been directed in recent years toward wear-resistant coatings for titanium ranging from anodic coatings to hard plating. Hamilton Standard, as part of a Navy-sponsored titanium, propeller system development program, has been developing a diffused electroless nickel coating to provide adequate wear and scuffing resistance to permit its application on titanium gears. Over the past two years, titanium gears with this coating have been successfully tested in the laboratory, at gear-tooth stress levels approximately equivalent to 75% of those used for high strength steel gearing, for 350 million cycles without failure. The results, to date, have been quite promising and there are definite indications that further improvements in the coating properties will enable satisfactory operation at higher tooth stresses. Although a considerable amount of further development is required, it now appears that the availability of titanium gearing for future applications may be attainable.

TITANIUM - CAST

The casting of titanium alloys has recently emerged from the basic development stage. Limitations still exist concerning the alloys cast, the degree of part complexity attainable, and the high cost. However, titanium castings are included within the scope of this study because of their potential application for cast gearbox housings. Casting has been limited to Ti-6Al-4V and Ti-5Al-2.5Sn, and static mechanical properties comparable to wrought material have been obtained. Further work must be done in the determination of fatigue strengths, establishment of realistic soundness standards, and improvement of the casting process to enable the economical production of reliable castings. Ti-6Al-4V has been selected as currently having the greatest potential. Since there is no strength advantage obtainable through heat treatment, it would be used in the annealed condition.

MAGNESIUM - CAST

Magnesium alloy castings, primarily the aluminum-zinc alloys AZ91 and AZ92, have previously been used extensively for propeller gearbox housings. Recently, the British developed a new magnesium base casting alloy which involves a new principle of heat treatment that makes it possible to combine high strength and good ductility with virtually a complete absence of microporosity. The alloy, ZE63A, a zinc-rare earth composition, derives its excellent properties and soundness from a unique treatment process of heating in hydrogen, which transforms large-size zinc-rare earth intermetallic precipitates at the grain boundaries to smaller rare earth hydrides. The smaller hydride precipitates are less detrimental

to such properties as fatigue strength and soundness. For practical fabrication, the maximum section thickness that can be effectively hydrided appears to be 1 in. The castability of the alloy is excellent and reportedly is better than that of AZ92. Two major deterrents to using magnesium alloys are the coefficient of expansion and the need for corrosion protection. The large magnesium coefficient of expansion changes center-to-center locations of gearing, which dictates slightly heavier gears to accommodate these changes. Corrosion of magnesium alloys is of critical concern and requires careful attention to both application of protective coatings and inspection in service. However, the coatings have been demonstrated to be adequate, and the concern over corrosion should not be an overriding factor. The ZE63A alloy is considered to possess the optimum potential of the magnesium casting alloys.

ALUMINUM - WROUGHT

Consideration was given to the use of high-strength wrought aluminum alloys. A great quantity of these alloys has been used in propeller components over the years. AA 7076 for propeller blades and AA 2014 for a multiplicity of parts made from bar stock and forging are currently in production.

Comparison of the strongest aluminum alloys with other high-strength alloys shows that, on a static strength-to-weight basis, these aluminum alloys are not far behind the stronger titanium alloys. The problem, however, is that the high-strength aluminum alloys are highly sensitive to stress corrosion and are thus unsuitable for aircraft application without special heat treatments. These special (controlled overaging) heat treatments reduce or eliminate the stress corrosion problem; however, they also reduce strength to the point that the alloys are no longer competitive with titanium, especially on a fatigue basis.

ALUMINUM - CAST

Until quite recently, even the highest-strength cast aluminum alloys, such as AA-C355-T61 and AA-A356-T61, could not compete with cast magnesium alloys such as ZE63A on a strength-to-density ratio basis. However, during the past few years, a high-strength proprietary alloy, K01, has been developed and tested by Electronic Specialties Corporation, Pomona, California. Quoted typical static mechanical properties represent approximately a 50% increase over typical strengths measured on the strongest C355 or A356 castings. Comparison with ZE63A reveals that they are approximately equivalent on a tensile strength-to-density basis, and that K01 is superior in a yield strength-to-density comparison. Dynamic properties, such as fatigue strength, do not follow the same trend based on preliminary K01 tension data. The typical endurance limit of K01-T6 appears to be less than one-half that of ZE63A, although further testing of K01 is needed to define this property better.

Until the question of the dynamic properties of K01 is resolved by further testing, the alloy must still be rated inferior to ZE63A. By 1970-1975, however, it may well be that methods of raising the fatigue strength will make K01 a very attractive candidate for gearbox housing and other casting applications.

BERYLLIUM - WROUGHT

Unalloyed beryllium, because of its unique features such as low density, high modulus, and acceptable strength-to-weight ratio, continues to command the attention of those concerned with developing lighter weight structural elements for aircraft. Beryllium's density is approximately one-quarter that of steel and one-half that of titanium, and, when compared on a strength-to-weight basis, it is stronger than steel and only slightly weaker than titanium. The greatest advantage of beryllium is its phenomenal stiffness-to-weight ratio, which is six to seven times greater than that of other commonly used structural materials.

The largest barrier to wider application of beryllium in aerospace structures is its low total elongation-to-failure in the short transverse direction. Room temperature ductility in the longitudinal and long transverse directions has been increased markedly by cross-rolling of sheet and by development of biaxial forging processes. However, at present, there is little that can be done about its short transverse ductility, except to minimize design strains in that direction.

The use of beryllium in a propeller system would normally be limited to extrusions and forgings because of the configurations required. Beryllium extrusions are produced in varied configurations. Extruded tubing, which has been produced in 1.5 in. to 5 in. outside diameter with wall thicknesses of 0.090 in. to 1.5 in., would be excellent for the manufacture of blade spars where specific stiffness is important, except that the very low, short transverse elongation (typically 0.25 to 0.75%) eliminates any possibility of tube flattening to form the airfoil section. Forged beryllium also exhibits a high amount of anisotropy due to mechanical working. Sophisticated techniques for forging beryllium to obtain semirandom or random crystal orientation are in early stages of development. Biaxial forging has been studied by determining the mechanical properties of a series of combinations of a uniaxial forging reduction (by forward extrusion), followed by a biaxial forging reduction (by upset forging against the extrusion direction). The results demonstrated fairly isotropic properties in two directions, but, as in the case of extrusions and sheet stock, the elongation is very low in a third direction. Early attempts with triaxial forging have produced three-dimensional properties which are lower than typical values normally encountered in the anisotropic material.

The primary effort today with beryllium concentrates on developing reproducibility of forging or extrusion characteristics by relating them to ingot characteristics such as chemistry or grain size. Once process control is developed, effort may

then be directed toward establishing statistically significant mechanical properties. Because of the lack of short transverse ductility in beryllium products to date and because of the apparent inability to improve this property within the near future, beryllium has not been selected for application in the major structural components of the propeller system for this study.

In an effort to solve the problems preventing the use of beryllium, a 68Be-32Al alloy, known as Lockalloy, is being developed. The purpose of alloying was to increase ductility and formability while maintaining as much of the high strength, high elastic modulus, and low density of pure beryllium as possible. While neither yield strength-to-density nor modulus-to-density ratios of Lockalloy approach those of beryllium, Lockalloy's modulus-to-density ratio surpasses those of all other contending materials and its yield strength-to-density ratio is second only to titanium alloys among the other contenders. Unfortunately, the forgeability of Lockalloy is as yet poor, and problems are encountered in fabricating even rather simple shapes.

Nevertheless, extrusions and sheet metal are in current production and, for 1970+ applications requiring high modulus-to-density or strength-to-density ratios, this material could possibly be considered.

COMPOSITES

Composite structures have existed for many years, but only recently have they gained any extensive application potential for aircraft. Presently, only glass-reinforced plastics are extensively used, providing high strength-to-weight ratios, excellent corrosion resistance, and low fabrication and maintenance costs. To date, more extensive application of these materials has been ruled out by their low modulus, the rapid degradation of properties at high temperatures, and the need for protecting the surface of the resin matrix against the adverse effects of erosion, moisture, and ultraviolet light. Work on composition of higher strength and higher modulus-to-density ratios is expanding steadily. It is devoted to three classes of materials: metal fibers in metal matrices, metal and inorganic fibers in organic matrices, and ceramic and inorganic fibers in metal matrices. A further distinction may be made according to whether the reinforcement is provided by continuous or discontinuous fibers.

The changing status of composite materials makes the selection of one material as the optimum for application in 1970-1975 essentially impossible. Two major reasons account for this difficulty: (1) both reinforcing and matrix materials are improving continuously, either by bettering existing ones or by adapting new ones to composites, and (2) the technique of designing with composites is becoming more sophisticated as analytical techniques for determining the reaction of various composite materials to different types of stressing are established.

Several different reinforcing materials are shown in Table IV, with typical values of specific strength and stiffness given for comparison.

Boron has received the major emphasis to date because good-quality filament³ have been available in quantity and at lower cost than other filament materials. The Air Force has established standards for boron filament: 400,000-psi minimum tensile strength, 55×10^6 -psi minimum elastic modulus, 0.004 \pm 0.0001-in. diameter, and 2.70-g/cc (.099 lb/cu in.) maximum density. To achieve lower costs, improved production techniques are being investigated. Speeding up deposition rates and windup processes, improving reliability, and eliminating costly reprocessing are advances that are needed to effect lower costs.

Next to boron, graphite is the most widely publicized filament. Produced in yarn form at a density of 1.38 g/cc (0.056 lb/in.³), graphite provides the highest specific stiffness of any reinforcing material to date (Table IV) and is surpassed only by S-glass with regard to specific strength. The graphite fibers have great promise but as yet have not produced the high composite properties of boron, particularly in the cross-ply direction and in interlaminar shear. Also, graphite has a high rate of solution in some metals and a high sensitivity to oxygen. These are problems that need to be solved for use in metal matrices.

Silicon carbide has approximately the same mechanical properties as boron but is 20% denser. However, it is compatible with metals at elevated temperatures and is resistant to oxidation, thus offering definite advantages when considering metal matrices. Many other continuous-filament materials are in the development stage and may eventually compete with the three prominent materials discussed. These include boron carbide, boron nitride, alumina, beryllia, aluminum boride, titanium boride, and beryllium.

Although these new filament materials are receiving the majority of attention, improved glass fibers should not be ignored. Despite their low modulus compared with boron and graphite, S-glass and the newer 970-S36 are superior to the widely used E-glass and offer a much higher specific strength than any of the other filament materials.

The ultimate in reinforcement strength is obtained with single crystals grown in threadlike lengths and known as "whiskers". In this form, the whiskers can reinforce both metals and resins. Silicon carbide and alumina whiskers are used predominantly now, followed by boron carbide and silicon nitride. Also, graphite whiskers have been experimentally produced with the highest specific stiffness of any reinforcing material. However, the exploitation of the extremely high strengths and moduli of whiskers in real structures has been impeded by the practical difficulties involved in properly incorporating them into composite structures. Whiskers, being quite rigid and anisometric, can be incorporated principally in randomly

TABLE IV TYPICAL PROPERTIES OF REINFORCING MATERIALS (ROOM TEMPERATURE)												
PROPERTY	UNITS	FILAMENTS						WHISKERS				
		S-GLOSS	GRAPHITE	BORON	BERYLLIUM	SILICON CARBIDE	GRAPHITE	SILICON CARBIDE	ALUMINUM OXIDE			
DENSITY (P)	LB/CU. IN.	0.072	0.084	0.09	0.066	0.128	0.080	0.118	0.143			
MODULUS OF ELASTICITY (E)	10 ⁶ PSI	13	30	88	38	70	142	122	60			
ULTIMATE TENSILE STRENGTH (UTS)	10 ³ PSI	680	285	400	160	380		1680	600-1200			
SPECIFIC STRENGTH $\left(\frac{UTS}{P}\right)$	10 ⁶ IN.	9	5.3	4.4	2.4	2.8		14.3	4.2-8.4			
SPECIFIC STIFFNESS $\left(\frac{E}{P}\right)$	10 ⁶ IN.	180	925	610	180	840	2370	1080	420			

oriented fashion in a matrix, and with only relatively low volume percentages. A low whisker content, together with the three-dimensional randomness, results in composites with mechanical properties much lower than those of the individual whiskers. The means of providing a high reinforcement content and a composite having a significant percentage of the reinforcement properties is to have a high degree of whisker alignment. To effect alignment, several methods are being investigated, including fluid techniques, such as slurry extrusion and vortex spinning, and magnetic coatings. To date, whiskers have been evaluated in systems where the matrix is introduced in the fluid state, such as metal casting and injection molding of thermoplastics, where the whiskers would compete with chopped-glass composites.

Although the reinforcing medium is the element providing the superior strengthening of composites, the matrix material has several important functions. The matrix serves to transfer load from filament to filament, to provide fiber separation, to protect fibers from abrasion, and to bind them in a rigid shape. Thus, the matrix is essential to composite integrity and is the subject of considerable research, particularly in terms of fiber-matrix interaction.

Differences in fabrication techniques have resulted in different development programs being conducted on resin and metal matrix composites. The well-developed processes of filament winding and hand layup, used extensively for glass fiber reinforced resins, have been successfully adapted to the manufacture of reinforced resins such as boron/epoxy and graphite/epoxy. The optimum nonmetallic matrix is one possessing the maximum load transfer characteristics, which is a direct function of interfacial bond strength and the matrix modulus. Based upon these parameters, the epoxy resins are superior to other resin systems at temperatures up to the range of 350° to 450° F. They possess a high modulus ($E = 5 \times 10^{10}$), high interfacial strengths, and excellent handling characteristics. The latter makes them readily applicable to processing techniques, such as wet layup, filament winding, and tape prepegs. For applications above 350° to 450° F, several new families of high-performance resins, including epoxyated novolacs, phenolics, and the polyimides, are available. However, for propeller components which operate at temperatures less than 350° F, selection of a resin matrix system should be confined to the epoxies.

Metal matrices have several potential advantages over resin matrices: (1) metals can operate continuously at temperatures above 700° F; (2) the inherent high shear strength of metals allows better load transfer between reinforcements; (3) metals can withstand triaxial stresses better than resins and, therefore, contribute more when the composites are subjected to complex loading situations; (4) metals have higher resistance to impact and damage by foreign objects; and (5) component processing steps, such as making access cutouts, drilling attachment holes, etc., can be accomplished more easily with metals. The major problem with metal matrix

composites is one of fabrication. Several methods have been and are being investigated for metals such as aluminum, titanium, nickel, and cobalt. The well-known metal fabrication techniques which are readily applied to metal matrix composites may be separated into three general categories based upon the physical state of the metal during processing.

Solid state processes are powder metallurgy and diffusion bonding. Both processes are limited to a maximum filament content: 20-30 vol % for powder metallurgy and 45-55 vol % for diffusion bonding. Evaluation has shown that the strengthening efficiency of the powder metallurgy process is susceptible to many variables and is not yet capable of providing reproducible results. Considerable effort has been expended toward developing diffusion-bonded components, resulting in substantial progress to date. Problems encountered have been chemical reactions between filament and matrix materials and maintaining consistent filament spacing. Methods of alleviating these are being developed and optimized.

Liquid state processes are casting, vacuum infiltration, and plasma spraying. The major detriments of the casting and vacuum infiltration processes are reactions with the molten metal, filament spacing, and filament wetting. Because these problems have been difficult to solve, the casting and vacuum infiltration processes have been deemphasized in comparison with plasma spraying. Plasma spraying is unique in that the metal remains liquid for only a very short time after contacting the filaments. When sprayed onto a fiber mat or filament wound on a mandrel, several advantages are obtained: the short-time contact with molten metal limits chemical reactions, and the woven mat or prewound filament provides consistent filament spacing. Also, filament contents up to 75 vol % are practical with this manufacturing process.

Molecular processes are electrodeposition and vapor deposition. These processes are limited to 50 vol % filament content, and problems have been encountered with filament spacing and bending between the matrix and filament resulting in lower strengthening efficiencies than expected.

The relatively low temperatures required for a propeller application narrow the choice of an optimum metal matrix down to alloys of titanium or aluminum. Tests with many alloys have demonstrated that the matrix contributes to the strength of the composite in proportion to its yield strength. However, the selection of an alloy for the matrix is highly dependent upon the manufacturing process used to make the composite. The type of components involved in a propeller system could be manufactured most easily from diffusion-bonded components or plasma-sprayed tape which could be employed in a layup construction.

Most of the development to date has been with aluminum. Fairly large diffusion-bonded laminates of aluminum, using high-strength steel and boron filaments, have been produced with excellent results. The plasma spray process results in an end product in the form of unidirectional tape which can be employed essentially like boron-epoxy prepreg tape. Multiple layers can then be joined by diffusion bonding or brazing. AA 6061 appears to be one of the better choices for the matrix material for several reasons. The lower alloy content, compared to the AA 2024 and AA 7075 alloys, tends to limit chemical reaction with the filament materials, and the material has better ductility, which is important to the plasma spray process.

Also, AA 6061 has better corrosion resistance than the aluminum copper alloys and has a high melting point. This is important when diffusion bonding or brazing the composite tapes together for a component structure. AA 6061 has good cryogenic properties, is resistant to stress corrosion cracking, and is more easily formed than the AA 2024 and AA 7075 alloys. Other alloys evaluated for plasma-sprayed composites have included AA 1100, 360, and 380. However, the AA 6061 has definitely been demonstrated as possessing the best combination of strength and ductility.

The configurations of propeller components essentially necessitate the use of long filaments rather than whiskers. Therefore, boron, S-glass, and graphite filament reinforcements have been selected because of their production availability in continuous lengths. For the metal matrix application, silicon carbide-coated boron filament will be used to eliminate oxidation of the filament and reactions with the matrix material. For a nonmetallic matrix system with boron, S-glass, or graphite filaments, the epoxy resin has been selected because the substantial amount of available strength data will permit a realistic design.

Three nonmetallic composites are selected because of the variation in strength due to orientation and the different specific strength. The graphite/epoxy composite, though stronger in the filament direction on a strength-to-weight comparison, is weaker in the cross-ply direction, and the S-glass epoxy has the greatest specific strength. This will be illustrated in the listing of mechanical properties. A plasma-sprayed boron-aluminum (AA 6061) composite has been selected as a representative metal matrix system. This selection is based upon several advantages: (1) the process is simple, (2) the process yields good fiber spacing because the monofilament winding technique allows careful placement of the fibers which are retained until bonding by the plasma spray, (3) good filament-matrix bonding is achieved without fiber degradation, and (4) the use of monolayer tapes as an intermediate product allows considerable flexibility in hardware fabrication.

SUMMARY - MATERIALS SELECTED

The above review of potential materials to effect a significant weight reduction in propeller systems for 1970-1975 provides the following selections, based on the criterion of the material within its particular class possessing the highest degree of potential weight reduction and the least degree of technical jeopardy. These materials range from the presently used steels which involve no technical jeopardy to composite materials where, until fabrication and design parameters are adequately developed, technical jeopardy certainly does exist. This summary discusses each of the selected materials with regard to potential problems and indicates the type of development required to alleviate or eliminate these areas of technical jeopardy.

Steel

Vacuum-melted D6A steel (AMS 6431) has been selected as the optimum ferrous material. This material is well established and has undergone extensive testing and application in propeller components. Also, the material's characteristics with regard to heat treating and induction hardening of raceways have been firmly defined. Therefore, D6A steel is used as a basis for comparison with other materials (refer to Table II).

One of the newer generations of high-strength steels, AFC-77, has been included because of its substantially higher ultimate strength, which provides greater latitude of stressing within the confines of a Goodman diagram. This material requires the determination of more statistically reliable mechanical properties to provide a basis for the establishment of realistic design strengths. The lower hardenability of this material would require lower contact stresses in areas such as the blade retention. This material may provide a small degree of weight savings in parts requiring the use of steel.

Titanium

Forged Ti-6Al-6V-2Sn and cast Ti-6Al-4V have been selected as the best titanium alloys for use in a lightweight propeller system. Forged Ti-6Al-6V-2Sn or modifications now being developed are the strongest alpha-beta alloys available, considering static and dynamic properties. The material is heat treatable to strength levels in excess of 180,000-psi UTS in sections less than 1 in. thick. Several minor problems exist with regard to titanium forgings of a blade spar or a barrel. However, solutions are within reach of the present state of the art, and with continuing development, any technical jeopardy should be eliminated by 1970. These problems include the optimization of forging practice to provide the maximum amount of working in the metal, the optimization of tube processing parameters, and the adaptation of heat-treat equipment to eliminate the formation of alpha case.

Cast Ti-6Al-4V is selected as the most promising titanium casting material. Casting of titanium is presently limited to small and relatively simple shapes. Also, extensive precautions are required to prevent the highly active molten metal from reacting with the mold or the atmosphere. Existing government programs should eventually develop structurally reliable titanium alloy castings, thereby eliminating any large degree of technical jeopardy by 1970-1975.

Magnesium

A relatively new alloy, ZE63A, has been selected as the optimum magnesium casting alloy. This material, developed by the British, provides higher strengths than the normally used AZ92. It has a sounder structure and possesses excellent castability. The material derives its high strength from a unique hydriding heat-treat process. This hydriding treatment converts insoluble zinc-rare earth intermetallics to hydrogen rare earth compounds which, being smaller, reduce the amount of brittle precipitate existing at the grain boundaries. More effort will be required to generate a larger amount of statistically reliable strength properties before this material can be utilized to its full potential. However, there appears to be little technical jeopardy in developing this material for propeller system application.

Composites

Several different composite materials have been selected as being representative of the better materials available in the immediate future and expected to be developed for application in 1970-1975. Boron, S-glass, and graphite filament reinforcements have been selected for nonmetallic matrix and silicon carbide-coated boron filaments for metal matrix composites. Epoxy resins have been selected as the optimum nonmetallic matrix, and plasma-sprayed aluminum (AA 6061) has been selected as the metal matrix.

With composites, the designer has an essentially unlimited range of raw materials at his disposal, so the problem becomes one of how to use them. The highly directional properties of fibrous composites make them both promising and a problem. They cannot be considered as simple substitutions for existing metal components which were originally designed on the basis of the properties of isotropic materials. The designer must now take advantage of the unidirectional properties as much as possible, because the great gains of unidirectional strength and stiffness are reduced if the structure must carry multidirectional loads. The maximum structural efficiency when using composites depends on how accurately and economically the reinforcement is oriented and proportioned to sustain design loads. This task requires far more knowledge of failure modes and constituent deformation. Toward this end, almost every company concerned with advance composites has programs to convert the basic specimen properties data to a more fundamental understanding of the interaction of fiber and matrix.

With metal matrix composites, these problems are a little easier to resolve because of the comparatively good transverse strength of the matrix material. The problem area here, particularly with the plasma-sprayed tapes, is one of finding proper techniques for fabricating the actual individual component which would be built up from the tapes. The two processes with the greatest potential are brazing or diffusion bonding. They possess the capability of being developed into a highly reproducible and economical manufacturing process for making hardware. The following limitations are influential in determining the character of the fabrication process: (1) bonding must be conducted at elevated temperatures, 900° F to 1000° F, in a protective atmosphere to prevent oxidation of the composites; (2) bonding of large components must be accomplished at relatively low pressures, 25 to 1000 psi (otherwise, press tonnage requirements and die costs may become exorbitant); and (3) shapes that can be formed are fairly restrictive due to stresses imposed by bending fibers around small radii, the limit for plasma-sprayed tape being a bend radius of about 3/4 in. The braze-bonding technique is preferred because it allows bonding at the lowest possible pressures. Also, the requirements for uniform pressure over a large area to assure good densification are far less stringent for brazing than for solid-state bonding, since all voids are readily filled by the flow of braze material.

These new advanced filament composites have dramatic increases in strength- and stiffness-to-weight ratios over either steel or titanium. When the loading is essentially unidirectional with the reinforcing fibers, and thus the matrix material is not highly stressed, the epoxy matrix appears preferable because of its lighter weight. However, metal matrix offers the advantage of higher strength and modulus where needed. Also, the design allowables of the epoxy matrix are normally adjusted downward, when used in a structural component, to allow for service environmental effects of moisture absorption and for the gradual decrease of its modulus under continuous cyclic stressing. Composites are being developed at a very rapid pace in the aircraft industry, and a reasonable degree of technical jeopardy still exists. However, the large weight improvements being projected should ensure continued evolution of these materials, and they are therefore considered to be feasible for use in propeller systems in 1970-1975.

COMPONENT DESIGN STUDIES

POINT DESIGN SIZING CRITERIA

This section discusses the various design studies and parametric studies conducted to determine the lightest weight concepts and configurations for the different components of the propeller system. With the exception of some parametric studies conducted early in the program, the component designs and subsequently, the system designs, are all based upon the following point design sizing criteria:

Structural

2000-hp, 1160-prpm torque limit
E. F. = 4(+25% higher order)
20:1 gear ratio
400-kn maximum velocity

Aerodynamic

35-psf thrust disk loading
1400-hp, 6000-ft, 95°F hover design point
900-fps hover tip speed
14.8-ft-dia/4-way/120AF/0.4C_{L1}
0.78 figure of merit (existing technology)
60% prpm for cruise
82% 250-kn cruise efficiency (S. L., standard day)

GEARBOX

Gear Sizing Trade-Off Study

Initial gear train parametric studies to define the optimum gear sizing were conducted using a two-stage, in-line, star-epicyclic configuration. For this configuration, studies were conducted to evaluate changes in the total gear train weight when certain significant parameters were varied. The parameters chosen were: (1) the second-stage gear ratio, (2) the number of planets in the second stand, and (3) gear face-width-to-pitch diameter ratios. The basic assumptions for these studies were as follows:

Engine shp - 2,000
Engine rpm - 19,000
Gear ratio 20:1
Bearing B₁₀ AFBMA Life Calculation of 600 hours air melt
Gear material, consumable electrode vacuum-melt steel

Only the gears, bearings, interconnecting shafting, and planet gear supports were considered in the weight comparisons.

The following discussion, together with Figures 18 through 20, summarizes the weight relationship to the above parameters. It should be noted that these figures are presented only to show the relative weight variations associated with each individual parameter and not the final study weights. These initial parametric studies were completed before the final propeller sizing from the aerodynamic studies was defined, and prior to the detailed optimization of the components.

Figure 18 shows the variation of both the first- and the second-stage gear train weight versus gear ratio split. To understand the figures better, first consider a given total gear train of constant torque input to the first stage and known overall gear ratio. If the first-stage ratio is increased by 20% and the second-stage gear ratio is decreased by 20%, the torque input to the second stage is increased by 20%. The larger gear ratio and higher output torque of the first stage will require larger (and heavier) gears. However, this is the low-torque stage and, as Figure 18 indicates, the increase in weight is minimal.

The second stage (high-torque stage) requires a slightly larger diameter sun gear because of the higher torque, but the ring gear and planets can be made much smaller due to the smaller gear ratio. This effect can be seen both in Figure 18 and in the following.

A relationship for gear tooth Hertz stress can be written for two gears in contact as shown below:

$$S_C = K \sqrt{\frac{W_t}{F} \left(\frac{D_1 + D_2}{D_1 D_2} \right)} = K \sqrt{\frac{2Q}{FD^2} \left(\frac{R + 1}{R} \right)} \quad (2)$$

- S_C = Hertz stress
- K = Constant dependent on tooth geometry and material
- W_t = Tangential tooth load, gear
- F = Gear face width
- D_1, D_2 = Pitch diameters of meshing gears
- $R = \frac{D_1}{D_2}$ = Gear ratio

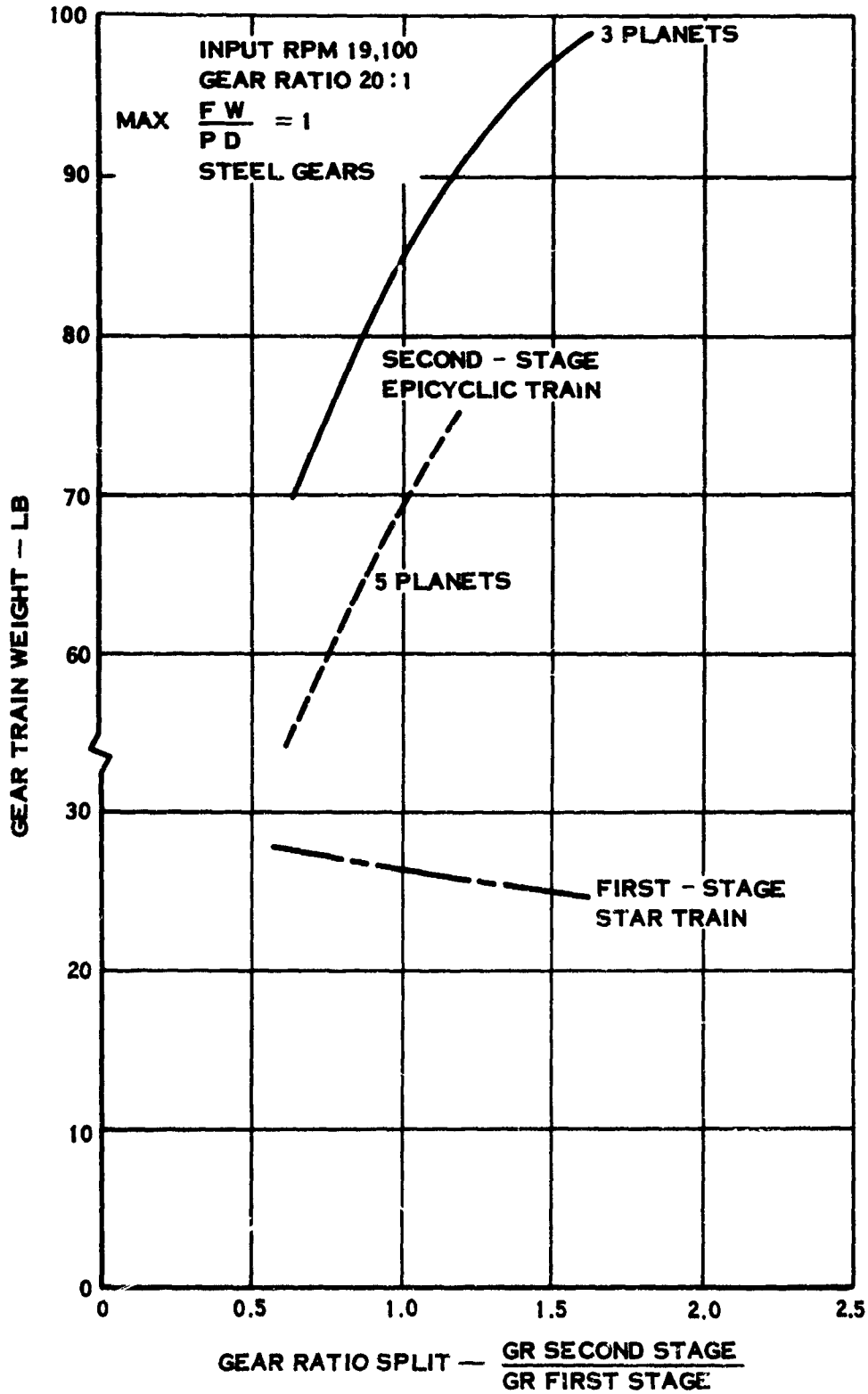


FIGURE 18. GEAR RATIO SPLIT-WEIGHT COMPARISON

$$Q = \frac{PD_2}{2} = \text{Torque}$$

or for a constant face-width-to-pitch-diameter ratio (F/D_2),

$$S_C = K \sqrt{\frac{2D_2}{F}} \cdot \sqrt{\frac{Q}{(D_2)^3} \frac{R+1}{R}} \quad (3)$$

For a constant gear ratio the 20% higher torque would require an increase in diameter of only $(1.2)^{1/3} = 1.063$. However, the diameter of the ring gear and planets is reduced by nearly 20% to produce the gear ratio decrease. This effects a definite weight saving.

Figure 19 shows the results of a parametric study to determine the variation of total gear train weight with different numbers of planet gears in the second stage. For a constant output torque and face-width-to-pitch-diameter ratio, increasing the number of planets produces a lighter second stage. This is because the load per mesh is lower, thereby permitting a smaller sun gear pitch diameter for the same ratio of face-width-to-pitch diameter. The smaller sun gear reduces the ring gear diameter, planet gear centrifugal load, and carrier size. As noted on the curve, a gear ratio of approximately 3.3 or less is required to use seven planets in the planetary gear train.

The third basic parametric study was to ascertain the effect of a variation of face-width-to-pitch-diameter ratio on total gear train weight. Figures 20 and 21 show that the gear train weight increases as the ratio of face-width-to-pitch diameter of the sizing gear (MAX F/D) increases.

This can also be seen from the previous relationship, where, for a constant Hertz stress, torque, and gear ratio, FD_2^2 is constant. Also, gear weight should be proportional to $D_2 F t$ (t is gear rim thickness) or $D_2^2 F t/D_2$. Therefore, weight is proportional to t/D_2 . If t is constant and the supporting gear webs have only a secondary effect on weight, which is generally true, gear weights decrease as the diameter increases.

Figures 20 and 22 show the interrelated effect of varying gear ratio split and face-width-to-pitch diameter, that is, the change of the overall gear train diametral envelope. The figures graphically demonstrate that the largest gear envelope generally produces lighter weight.

This initial parametric study of the 20:1 gear train was conducted to determine the weight trends of the previously discussed parameters. It was shown that, in general, the lightest weight gear train should (1) have the majority of the gear reduction in

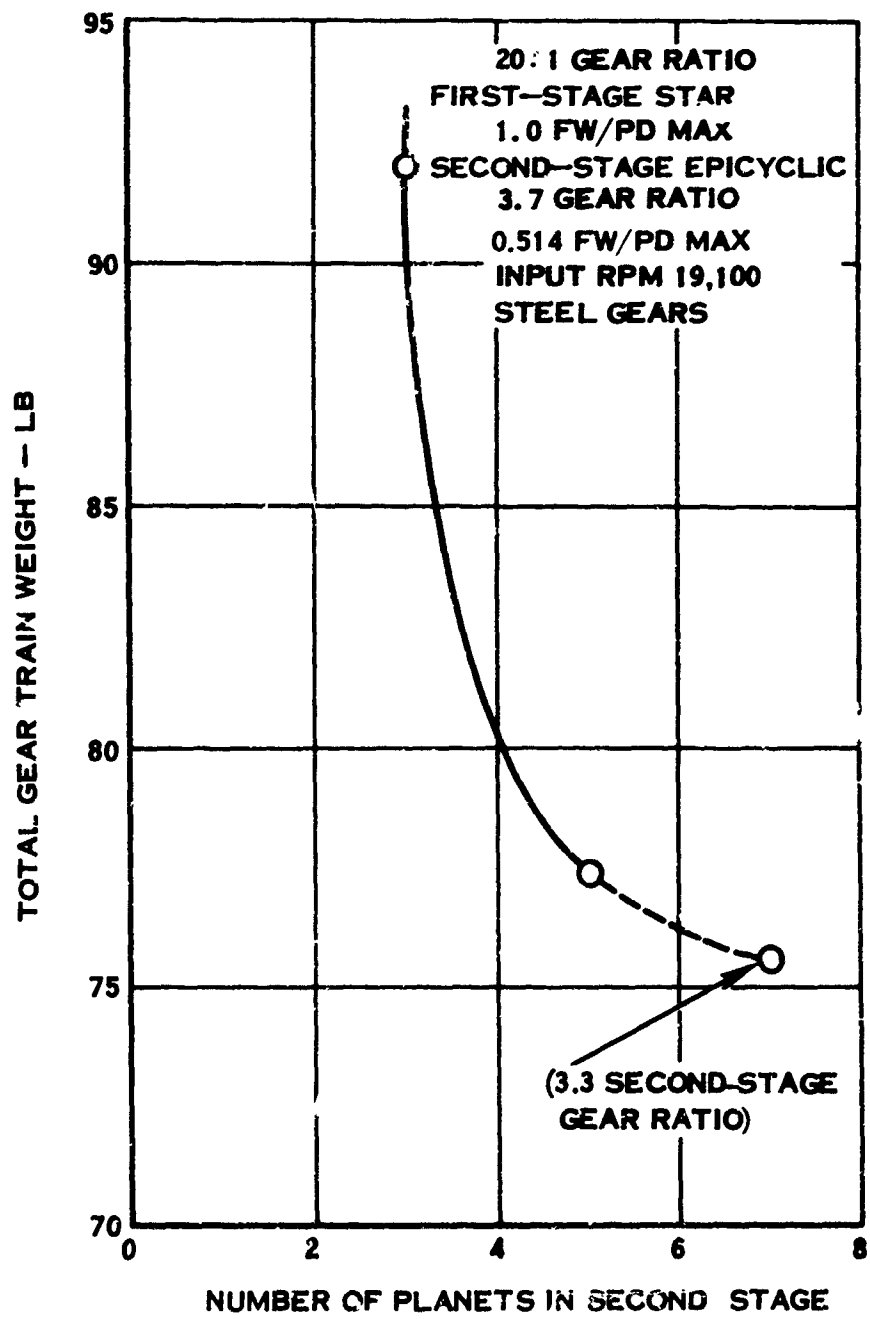


FIGURE 19. EFFECT OF NUMBER OF PLANET GEARS

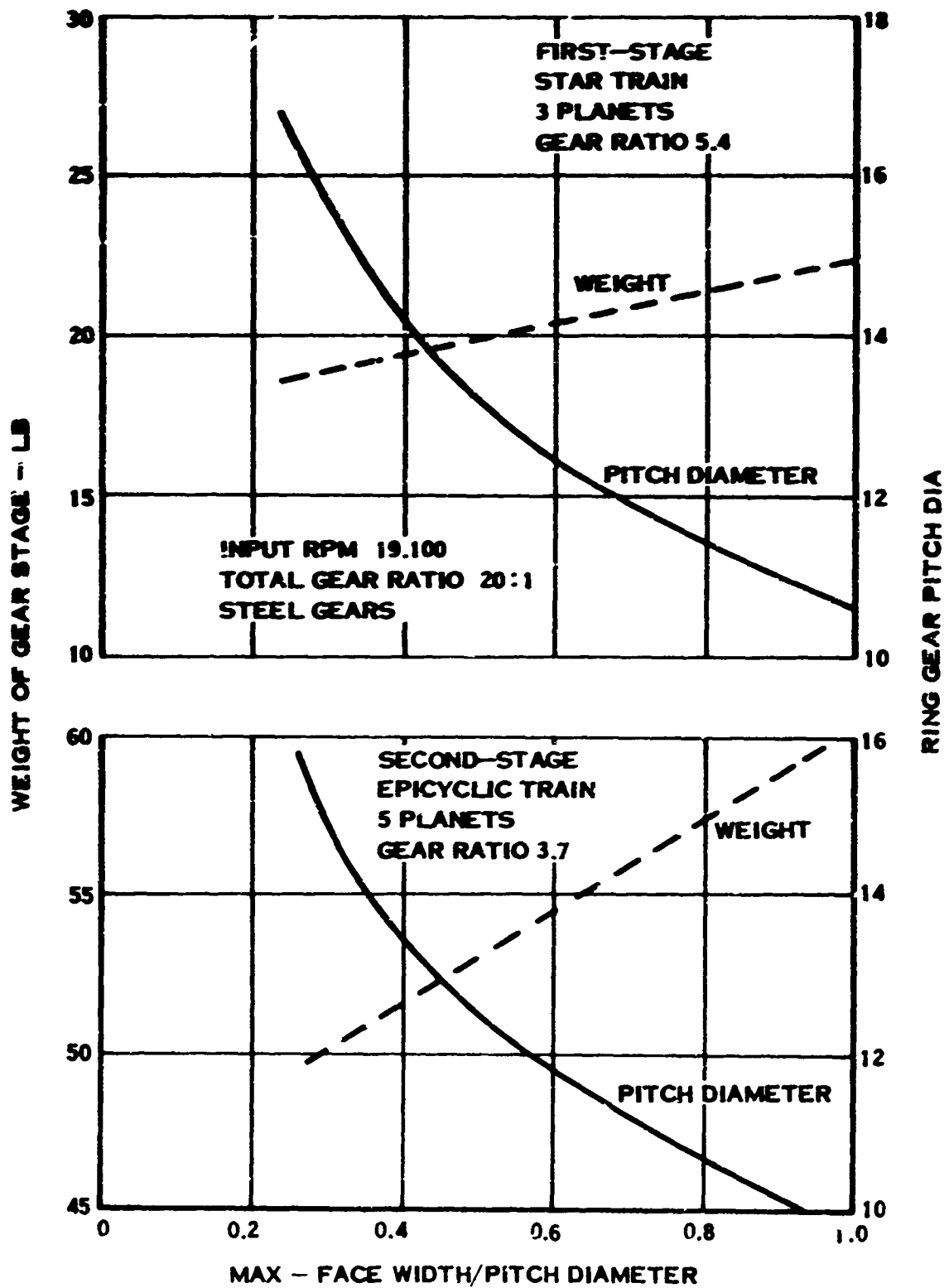


FIGURE 20. EFFECT OF GEAR SIZE ON WEIGHT

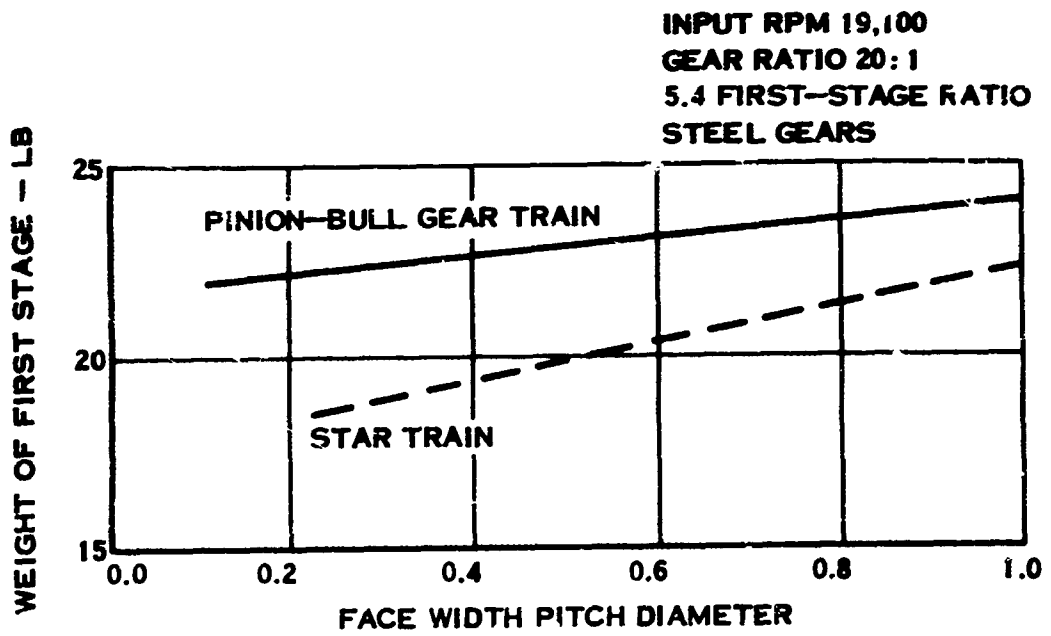


FIGURE 21. FIRST-STAGE GEAR TRAIN WEIGHT TREND

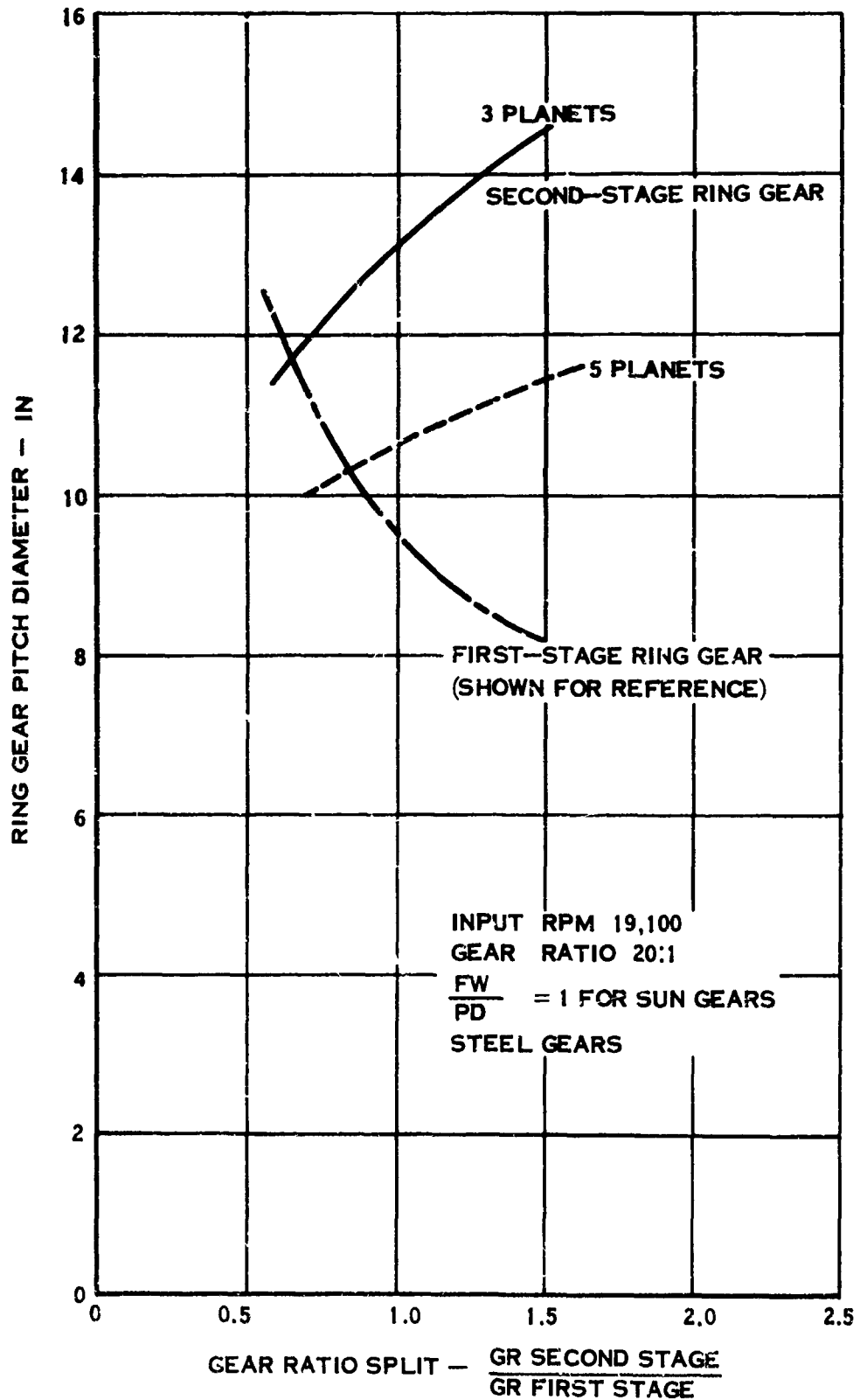


FIGURE 22. EFFECT OF GEAR RATIO SPLIT ON GEAR SIZE

the first stage (low-torque stage); (2) use the largest number of planet gears possible; (3) have as large an envelope as possible, thus enabling the use of gears of lower face-width-to-pitch-diameter ratio.

Gear Train Configurations

Under this phase, several different gear train configurations were designed and compared in order to ascertain which gearbox was the most favorable in terms of the following characteristics:

1. Weight
2. Envelope
3. Efficiency
4. Simplicity of providing opposite rotation
5. Simplicity of providing cross-shaft drive

The basic assumptions established for use in this comparison study are listed below in tabular form. Gearbox housing comparisons, overrunning clutch, decoupling, and accessories were not considered in this phase of the study.

Engine shp	2,000
Engine rpm	19,000
Overall gear ratio	20:1
First-stage ratio	5:4
Max face-width-pitch to diameter ratio	1.00
Gear material	CEVM Steel
Bearing life	600 hours air melt

A summary of the several configurations, their advantages, and their disadvantages are discussed in the following paragraphs. Table V is a compilation of the specific design data for the gear trains.

In-Line Star-Epicyclic (Figure 23)

The selected gear train for this concept incorporated a gear ratio of 5.4 in the first stage and 3.7 in the second stage. This gear ratio split, together with a face-width-to-pitch-diameter ratio of 0.522, resulted in a ring gear pitch diameter of 12.96 in. for the first stage. It was felt that this pitch diameter plus the diameter increase required for ring gear backing and housing would result in approximately the maximum envelope that would still allow for annular ducting to the engine inlet. The gear ratio split was selected on the basis of the earlier parametric studies, and the requirement that three planets be used in the first stage was based on allowing room for the insertion of three idlers for reverse rotation.

TABLE V. DATA SUMMARY OF GEAR TRAIN CONFIGURATIONS

FIGURE NO	CONFIGURATION	PROP ROTATION	FIRST STAGE					SECOND STAGE					TOTAL				SHIPSET SYSTEM	
			MAX P/D	NO PLANETS	GEAR RATIO	RING OR BULL P.D. (IN)	WT. (LB)	MAX P/W	NO PLANETS	GEAR RATIO	RING OR BULL P.D. (IN)	WT. (LB)	MAX ENVELOPE GEAR P.D. (IN)	EQUN. MEMES W O X-S	BASIC WT. (LB)	RH WT. INCL. X-S DRIVE	LH WT. INCL. X-S DRIVE	RH & LH WITH X-S DRIVE
21	IN-LINE STAR-EPICYCLIC)	RH	0.522	3	5.4	12.96	20.0	0.516	5	3.7	12.10	13.2	3	73.2	84.7	84.7	183.4	152.4
	IN-LINE STAR WITH IDLERS EPICYCLIC)	LH	0.989	6	5.4	12.96	28.0	0.516	5	3.7	12.40	33.2	4	79.2	84.7	84.7	179.2	161.2
23	OFFSET PINION (BULL-EPICYCLIC)	RH	0.613	-	5.4	15.20	22.9	0.516	5	3.7	12.40	33.2	2	76.1	83.6	83.6	179.2	161.2
	OFFSET PINION, BULL, IDLER EPICYCLIC)	LH	1.00	-	5.4	15.20	31.9	0.516	5	3.7	12.40	33.2	3	68.1	83.6	83.6	179.2	161.2
24	DIFFERENTIAL OFFSET WITH IDLER	RH	1.00	-	2.0	6.00	18.9	0.94	7	10.0	12.00	86.6	7.5	103.8	113.5	113.5	221.7	201.7
	DIFFERENTIAL OFFSET	LH	0.82	-	2.0	6.00	11.6	0.94	7	10.0	12.00	86.6	6.5	94.2	108.2	108.2	221.7	201.7
25	ROLLER GEAR	RH	0.97	16	20.0	22.0	97.3						3	97.3	112.8	112.8	230.1	210.1
	ROLLER GEAR WITH OFFSET	RH	0.82	-	2.0	6.00	11.6	1.0	12	9.0	13.50	90.8	4	102.4	112.4	112.4	230.1	210.1
	ROLLER GEAR WITH OFFSET AND IDLER	LH	1.00	-	2.0	6.00	16.9	1.0	12	9.0	13.50	90.8	5	107.7	117.7	117.7	230.1	210.1
27	COMPOUND STAR	RH	1.00	3	20.0	23.04	77.7						2	77.7	93.7	93.7	189.3	169.3
	COMPOUND STAR WITH OFFSET	RH	0.82	-	2.0	6.00	11.6	1.0	3	10.0	18.30	70.4	3	82.0	92.0	92.0	189.3	169.3
	COMPOUND STAR WITH OFFSET AND IDLER	LH	1.00	-	2.0	6.00	18.9	1.0	3	10.0	18.30	70.4	4	87.3	97.3	97.3	189.3	169.3
29	SPLIT POWER (EPICYCLIC-STAR)	RH	0.366	3	5.0	13.81	35.9	0.35	5	3.80	14.0	33.6	4	69.8	88.0	88.0	176.7	155.7
	SPLIT POWER (STAR-EPICYCLIC) WITH OFFSET	RH	0.15	5	3.0	14.00	30.3	0.286	7	3.00	14.0	32.0	5	72.2	88.2	88.2	176.7	155.7
	SPLIT POWER (STAR-EPICYCLIC) WITH OFFSET AND IDLER	LH	0.18	5	3.0	14.00	30.3	0.286	7	3.00	14.0	32.0	6	80.8	90.5	90.5	176.7	155.7

* TOTAL WEIGHT INCLUDES 12.9 LB FOR OFFSET PINION-BULL STAGE.
 ** ADDITIONAL 3.3 LB REQUIRED FOR REVERSE NOTATION.

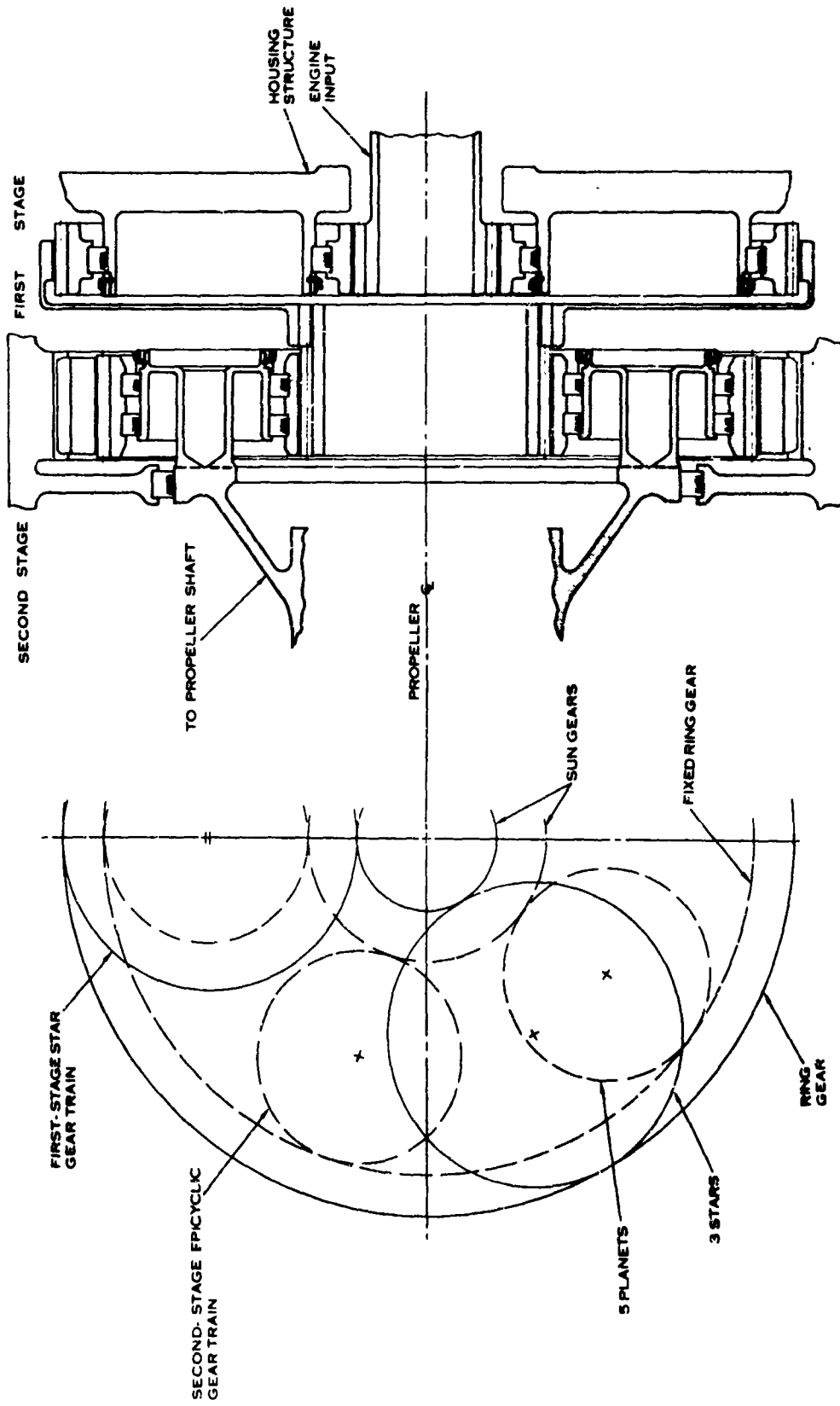


FIGURE 23. IN-LINE (STAR-EPICYCLIC) GEAR TRAIN

To provide for the addition of a cross-shaft drive to this concept required the incorporation of a 2:1 gear ratio angle drive bevel mesh between the engine and the star stage sun gear. This added 15 lb to the basic gear train weight.

Offset (Pinion-Bull) Epicyclic (Figure 24)

The pinion-bull stage inherently has one less equivalent power mesh (hence, one less mesh producing a power loss) than the star train and, therefore, can be designed for higher efficiency from a power loss standpoint. The number of equivalent power meshes can be determined by summing the product of the tooth load and the relative velocity of the engaging teeth for each mesh and by dividing by the product of the input gear tooth load and meshing velocity (Reference 40). For a star gear train, the number of equivalent power meshes will be equal to the actual number of meshes (Z) transmitting full power. In a planetary gear train, the relative velocity between the planet-ring mesh and the planet-sun mesh is one-half the absolute pitch line velocity; therefore, the total is equal to one equivalent power mesh. In gear trains such as the split power configuration, to be discussed later, some of the meshes have high relative velocities which increase the relative power (relative meshing velocity times the tooth load) at the mesh actually more than the transmitted power. This results in a large number of equivalent power meshes.

The offset design allows a local scoop-type air inlet to be incorporated in the nacelle under the pinion and to be flared into a full annular engine inlet behind the gearbox. The in-line design normally utilizes an annular air inlet which usually limits the size of the gearbox envelope diameter. The previous gear sizing study showed that an increase in diameter has a beneficial influence on weight.

The pinion-bull first stage allows the addition of cross-shaft drive with a lower weight penalty than would be the case with a star stage. Although accessory mounting was not considered in this phase of the study, it should be noted that accessories can usually be added to an offset configuration with less weight penalty than for the in-line version.

Modification of this concept for opposite rotation is accomplished by opening up the center distance between the pinion and the bull gear enough so that an idler gear can be inserted as an intermediate mesh.

Differential Gear Train With Offset

A fixed planet differential drive, with 20:1 gear ratio, which did not include an offset first stage was studied briefly. The concept was found to be heavier than the one studied previously because the high planet bearing loads from the high first-stage tooth loads and the high second-stage rpm inherent in this type of train required over 20:1 planets to mount adequate bearings. Also, the overall diametral

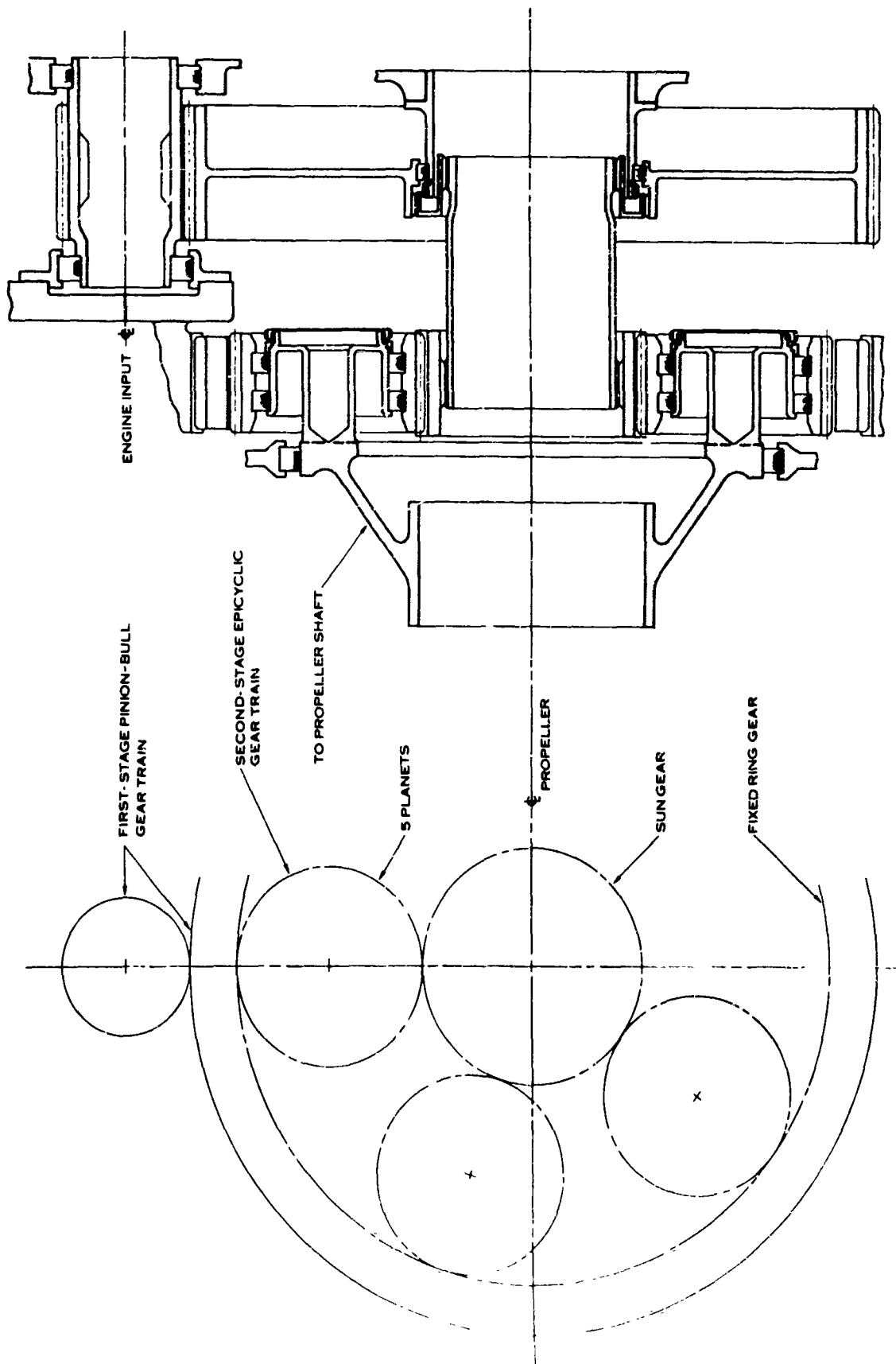


FIGURE 24. OFFSET (PINION, BULL-EPICYCLIC) GEAR TRAIN

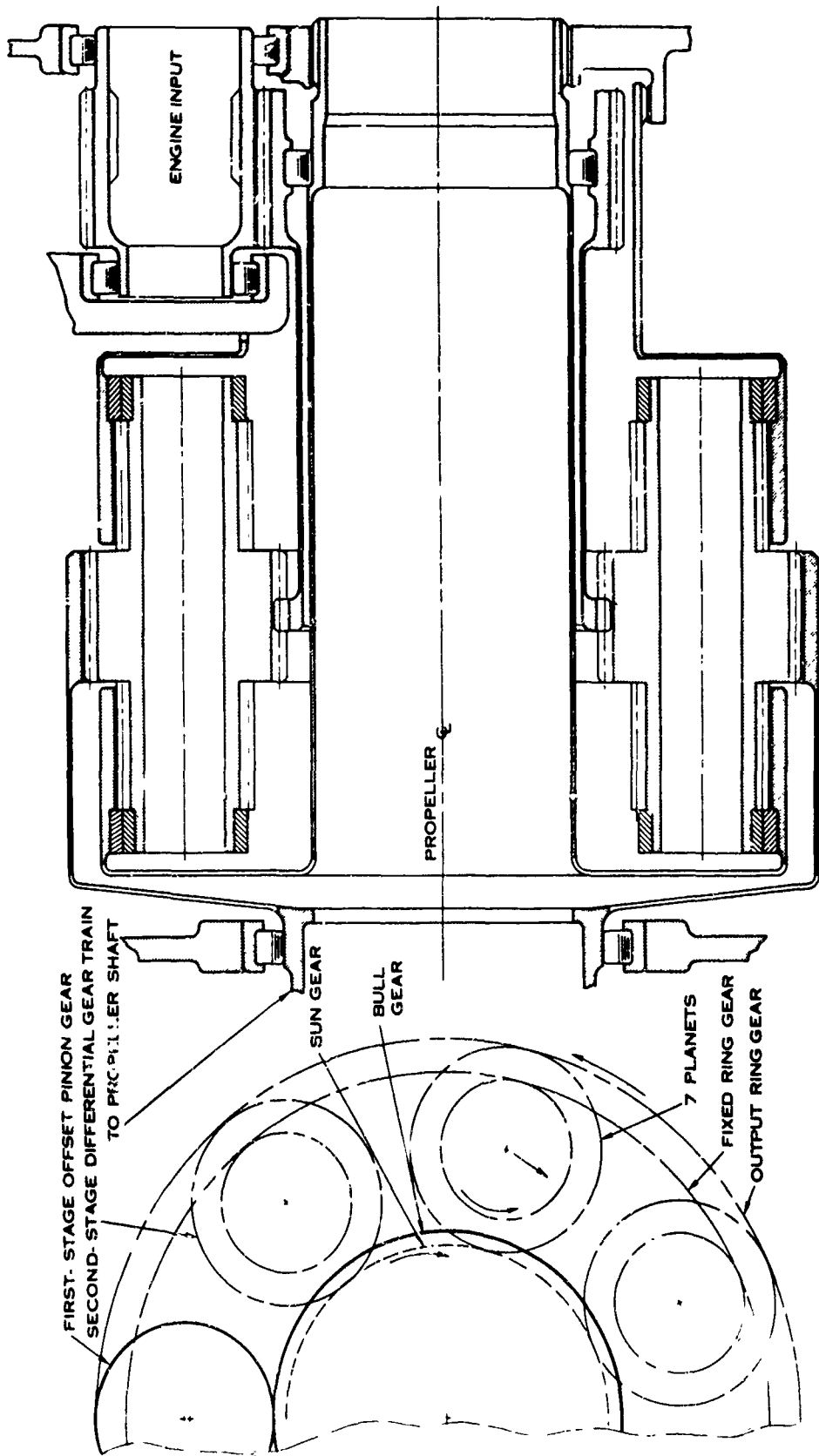


FIGURE 25. DIFFERENTIAL GEAR TRAIN WITH OFFSET

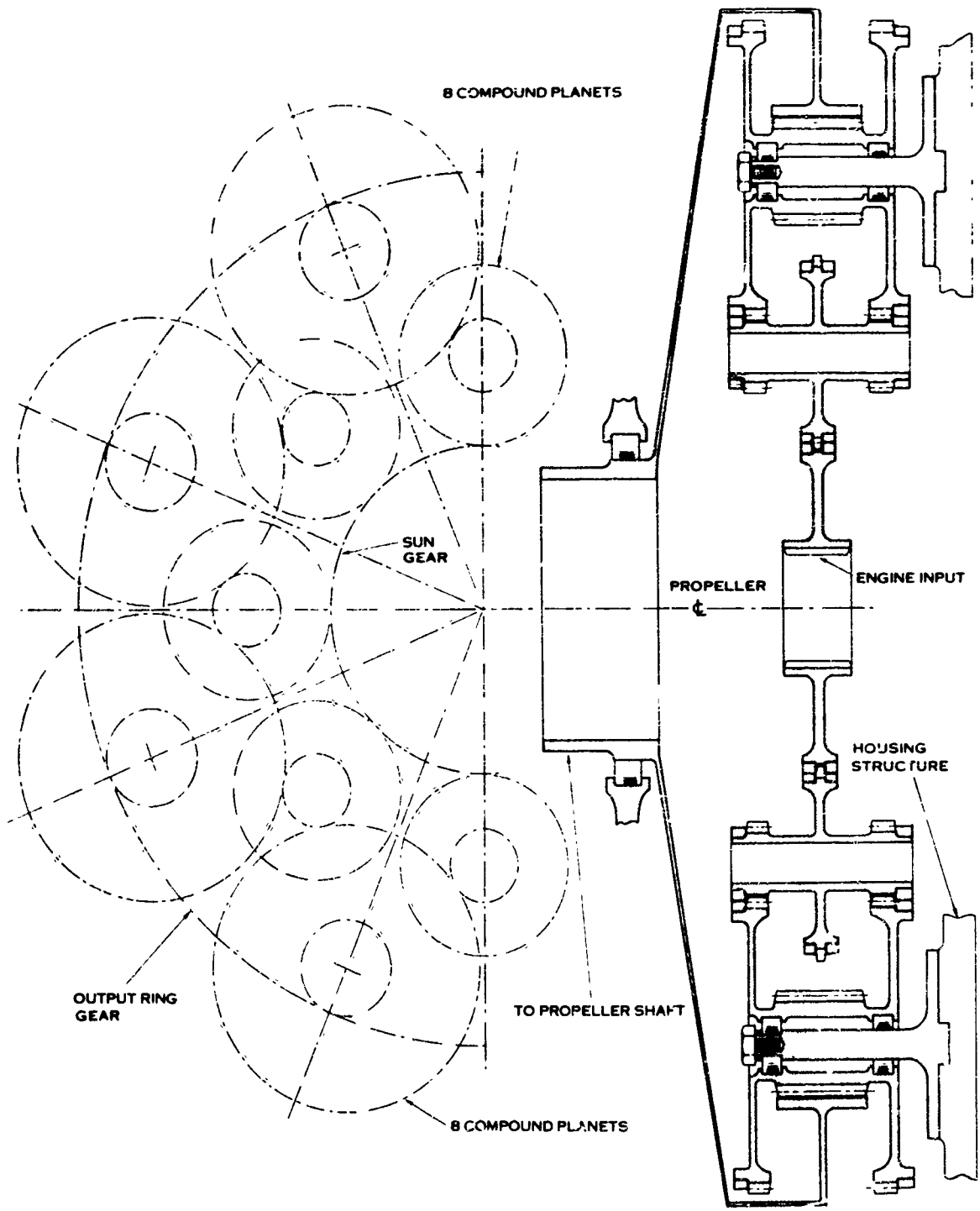


FIGURE 26. ROLLER GEAR TRAIN

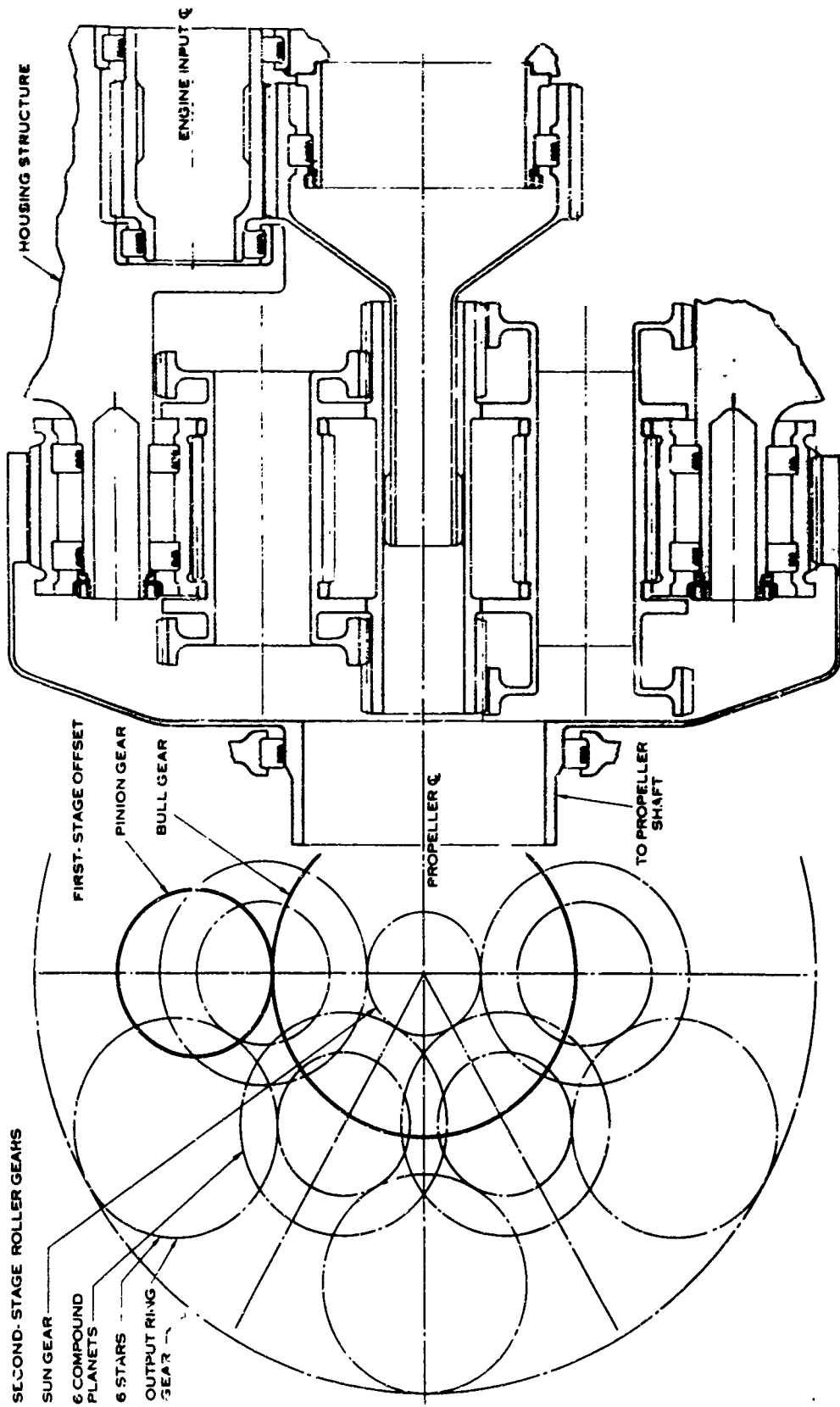


FIGURE 27. ROLLER GEAR TRAIN WITH OFFSET

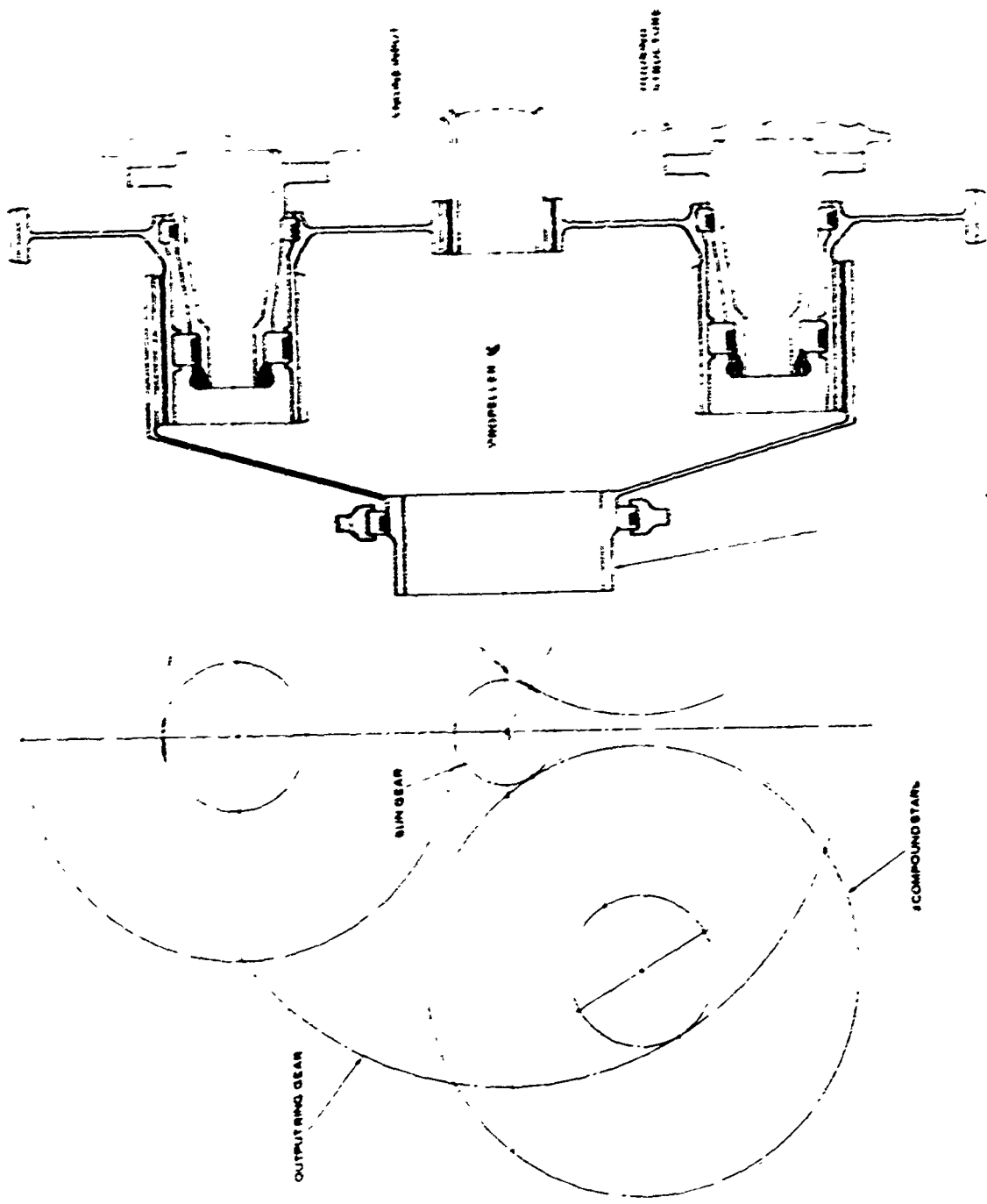


FIGURE 28. COMPOUND STAR GEAR TRAIN

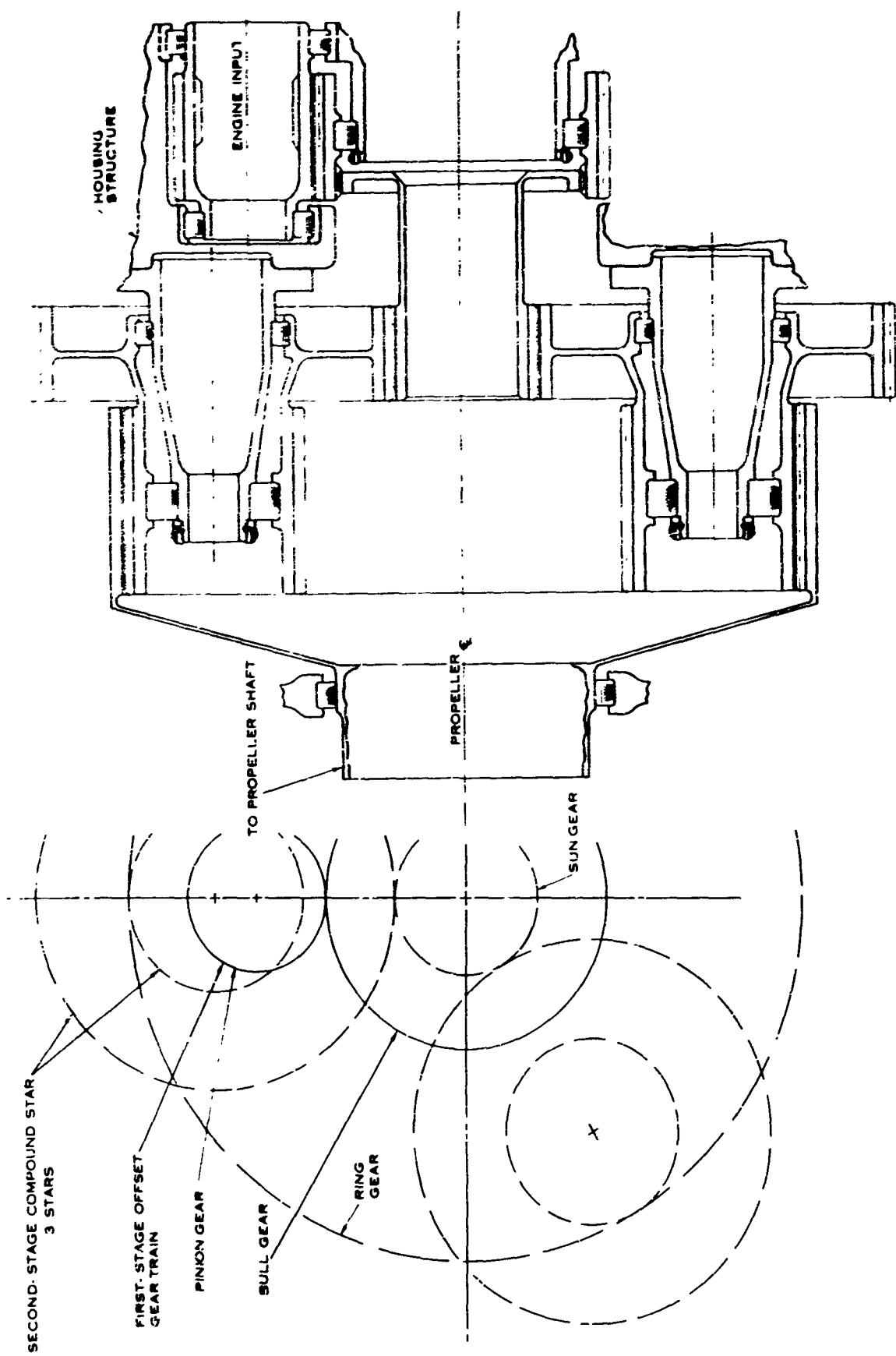


FIGURE 29. COMPOUND STAR GEAR TRAIN WITH OFFSET

Split Power

A split-power epicyclic-star gear train (Figure 30) was designed, wherein 70% of the output torque is taken off the second-stage ring gear and the remaining 30% of the output torque is taken off the first-stage planet carrier. This concept, as a righthand gearbox without cross-shaft drive provision, is the lightest system but does not include opposite rotation. The addition of cross-shaft drive increased the weight by 15.5 lb. In an attempt to reduce this weight penalty and to incorporate provisions for opposite rotation without requiring a new gear train, a second concept was studied. This concept (Figure 31) utilized an offset pinion-to-bull (2:1 gear ratio) driving a 10:1 split-power star-epicyclic-gear train. In this second system, 59.4% of the output torque is taken from the second-stage ring gear, with the remaining torque being taken from the first-stage planet carrier. The weight of this system with cross-shafting was the lightest of all the systems conceived. The major disadvantage of this concept is the large number of equivalent power meshes. It has five equivalent full-power meshes versus two for the offset-epicyclic train. This makes it virtually impossible to limit the maximum gear train power loss to 1%.

Summary - Gear Train Configurations

Table VI is presented as a comparison of the several gear train configurations studied. The parameters of this table are the weight and envelope values (shown in Table V) as a ratio of those values for an "Offset, Two-Stage (Spur, Epicyclic)" configuration. It should be noted that the weight and power loss parameters are given for a twin-propeller shipset system. The weight parameter includes the weight of the gears, bearings, bearing supports, and connecting shafts; but it does not include housing, propeller tailshaft, or other components of an integral gearbox propeller. The cross-shaft drive weight includes power takeoff gearing in the integral gearcase, but does not include the aircraft cross-shafting, wing box or other components of the transmission system. Parameters for a shipset are not listed for those configurations that required a new gear train to provide opposite rotation.

The conclusion reached in this phase of the study is that the gear trains using differential, compound star, and roller gears were appreciably heavier than the other trains, which showed little relative weight difference. The offset, two-stage, spur-epicyclic gear train was selected as the optimum configuration for an application with cross shafting. It is the lightest configuration with provision for opposite rotation and cross-shaft drive which affords the possibility of obtaining 99% power transmission efficiency.

Although the split power with offset first-stage configuration is slightly lighter, the power loss associated with over twice the equivalent power meshes greatly over-

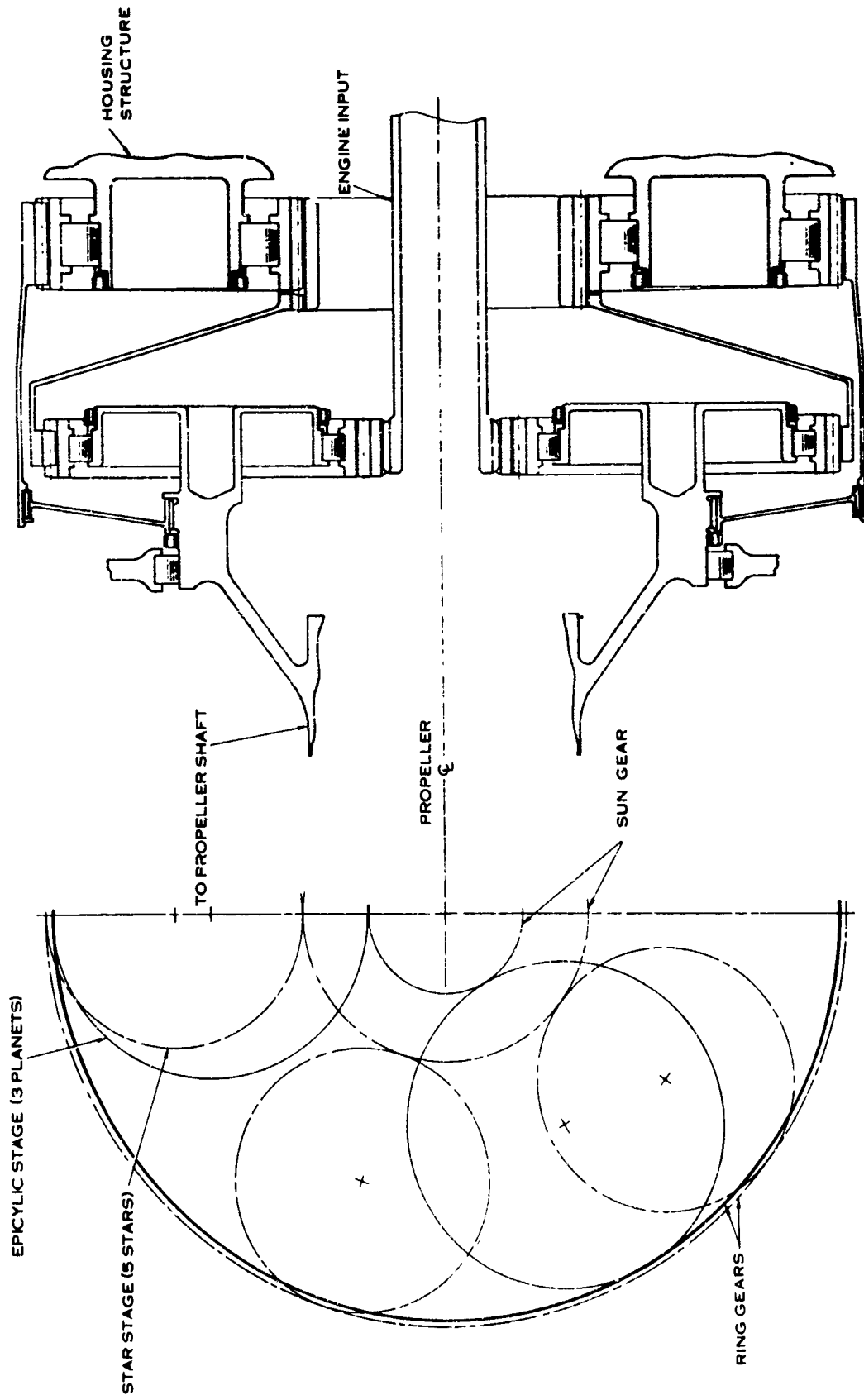


FIGURE 30. SPLIT-POWER GEAR TRAIN

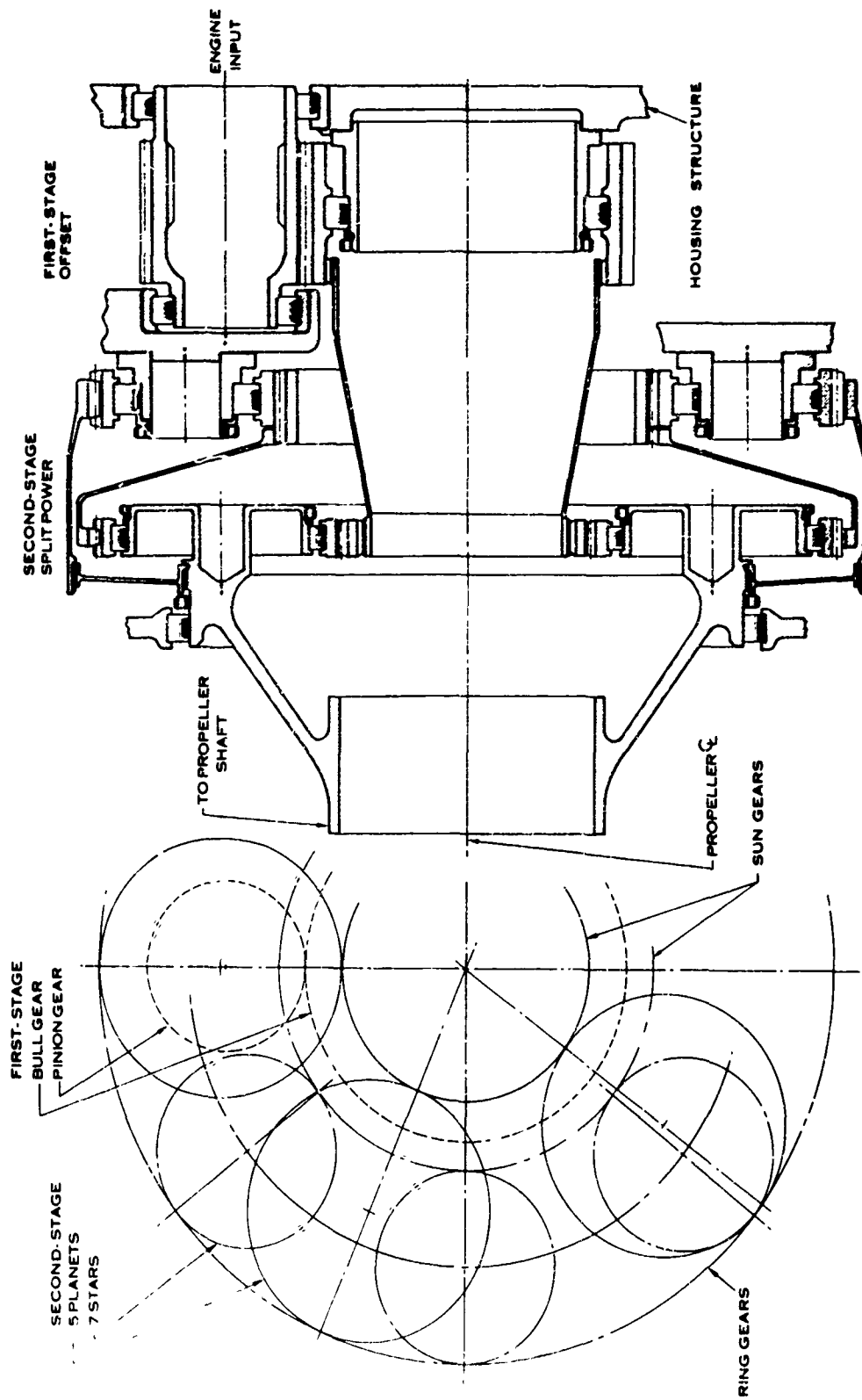


FIGURE 31. SPLIT-POWER GEAR TRAIN WITH OFFSET

TABLE VI. SUMMARY OF GEAR TRAIN CONFIGURATIONS

CONFIGURATION (FIRST STAGE, SECOND STAGE)	DIAMETER OF ENVELOPE PARAMETER, IN./IN.	BASE WEIGHT PARAMETER, LB/LB.	WEIGHT PARAMETER IF PROVISIONS FOR OPPOSITE ROTATION ARE ADDED TO THE BASE	WEIGHT PARAMETER IF A CROSS-SHAFT DRIVE IS ADDED TO THE BASE	WEIGHT PARAMETER FOR ONE SHIPMENT WITH/ WITHOUT CROSS SHAFTING	NO OF EQUIVALENT POWER MESHES PER SHIPSET	
IN-LINE TWO-STAGE (STAR - EPICYCLIC)	0.85	0.96	1.04	1.17	2.41	2.00	7
OFFSET TWO-STAGE (SPUR - EPIC\ CLIC)	1.0	1.0	1.12	1.11	2.34	2.12	5
OFFSET TWO-STAGE (SPUR, DIFFERENTIAL)	0.79	1.29	1.36	1.42	2.91	2.65	14
IN-LINE SINGLE STAGE (ROLLER GEARS)	1.45	1.28	NEED NEW GEAR TRAIN	1.48	N/A	N/A	N/A
OFFSET TWO-STAGE (SPUR, ROLLER GEARS)	0.89	1.35	1.42	1.48	3.03	2.76	9
IN-LINE SINGLE STAGE (COMPOUND STAR)	1.52	1.02	NEED NEW GEAR TRAIN	1.22	N/A	N/A	N/A
OFFSET TWO-STAGE (SPUR, COMPOUND STAR)	1.20	1.08	1.15	1.21	2.49	2.22	7
IN-LINE SINGLE STAGE (SPLIT POWER)	0.92	0.91	NEED NEW GEAR TRAIN	1.12	N/A	N/A	N/A
OFFSET TWO-STAGE (SPUR, SPLIT POWER)	0.92	0.99	1.06	1.12	2.31	2.04	11

shadows this weight difference. For example, the split-power configuration would be expected to be approximately 1% less efficient than the selected configuration, and this results in approximately a 60-lb loss in static thrust per propeller, which is many orders of magnitude larger than the slight weight savings. For the non-cross-shafted gearbox application, the offset spur-epicyclic gearbox was also selected as the optimum configuration. Here again, the split-power version is slightly lighter, but its lower gearbox efficiency offsets this advantage. The in-line (star-epicyclic) is also less efficient and slightly lighter than the selected offset configuration. The power loss would probably still be sufficient to overcome the weight advantage, but since the non-cross-shafted version is not considered to be a VTOL, the trade-off is much more dependent upon the aircraft mission. Also since the propeller control inputs to the in-line gearbox become more complex, this was assessed as negating the small weight advantage.

It should be noted, however, that the gearbox configuration selected in this study is based primarily on optimizing the integral gearbox propeller system itself. There may be overriding airframe installation and/or performance requirements (especially for non-VTOL aircraft) for a specific aircraft design which would lead to the selection of an in-line rather than an offset installation.

Gearing and Gear Tooth Shapes

The selection of the gear tooth shape and the gear material to use with the two-stage, spur-epicyclic gear train configuration to obtain the lightest weight gearing is discussed below.

The use of involute spur gears in both high-speed and planetary stages has been successful in previous integral gearbox propeller systems and is shown in the system design.

The selection of gear tooth geometry, tolerances, stress levels, and mounting arrangements which will provide a flexible system is a necessary consideration to ensure that design calculations will reasonably approximate actual operating loading conditions.

During the detailed design of the gearing, the magnitude of the involute profile modification would be determined from an analysis of the gear tooth deflections under loading conditions. The standard involute gear tooth proportions would also be modified after analyzing the gear center distance and scoring parameter change under load. These analyses have been successfully used on previous aircraft gearing and would not change the gear sizing discussed below, but they would provide detailed design refinements.

The Hertz stress levels of helical gears are reduced by the cosine of the helix angle. For a given diametral pitch (rotational), the bending stress remains the same as that of an equivalent spur gear. The reduction in normal tooth section and the increase in normal tooth load are offset by the increase in face width engagement and contact ratio.

The selection of the helix angle of the helical gear should be large enough to provide two or more teeth in contact to obtain the desired increase in contact ratio. For the pitch sizes used in this gearbox, a 30° helix angle would be required, which would produce very high axial gear forces. Therefore, if helical gearing were desired, herringbone gears (double helical) would be used to eliminate the need for large gear thrust bearings. Herringbone gears could be used in the first-stage gear trains of the design shown herein with essentially no change in weight.

In an attempt to reduce the gear train weight further, a study of the literature was conducted on circular arc tooth forms (Novikov gears). The conclusions of this study are presented in Appendix IV, and a brief synopsis is included below.

Gear teeth for propeller gearbox systems are usually designed for structural adequacy relative to two potential failure phenomena: tooth bending and surface durability (primarily Hertz stress) under both steady and dynamic loads. However, the majority of investigations of the Novikov tooth shape that were examined have used only the surface and beam strength criteria under steady loads to rate the Novikov tooth form. From the literature surveyed, the Novikov gear form at first appeared to have a substantial advantage over the involute tooth relative to Hertz contact stress, but this advantage is substantially lost when consideration is given to tooth bending and dynamic loadings. Based on steady transmitted load, the circular arc tooth form may, however, have significant weight advantage over the involute in applications where wear of contact stress is the limiting design criterion. The two tooth forms are comparable when static beam strength is the criterion. However, the circular arc appears to be at a disadvantage when the effects of dynamic load are included.

Some weight advantage may be possible, depending on the particular configuration and operating requirements. However, in propeller gearbox systems where the dynamic loadings are usually a significant part of the sizing loads, the weight saving would, at best, be small and would require considerable research to determine its magnitude accurately. Therefore, the circular arc tooth form was not incorporated in the proposed gear train concept.

To obtain a minimum-weight gear train, an assessment of titanium versus vacuum-melted steel as a gear material was made. For this comparison, two offset-epicyclic gear trains were designed for the following criteria:

Engine horsepower	2000
Engine rpm	23,300
Face-width-to-pitch diameter	1.0 max
First-stage ratio	5.4
Overall gear ratio	20:1
5 planets in the second stage	

Weight comparison of the gears is shown in Table VII.

From test work currently in progress, hard-surfaced, diffused-nickel-coated titanium appears to be a feasible gear material for the 1970-1975 time period. Titanium has therefore been selected as the optimum gear material for the study.

The calculated stresses on the gears have been determined by the equations presented below. Relatively conservative stress allowables of approximately 100,000 psi static Hertz stress and 55,000 psi dynamic bending stress for titanium gears were used as a basis for the 1970-1975 time period. For comparison, 150,000 psi static Hertz stress and 65,000 dynamic bending stress were used for steel gears.

A. Hertz Stress

$$S_C = 0.564 \left[\frac{W_t}{F_e \cos \phi \sin \phi} \left(\frac{1}{R_{p1}} + \frac{1}{R_{p2}} \right) \left(\frac{1}{\frac{1-\mu_1}{E_1} + \frac{1-\mu_2}{E_2}} \right) \right]^{0.50} \quad (4)$$

where:

- W_t = tangential tooth load (pounds) = $\frac{\text{torque}}{\text{pitch radius}}$
- F_e = minimum effective face width (in.)
- ϕ = pressure angle
- R_{p1} and R_{p2} = pitch radius
- $\mu_1 = \mu_2$ = Poisson's ratio
- $E_1 = E_2$ = modulus of elasticity

B. Bending Stress

$$S_B = \frac{1.5 (W_d) (K_t)}{(F) (X)}$$

TABLE VII
GEAR WEIGHT COMPARISON

	TITANIUM				STEEL			
	FACE WIDTH (IN)	PITCH	PITCH DIA (IN)	WT (LB)	FACE WIDTH (IN)	PITCH	PITCH DIA (IN)	WT (LB)
PINION	2.80	7.5	2.80	1.65	2.70	8.05	2.61	2.05
IDLER	2.80	7.5	6.94	3.72	2.70	8.05	6.40	5.50
BULL	2.25	7.5	15.05	7.78	2.10	8.05	14.05	13.05
SUN	1.53	8.0	5.38	1.45	1.50	8.6	4.98	2.20
PLANETS	1.53	8.0	4.63	7.53	1.50	8.6	4.28	8.71
RING	1.00	8.0	14.62	3.80	1.00	8.6	13.54	4.30
TOTAL				25.93*				35.81

*APPROXIMATELY 3.17 LB OF THIS WEIGHT IS THE RESULT OF THE TITANIUM GEAR RIMS BEING DESIGNED TO BE 30 PERCENT THICKER THAN EQUIVALENT STEEL GEAR RIM. THIS WAS PRIMARILY DONE TO BE CONSERVATIVE BECAUSE OF THE PRESENT LACK OF EXPERIENCE WITH FULL SCALE TITANIUM GEAR-IRIG. IT IS BELIEVED THAT AS DEVELOPMENT PROGRESSES WITH FULL-SCALE TITANIUM GEARS, TITANIUM RIM THICKNESSES COULD EVENTUALLY APPROACH THOSE OF STEEL.

where:

$$\begin{aligned} K_t &= \text{stress concentration factor} \\ F &= \text{face width (in.)} \\ X &= \text{tooth form factor} \\ W_d &= \text{dynamic load (lb)} \\ W_d &= \frac{0.05 V_p (F C_B + W_t)}{0.05 V_p + (F C_B + W_t) 0.50} + W_t \end{aligned}$$

where:

$$\begin{aligned} V_p &= \text{pitch line velocity} \\ F &= \text{face width} \\ C_B &= \text{deformation factor} \\ W_t &= \text{tangential tooth load (lb)} \\ W_t &= \frac{\text{torque}}{\text{pitch radius}} \end{aligned}$$

As an example, the calculated stress levels for the input pinion-idler mesh are 100,530-psi Hertz and 53,820-psi bending when:

$$\begin{aligned} \text{torque} &= 5410 \text{ in.-lb} & E_1 = E_2 &= 16.5 \times 10^6 \\ \text{rpm} &= 23,300 \text{ (input)} & \mu_1 = \mu_2 &= 0.30 \\ K_t &= 1.15 & \phi &= 25^\circ \\ X &= 0.095 \\ C_B &= 405 \\ F &= 2.8 \end{aligned}$$

Based on a current development program for titanium gears, it is of importance to note that sliding velocities, pitch line velocity, scoring parameters and flash temperature values for the study gearbox design are lower values than those of titanium gears presently being tested.

The design of the planetary system incorporates a nonsequential, nonsimultaneous, hunting tooth arrangement, with a flexible planet carrier and a floating sun gear to ensure load distribution and to decrease vibratory effects due to gear meshes. Figure 32 shows the order of gear meshing of the planetary arrangement.

With this system, no two planets pick up the load simultaneously, nor does one planet engage with the sun and ring at the same instant. Although it is shown above that planet A engages with the sun and ring simultaneously, the planet gear with 43 teeth cannot engage at the same instant due to the odd number of teeth. The order of meshing with planet A engaging first is (A-D-B-E-C-A, etc.) for the sun gear and (A-C-E-B-D-A, etc.) for the ring gear. The sun gear's ability to float between the meshes makes allowance for tooth errors and for positioning of the sun due to tolerances and thermal changes.

Data for the power gear train are shown in Table VIII.

As can be seen, a 2.8-in. face width is indicated for the first-stage pinion-idler mesh. The pinion could be smaller in face width and/or diameter when meshed with the bull, which would result in a weight reduction. However, the present design allows for interchangeability of pinion gears for a right-hand or left-hand gearbox.

Propeller Barrel Mounting

The propeller barrel mounting system used in today's integral gearcase propellers incorporates the use of a relatively long tailshaft. The tailshaft is an integral part of the propeller barrel and is supported in the gearcase by bearings attached to the front and rear of the housing (see Figure 33A). The propeller moments are reacted by the two roller bearings at each end of the tailshaft, and propeller thrust loads are reacted by a thrust bearing which may be positioned at either end of the gearcase. This design has been thoroughly proven in service and is in production.

Experience, however, has indicated that, in its present form, this design does impose certain restraints on the packaging and sizing of other propeller components. The conventional approach requires that the tailshaft pass through the sun gear, thereby possibly limiting the tailshaft diameter and dictating the inner diameter of the rear roller bearing and propeller hydraulic actuator envelope diameter.

Two new concepts have evolved from this study which eliminate the long tailshaft and any possible compromise of the design of other propeller components. The first concept utilized large-diameter, duplexed, angular-contact ball bearings (Figure 33B). This type of bearing negates the need for the long tailshaft, since the contact angle produces a large effective wheelbase(A) with which to react the propeller moments. Propeller thrust would also be reacted by the ball bearings. The evaluation of this design approach, however, indicated a weight penalty associated

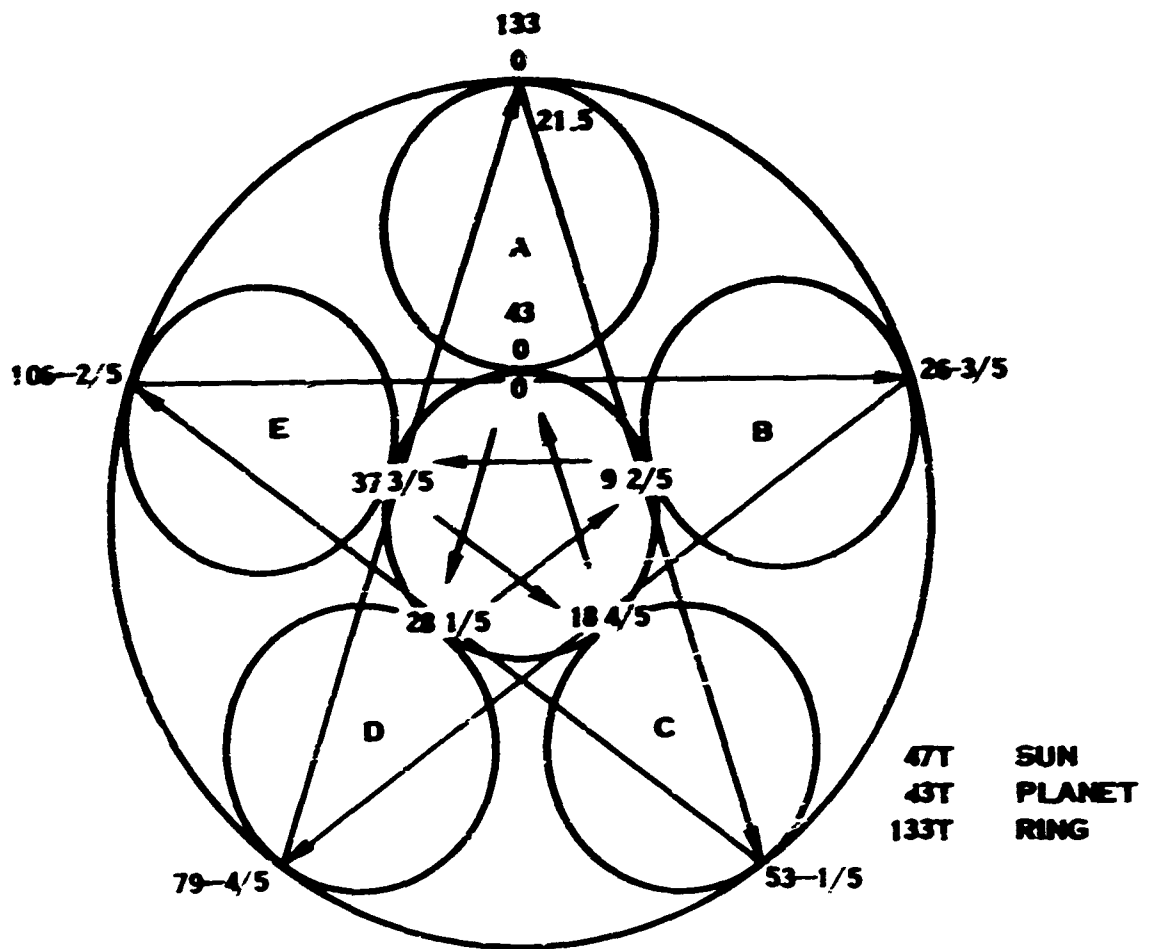


FIGURE 32. PLANETARY SYSTEM MESHING SEQUENCE

TABLE VIII. GEARING DATA							
GEAR	NUMBER OF TEETH	DIAMETRAL PITCH	PRESSURE ANGLE	PITCH DIA., IN.	FACE WIDTH, IN.	RPM	MESH VELOCITY (FT/MIN)
INPUT PINION	23	8	25	2.875	2.8	23,300	17,537
REVERSING IDLER	53	8	25	6.625	2.8	10,111	17,537
BULL GEAR	120	8	25	15.00	2.4	4,466	17,537
SUN	47	9	25	5.222	1.57	4,466	4512
PLANET	43	9	25	4.778	1.57	1,165 CAGE	4512
RING	133	9	25	14.778	1.1	00	4512

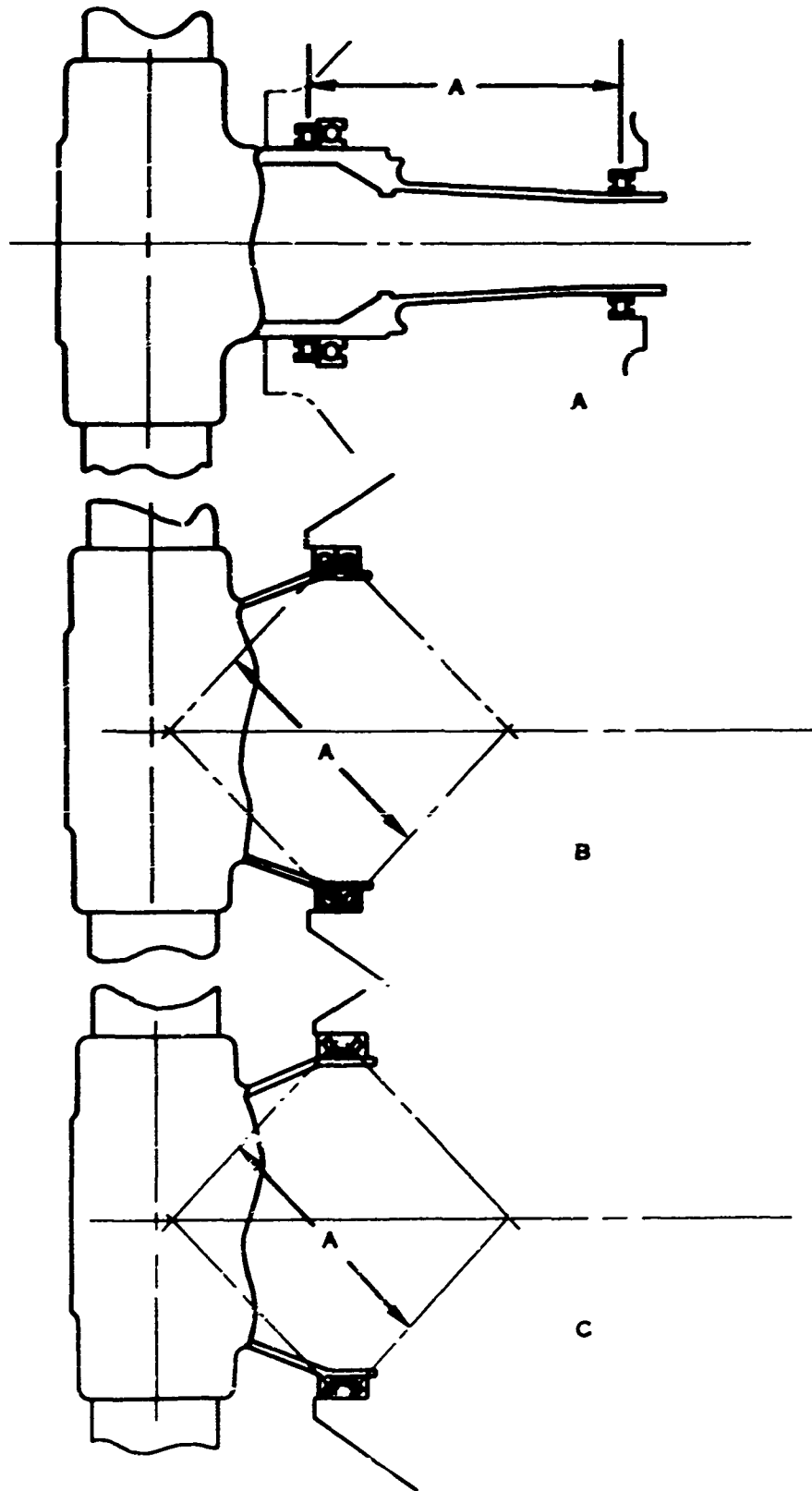


FIGURE 33. BARREL MOUNTING CONCEPTS

with the use of ball bearings in place of roller bearings with a higher capacity-to-weight ratio. Another concern was that, from a structural standpoint, the effective wheelbase of the duplexed ball-bearing design is a sensitive function of the contact angle. Any wear of the bearing or loss of preload which might adversely affect the contact angle and decrease the effective wheelbase (A) would reduce the bearing load-carrying capacity and life.

The second new concept was selected as optimum in the study and is similar to the above concept except that the ball bearings were replaced by large-diameter, duplexed, tapered roller bearings (Figure 33C). The tapered rollers do not have the structural disadvantage of the ball bearing, since any wear of the races does not affect the contact angle and therefore does not alter the effective wheelbase of the bearing. Preload is applied to the duplexed, tapered roller set to eliminate backlash in the system. Only a small load is required to accomplish this, and any loss of this preload will not influence the effective wheelbase of the bearing. This concept was evaluated and found to be approximately 20% lighter than the long tailshaft concept. This weight assessment considered only the effects on the tailshaft, bearings, bearing mounting, and the second-stage planet carrier. It appears reasonable to assume, however, that the permitted use of a larger diameter bearing might also contribute some additional weight saving in the front housing.

Bearings

The design criterion selected for the gearbox bearings was to use a minimum B10 life of 3000 hours, based upon the AFBMA life calculation (References 41 and 42) adjusted by a factor of 5.

The factor of 5 is approximately twice that used in present design practice and adjusts the calculation to represent a conservative estimate of the improvements being projected in bearing materials.

Reports by two bearing manufacturers (References 43 and 44), based on current testing of ball bearings manufactured from Crucible 52 CB material, exhibited a minimum test life of approximately 15 times the AFBMA calculation. Each test group consisted of a homogeneous lot, with a minimum of 30 test bearings, run either to failure or to 200 million revolutions, at which time the tests were suspended. From these reports and the further testing that is being conducted, it is concluded that the actual life factor for vacuum-melt 52 CB material for future applications would probably be at least 10, which would make the B10 life of the bearings used in the study at least 6000 hours. Therefore, the material factor utilized in this gearbox design is considered to be conservative and in no way a jeopardy for designs of the 1970's.

Thin bearing races of consumable electrode, vacuum-melt bearing steel have been incorporated in the design and would either be bonded or mechanically joined to the titanium gears. The thickness of the race would be determined by the magnitude of the subsurface shear stress, which must be below the allowable shear stress of the bond at the junction of the race and foundation material. Where possible, the bond has been extended beyond the roller contact area to increase the bond shear area. Development testing would be required to establish the proper detailed design and manufacturing practice. However, this is considered to be of minimum technical jeopardy.

The design loads, speed, dynamic capacity, and B10 life for the major bearings used in the study gearbox design are tabulated in Table IX. The mean effective loads and speeds listed were considered to be representative of the bearing loading spectrum for twin-propeller V/STOL systems.

Gearbox Housing

Present-day aircraft gearcase housings are made primarily of cast magnesium alloy. This cast material has the disadvantage that the large size of the housing generally results in wall thicknesses which in many areas are dictated, not by stress or deflections, but by manufacturing process limitations (Figure 34). The possible need for providing accessory mounting pads was not considered for any of the housings conceived during the study.

The incorporation of a tapered roller bearing barrel retention would afford additional freedom to the housing design, since the tailshaft loads would then not have to be reacted by the rear housing. One of the minimum-weight housing concepts considered in this study was a back-to-back conical housing which had the benefit of very short load paths (Figure 35). The propeller loads are reacted through the forward housing and enter directly into the nacelle ring mounting structure, which is at the junction of the forward and rear housings. This concept proved to be lighter than locating the mounting pads on the rear housing, and thus nacelle mounting at the front ring was maintained on all concepts. The pinion bearing and cross-shaft loads are reacted in housings which are cantilevered off the rear main ring structure. A fiberglass cover can be used to enclose the aft end, since its only function is oil containment. This concept, when compared to a magnesium casting, was found to be approximately 50% lighter using either forged and machined magnesium or titanium as the material. However, this double conical concept became less efficient when consideration for an idler gear and control mountings was included, to provide needed additional strength and deflection capacity for the fiberglass skin.

A strut-type housing utilizing channel beam sections for struts was then studied (Figure 36A), to provide the control mounting pad requirements. Oil containment

TABLE IX. BEARING DATA

BEARING	LOAD(LB)	RPM	DYNAMIC CAPACITY (LB)	DESIGN B10 LIFE (1)
FORWARD PINION	1,490 ⁽²⁾	19,800 ⁽³⁾	10,420	3000
AFT PINION	1,490 ⁽²⁾	19,800 ⁽³⁾	10,420	3000
IDLER GEAR	238 ⁽²⁾	8,000 ⁽³⁾	2,670	35,000
BULL GEAR	2,985 ⁽²⁾	3,680 ⁽³⁾	13,000	3000
PLANET	3,840 ⁽²⁾	3,130 ⁽³⁾	15,550	3000
CROSS-SHAFT FORWARD	420 ⁽⁴⁾	10,650 ⁽⁵⁾	5,950	22,500
AFT BEARING	420 ⁽⁴⁾	10,650 ⁽⁵⁾	5,950	22,500
PROPELLER MOUNTING	(6)	1,165	COMPUTER CALCULATION (REFERENCE 45)	3325/SET (7)

NOTES :

- (1) AF BMA CALCULATION METHOD CORRECTED FOR IMPROVEMENTS PROJECTED FOR 1970 BEARING MATERIALS.
- (2) MEAN EFFECTIVE LOAD = 70%(GEAR TOOTH LOAD)
- (3) MEAN EFFECTIVE SPEED = 85%(SPEED)
NOTE : 100% INPUT SPEED = 23,300 FOR PINION
- (4) MEAN EFFECTIVE LOAD = 45%(GEAR TOOTH LOAD)
- (5) MEAN EFFECTIVE SPEED = 91.5%(SPEED)
NOTE : 100% CROSS-SHAFT SPEED = 11,650 RPM
- (6) MEAN EFFECTIVE DESIGN LOAD = 4170-LB THRUST 57,200 IN-LB (1-P MOMENT)
- (7) ADJUSTED VALUE BASED ON THE DUPLEX COMBINATION. CONSIDERING EACH INDIVIDUAL BEARING ROW SEPARATELY. THE LIFE FOR THE FORWARD ROW IS 6480 HOURS AND THE LIFE FOR THE AFT ROW IS 5850 HOURS.

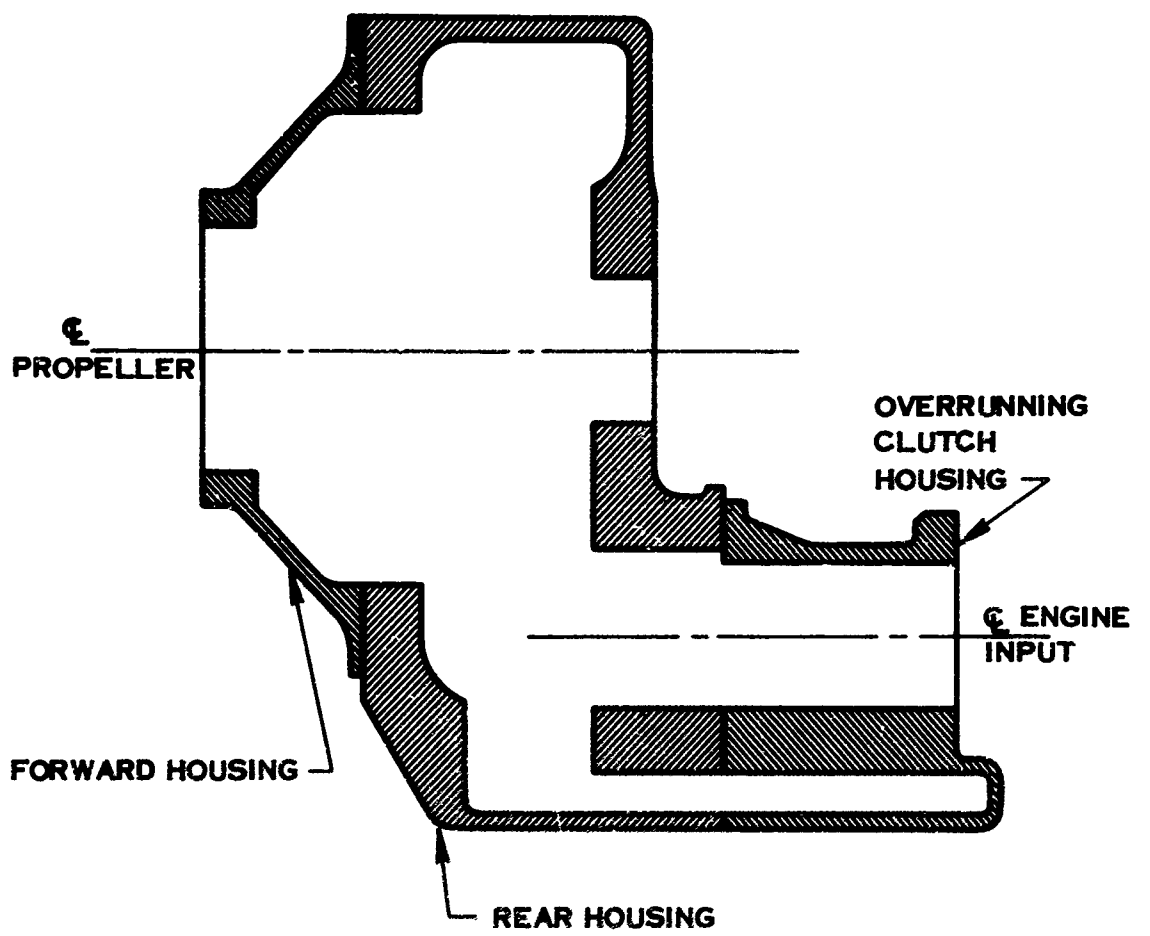


FIGURE 34. CAST MAGNESIUM HOUSING

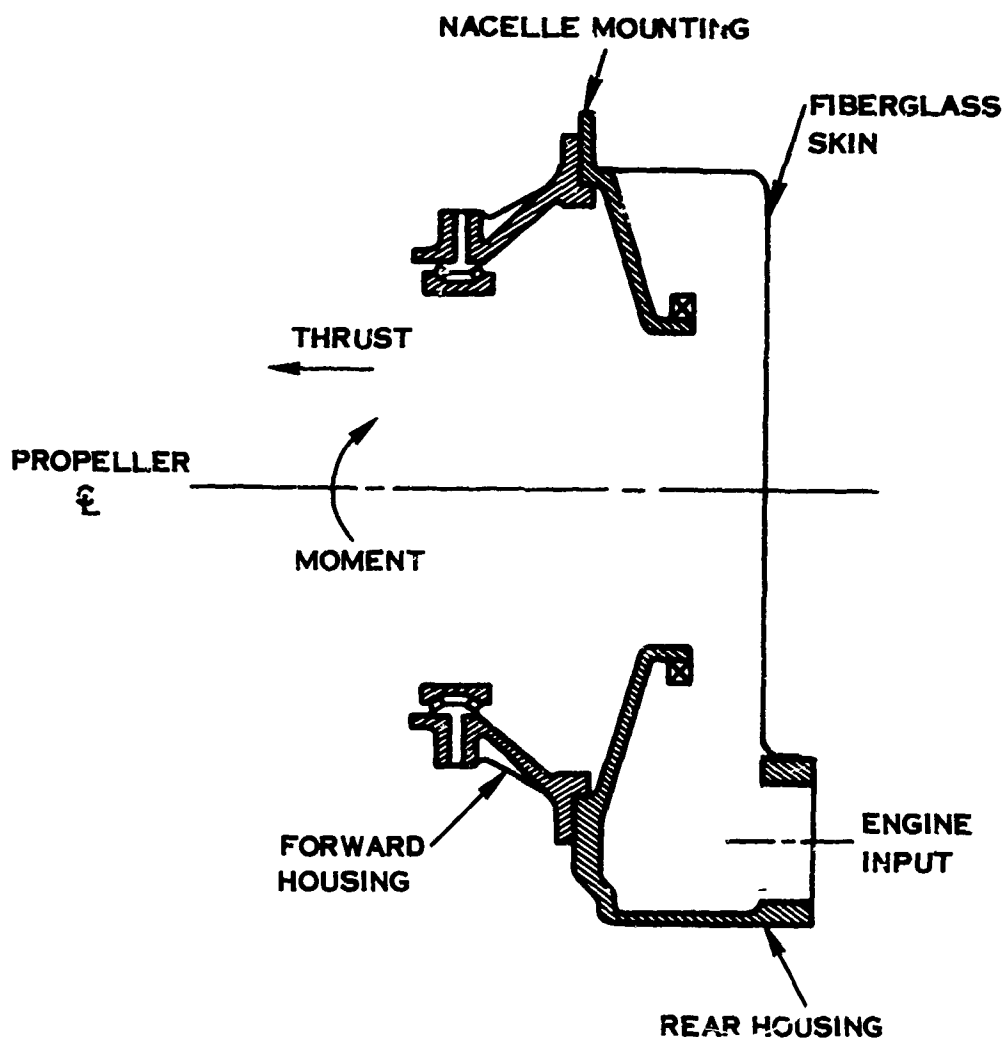


FIGURE 35. BACK-TO-BACK CONE HOUSING CONCEPT

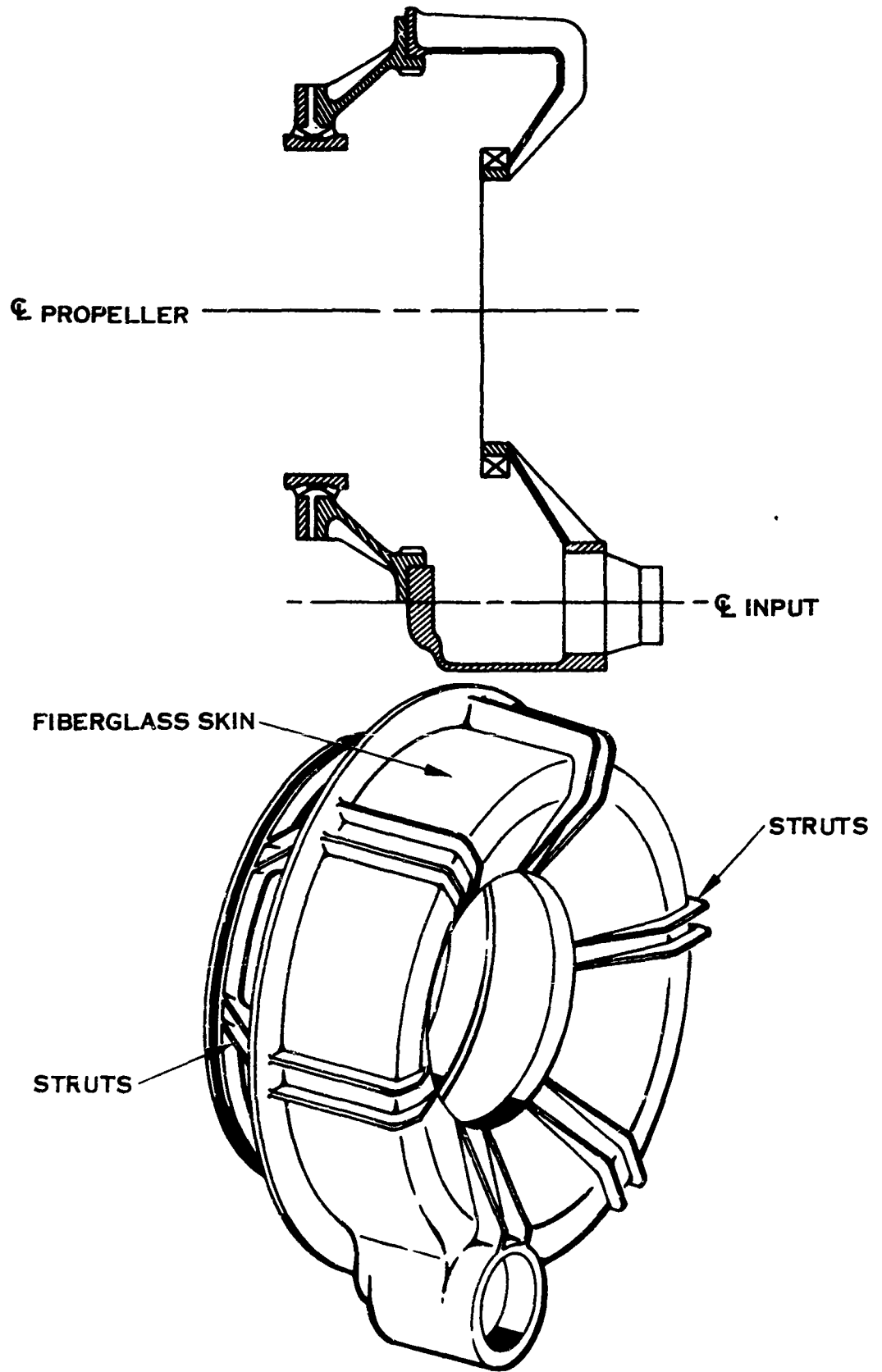


FIGURE 36. STRUT HOUSING CONCEPT

in the rear housing is accomplished by the use of a fiberglass shell bonded to the inside of the struts.

A third housing concept was evolved that consisted of a forged titanium front housing and a welded plate and ring structure for the rear main housing (Figure 37). This concept proved to be the lightest overall titanium housing configuration of any conceived under this study, since it permits a most efficient distribution of material, with localized reinforcement only where needed for structure and/or bosses. Forged and machined magnesium could also be used in this concept and would be slightly lighter than the titanium. However, the titanium is preferred because of the virtual elimination of changes in gear center distances due to differential thermal expansion. This allows the use of high diametral pitch gears with the attendant advantage of reduced gear weight.

Another favorable feature of the welded plate housing concept is that it permits the use of tubing for lubrication lines. The tubes can be positioned to give a direct connection to the areas where lubrication is required. This is in contrast to the conventional housing concept, which requires cored or drilled passages with inherently heavier sections to accommodate the lube lines and plugs.

Overrunning Clutch

An overrunning clutch is provided on the engine input to the gearcase to allow the engine to be shut down and still maintain propeller operation via use of the cross-shaft system. To fulfill this function, two types of overrunning clutches were studied: (1) sprag and (2) spring.

In the sprag clutch, shaped sprags operate in the annular race between two cylindrical races (Figure 38B). The rotation of the outer race (driver) produces an initial friction force on the sprags, causing them to pivot and in so doing, to wedge between the outer and the inner races. In this position, the load is then able to be transmitted from the driver (engine) to the driven (propeller) member. If the driven or inner member attempts to overrun, the sprags will pivot, unlock the load, and permit freewheeling of the inner member.

The spring clutch utilizes a spring wrapped in the annular space between two circular races (Figure 38A). One end of the spring is mechanically driven by the inner race, while the opposite end has a slight rubbing interference fit on the outer member. Rotating the spring in the same direction as the helix of the spring causes the free end to rub against the outer member; this frictional force expands the spring, and it tightens against the driven member to drive it.

The expansion of the initially engaging coil will not, in itself, produce a sufficient force to drive the gear, but the compressive force in that coil causes expansion of

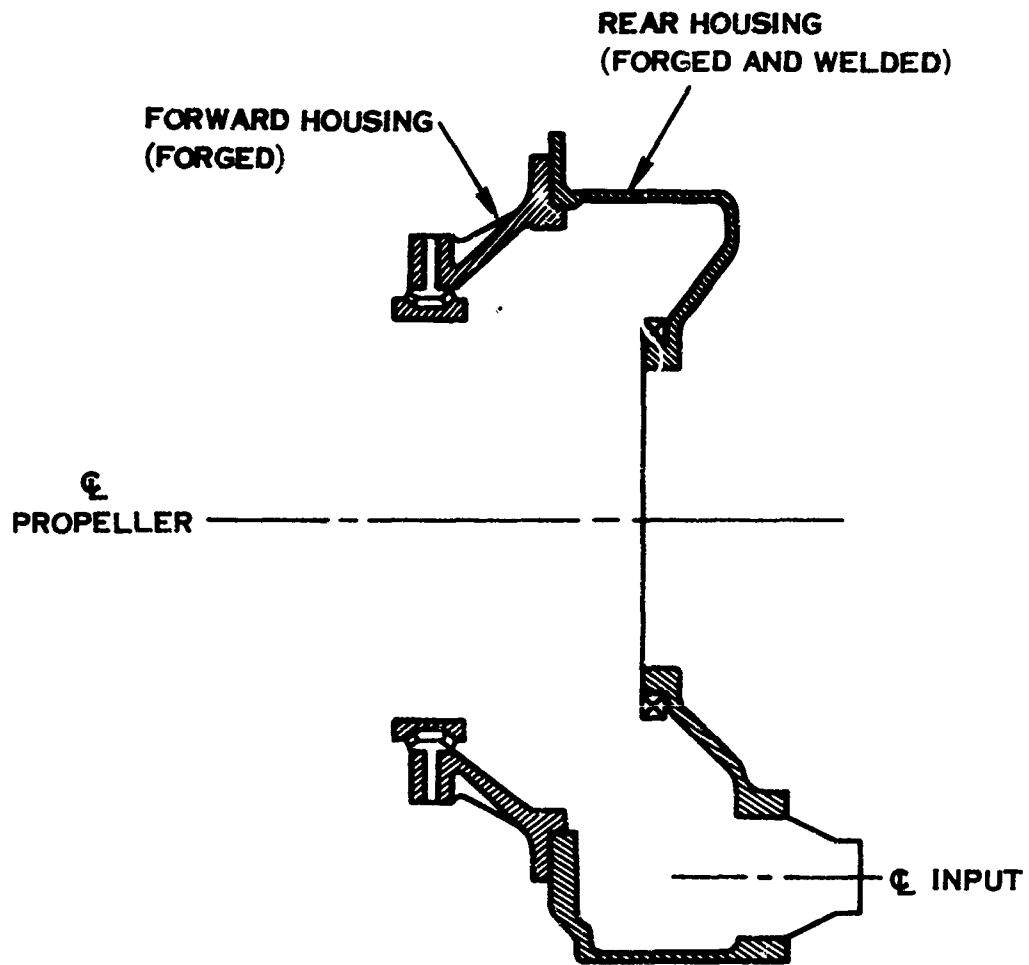
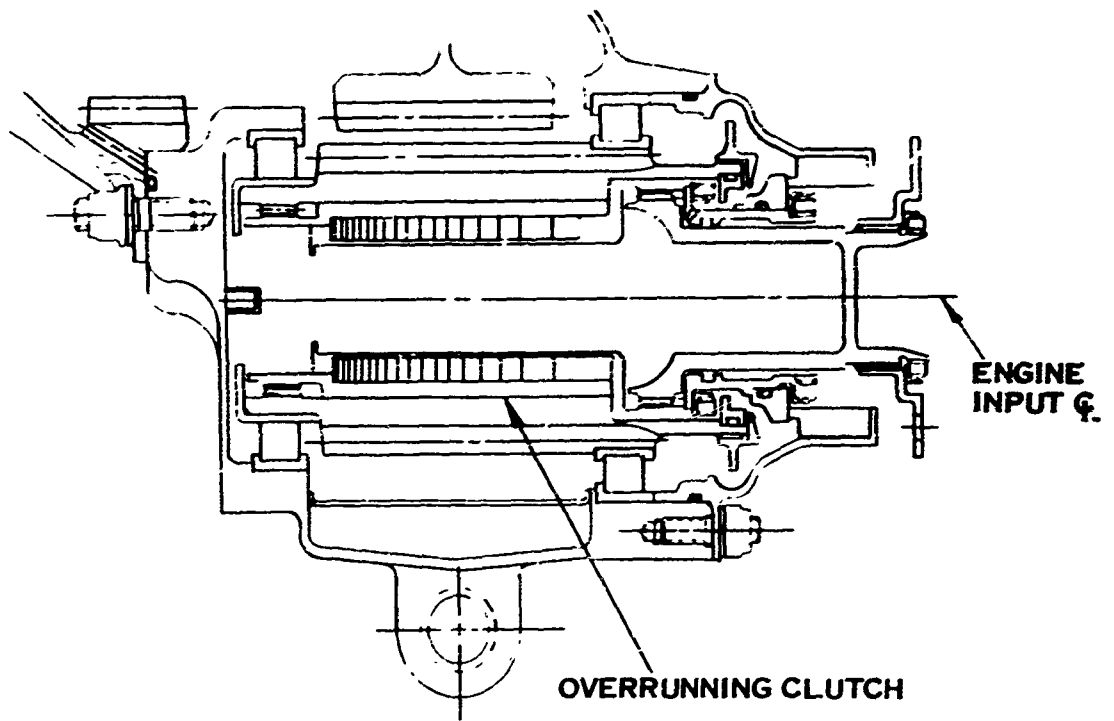
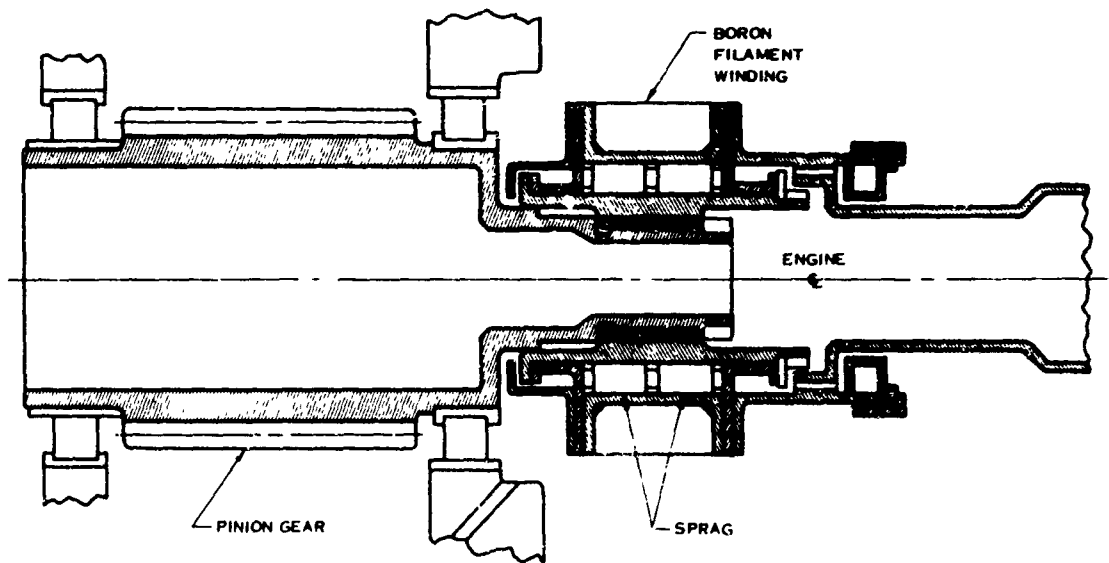


FIGURE 37. TITANIUM HOUSING CONCEPT



A. SPRING TYPE



B. SPRAG TYPE

FIGURE 38. OVERRUNNING CLUTCH CONCEPTS

the succeeding coils until the required load to drive the pinion gear is produced. Whenever the outer member attempts to overrun the inner member, the rubbing force on the spring coils is in the opposite direction to that of the helix, and the spring loosens and will not drive.

The spring concept requires a smaller envelope for packaging and therefore could be placed within the pinion gear, minimizing the overall gearbox envelope and weight. The rubbing action of the spring and resultant burst load induced by the spring have been contained within a steel sleeve. Additional weight saving could have resulted by incorporating a boron wrapping around the sleeve, thereby permitting the use of a lighter sleeve.

Cross-Shaft Decoupler

To feather a propeller connected to a cross-shaft system and still be able to operate the remaining propellers, a cross-shaft decoupler is required. The location of the decoupler is dependent upon the specific requirements of the aircraft -- either to shut down just the propeller reduction gearbox or both the propeller reduction gearbox and the wing box, or even the complete wing transmission system. Since the scope of this study did not entail the design of a wing box or a cross-shafting system, the decoupler has been positioned on the main gear train. To perform this decoupling function, both a jaw-type and a spring-type decoupler were conceived.

The jaw type (Figure 39) contains several advantages which are not found in the spring concept (Figure 40). Cross-shaft torque is transmitted by the positive action of the curvic gear teeth, whereas the spring concept relies on the friction of the system. In the spring type, any slippage in the system, as power direction is reversed, will distort the phasing of the propellers. In contrast to this, the positive action of the jaw-type decoupler keeps the propeller phasing fixed.

The decoupler must be capable of transmitting power in both directions. The jaw-type decoupler accomplishes this by being able to carry load on either side of the curvic teeth, whereas the spring concept requires two effective spring elements and two separate load paths between the cross-shaft gear and the output drive flange.

The jaw-type decoupler was also slightly lighter, but it was selected primarily for the reasons discussed above.

The coupling and decoupling actions of the jaw-type decoupler are described below. A signal from the cockpit to couple the cross shaft is fed to the speed indicator and coupling control. Here the speed of the cross shaft is compared to gear speed in such a fashion that the jaw teeth will not engage until the two speeds are equal.

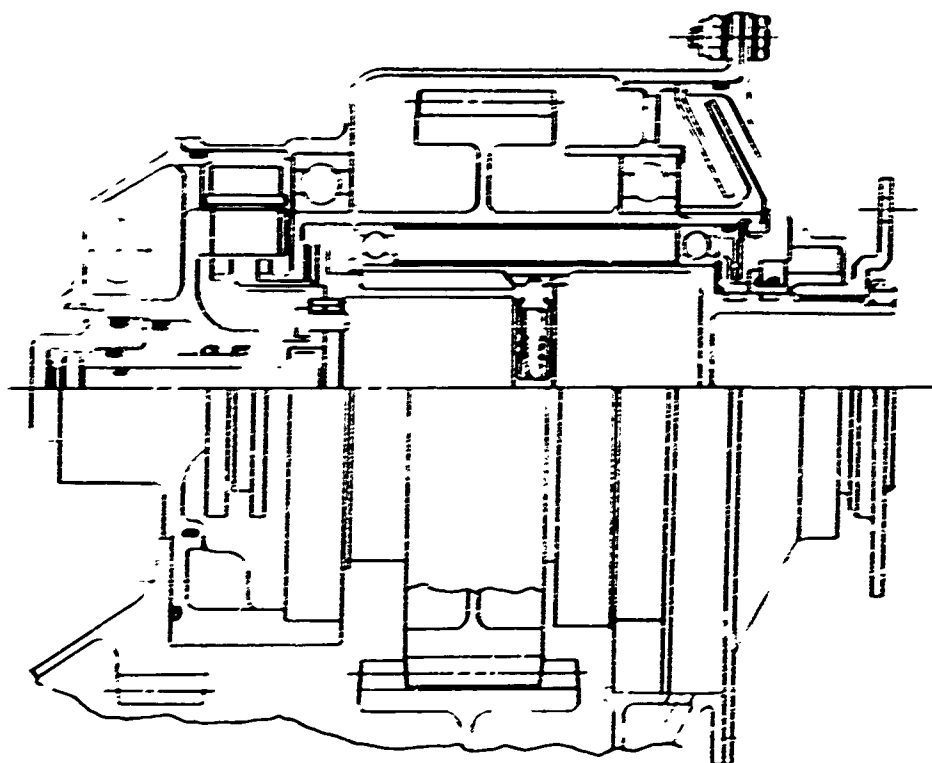


FIGURE 39. JAW-TYPE DECOUPLER

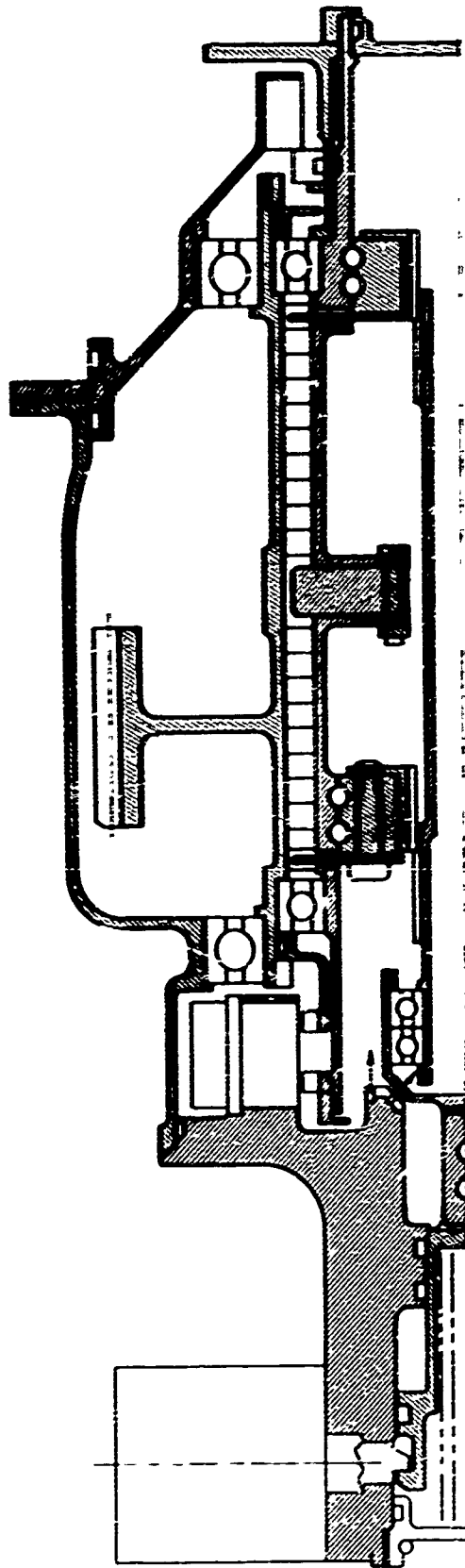


FIGURE 40. SPRING-TYPE DECOUPLER

Upon equalization of the speed, a signal is transmitted to the solenoid to actuate coupling of the jaw teeth. This is accomplished by having the solenoid activate a check valve, thus allowing aircraft hydraulics to enter a servo piston. The movement of the servo unlocks the moveable jaw by physically disengaging it from the detent; continued movement engages the teeth of the jaws and allows the system to lock into an engaged position detent. For decoupling, a second solenoid is used, which, when actuated, allows aircraft hydraulics to flow into the opposite side of the servo piston and to force the jaws to disengage. When the solenoid is de-energized, the detent holds the jaws apart.

Lubrication System

To satisfy the design requirements of being able to distribute and scavenge oil in the horizontal and vertical modes, two types of pumping systems were studied. A conventional constant-displacement gear pump with two scavenge elements and its required gear train drive was compared to a "Schleuder pump" for distributing the lube oil and two ejectors for scavenging the hot oil. The Schleuder and ejector concept shown in Figure 41 was clearly the lighter system and had advantages of less moving parts and simplicity of design. The "Schleuder pump" is basically a stationary tube projected into a volume of rotating fluid. The rotation is provided by the idler gear. The rotating fluid has a velocity head and a centrifugal head associated with it. When the fluid contacts the stationary tube, the velocity head is converted to a static head or pressure. The theoretical pressure created by only the velocity of the rotating fluid in the design studied is 280 psi for 100-percent rpm and 100 psi for the 60-percent rpm condition. The 100-psi pressure level would be more than adequate for the lubrication of the gearbox. Theoretical analysis has shown that this concept is feasible, but a limited amount of additional detailed design and testing would be required to determine the optimum configuration. The use of a Schleuder pump is not a completely new concept; for instance, the variable camber VC82S propeller control incorporates a Schleuder pump for scavenging and is operating successfully.

The total lube oil flow for this gearbox is based on the requirements of 20 quarts per minute for heat rejection in the gearbox and 3 quarts per minute for heat rejection in the actuator. Of the oil which is picked up by the Schleuder pump inlet, 10 quarts per minute are diverted to ejectors (jet pump) for scavenging the sump areas. The scavenged air-oil mixture is discharged into the rotating idler gear cavity.

Based on an efficiency of 20% for this ejector, a supply flow of 9.2 quarts per minute to the ejector would be required to scavenge 32.2-quarts-per-minute flow from the sump into the rotating idler gear. To ensure that the Schleuder is always immersed in oil, 10 quarts-per-minute supply flow would be used so that 35 quarts per minute would be provided to the idler gear, which is more flow than is removed by the Schleuder. The excess oil is allowed to spill out of the gear and into an annulus provided on the baffle. This moving fluid is then directed through the baffle

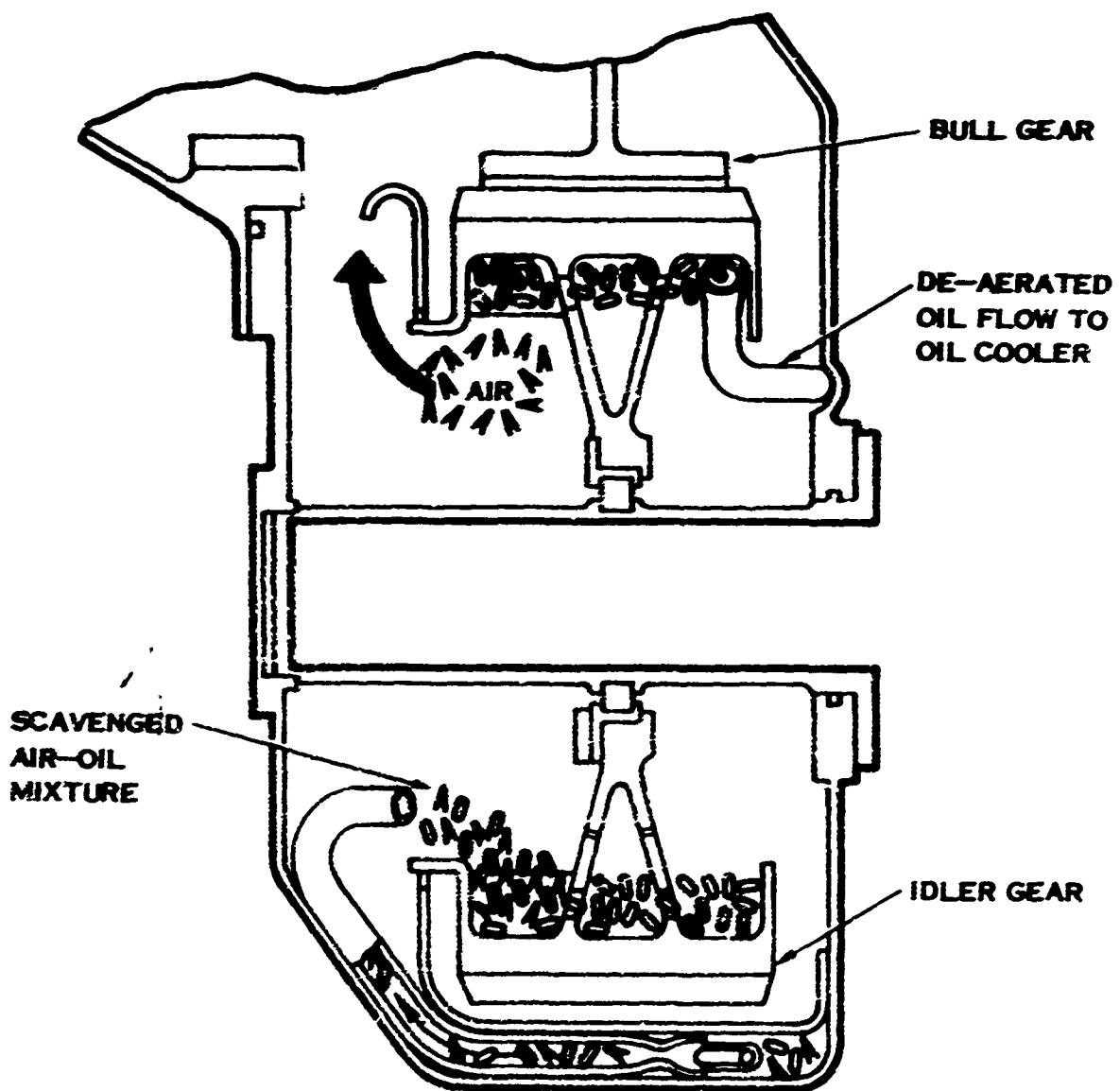


FIGURE 41. CENTRIFUGAL PUMP AND AIR-OIL SEPARATOR

and is allowed to reenter the sump area. The incoming fluid is initially brought up to the speed of the gear by vanes which are physically a part of the gear. The oil then translates across the inner surface of the gear through a baffle, which isolates this oil from additional incoming scavenged oil and allows the centrifugally loaded oil to centrifuge any air which is entrapped. The oil, after passing through the air-oil separator chamber, is passed through a second baffle into the area in which the Schleuder is located.

The effect of placing the scavenged oil into the rotating field is to increase the buoyancy force, by centrifugal action, to approximately 300 times the force of a 1"g" field. The dwell time necessary for air-oil separation is therefore decreased by a factor of 1/300 over the dwell time in a static tank. For the gearcase conceived, a separate tank for separation would have required approximately a 6-quart capacity for a 15-second dwell time. The rotating separator requires only 0.05 second for air disentrainment and a volume capacity of only 0.019 quart. This rotating separator saves not only oil weight but also the weight of the tank, hydraulic lines, and mounting hardware.

The 23 quarts per minute required for heat rejection is passed through a filtration system upon leaving the Schleuder (Figure 42). This filter assembly will consist of two filter elements. The primary stage will provide 10-micron absolute filtration (nominal of 1 micron), and the secondary stage will provide 18-micron absolute filtration (3 microns nominal), together with a high-pressure relief valve. The oil normally will pass through the primary and secondary stages before continuing on in the system. Deterioration of the primary system will not contaminate the gear train or the actuator, since the second stage will filter. Clogging of the primary filter will cause the relief valve to open, thus bypassing the flow around the primary and into the secondary filter. A differential pressure indicator will be inserted into the system for indicating failure of the primary filter.

The lubricating fluid is then directed to the heat exchanger before being used for cooling of the propeller assembly.

Two concepts for mounting an integral heat exchanger and fan were studied. A modular concept, where an axial flow fan and cooler were mounted on the aft end of the gearcase and driven off the idler gear, was the first system considered. This system had several disadvantages: (1) the air supplied to the fan had to be ducted around the gearcase, (2) it required additional mounting structure which added weight, and (3) accommodating the length of the package required that the distance between the engine and gearcase be increased, also adding weight.

The concept selected for minimum weight (Figure 43) incorporates an axial flow fan with integral drive gear on its outer periphery which is driven directly by the first-stage bull gear. Because of the proximity of the nacelle cover to the gearcase, the

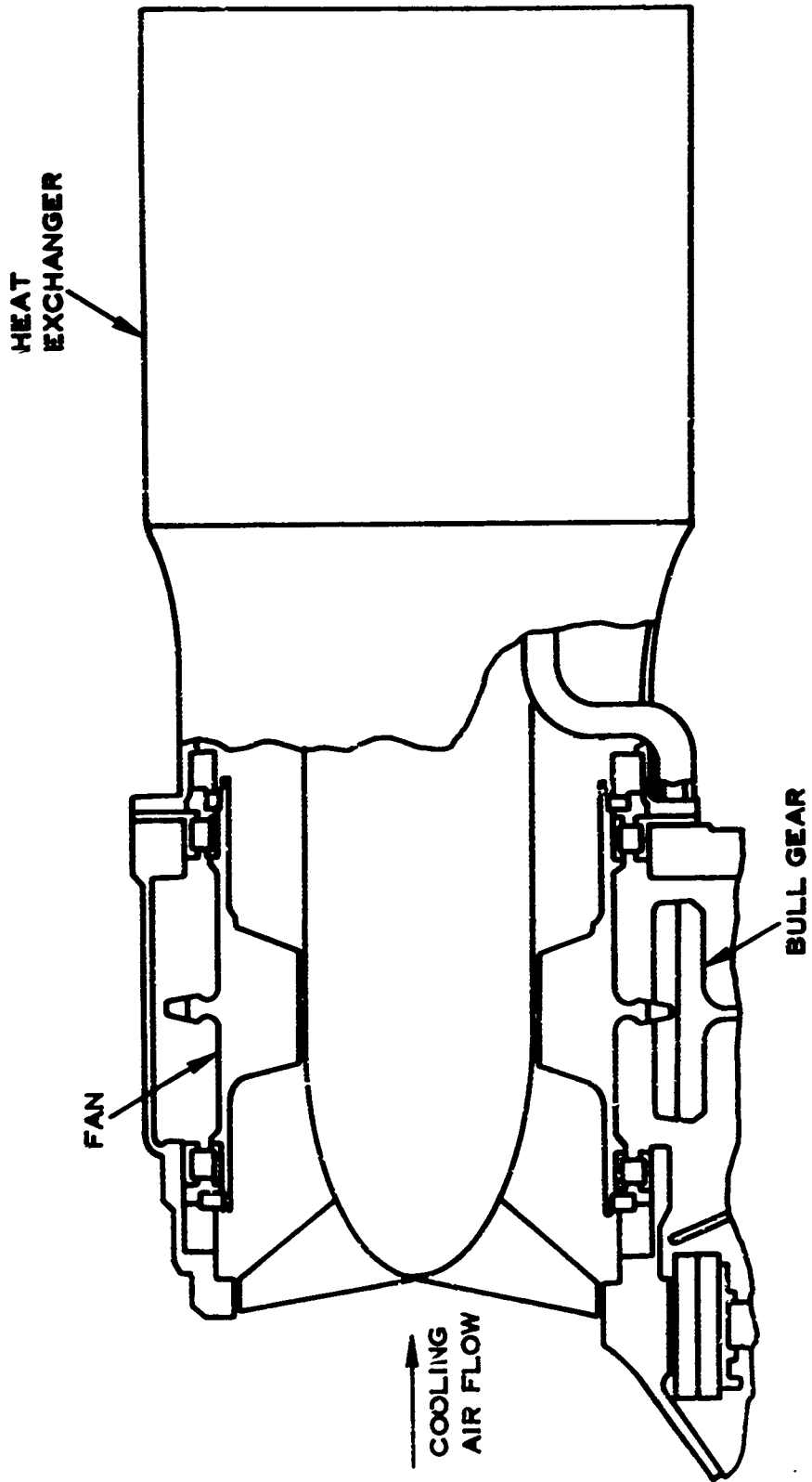


FIGURE 43. INTEGRAL OIL COOLER AND FAN

design has a simple air entry, and the air exit may be ducted out along the side of the nacelle aft of the gearcase mounting structure. The high-speed fan ensures sufficient cooling airflow when the aircraft is in the vertical hover mode, and it increases the air pressure available to the heat exchanger over that available by using only propeller slipstream. The fan exits the air directly into the spiral-wrapped heat exchanger mounted on a pad coaxial with the fan. The exchanger consists of two corrugated sheets laid perpendicular to each other and separated by parting sheets. The combined sheets are then rolled into a cylinder (Figure 44). This configuration lends itself to simple cantilever mounting off the gearbox.

Part of this cooled oil is then directed by tubing to the spray bars for cooling of the cross-shaft bull, pinion-idler, and idler-bull gear meshes. A flow of 3 quarts per minute is fed directly into the actuator to top off the hydraulic sumps. The returning oil is discharged from the actuator into the rotating planet carrier. This returning oil, and oil from the sun spline, is then used to lubricate the propeller mounting bearings, the planet bearings, and the planet-sun meshes. The remaining oil is sprayed onto the aft sun-quill spline. The overflow from this flooded spline connection flows outward into the bull gear quill spline and continues on to lubricate the bull gear bearing before draining back to the sump.

The incorporation of baffling ensures that the oil is directed away from the rotating gears, thereby reducing windage losses from the churning action of the oil.

Horizontal mode scavenging is natural for this housing contour. Vertical mode scavenging is accomplished by contouring the aft face of the housing so that the same sump area is also the low point on the gearcase, and by the addition of two slinger pumps. These pumps consist of rotating plates, which centrifuge the oil up and out of the low areas and back to the main gearcase and sump area.

For visual inspection of the oil level, a sight glass has been incorporated into the gearbox rear housing. Oil can be added to the gearbox through a combination breather and filler plug. A screen in the gearbox beneath the plug keeps foreign particles from entering, and a combination chip detector and drain plug has been incorporated in the sump area.

BARREL AND RETENTION

Retention

The blade retention supports the blade at the interface between the inboard portion of the blade (shank end) and the barrel structure. The normal retention consists of the blade shank, an antifriction bearing to react blade loads and to permit blade pitch angle change, the barrel shank arm structure in the barrel, a clamp ring to position the blade statically, and a seal to retain oil in the barrel. (See Figure 45.)

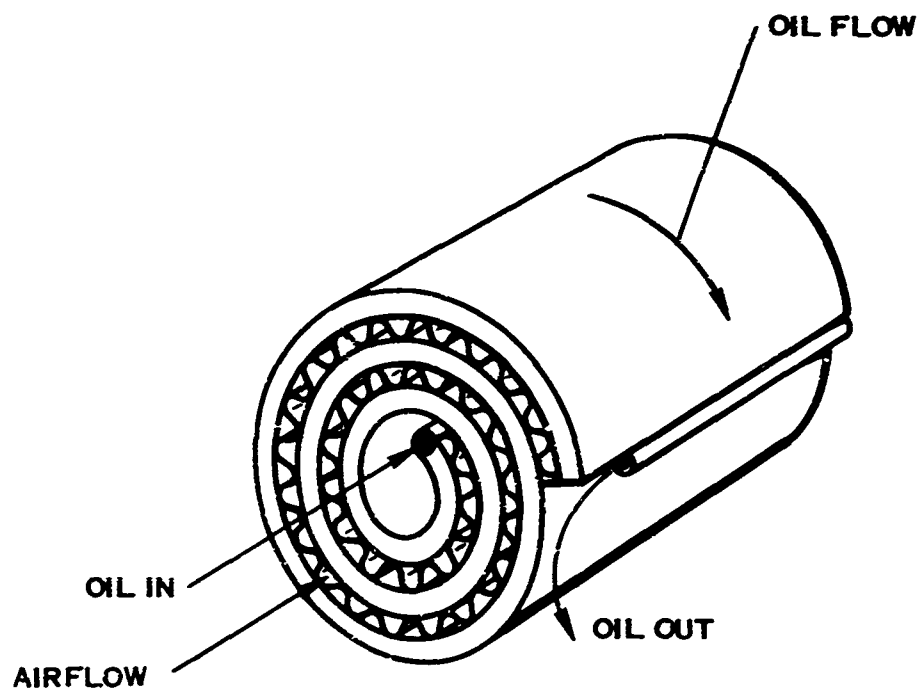


FIGURE 44. HEAT EXCHANGER

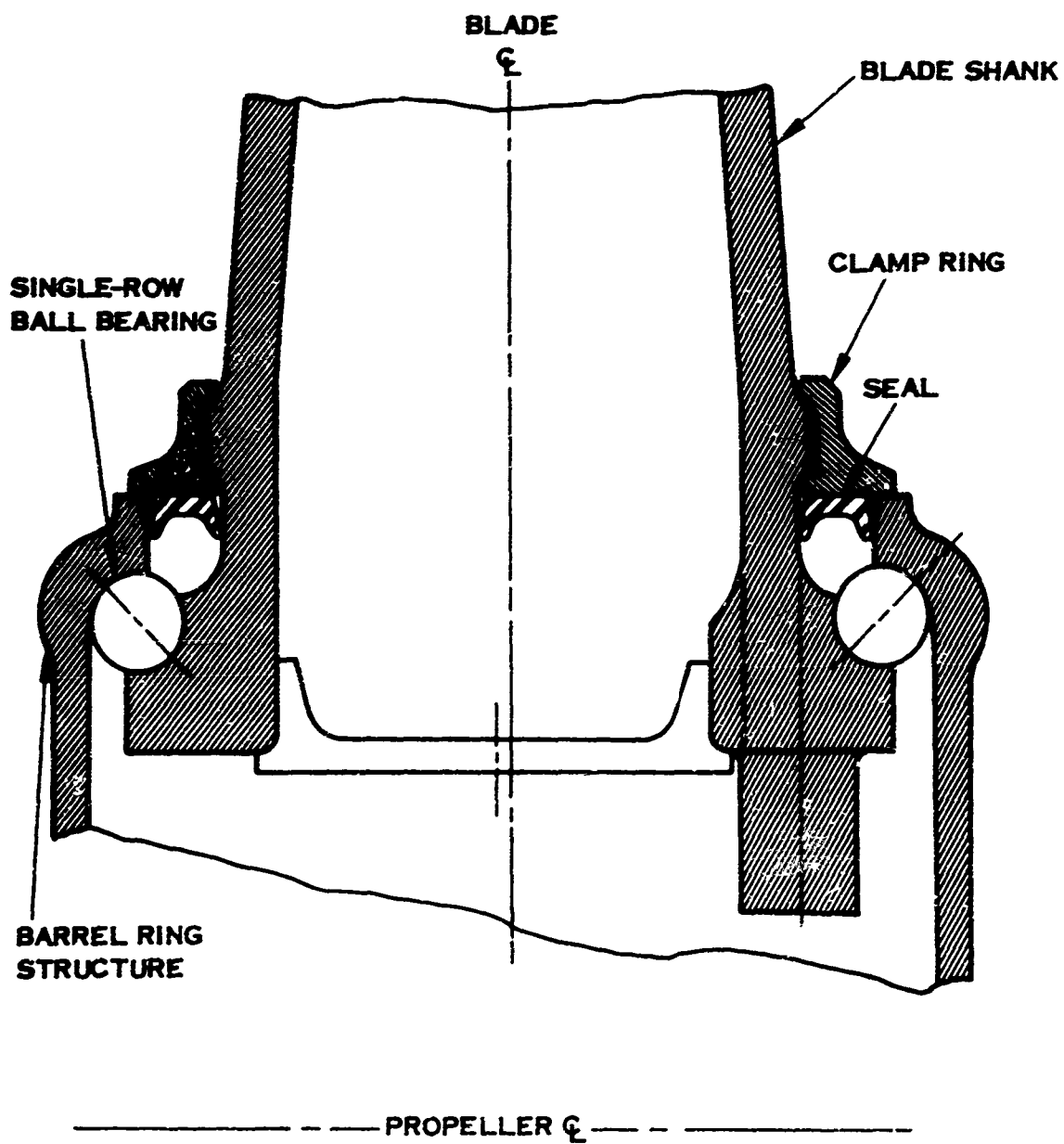


FIGURE 45. INTEGRAL BALL RACE BLADE RETENTION

The blade retention must react the following blade loads: (1) steady axial load from centrifugal force on the rotating blade, (2) transverse side loads from lateral aerodynamic and inertia loads on the blade, and (3) both in-plane and out-of-plane steady and cyclic bending moments from aerodynamic and inertia loads on the blade.

With the conventional integral ball race blade retention shown in Figure 45 as an established inherently lightweight design, a parametric study was conducted to determine the effect of number of bearing races, ball diameter, mean bearing diameter, and race spacing on retention stiffness and weight, axial, moment, and "rocking" capacities. Retention length, gross barrel arm and blade shank stressing, and ball race contact stressing were held constant during the study. For a retention with the best balance between stiffness/weight, axial capacity/weight, and "rocking" and moment capacity/weight, it was found that small race spacing on one or two bearing rows is superior and that the mean bearing diameter/ball diameter ratios should lie between 12 and 16. The smallest ball size which meets the axial load requirements should also be selected to provide a more uniform load distribution around the retention bearing race and to decrease the local stress concentrations in the retention and mating parts. This parametric retention study is described in detail in Appendix VII.

An alternate retention concept incorporating a tapered roller instead of a ball bearing was studied (reference Figure 46). Results of this study revealed that a slight weight reduction was possible by utilizing this bearing concept for the basic retention, but the concept represented a more complex design problem to provide the desired feature of quick blade removal.

The use of materials other than steel for the blade spar and barrel to obtain weight reductions requires that the basic integral ball race retention design be revised as shown in Figure 47. Hardened steel ball races must be added to both the blade shank and the barrel.

Blades of titanium or composite boron filament construction result in significant weight reduction, which reduces centrifugal blade load on the retention. This load reduction is sufficient to permit the blade to "rock" on the retention under the influence of aerodynamic blade moments, which are unaffected by reduced blade weight. To prevent blade "rocking" or unloading of the balls on one side of the retention, the basic bearing design was revised to react axial loads in both directions. This is accomplished by extending hardened steel races around the ball to establish a four-point contact bearing as shown in Figure 48.

Since the resulting centrifugal load from the lightweight blades supports approximately 90% of the maximum blade moments, the extended races need to support only the remaining 10% of the maximum moment. The conventional blade clamp is replaced by a retention nut which provides a small bearing preload and which

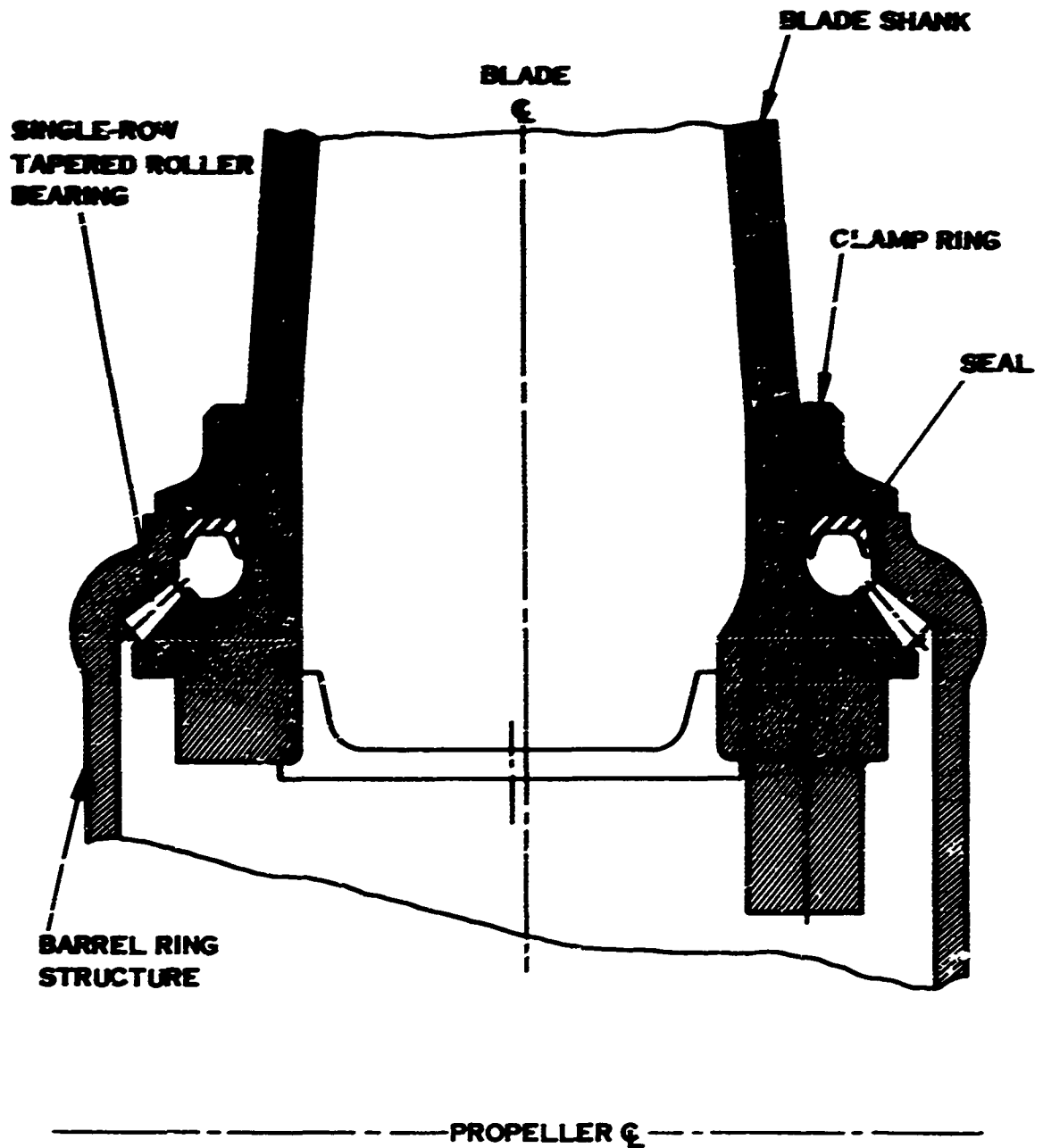


FIGURE 46. TAPERED ROLLER BEARING
 BLADE RETENTION

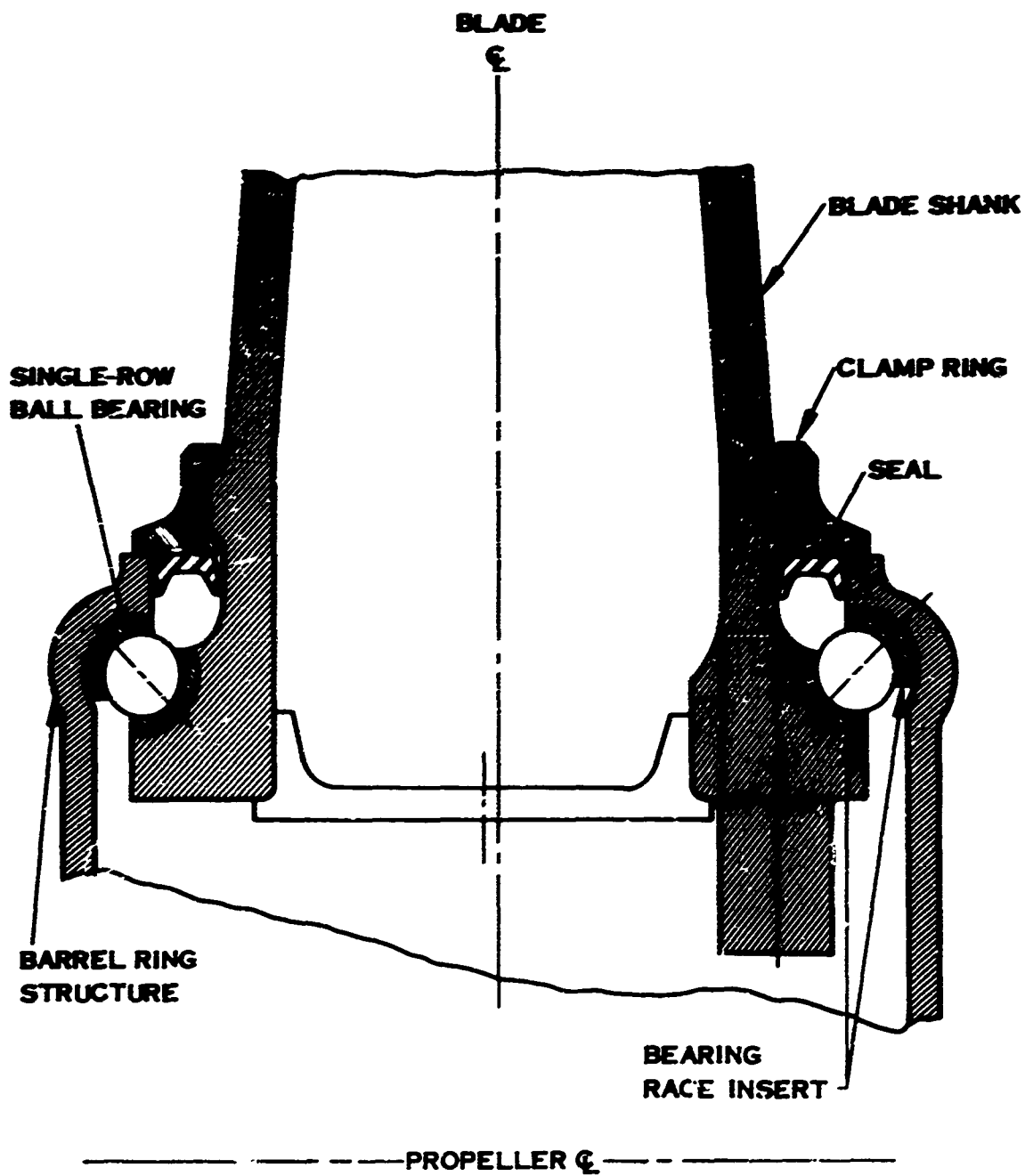


FIGURE 47. BALL RACE BLADE RETENTION WITH INSERTS

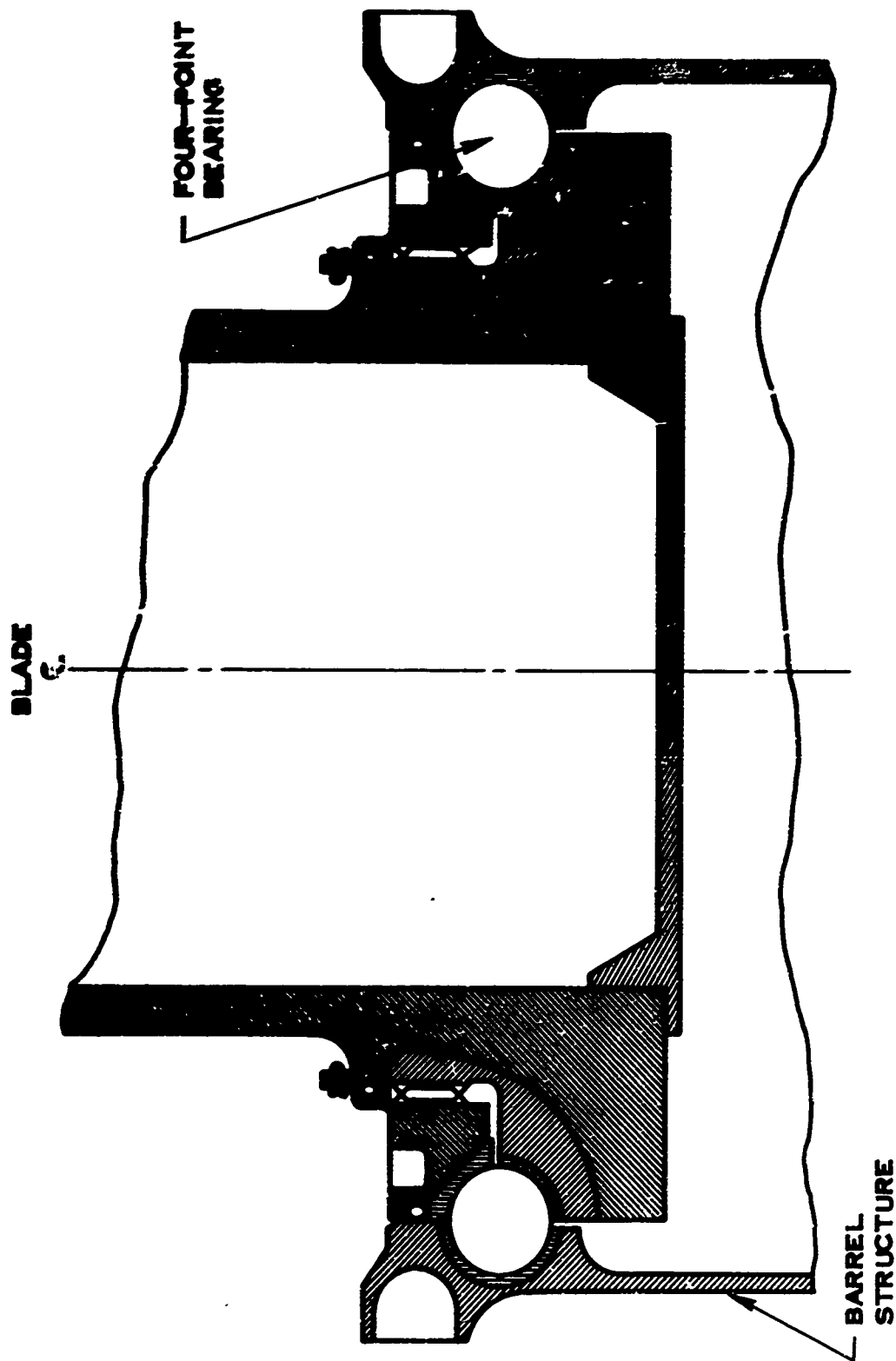


FIGURE 46. FOUR-POINT BEARING RETENTION

supports the blade statically. To avoid the undesirable use of machined threads on the blade shank, a separate titanium collar ring is formed on the blade to accommodate the retention bearing.

Barrel

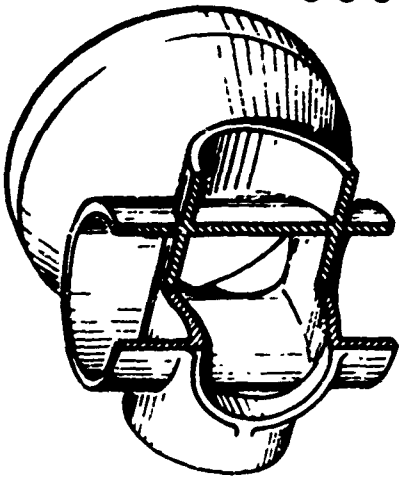
The propeller barrel consists of three major elements: the blade retention, the hub structure, and the tailshaft. The blade retention supports each blade shank in a ring structure, as discussed in the previous section. The barrel is the primary structure supporting the retention rings and the tailshaft transmits drive torque to the propeller and mounts the barrel on antifriction bearings in the gearbox.

Four basic approaches were taken in this study to reduce barrel weight:

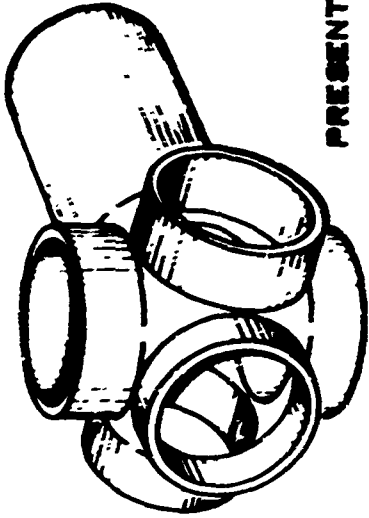
1. Reduction of centrifugal load on the barrel by utilization of lightweight blade construction.
2. Optimization of conventional barrel design concepts by parametric study.
3. Study of new structural shapes.
4. Use of high strength-to-weight material.

A four-way propeller was chosen for this study because of the theoretical performance considerations listed earlier in the "Aerodynamic Studies" section of this report. Since centrifugal blade loads represent a major loading on the barrel retention and hub structure, reduction in blade weight results in an inherently lighter barrel structure. Conventional barrel structures consist basically of forward and rear ring structures supporting cylindrical blade arms (Figure 49). Web structure is blended between blade arms and rings to make a closed structure. The rear ring blends into the tailshaft, and the forward ring incorporates a bolt circle for mounting the pitch change mechanism. A parametric study was conducted on a barrel of conventional design to determine load capacity-to-weight ratio as a function of barrel and retention radius and fore-and-aft ring spacing. This parametric study is contained in Appendix VI. Results of the study showed that the barrel diameter should be small with a retention as large as possible consistent with barrel diameter and that the fore-and-aft ring spacing should be as small as possible consistent with retention diameter. Since conventional barrel design practice has generally complied with these criteria, there was no significant weight saving potential (other than with material change) to be gained by selecting a conventional barrel structure for this propeller.

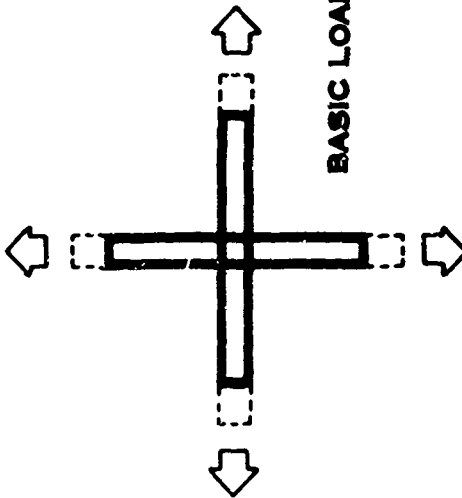
A new barrel structural concept was studied which consists basically of two crossed cylinders, arranged in such a manner that the walls of each cylinder are continuous through the other (Figure 49). The blade retentions are located at the four outer ends



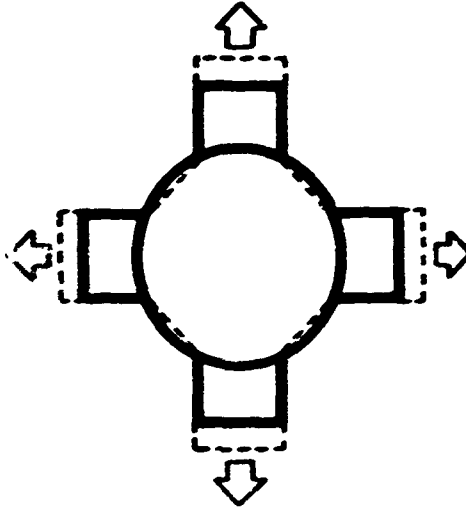
CROSSED-CYLINDERS CONCEPT



PRESENT TYPE



BASIC LOAD PATH



LOAD PATH FORCES BENDING

FIGURE 49. BARREL CONCEPT

of the cylinders. This basic configuration provides an efficient structure for reacting centrifugal blade loads and blade moment loads in the continuous cylindrical beams. This basic cylinder structure was then modified to incorporate: (1) a tailshaft, (2) a reinforced hole in the forward face for mounting the pitch change mechanism, and (3) small reinforced holes in the rear of the cylinders to provide access to the blade pitch change links (reference Figure 50).

A second concept of a monocoque design was studied, consisting of a shell structure generated by connecting each point in the blade retention ring with a straight line to its corresponding point on the adjacent retention ring (reference Figure 51). This concept was also shown to be lighter than conventional barrels and to provide good access to the blade for pitch change. However, this design was found to contain additional oil weight; accordingly, the crossed-cylinder design was established as the preferred concept. For a three-way propeller, the crossed-cylinder concept would change from an "X" structure to a "Y". A discussion of the structural features of both concepts is provided in Appendix VI.

The crossed-cylinder barrel was initially designed using the same allowable stress and stiffness values used in conventional steel barrels. The use of titanium was evaluated, and the barrel was redesigned for the lower density material. A titanium barrel of conventional design for this propeller weighs approximately 33 % less than a conventional steel barrel, and a titanium barrel incorporating the new crossed-cylinder design weighs approximately 44% less than the steel barrel of conventional design. Therefore, the latter barrel design was selected as the basic configuration for this study. With successful progress being made on the current development program on titanium barrels of conventional design, little technical jeopardy is involved in proposing titanium as the barrel material for the near future.

The large conical tailshaft was selected for this barrel based on the propeller mounting trade-off studies. The larger diameter shaft is a lighter weight structure for reacting propeller moments and readily adapts to the lightweight planet carrier concept. Furthermore, the large-diameter barrel tailshaft was easily adaptable to the new barrel structure and provided better access to the blade pitch change links.

BLADES

Blades represent 35% of the total weight of one of today's advanced propeller-gearbox systems. Blade weight also sets the design loads for other major components, such as barrel, actuator, gearbox, and support structure. It thus represents the single, most determining factor on total system weight. Therefore, in seeking to define the maximum weight reduction potential for the 1970-1975 propeller system, prime attention must be directed toward blade weight reduction. This requires not only the evaluation of those new materials which appear to be feasible for use in that time period, but also a detailed evaluation of composite blade structures to utilize the advanced material properties best.

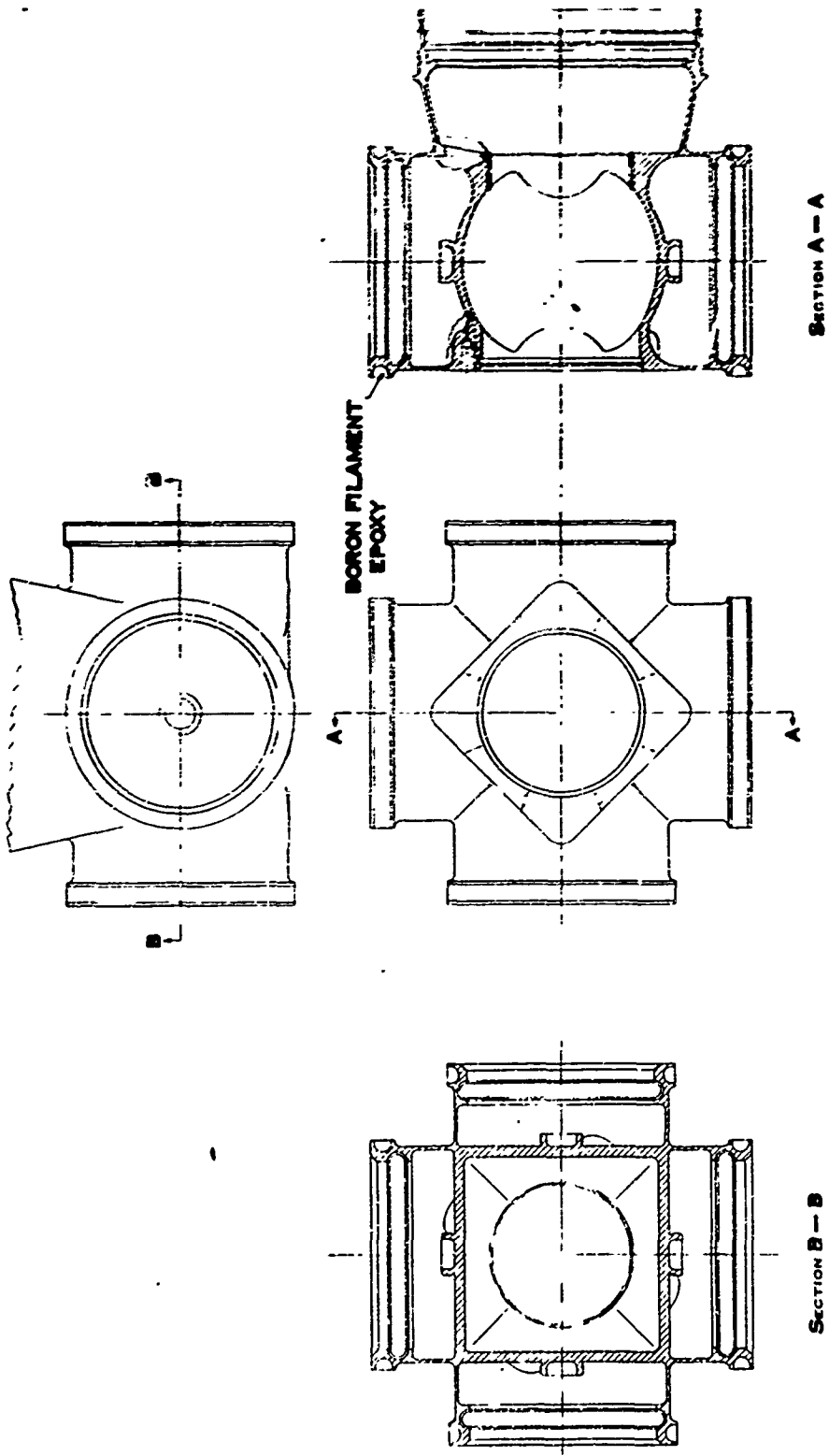


FIGURE 50. CROSSED-CYLINDER BARREL

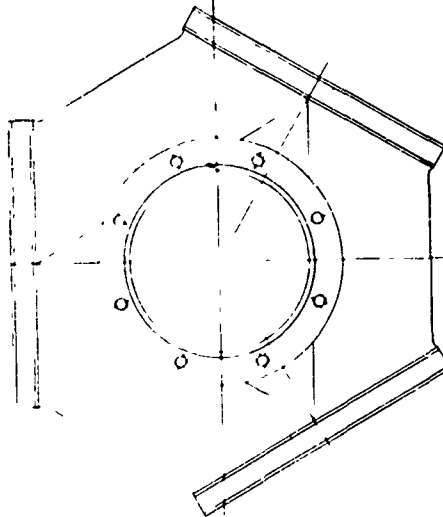
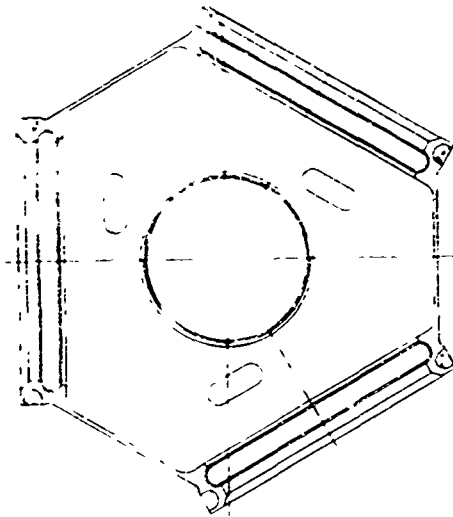
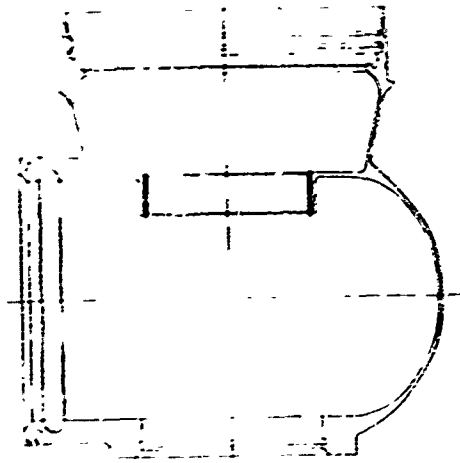


FIGURE 51. SHELL STRUCTURE BARREL CONCEPT

This section presents the results of such an evaluation, based upon quite searching design analysis studies. The methodology is that currently used to design production V/STOL blades, and it is one which analyzes all primary and secondary structural actions, considers the unique and often conflicting requirements at varied operating conditions, and arrives at a balanced structural design consistent with the desired aerodynamic blade shape. An important input is the definition, based on past experience, or proper design stress limits and safety factors specific to the complex structural environment of propeller blades.

All weight projections emanating from this study are predicated on such analysis. It is recognized, however, that there may be a degree of conservatism in such projections, in that no assumptions were made for any progress on the learning curve of structural design tailoring, as a parallel to the introduction of the advanced materials.

The detailed blade design process described above is in direct contrast to the generalized form of blade structural analysis presented in Appendix IX. The latter is basically a more theoretical parametric analysis which must, inherently, be more general and which tends to indicate more optimistic blade weights. These may be construed to be "ideal" weights. Such "ideals" are never fully attainable, but they serve the useful purpose of setting targets for further potential refinements, over and above those indicated by today's established design criteria. A comparison of the projected blade weights in Table X to the "ideal" weight values plotted on the parametric weight charts in Appendix IX affords some indication of the extent of the remaining weight margin. It is reasonable to presume that a sizeable portion of this margin can be gained by a progressive refinement of blade design methods; but, to be conservative, the following blade weight projections do not include this potential.

Tables X and XI summarize the most promising blade designs generated by this study. The optimum blade configuration which was selected as common to each of these designs is presented in Figure 52.

Blade A, included solely for comparison purposes, is a steel spar, fiberglass shell blade of the type presently used on the XC-142, X-22, AH-56A, and P-2H. This is a blade that could be built today with no advancement in materials state of the art.

Blade B uses the same basic materials, but assumes a reasonable advancement in material properties for the 1970-1975 period. Approximately a 30% decrease in the blade fill density and 15% increase in the allowable steel spar fatigue strength were assumed, and S-glass was substituted for the present E-glass shell. From Table X, it is seen that these improvements would lower the individual blade weight from 62 lb to 54.3 lb (a 12.5% reduction). The corresponding reductions in blade centrifugal load, centrifugal twisting moment (CTM), and polar moment of inertia

TABLE X. BLADE PROPERTIES

	A (TODAY'S STEEL SPAR)	B (1975 STEEL SPAR)	C (TITANIUM SPAR)	D BORON EPOXY SPAR)	E BORON-ALUMINUM SPAR)
BLADE WEIGHT (LB/BLADE)	62.0	54.3	45.7	40.8	37.2
CENTRIFUGAL LOAD (LB/BLADE) 1160 PRPM	75600	66500	55200	50100	45000
MAX CTM (IN-LB/BLADE) 1160 PRPM	9150	8400	7700	7300	6950
I_p - (LB-FT / BLADE)	615	560	465	420	390
MAX STEADY BENDING MOMENT (IN-LB/ BLADE) 1160 PRPM, 2000 HP	69000	66000	65000	75000	73000
MAX 1 X P SHANK MOMENT (E.F. 4.0, 150K, 1050 PRPM 2000 HP)	55,000	57000	57000	53000	52000

TABLE XI. BLADE FREQUENCY SPECTRUM

	(PRPM)				
	A (TODAY'S STEEL SPAR)	B (1975 STEEL SPAR)	C (TITANIUM SPAR)	D (BORON EPOXY SPAR)	E (BORON-ALUMINUM SPAR)
2P FLATWISE	1020	990	960	1420	1230
EDGEWISE	1370	1620	1330	2100	1930
3P FLATWISE	610	590	560	870	750
EDGEWISE	980	1010	980	1320	1230
4P FLATWISE	440	430	410	640	540
EDGEWISE	730	750	720	970	900
SECOND FLATWISE	1680	1690	1630	2440	2130
ASSUMED OPERATING RANGE :					
	TAKEOFF	1160 PRPM MAX			
	CRUISE	696 PRPM MIN			

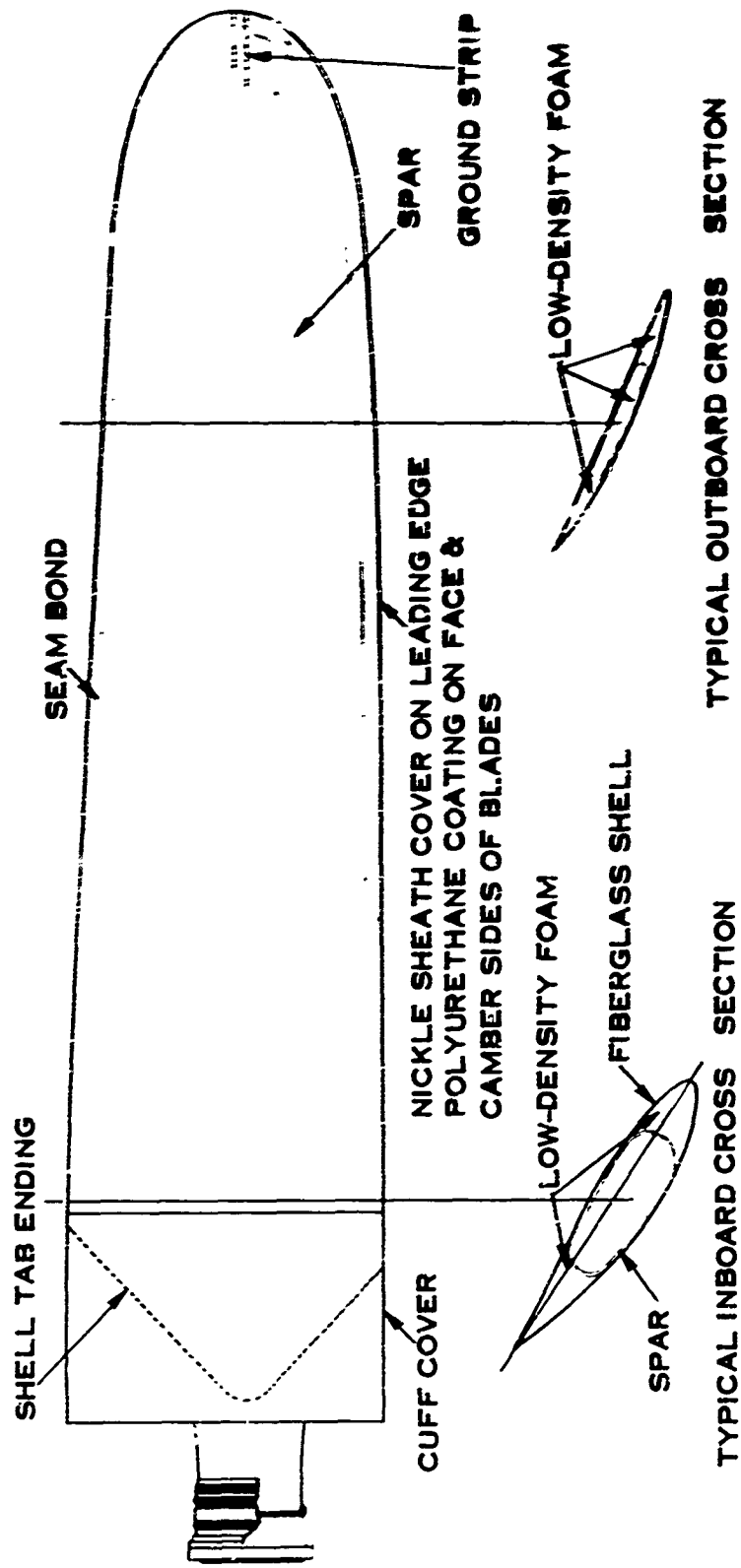


FIGURE 52. LIGHTWEIGHT BLADE DESIGN (STRUCTURAL SPAR - FIBERGLASS COVER)

(1p) represent a source of added, substantial weight reductions in the propeller barrel, actuator, and support structure.

Blade C uses the same materials as Blade B except that a titanium spar has been substituted for the steel core. This blade weighs 45.7 lb, which is a 26% reduction from the weight of the present-day steel core blade.

It is interesting to note that the present-day steel spar blade, the advanced steel spar blade, and the titanium spar blade are shown to have the same basic frequency spectrum (see Table XI), with the 2P flatwise frequency falling well below the operating takeoff rpm. This type of spectrum is typical of today's propellers.

The final two blades, D and E, use the more advanced boron filament composite materials in their construction. Both a monocoque construction and a spar and shell construction were investigated with these materials. The fact that fabrication processes with the boron filament composites are more tractable to the attainment of a desired, nonuniform distribution of material than are those with steel or titanium affords the prospect of some improvement in the generally poorer structural efficiency of monocoque blade construction by concentrating material at critical locations. However, the evaluation showed that spar-and-shell type construction was still the most efficient structure. By using a fiberglass shell over the boron composite spars, the full-strength levels of these boron materials may be realized; and since the spar material is protected by the shell, it is not necessary to derate the design allowable stress levels because of possible surface damage.

Blade D uses a boron-filament-reinforced epoxy composite material for the spar. All other materials are the same as in blades B and C. The blade weight is 40.8 lb, which is a weight reduction of 34% over the present-day steel core blade.

Blade E uses a boron-filament-reinforced aluminum matrix composite material for the spar. This blade weighs 37.2 lb, which amounts to a 40% reduction over the steel spar blade of today's technology.

Examination of the frequency spectrum of the boron composite spar blades reveals a characteristic change from the other blades: the 2P first-mode frequencies fall well above the operating takeoff rpm. This would be a definite advantage for these propellers, since there would then be no necessity for a 2P rpm restriction.

Blade C, the titanium spar version, has the advantage of involving the least state-of-the-art advancement. The only major development required would be in the retention area, and this does not present any major problems. Hamilton Standard has done considerable work on developing steel raceway inserts on titanium blades and barrels, and no major obstacles have been encountered.

Blades D and E represent the greatest weight-saving potential, but they do require the greatest amount of development. The boron-epoxy and boron-aluminum materials are both still in their early stages of development; however, with an accelerated effort, their evolution could closely parallel that of the titanium spar.

The major technical jeopardy will probably be in the retention area of the boron composite blades. Loading patterns in the retention area are quite complex and involve combinations of tension, compression, bearing, and torsion as well as the Hertz-type stress in the bearing areas. To take full advantage of the boron composites for the spar, the spar needs to be configured to handle these omnidirectional loads with a basically unidirectional filament composite material. A promising solution for the retention is shown in the "System Design" section of this report, page 160. In order to be ready for the 1970-1975 period, this type of development which involves the need for new basic skills in material handling and forming, should be started immediately. In addition to the manufacturing process development required for these new materials, environmental development testing for foreign object damage, erosion, temperature extremes, weathering, lightning damage, etc., is required to determine their effect on the blade and its allowable stress levels. From the data generated by this study, however, it seems certain that this new technology can be achieved in an orderly fashion and that the introduction of boron composite blades can be looked to for very substantial reductions in propeller blade weights before 1975.

COLLECTIVE PITCH CHANGE MECHANISM

The hydraulic collective pitch change actuator is a hydraulic servo actuator designed to react blade twisting moment loadings so as to maintain any selected blade angle for all operating conditions. These twisting moments include frictional twisting moments (FTM) caused by rolling friction in the blade retention, centrifugal twisting moment (CTM), and aerodynamic twisting moment (ATM). ATM and CTM vary with blade angle and rpm, and ATM also varies with airspeed. The total twisting moments (TTM) which determined the design loads are shown in Figure 53. Reliability, weight reduction and maintainability, and the ease of disassembly of the actuator without requiring the removal of blades or other major structure are the prime objectives in the actuator design (Figure 54).

Description

For ease of actuator removal, breach thread is used to attach the actuator cylinder to the yoke which supports the rod ends of the blade links. The actuator cylinder is splined to a tube that is bolted to the barrel, and the yoke is directly splined to the barrel, thus locking the breach thread. To remove the actuator from the propeller

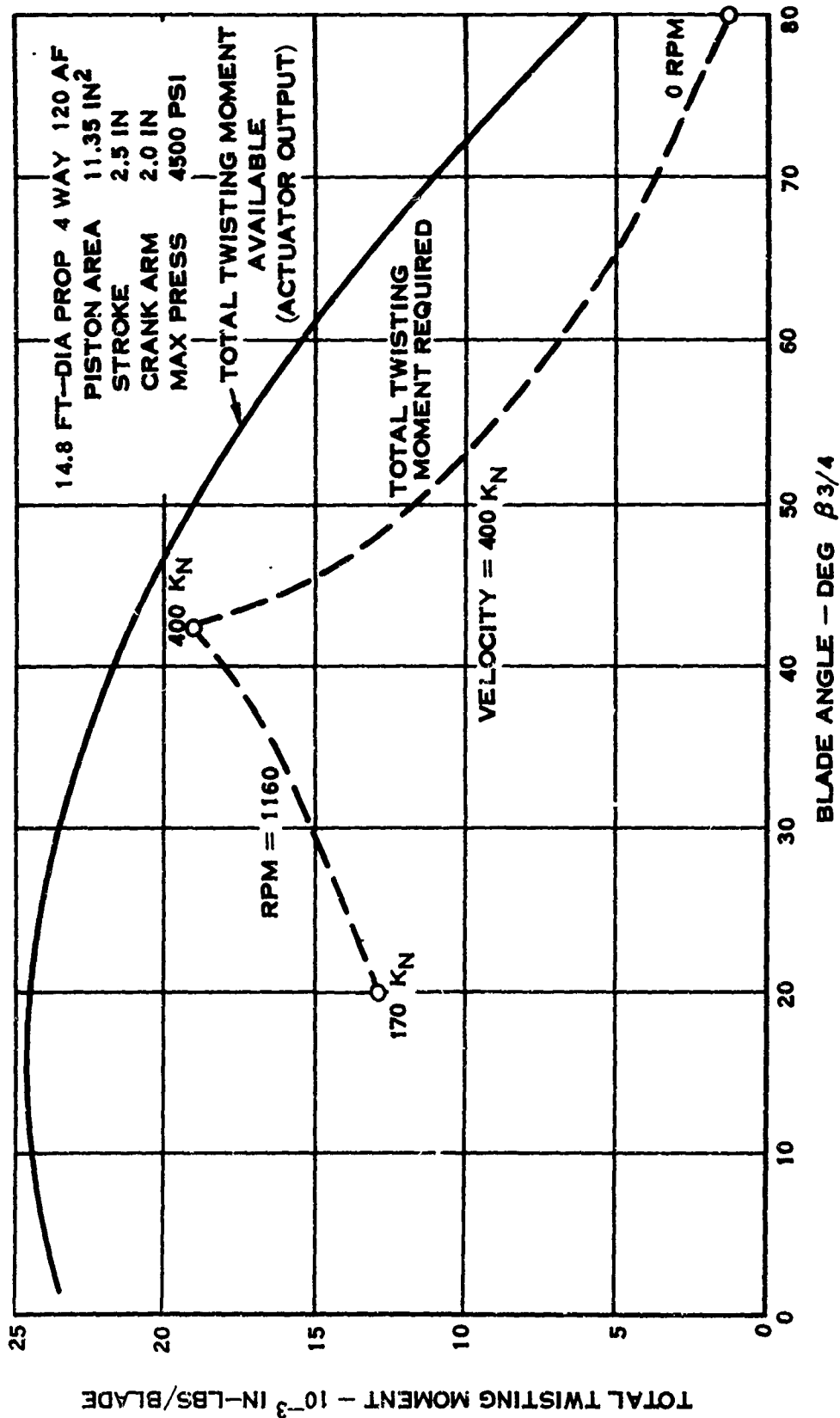


FIGURE 53. BLADE TWISTING MOMENT VS BLADE ANGLE

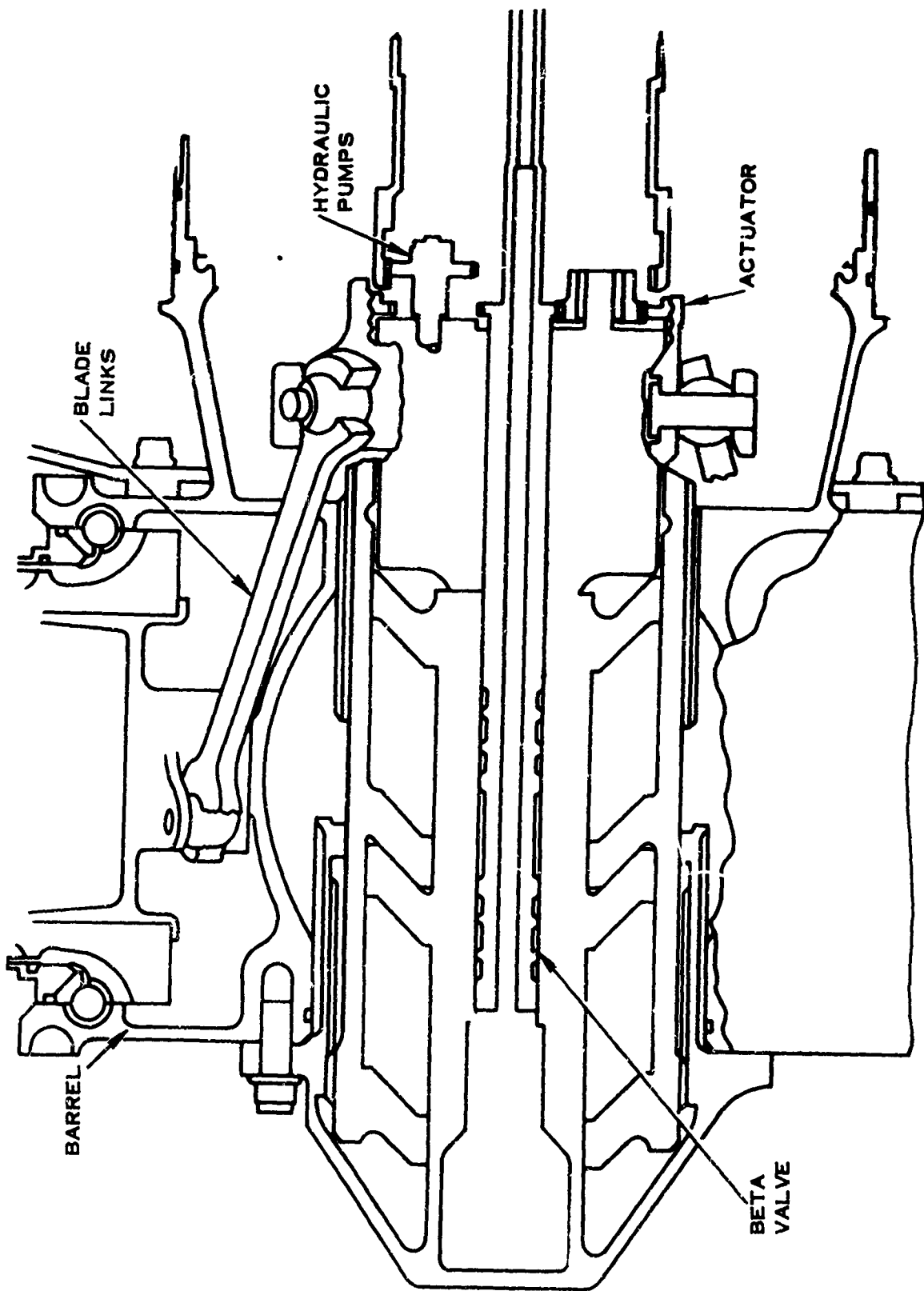


FIGURE 54. COLLECTIVE PITCH ACTUATOR

assembly, the spinner and the front bulkhead bolts are removed, and the spline tube as well as the cylinder is rotated a portion of a turn to free the breach thread. The actuator, beta valve, pump housing, and pump drive are then removed as one unit.

For high reliability, the actuator hydraulic chambers, blade links, pumps, beta valve, and control input are dualized. This provides for two completely independent hydraulic systems and redundant major structural components where practical, each capable of supporting the maximum blade loads over the entire operating range.

The actuator is positioned by a servo valve which consists of two four-way valves physically coupled together to meter oil to the high and low pitch sides of the actuator. The hydraulic power is provided by two gear pumps which form an integral part of the nonmoving actuator. These pumps operate at 9500 rpm and deliver 15 quarts per minute each to provide for a minimum pitch change rate of 30 deg/sec. Dual system-out indicators are provided to detect the failure of either system's supply pressure. In the event of a failure of both hydraulic systems, a pitchlock mechanism prevents the blades from moving toward low pitch. The propeller then continues to operate at fixed pitch.

The actuator weight was optimized by considering loading paths, trade-off studies of geometric considerations (actuator diameter versus stroke, blade arm length, and working pressures), and actuator construction. Links connecting the blade trunnions with the actuator yoke were chosen over a scotch yoke design to minimize the hole required in the barrel to insert the actuator and thus to produce a lighter barrel design. The titanium blade links are a dual redundant structure having spherical rod ends with reinforced Teflon-coated bearings. Loads from the links produce a torsional component on the yoke which is reacted through the yoke spline to the barrel.

As part of the actuator study, two parametric studies evolved in order to determine the effect of (1) pressure and (2) blade trunnion radius on the actuator weight. The influence of pressure on the weight per inch of length for various center-body diameters (Figure 55) indicates that, for decreasing center-body diameter and increasing allowable pressure, the wet weight per inch of actuator decreases. The physical requirements of the beta valve, hydraulic lines, and hydraulic pump drive shafts dictated that the center-body diameter be 2.3 in. For the study design system loadings, this center-body diameter dictated that a pressure of 4500 psi be used.

Increasing the blade trunnion arm length on a blade with constant total twisting moment loadings reduces the pressure load required in the actuator but at the same time increases the linear stroke of the actuator required. Figure 56 indicates the effect of blade arm length on weight for a constant pressure level. This weight study included the cylinder, piston, bulkheads, barrel extension, and splined blade

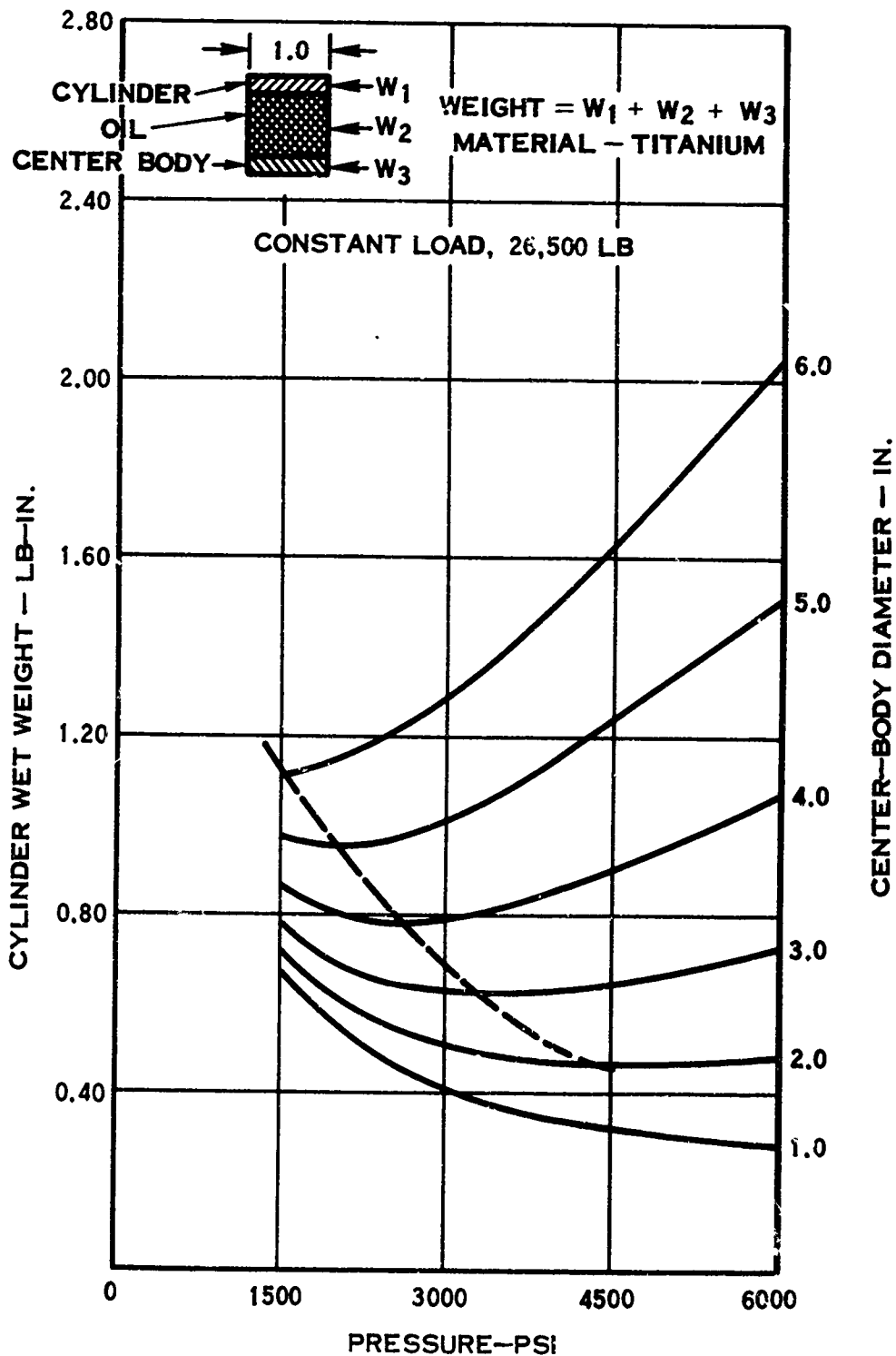


FIGURE 55. ACTUATOR WET WEIGHT PER INCH OF LENGTH

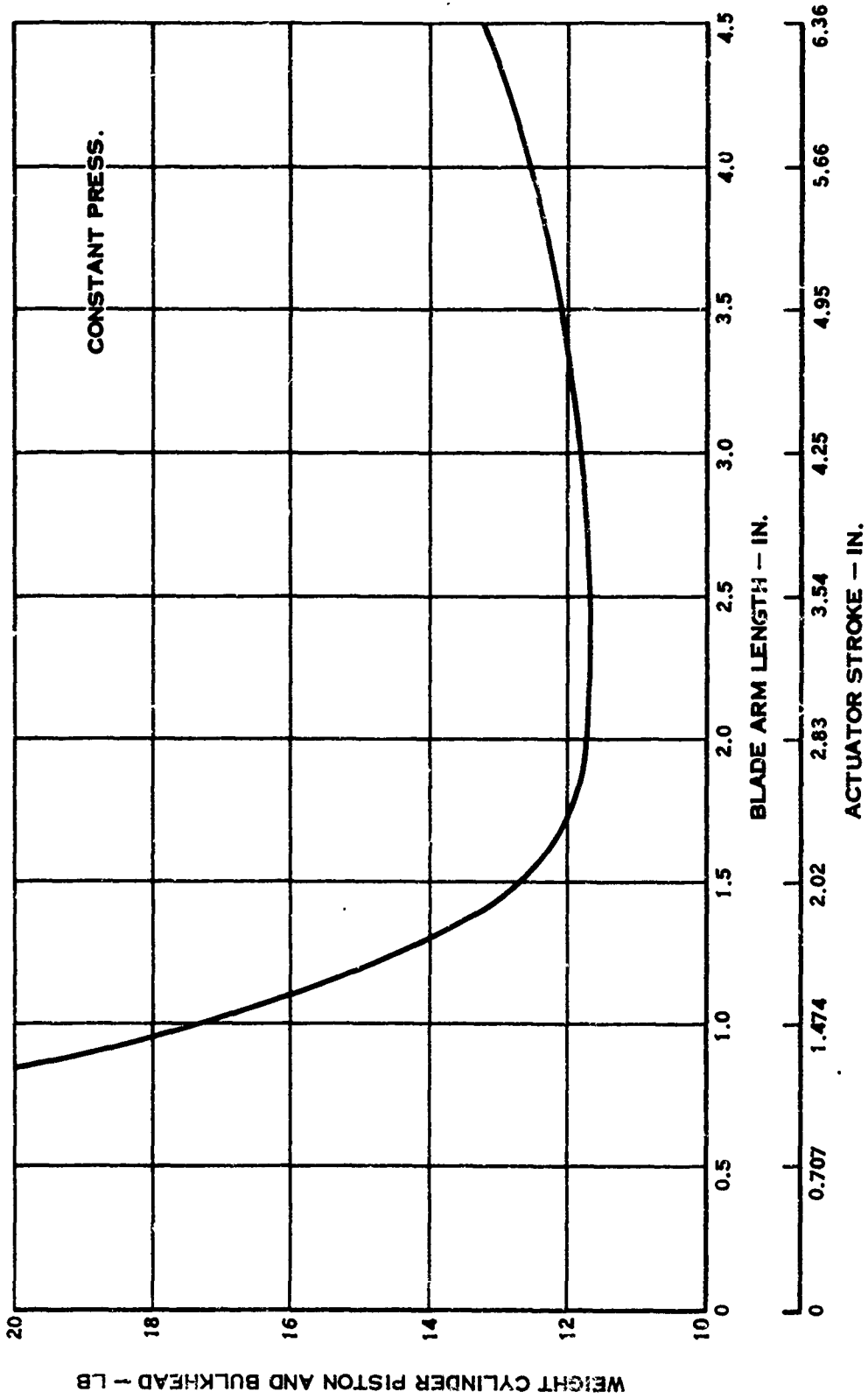


FIGURE 56. ACTUATOR STROKE VS ACTUATOR WEIGHT

shank. As the blade arm shortens, piston diameter and bulkheads increase (for constant pressure), as does the total load carried by the blade links; thus, the curve asymptotically approaches infinity as the blade length shortens. Conversely, as the blade arm lengthens, the actuator and barrel extension required length also increase; thus the curve (Figure 56) also indicates higher weight for large blade arm lengths. For the USAAVLABS system, a 2.00 blade arm was used.

With respect to the materials, an all-titanium actuator would be light, but it has the disadvantage that with the cylinder diameter used and the pressure of 4500 psi, the radial deflection could be as large as 0.01 in. This would exceed the normal seal capacity to prevent extrusion. Thus, cylinder stiffness becomes the limiting structural criterion.

To provide the necessary cylinder hoop stiffness, boron filaments in an epoxy matrix are filament wound on the outside diameter of the titanium cylinder. The bulkheads and pistons are all titanium, and the cylinder uses a titanium shell with boron filament winding. The titanium on the cylinder is sized to react axial loads primarily. Approximately 1 lb of boron filament is used on the actuator cylinder to limit deflections, and it provides weight savings of approximately 5 lb over an all-titanium cylinder. This also permits the cylinder outside diameter to be smaller, thus enabling a smaller hole in the barrel and additional barrel weight saving. The inside diameters of the cylinders and all wear surfaces on the titanium would be coated to prevent fretting or galling.

An in-place pitchlock has also been incorporated in the actuator system to prevent loss of blade angle in the event that both of the actuator hydraulic systems malfunction. The in-place pitchlock feature (Figure 57) utilizes a threaded member to convert the rotary signal of the propeller control to an axial positioning of the actuator servo valve. Should the hydraulic pressure drop to a level that is not sufficient to tend to move the actuator in a direction to decrease blade angle. However, in this concept, the actuator reacts through the threaded member and closes the pitchlock "gap". The blades are then mechanically held in position due to the irreversible nature of the thread.

By having the actuator hydraulic pumps rotating with the propeller, a high-pressure oil transfer bearing is eliminated, and the pumping system becomes an integral part of the actuator. These pumps operate at 9500 rpm and deliver 15 quarts per minute each to provide a minimum pitch change rate of 30 deg/sec. Included with each rotating pump are a high-pressure relief valve, regulating valve, double valve to the system-out indicator, check valve for auxiliary pump and ground handling, and actuator cooling valve. The regulating valve keeps pump outlet pressure at about 150 psi above actuator pressure. This restrains the pumps so that little power is consumed in the low actuator pressure operating regime. The high pressure relief valve is set at 4500 psi. The actuator cooling valve has its longitudinal axis radially out from

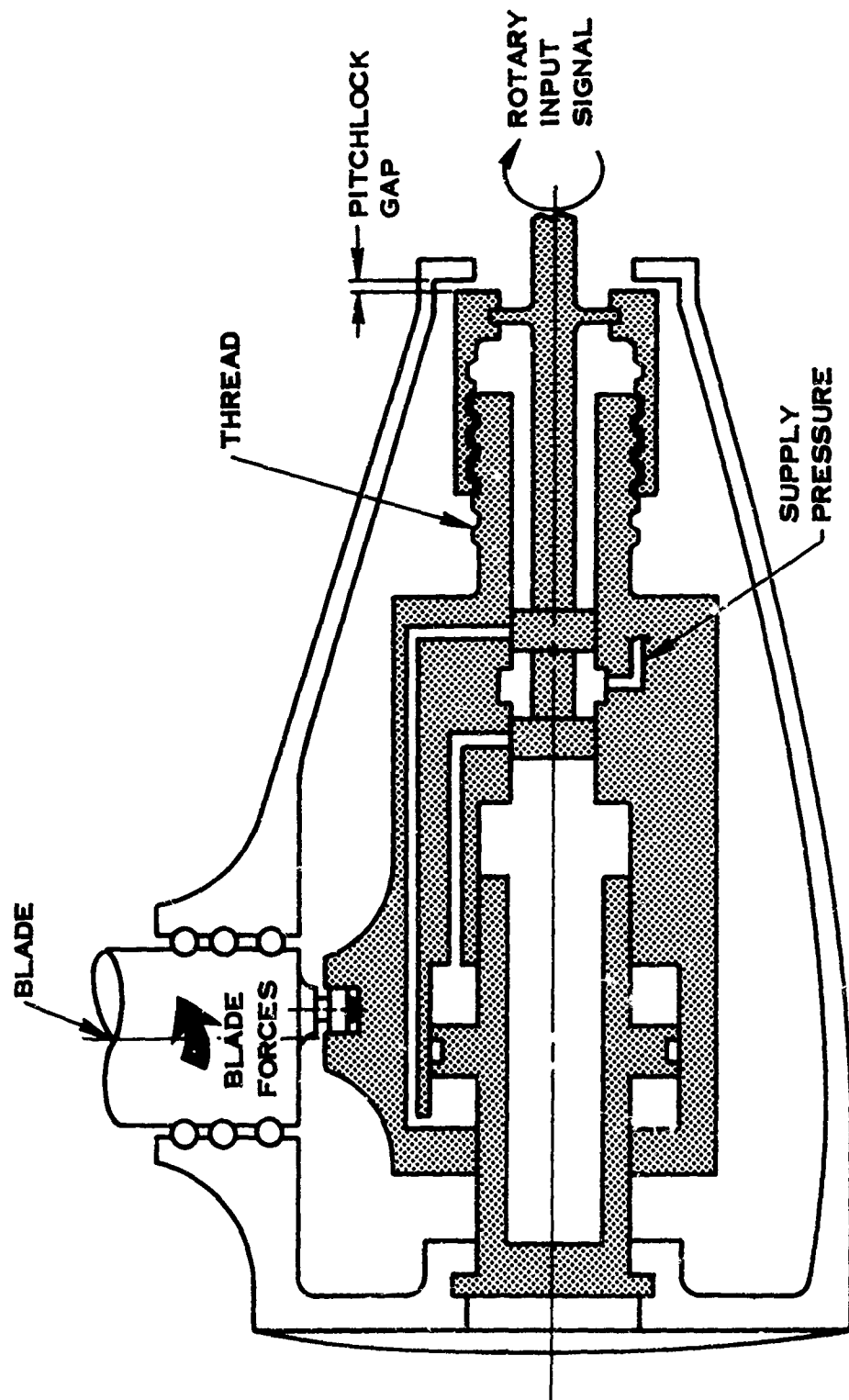


FIGURE 57. IN-PLACE PITCHLOCK CONCEPT

the rotational axis of the propeller, and its setting is a function of propeller rpm. When the propeller is not rotating, the valve closes off and prevents leakage to the gearbox. During normal operation, it takes the outflow from the regulating valve and dumps a portion of low-pressure hot oil into the gearbox. Cooler gearbox oil replenishes the system by providing low-pressure lube oil through the center of the beta valve. In the event that this replenishing oil is blocked off, the actuator cooling valve shuts off, and the propeller continues to operate with no exchange of oil between the gearbox and the propeller. All this valving is included in the pump housing, and it is removed with the actuator during disassembly.

A summary of the actuator design data is listed in Table XII.

Ball Screw Actuator

As part of the propeller actuator component studies, a brief study of a ball screw actuator was conducted. This type of actuator utilizes the control system to activate hydraulic motors which, in turn, change the propeller blade angle by use of a gear train and a power screw (Figure 58).

The ball screw actuator would provide redundant load paths, with each capable of carrying the full load. Failure of one of the paths results in the reduction of the pitch change rate to one-half the normal rate.

The combined weight of the ball screw (to change blade angle), the main actuator thrust bearings (to react the propeller loads), and the hydraulic motor (required for input signal), without consideration for the gear train, input shafts, and redundant drive system, is equal to the weight of a hydraulic actuator system. Therefore, with no indicated weight advantage, the study of the ball screw actuator system was not pursued further.

TABLE XII. CYCLIC PITCH ACTUATOR DESIGN DATA

PISTON AREA	11.35 IN.²
MAXIMUM OPERATING PRESSURE*	4500 PSIG
MAXIMUM NORMAL OPERATING PRESSURE	2250 PSIG
CENTER-BODY DIAMETER	2.3 IN.
ACTUATOR STROKE	2.57 IN.
BLADE ANGLE RANGE	90°β
BLADE FEATHER ANGLE	81°β 3/4
BLADE CRANK RADIUS	2.00 IN.
MAXIMUM TOTAL TWISTING MOMENT	19,200 IN.-LB/BLADE

***ONE SYSTEM OUT**

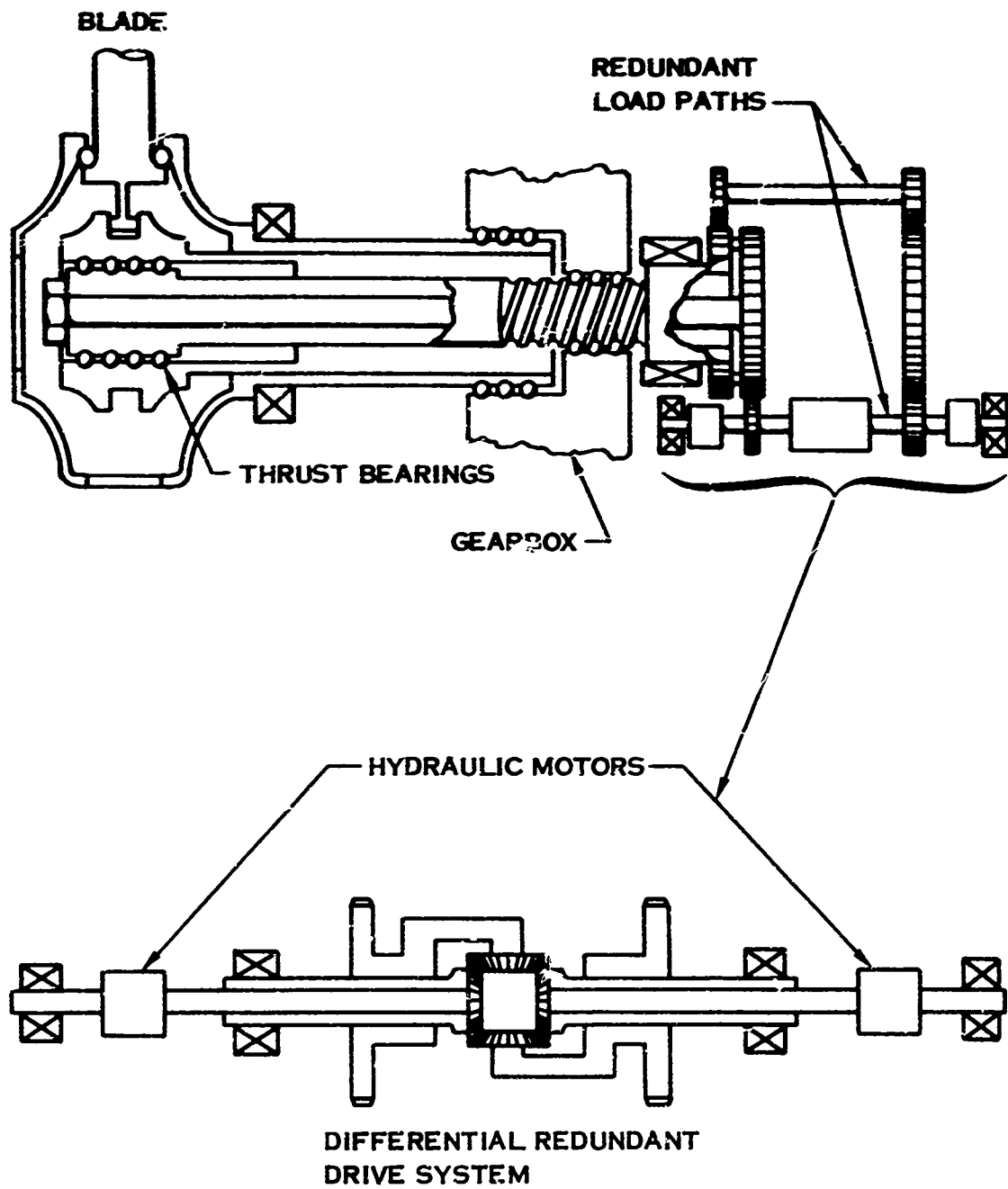


FIGURE 58. BALL SCREW ACTUATOR

CYCLIC PITCH CHANGE MECHANISM

Introduction

Cyclic pitch, the variation of blade angle with rotational position of a propeller, can be used to produce pitch control moments for the aircraft. This pitch control used in hover could allow the elimination of a tail propeller, fuselage gearbox and associated shafting. However, a total analysis, including the hover performance loss when cycling blade pitch and an assessment of the complexity and reliability of the cyclic pitch systems, is needed to fully evaluate whether adding a cyclic pitch capability to the propeller is desirable. This study did not attempt to make such an analysis; it was concerned solely with design concepts to define the best mechanical implementation of blade angle cycling pitch for minimum weight and maximum reliability of the propeller system.

Another potential use for cyclic pitch to consider is to produce a moment in flight to cancel or minimize propeller 1P moment. The 1P moment is encountered in flight when the propeller disc is not perpendicular to the velocity vector of the inflow airstream. 1P moment is generally the major structural design consideration for the blade and barrel construction, and its reduction could have a marked effect on blade weight as well as on the weight of the entire propeller system. Although the cyclic pitch mechanisms for minimizing 1P would be similar to those used to produce control moments, only the latter were considered in detail for this study.

For the specific disc loading considered in this study, the desired pitch control moments at the hover design point are of the same magnitude as the design 1P moments. For these conditions the structural loadings to which the blade, retention, and barrel must be designed are essentially the same to react the control moments as the 1P moments. Specifically for the point design, the 1P moment is 106,000 in-lb per propeller, and the maximum pitch control moment induced into the propeller shaft is 116,000 in-lb. Thus, for this design, very little weight was added to the blade and barrel to superimpose the capability of providing control moments. The weight added to the specific cyclic pitch propeller design described in this report was primarily that due to the additional mechanism required in the pitch change actuation system.

It should be noted that if different assumptions of the design requirements were made, the weight increase could be higher than that discussed above. For example, since there would be more power (and thrust) available during operation at sea level standard day conditions, the aircraft could be designed to accommodate extra payload. Therefore, the maximum operating gross weight would increase, and higher cyclic pitch propeller control moments for the aircraft would be required. This would increase the propeller structural loading requirements; hence the weight would increase. Another example is that the same magnitude of aircraft control moments

required for hover may also be required to be provided in transition by the cyclic pitch propeller. In this case the cyclic pitch moments can add vectorially to the 1 P moments encountered in transition which could also increase the propeller structural requirements and weight.

Discussion

Several concepts were considered, and the cyclic pitch design deemed optimum is that shown in Figure 59. A change in location of the collective pitch control as well as of the pump housing was necessary. When the entire design adaptation to cyclic pitch is considered, this concept showed a difference in weight of only 23 lbs per nacelle over the noncyclic design. Its major advantages are its relative mechanical simplicity--all linkages and moving parts are enclosed within the barrel and gearbox, providing adequate lubrication and protection from contamination and minimized load paths to support the blade twisting moment loads--and its mutual compatibility with the gearbox, actuator, and barrel designs which optimized collective pitch propeller design.

For purposes of the design analysis, a maximum aircraft pitching moment requirement was estimated, equivalent to a propeller thrust vector shift to the 25% blade radius. The corresponding cyclic angle amplitude of ± 10 deg. blade angle was calculated by the analysis discussed previously in the "Aerodynamic Studies" section. Since the maximum control moment requirement is considered to be only a short duration, it was also necessary to define a representative steady-state condition. This was estimated as being equivalent to a 10% thrust axis offset, which would require a cyclic blade angle of ± 4 deg. or less.

Selected Design Concept

Figure 59 describes the new cyclic pitch actuator concept which was selected as the optimum design concept. The basic actuator is essentially the same as the propeller actuator previously discussed for purely collective pitch change. The major difference is that the connection between the translating actuator cylinder and the links to the crank arm on each blade is made through a moveable ball joint. The axial positioning of the actuator determines the propeller collective pitch in the usual manner, but rotational displacement of the ball joint allows the rear plane of the blade links to be tilted relative to the plane of the propeller disc. Then, with propeller rotation, the axial location of each blade link varies cyclically, forcing a periodic blade angle excursion about the collective pitch setting. Adjustment of the angular positioning of the ball joint will control the magnitude of the generated moment in a manner analogous to that of tilting the swashplate on a helicopter rotor.

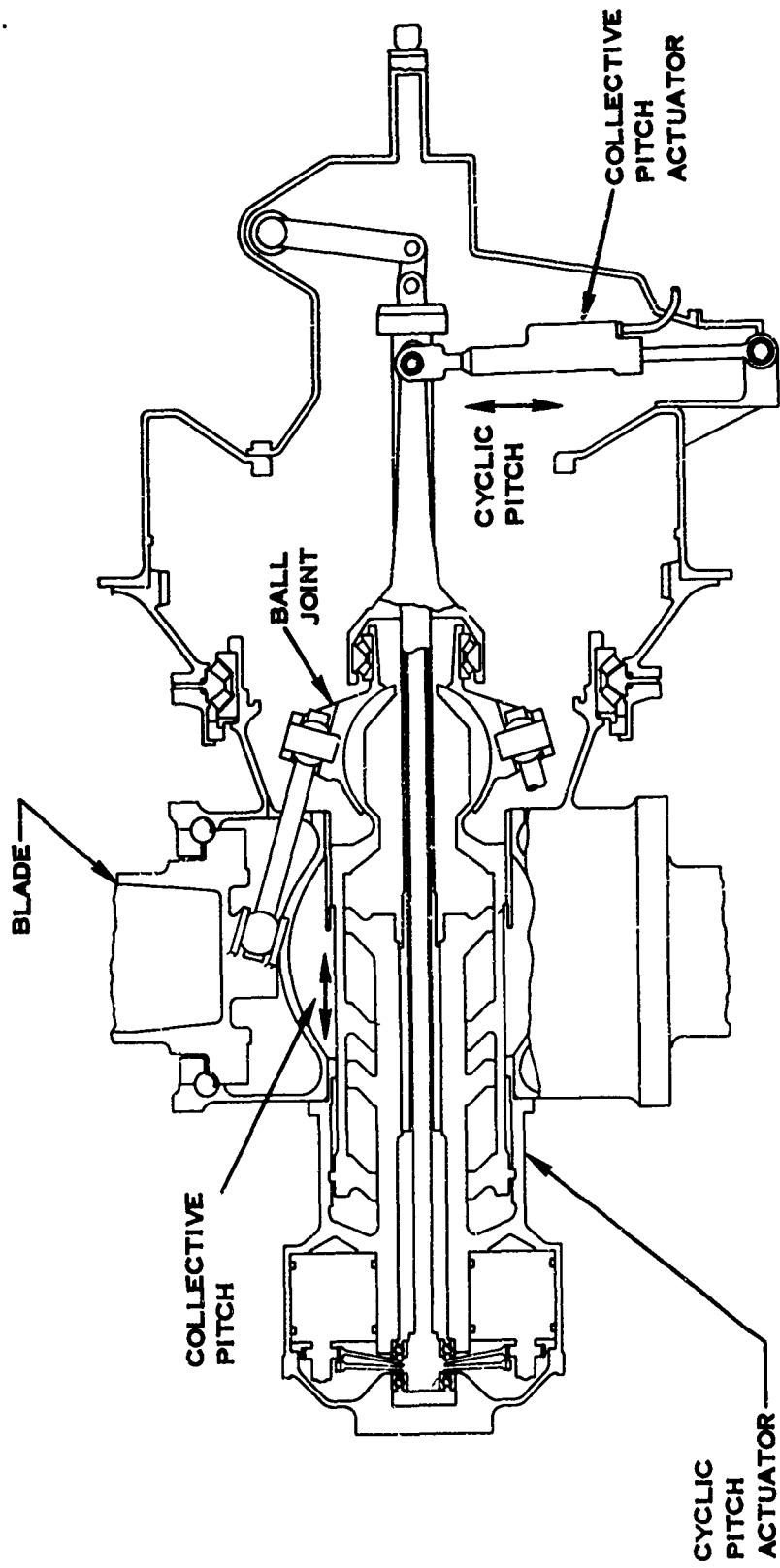


FIGURE 59. BALL JOINT CYCLIC PITCH ACTUATOR CONCEPT

Loading

The first consideration in analyzing the loading imposed by monocyclic pitch was the inertia of the propeller mechanism. This includes the ball joint, blade links, and blades. The blades contribute the major portion of the mass moment of inertia.

For the design point propeller, this moment of inertia about the longitudinal axis of the blade is 3.6 lb-ft². With the maximum angular acceleration imposed by ± 10 deg. cyclic pitch at 1160 propeller rpm, the blade inertia torque is 60 in.-lb. This is negligible when considering that just the cyclic torque produced by the retention friction is over 1000 in.-lb (Figure 60).

The titanium link arms are the same as those used in the noncyclic propeller. The maximum load requirement for the blade links is the same as that for the collective pitch actuator design, which is 10,000 pounds per link in high-speed flight. The rod end bearings in the ends of the blade links, however, are subjected to increased motion when providing cyclic pitch. The maximum blade link load is lower (2000 lb per link) when in hover where cyclic pitch is used. The wear of the rod ends operating continuously for 1000 hours of cyclic pitch operation was estimated to be approximately 0.002 in. This wear could result in an error in blade angle, but it is only of the same magnitude as the backlash existing in present-day propeller design practice, using a scotch yoke mating with a blade crank pin.

The ball joint design is also capable of being packaged in a small envelope, because lower blade twisting moment loads occur in the blade range of cyclic pitch than at the high speed cruise conditions. The total calculated axial load on the ball joint during cyclic pitch operation has a maximum value of approximately 8,000 lb. This load must be supported during relative motion of the ball and socket mating surfaces. The ball joint design was found to be structurally adequate to support the maximum collective actuator axial loads of approximately 40,000 lb in the noncyclic flight range.

Redundant lubrication of the ball joint has been conceived. A reinforced Teflon coating is used for backup to a unique lubrication system incorporated in the ball joint which provides a hydrostatic oil pressure over the moving surfaces. This is accomplished with piston pumps that reciprocate only during cyclic action. The pumps have oil flow supplied by the gearbox lube system plus the centrifugal pressure head provided by propeller rotation, and they can provide flow up to 0.48 in.³/sec at a cyclic amplitude of ± 10 deg. This provides enough lubrication flow to dissipate friction heat, and the developed pressure will support the axial loads.

A Hooke's joint design using anti-friction bearings to reduce friction could have been used in this concept rather than a ball joint. However, in that case, the structure involved in transmitting the maximum collective pitch actuator loads would necessitate large, heavy gimbal rings and a large weight penalty.

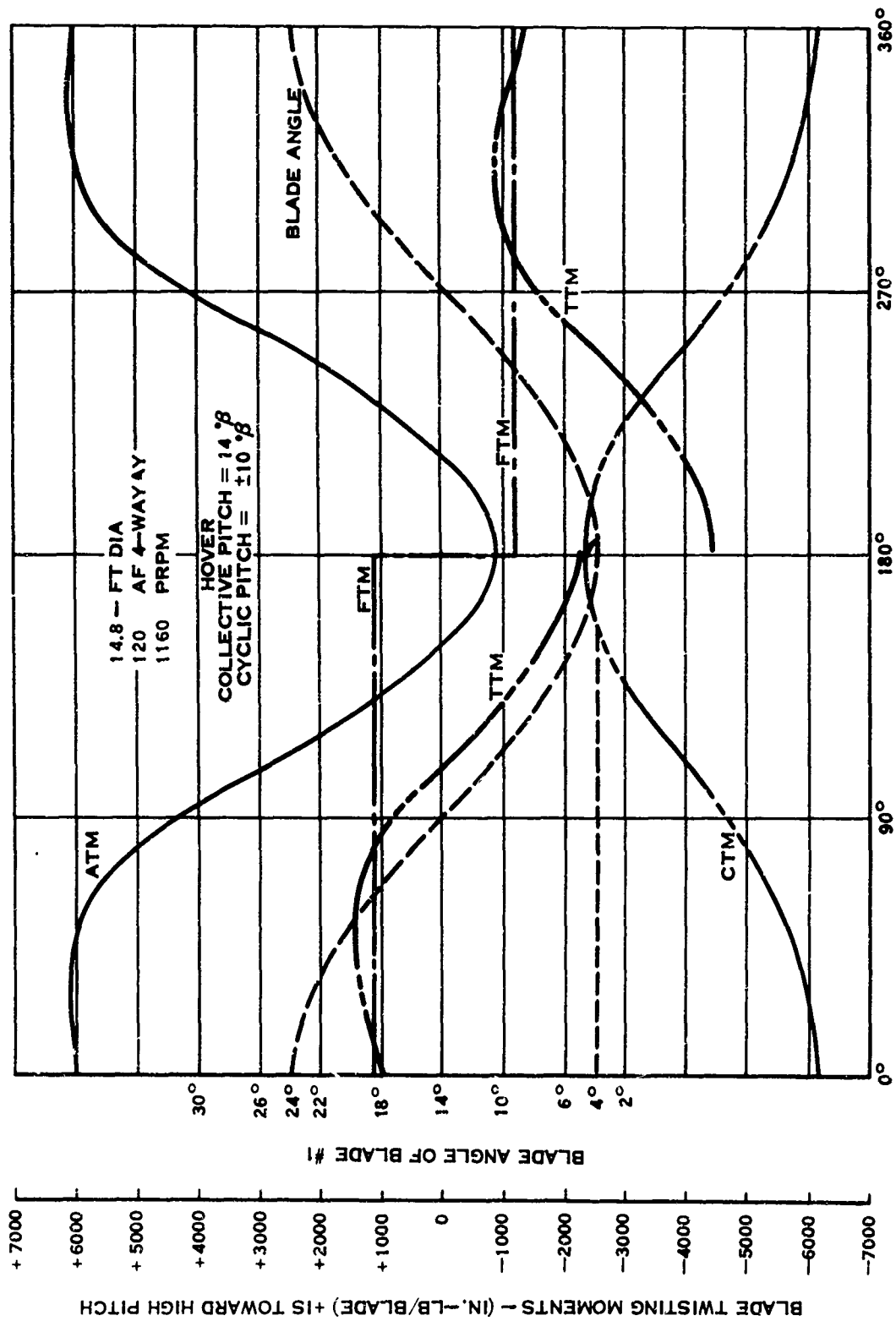


FIGURE 60. CYCLIC BLADE TWISTING MOMENTS

The ball joint must also react a component load from the link arms, which impose a torque about the propeller axis. This torque has a maximum value of 5500 in-lb and is transmitted by two needle bearings (similar to cam rollers) fixed in the outer socket and rolling in slots in the ball. The torque is then reacted through a spline directly into the barrel.

The blade retention was increased slightly (7-in. diameter to 7.5-in. diameter) to account for the increased number of pitch change cycles. During cyclic pitch operation, as the blade oscillates to either side of the collective pitch angle, each ball in the retention rolls over a given point on the retention bearing races twice.

The cyclic pitch signal to the ball joint is provided by a tapered roller bearing set, redundant load path lever arms, and a dual servo actuator. This load path reacts a moment produced on the ball joint by the blade links which is due to both FTM, and the nonlinearity of CTM and ATM with blade angle. Figure 60 shows the twisting moment of blade #1 as it cycles ± 10 deg. through one complete propeller rotation. Figure 61 shows the total twisting moments of each of the four blades and their summation as the propeller rotates through 360 deg.

Friction in the ball joint also has to be reacted by the cyclic input lever. This is a moment which is in a plane perpendicular to the axis of the cyclic input lever and has a maximum value of 400 in-lb.

A summary of the Ball Joint Cyclic Pitch Actuator design data is listed in Table XIII.

Cyclic Servo Actuator

The cyclic servo actuator is designed with the same double redundancy philosophy as the collective pitch actuator, and it also has a moving cylinder with a direct feedback. Each actuator pressure chamber is sized to take the entire load, as is each lever arm to the ball joint. The cyclic pitch servo actuator reacts its load through a grounded pivot mounted to the gearbox housing. The actuator cylinders are pinned to the input lever connected to the ball joint.

The cyclic actuator hydraulic supply pressure is 3000 psi. This was considered to be supplied by the aircraft hydraulic system, but it could also be supplied by propeller-mounted hydraulic pumps. If aircraft hydraulics are used, the cylinders would be designed so that any leakage was directed out of the gearbox and was not mixed with propeller oils.

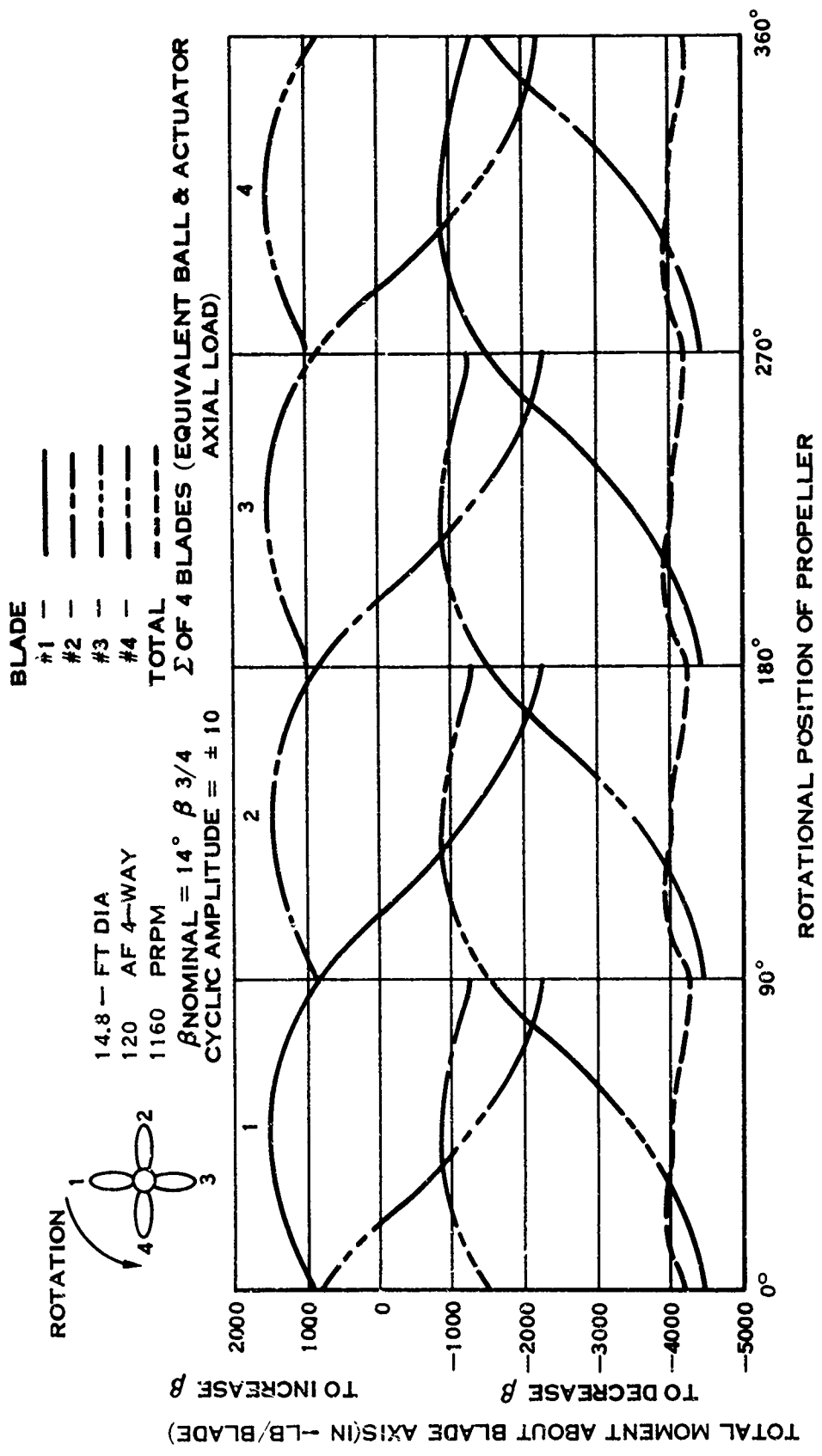


FIGURE 61. SUMMATION OF CYCLIC BLADE TWISTING MOMENTS

TABLE XIII. CYCLIC PITCH ACTUATOR DESIGN DATA

COLLECTIVE PITCH

PISTON AREA	11.35 IN ² EACH
MAX OPERATING PRESSURE	4500 PSIG
MAX NORMAL OPERATING PRESSURE	2250 PSIG
CENTER BODY DIAMETER	2.3 IN.
ACTUATOR STROKE	2.57
BLADE ANGLE RANGE	90°
BLADE FEATHER ANGLE	81° β 3/4
BLADE CRANK RADIUS	2.0 IN.
MAX TOTAL TWISTING MOMENT	19,200 IN-LB/BLADE

CYCLIC PITCH

CYCLIC BLADE ANGLE EXCURSION (MAX)	±10°
PISTON AREA	.307 IN ² EACH
MAX OPERATING PRESSURE	2500 PSIG
NORMAL OPERATING PRESSURE	550 PSIG
ACTUATOR STROKE	1.3 IN.

Other Cyclic Mechanisms

The above-discussed cyclic pitch system was considered to be of optimum design. Several other cyclic mechanisms were considered and are described below.

Figure 62 shows a concept of a nonrotating actuator with a ball and a rotating, tilting swashplate. A basic disadvantage of this configuration is the size of the duplexed tapered roller bearings which must react the full actuator collective and cyclic blade loads while rotating at propeller speed. The cyclic input bearings in the selected design react only the differential moments between blades and also rotate at propeller speed. The required bearing capacity for the nonrotating actuator would be approximately 17 times that of the concept used, which would cause at least a 25-lb weight penalty.

A second disadvantage to this concept is that the actuator loads must be grounded across the main propeller mounting bearings into the hub structure. This additional thrust loading increases the required capacity of the main bearings by a factor of 2.85 times that of the selected system, and it would produce an additional weight penalty of approximately 22 lb.

The nonrotating cyclic actuator design was not pursued further because it had these apparent weight disadvantages.

Figure 63 shows another cyclic pitch concept which uses linkages to provide a cyclic input that does not stroke with the collective actuator. However, the design has 12 more pivot points than the selected design, with each reacting the total blade loads. The added complexity and additional structural pivots were the primary reasons for discarding this concept.

A planetary gear train located within the blade shank seemed to be an interesting concept and is shown in Figure 64. The gear train is used to sum collective angle and also to cycle blade angle. This system requires a 7.00-in. ring gear, six planets with a 2.00-in. diameter, and a 3-in. sun gear, all with face widths of 1.5 in. A collective pitch actuator with inputs to the planet cage would have a stroke of 2.75 in. and would require dual areas of 14 in.² each. The cyclic input of the sun gear must essentially go through a swashplate similar to that of the selected design. The cyclic input must also go through a bearing to take out propeller rpm, but it does not have to translate with collective pitch. This system has the disadvantage of being heavier and more complex than the selected system.

One of the concepts considered for providing a cyclic pitch to minimize 1P loads was a self-regulating propeller in which the propeller hub was gimballed to the propeller shaft. An anticipated advantage was that a major portion of the 1P moment would be automatically eliminated by allowing the plane of the propeller disc to adjust to the free airstream inflow to the propeller. This configuration is shown in

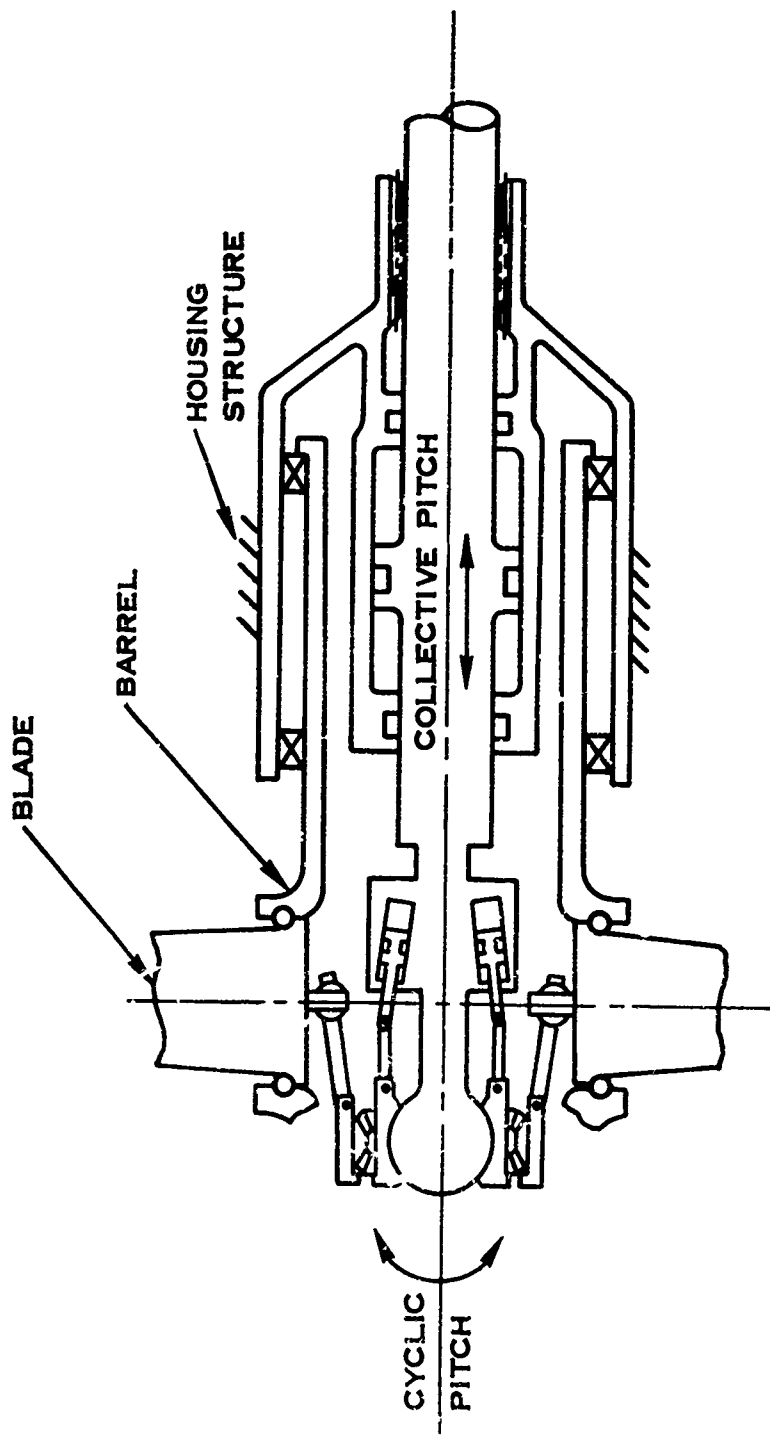


FIGURE 62. NONROTATING CYCLIC ACTUATOR

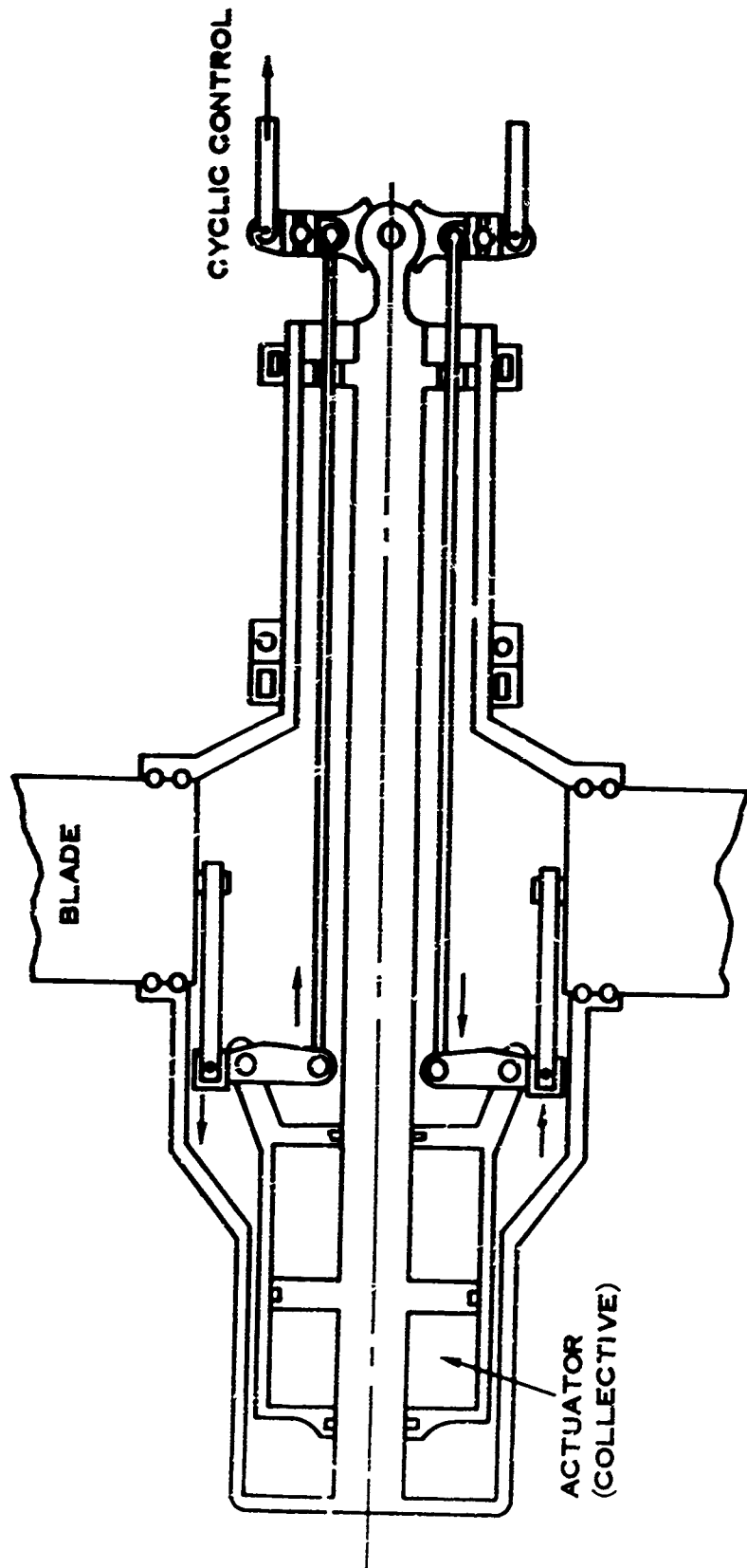
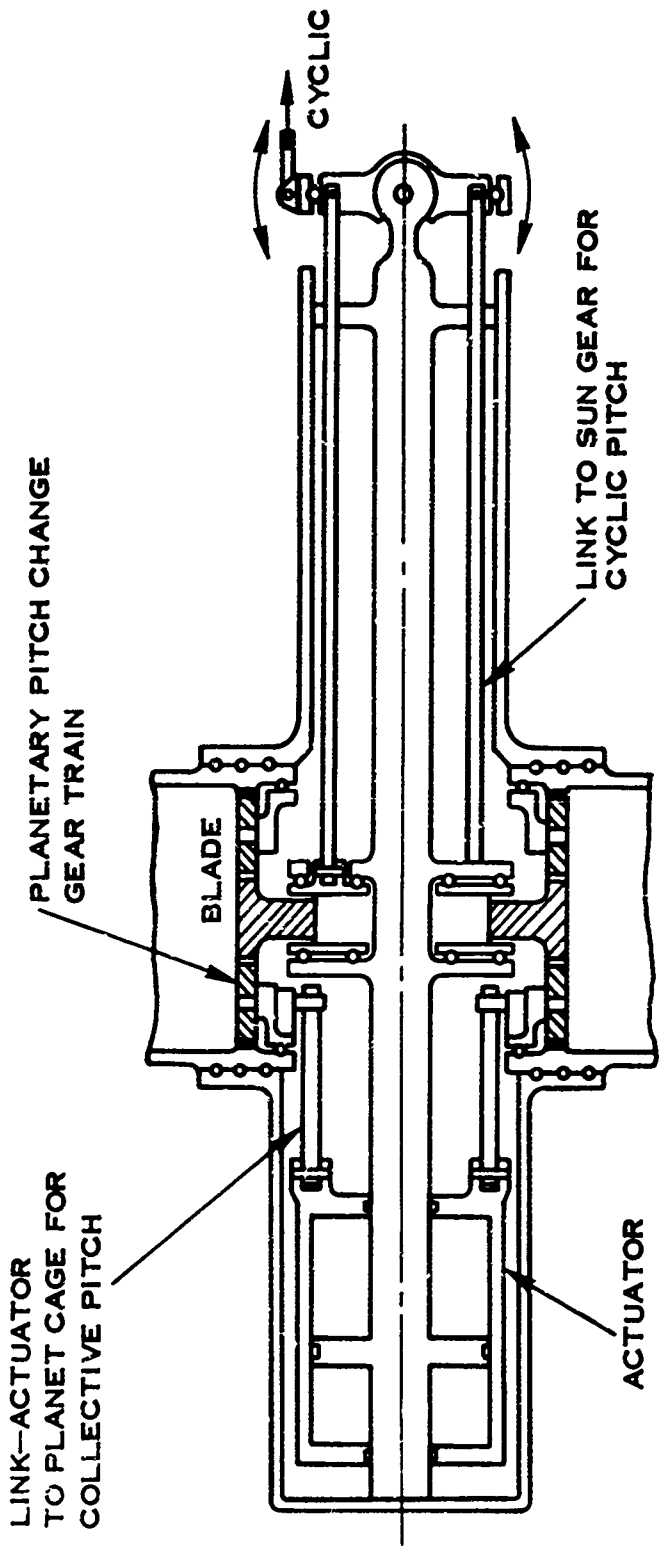


FIGURE 63. CYCLIC PITCH ACTUATION WITH LINKAGE



NOTE : RING GEAR MAY BE ATTACHED TO THE ACTUATOR AND THE CAGE TO THE BLADES AS AN ALTERNATE DESIGN

FIGURE 64. CYCLIC PITCH ACTUATION USING A PLANETARY GEAR TRAIN

Figure 65. The gimbale joint must have the angular degrees of freedom of a ball joint, be driven torsionally about the propeller axis, and must transmit full propeller torque (approximately 108,000 in.-lb). This design must also avoid possible whirl flutter instability. A mathematical discussion of the criteria for stability is discussed in Appendix VIII. The stability criteria for a monocyclic mechanism depend on the ratio of blade angle cyclic excursion to angular rotation (tilting) of the propeller disc. For an aircraft with a V_{max} of 410 kn this ratio must be 6.0 to be stable. Specifically, for a blade crank arm radius of 2.0 in. selected for the propeller design, the blade link would have to be attached to the blade external to the barrel at a radial location 12 in. from the propeller axis of rotation. This would require an extensively modified large barrel or external blade linkage. These conditions appeared to negate any weight advantages that would be accrued by the elimination of the major portion of 1P by using the gimbale propeller concept.

The controlled cyclic pitch (such as the selected design concept) is not subject to the stability described above. Also, the selected cyclic control system could be used with a feedback loop from a 1P moment sensing device to automatically minimize induced 1P moments in flight. This would be the preferred method.

CONTROL SYSTEM

The rpm control system for the propeller consists of an rpm-sensitive valve which meters oil to the beta valve servo piston in proportion to the rpm error. The servo piston moves as long as there is an rpm error present, and at a rate proportional to the rpm error magnitude. The beta valve position is then changed by a linkage connected to the servo piston. Displacement of the beta valve causes the actuator cylinder, and thus the blades, to move. Output of the servo piston is also connected to the speeder spring platform and the speed-setting servo through a summing link. This, in combination with the speed-setting pilot valve, provides a lead time constant which cancels the effect of the long engine-propeller lag time constant, thus allowing high system gains and less rpm overshoot during transients. The same hardware also provides a delay in speed setting. Since this delay is the same as the lead time constant, which is matched to the engine-propeller time constant, torque dips are minimized when power and rpm settings are changed in the coordinated mode.

The overspeed governing system provides protection against failure of the main governor. If the main governor fails and calls for a decrease in pitch, the resulting motion of the beta valve actuator servo moves the speeder spring platform of the overspeed governor as well as that of the main governor, thus resetting the governor and bringing it into play before the propeller reaches the steady-state rpm setting of the overspeed governor. Studies have shown that this feature prevents rpm overshoots greater than 2% over the overspeed governor setting. Since the overspeed governor is a true governor for this mode of failure of the main governor, the propeller will continue to operate at the increased rpm.

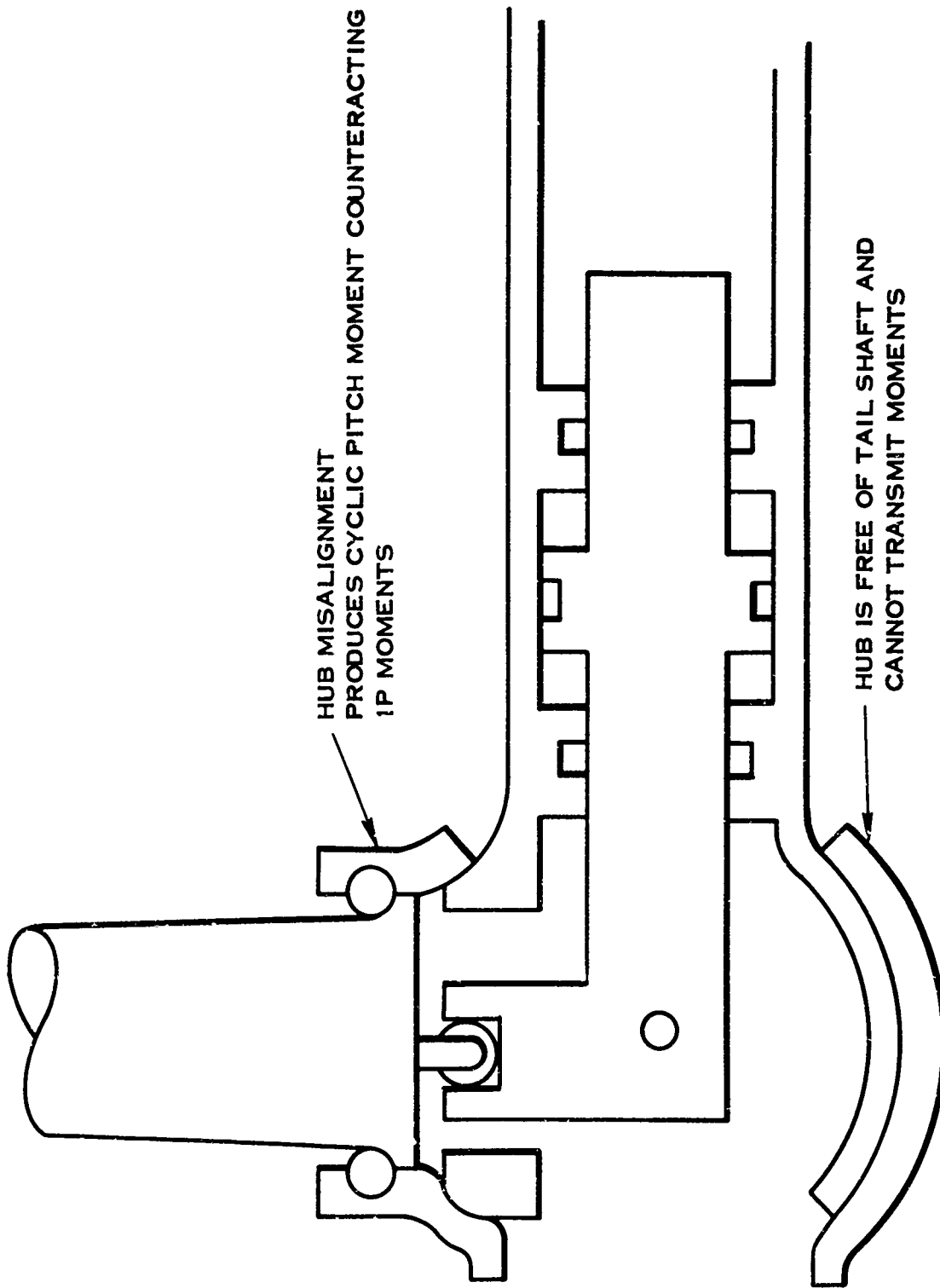


FIGURE 65. GIMBALED PROPELLER CONCEPT

Feathering of the propeller is initiated by rotating the feather valve. This action bypasses the governor output and directs supply oil to the beta valve actuator servo piston which moves the beta valve to increase pitch.

The beta control mode is accomplished mechanically and bypasses all the hydraulic functions of the control. This ensures additional propeller reliability by providing direct control of the beta valve with the input linkage. In cases where the hydraulic supply of the control has failed, the blade angle can be increased by activating the beta valve to correct an overspeed condition.

Hydromechanical Control

Figure 66 depicts the hydraulic schematic of the propeller control. It is similar to that used on the Hamilton Standard VC82S propeller system, in that it incorporates a mechanical lead network, but linkage and valving have been greatly simplified for this concept.

Redundant beta valves (distributor valve) in the propeller actuator are positioned by the control output. Failure of the actuator signal to reposition these valves will cause the propeller to lock pitch, as described previously.

Use of new concepts for the control (Figure 67), such as modular construction, hydraulic wiring, and miniaturization of components, yields large-percentage weight savings while increasing reliability and ease of field maintenance. "O" seals have been eliminated except for external sealing. Titanium is incorporated in place of steel wherever possible throughout the control to take advantage of titanium's inherent high strength-to-weight ratio and corrosion resistance.

One of the major weight reductions accomplished in the control is the elimination of the conventional forged or cast control housing, which has valve bores and drilled interconnecting passages. The new housing concept consists of an aluminum mounting plate of sandwich construction. Hydraulic tubing is integrally brazed between the plates of the housing and forms a light, rigid "wiring board" which distributes hydraulic flow to all the modular control units. The rear face of the mounting plate is used for mounting various components, and a "spider" structure is used for support of linkage. All units are mounted by studs and locknuts, thus eliminating lockwiring.

Sealing between modules and the control housing is performed by soft metal gaskets. To provide a known preload at the gasket interface, the mounting surface of the housing is slightly recessed except for small rings of material around the hydraulic line endings and studs.

A typical valve module is shown in Figure 68. It is comprised of a steel container,

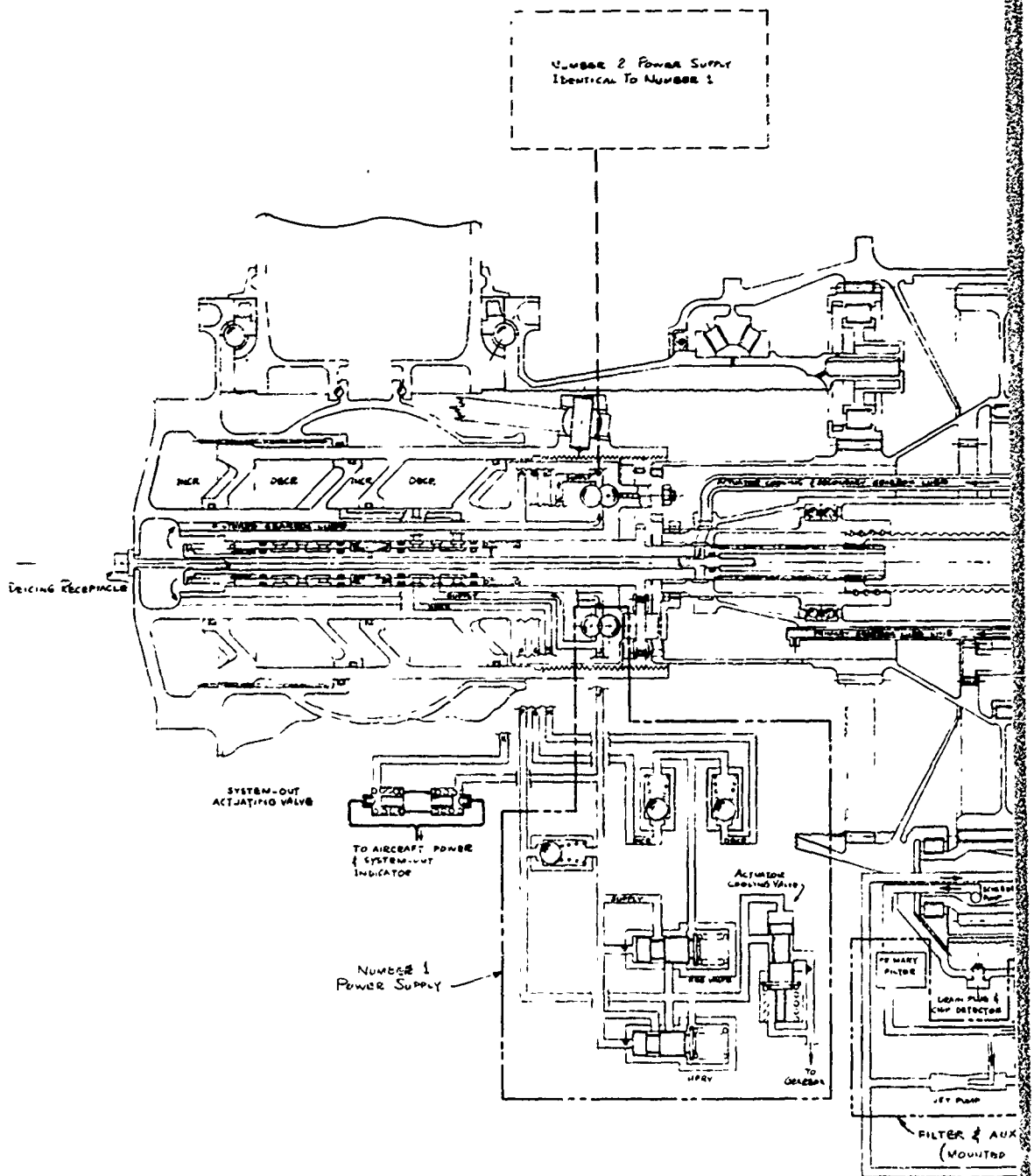
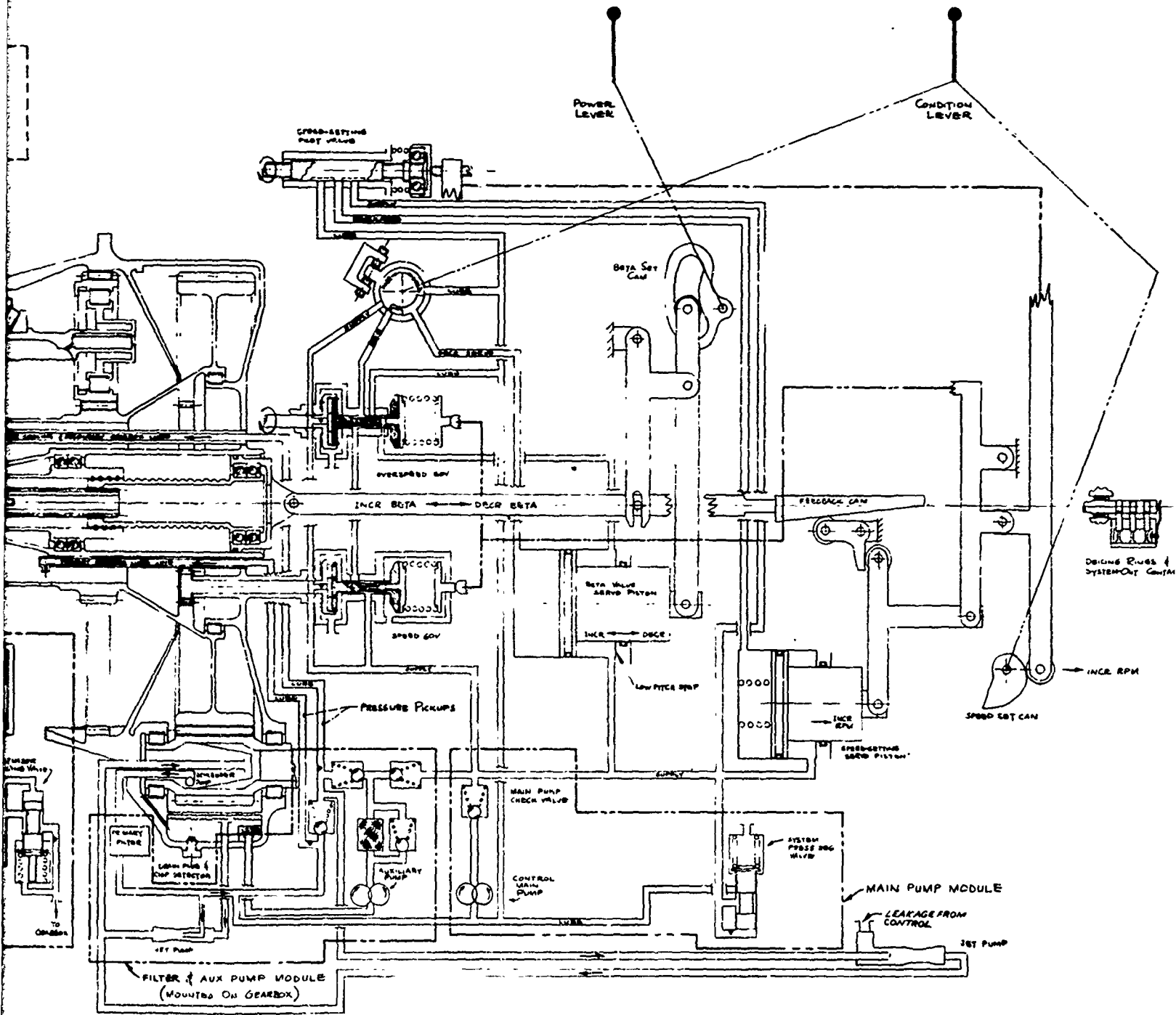


FIGURE 66. HYDROMECHANICAL PROPELLER CONTROL SCHEMATIC



PEPELLER

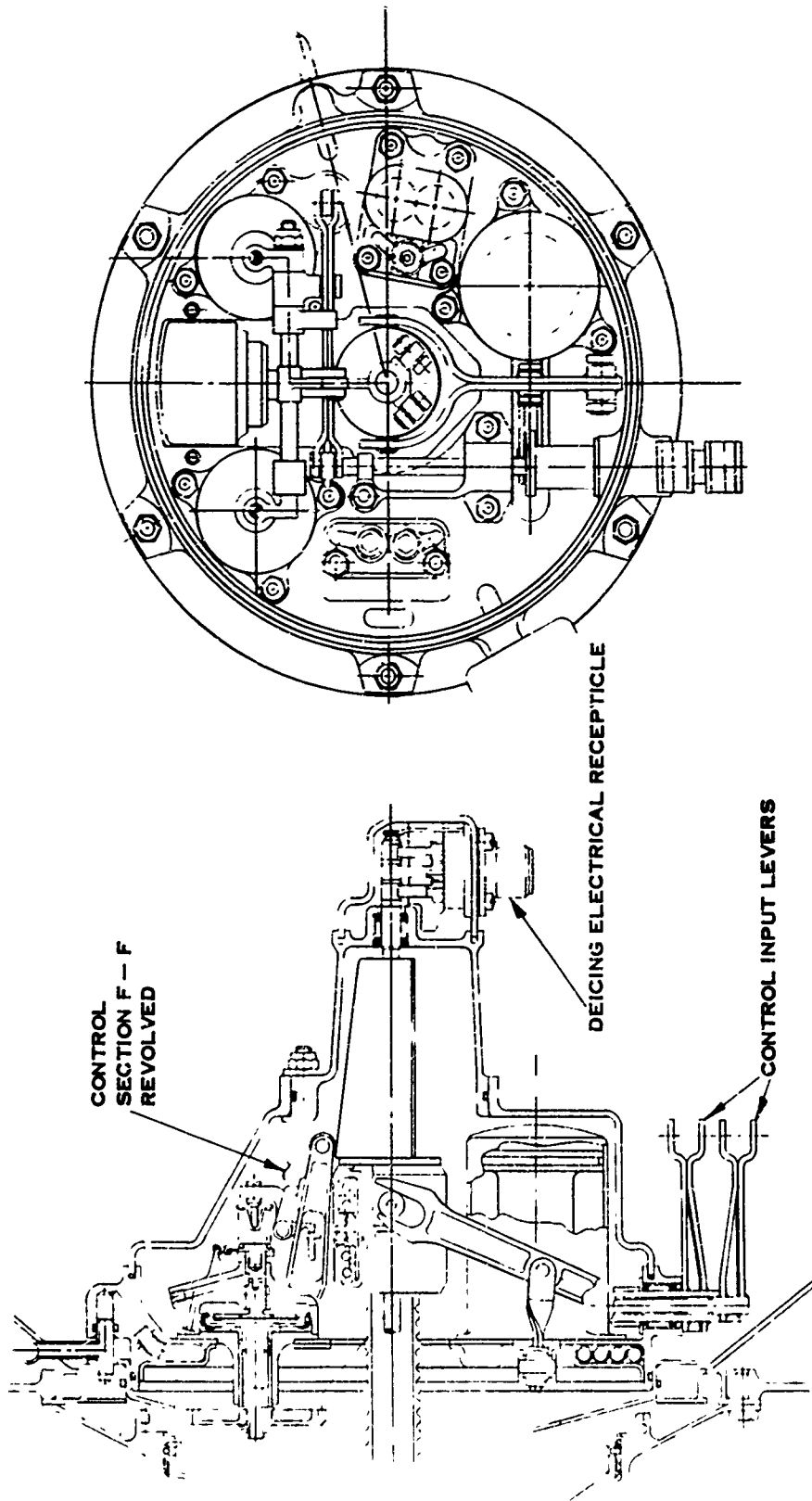


FIGURE 67. CONTROL ASSEMBLY

sleeves, and tubes joined by nickel brazing into one rigid assembly. Within the module container, hydraulic input and output lines are brazed to the container next to the stud locations to ensure adequate transfer of the stud loading to the sealing surfaces at the metal gasket interface. For redundant joint sealing and additional vibration damping, the modules would be encapsulated with a relatively low density, high-temperature epoxy compound (similar to Stycast 2662) with good strength and adherence characteristics.

Although the components within the modules are not intended to be line-replaceable units, all valves within a module could be disassembled and inspected by removing their sealed threaded plugs. The modules could be operated at temperature levels up to 400°F with the elimination of "O" seals. (Maximum oil temperature is 300°F.)

For the early 1970's, the material used for the module valves and tubing would be a combination of AISI 347, a carbon-stabilized stainless steel, and a nickel-alloy braze which allows liberal clearance gaps between parts for brazing.

During assembly and brazing, a ceramic fixture holds the sleeves in position. Brazing material is applied in a powder form over a dip coating of a volatile oil which vaporized during brazing. After brazing, the valve bores are sized to their finished diameters and are nitrided.

Work is currently in progress to obtain a satisfactory means for brazing titanium. Current brazing materials yield a brittle interface which affects the fatigue strength of the joints. Silver alloys are showing the greatest promise; however, at operating temperatures higher than 300°F, MIL-L-7808 oil breaks down, due to the catalytic action of silver. It is expected that significant advances in this regard can be made, such that, by 1975, titanium will eventually replace steel for the modules.

The main control pressure pump and valve module would be constructed in a manner similar to the module described above. The pump is a constant-displacement gear-type pump which is operated at approximately 15,000 rpm (at takeoff). This is a higher speed than has previously been used, and it will greatly reduce pump size and weight. Speeds of 15,000 rpm are considered to require only a small improvement in today's state of the art. For a constant pump output flow rate, increasing the speed allows tooth height and/or gear outside diameter to be reduced. Reducing these dimensions tends to offset the problem of filling the gear pump teeth cavities at high speeds, and it reduces the pump inlet pressure required for proper tooth filling. Should inlet pressurization cease, the pump is capable of operating at approximately 70% volumetric efficiency for several hours. However, cavitation would probably occur under this severe operating condition. Pressurization to 20 psi should ensure proper operation without the need to resort to additional measures such as helical gears. Pump gear centerlines would be oriented so that

by interchanging the drive gear and idler gear, a minimum of change would be required to accommodate propellers of opposite directions of rotation. Should the pump drive gear spline fail due to a jammed pump, a journal bearing is provided between the gear and the pump shaft to allow gear rotation without damage to the gearbox components.

A new concept for the propeller governor is shown on the control package. The new concept has improvements in simplicity, weight, and volume. Basically, the governor flyweights have been replaced by a rotating disk of oil behind an axially movable, double-layered, flexible metal diaphragm. Hydraulic force generated by the centrifugal force of the rotating oil is opposed by the conventional speeder spring and associated speed-setting linkage. The gear ratio between bull gear and governor drive allows the governor to be driven at approximately 15,000 rpm and ensures a small governor with large hydraulic force output. The lack of friction in converting from a rotating to an axial force by means of fluid pressure ensures excellent speed sensitivity and accuracy. A hydrostatic/hydrodynamic thrust bearing at the speeder spring end of the governor would be employed rather than the conventional high-speed ball bearing. An antitorque link connected to the stationary spring seat is used during governor startup to prevent spring windup before hydraulic pressure is established between the thrust bearing seats. When synchronizing and synchrophasing are required, the antitorque link is replaced by a lever which is positioned by the synchronizing control and applies a varying load input to the speeder spring for small speed corrections. Governor metering is accomplished with the conventional spool valve, but due to the elimination of "O" seals, it has a much smaller envelope.

Nonregulatory on-off hydraulic switching functions, such as the feather valve shown in Figure 66, have been incorporated into a rotary-type disk valve. A small center disk of approximately 0.5 in. outside diameter surrounds the shaft, and it is sandwiched between two end plates. Fluid metering is accomplished by relative rotation between the shaft and the disk. An adjustment screw on the outer disk allows adjustment of the valve. This type of valve greatly reduces size compared to the conventional spool type and also eliminates "O" seals.

Shafting, feedback cam roller supports, lever pivots, control cover, and brush block are supported and positioned by a lightweight aluminum spider housing mounted to the control mounting plate by self-locking nuts and studs. Included in the control at the lower aft part of the spider housing is a jet pump and check valve module. Normal component and gearcase leakage is scavenged and returned to the main gearcase in either the VTOL or the cruise attitude.

Input levers and control linkage are primarily constructed of sheet metal and are laminated or doubled for redundancy. Input levers are welded to the coaxial shafts to form an integral, strong, lightweight configuration. For reliability, pins to

support linkage bearings will be electron-beam welded to the levers or will be trapped by adjacent hardware, thus eliminating loose pieces such as clevis pins, washers, and cotter pins.

An axial-type feedback bar cam was selected in preference to a rotary type for simplicity and ease of control assembly and disassembly.

By utilizing the center area along the propeller axis, electrical wiring for propeller deicing can be enclosed within a hollow tube which supports the wires from the rear of the control package to the front of the propeller. The rear end of the tube attaches to small-diameter beryllium-copper sliprings contained within a sealed rear slip-ring brush block for redundancy. A small carbon button at the centerline of the aft end of the tube makes contact with a flexible spring to transmit the system-out signal. Assembly of the slipring tube can be performed from the forward end of the propeller. Inspection of the sliprings and brush block assembly can be accomplished, without removing the control, by removing three self-locking nuts that retain the brush block assembly.

The control cover is fabricated from fiberglass reinforced plastic. The control cover can be moved rearward over the brush block assembly by removing the cover self-locking nuts to inspect the internal parts of the control without removing the propeller system from the engine.

Electromechanical Control

Although an electrohydraulic propeller control was not the selected control for use with the study propeller, a system has been conceived for comparison. The control can be a relatively small, lightweight unit attached to the aft end of the gearbox, and it can produce a mechanical output which actuates the beta valves in the propeller pitch change hydraulic actuator.

The control system would comprise three basic elements: sensors, electronics package (including power generation, computation and output power circuits), and output electromechanical coupler (Figure 69). The speed sensor, power generator, and computation would be contained in a single unit mounted on the aft part of the propeller gearbox. Two separate channels would be utilized, with the power generator, computer, lever position sensor, and motor electrical windings repeated in each channel. A comparator in the electronic package will permit both channels to function when their signals agree. When they do not, a comparison is made with the last control signal (held in storage), and the channel whose signal is closest to the last signal is activated and the other channel is deactivated.

The position sensors for power lever and condition lever would be located at the control for maximum reliability and would connect to the electronic package with

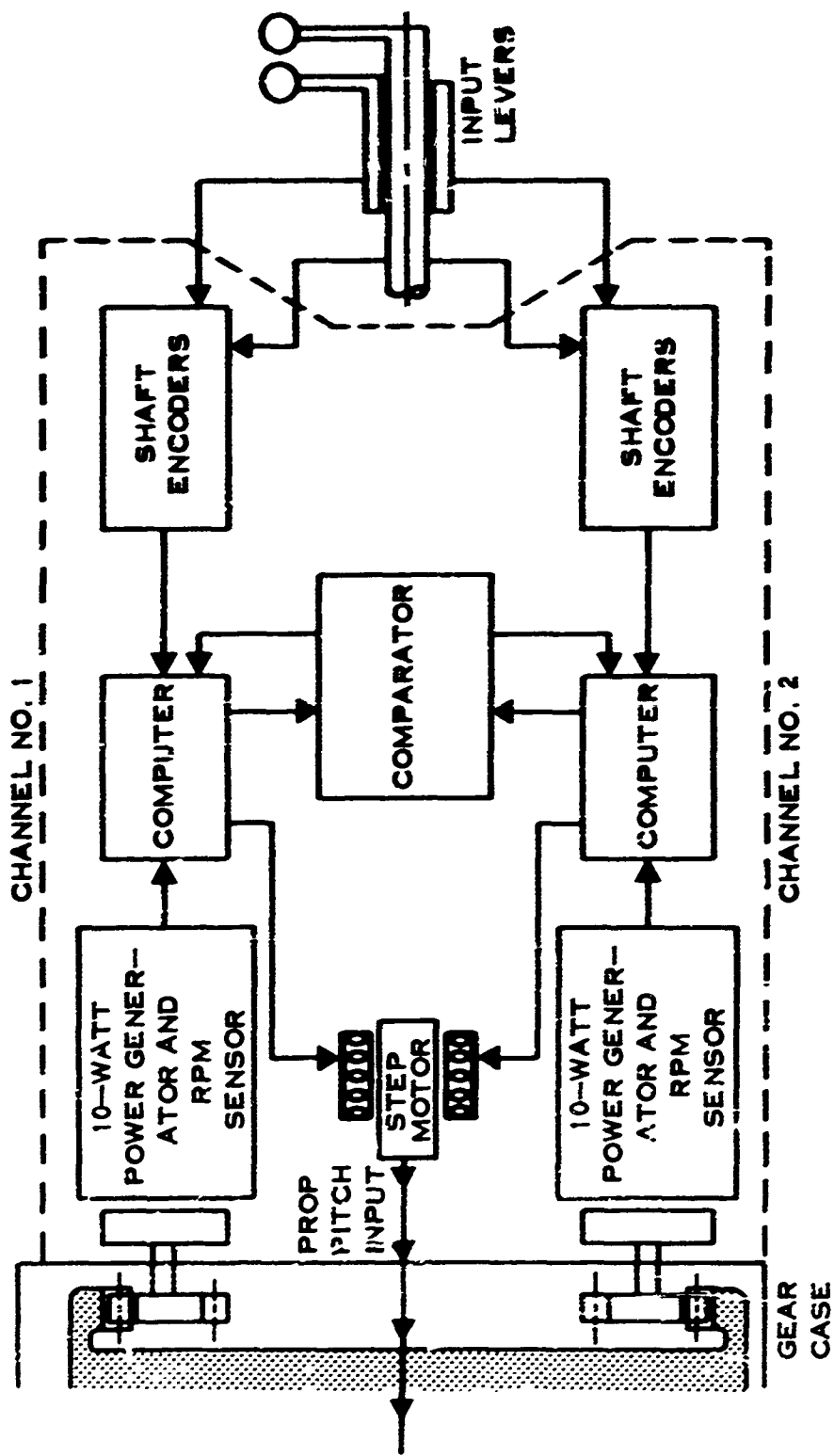


FIGURE 69. ELECTROMECHANICAL CONTROL CONCEPT

redundant permanent-type wiring to avoid receptacles. It is anticipated that the entire control could be line-replaced and that any component replacement wiring could be done at a depot level maintenance facility.

Sensors and Power Generator

Propeller speed, speed lever command, and condition lever command must be sensed. The propeller speed would be sensed by a pulse generator driven by the propeller rotation but mounted to the nonrotating portion of the propeller system. Sufficient power would be extracted from the pulses generated for speed sensing to provide the low wattage required for the computer plus approximately 10 watts of pulse power required for the step motor. Two redundant pulse generators provide redundant power, speed, and phase signals to two completely separate electronic channels.

Sensors for the position of power lever and condition lever would be two solid-state optical encoders mounted in an encapsulated package, and solid-state low-speed multiplexers would sequentially sample the encoders and pass information through redundant, physically isolated paths to the computer.

Computer

The computer would be entirely contained in the rear portion of the speed sensor package and would comprise 500-1000 integrated circuits. All signal conversion, power source regulation, computation, and output circuits would be in the assembly.

Electromechanical Coupler

The output coupler will comprise a stepping motor and mechanical positioner located in the stationary part of the propeller. The coupler drives the input to the propeller in the same fashion as in the hydromechanical system. Its electrical windings would be made redundant and would be driven from the redundant computers. Circuit magnetic bias in the motor will lock the rotor with a torque equal to rated torque except when the motor is stepping. This provides a fixed input characteristic to the hydromechanical propeller in the event of an "open" control failure.

Environmental Tolerance

Vibration, temperature, and RFI (Radio Frequency Interference) characteristics present problems for electrical equipment in a combat powerplant environment. The use of solid-state circuits and completely encapsulated wiring has been demonstrated to be adequate for vibration in powerplant environments, and the motor would employ potted windings, no brushes, and no connectors to assure vibration tolerance.

The temperature of the solid-state electronics would be limited by their insulation from the surrounding parts of the stationary propeller and by cooling air provided from the gearcase oil cooler through a small air duct. This should limit the maximum temperature of the computer to less than 200°F. Temperature is not a problem for the output coupler or the input sensors. RFI susceptibility would be controlled by using digital transmission of a command signal and by limiting the bandwidth of signals. RFI generator would be controlled by eliminating the fast rise times of high-power signals.

Fail-Safe Features

Fail-safe features would be required, such that no failure would jeopardize the safety of the aircraft and its passengers.

The completely redundant dualized system provides inherent ability to handle any "open" failure, and a comparator circuit is used to provide protection from short-circuit failures.

Speed condition commands would be stored in the computer. As these sensors were sampled, the new commands from the redundant sensors would be compared by the computer. In the event of disagreement, the value closest to the previous command would be selected, and the other system would be shut down.

The comparator has the ability to detect the rise time of the signals and to shut down either system when the signal rise is essentially instantaneous, as is the case of an electrical failure.

Reliability

The low reliability level of a electromechanical control in comparison to a hydro-mechanical control is a major problem. The improvement of the electromechanical control reliability level requires the elimination of critical fits and motions, the use of components of high inherent reliability, the employment of conservative design, and the use of redundancy in critical components. The electromechanical control does have the advantage of few moving parts (and those that do move do so on a very low duty cycle) and therefore, failures accentuated by wear should not be present. However, the probability of initial failures (infant mortality) in the electrical components is high, and therefore a "burn in" period of operation after manufacture would also be mandatory to provide a reasonable level of reliability.

Electronic Control Conclusions

Electronic controls are receiving considerable emphasis for engine fuel controls at Hamilton Standard Division and elsewhere in industry. Electronics is an area

of tremendous growth, and the use of electronics for specific functions should continue to be considered where their unique advantages of microminiaturized computing ability, ease of readout, and integration into other electronic circuits (such as stabilization or integrated data systems) warrant their use. It is estimated, however, that in the 1970's, electronics for propeller controls will continue to show a negligible advantage in weight and volume and a considerably lower overall reliability. (Mission reliability can be markedly improved by redundant circuitry, but it is estimated that unit reliability in the environment of a propeller control will not approach that of a hydromechanical device in this time period).

Fluidic Control

Fluidic systems have the potential for providing improvements in reliability, cost, weight, and frequency response over conventional hydromechanical controls and therefore warrant some study. The major disadvantage of fluidic systems, however, is the greater standby power consumption required over hydromechanical systems. This limits their use in providing large power actuation functions. It does not appear desirable, therefore, to replace the propeller actuator and associated hydraulic power pressure regulators with fluidic components.

It does appear that even further improvements over miniaturized hydromechanical controls in volume and weight could be realized by replacing the lead network (and possibly the governor) with fluidic components with at least equal reliability to hydromechanical components, although this change would not have a major impact on the overall system weight or volume. It is recommended that additional studies in this area be pursued.

Synchrophasing

Synchronization and synchrophasing of engines, if desired, could be accomplished with a fluidic system as shown in Figure 70 by biasing the slave engine governor through a small lever and bellows assembly attached to the spring seat. A centrally located master fluidic control, supplied by air pressure, compares the speeds of the master and slave engines and by means of a digital-to-analog converter, modifies pressure to the slave governor bellows to effect proper slave synchronization and synchrophasing. This concept has been laboratory tested at the UAC Research Labs with excellent results.

DEICING SYSTEM

Deicing power for the two propellers is assumed to be supplied from one phase of the aircraft main electrical system. The higher the voltage, the lower would be the current requirement for the deicing system. Therefore, a 208-vac supply is recommended. The blades would be deiced from the spinner radially to

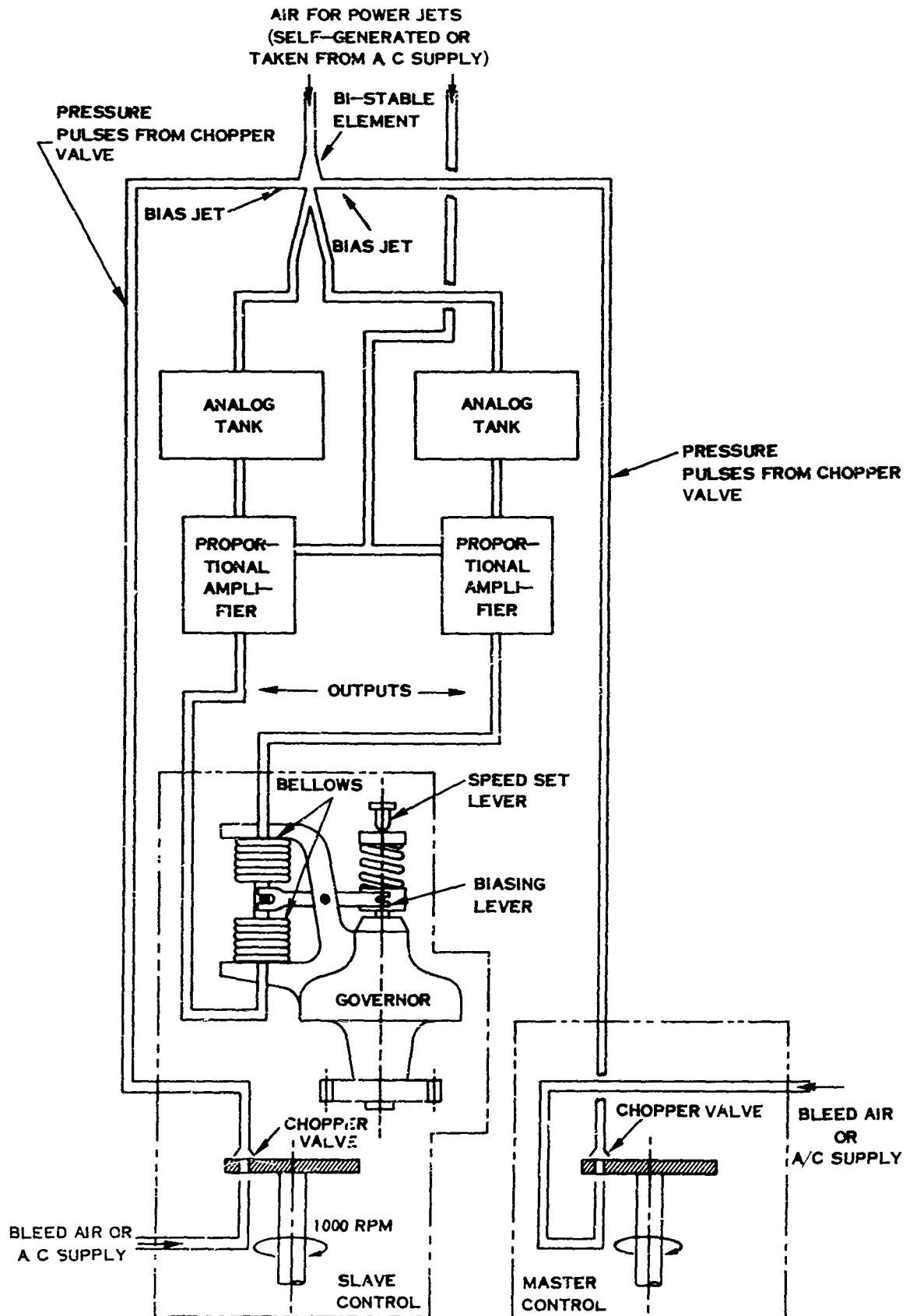


FIGURE 70. SYNCHROPHASING SCHEMATIC

approximately 23% of the blade radius, and from the blade leading edge back to 20% blade chord. The average watt density would be 6 watts per square in.

On this basis, each propeller would require 2076 watts for blade heating. A typical blade heater is shown in Figure 71.

Should spinner deicing be required, another 2076 watts would be required for heating the spinner. The spinner heated area extends from the tip to the 12-in. station with power densities varying from 9.0 to 3.5 watts per square inch (Figure 71). A thermostat is located near the spinner and blade heaters to switch off the current in the event of an overtemperature condition at the heater.

The power requirements for each propeller are summarized in Table XIV. Power would be cycled by a timer so that power would be supplied to only one propeller's set of blades or spinner at any given time. The cyclic time would be 30 sec. on and 90 seconds off. The power would be supplied to the spinner (#1 prop) for 30 sec., then to the blades (#1 prop), then spinner (#2 prop), then blades (#2 prop); then repeat cycle. In this manner, the total deicing power requirement is 2076 watts.

The timer would be powered by the aircraft 28-vac system. The timer activates the deicer relay to a specified propeller heater zone and current flows through a brush block slipring assembly mounted on the control housing. Three #14 or #16 Teflon-coated lead wires (2 power and 1 ground) conduct the current to the spring loaded electrical contacts mounted on the inner spinner surface adjacent to the blade shanks. The current is then conducted through thermostats to the spinner and blade heaters. The spinner-to-actuator contact will be by means of spring-loaded contacts to provide for quick spinner removal. The electrical schematic shown in the next section includes the above deicing system.

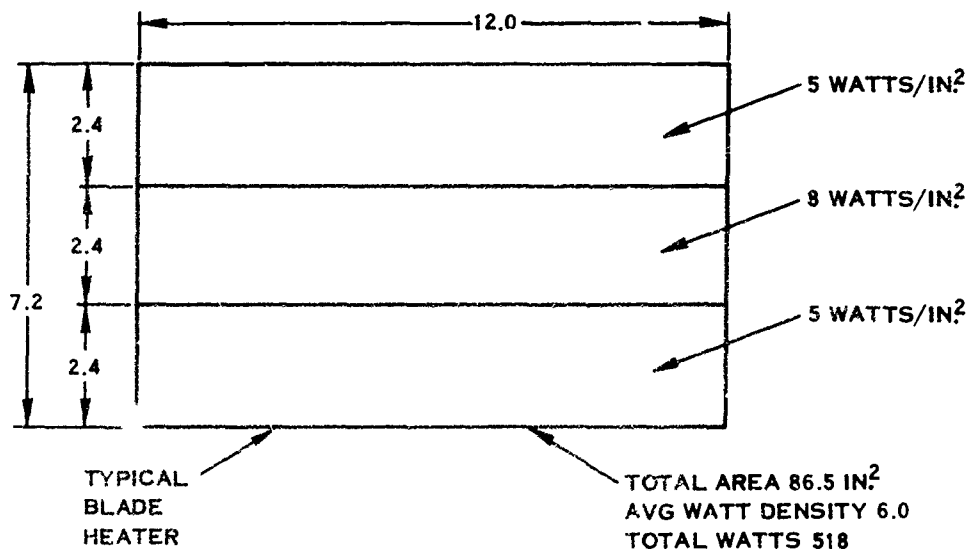
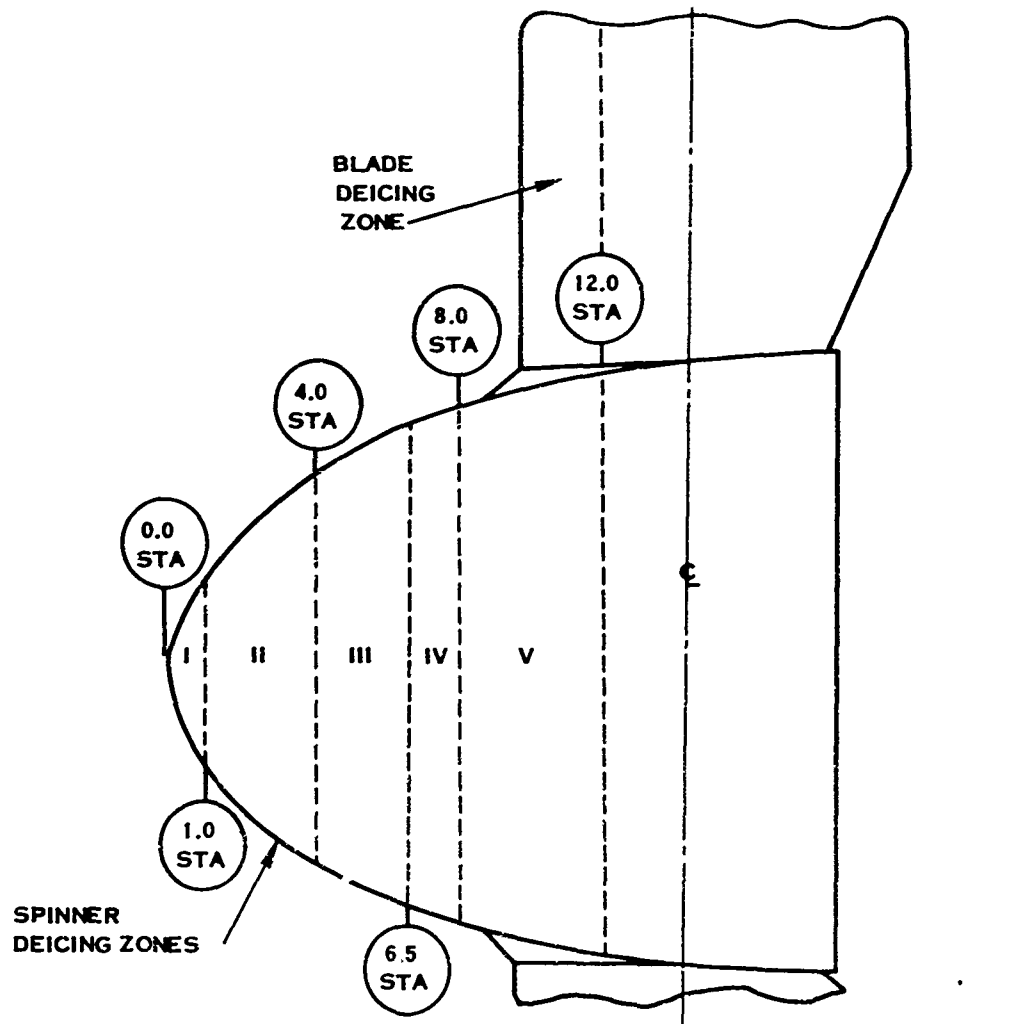


FIGURE 71. BLADE AND SPINNER DEICING ZONES

TABLE XIV. DEICING POWER REQUIREMENTS			
	AREA (SQ IN.)	WATT DENSITY (WATTS/IN.²)	POWER (WATTS)
BLADES	346	6.0	2076
SPINNER ZONES			
I	3	9.0	27
II	78	7.7	604
III	76	5.2	396
IV	81	5.0	405
V	184	3.5	644
TOTAL SPINNER	422	4.9	2076

SYSTEM DESIGN

The previous section described the various concepts and materials studied for use in the integral gearbox (IGB) propeller system components. The concepts and materials found to be feasible and to offer the best potential for weight reduction were defined. This section presents three different propeller system designs using the previously optimized components. The three specific system designs are:

Collective Pitch IGB Propeller System With Cross-Shaft Drive
Cyclic Pitch IGB Propeller System With Cross-Shaft Drive
Collective Pitch IGB Propeller System Without Cross-Shaft Drive

DESCRIPTION

The major components of the three system designs presented are described in the following pages.

Integral Gearbox Assembly

The integral gearbox assembly will be identical for both propeller systems used with cross shafting, and only minor changes are made to the gearbox used with the non-cross-shafted propeller system.

The primary requirements of the gear train are that it transmit 2000 hp through a 20:1 speed reduction with a maximum desired 1% loss and that it incorporate provisions for opposite rotation.

The gear train (Figure 72) is a two-stage configuration with a pinion-bull gear train driving an epicyclic (planetary) gear train. The engine input power is transmitted to the driving inner sleeve of the overrunning clutch by a splined connection. This spline allows for small eccentricities and deflections that change the location of the engine output shaft and the gearcase input. The clutch has been integrated within the first-stage pinion gear, thereby eliminating the need for separate clutch mounting bearings and additional housing. The overrunning clutch is a spring-type clutch that drives a steel cylinder insert in the pinion gear rim. The sleeve isolates the high bursting loads of the driving spring from the pinion gear rim loading. A spline connects the sleeve to the pinion gear. Lubrication of the clutch area is achieved by a spray bar depositing oil in an annulus that causes the input spline, output splines, and clutch spring to be submerged in oil.

The pinion gear meshes either with an idler gear for the left-hand gearbox rotation configuration or directly with the bull gear for the right-hand rotation configuration. The first-stage gear ratio is 5.22:1.

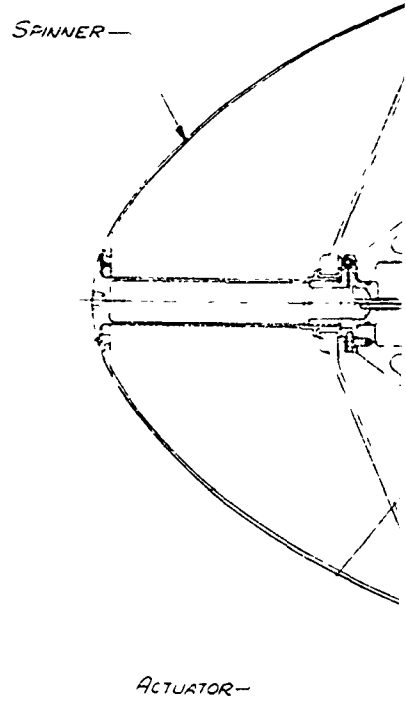
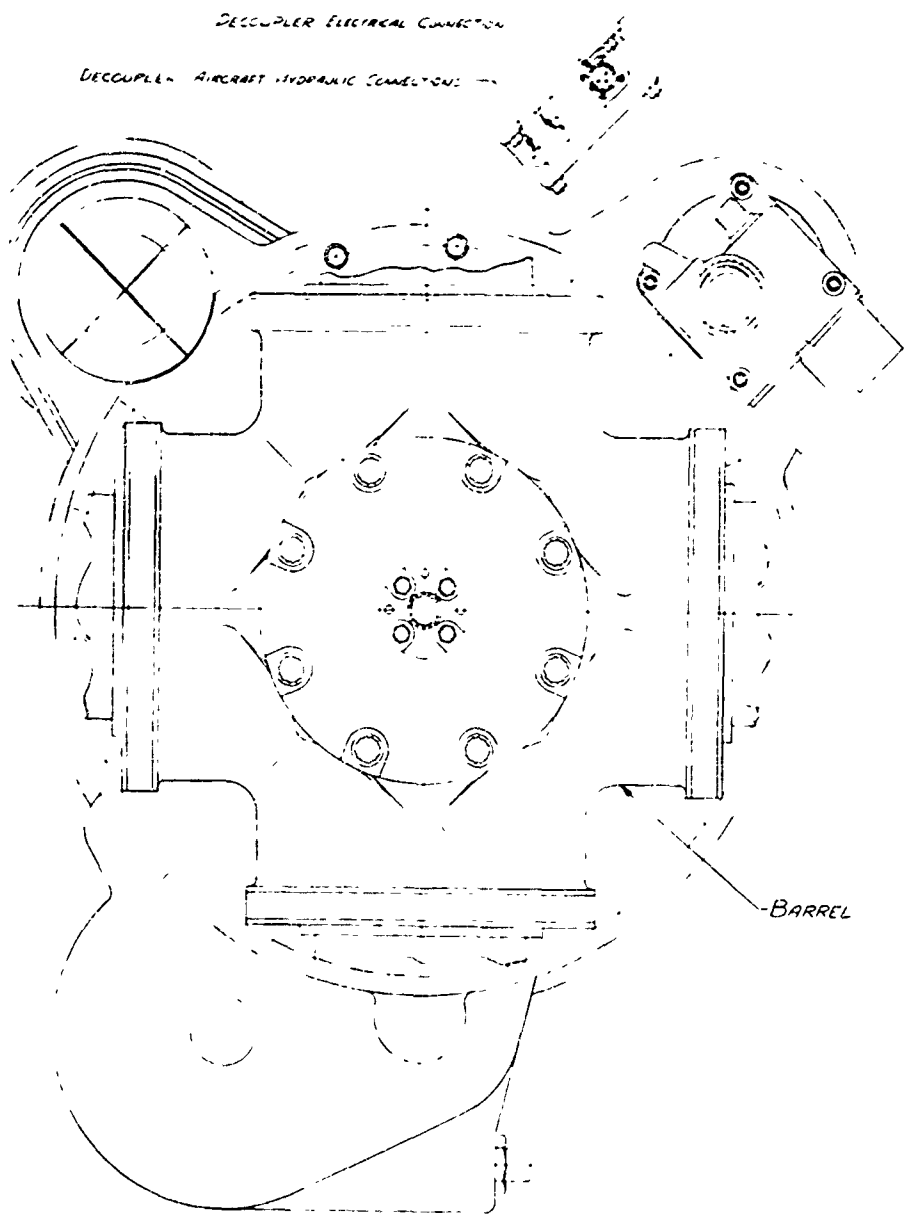
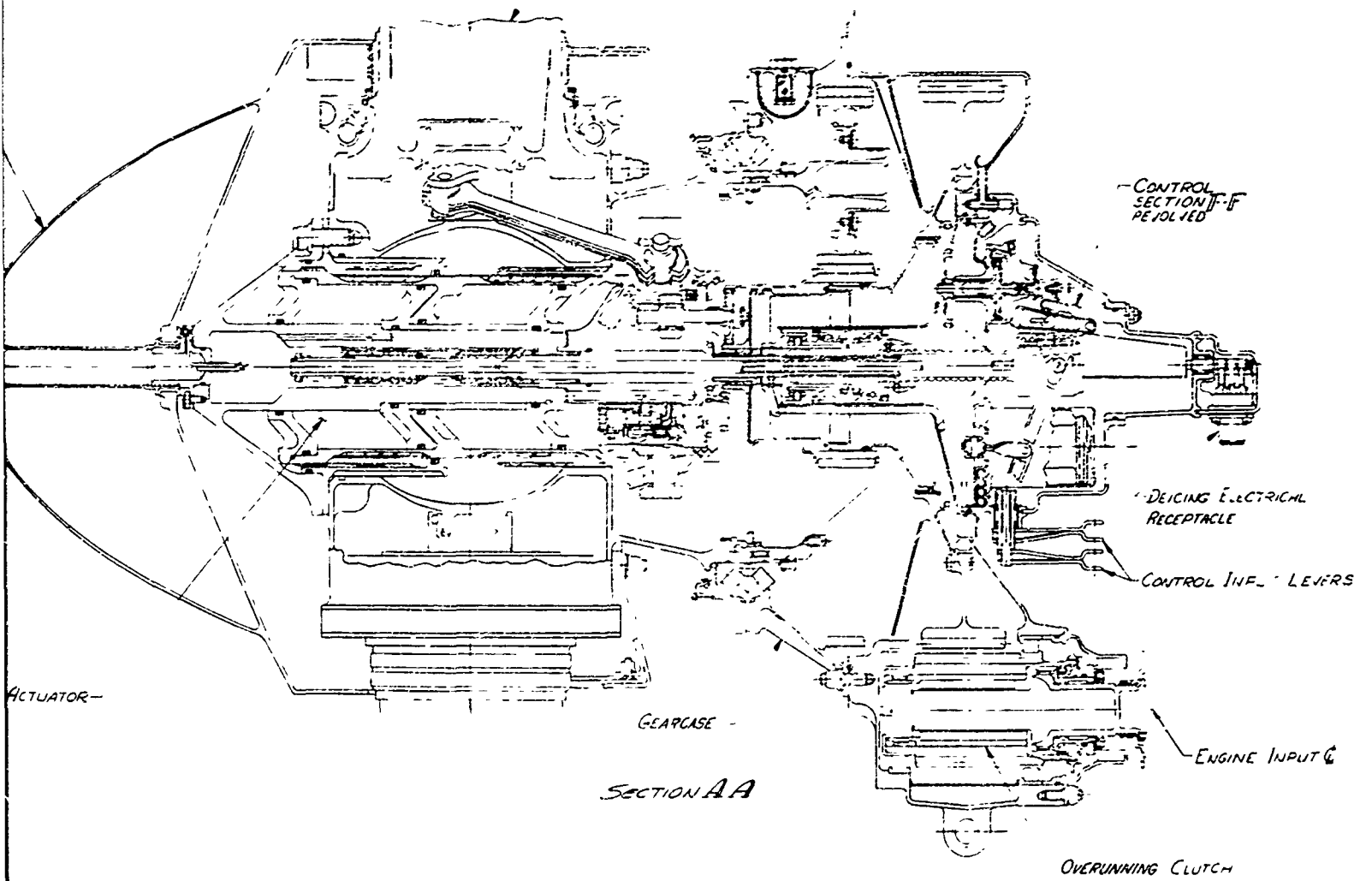


FIGURE 72. COLLECTIVE PITCH IGB PROPELLER SYSTEM WITH CROSS-SHAFT DRIVE

BLADE

← FACELLE MOUNTING SURFACE



CONTROL SECTION J-F REWIRED

DEICING ELECTRICAL RECEPTACLE

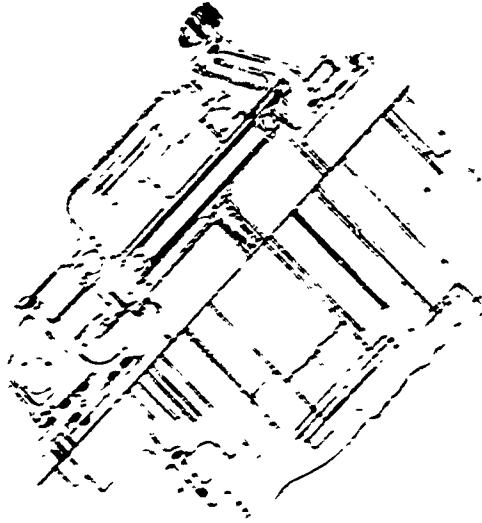
CONTROL INFL. LEVERS

ENGINE INPUT

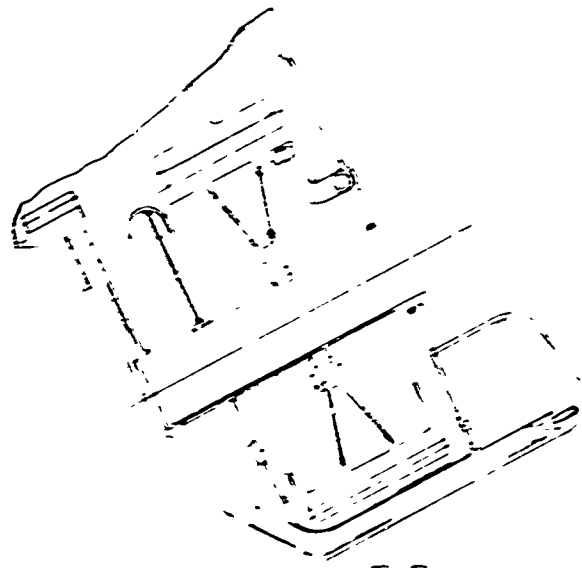
GEARCASE

SECTION AA

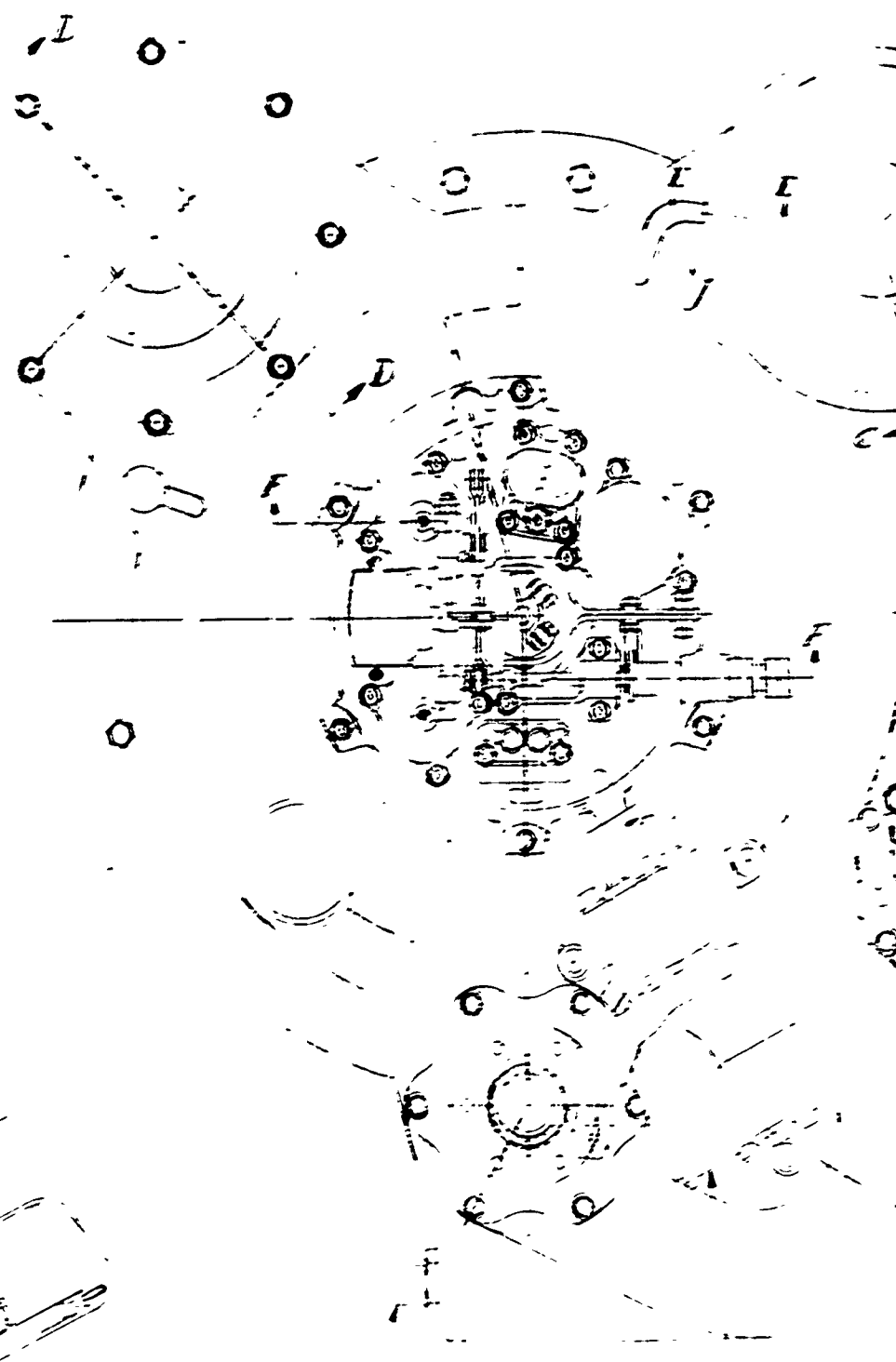
OVERRUNNING CLUTCH



SECTION D-D
CROSS-SHAFT AND DECOUPLER

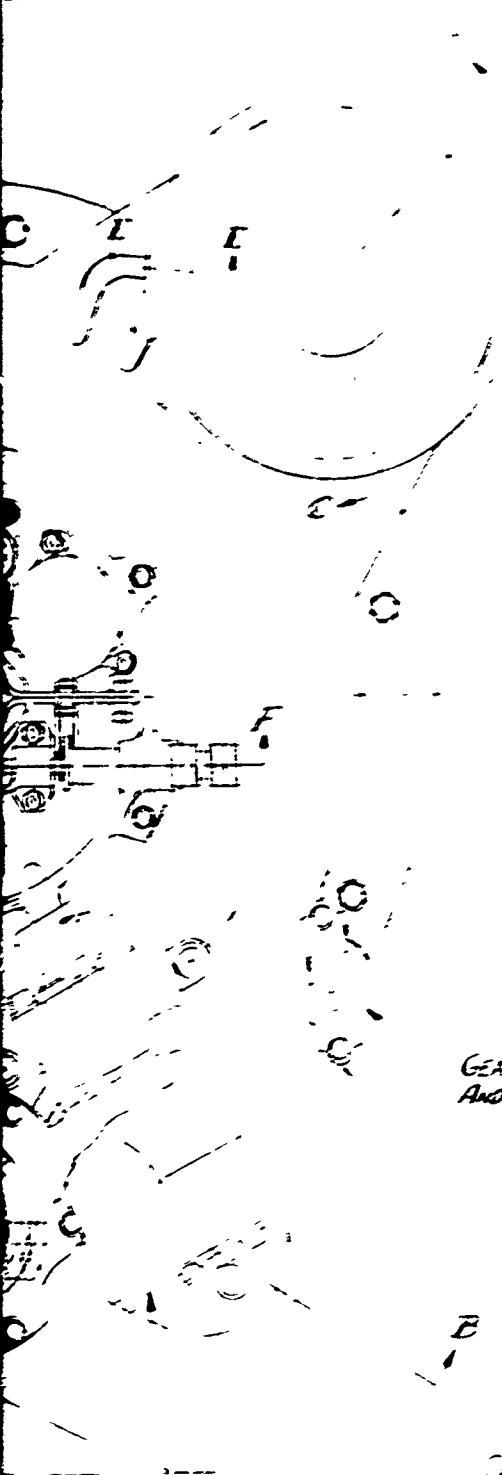


SECTION E-E
LEFT-HAND IDLER

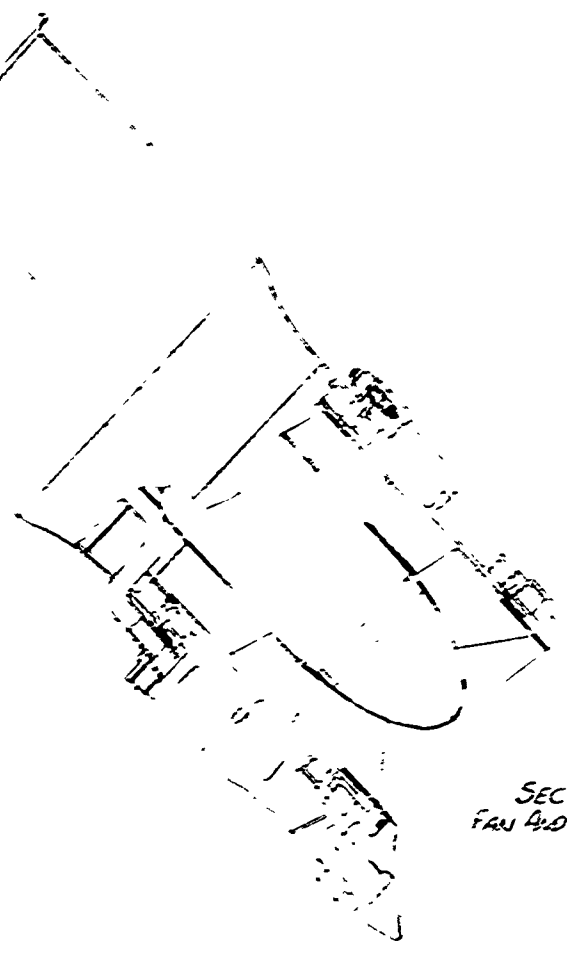


THE DETECTOR
AND DOOR PINS

FIGURE 72(CONT).



GEARCASE FILTER
AND INDICATOR



SECTION E-C
FAN AND HEAT EXCHANGER

FIG. 2. P. 10. 4. 10. 10. 10. 10. 10. 10.

The idler and the bull gears are mounted on single bearings to permit the gears to adjust their angular alignment automatically and to ensure a more uniform load distribution along the tooth profile. The idler gear mounting shaft is used as the inner race of the idler mounting bearing, thereby reducing weight and simplifying the assembly procedure. The position of the idler gear center with respect to the pinion and bull gear centers is selected so that the summation of the gear loads at the two meshes tends to make them cancel each other, thus reducing the required bearing capacity and weight.

A doweled and bolted flange connection is utilized for transmitting the torque from the bull gear to the sun gear quill spline to allow for assembly. The splined titanium quill shaft allows the sun gear to adjust its angular and radial position as it meshes with the planet gears. The second stage has a 3.84:1 gear ratio.

The planet gears are mounted on a planet carrier with spokes designed to deflect a sufficient amount so that there is essentially equal torque sharing among the five planets. In addition to a net lateral deflection, the spokes are designed so that angular deflections are cancelled, leaving the net slope of the planet bearing unchanged. This ensures that the planet loads will only produce deflections of the spokes in such a manner that the planet gear is not misaligned.

The selection of titanium material for the gearcase as well as for the gears virtually eliminates the effect of thermal expansion on gear center distance. This also permits the planetary ring gear to be made an integral part of the front housing.

The use of the large-diameter tailshaft enables the planet carrier ring structure to mate directly with the tailshaft, close to the point of loading on the planets. The moments which must be reacted by the ring are thereby reduced. The placement of the carrier-tailshaft spline connection beneath the tailshaft bearings has the additional advantage of increasing the stiffness of that section. The planet carrier is mechanically held to the propeller tailshaft by a large spanner nut, and is locked in position by a splined lock cup.

The propeller tailshaft mounting concept selected for the system was the duplexed tapered roller bearing configuration. In addition to the weight saving, this design has a larger area available at the rear of the actuator which is used to advantage in the cyclic pitch design.

External sealing is accomplished by using carbon face seals for the high-speed input shaft, cross-shaft, and fan shafts and a lip seal at the low-speed propeller tailshaft. The lip seal may be removed for replacement without disassembly of the propeller by removing the front housing ring and by cutting the seal. A split lip seal is used for replacement until the propeller is overhauled. This concept is presently being used on the AH-56A propeller system.

For cruise operation of a cross-shafted propeller system, a decoupler has been included in the system in order to feather the propeller. To actuate the decoupler mechanism for either decoupling or recoupling in flight, two solenoid valves using aircraft hydraulic supply pressure and a speed indicator with a coupler control are utilized (Figure 72). A signal from the cockpit to couple the cross-shaft is transmitted to the speed indicator and coupling control. Here, the speed of the cross-shaft is compared to the speed of the cross-shaft drive gear. When the speeds are equal, the signal is then transmitted to a solenoid valve. The solenoid valve then allows aircraft hydraulic pressure to enter into a servo piston. The movement of the piston unlocks the moveable jaw member by physically disengaging it from a detent; then continued movement engages the teeth of the jaws and the moveable jaw member is locked in the engaged position by a detent. For decoupling, a second solenoid valve is used, which, when actuated, allows aircraft hydraulics to flow into the opposite side of the servo piston and to force the jaws to disengage. The use of the servo system ensures rapid engagement and disengagement of the coupling.

Lubrication of the decoupler jaw teeth, splines, and inner bearings is accomplished by incorporating dams and submerging these parts in oil. For the sizing of the cross-shaft gear and decoupler system, the torque capacity was based on transmitting one-half engine power at a cross-shaft speed equal to one-half engine rpm.

The right-hand version of the gearbox assembly will be identical to the left-hand configuration shown in Figure 72 except in the following areas: (1) the pinion gear center location is changed, which brings the pinion into mesh with the bull gear; (2) the idler gear is retained to drive the pumping system, but its center is also changed so that it meshes only with the pinion gear, and its face width is decreased to reduce weight.

Based on test programs currently being conducted by bearing manufacturers on the use of Crucible 52 CB bearing steel material, the bearings for this study were designed for an AFBMA air-melt-calculated B_{10} life of 600 hr. A conservative factor of 5 was applied to the life calculation to account for the increased life obtainable with these advanced bearing materials, which would result in an expected B_{10} life of at least 3000 hr for the bearings.

Integration of the fan and heat exchanger into the gearcase has actually increased the weight usually furnished by the propeller manufacturer, but it has reduced the weight of the total propulsion system. The air inlet ducting to the fan has been eliminated, and the use of the axial flow fan allows the heat exchanger to have a smaller volume.

The proposed pumping and scavenging systems shown for this gearbox design have fewer moving parts and are lighter than the constant-displacement gear pumps

presently in wide use. The scavenged lube oil is supplied to the rotating idler gear internal annulus. The rotation of the gear provides a centrifugal field that centrifuges the oil from the scavenged air-oil mixture which, because of the almost immediate air-oil separation, eliminates the need for large external oil tanks presently in use. The rotating gear is also used as a centrifugal pump to provide lube system pressure and flow. A portion of the pump flow is diverted to a jet pump located in the wet sump area to provide scavenging. The scavenged discharge from the jet pump flows into the rotating idler gear. Initial operation of the pump is accomplished by having the pump area flooded when the system is shut down.

The forward and rear gearbox housings are joined at a bolted flange connection. This same flange would be designed to be a mounting ring for attaching the propeller system to the aircraft nacelle structure. The cross-shaft power takeoff and cooling fan are positioned 45 deg from a vertical plane in order to reduce the overall gearcase height and nacelle size. A preliminary nacelle layout is shown in Figure 73.

The integral gearbox with cross-shaft drive described above can be used with either the propeller providing collective pitch change or the propeller providing cyclic pitch (Figures 72 and 74). For aircraft installations where cross shafting is not required, the only change to the integral gearbox is to remove the cross-shaft drive gear and decoupler and to remove the provisions for these in the housing (Figure 75).

Propeller Assembly

The propeller assembly consists of four major components: blades, barrel, pitch change actuator, and spinner.

Significant reductions in blade weights primarily due to using advanced materials for the blade spar have been projected in a previous section. Since the blade weight imposes the main sizing requirements for the barrel and actuator, these components will also possibly be substantially lighter.

The spar made of boron filaments in an aluminum matrix has been shown to offer the highest potential for future weight reduction, and that is the blade spar specifically shown in the drawings of the system design (Figure 72 through 75).

A titanium spar also offers a significant improvement in blade weight over that of the steel spar blade. The titanium spar is presently being developed and could feasibly be used in the next-generation V/STOL propellers. The only modification required to the design shown in order to substitute a titanium spar for the boron spar, would be to make the titanium blade retention bearing race, which is shown attached to the boron spar, integral with the titanium spar. Both blade spars would be covered with the airfoil-shaped fiberglass shell.

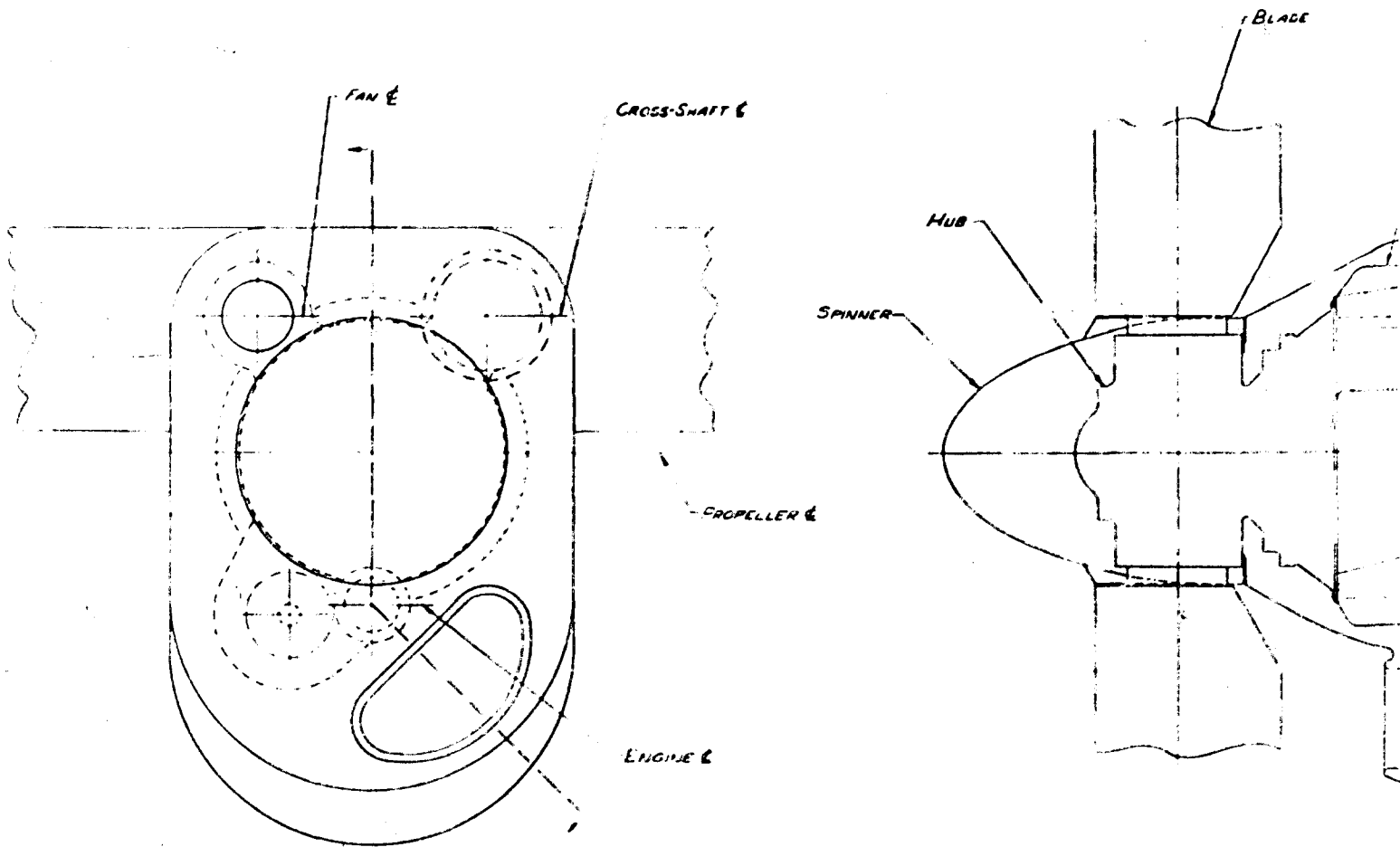


FIGURE 73. PRELIMINARY NACELLE LAYOUT

BLADE

GEAR CASE

DECOUPLER

PROPELLER MOUNT

HEAT EXCHANGER

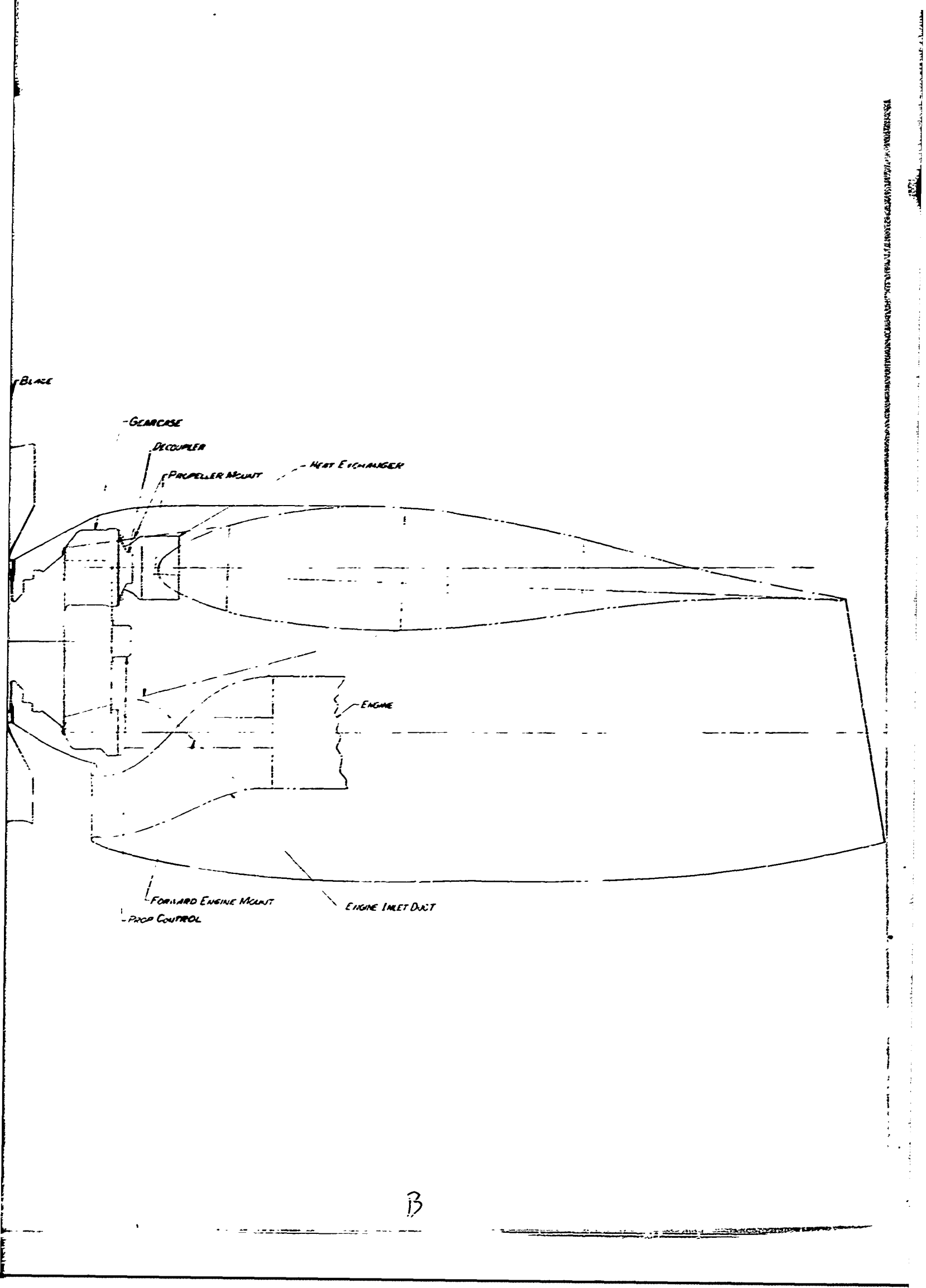
ENGINE

FORWARD ENGINE MOUNT

PROP CONTROL

ENGINE INLET DUCT

B



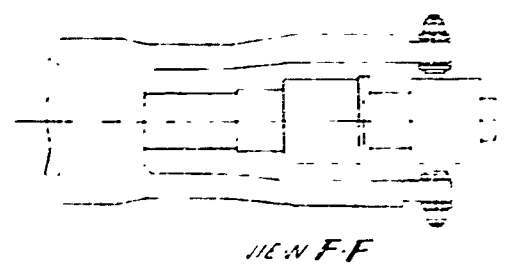
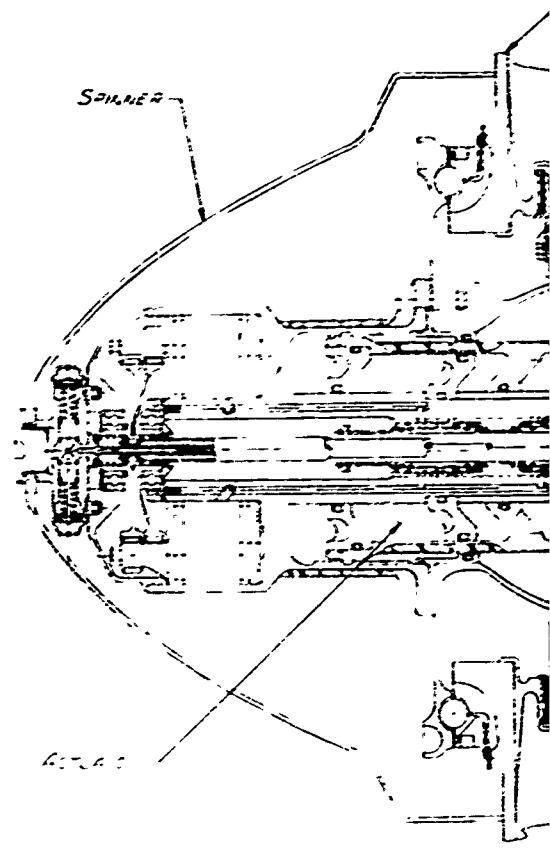
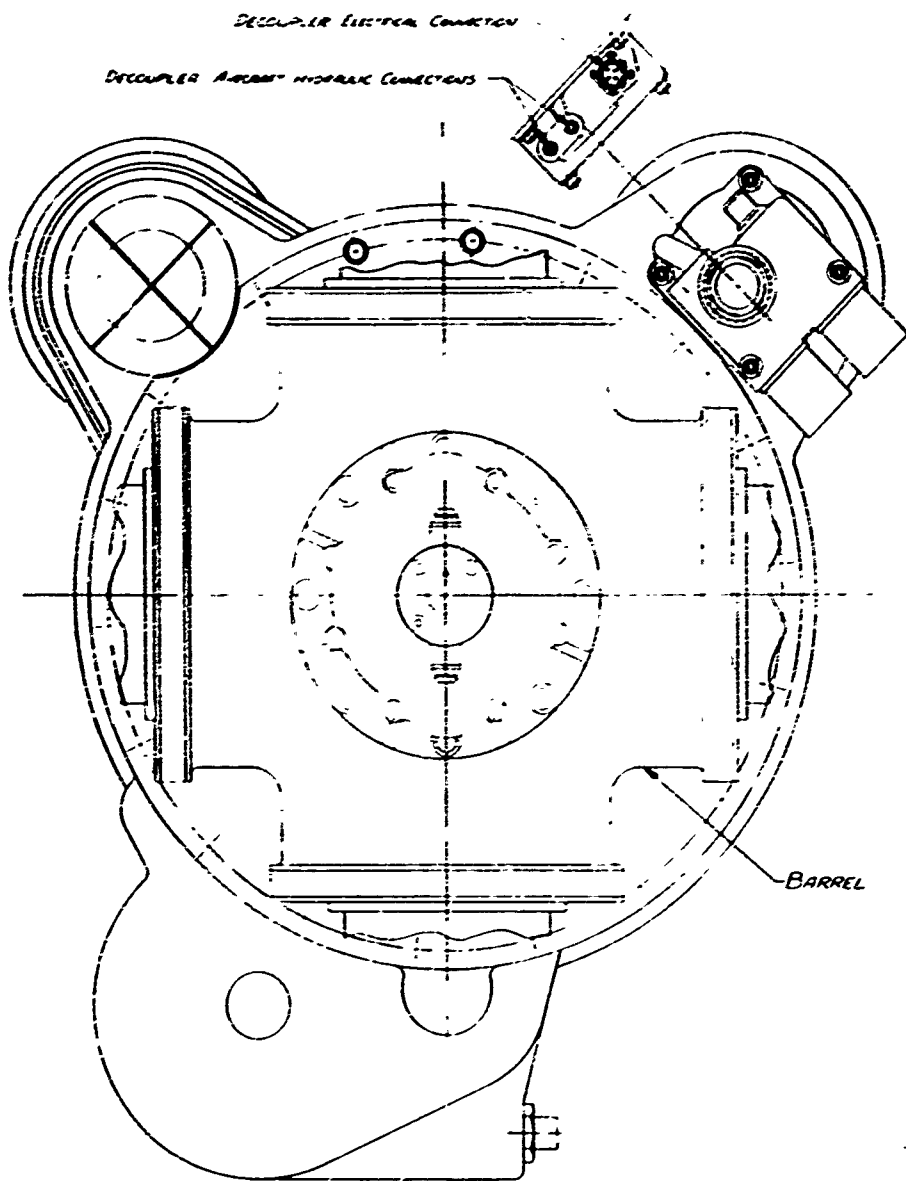
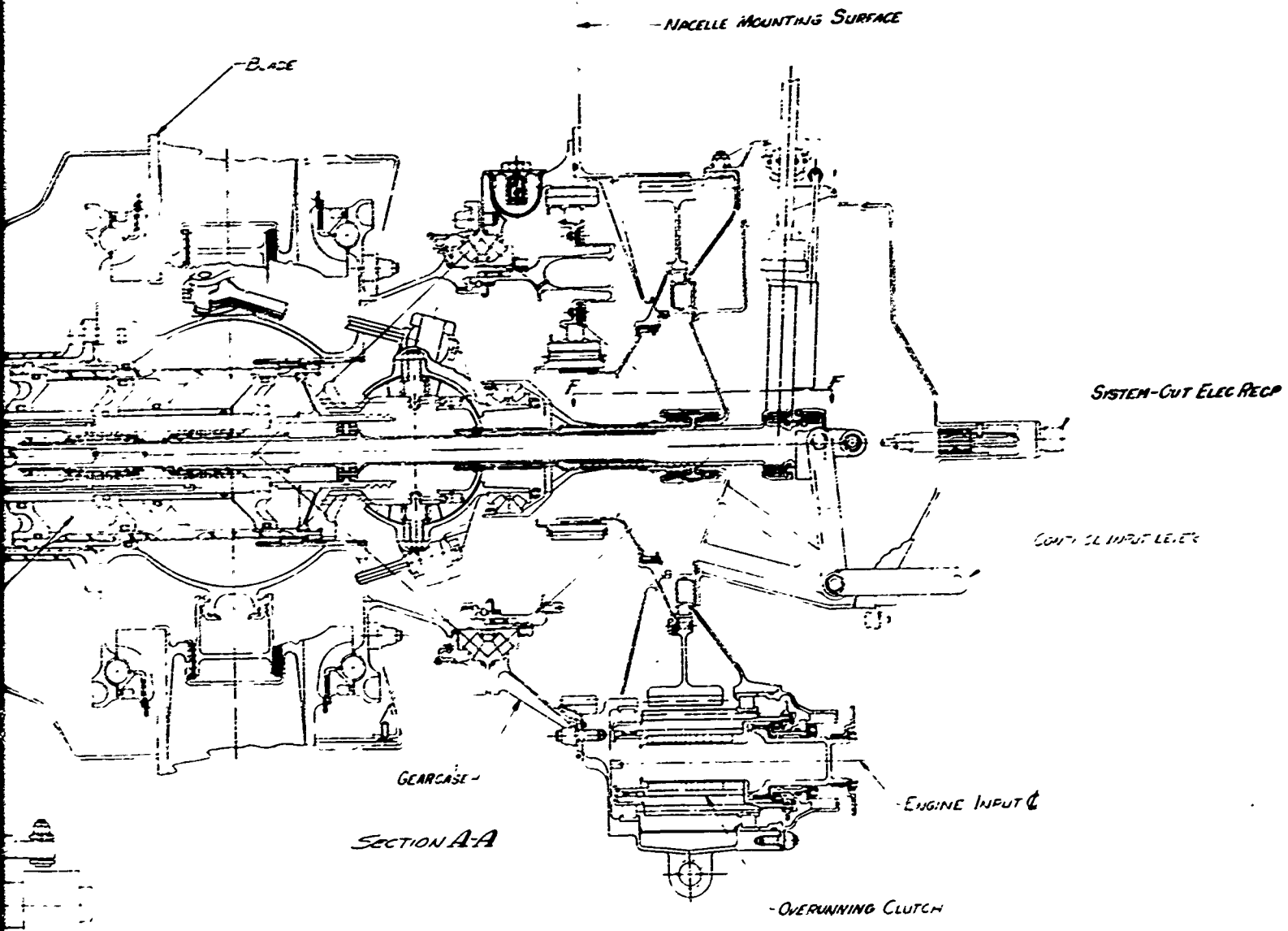


FIGURE 74. CYCLIC PITCH IGB
 PROPELLER SYSTEM
 WITH CROSS-SHAFT
 DRIVE

A



D

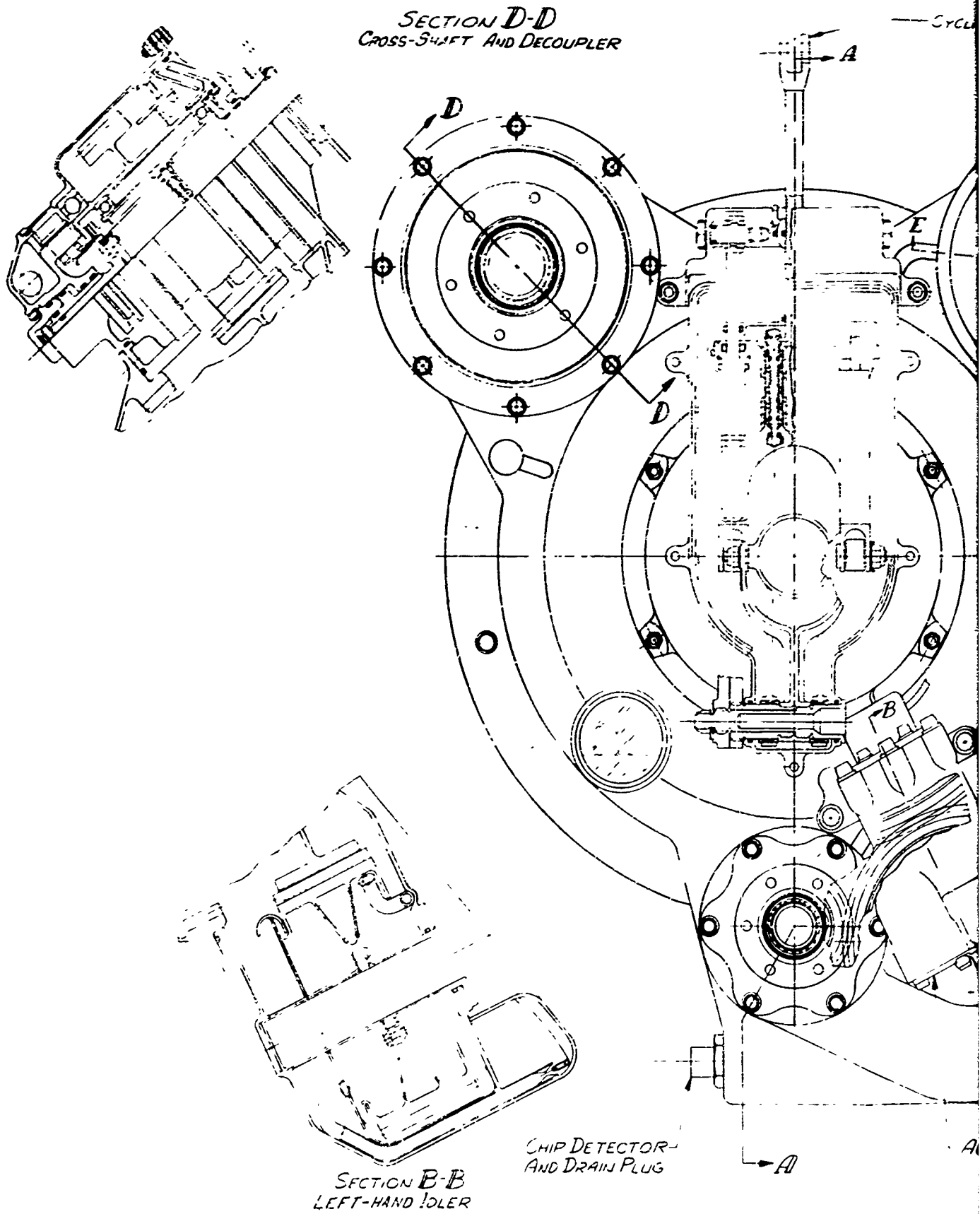
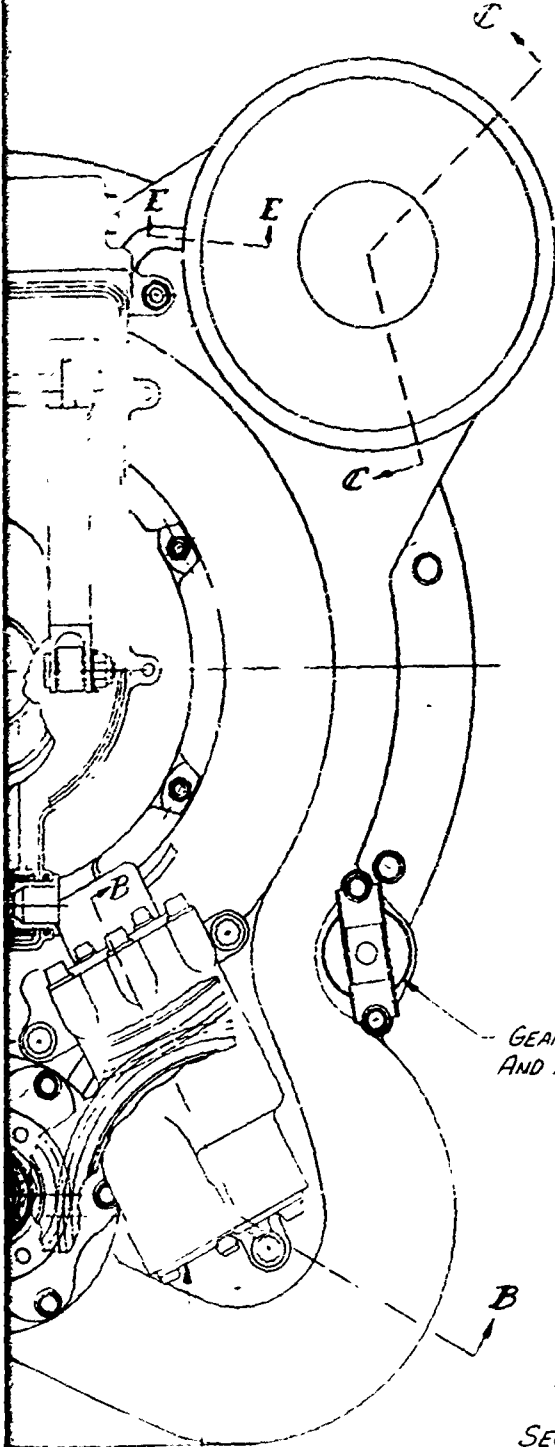


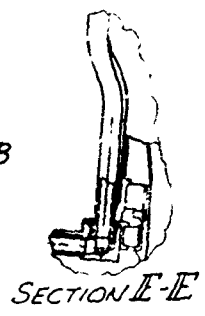
FIGURE 74(CONT).

A

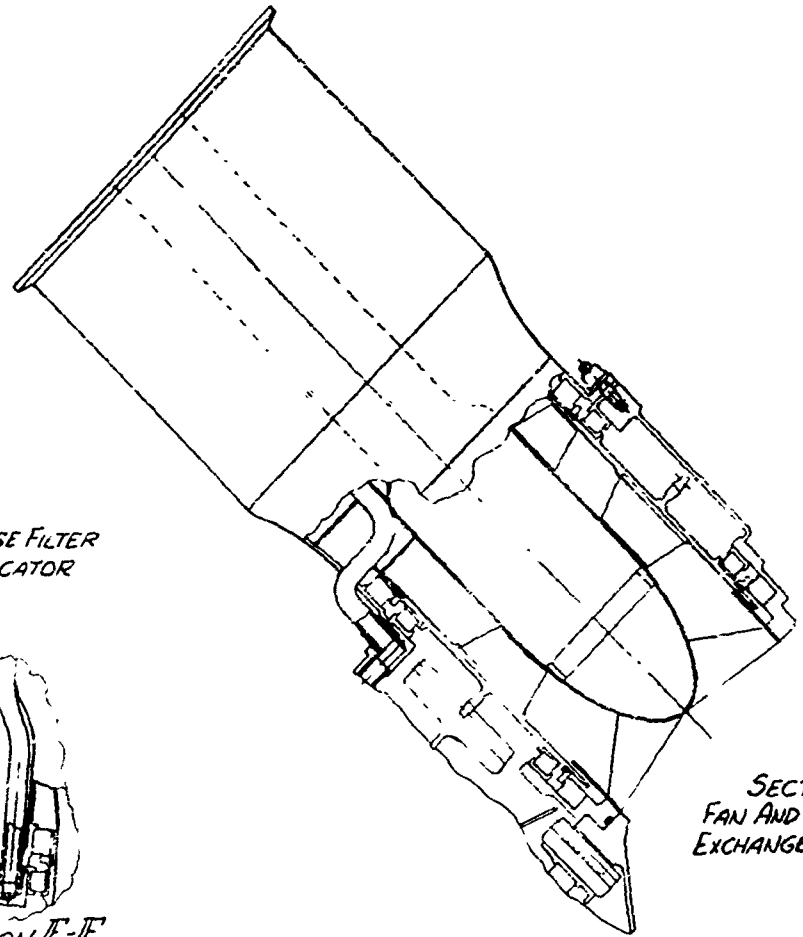
CYCLIC PITCH INPUT LEVER
A



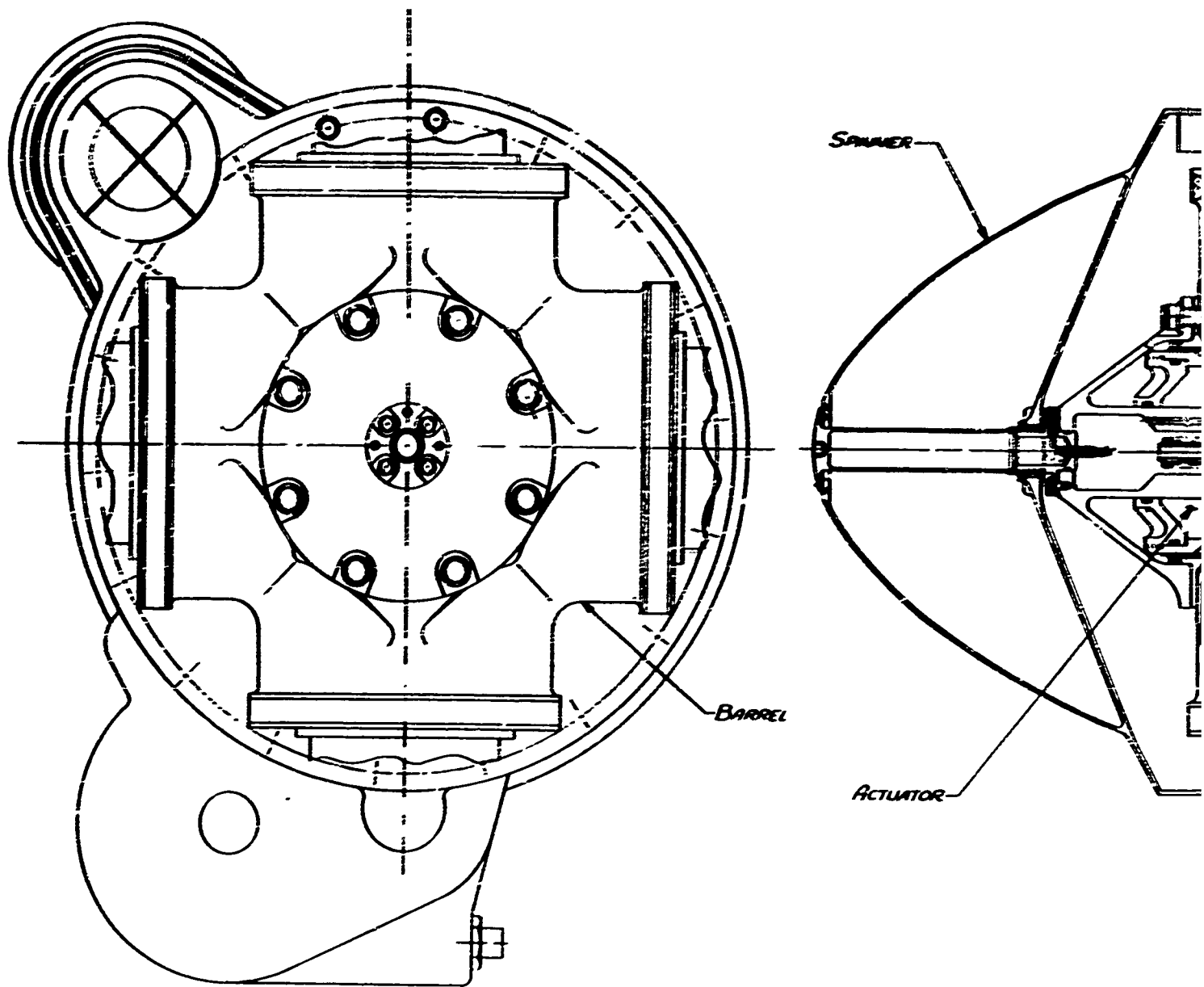
GEARCASE FILTER AND INDICATOR



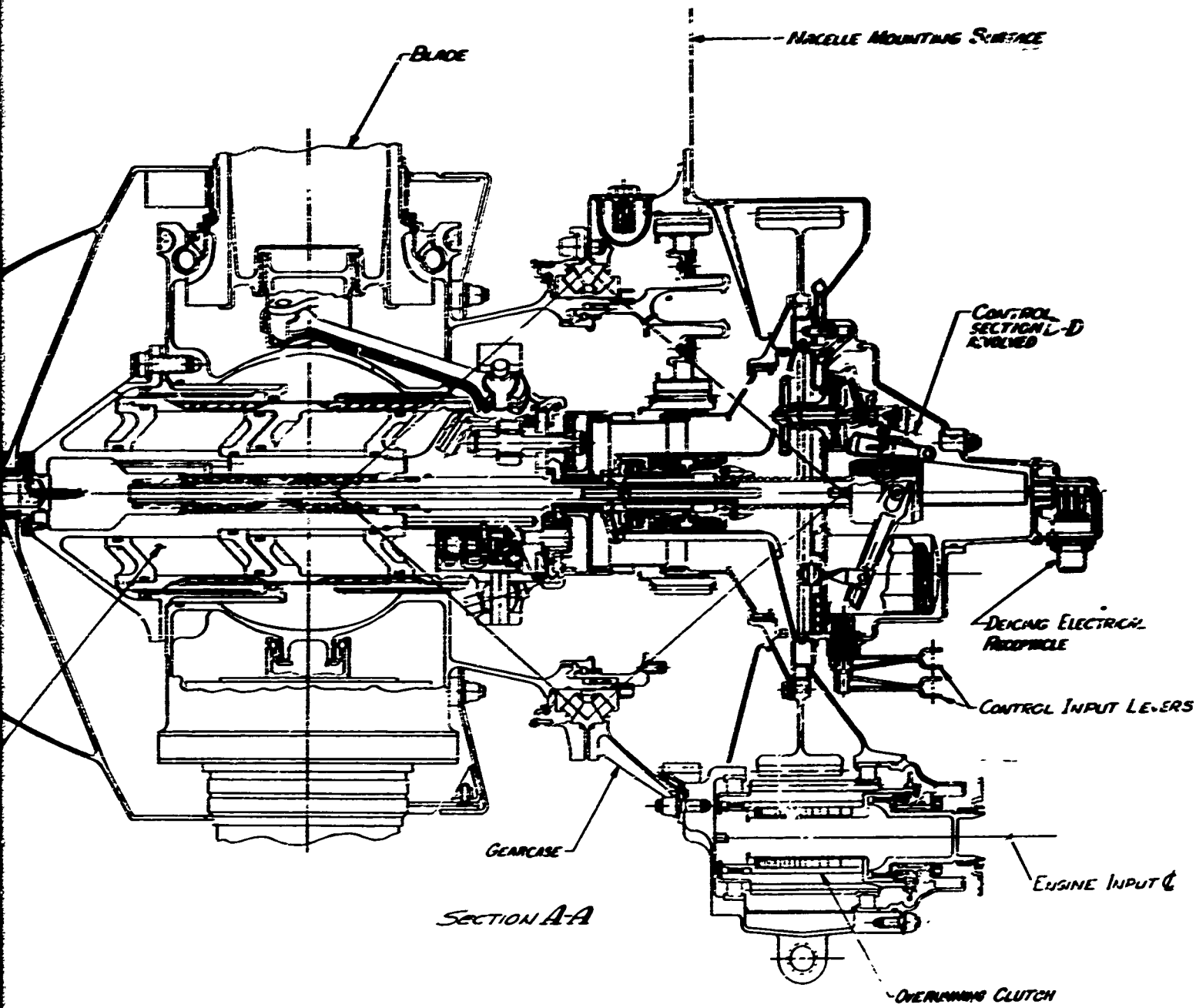
AUX PUMP AND MOTOR

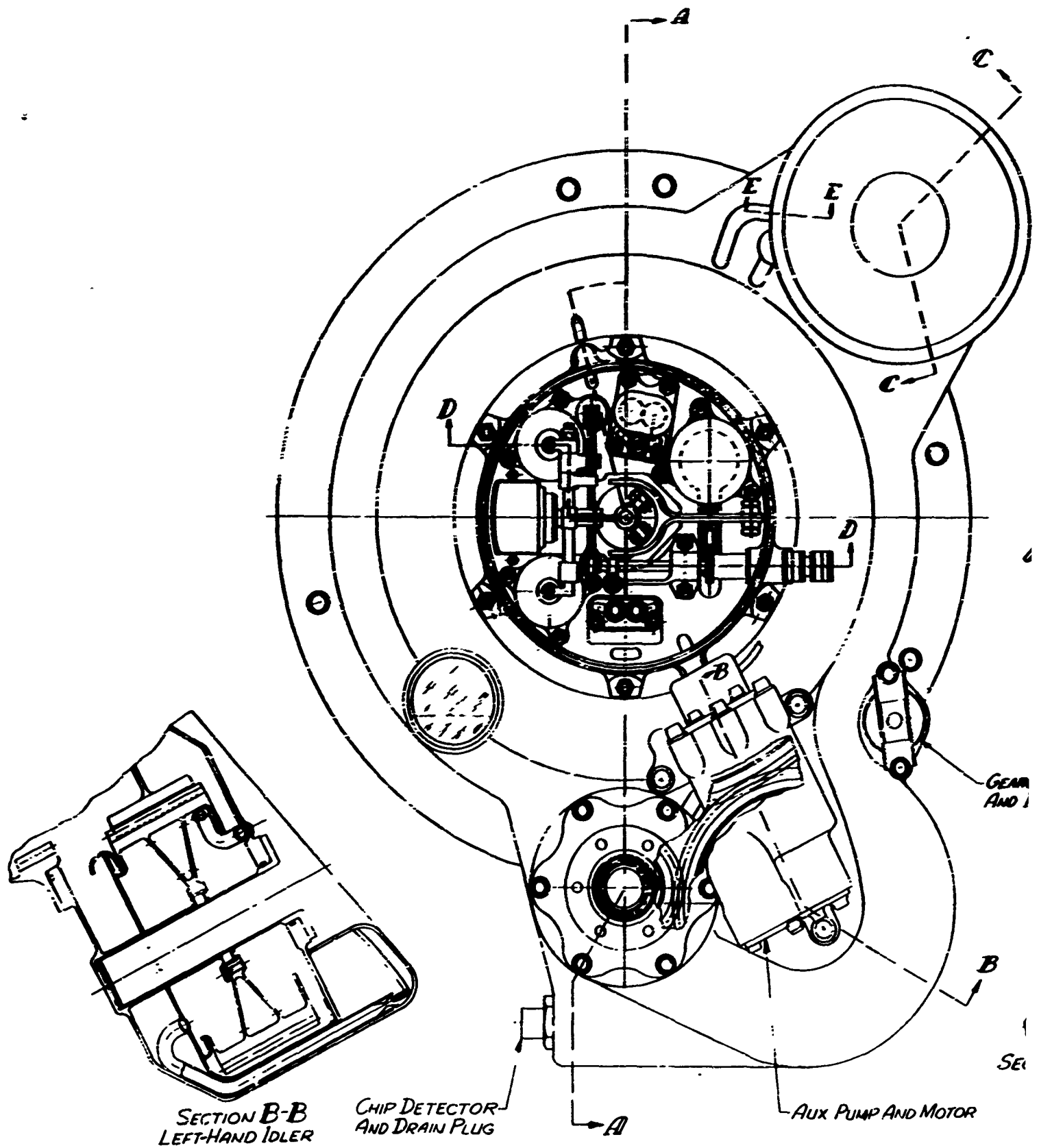


B



**FIGURE 75. COLLECTIVE PITCH IGB
PROPELLER SYSTEM
WITHOUT CROSS-SHAFT
DRIVE**



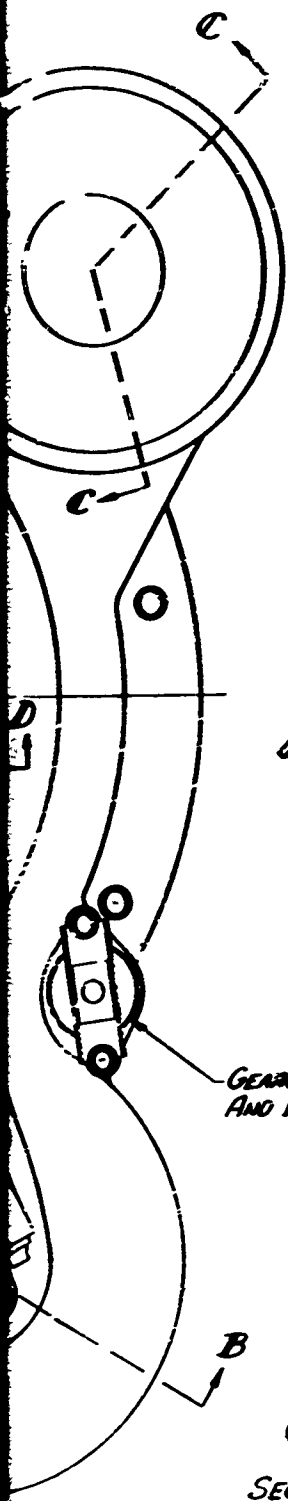


SECTION B-B
LEFT-HAND IDLER

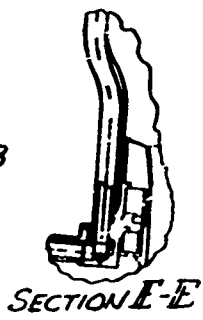
CHIP DETECTOR
AND DRAIN PLUG

AUX PUMP AND MOTOR

FIGURE 75(CONT).

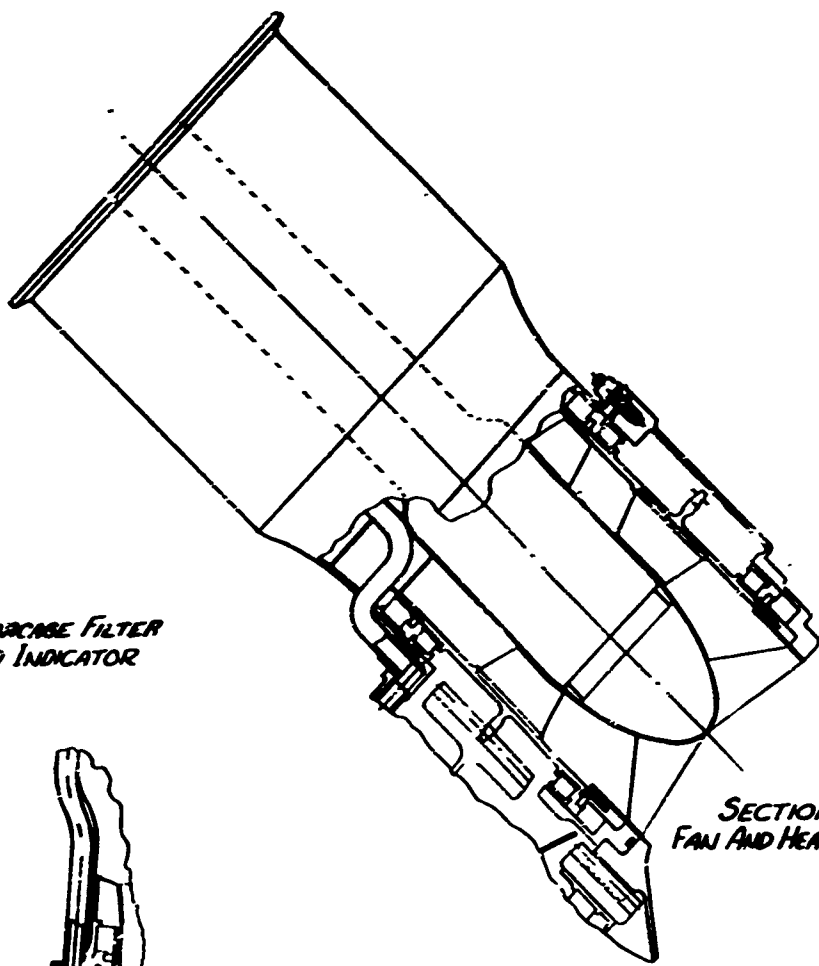


GEARCASE FILTER
AND INDICATOR



SECTION E-E

PUMP AND MOTOR



SECTION C-C
FAN AND HEAT EXCHANGER

The torque output of the gearbox planet carrier is transmitted through a splined connection to the barrel tailshaft. The tailshaft is integral with the cross-cylinder barrel concept and reacts the propeller loads into the gearcase structure through the tapered roller bearings. The cross-cylinder barrel concept consists of two continuously interacting perpendicular cylinders that form the four blade retentions at their extremities. The normal ball-bearing blade retention has been modified to a four-point bearing design to increase its capability to react blade moments.

Movement of the actuator cylinder is controlled by beta valve displacement, which is accomplished by converting the propeller control output signal by means of a system of bearings, ball-screw, and moveable threaded members. Fore-and-aft axial control output motion is first introduced from the nonrotating control into the rotating propeller by a redundant set of duplexed ball bearings. With a double-lead, dual-load-path ball screw, the axial position of the control output adds or subtracts a given number of revolutions from the ball screw, thus causing the pitch lock nut threaded to the actuator to rotate relative to the actuator and to translate to a new axial position. This axial motion is transmitted through two flanged idler gears to displace the beta valves that meter hydraulic fluid to the actuator. Motion of the actuator (and therefore the nut) nulls the displacement of the beta valve and closes the metering passages. A loss of hydraulic pressure would allow the blades to move toward low pitch, closing the gap between the actuator nut and the stop and causing the blades to lock pitch.

Beta valves are dualized for redundancy, and they contain a centering device so that override of either valve can occur in the event one of the valves is jammed. If an override occurs, that system pressure is automatically dumped to drain, to allow the remaining system to continue to control the actuator. The double-lead ball screw allows preloading within the assembly for removal of backlash and also serves in a redundant manner. Misalignment of the input system from the beta valves to the control is prevented by incorporation of a universal joint at the forward end of the ball screw.

The beta valves meter fluid to the actuator from the actuator-mounted high-pressure pumping system. The motion of the actuator cylinder produces a displacement in the blade links, which are connected to the offset blade trunnion arm. The axial movement of the links thereby produces a rotatory motion of the blades about the blade axis.

The side loads generated by the blade trunnion are reacted in the actuator cylinder by the incorporation of a spline connection between the cylinder and the barrel.

The additional pitch change mechanism required to incorporate provisions for cyclic pitch consists primarily of a moveable ball joint between the collective pitch actuator and the blade links, and a lever and servo actuator to provide the force to pivot the ball joint (Figure 74).

To improve the airflow into the propeller and provide better pressure recovery, a fiberglass spinner has been included in the system. The single-point retention of the spinner allows for the quick removal of the spinner and also ensures mechanical connection of the deicing leads. Lateral loads of the spinner shell are reacted by the front bulkhead and through the slip joint connection of the spinner to the rear bulkhead, while fore-and-aft loads are reacted by the front bulkhead.

Control System

Non-Cross-Shafted System

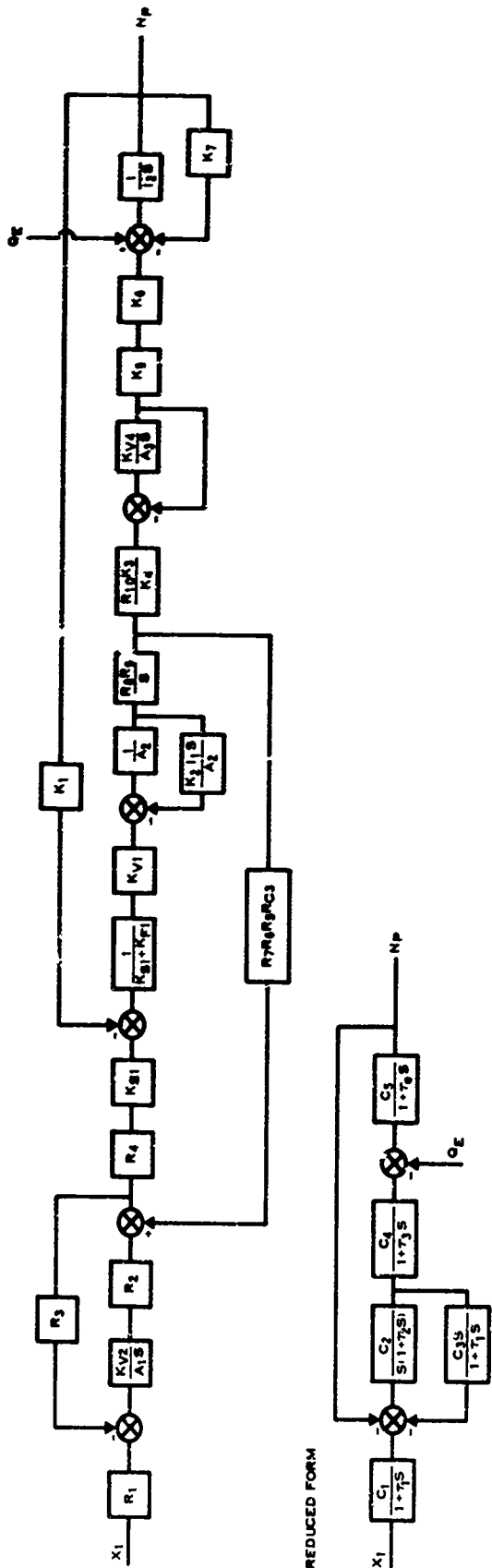
The rpm control system for this propeller consists of an rpm-sensitive valve (governor) which meters oil to the beta valve servo piston in proportion to the rpm error. The servo piston moves as long as there is an rpm error present, and at a rate proportional to the rpm error magnitude.

The output of the beta valve servo is connected to the main beta valve actuating rod. Motion of this rod, through a linkage mechanism, displaces the beta valve located in the main actuator, which in turn meters oil to the main actuator. The beta valve is pulled by motion of the main beta actuating rod, which is connected to a cam and a cam follower.

The cam follower, through a linkage, resets the governor speeder springs and displaces the speed-setting pilot valve. Oil metered by the speed-setting pilot valve moves the speed-setting servo piston, and the resulting motion is summed with the motion of the cam follower, thus nulling the speed-setting pilot valve and returning the speeder spring to its original position.

The rate of displacement of the pilot valve determines the value of the lead time constant (τ_l), which is sized to cancel the effect of the long engine-propeller lag time constant (τ_e). This allows high system gains which provide improved steady-state and transient characteristics. The linear block diagram representation of this system is shown in Figure 76, which presents characteristics that define the propeller response under engine power transients.

The overspeed governing system provides protection against failure of the main governor. If the main governor fails and calls for a decrease in pitch, the resulting motion of the beta valve actuator servo moves the speeder spring platform of the overspeed governor as well as that of the main governor, thus resetting the governor and bringing it into play before the propeller reaches the steady-state rpm setting of the overspeed governor. Studies have shown that this feature prevents rpm overshoots greater than 2% over the overspeed governor setting. Since the overspeed governor is a true governor for this mode of failure of the main governor, the propeller will continue to operate at the increased rpm.



TYPICAL SYSTEM VALUES

C_1	- 4640 $\frac{\text{RPM}}{\text{IN.}}$
C_2	- 0.03 IN./RPM
C_3	- 100 RPM/IN.
C_4	- 21,100 $\frac{\text{FT-LB}}{\text{IN.}}$
C_5	- 0.001 $\frac{\text{RPM}}{\text{FT-LB}}$
T_1	- 0.5 SEC
T_2	- 0.001 SEC
T_3	- 0.01 SEC
T_4	- 0.1 SEC

SYMBOLS

K_8	- DEG/IN. - PITCH CHANGE LINKAGE
K_9	- FT-LB/DEG - BLADE AERODYNAMIC GAIN
K_7	- FT-LB/RPM - BLADE & ENGINE CHARACTERISTIC
X_1	- IN. - SPEED-SET CAM RISE
O_e	- FT-LB - ENGINE TORQUE
N_p	- RPM - PROPELLER ROTATIONAL SPEED
A_1	- IN. ² - SPEED-SETTING SERVO
A_2	- IN. ² - BETA VALVE ACTUATOR SERVO
A_3	- IN. ² - PITCH CHANGE PISTON
I_1	- $\frac{\text{LB/SEC}^2}{\text{IN.}}$ - BETA VALVE POSITIONING SYSTEM INERTIA
I_2	- $\frac{\text{LB-FT/SEC}}{\text{RPM}}$ - ENGINE, GEARBOX, & PROPELLER INERTIA

SYMBOLS

R_1 THRU R_{10}	- LINKAGE RATIO, GEAR RATIO, CAM RATIO
K_{V1}	- $\frac{\text{IN.}^3/\text{SEC}}{\text{IN.}}$ - MAIN GOVERNOR GAIN
K_{V2}	- $\frac{\text{IN.}^3/\text{SEC}}{\text{IN.}}$ - SPEED-SETTING PILOT VALVE GAIN
K_{V4}	- $\frac{\text{IN.}^3/\text{SEC}}{\text{IN.}}$ - BETA VALVE GAIN
K_{S1}	- LB/IN - SPEEDER SPRING RATE
K_{F1}	- LB/IN - RPM SENSOR RATE
K_1	- LB/RPM - RPM SENSOR RATE
K_2	- $\frac{\text{IN.}^3/\text{SEC}}{\text{PSI}}$ - BETA VALVE ACTUATOR
K_3	- IN./RAD - BALL SCREW
K_4	- IN./RAD - PITCHLOCK SCREW

FIGURE 76. CONTROL BLOCK DIAGRAM

Feathering of the propeller is initiated by rotating the feather valve. This action bypasses the governor output and directs supply oil to the beta valve servo piston, which moves the beta valve to increase pitch.

The beta control mode is accomplished mechanically and bypasses all the hydraulic functions of the control. This mode covers the range of blade angle control from the low-pitch stop (i.e., the minimum governing angle) to full reverse. Since the low-pitch stop angle is determined by the stop on the beta valve actuator servo, the beta valve is positioned directly by the input linkage. Thus, by coordinating power and blade angle, reasonable rpm control can be maintained for ground handling and reverse thrust.

Operation of this control is similar to that used on the VC82S-1 propeller system which has been successfully engine tested on the T56-A18. Excellent transient and steady-state performance has been observed. Although the engine-propeller inertial time constant (τ_e) on the study propeller is shorter than that on the VC82S-1, this would only improve the propeller transient characteristic. No other unusual dynamic characteristics were found in investigating the propeller-engine system.

Cross-Shafted (VTOL) System

The cross-shafted (VTOL) control system either with or without cyclic pitch contains essentially the same hardware as the non-cross-shafted system, but it must be different in its mode of control. In the non-cross-shafted system, the isochronous main governors maintain rpm on each propeller system independently while power is controlled by the pilot. This system automatically accommodates any change in the propeller operating environment, such as air-speed, power level, and density, and continues to operate at its set rpm. When the two systems are cross-shafted together, several major problems arise. If two isochronous governors are trying to control a common rpm, and the two governors are not set at exactly the same rpm setting, one governor will increase blade angle while the other will decrease blade angle, causing a severe torque and thrust mismatch.

To stabilize this system, either (1) a trim device can be added to average the settings of both governors and to provide the necessary bias to force both to increase or decrease pitch together, (2) the cross shafting can be decoupled before entering the propeller governing mode, (3) the main governors can be modified from an isochronous mode to a droop mode, or (4) one control can be a "master" controlling both propellers. In the first system, a failure mode arises where one governor failure can cause either overloading or unloading of that propeller system with the remaining shp shifted to the second propeller, i.e., a failure which causes decreased pitch will unload that side, but the other system will increase pitch to absorb the increased shp and to maintain rpm. This will cause a thrust mismatch and a yaw moment on the aircraft.

The second system is undesirable for STOL operation where safety requires the use of the cross-shafting.

In the third system, the estimated droop which can be tolerated for reasonable stability is perhaps 0.5 deg per percent rpm. In an STOL mode, the blade angle increases from approximately 14 deg statically to 22 deg at 150 KTAS, which is an increase in rpm of 16%, and the V_{max} flight blade angle is approximately 42 deg which would result in a further increase in rpm of 40%. Therefore, it appears desirable to use some form of common governor output feeding both propeller systems. This can be accomplished by cross-coupling the collective blade angle outputs to each other, either across the aircraft or by moving the two controls to a more central location.

Each control system would continue to have an isochronous governor, but the overspeed governors would be deleted. For safety, each governor could provide sufficient output through its servo to drive both propeller systems. Each servo governor output would also be provided with a "no-back" device such that the mechanical collective pitch signals could not feed back through the control of either system.

In the event of an "open" failure (such as loss of a control systems hydraulic power) or a "short" failure (such as a governor drive fracture), an electrical pressure balance cutout switch located across the metered servo output pressures would be activated to dump both system supply pressures by means of electrical solenoids, and a system-out indication is provided. If this shutoff system should be non-operative during a "short" failure, the two governors' outputs would cancel each other, and the rpm would shift less than 1%. The two systems can be shut down, and the pilot can revert to an emergency beta mode of operation by using the collective pitch lever.

During VTOL operation, the pilot can set the propeller governors to a "topping" setting (approximately 103%), and the governors are prevented from operating by locking the output servo pistons in "full decrease" position with the electrical dump solenoids. This precludes any possible governor, overspeed governor, or secondary hydraulic control failure from affecting the VTOL operation, and the system now operates in a conventional beta (helicopter) mode. The pilot (and/or stabilization system) is given limited direct mechanical blade angle authority from essentially flat pitch to the maximum static thrust blade angle. He can feed direct collective pitch signals to the two controls for altitude control, and he can feed differential collective pitch to each for roll control, while the fuel control maintains rpm by increasing or decreasing fuel flow.

During transition, as the wing tilt angle is lowered, the pilot maintains blade angle authority until the wing is horizontal and forward flight is established.

The pilot can now fly a forward beta mode at the transition airspeed or below, which is "velocity stabilized" (i.e., any change in aircraft attitude which tends to increase or decrease airspeed will also cause a change in propeller/engine rpm, and therefore fuel flow, so as to increase power if airspeed is decreasing and to decrease power if airspeed is increasing). This would be advantageous in providing attitude compensation for landing and maneuvers. However, a beta mode also imposes some important limitations on the pilot. If the blade angle is reduced too rapidly, overspeeds can occur; if the blade angle is increased too rapidly, an overtorque situation may develop. Because of these limitations, it is not considered to be desirable to provide a normal beta mode over the entire flight regime, even though protective systems could be provided to limit the pilot's collective pitch authority.

After a steady-state level-flight attitude has been established, the operating mode can be converted to the governing mode and the control governors can be reset downward to the desired governing rpm.

As the governor rpm is reset below the operating rpm setting of the fuel control, the propeller will begin to increase blade angle, the rpm will drop, the fuel control will increase fuel flow, and independent propeller governing operation will occur at the maximum scheduled fuel-flow setting.

It is suggested that the fuel control power lever be provided with a schedule such that at its maximum setting, 100% rpm is set with any power available between 100% and flight idle power; it is further suggested that as the power lever is retarded, the rpm and maximum available shp be reduced in a coordinated fashion such that the fuel control (power turbine, N₂) rpm exceeds the final desired propeller rpm at any desired operating flight condition by a few percent. It is also suggested that the power lever and the propeller rpm (condition) lever be located side by side, and such that when they are in alignment, the N₂ rpm is set a few percent above the propeller control rpm setting. This allows a coordinated shp/rpm governing mode from flight idle to 100% shp.

In a VTOL beta mode, the power lever is set at 100% rpm and 100% available shp, and the propeller condition lever is set at approximately 103%. The fuel control is controlling rpm and is modulating fuel flow (power as a function of the pilot's collective pitch setting).

To enter the governing mode, the propeller rpm lever is retarded to a position in alignment with the power lever, where its setting is slightly less than 100%. This allows propeller governing at essentially 100% rpm and 100% shp. As the two levers are retarded simultaneously, any coordinated rpm/shp condition can be set on propeller governing, and the fuel control N₂ governor acts as an rpm topping governor at a few percent above the propeller governor setting.

If the condition lever is retarded independently, the propeller will govern rpm, but the power level may remain high; or if the power lever is retarded independently so that the N₂ fuel control governor is set below the propeller governor setting, the propeller rpm will reduce and the fuel flow will reduce toward flight idle power. In either case, moving the remaining lever to the coordinated position will establish the desired power and rpm in the governing mode.

The collective pitch lever should remain locked in its beta mode position, where it acts as a flight low-pitch stop. Power can be controlled by the power lever for any power increase up to 100% power, since at any increased position the N₂ governor will continue to run underspeed relative to the propeller governor.

For an STOL takeoff, the propeller can also be placed in the propeller governing mode by locking the collective pitch at zero thrust, setting the propeller governor to 100% rpm, and then advancing the power lever past a gate at 100% rpm to approximately 103%. At this position, the fuel control will schedule maximum shp, while the propeller governor will increase blade angle during takeoff at essentially 100% rpm to absorb full power and will continue to increase blade angle as airspeed is increased.

To convert from the governing mode to the beta mode at the transition airspeed, the collective pitch can be advanced a few degrees until a slight reduction in rpm occurs, indicating that the governor servo output is bottomed and that collective authority has been established. The condition lever can then be advanced to its maximum position (103%). Since blade angle cannot decrease, rpm will not increase from the propeller governor action, and shp will remain at the scheduled value. The system is then on beta control at a part-power/rpm condition; and if 100% rpm beta mode is desired, such as prior to conversion to a VTOL or an STOL landing, the power lever can be advanced to its 100% setting and collective pitch can be modified as necessary to maintain the desired power absorption.

In the event that both governors are inoperative or that the cross-shaft must be shut down, an emergency beta flight mode can be established by locking both governors out through the dump solenoids. The collective pitch lever can then be lowered through its authority of perhaps 24 deg to allow a reduction in airspeed and an STOL landing, although reverse thrust may not be available.

To allow one propeller system to be shut down and feathered in flight, a decoupler is provided in the common governor servo output between the two controls. This allows the desired control to feather its system through the feather valve action. This decoupler can be electrically energized simultaneously or sequentially with the cross-shaft decoupler. The entire cross-shaft can also be decoupled at transition velocity or below by first reverting to the beta mode.

Although this approach to a cross-shafted installation does require system coordination among the airframe, the fuel control, and the propeller control, it has a number of advantages:

1. VTOL operation control is direct, with maximum reliability from the propeller controls.
2. VTOL operation is similar to helicopter operation.
3. A beta flight mode can be used in an emergency.
4. A propeller governing mode can be selected over the entire flight regime.
5. The fuel control does not require a switch in operating mode, including reversing and ground handling.
6. The cross-shafting system can be shut down in flight if necessary.

Maintainability and Reliability Assessment

An electrical wiring schematic for the KGB propeller system is shown in Figure 77. An assessment of the system design features that should improve maintenance and reliability over existing production turboprop systems, such as the 54H60 propeller used on the C-130 and P-3 aircraft, is presented below. It should be noted that certain improvements have already been incorporated on first-generation V/STOL aircraft (XC-142, X-22), such as the fiberglass-covered steel spar blade and the integral propeller reduction gearbox. These improvements not only offer significant weight reductions but also offer improvements in maintainability and reliability. Examples of these are that impact damage to the fiberglass blade shell can be repaired in the field and that the integral gearbox concept isolates the propeller-induced moments from the gear train and permits a more accessible control location. Also, the recently developed pusher propeller for the AH-56A introduced the "modular packaging" concept wherein major components (blades with quick-disconnect retention, pitch change actuator, integral gearbox, spinner, and cooling fan) can be easily removed and replaced without special tools or rerigging.

The system designs presented herein are considered to provide improvements in maintainability and reliability over present production turboprop systems. Those significant improvements are listed below.

Modular Packaging

Modular packaging allows a number of propeller system items to be packaged

as separate interchangeable components. Line replaceable units (LRUs) of the proposed design which can be easily removed and replaced in a matter of minutes are:

1. Spinner
2. Lube Oil Heat Exchanger
3. Blade Pitch Change Actuator
4. Integral Gearbox
5. Propeller Blades
6. Control
7. Deicer Brush Block Assembly

Oil Filters

The oil filters utilize throwaway cartridges and a differential pressure sensor to indicate when clogging has reached a critical point.

Lip Seals

Split lip seals can be installed without removing or disassembling the integral gearbox propeller system.

Chip Detectors

Chip detectors are connected to a cockpit indication.

Blade Retention

Quick-disconnect blade retention makes blade replacement in the field a rapid and simple process.

Blade Weight

Blade weight reduction has been accomplished through the use of advanced materials which will in itself reduce maintenance because the lighter blade weight makes handling and transporting the blades easier.

Blade Repairs.

The blade can be removed for overhaul on an "on-condition" basis; i.e., only when exterior surface deterioration makes overhaul more practical or when spar damage is evident. Field patch repairs of the fiberglass blade return it to a like-new condition, provided the metal spar is not damaged.

Pitch Change Actuator

The pitch change actuator provides system-out indication when one of the tandem hydraulic cylinders or valves fails to function.

Fan and Heat Exchanger

The integral fan and heat exchanger does not require lube oil line connections to be made during gearbox installation.

Although current state-of-the-art VTOL propellers have been designed with dual pitch change actuators, a double failure has occurred which negated the protection usually afforded by dual systems. The addition of a simple, mechanical pitchlock device in the study design will greatly reduce the effect of a double actuator failure. Mechanical pitchlock will also reduce the effect of propeller hydraulic oil loss due to combat damage for a military aircraft.

Control Signal Linkage

Mechanical dualization of all control signal linkage will increase VTOL propeller reliability.

Propeller Bearings

Bearing manufacturers expect the vacuum-melt material factor to increase from the current value of approximately 3 to a value of approximately 15 in 1975, due to improved materials. Naturally, a part of this material improvement factor has been applied to reduce propeller weight. Critical bearings have been designed for an air-melt B₁₀ life of 600 hr and have used a factor of only 5 to arrive at a vacuum-melt B₁₀ life of 3000 hr. However, since a material factor of 15 should be applicable by 1975, the actual vacuum-melt B₁₀ life will be 9000 hr. Thus, a part of the bearing material improvement has been applied to improve propeller bearing reliability by a factor of 3 over currently designed VTOL integral gearcase propellers.

Deicing System

Deicing brushes have historically had a relatively high premature removal rate due to relatively high contact velocities and occasional contamination with oil from lip seals. Location of deicing brushes as shown on the study design will reduce the contact velocities, reduce oil contamination, and improve the reliability of the deicing system.

Control Valves

Miniaturization of control valves and elimination of the majority of "O" seals will result in improved control reliability. Many premature removals of propeller controls have been caused by "O" seal deterioration and leakage. The improved design will eliminate a substantial portion of this failure mode.

WEIGHT SUMMARY

A weight breakdown by major components is presented in Table XV for the three system designs discussed above representing the lightest weight potential found during the study. For comparison, the weights of a first-generation VTOL propeller system (XC-142) and the estimated weights of a 2000-shp, 14.8-ft diameter VTOL propeller system based on today's state of the art (SOTA) are also listed in the table.

The propeller components in the weight column listed "1965 SOTA ..." were estimated by using the weight of "today's" steel spar fiberglass-covered blade listed in the above section concerning the blade component design and by adjusting the XC-142 barrel and actuator weight due to the lighter blade. The gearbox components were estimated by adjusting the XC-142 system weights by the ratio of the gearbox output torque to the 0.84 exponent (Reference 1).

Since the table presents the lightest weight potential for 1970-1975, the blade weight shown represents the spar-shell design with a boron-aluminum composite material for the spar. However, as discussed previously in this report, a titanium spar could be used which also will result in a significant weight improvement for the future.

If a titanium spar, fiberglass-covered blade were used, the following changes would have to be made to the 1970-1975 weight breakdown in the table:

Blade and Retention	Add 36.2 lb
Barrel	Add 2.0 lb
Actuator	Add 0.7 lb
Total Weight (Dry and Wet)	Add 38.9 lb

The non-cross-shafted design is shown with the same overrunning clutch as is used with the two cross-shafted designs, since the clutch could be used as a propeller-to-engine decoupler if the IGB propeller were used with a single-shaft engine. If the clutch is not required, the engine output shaft would be connected directly to the pinion gear and the system would be 3.4 lb lighter than shown in the table.

An assessment of the potential reductions in IGB propeller system weight for the 1970's and the primary causes of the weight reductions are summarized in Table XVI.

TABLE XV
WEIGHT SUMMARY AND COMPARISON

COMPONENT	XC-142 3400 SHP 15.6 FT DIA.	1965 SOTA ESTIMATED FOR COMPARISON 2030 SHP, 14.8' DIA	1970-75 SOTA 2000 SHP, 14.8 FT DIA.		CYCLIC PITCH WITH CROSS- SHAFT DRIVE
			COLLECTIVE PITCH NON- CROSS- SHAFTED	WITH CROSS- SHAFT DRIVE	
BLADES & RETENTION	311.0	276.0	164.1	164.1	166.1
BARREL	92.0	76.0	30.5	30.5	31.5
ACTUATOR & LINKAGE (5)	100.8 ⁽³⁾	89.5	34.2	38.7	52.9
GEARING	208.0	140.0	63.9 ⁽²⁾	71.9 ⁽²⁾	71.9 ⁽²⁾
GEARCASE	107.0	72.0	24.1	26.3	26.3
OVERRUNNING CLUTCH	26.0	18.0	3.4	3.4	3.4
LUBE SYSTEM					
PUMPS	20.0	13.0	1.8	1.8	1.8
FAN & HEAT EXCHANGER	27.0 ⁽³⁾	15.9	11.6	11.6	11.6
EXTERNAL OIL TANKAGE	15.0 ⁽³⁾	10.8	0	0	0
CONTROL (4)			7.0		
DECOUPLER	13.0	9.0	0	5.0	5.0
SPINNER	22.0 ⁽³⁾	18.0	8.5	8.5	9.1
DEICING	7.4	7.4	5.6	5.6	5.6
TOTAL DRY WEIGHT	949.2 LB	755.6 LB	354.7 LB	367.4 LB	385.2 LB
OIL WEIGHT	49.0 ⁽³⁾	36.0	20.7	20.7	21.0
TOTAL WET WEIGHT	998.2 LB	791.6 LB	375.4 LB	388.1 LB	406.2 LB
NOTES					
(1) WEIGHTS ARE REPRESENTATIVE OF SYSTEMS WITH PROVISIONS FOR THE SAME FUNCTIONAL REQUIREMENTS (IE. IGB PROPELLER CONFIGURATION, SELF-CONTAINED HYDRAULICS FOR ACTUATOR AND IN-PLACE PITCHLOCK, COMPLETE GEARBOX LUBE SYSTEM, POWER TAKEOFF FOR CROSS-SHAFTING BUT SHAFTING AND WINGBOX ARE NOT INCLUDED)					
(2) LEFT-HAND ROTATION CONFIGURATION WEIGHTS ARE SHOWN. RIGHT-HAND CONFIGURATION WOULD BE 2.4 LB LIGHTER.					
(3) ESTIMATED WEIGHT REPRESENTATIVE OF PRESENT TECHNOLOGY.					
(4) WEIGHTS LISTED ARE FOR A NACELLE SYSTEM AND CROSS-SHAFTED SYSTEMS ARE ASSUMED TO USE A REMOTELY MOUNTED MASTER CONTROL FOR COMPARISON WITH PRESENT TECHNOLOGY SYSTEMS. THE 1965 SOTA MASTER CONTROL IS ESTIMATED TO BE 16 LB, AND THE 1970-1975 SOTA WOULD BE 7.5 LB.					
(5) THE WEIGHT OF AN AUXILIARY PUMP AND MOTOR IS CONSIDERED TO BE G.S.E. AND NOT FLIGHT HARDWARE AND IS NOT INCLUDED. 1965 SOTA AND 1970-1975 SOTA UNITS ARE ESTIMATED TO BE 5.2 LB AND 4.2 LB RESPECTIVELY.					

TABLE XVI WEIGHT REDUCTION 1975 TECHNOLOGY VS. 1965				
COMPONENT	STUDY WEIGHTS (WT. REDUCTION) LB	PERCENT REDUCTION OF COMPONENT	PERCENT REDUCTION OF SYSTEM DRY WEIGHT	PRIMARY REASONS FOR WEIGHT REDUCTION
BLADES & RETENTION	164.1 (111.0)	35	12.6	BORON-ALUMINUM BLADE SPAR LIGHTER BLADE FILL
		6	2.1	
		41%	14.8%	
BARREL	30.5 (23.2)	25	2.8	LIGHTER BLADES TITANIUM HIGH PRESSURE ACTUATOR 1975 CONCEPT
		15	1.7	
		5	0.5	
		20	2.3	
		69%	7.3%	
ACTUATOR & LINKAGE	38.7 (30.8)	22	2.6	LIGHTER BLADE HIGHER PRESSURE TITANIUM & FILAMENT WINDING HIGH SPEED PUMPS POSSIBLE WITH LARGE TAILSHAFT AND MODULAR PACKAGING
		6	0.9	
		18	2.1	
		9	1.1	
		57%	6.7%	
GEARING	71.9 (69.1)	24	4.4	GEAR RATIO SPLIT, L/D STUDIES AND LARGER ENVELOPE INCREASED BEARING LIVES NEW TITANIUM PLANET CARRIER DUPLEX TAPERED BEARING PROP MOUNTING & LARGE DIA. SHAFT TITANIUM GEARS
		7	1.4	
		4	0.7	
		4	0.7	
		10	1.8	
		49%	9.0%	
GEARCASE	28.3 (43.7)	33	3.1	FORWARD BOLT CIRCLE GEARBOX MOUNTING AND ENGINE NOT SUPPORTED BY GEARBOX TITANIUM STRUCTURE
		31	3.0	
		64%	6.1%	
OVERRUNNING CLUTCH	3.4 (14.8)	81%	1.9%	INTEGRATED SPRING CLUTCH
LUBE SYSTEM				
PUMP	1.8 (11.2)	86%	1.5%	CENTRIFUGAL LUBE SUPPLY PUMP AND EJECTOR SCAVENGE
FAN & HEAT EXCHANGER	11.8 (4.3)	27%	0.6%	FAN AND DRIVE INTEGRATED, INLET DUCTING ELIMINATED
GEARBOX OIL TANKAGE	NONE	100%	1.4%	SUFFICIENT WET SUMP IN GEARBOX
DECOUPLER	5 (4)	44%	0.5%	INTEGRATED DESIGN AND TITANIUM
SPINNER	8.3 (9.3)	18	0.5	SINGLE POINT ATTACHMENT AND SIMPLIFIED DESIGN "B" GLASS
		35	0.9	
		53%	1.4%	
DEICING	5.8 (1.8)	24%	0.2%	SMALLER MAIN SLIP RINGS, BUT BLADE BRUSH BLOCKS FOR EASE OF REMOVAL ARE SLIGHTLY HEAVIER
TOTAL DRY WEIGHT	367.4 (388.2)	51.4%	51.4%	
OIL WEIGHT	20.7 (15.3)	38%		AIR-OIL SEPARATOR
TOTAL WET WEIGHT	388.1 (403.5)	51%		

PERFORMANCE SUMMARY

The performance of the IGB propeller designs described in this report is presented in the following tables and curves:

- Table XVII presents the propeller efficiency and/or thrust for specific operating conditions. Note that both the 14.8-foot-diameter point design propeller and a propeller with a higher figure of merit projected for the 1970 time period are listed.
- Figures 78 through 83 include the blade characteristic chart and performance curves for calculating propeller thrust at other operating conditions.
- Table XVIII presents the estimated pressure recovery for hover and cruise conditions.
- Figure 84 presents the calculated thrust and control moments for the cyclic pitch propeller design.
- Tables XIX, XX, and XXI and Figures 85 and 86 present data concerning the propeller noise estimation. The sound pressure levels produced by 14.8-ft (point design) and 12.8-ft-(presented for comparing the effect of a lower power design point at the same disk loading) diameter propellers were estimated at the operating conditions listed in Table XIX. The estimates are believed to be accurate to within ± 3 db for near-field and ± 10 db for far-field.
- The near-field levels listed in Table XX are estimated for a location one foot from the tip of the propeller in the plane of rotation in a free-field domain. Also shown are the propeller's operating parameters and the harmonic distribution of the noise generated at each condition.
- The maximum and minimum estimated overall noise levels for the 14.8-foot-diameter propeller are 130.4 db and 128.6 db; for the 12.8-foot-diameter propeller, 129.2 db and 128.0 db.
- Figures 85 and 86 show the maximum and minimum octave band plots of the noise of the two propellers. These curves were obtained by summing the harmonics presented in Table XX within each octave band. It is shown that the low-frequency noise is the most prominent, while the levels in the 500-Hz center band and above are much lower and contribute little to the character of the noise.
- It should be noted that it is difficult for the human ear to distinguish between two sounds differing by less than 5 db; therefore, all of the levels

TABLE XVII. PERFORMANCE SUMMARY

		TODAY'S SOTA		80 FM	
PROPELLER DESIGN NUMBER OF BLADES PROPELLER DIAMETER ACTIVITY FACTOR INTEGRATED DESIGN C ₁					
		4	4	4	4
		14.8	14.8	15.0	15.0
		120	120	120	120
		.400	.400	.400	.400
CONDITION	PROPELLER SHP	TIP SPEED (FPS)	ALTITUDE FT	AIRPLANE SPEED (KTAS)	PROPELLER THRUST OR EFFICIENCY
HOVER	1400	900	6000' 95°F	0	6025 (.776)
HOVER	2000	900	S.L. SD	0	8410 (.773)
CRUISE	643	540	S.L. SD	250	.829
CRUISE	643	630	S.L. SD	250	.805
V _{MAX}	1500	720	S.L. SD	350	.790
V _{MAX}	1500	810	S.L. SD	350	.755
V _{MAX}	2000	720	S.L. SD	350	.836
V _{MAX}	2000	810	S.L. SD	350	.814
V _{MAX}	2000	810	S.L. SD	400	.622
V _{MAX}	2000	900	S.L. SD	400	.552
					6190 (.800)
					8590 (.797)

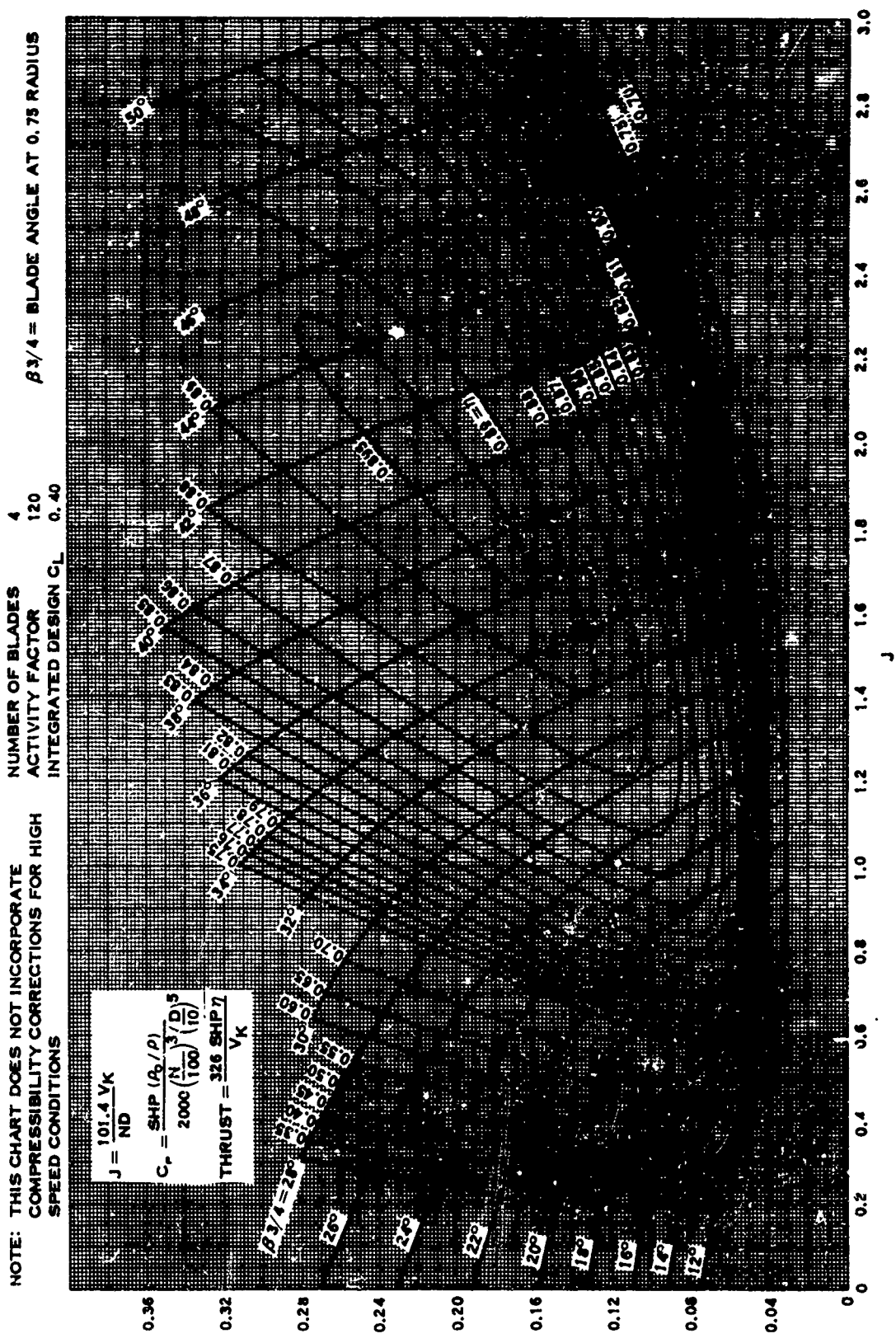


FIGURE 78. PROPELLER EFFICIENCY MAP BASED ON STRIP ANALYSIS CALCULATIONS

4 WAY/120 AF/0.40CL₁
 (0.78 TIP MACH NO.)

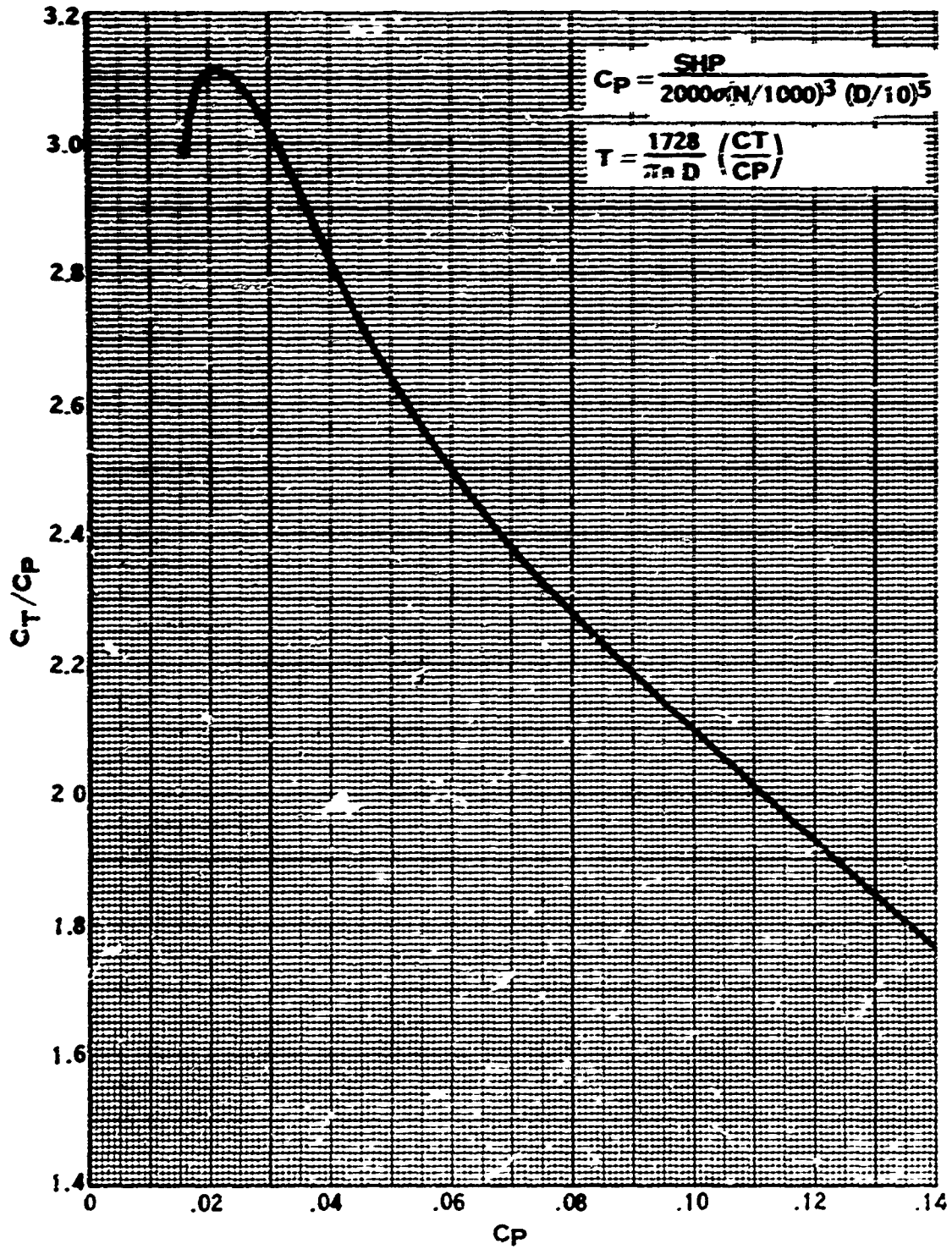


FIGURE 79. STATIC PROPELLER PERFORMANCE

COMPRESSIBILITY - FT X η INCOMPRESSIBLE
 MN - AIRPLANE MACH NUMBER

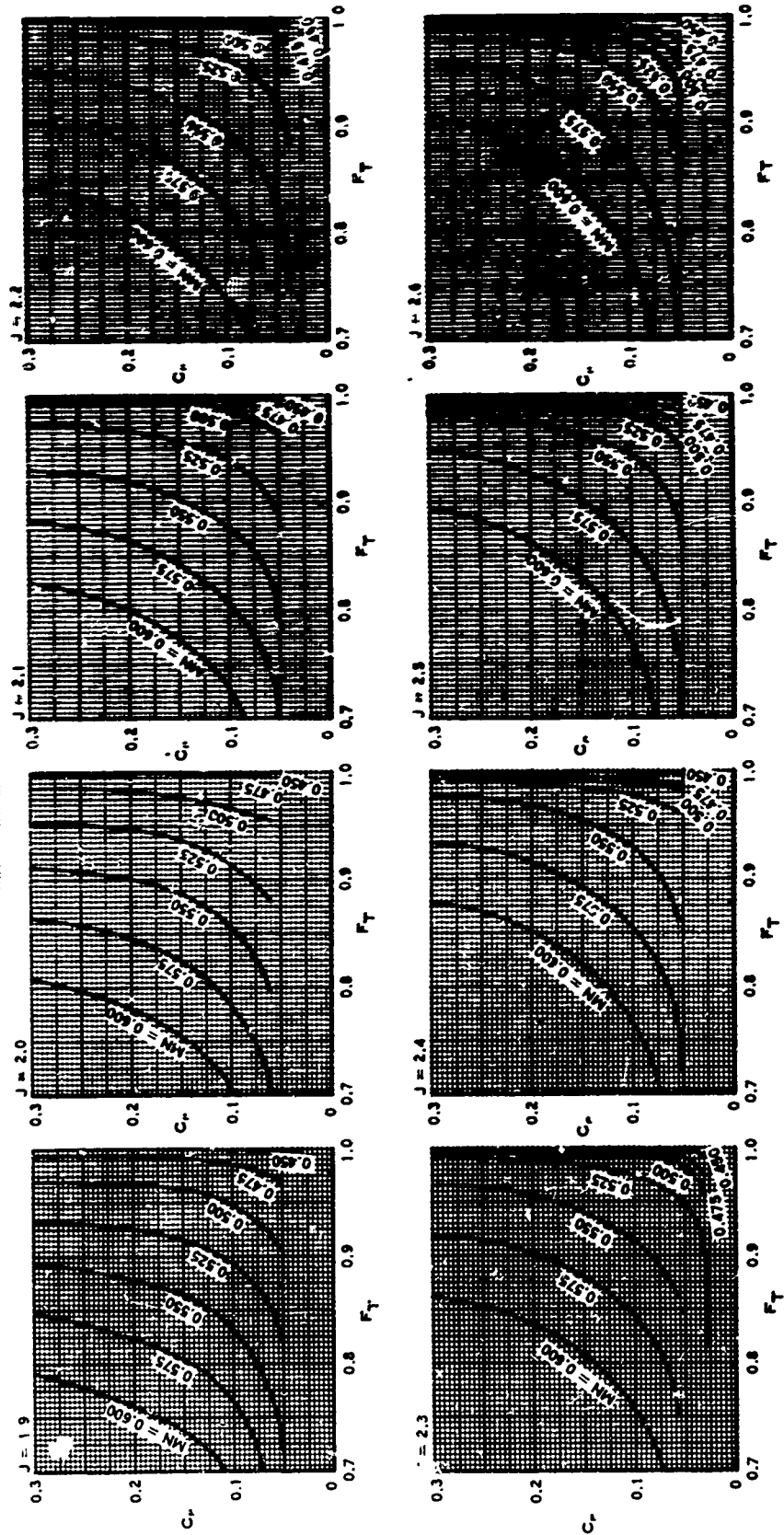


FIGURE 80. COMPRESSIBILITY CORRECTION FACTORS FOR THE 4-WAY/120 AF/0.40 C_{L1} EFFICIENCY MAP

$\eta_{\text{COMPRESSIBLE}} = F_T \times \eta_{\text{INCOMPRESSIBLE}}$
 MN = AIRPLANE MACH NUMBER

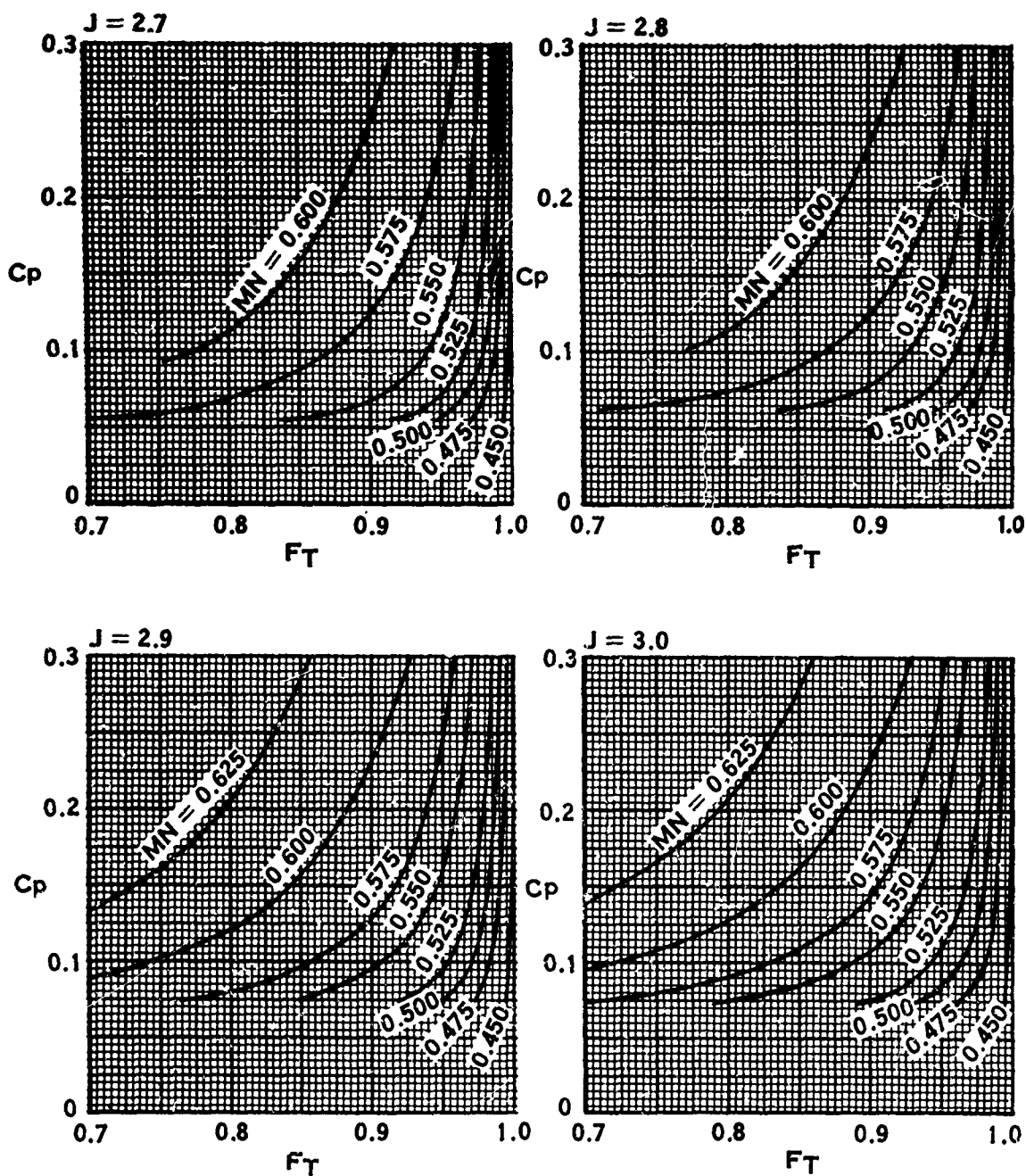


FIGURE 80 (CONT). COMPRESSIBILITY CORRECTION FACTORS FOR THE 4-WAY/120 AF/0.40 C_{L_i} EFFICIENCY MAP

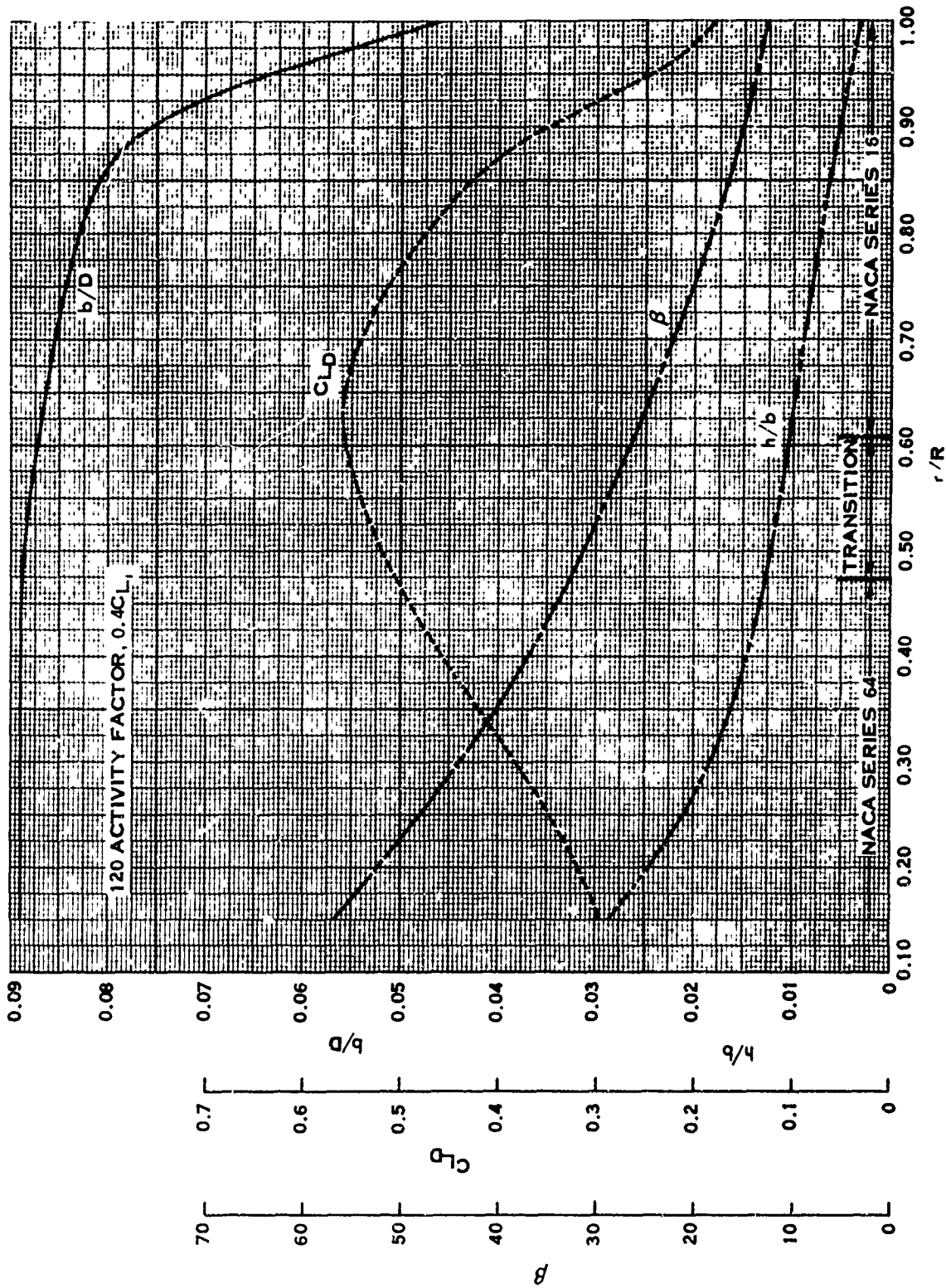


FIGURE 81. BLADE CHARACTERISTICS

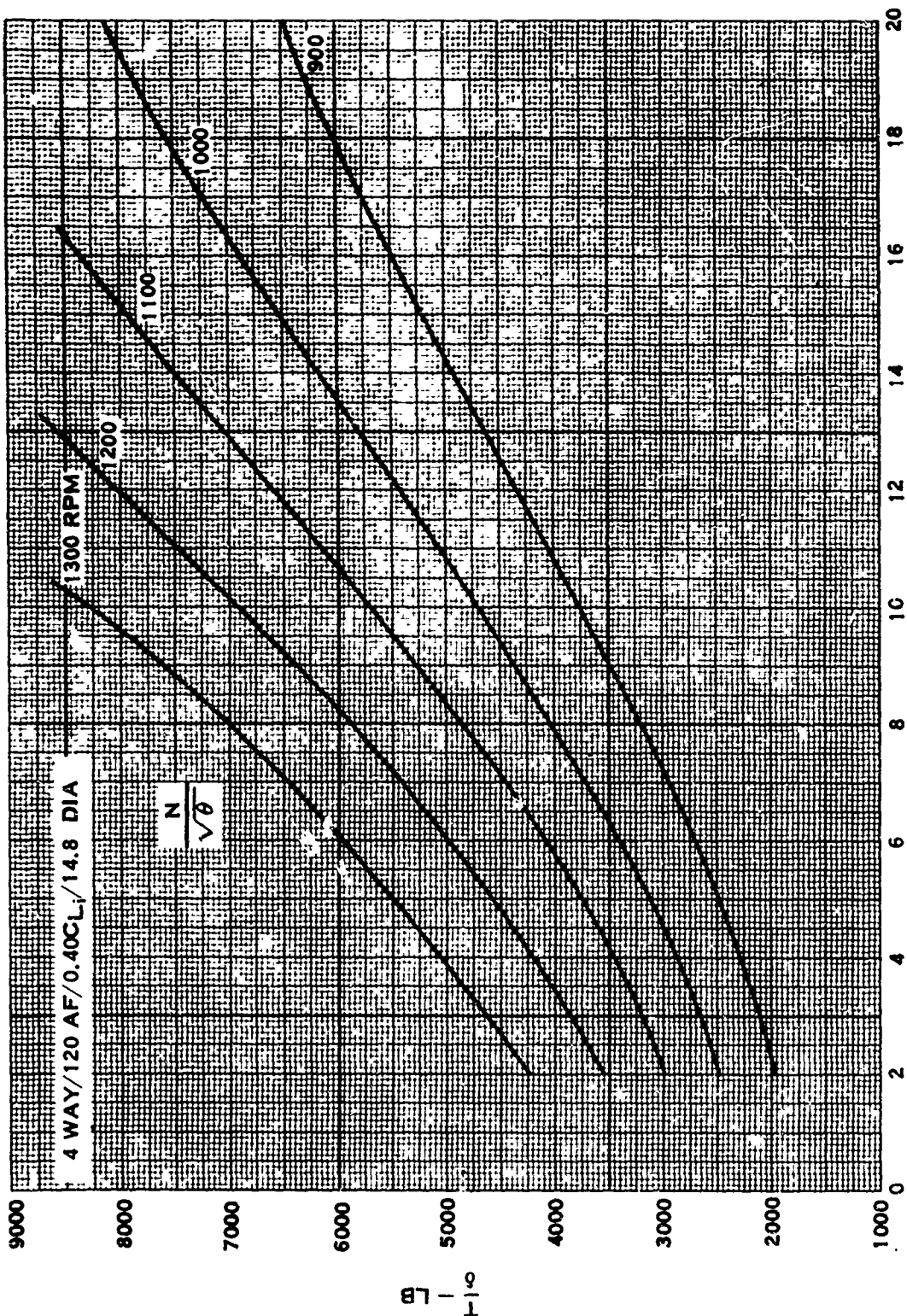
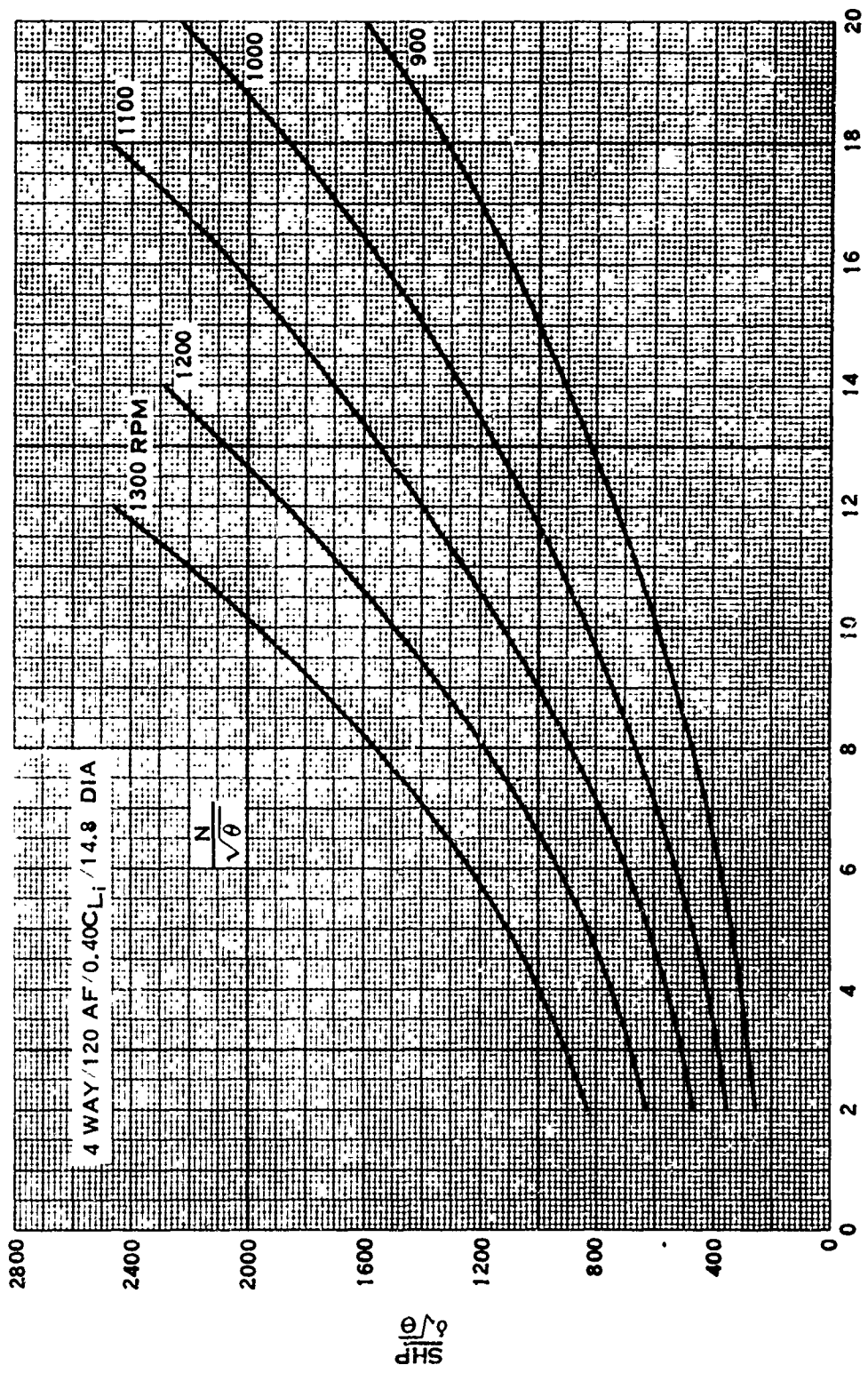


FIGURE 82. BLADE ANGLE AT .75 RADIUS - DEG.
 (THRUST VS BLADE ANGLE)



BLADE ANGLE AT .75 RADIUS - DEG.

FIGURE 83. STATIC PROPELLER PERFORMANCE
(HORSEPOWER VS BLADE ANGLE)

TABLE XVIII. ESTIMATED PRESSURE RECOVERY					
ATTITUDE	SHP	PRPM	ALTITUDE	SPEED (KTAS)	PRESSURE RECOVERY*
HOVER	1400	1160	6000 FT, 95° F	0	1.0058
HOVER	2000	1160	SL, STD	0	1.0061
CRUISE	643	700	SL, STD	250	1.0017
CRUISE	643	815	SL, STD	250	0.9993
CRUISE	643	930	SL, STD	250	0.9963

*INTEGRATED FROM SPINNER CUTOFF ($r/R = 0.098$) TO THE ESTIMATED RADIALLY OUTWARD LOCATION OF THE ENGINE AIR-INLET ($r/R = 0.208$)

$\frac{T}{A} = 35.0$ AT ZERO CYCLIC PITCH, 1400 HP, 6000 FT, 95°F

$900\pi n D$

4-WAY/14.8 - FT DIA/120 AF/0.4C_L PROPELLER

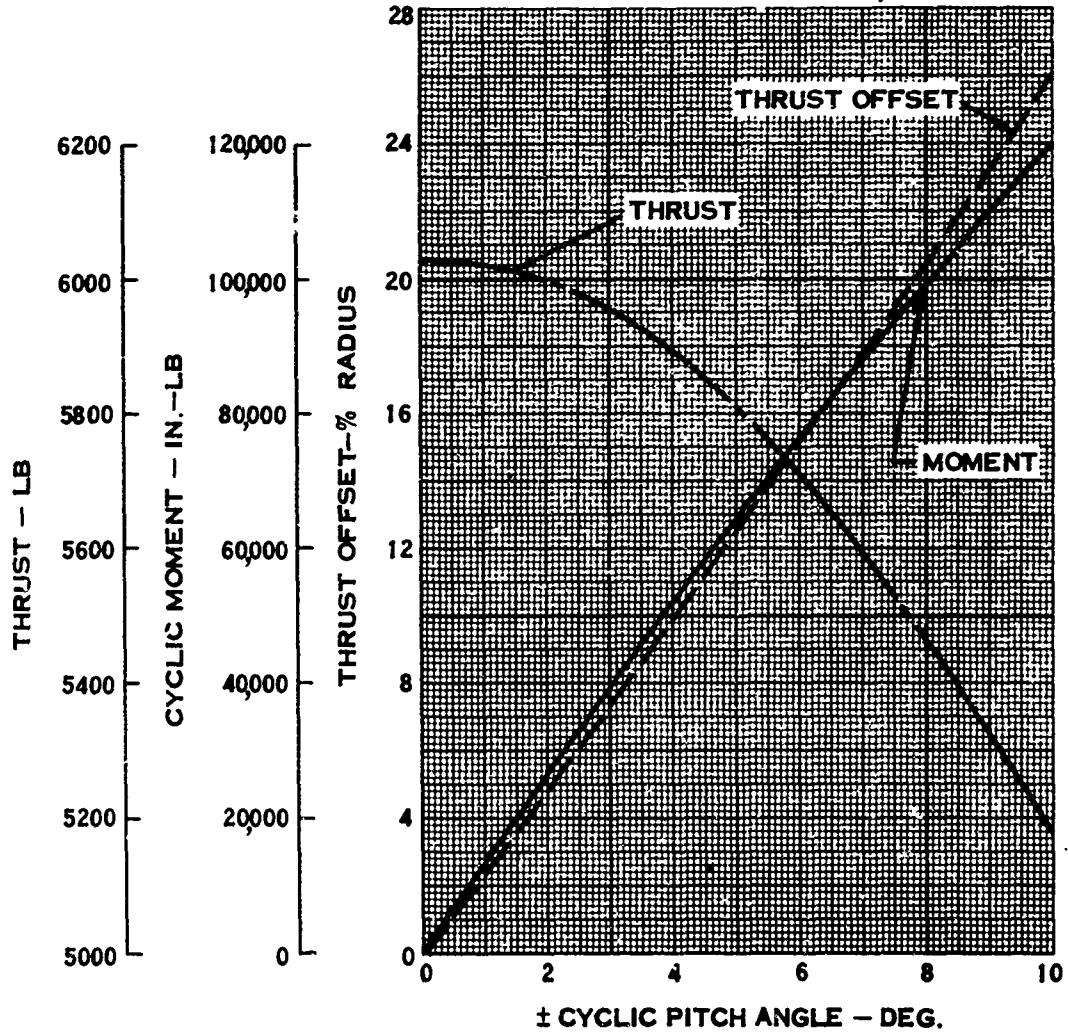


FIGURE 84. STATIC PROPELLER CYCLIC PITCH PERFORMANCE

TABLE XIX. OPERATING CONDITIONS FOR NOISE ESTIMATES

VELOCITY (KN)	HORSEPOWER	TIP VELOCITY (FT/SEC)	ALTITUDE (FT)	PROPELLER DIAMETER (FT)	NUMBER OF BLADES
0	1050	900	6000 AT 95°F	12.8	4
0	1400	900	6000 AT 95°F	14.8	4
250	643	450	SEA LEVEL	14.8	4
250	643	540	SEA LEVEL	14.8	4
250	643	630	SEA LEVEL	14.8	4
250	482	450	SEA LEVEL	12.8	4
250	482	540	SEA LEVEL	12.8	4
250	482	630	SEA LEVEL	12.8	4

TABLE XX. NEAR FIELD NOISE ESTIMATES

HOVER CONDITION

12.8 FT DIA, 1050 HP, 900 FT/SEC TIP SPEED 6000 FT ALT, 95°F

O.A.	137.82 DB	6	119.8
FUNDAMENTAL	134.3	7	118.8
2	130.8	8	118.8
3	127.8	9	118.8
4	124.8	10	118.8
5	121.8		

CRUISE CONDITION

250 KN, 482 HP, 450 FT/SEC TIP SPEED, 12.8 FT DIA, SEA LEVEL, STD DAY

O.A.	128.02 DB	6	107.0
FUNDAMENTAL	125.0	7	107.0
2	114.0	8	107.0
3	110.0	9	107.0
4	108.0	10	107.0
5	107.0		

250 KN, 482 HP, 540 FT/SEC TIP SPEED, 12.8 FT DIA, SEA LEVEL, STD DAY

O.A.	129.12 DB	6	108.1
FUNDAMENTAL	126.6	7	108.1
2	116.1	8	108.1
3	112.1	9	108.1
4	110.1	10	108.6
5	109.1		

250 KN, 482 HP, 630 FT/SEC TIP SPEED, 12.8 FT DIA, SEA LEVEL, STD DAY

O.A.	129.22 DB	6	110.2
FUNDAMENTAL	126.7	7	109.2
2	119.7	8	109.2
3	116.2	9	109.2
4	113.2	10	109.2
5	111.2		

TABLE XX—CONTINUED

HOVER CONDITION

14.8 FT DIA, 1400 HP, 900 FT/SEC TIP SPEED, 6000 FT ALT, 95°F

O.A.	137.7 DB	6	119.7
FUNDAMENTAL	134.2	7	118.7
2	130.7	8	118.7
3	127.7	9	118.7
4	124.7	10	118.7
5	121.7		

CRUISE CONDITION

250 KN, 643 HP, 450 FT/SEC TIP SPEED, 14.8 FT DIA, SEA LEVEL, STD DAY

O.A.	128.6 DB	6	107.6
FUNDAMENTAL	125.6	7	107.6
2	114.6	8	107.6
3	110.6	9	107.6
4	108.6	10	107.6
5	107.6		

250 KN, 643 HP, 540 FT/SEC TIP SPEED, 14.8 FT DIA, SEA LEVEL, STD DAY

O.A.	129.4 DB	6	109.4
FUNDAMENTAL	126.9	7	109.4
2	118.4	8	109.4
3	113.9	9	109.4
4	111.4	10	109.4
5	109.9		

250 KN, 643 HP, 630 FT/SEC TIP SPEED, 14.8 FT DIA, SEA LEVEL, STD DAY

O.A.	130.4 DB	6	110.4
FUNDAMENTAL	127.9	7	110.4
2	120.4	8	110.4
3	116.4	9	110.4
4	113.4	10	110.4
5	111.4		

NOTE O.A. INDICATES OVERALL NOISE LEVEL
FUNDAMENTAL 2,3... INDICATES THE HARMONIC ORDER

TABLE XXI. FAR FIELD NOISE ESTIMATES (1000 FT)

HOVER CONDITION

6000 FT ALT, 95°F V = 0 KN

12.8 FT DIA	1050 HP	O.A. = 62.26 DB
14.8 FT DIA	1400 HP	O.A. = 62.12 DB

CRUISE CONDITION

250 KN, 482 HP, 1000 FT ALT, STD DAY, 12.8 FT DIA

V _T * 450	O.A. 68.02 DB
V _T 540	O.A. 69.12 DB
V _T 630	O.A. 69.22 DB

250 KN, 482 HP, 1000 FT ALT, STD DAY, 14.8 FT DIA

V _T 450	O.A. 68.6 DB
V _T 540	O.A. 69.4 DB
V _T 630	O.A. 70.4 DB

* V_T INDICATES PROPELLER TIP SPEED IN FEET PER SECOND

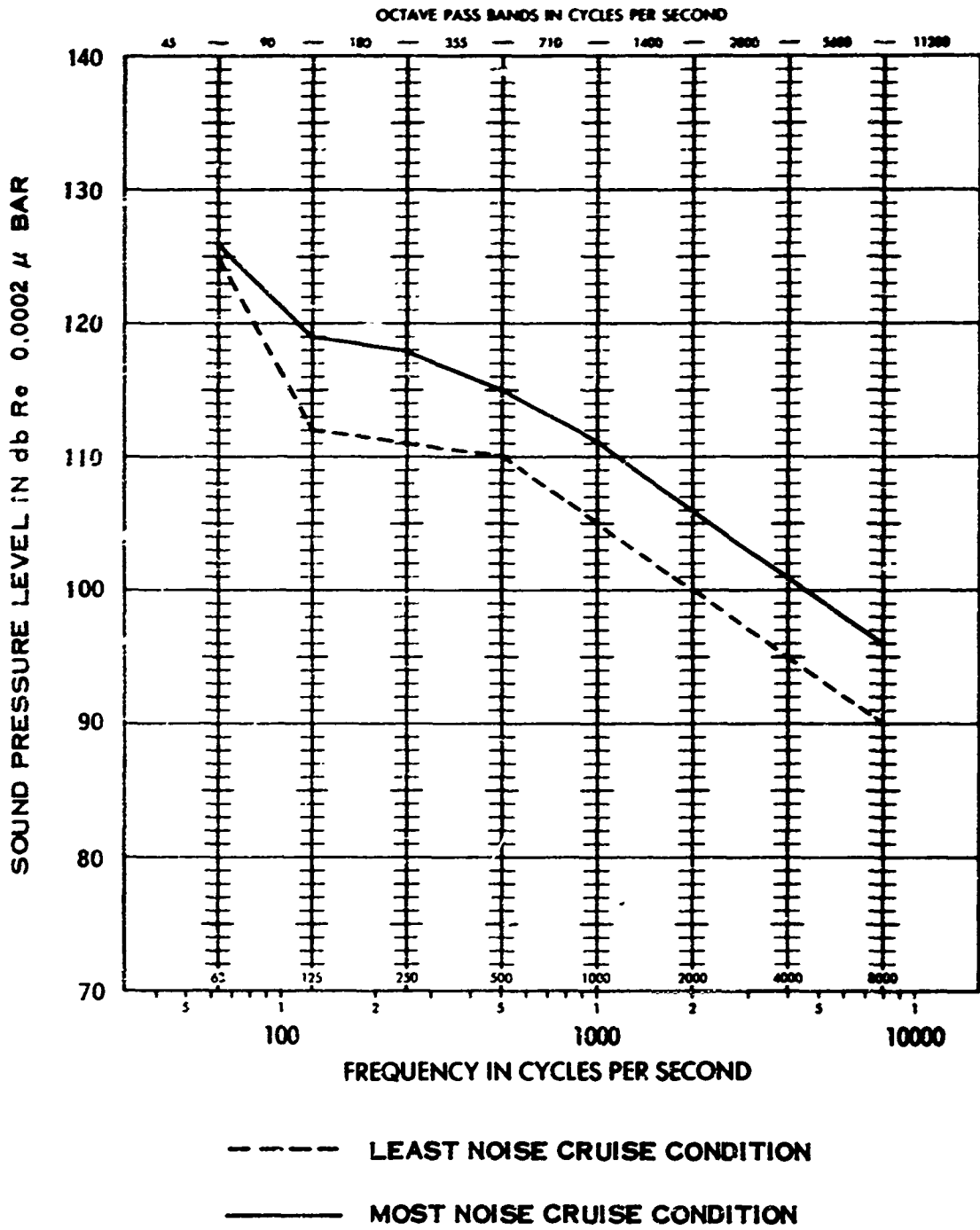


FIGURE 86. NOISE ESTIMATES FOR 12.8-FOOT-DIAMETER PROPELLER

estimated for cruise conditions would sound the same to anyone inside the aircraft, providing the tip of the propeller is the same distance from the fuselage in every case.

The far-field overall levels are summarized in Table XXI. These levels were estimated for a location 1000 feet from the tip of the propeller in the plane of rotation.

SCALING FACTORS

The system weights listed in the previous weight summary would vary if the sizing criteria were changed. This section presents scaling factors that can be applied to the previous system weights for estimating the effect on weight of changing the following significant design sizing parameters.

Hover Design SHP or Propeller Diameter

The point design is based on a 14.8-foot diameter, a 1400 design shp (hover at 6000 ft, 95°F), and a 0.78 figure of merit (FM), which produce 35 lbs of thrust per square foot of disk loading at the hover design point. If either the hover design shp or the figure of merit is changed, then the diameter will also be changed to keep the same 35 lb/ft² disk loading as shown in Figure 87. The scaling factor (WD) for these variables is presented in Figure 88.

Gear Ratio

The point design was based on a 20:1 reduction gear ratio to reduce the engine power turbine rpm to the desired propeller rpm. For the 14.8-foot-diameter propeller and the 900-fps hover speed point design propeller, the power turbine rpm would then be 23,250 rpm. If the propeller diameter or engine turbine speed is changed, then a different gear ratio may be required. The effect of different gear ratios is small, and the scaling factor (WGR) can be determined from Figure 89.

Gearbox Torque Limit

The hover design shp is a critical parameter for sizing the propeller from a performance viewpoint; however, from a structural viewpoint, the requirement for a power capacity higher than the hover design shp is usually specified. The major effect of propeller system weight is not actually the power capacity; it is the maximum continuous output torque of the integral gearbox. The point design was based on the sea-level, standard-day assumed engine takeoff rating of 2000 hp and 1160 propeller rpm, which is a torque limit of 9050 ft-lb for the propeller reduction gearbox output shaft. Scaling factors for other torque limit values (W_{TL}) are given in Figure 90.

"g" Loading

The effect of maneuver "g" forces can indirectly influence the structural design of the propeller. The "g" loading essentially increases the gross weight of the aircraft, and thus the angle of attack of the wing must increase to maintain equilibrium. This will change the air inflow environment of the propeller, and it can impose a

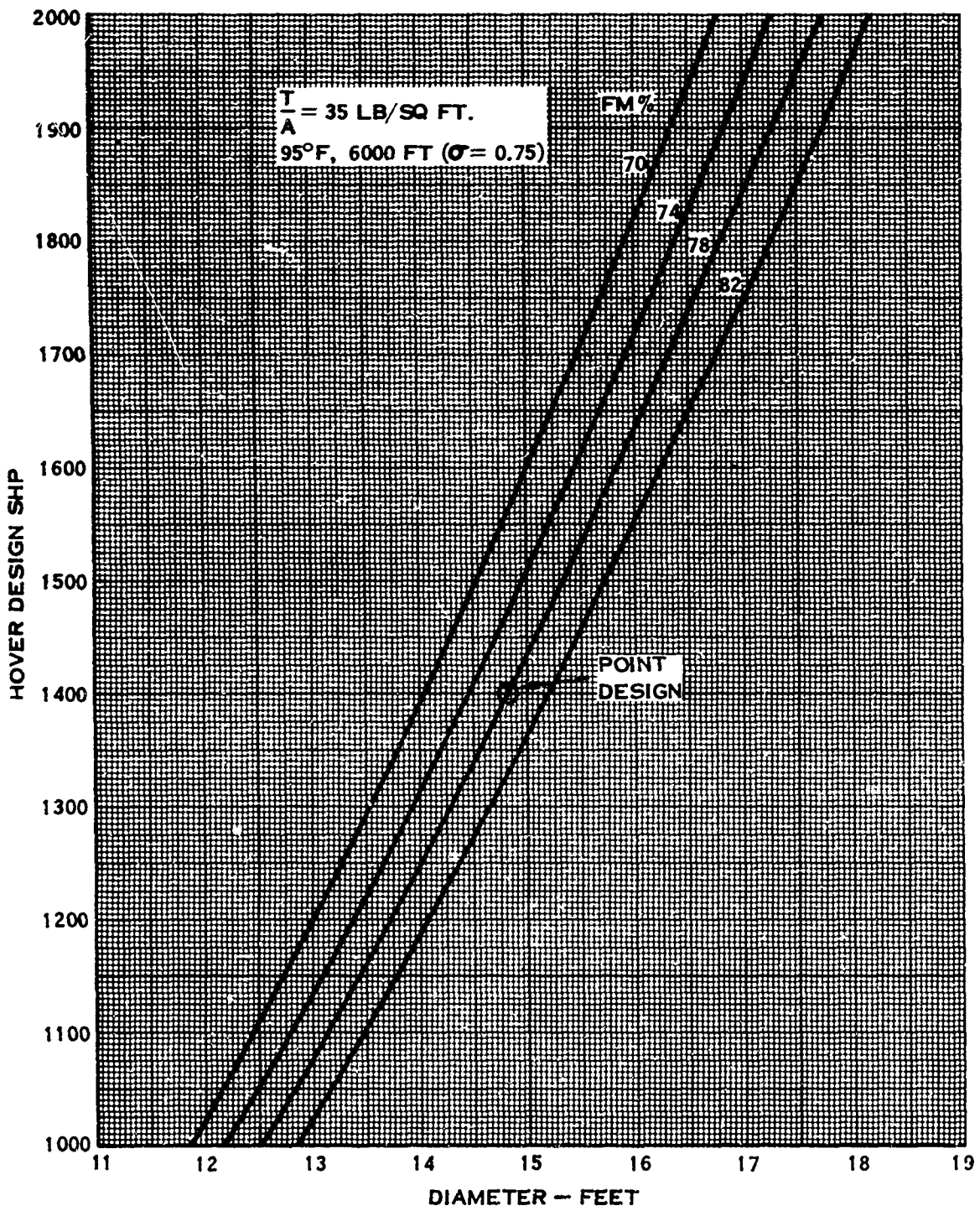


FIGURE 87. VARIATION OF SHAFT HORSEPOWER WITH PROPELLER DIAMETER

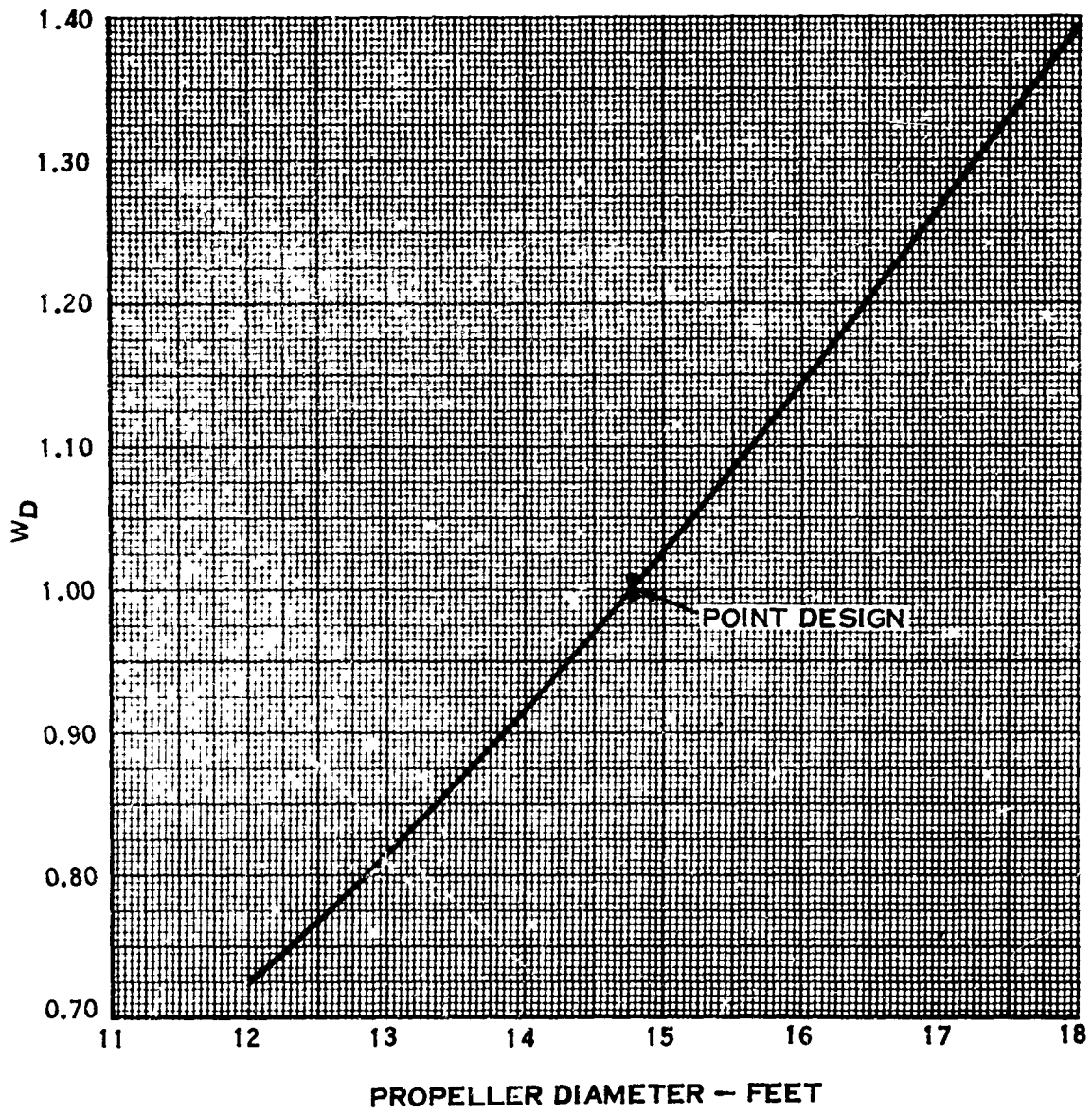


FIGURE 88. DIAMETER — WEIGHT FACTOR

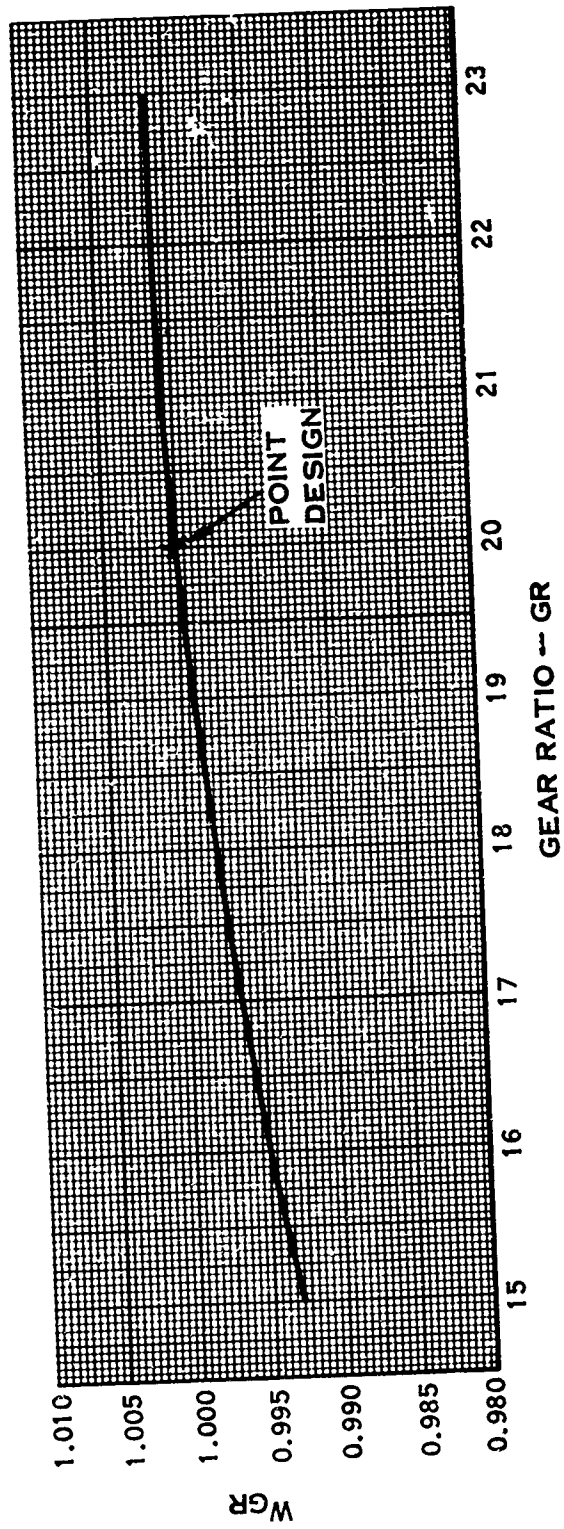


FIGURE 89. GEAR RATIO -- WEIGHT FACTOR

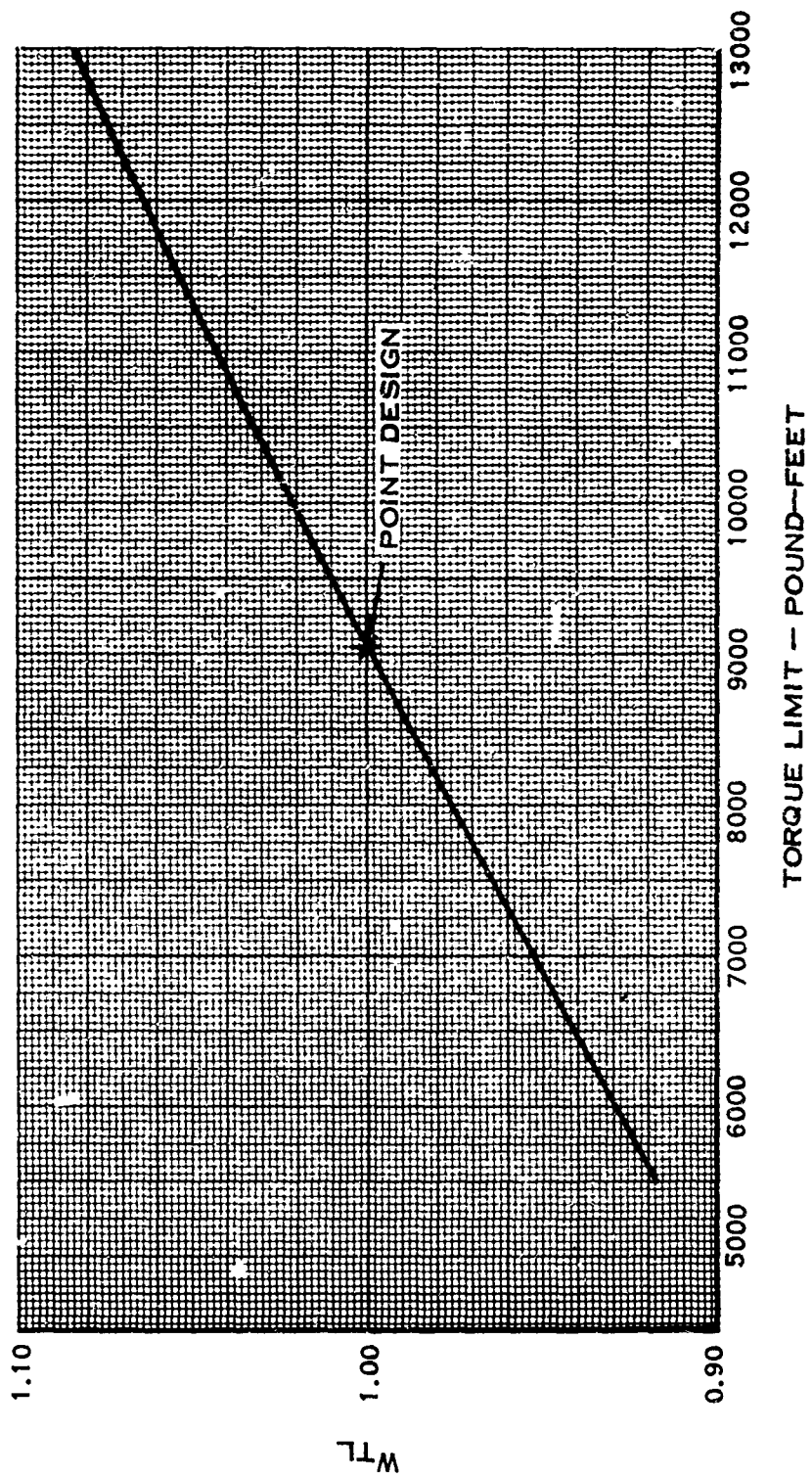


FIGURE 90. TORQUE LIMIT - WEIGHT FACTOR

higher operating excitation factor (E. F.). The frequency of occurrence of "g" loadings and equivalent E. F. 's can be estimated for the life of the aircraft and superimposed upon the normal (1 "g") operating E. F. resulting from the aircraft geometry. Both the frequency of occurrence and the magnitude of the "g" loading are significant, since the determining factor is usually the fatigue stress allowable versus number of stress cycles of the blade structural material.

The point design was based upon an E. F. of 4.0 plus 25% for higher order excitations. This design E. F. is higher than that calculated using the previously defined aircraft geometry, and it would allow margin for a 6.25 "g" loading. The frequency and proportionment of "g" loads were calculated using MIL-A-8866 (ASG), Table IV. Scaling factors for other magnitudes of "g" loading (W_g) are presented in Figure 91.

Total Activity Factor

The point design is based on a total activity factor of 480. Scaling factors (W_x) to show the effect of activity factor on the propeller system weight are shown in Figure 92. Note that curves in the "Aerodynamic Studies" section of this report show that there would be a change in thrust per horsepower if the activity factor is changed. Thus, propeller diameter or hover design shp should be changed to maintain the hover thrust disk loading of 35 lb/ft².

Number of Blades

A study of the weight of a 3-way/160 AF propeller was made for comparison with the point design 4-way/120 AF (note that the same total propeller solidity was compared). The lower total blade weight for the 3-way propeller would have resulted in a propeller system weight approximately 4 percent lighter than the 4-way propeller, except that in this case the increased weight of the 3-way barrel, actuator, and spinner caused the 3-way propeller to be approximately 0.4 percent heavier than the 4-way propeller. Because of this, it was concluded that, for the purposes of this study, there was essentially no weight difference between 4-way and 3-way propellers of the same total solidity.

The scaling factors are used as independent variables in the following equation, which defines the propeller system weight if the design sizing criteria are changed:

$$\text{Weight} = \left[\text{Weight of Point Design} \right] (W_D)(W_{GR})(W_{TL})(W_g)(W_x)$$

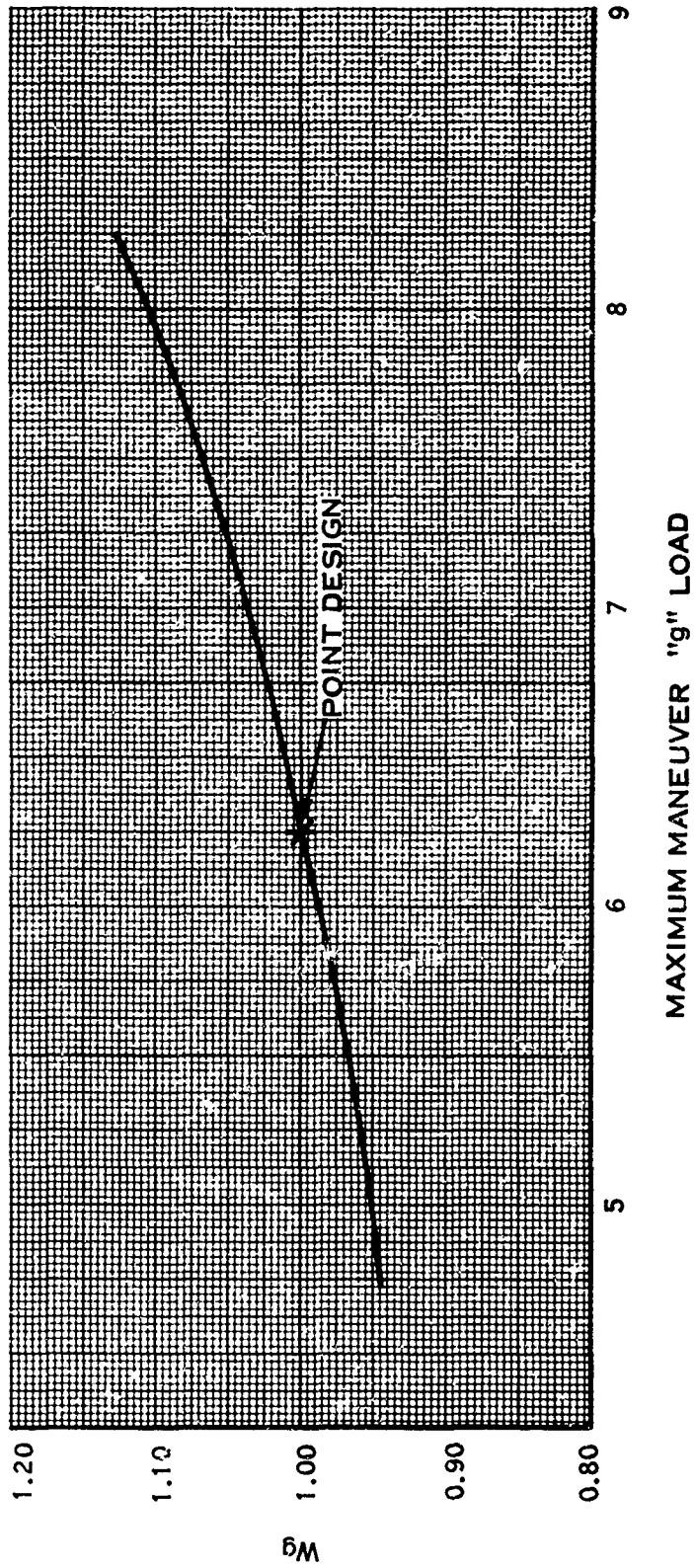


FIGURE 91. "g" LOADING - WEIGHT FACTOR

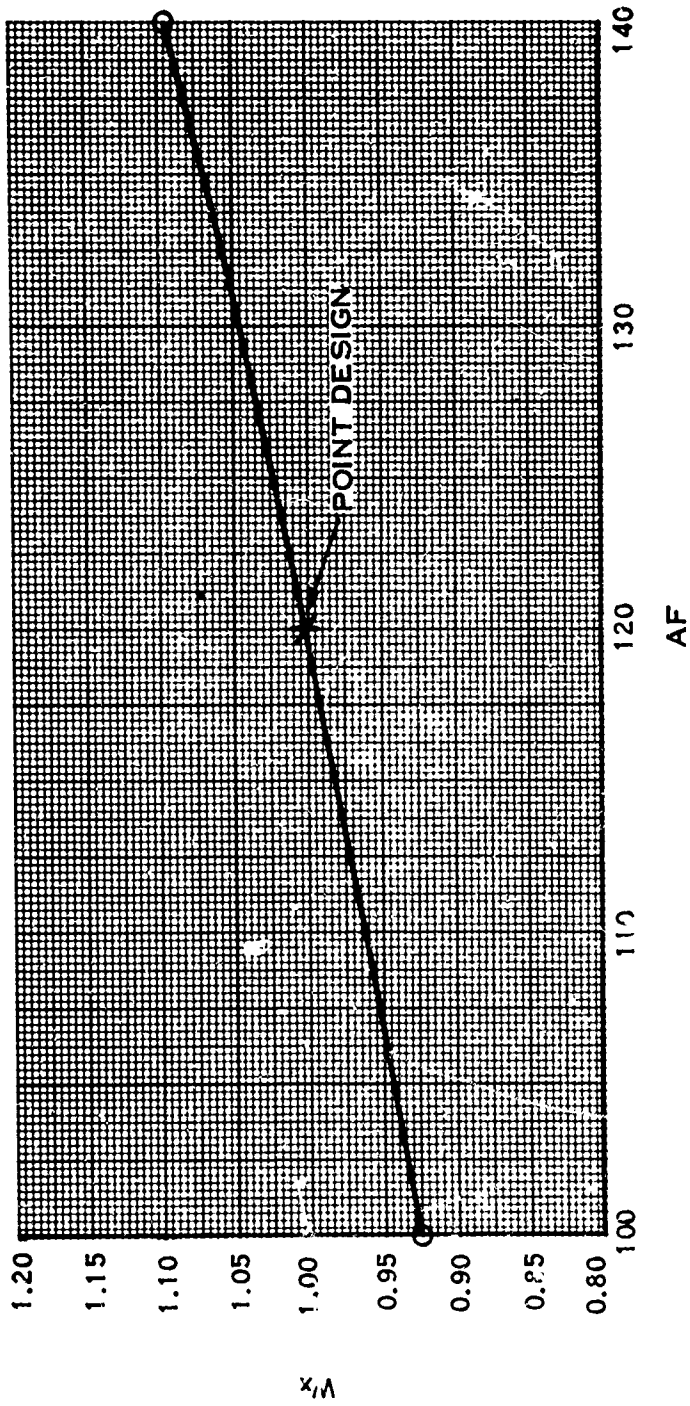


FIGURE 92. ACTIVITY FACTOR - WEIGHT FACTOR

Sample Calculation

Given: Engine with 1500 shp (sea level, standard day) and 1050 shp (6000 feet, 95°F) rating. Use 1050 shp for hover design point and 1500 shp for hover torque limit. No change in gear ratio from that of the point design. From Figure 87 (assuming 0.78 FM), the propeller diameter will be 12.8 feet; Figure 88 defines $W_D = 0.795$.

$$WGR = 1$$

The new torque limit will be lower than that of the point design (9050 ft-lb) because of both the smaller propeller diameter (higher propeller rpm for the same tip speed) and the lower maximum shp.

$$\text{Torque Limit} = 9050 \times \frac{12.8}{14.8} \times \frac{1500}{2000} = 5880 \text{ ft-lb}$$

$$\text{From Figure 90, } W_{TL} = 0.926$$

$$W_g = 1$$

$$W_x = 1$$

$$\text{Weight} = 388.1 (0.795)(1)(0.926)(1)(1)$$

$$\text{Weight} = 286 \text{ lb IGB Propeller Wet Weight}$$

CONCLUSIONS AND RECOMMENDATIONS

1. It is concluded that significant reductions can be made in the weight of future advanced V/STOL propeller systems. Over 50% weight reduction is projected for the 1970-1975 V/STOL propeller systems when compared to systems presently available. This weight reduction should have a major influence on improving V/STOL mission and cost effectiveness.

2. The major contributions to reducing the propeller system weight are proportioned as shown below:

Approximately 20% system weight reduction is feasible by incorporating a boron/aluminum metal blade spar. (As an alternate, approximately 13% reduction would be realized by use of a titanium spar.)

Approximately 20% system weight reduction is feasible through the implementation of new design concepts and packaging arrangements.

Approximately 10% system weight reduction is feasible by the substitution of titanium for steel in the propeller barrel, actuator, and gearbox, including some selective reinforcements using boron composites.

3. The technology development for the application of titanium in the propeller system is now being actively pursued, and with the logical continuation of present development, the timetable for incorporating titanium can be clearly projected. Use of titanium in all recommended areas of the propeller system, with the exception of the gears, should be practical by 1970. Significant advances in titanium gearing have been realized recently; with continued development, titanium should prove to be a suitable gear material before 1975.
4. Intensive R&D activity over the last two to three years has advanced industry's knowledge of a number of composite materials considerably beyond the laboratory stage. Of these, the boron/aluminum composite appears to promise the maximum in weight reduction for an advanced blade structure. Existing knowledge is sufficient to justify exploratory development leading to the application of boron/aluminum blade spars during the early 1970's.
5. The various new concepts for design packaging shown in this report are considered to be natural extensions and refinements of present V/STOL propeller technology and will be available for use by 1970.

6. The cyclic pitch propeller configuration presented in the report was found to be of the lightest weight and the highest potential reliability of all the cyclic pitch concepts studied. The recommended concept added little weight to the basic propeller system, achieved a desired basic design simplicity, and packaged the additional mechanism inside the propeller system to keep it protected and free from contamination.

7. For the early attainment of the maximum weight reductions of the propeller systems shown herein, it is recommended that appropriate R&D effort be initiated on the major, long-lead-time items. Specifically, prime emphasis should be placed on expediting the basic technological development of the boron/aluminum blade spar and titanium gears. Initial development of cyclic pitch mechanisms should also be pursued.

APPENDIX I
PRESENT-DAY TURBOPROP SYSTEMS

Table XXII presents data on present-day turboprop propeller and gearbox systems which were furnished by six U. S. manufacturers and four foreign manufacturers.

The propeller systems representing the conventional turboprop and gearbox installations are plotted in Figure 93. As can be seen from the generalized plot, there is a large amount of scatter in the data. A previously developed generalization is also shown on the plot (shaded band) for reference. The specific weight indicated by the plot for the point design size propeller of this study (4-lb thrust/hp at sea level, standard day) is approximately 0.55 lb per hp.

TABLE XXII - PRESENT DAY TURBOPROP SYSTEMS

	A	B	C	
1.0	<p>PROPELLER DESCRIPTION</p> <p>DATE OF FIRST QUALIFICATION OR CERTIFICATION PROPELLER DIAMETER (FEET)</p> <p>PROPELLER MOUNTING SIZE DIRECTION OF PROP ROTATION NUMBER OF BLADES PER PROPELLER</p> <p>BLADE A.F. BLADE C.L.I. BLADE MATERIAL</p> <p>BARREL MATERIAL- SPINNER MATERIAL TYPE OF CONTROL</p> <p>TYPE OF BLADE PITCH CHANGE ACTUATION SINGLE OR DUAL HYDRAULIC SYSTEM TYPE OF DEICING</p> <p>FEATHERING AVAILABLE REVERSING AVAILABLE PITCH-LOCK AVAILABLE SYNCHROPHASING AVAILABLE</p> <p>GEARBOX DESCRIPTION</p> <p>GEAR RATIO DESCRIPTION OF GEAR TRAIN TYPE OF GEARING GEARBOX EFFICIENCY PROVISIONS FOR MOUNTING WHICH ACCESSORIES</p> <p>SPECIAL FEATURES HOUSING MATERIAL</p> <p>WEIGHT DATA - COMPONENTS (LBS)</p>	<p>1959 13.5</p> <p>NO. 60 SPLINE RH 4</p> <p>178 0.479 ALUMINUM</p> <p>STEEL FIBERGLASS IOC, BETA</p> <p>HYDRO-MECH SINGLE ELECTRICAL</p> <p>YES YES YES YES</p> <p>13.54</p> <p>STARTER, GENERATOR TURBOCHARGER TACH. NEGATIVE TORQUE SENSOR (NTS)</p>	<p>1959 13.5</p> <p>NO. 60 SPLINE RH 4</p> <p>163 0.286 ALUMINUM</p> <p>STEEL FIBERGLASS IOC, BETA</p> <p>HYDRO-MECH SINGLE ELECTRICAL</p> <p>YES YES YES YES</p> <p>13.54</p> <p>STARTER, GENERATOR TURBOCHARGER TACH. NEGATIVE TORQUE SENSOR (NTS)</p>	<p>1959 13.5</p> <p>NO. 60 SPLINE RH 4</p> <p>163 0.286 ALUMINUM</p> <p>STEEL FIBERGLASS IOC, BETA</p> <p>HYDRO-MECH SINGLE ELECTRICAL</p> <p>YES YES YES YES</p> <p>13.54</p> <p>STARTER, GENERATOR TURBOCHARGER TACH. NEGATIVE TORQUE SENSOR (NTS)</p>
2.0				
3.0				

TABLE XXII - CONTINUED

	A	B	C
BLADES	539	532	552
HUB	327	320	320
SPINNER	60	44	44
AFTERBODY	17	36	36
CONTROL	106	120	120
GEARBOX	598	598	598
CLUTCHES	NONE	NONE	NONE
HYDRAULIC OIL	45	45	45
LUBRICATING OIL	NO DATA	NO DATA	NO DATA
PERFORMANCE DATA			
TAKE OFF (STATIC SL-SD)			
THRUST	8810	7980	7620
SHIP	4591	4591	4591
PROP RPM	1020	1020	1020
CRUISE			
ALTITUDE (FEET)	10,000	10,000	25,000
EFFICIENCY	.893	.888	.922
KNOTS (TRUE)	300	300	330
SHIP	3800	3800	1760
PROP RPM	1020	1020	1020
VMAX (LEVEL FLIGHT)			
ALTITUDE (FEET)	15,000	10,000	0 8000
EFFICIENCY	0.908	.912	
KNOTS (TRUE)	350	380	364 KIAS
SHIP	3100	3710	4000
PROP RPM	1020	1020	1020
STRUCTURAL DATA			
MAX CONTINUOUS AQ AND THE OPERATING CONDITION AT WHICH IT OCCURS (AT ONE G)			
	1301.7 AQ AT	1600 AQ AT	1870 AQ AT
	155 000 LBS AT	142 000 LBS AT	66 100 LBS AT
	140 KNOTS	175 KNOTS	364 KIAS
MAX MANEUVERING "G" LEVEL	3G	3G	3G
VMAX (PLACARD)	360 KIAS	403 KIAS	364 KIAS

		TABLE XXII - CONTINUED				
		D	E	F	G	H
1.0	PROPELLER DESCRIPTION					
	DATE OF FIRST QUALIFICATION OR CERTIFICATION	1962	1962	1962	1962	1962
	PROPELLER DIAMETER (FEET)	14.5	14.5	14.5	14.5	14.5
	PROPELLER MOUNTING SIZE					
	DIRECTION OF PROP ROTATION					
	NUMBER OF BLADES PER PROPELLER	NO. 60 SPLINE RH 3	NO. 60 SPLINE RH 3	NO. 60 SPLINE RH 3	NO. 60 SPLINE RH 3	NO. 60 SPLINE RH 3
	BLADE A.F.					
	BLADE CLI					
	BLADE MATERIAL					
	BARREL MATERIAL	120	120	120	120	120
	SPINNER MATERIAL	ALUMINUM	ALUMINUM	ALUMINUM	ALUMINUM	ALUMINUM
	TYPE OF CONTROL	0.654	0.654	0.654	0.654	0.654
	TYPE OF BLADE PITCH CHANGE ACTUATION	STEEL FIBERGLASS IOC	STEEL FIBERGLASS IOC	STEEL FIBERGLASS IOC	STEEL FIBERGLASS IOC	STEEL FIBERGLASS IOC
	SINGLE OR DUAL HYDRAULIC SYSTEM					
	TYPE OF DE-ICING	HYDRO-MECH SINGLE ELECTRICAL	HYDRO-MECH SINGLE ELECTRICAL	HYDRO-MECH SINGLE ELECTRICAL	HYDRO-MECH SINGLE ELECTRICAL	HYDRO-MECH SINGLE ELECTRICAL
	FEATHERING AVAILABLE	YES	YES	YES	YES	YES
	REVERSING AVAILABLE	YES	YES	YES	YES	YES
	PITCH-LOCK AVAILABLE	YES	YES	YES	YES	YES
	SYNCHROP USING AVAILABLE	YES	YES	YES	YES	YES
	GEARBOX DESCRIPTION					
	GEAR RATIO					
	DESCRIPTION OF GEAR TRAIN					
	TYPE OF GEARING	13.44 SIMPLE REDUC- TION & PLAN- ETARY SPUR AND HELICAL 97.9 2 PUMPS 1 GENERATOR TANDEM MOUNT- ED ACCESSORY GEARBOX ALUMINUM	13.44 SIMPLE REDUC- TION & PLAN- ETARY SPUR AND HELICAL 97.9 2 PUMPS 1 GENERATOR TANDEM MOUNTED ACCESSORY GEARBOX ALUMINUM	13.44 SIMPLE REDUC- TION & PLAN- ETARY SPUR AND HELICAL 97.9 2 PUMPS 1 GENERATOR TANDEM MOUNTED ACCESSORY GEARBOX ALUMINUM	13.44 SIMPLE REDUC- TION & PLAN- ETARY SPUR AND HELICAL 97.9 2 PUMPS 1 GENERATOR TANDEM MOUNTED ACCESSORY GEARBOX ALUMINUM	13.44 SIMPLE REDUC TION & PLAN ETARY SPUR AND HELICAL 97.9 2 HYD. PUMPS TANDEM MOUNTED ACCESSORY GEARBOX ALUMINUM
	GEARBOX EFFICIENCY					
	PROVISIONS FOR MOUNTING WHICH ACCESSORIES					
	SPECIAL FEATURES					
	HOUSING MATERIAL					
2.0						

		TABLE XXII -- CONTINUED						
		D	E	F	G	H		
30	WEIGHT DATA COMPONENTS (LBS)							
	BLADES	348	348	348	348	348	348	
	HUB	263	263	263	263	263	263	
	SPINNER	37	37	37	37	37	37	
	AFTERBODY	20	20	20	20	20	20	
	CONTROL	72	72	72	72	72	72	
	GEARBOX	413	357	413	413	413	357	
	CLUTCHES	NONE	NONE	NONE	NONE	NONE	NONE	
	HYDRAULIC OIL	34	34	34	34	34	34	
	LUBRICATING OIL	NO DATA	NO DATA	NO DATA	NO DATA	NO DATA	NO DATA	
	PERFORMANCE DATA							
	TAKE OFF (STATIC SL 50)							
	JUST	8530	8710	8620	8620	8888	8888	
	541P	2655	2970	2765	2765	3095	3095	
	PROP RPM	1160	1160	1160	1160	1160	1160	
	CRUISE							
	ALTITUDE (FEET)	S.L.	10,000	10,000	10,000	S.L.	S.L.	
	EFFICIENCY	.898	.89	.89	.892	.892	.892	
	KNOTS (KTAS)	270	174	174	200	215	215	
	SHF	2045	895	895	1580	1800	1800	
	PROP RPM	1015	854	854	1015	1015	1015	
	VMAX (LEVEL FLIGHT)							
	ALTITUDE	S.L.	S.L.	S.L.	S.L.	S.L.	S.L.	
	EFFICIENCY	.833	.90	.90	.71	.71	.915	
	KNOTS (KTAS)	315	230	228	324	300	300	
	SHF	2937	2667	2340	1800	2200	2200	
	PROP RPM	1160	1015	1015	1160	1015	1015	
	STRUCTURAL DATA							
	MAX CONTINUOUS AQ AND THE OPERATING CONDITION							
	AT WHICH IT OCCURS AT ONE G	1140 AQ, 72000	-850, 25000	-840, 25,000	1150, MIN. G.W.	580, 46,000 LB.		
		LB, 139 KIAS	LB, 291 KIAS	LB 218 KIAS	341 KIAS	140 KIAS		
	MAX MANEUVERING 1 G ¹ LEVEL							
	VMAX (PLACARD)	350 KIAS	291 KIAS	341 KIAS	341 KIAS	270 KIAS		

TABLE XXII - CONTINUED

	I	J	K	L	M
PROPELLER DESCRIPTION					
DATE OF FIRST QUALIFICATION OR CERTIFICATION	1963				
PROPELLER DIAMETER (FEET)	10	7.5	8.5	8.5	8.5
PROPELLER MOUNTING SIZE	NO. 51 SPLINE	4.25 INCH B.C.	4.25 INCH B.C.	4.25 INCH B.C.	4.25 INCH B.C.
DIRECTION OF PROP ROTATION	RH	RH	RH, LH	RH, LH	RH
NUMBER OF BLADES PER PROPELLER	3	3	3	3	3
BLADE A.F.	125	109	109	109	109
BLADE C.L.I.	0.448	0.424	0.509	0.509	0.509
BLADE MATERIAL	ALUMINUM	ALUMINUM	ALUMINUM	ALUMINUM	ALUMINUM
BARREL MATERIAL	STEEL	STEEL	STEEL	STEEL	STEEL
SPINNER MATERIAL	FIBERGLASS	FIBERGLASS	FIBERGLASS	FIBERGLASS	FIBERGLASS
TYPE OF CONTROL	IOC	ENGINE OIL, BETA GEARBOX MTG	ENGINE OIL, BETA GEARBOX MTG	ENGINE OIL, BETA GEARBOX MTG	ENGINE OIL, RI, TA GEARBOX MTG
TYPE OF BLADE PITCH CHANGE ACTUATION	HYDRO-MECH SINGLE ELECTRICAL	HYDRO-MECH SINGLE ELECTRICAL	HYDRO-MECH SINGLE ELECTRICAL	HYDRO-MECH SINGLE ELECTRICAL	HYDRO-MECH SINGLE ELECTRICAL
SINGLE OR DUAL HYDRAULIC SYSTEM	YES	YES	YES	YES	YES
TYPE OF DEICING	YES	YES	YES	YES	YES
FEATHERING AVAILABLE	YES	NO	NO	NO	NO
REVERSING AVAILABLE	YES	NO	NO	NO	NO
PITCH-LOCK AVAILABLE	YES	NO	NO	NO	NO
SYNCHROPHASING AVAILABLE	YES	NO	NO	NO	NO
2.0 GEARBOX DESCRIPTION					
GEAR RATIO	12.4	20.9	20.9	15.0	24.1
DESCRIPTION OF GEAR TRAIN	SPLIT POWER	SIMPLE, REDUCTION & PLANETARY HELICAL & SPUR 97 - 98	SIMPLE REDUCTION & PLANETARY HELICAL & SPUR 97 - 98	2 STAGE PLANETARY SPUR 97	COMPOUND STAR
TYPE OF GEARING	STARTER, TACH GENERATOR	PROPELLER GOVERNOR, TACH GENERATOR, STARTER	PROPELLER GOVERNOR, TACH GENERATOR, STARTER	PROPELLER GOVERNOR, OVERSPEED GOVERNOR, TACH GENERATOR, GOVERNOR, TORQUE METER	TACH GENERATOR, STARTER, FUEL PUMP, GOVERNOR, OIL PUMP
GEARBOX EFFICIENCY					
PROVISIONS FOR MOUNTING WHICH ACCESSORIES					
SPECIAL FEATURES	NTS, POWER TAKE-OFF PAD				
HOUSING MATERIAL	MAGNESIUM	MAGNESIUM	MAGNESIUM	MAGNESIUM	MAGNESIUM

TABLE XXII - CONTINUED

	I	J	K	L	M
3.0 WEIGHT DATA - COMPONENTS (LBS)					
BLADES	142	55	70	70	70
HUB	115	69	74	75	75
SPINNER	10	7	9	9	7
AFTERGOOY	6	-	-	-	-
CONTROL	64	8	8	8	NO DATA
GEARBOX		121	125	78	NO DATA
CLUTCHES	NONE	NONE	NONE	NONE	NONE
HYDRAULIC OIL	15	-	-	-	NO DATA
LUBRICATING OIL	NO DATA	9	9	9	NO DATA
4.0 PERFORMANCE DATA					
TAKE-OFF (STATIC SL-SD)					
THRUST	3740	1730	2580	2880	2106
SH/P	1100	534	715	750	790
PROP RPM	1678	2000	2000	2200	1783
CRUISE					
ALTITUDE (FEET)	5000	15,000 (8°F)	S.L.	S.L.	15,000
EFFICIENCY	.91	.88	.88	.88	.88
KNOTS (K ³)	200	235	175	180	262
SH/P	480	245	330	275	575
PROP RPM	1475	2000	1770	1600	1783
VMAX (LEVEL FLIGHT)					
ALTITUDE (FEET)	5000	S.L.	S.L.	S.L.	S.L.
EFFICIENCY	.91	.88	.89	.89	.89
KNOTS (KTAS)	275	245	275	275	275
SH/P	910	433	810	810	810
PROP RPM	1678	2000	2000	2000	2000
5.0 STRUCTURAL DATA					
MAX CONTINUOUS AQ AND THE OPERATING CONDITION AT WHICH IT OCCURS (AT ONE G)	1760	632, 8500 LB.	-1200, 7000 LB.	1200, 7000 LB.	820, 9000 LB.
MAX MANEUVERING "G" LEVEL	6.0	100 KIAS	430 KEAS	430 KEAS	270 KIAS
VMAX (PLACARD)	390 KIAS	274 KIAS	430 KIAS, .7M	330 KEAS, .5M	270 KIAS

TABLE XXII - CONTINUED

	N	O	P	Q	
1.0	<p>PROPELLER DESCRIPTION</p> <p>DATE OF FIRST QUALIFICATION OR CERTIFICATION PROPELLER DIAMETER (FEET)</p> <p>PROPELLER MOUNTING SIZE DIRECTION OF PROP ROTATION NUMBER OF BLADES PER PROPELLER</p> <p>BLADE A.F. BLADE CLI. BLADE MATERIAL</p> <p>BARREL MATERIAL SPINNER MATERIAL TYPE OF CONTROL</p> <p>TYPE OF BLADE PITCH CHANGE ACTUATION SINGLE OR DUAL HYDRAULIC SYSTEM TYPE OF DEICING</p> <p>FEATHERING AVAILABLE REVERSING AVAILABLE PITCH-LOCK AVAILABLE SYNCHROPHASING AVAILABLE</p>	<p>1945 9.0 NO. 50 SPLINE RH 3</p> <p>156 0.485 ALUMINUM</p> <p>STEEL NONE BETA MOUNTED ON TRANSMISSION</p> <p>HYDRO-MECH SINGLE NONE</p> <p>NO-N/A YES NO NO-N/A</p>	<p>1945 10.0 NO. 50 SPLINE RH 3</p> <p>138 0.44 ALUMINUM</p> <p>STEEL NONE IOC, BETA</p> <p>HYDRO-MECH SINGLE NONE</p> <p>NO-N/A YES NO YES (CROSS-SHAFT)</p>	<p>1968 10.0 IGB MOUNT 3</p> <p>142 0.411 FIBERGLASS</p> <p>STEEL FIBERGLASS IOC, BETA</p> <p>HYDRO-MECH DUAL NONE</p> <p>NO-N/A YES NO NO-N/A</p> <p>1.39 FOR ANTI-TORQUE DRIVE RIGHT ANGLE</p>	<p>1965 7.0 IGB MOUNT RH LH 3</p> <p>157 0.458 FIBERGLASS</p> <p>STEEL FIBERGLASS BETA AIRCRAFT HYDRAULICS. MASTER CONTROL</p> <p>HYDRO-MECH DUAL NONE</p> <p>NO-N/A YES NO YES (CROSS-SHAFT)</p> <p>2.74 RIGHT ANGLE</p> <p>SPIRAL BEVEL 9%</p> <p>NONE INTEGRAL GEARCASE MAGNESIUM</p>
2.0	<p>GEAR BOX DESCRIPTION</p> <p>GEAR RATIO</p> <p>DESCRIPTION OF GEAR TRAIN</p> <p>TYPE OF GEARING</p> <p>GEARBOX EFFICIENCY</p> <p>PROVISIONS FOR MOUNTING WHICH ACCESSORIES SPECIAL FEATURES</p> <p>HOUSING MATERIAL</p>	<p>N/A</p> <p>PROPELLER SPEED RE- DUCTION IS PART OF VEHICLE TRAN- SMISSION</p>	<p>N/A</p> <p>PROPELLER SPEED RE- DUCTION IS PART OF VEHICLE TRAN- SMISSION</p>	<p>1.39 FOR ANTI-TORQUE DRIVE RIGHT ANGLE</p> <p>SPIRAL BEVEL N/A NONE INTEGRAL GEARCASE MAGNESIUM</p>	<p>2.74 RIGHT ANGLE</p> <p>SPIRAL BEVEL 9%</p> <p>NONE INTEGRAL GEARCASE MAGNESIUM</p>

TABLE XXII - CONTINUED

	R	S	T	U	V
1.0	PROPELLER DESCRIPTION				
	1964	1964	14.0	13.5	13.5
DATE OF FIRST QUALIFICATION OR CERTIFICATION	8.0	15.625	IGB MOUNT RH	IGB MOUNT	NO 60 SPLINE RH
PROPELLER DIAMETER (FEET)	IGB MOUNT RH	IGB MOUNT RH LH	IGB MOUNT RH	IGB MOUNT	IGB MOUNT
PROPELLER MOUNTING SIZE	3	4	1	8	6
DIRECTION OF PROP ROTATION					
NUMBER OF BLADES PER PROPELLER					
BLADE A.F.	145	105	120	110	107
BLADE CLI.	0.00	0.500	0.854	VC .200	VC .250
BLADE MATERIAL	FIBERGLASS	FIBERGLASS	ALUMINUM	FIBERGLASS	FIBERGLASS
BARREL MATERIAL	STEEL	STEEL	STEEL	STEEL	STEEL
SPINNER MATERIAL	NONE	NONE	FIBERGLASS	NONE	NONE
TYPE OF CONTROL	BETA, AIRCRAFT HYDRAULICS	BETA, AIRCRAFT HYDRAULICS	IOC, IGC MOUNTED	IOC, IGC MOUNTED	IOC
TYPE OF BLADE PITCH CHANGE ACTUATION	HYDRO-MECH DUAL	HYDRO-MECH DUAL	HYDRO-MECH SINGLE	HYDRO-MECH SINGLE	HYDRO-MECH SINGLE
SINGLE OR DUAL HYDRAULIC SYSTEM	NONE	ELECTRICAL	ELECTRICAL	NONE	NONE
TYPE OF DEICING					
FEATHERING AVAILABLE	NO-N A	YES	YES	YES	YES
REVERSING AVAILABLE	NO-N A	YES	YES	YES	YES
PITCH-LOCK AVAILABLE	NO-N A	NO	YES	YES	YES
SYNCHROPHASING AVAILABLE	YES	YES	YES	YES	YES
	(CROSS SHAFT)	(CROSS SHAFT)			
2.0	GEARBOX DESCRIPTION				
GEAR RATIO	5.25	11.05	12.08	13.5	12.08
DESCRIPTION OF GEAR TRAIN	RIGHT ANGLE	PINION-BULL 1ST STAGE, EPICYCLIC 2ND STAGE, RIGHT ANGLE CROSS-SHAFT DRIVE	PINION-BULL 1ST STAGE, EPICYCLIC 2ND STAGE,	PINION-BULL 1ST STAGE, EPICYCLIC 2ND STAGE	PINION-BULL 1ST STAGE, EPICYCLIC 2ND STAGE
TYPE OF GEARING	SPIRAL BEVEL	SPUR, SPIRAL BEVEL	SPUR	HERRINGBONE	SPUR
GEARBOX EFFICIENCY	99%	98% - 99%	98% - 90%	NO DATA	98%-99%
PROVISIONS FOR MOUNTING WHICH ACCESSORIES	NONE	ALTERNATOR	ALTERNATOR	ALTERNATOR	ALTERNATOR
SPECIAL FEATURES	INTEGRAL GEARCASE	INTEGRAL GEARCASE CLUTCH, DECOUPLER, INTEGRAL GEARCASE CROSS-SHAFT GEAR- CASE	INTEGRAL GEARCASE	INTEGRAL GEARCASE	INTEGRAL GEARCASE MODIFIED FOR SHAFT MOUNT PROPELLER
HOUSING MATERIAL	MAGNESIUM	MAGNESIUM	MAGNESIUM	MAGNESIUM	MAGNESIUM

TABLE XII CONTINUED

	N	B	V	U	V
WEIGHT DATA COMPONENTS (LBS)					
1.0					
BLADES	50	780	348	300	441
HUB	51	126	340	314	374.6
SPINNER		75	61		
AFT BODY	32	94	41	77	67.4
COP MOL	81	488	338		340
GEARBOX	HOME	30	HOME	HOME	10348
CLUTCH	4	12	10	20	16
HYDRAULIC OIL	4	4	6	24	6
LUBRICATING OIL					
PERFORMANCE DATA					
4.0		3100 100" P			
TAKE OFF STATIC RL. (D)					
THRUST	3030	9470	6470	10410	8836
SHIP	950	2753	2753	3110	2783
PROP RPM	2400	1232	1160	1107	1186
CGUIRE					
ALTITUDE (FEET)		N.L.	10,000	75,000	75,000
EFFICIENCY		77	80	84	88
KNOTS (TRUE)	N.A.	230	178	300	400
SHIP		997	833	7100	1010
PROP RPM		925	854	1107	1041
VMAX LEVEL FLIGHT					
ALTITUDE (FEET)		N.L.	51	75,000	75,000
EFFICIENCY		654	90	87	916
KNOTS (TRUE)	N.A.	305	228	400	400
SHIP		3100	2100	2000	1887
PROP RPM		1737	1015	1107	1046
STRUCTURAL DATA					
VMAX CONTINUOUS AQ AND THE OPERATING CONDITION AT WHICH IT OCCURS					
VMAX MANEUVERING "G" LEVEL					
VMAX FLAGARD					
		400 KIAS	700 KIAS	1000 100 KIAS AG	(PERMITS AQ) 1000

TABLE XVII (CONTINUED)		W		N		V		F	
PROPELLER DESCRIPTION	18	19	1017	1017	10				
DATE OF FIRST QUALIFICATION OR CERTIFICATION									
PROPELLER DIAMETER FEET									
PROPELLER MOUNTING RIFLE									
DIRECTION OF PROP ROTATION									
NUMBER OF BLADES PER PROPELLER	4	4	4	4	4				
BLADE A.P.	170	175	170	170	161				
BLADE C/L	0.5	0.509	0.55	0.55	0.5				
BLADE MATERIAL									
WHEEL MATERIAL	STEEL	STEEL	STEEL	STEEL	STEEL				
SPINNER MATERIAL	ALUMINUM	ALUMINUM	ALUMINUM	ALUMINUM	ALUMINUM				
TYPE OF CONTROL	JA ENGINE OIL	JA ENGINE OIL	JA ENGINE OIL	JA ENGINE OIL	JA ENGINE OIL				
TYPE OF BLADE PITCH CHANGE ACTUATION	HYDROMECHANICAL	HYDROMECHANICAL	HYDROMECHANICAL	HYDROMECHANICAL	HYDROMECHANICAL				
SINGLE OR DUAL HYDRAULIC SYSTEM	SINGLE	SINGLE	SINGLE	SINGLE	SINGLE				
TYPE OF DRIVING	ELECTRICAL	ELECTRICAL	ELECTRICAL	ELECTRICAL	ELECTRICAL				
FEATHERING AVAILABLE	YES	YES	YES	YES	YES				
REVERBERG AVAILABLE	YES	YES	YES	YES	YES				
PITCH LOCK AVAILABLE	YES	YES	YES	YES	YES				
SYNCHRONIZING AVAILABLE	YES	YES	YES	YES	YES				
GEARBOX DESCRIPTION									
GEAR RATIO	15.0	15.0	15.0	15.0	15.0				
DESCRIPTION OF GEAR TRAIN	EPICYCLIC GEAR ROUND PLANETS HELICAL	EPICYCLIC GEAR ROUND PLANETS HELICAL	EPICYCLIC GEAR ROUND PLANETS HELICAL	EPICYCLIC GEAR ROUND PLANETS HELICAL	EPICYCLIC GEAR ROUND PLANETS HELICAL				
TYPE OF GEARING	EPICYCLIC GEAR	EPICYCLIC GEAR	EPICYCLIC GEAR	EPICYCLIC GEAR	EPICYCLIC GEAR				
GEARBOX EFFICIENCY	90.5-99	90.5-99	90.5-99	90.5-99	90.5-99				
PROVISIONS FOR MOUNTING WHICH AGGENROMEN	NONE	NONE	NONE	NONE	NONE				
SPECIAL FEATURES	TORQUEMETER	TORQUEMETER	TORQUEMETER	TORQUEMETER	TORQUEMETER				
HOUSING MATERIAL	MAGNESIUM	MAGNESIUM	MAGNESIUM	MAGNESIUM	MAGNESIUM				

TABLE XXII CONTINUED		AA	AN	AG
1.0	PROPELLER DESCRIPTION			
	DATE OF FIRST QUALIFICATION OR CERTIFICATION	1984	1983	13
	PROPELLER DIAMETER (FEET)	18	27.5	
	PROPELLER MOUNTING RIZE	NO. 70 DPHLINE	475 HG	NO. 415 BRAC
	DIRECTION OF PROP ROTATION	MH	MH	1,11
	NUMBER OF BLADES PER PROPELLER	3	3	4
	BLADE A.P.	173	110	126
	BLADE C/LI	240	08	0.324
	BLADE MATERIAL	STEEL	AL.	DURAL
	BARNEL MATERIAL	STEEL	STEEL	STEEL
	SPINNER MATERIAL	ALUMINUM & MAGNESIUM	ALUMINUM	ALUMINUM
	TYPE OF CONTROL	CONSTANT SPEED AND WETA	ENGINE OIL, GEARBOX MOUNTED	ENGINE OIL
	TYPE OF BLADE PITCH CHANGE ACTUATION	ELECTROMECHANICAL	HYDRAULIC	HYDRAULIC
	SINGLE OR DUAL HYDRAULIC SYSTEM		RIMBLE	SINGLE
	TYPE OF DEICING	ELECTRICAL	ELECTRICAL	ELECTRICAL
	FEATHERING AVAILABLE	YES	YES	YES
	REVERSING AVAILABLE	YES	YES	NO
	PITCH LOCK AVAILABLE	YES	NO	YES
	SYNCHROPHASING AVAILABLE	YES	NO	YES
2.0	GEARBOX DESCRIPTION			
	GEAR RATIO	11.0	15.0	10.7
	DESCRIPTION OF GEAR TRAIN	3 STAGE EPICYCLIC	2 STAGE EPICYCLIC	COMPOUND STAN
	TYPE OF GEARING	SPUR	SPUR	HELICAL
	GEARBOX EFFICIENCY	90-95	PRIME GOV. O/SPEED GOV.	90-95
	PROVISIONS FOR MOUNTING WHICH ACCESSORIES	TORQUEMETER	MAGNESIUM	NONE
	SPECIAL FEATURES	MAGNESIUM & AL		TORQUE METER
	HOUSING MATERIAL			MAGNESIUM

TABLE 9-10 (CONTINUED)

INHERENT JET ENGINE DATA

PROPELLER DESCRIPTION	AE	AF	AG	AH	AI	AJ	AK
DATE OF FIRST QUALIFICATION OR VERIFICATION	10	11	12	13	14	15	16
PROPELLER DIAMETER (IN)	NO. 4 BRAC	NO. 4 BRAC	NO. 4 BRAC	NO. 4 BRAC	NO. 4 BRAC	NO. 4 BRAC	NO. 4 BRAC
PROPELLER MOUNTING RIFE	10	11	12	13	14	15	16
CHUCK TYPE AND POSITION	NO. 4 BRAC	NO. 4 BRAC	NO. 4 BRAC	NO. 4 BRAC	NO. 4 BRAC	NO. 4 BRAC	NO. 4 BRAC
NUMBER OF BLADES PER PROPELLER	10	11	12	13	14	15	16
BLADE A7	10	11	12	13	14	15	16
BLADE L1	10	11	12	13	14	15	16
BLADE MATERIAL	10	11	12	13	14	15	16
BARREL MATERIAL	10	11	12	13	14	15	16
SPINNER MATERIAL	10	11	12	13	14	15	16
TYPE OF CONTROL	10	11	12	13	14	15	16
TYPE OF BLADE PITCH CHANGE ACTUATOR	10	11	12	13	14	15	16
WINDS ON DIAL HYDRAULIC SYSTEM	10	11	12	13	14	15	16
TYPE OF DRIVE	10	11	12	13	14	15	16
FEATHERING AVAILABLE	10	11	12	13	14	15	16
REVERSING AVAILABLE	10	11	12	13	14	15	16
CHUCK AVAILABLE	10	11	12	13	14	15	16
SYNCHRONIZING AVAILABLE	10	11	12	13	14	15	16
GEAR BOX DESCRIPTION	10	11	12	13	14	15	16
GEAR RATIO	10	11	12	13	14	15	16
DESCRIPTION OF GEAR TRAIN	10	11	12	13	14	15	16
TYPE OF GEARING	10	11	12	13	14	15	16
WEAR AND EFFICIENCY	10	11	12	13	14	15	16
MOUNTING FOR MOUNTING WHICH ACCESSORIES	10	11	12	13	14	15	16
SPECIAL FEATURES	10	11	12	13	14	15	16
HOUSING MATERIAL	10	11	12	13	14	15	16

TABLE XXII - CONTINUED

	AD	AE	AF	AG	AH	AJ	AK
3.0	WEIGHT DATA - COMPONENTS (LB)						
	149	160	181	218	218	236	398
	138.0	140.0	168.0	206.0	206.0	286	296
	17.5	17.5	16.5	18.0	18.8	23.0	23.0
	---	---	---	---	---	---	---
	53.5	52.6	65.6	64.5	57.2	74.8	74.8
	195	215	218	218	218	270	270
	7.5	7.5	7.5	7.5	7.5	11.0	11.0
	NONE	NONE	NONE	NONE	NONE	NONE	NONE
4.0	PERFORMANCE DATA						
	TAKE-OFF (STATIC SL-SD)						
	3520	3690	5400	8880			N.A.
	1800	1700	1876	1910			
	1150	1395	1395	1395			
	CRUISE						
	20,000	20,000	20,000	20,000	13,000	20,000	N.A.
	0.88	0.88	0.88	0.88	0.88	0.88	
	283	318	260	270	300	200	
	900	1225	1160	1130	1130	1160	1390
	1264	1302	1302	1302	1302	1302	1066
	VMAX (LEVEL FLIGHT)						
	28,000	28,000	20,000	19,200	18,000	13,000	---
	---	---	---	---	---	---	---
	375	378	390	387	387	303	336
	---	---	---	---	---	---	---
	STRUCTURAL DATA						
	MAX CONTINUOUS AG AND THE OPERATING						
	CONTION AT WHICH IT OCCURS (AT ONE G)						
	2.5	2.5	2.0	1.5	2.5	2.61	2.5
	235 KEAS	235 KEAS	274 KEAS	227 KEAS	230 KEAS	210 KEAS	248 KEAS
	VMAX (PLACARD)						
							N.A.
							N.A.
5.0	STRUCTURAL DATA						

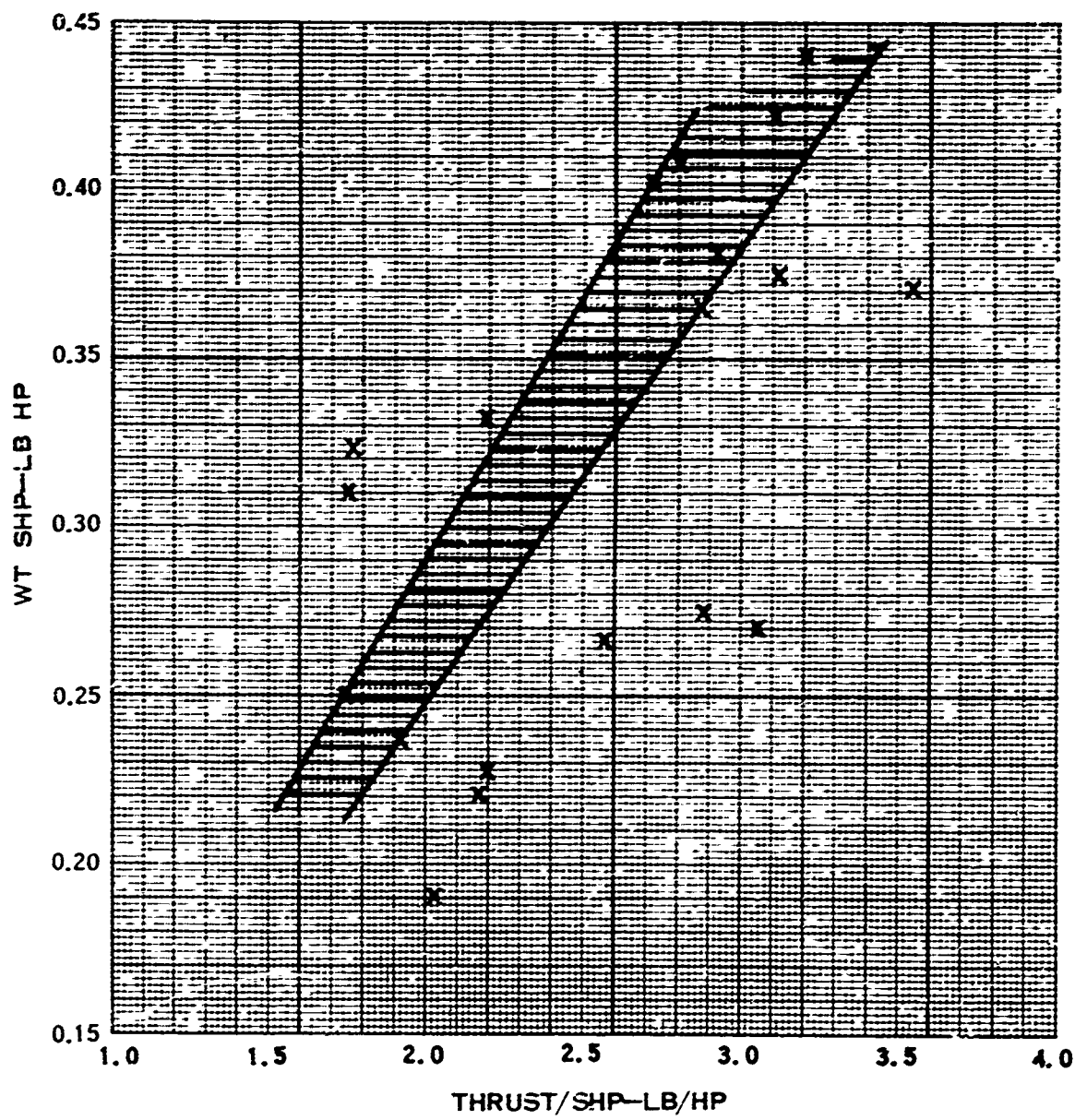


FIGURE 93. PRESENT-DAY TURBOPROP SYSTEM WEIGHTS

APPENDIX II
DERIVATION OF OPTIMUM AERODYNAMICS TRADE-OFF CRITERION

The aircraft component weight equation is

$$GW = (W_{fus} + fe) + PL + W_{wing} + W_{lg} + W_{eng} + W_{prop} + W_{fuel} \quad (5)$$

where GW = gross weight at takeoff

$W_{fus} + fe$ = weight of fuselage plus fixed equipment

PL = payload

W_{wing} = weight of wing and tail

W_{eng} = weight of engines

W_{prop} = weight of propellers and propeller reduction gearboxes

W_{lg} = weight of landing gear

W_{fuel} = weight of fuel

In differential form, nondimensionalized by the initial gross weight, the equation is

$$\frac{\Delta GW}{GW} = \frac{\Delta W_{fus} + fe}{GW} + \frac{\Delta PL}{GW} + \frac{\Delta W_{wing}}{GW} + \frac{\Delta W_{lg}}{GW} + \frac{\Delta W_{eng}}{GW} + \frac{\Delta W_{prop}}{GW} + \frac{\Delta W_{fuel}}{GW} \quad (6)$$

The following assumptions can be made:

Payload is constant, $\Delta PL = 0$

If the payload is constant, the fuselage weight is assumed to be constant. Also, fixed equipment weight does not vary with changes in gross weight. Therefore,

$$\Delta W_{fus} + fe = 0.$$

The engine weight is a fixed quantity since the horsepower is fixed; thus,

$$\Delta W_{eng} = 0.$$

The ratio of static thrust to gross weight is assumed to be a constant (1.07). The component weight equation can now be written,

$$\frac{\Delta GW}{GW} = \frac{\Delta T}{T} = \frac{\Delta W_{prop}}{GW} + \frac{\Delta W_{fuel}}{GW} + \frac{\Delta W_{wing}}{GW} + \frac{\Delta W_{lg}}{GW} \quad (7)$$

where T = static thrust.

The wing, tail, and landing gear terms vary with gross weight change and thus do not drop out. The ratio of wing, tail, and landing gear weight over gross weight is a constant. For a wing loading of 70 psf, a wing and tail density of 7 psf, a wing-to-tail area ratio of 2.7, and a landing gear weight to gross weight ratio of 0.035,

$$\frac{\Delta W_{wing}}{GW} + \frac{\Delta W_{lg}}{GW} = 0.172 \frac{\Delta GW}{GW} = 0.172 \frac{\Delta T}{T} \quad (8)$$

Combining equations (7) and (8) above,

$$0.828 \frac{\Delta T}{T} - \frac{\Delta W_{prop}}{GW} = \frac{\Delta W_{fuel}}{GW} \quad (9)$$

Since the desired form of the equation is to relate static thrust to propeller weight and 250-kn cruise efficiency, a relation between efficiency and fuel weight can be obtained from the Brequet range equation.

$$R = \frac{\eta}{SFC} \frac{L}{D} 375 \ln \frac{1}{1 - \frac{W_{fuel}}{GW}} \quad (10)$$

where η = cruise propeller efficiency (decimal)

SFC = engine specific fuel consumption, $0.5 \frac{\text{lb}}{\text{hp-hr}}$

L/D = aircraft lift to drag ratio in cruise

D = $qS (C_{D0} + C_{Di})$

where $C_{D0} S = \frac{1 \text{ ft}^2}{\text{ton GW}}$ and $C_{Di} = \frac{C_L^2}{0.8 \pi AR}$, $S = \frac{GW}{70}$

$L = GW + C_L q S$

Finally,

$$\frac{\Delta W_{\text{fuel}}}{\text{GW}} = \frac{W_{\text{fuel}}}{\text{GW}} - \left[\frac{W_{\text{fuel}}}{\text{GW}} \right]_{\text{ref}}$$

where $\left[\frac{W_{\text{fuel}}}{\text{GW}} \right]_{\text{ref}}$ is assumed to be 0.153. This was arrived at by assuming

a $\left[\frac{W_{\text{fuel}}}{\text{GW}} \right]_{\text{ref}}$ at takeoff of 0.180 which allows 15 percent of the fuel for taxi, hover, climb, descent, reserve, etc.

The range at the design point is thus

$$R = \frac{0.82}{0.5} \times 8.18 \times 375 \ln \left(\frac{1}{1-0.153} \right) = 831 \text{ miles}$$

Equations (9), (10), and (11) solved to yield a constant range of 831 miles can be plotted as a single line on a $\Delta \eta$ vs. $0.828 \frac{\Delta T}{T} - \frac{\Delta W_{\text{prop}}}{\text{GW}}$ plot.

Any point plotted to the right of this curve denotes a greater available range; a point to the left yields a lower range. The optimum propeller has been defined as the propeller which attains the maximum range.

It should be noted that a change in propeller weight affects the weight of fuel carried but not the overall gross weight. A change in static thrust affects both the fuel weight and the gross weight.

PROPELLER WEIGHT EQUATION

The equation used for the blade geometry optimization study for propeller weight is

$$W_{\text{prop}} = K \frac{D}{10}^{1.85} \left(\frac{B}{4} \right)^{0.7} \left(\frac{AF}{100} \right)^{0.6} \left(\frac{ND}{20,000} \right)^{0.5} (M+1)^{0.5} \left(\frac{\text{shp}}{10D^2} \right)^{0.12}$$

where K^* = 170 for h/b tip = 0.033
 K^* = 182 for h/b tip = 0.022
 D = diameter, ft
 B = no. of blades
 AF = blade activity factor
 N = propeller RPM

M = mach number at design point = 0
shp = propeller shaft horsepower

*The thinner blade geometry (h/b tip = 0.022) requires a higher K factor than the thicker blade, and thus a higher weight, since more blade structural material is required in the thin blades. This is primarily because the blade structural material for supporting the blade flatwise bending loads cannot be placed as far from the neutral axis on the thin blade as on the thicker blade.

The IGB propeller system weight predictions at the conclusion of the study were significantly less than those of the above equations, which were assumed early in the program for the aerodynamic studies. However, since the weight was a minor factor in the aerodynamic optimization and since the weight trends of the above independent variables were found to be similar, the same geometry would be selected for the optimum propeller blade.

PERFORMANCE PREDICTION METHODS

The current Hamilton Standard propeller performance calculation method is based upon an advanced form of the blade element theory. In this theory, the aerodynamic forces acting on a series of radial blade elements are calculated and then integrated over the effective blade length to establish the total forces. With the application of the propeller vortex theory and the Goldstein solution for the radial distribution of circulation for a finite number of blades, an analytical method was evolved which permits the efficiency of any propeller configuration operating at any imposed flight condition to be accurately calculated. This refined performance calculation method has been programmed for a Univac 1108 computer, which permits the examination of many blade configurations in a short time. Comparisons with experimental data on both full-scale and model propellers indicated an accuracy of $\pm 1/2\%$ in the vicinity of the design point and only slightly less accuracy for off-design points.

More recently, attempts have been made to apply this same method to the static case but with substantially poorer agreement with test data. It was quickly realized that the neglect of wake contraction and three-dimensional flow effects in the blade tip region was a major cause of the discrepancy between calculated and test results. In recognition of these deficiencies, empirical corrections based on Wright Field Rig #4 propeller testing are now applied to the strip analysis calculation method to achieve better agreement with test experience. The propeller static data from Rig #4, with extended shaft and with the protective side walls moved back to the house walls, have proven to be the most consistent and accurate available. These data correlate closely with hover test data from the XC-142 aircraft. Although the wall and blockage effects on Rig #4 have appeared to be modest, they are in a direction to make the predicted thrust levels slightly conservative.

It should be pointed out that while these empirical correction factors are applied to both three- and four-bladed propellers, they are derived almost exclusively from four-bladed propeller testing. Presently used static thrust theory predicts higher static propeller performance for a four-way propeller when compared to a three-way propeller of the same total solidity. As yet, there has been insufficient static test experience to fully substantiate this effect of number of blades. Therefore, for the purposes of the study, the performance estimates presented in this section to determine the optimum propeller are based on the theoretical advantage of four-bladed propeller performance.

APPENDIX III
MATCHING THE PROPELLER AND ENGINE FOR
OPTIMUM FLIGHT PERFORMANCE

Propellers optimized for VTOL missions are designed, of necessity, to obtain near-optimum static performance. This generally results in the propeller being oversized (too much solidity or camber) when operating in forward flight at 100% rpm. The oversizeness can be compensated for by lowering the propeller rpm, which results in higher propeller efficiencies.

To propel an aircraft at a constant velocity and altitude requires a specific amount of thrust, which can be determined from the aircraft drag characteristics. The thrust required is directly proportional to the product of propeller efficiency and engine shaft horsepower. Thus, if a lower rpm increases the propeller efficiency less horsepower (and fuel consumption) is required. However, as the rpm is lowered from the optimum free-turbine rpm, the specific fuel consumption increases. The object is to find the best rpm match of the propeller and engine to produce the required thrust at the lowest fuel consumption level. This appendix uses the propeller previously described in this report and a typical advanced-technology engine to determine the best rpm match for both sea level and 15,000-ft-altitude flight conditions.

The thrust required was estimated from the aircraft defined in the section on "Aerodynamic Studies" and is listed in Figure 94.

For a given operating condition (velocity, altitude, and aircraft drag), a plot of propeller efficiency required versus percent takeoff rpm can be determined from the propeller efficiency map, the compressibility correction curves and the thrust-horsepower relationship ($TV = \eta_p \text{ shp}$). The propeller efficiency, η_p , versus percent takeoff rpm is plotted in Figures 95 and 96 for three velocity conditions.

Engine efficiency (η_e) versus percent takeoff rpm is also plotted in Figures 95 and 96. For the convenience of this study, engine efficiency was defined as the ratio of engine shaft horsepower at the actual operating rpm to the horsepower available when operating at optimum free-turbine rpm, both at the same rate of fuel flow (Figure 99). This essentially defines the penalties for operating the engine at non-optimum free turbine speeds: i. e., for constant fuel flow, the power decreases; conversely, for constant power, the specific fuel consumption increases. For given operating conditions and the above-mentioned thrust-horsepower relationship, a plot of engine efficiency versus percent takeoff rpm can be determined from Figures 97, 98, and 99.

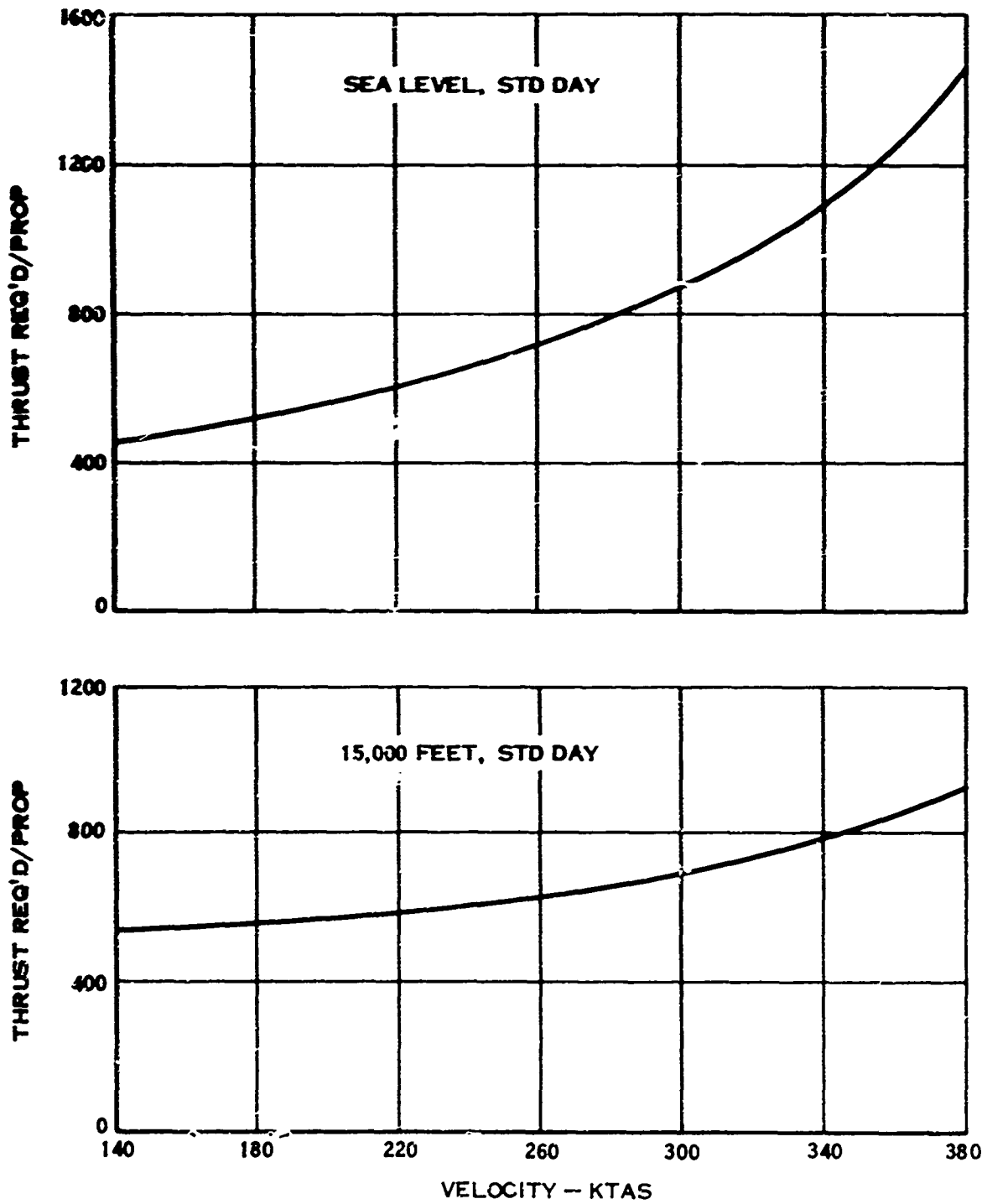


FIGURE 94. THRUST REQUIRED FOR VARIOUS AIRCRAFT SPEEDS

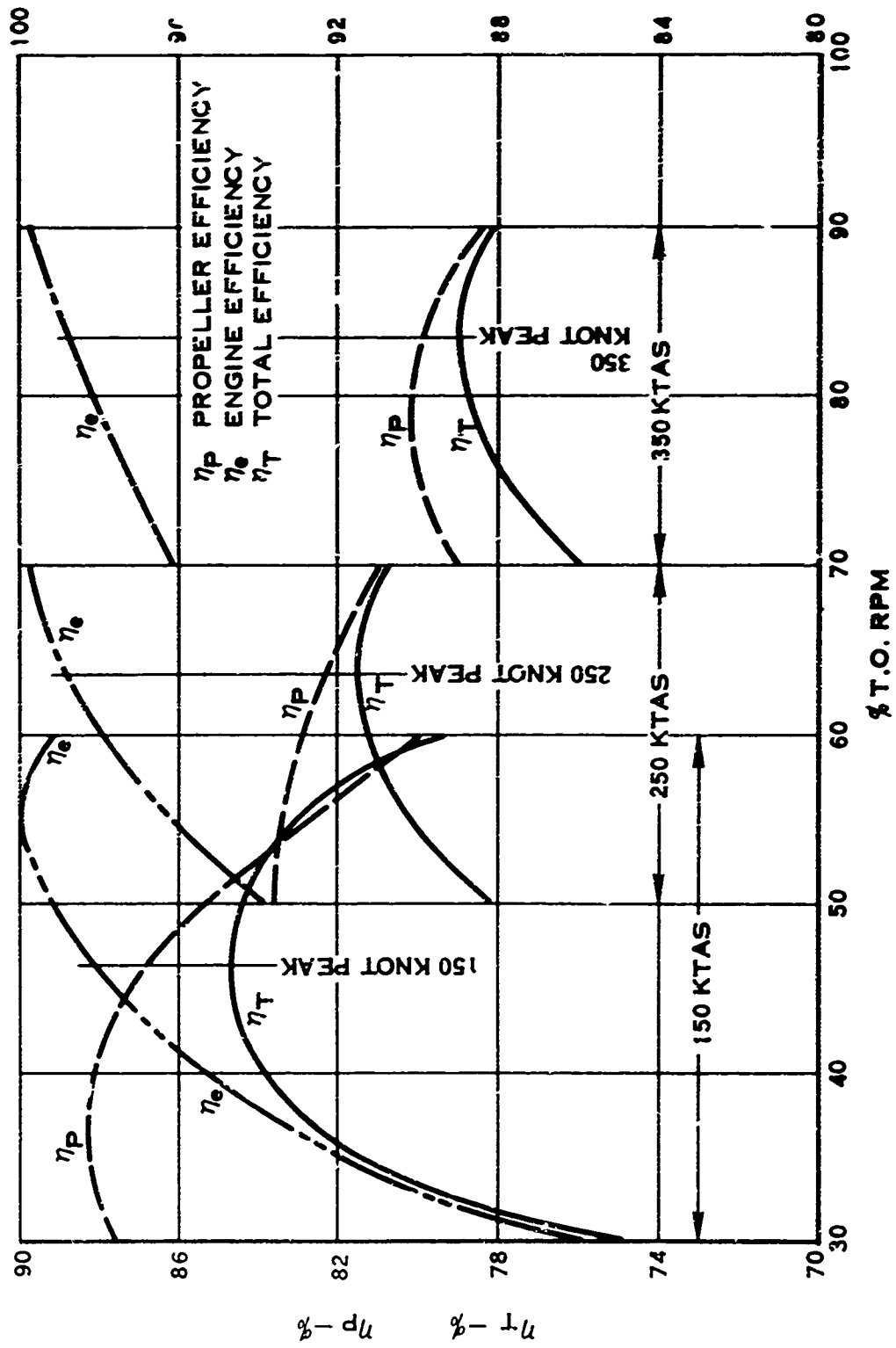


FIGURE 95. VARIATION OF PROPPELLER, ENGINE, AND TOTAL EFFICIENCY WITH RPM - SLSD

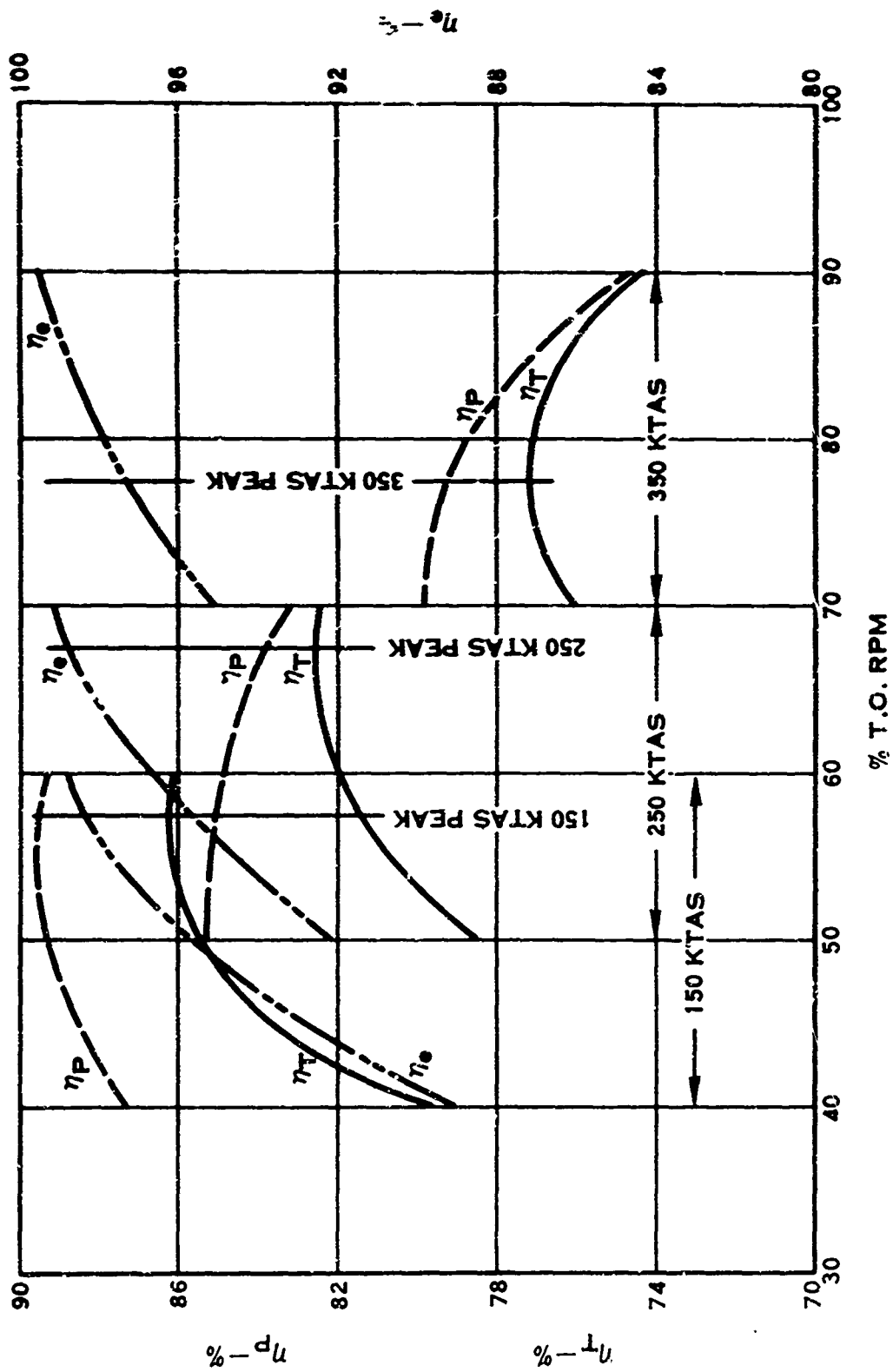


FIGURE 96. VARIATION OF PROPELLER, ENGINE, AND TOTAL EFFICIENCY WITH RPM — 15,000 r.p.m. PER DAY

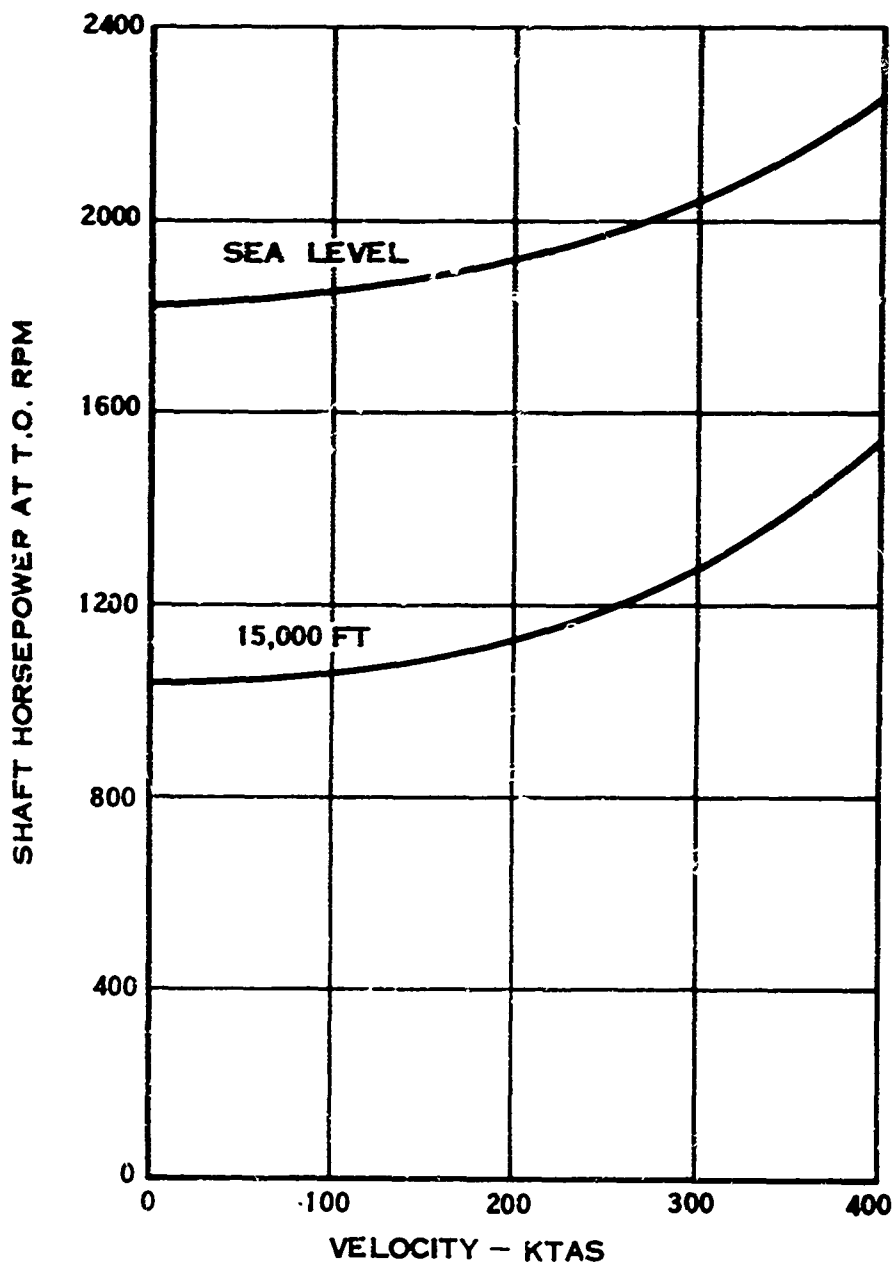


FIGURE 97. ENGINE MILITARY POWER RATING

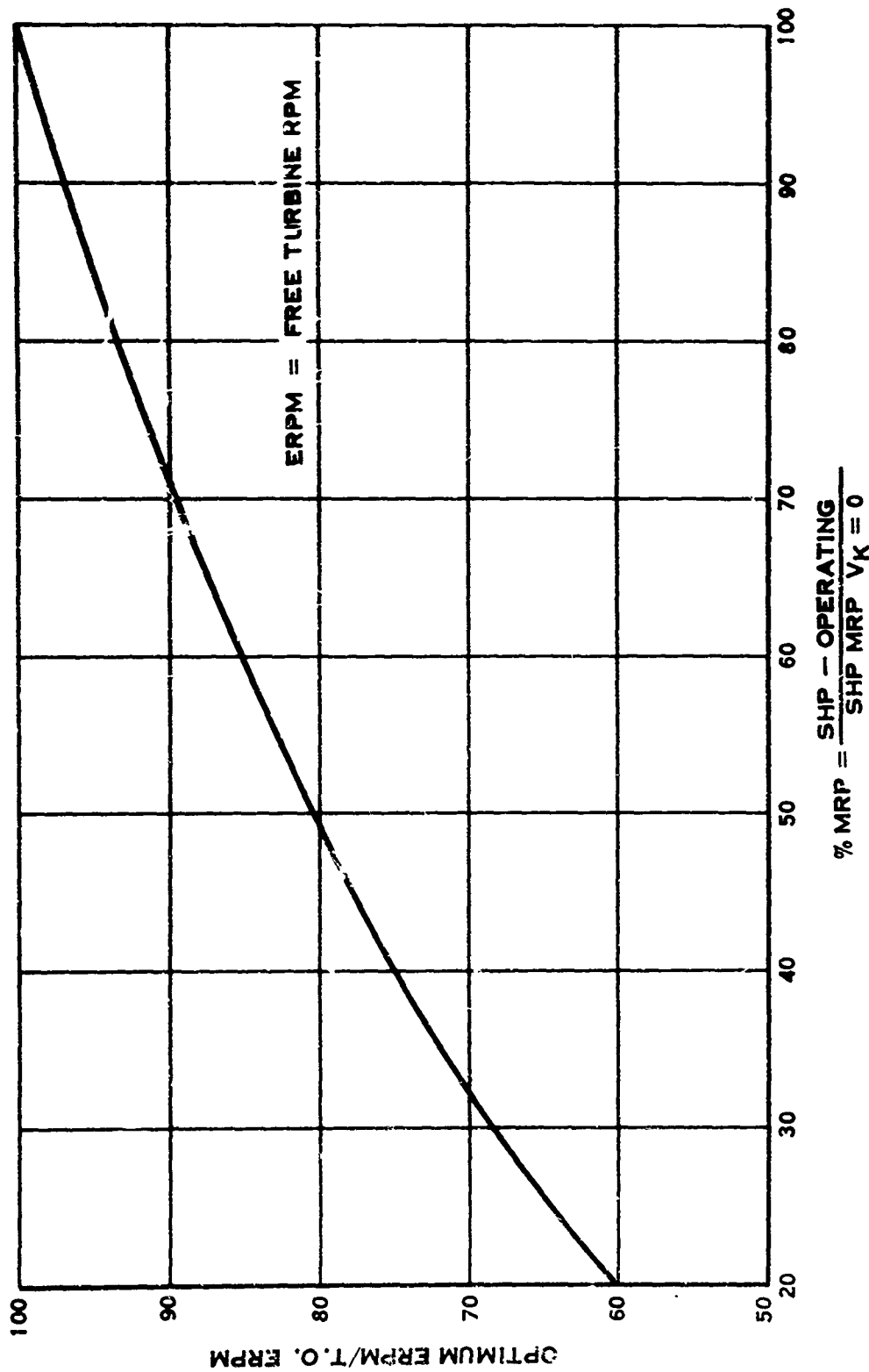


FIGURE 98. VARIATION OF OPTIMUM ENGINE RPM WITH SHP

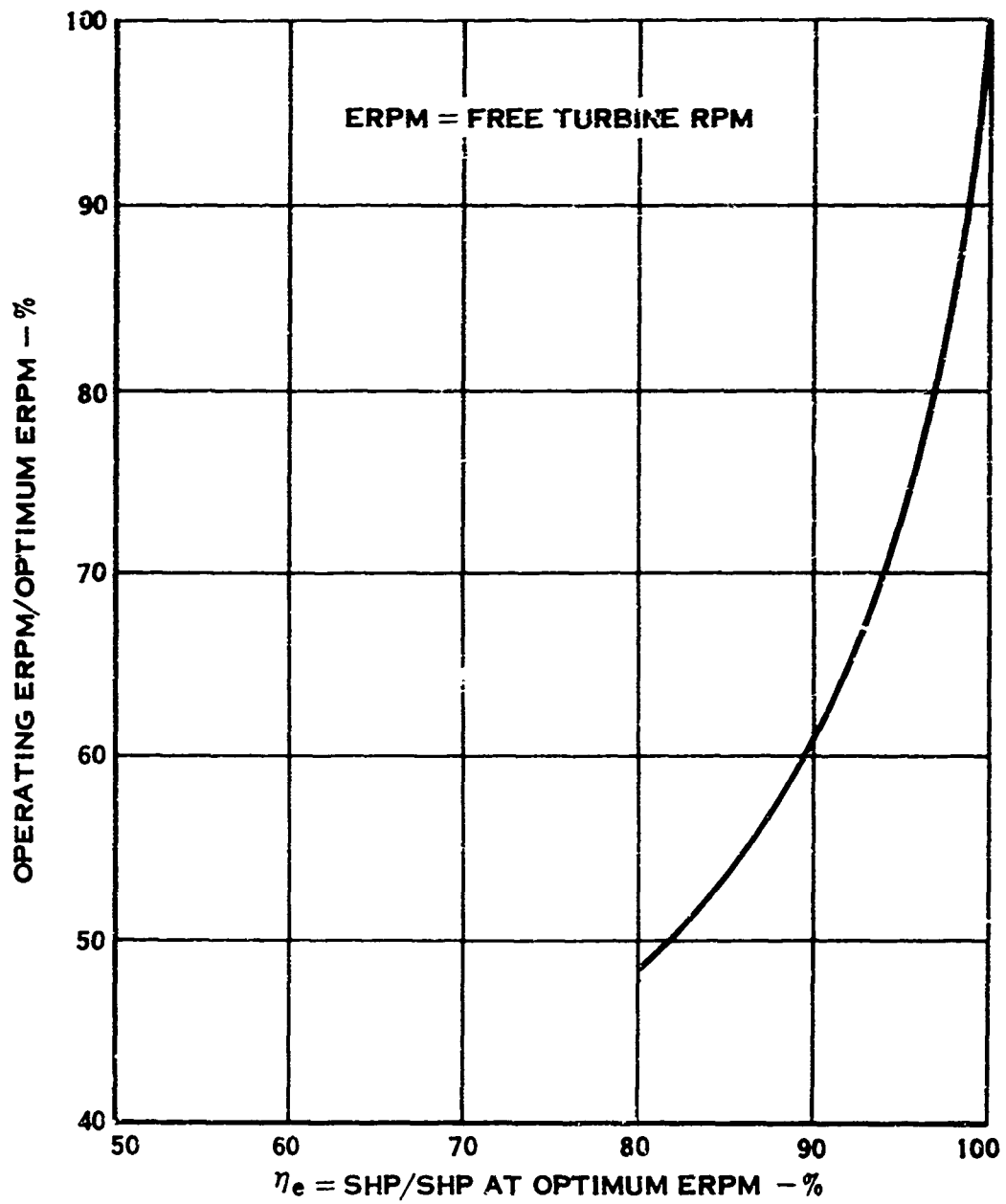


FIGURE 99. HORSEPOWER LOSS AT NONOPTIMUM ENGINE SPEEDS

The product of propeller and engine efficiency is defined as the total efficiency (η_T) as shown in Figures 95 and 96. Peak total efficiency defines the optimum rpm for the given operating condition, which is the best compromise between minimum power (maximum propeller efficiency) and best engine efficiency, to result in minimum fuel consumption.

Figures 100 and 101 summarize the optimum operating rpm and the resulting horsepower required for different flight speeds. Note that at sea level for speeds above 355 knots, the propeller has to operate at a slightly higher rpm than optimum because of the defined torque limit for the propeller (2000 hp, 100-percent rpm).

A sample calculation is shown below for a 250-kn (sea level, standard day) cruise condition at 60% rpm:

Calculation A. Propeller: From Figure 94, the thrust required is found to be $T = 685$ lb. This is converted to a thrust horsepower, $thp = T \times VKTAS/326 = 525$. An iterative procedure is used to determine the shp required. This necessitates finding a combination of C_p and shp such that $\eta_p \times shp = thp = 525$.

Assume $shp = 635$, then $C_p = 0.1325$, $J = 2.47$. From the efficiency map $\eta_p = 0.828$. The compressibility correction from the compressibility correction curves is $k_t = 1.0$. $\eta_{pshp} = C.828 \times 635 = 525$, thus the shp required is 635.

B. Engine: An iterative procedure is also used here. An engine efficiency is assumed; and, based on the shp required, an engine efficiency is calculated and compared to the assumed engine efficiency.

Assume $\eta_e = \frac{shp}{shp_{opt}} = 0.980$; then for $shp =$

635, $shp_{opt} = 648$. From Figure 99 at $\eta_e = 0.98$, the ratio $N_f/N_{fopt} = 0.855$ is obtained. $N_{fopt}/N_{mrp} = (N_f/N_{mrp})/(N_f/N_{fopt}) = 0.60/0.855 = 0.703$. From Figure 98 at $N_{fopt}/N_{mrp} = 0.703$, $shp_{opt}/shp_{mrp} = 0.329$ is obtained. From Figure 97 at 250 KTAS, the $shp_{mrp} = 1970$ is obtained. Then, to close the iterative loop, $shp_{opt} = 0.329 \times 1970 = 648$ and $\eta_e = 635/648 = 0.980$, as was assumed.

C. Total: The total efficiency is now $\eta_T = \eta_p \eta_e = 0.828 \times 0.980 = 0.811$.

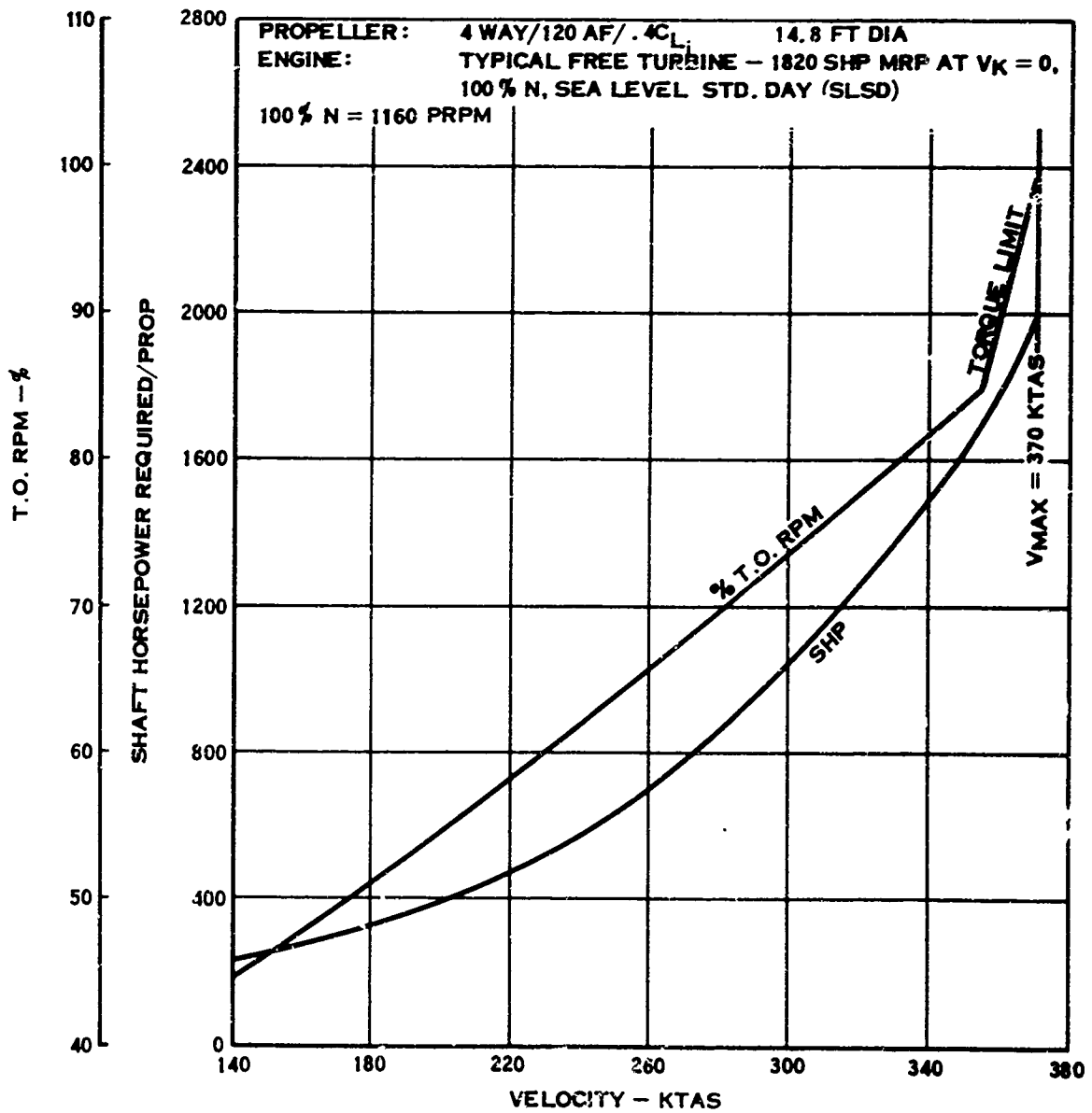


FIGURE 100. OPTIMUM FLIGHT OPERATING RPM - SLSD

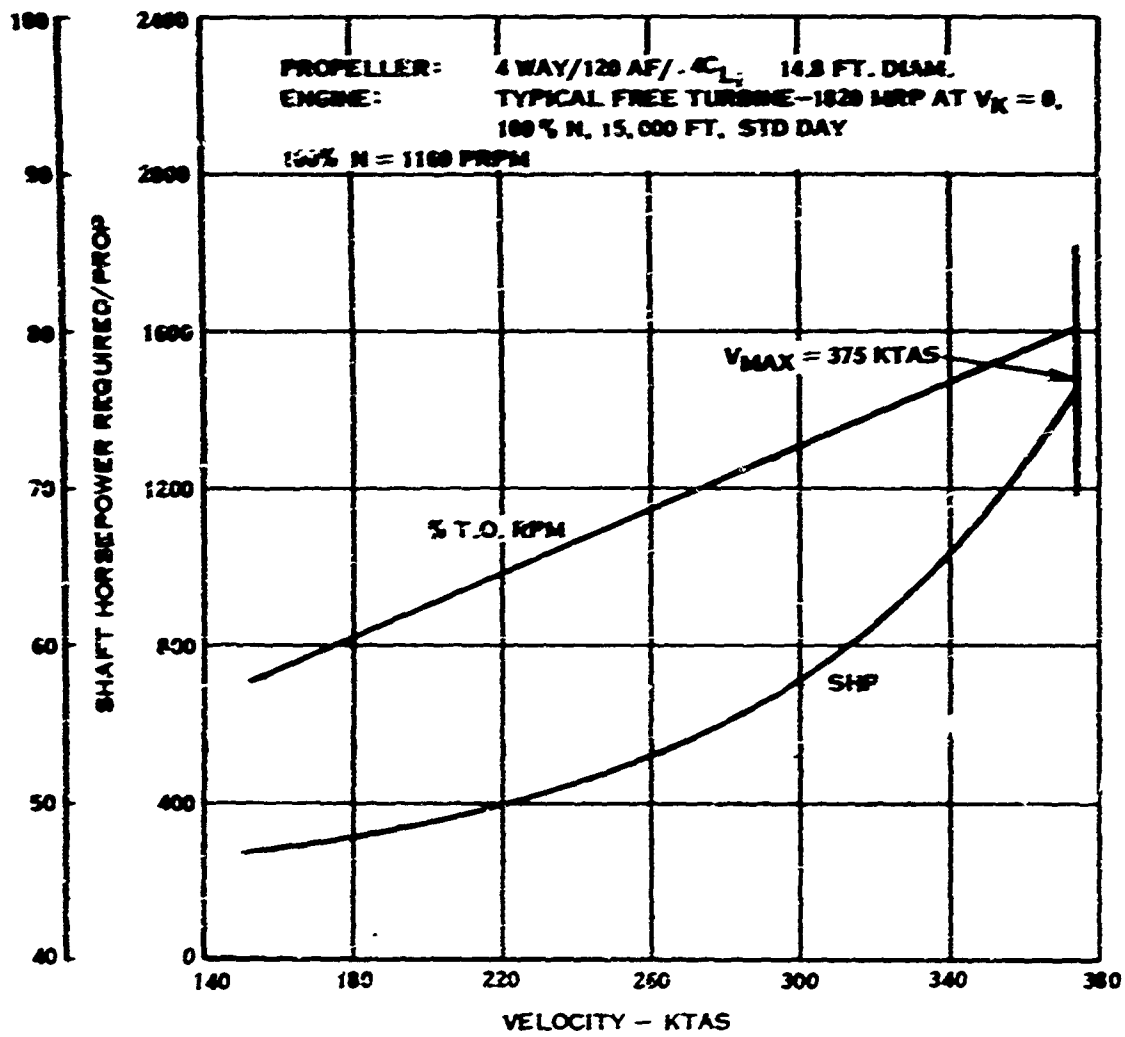


FIGURE 101. OPTIMUM FLIGHT OPERATING RPM - 15,000 FT, STD DAY

APPENDIX IV
FEASIBILITY STUDY OF NOVIKOV GEARS

INTRODUCTION

Minimum weight gears can certainly contribute to the general weight reduction objective for advanced V-STOL propellers. One effective way to achieve lower gear weight is to increase the tooth load capacity by using circular arc tooth shape. The past decade has seen renewed interest in the circular arc tooth form previously proposed by Gumbel (1916) and Wildhaber (1923), and more recently by Novikov (1956). See References 46 and 47, respectively. The majority of recent literature refers to the circular arc tooth form gear as the Novikov gear. This appendix summarizes the findings presented in recent literature and makes a comparison of involute and Novikov tooth forms for the gear drive proposed for the integral gearbox propeller previously described in this report.

STRENGTH

The analysis summarized in Table XXIII assumes involute gears made of AMS 6265 vacuum-melt, case-carburized steel with case hardness of Rc 60 minimum and core hardness of Rc 35-43 minimum, design contact stress of 150,000 psi, and design tooth bending strength of 65,000 psi at $R = -1$, 10^6 cycles and room temperature. No such strength data are available for Novikov gears.

LOADS

Gear teeth are usually designed for structural adequacy, under both steady and dynamic loads, relative to three possible failure modes: tooth bending, surface wear, and surface pitting. However, the majority of investigations examined in this survey have used only the surface and beam strength criteria under steady loads to rate the Novikov tooth form. The dynamic load was of little concern in the industrial and marine applications usually referred to, although in propeller gearbox gearing it is usually one of the primary loading considerations.

Wear

Although it has been claimed (see Reference 48) that Novikov teeth theoretically can take 3 to 5 times the involute tooth load on the flanks without detrimental pitting or wear, a more realistic study (see Reference 49) indicates that the Novikov tooth form can carry only 2 times the normal wear load limit of involute teeth. Contact stresses for Novikov and involute tooth forms for the proposed USAAVLABS propeller gear mesh are given in Table XXIII.

TABLE XXIII. COMPARISON OF DESIGN DATA AND STRESSES FOR NOVIKOV AND INVOLUTE PINION TEETH FOR THE USAVLABS PROPELLER *AR MESH

ITEM	NOVIKOV *		INVOLUTE *
H.P.	2,000		2,000
R.P.M.	23,000		23,000
DIAMETRAL PITCH	8.045		8.045
NUMBER OF TEETH	21		21
PRESSURE ANGLE	30° ⊕		30°
PITCH DIAMETER (IN.)	2.61		2.61
MATERIAL *	AMS 6265 VACUUM MELT, CASE CARBURIZED		RC 60 MIN.
TANGENTIAL LOAD (LB)	4,220		4,220
HELIX ANGLE	15° ⊕	20° ⊕	25° ⊕
NORMAL LOAD (LB)	3,000	5,100	5,250
CONTACT STRESS (KSI)	79.5 ⊕	107 ⊕	130 ⊕
FACE/DIAMETER RATIO	0.5 ⊕	0.5 ⊕	0.5 ⊕
BENDING STRESS (KSI)	169 ⊕	120 ⊕	95.5 ⊕
CONTACT RATIO	*0.89	1.22	1.55
FACE WIDTH (IN.)	1.30	2.61	1.30
DYNAMIC LOAD (KIPS)	15.3 ●	18.3 ●	15.3 ●
DESIGN STRENGTH * CONTACT (KSI)			150
FATIGUE (KSI) @ 10 ⁷ n, s=1, RT=1			65

- * FOR INVOLUTE GEARS ONLY; NO DATA AVAILABLE FOR NOVIKOV GEARS
- BASED ON BUCKINGHAM'S SHORT EQUATION, NOVIKOV, 1.5 X INVOLUTE
- * LESS THAN MINIMUM ALLOWABLE CONTACT RATIO OF 1.0; RECOMMENDED RATIO IS 1.2
- ⊕ BASED ON EQUATIONS AND DATA USED IN REFERENCE 50 (BOEING-VERTOL)
- * DATA LISTED FOR PURPOSE OF COMPARISON ONLY

Beam

Much of the literature (see Reference 48) indicates that the static beam strength of Novikov gears is greater than that of involute gears at helix angles less than 11 deg, and less than that of involute gears at helix angles greater than 11 deg. However, in Reference 50, it was claimed for a helicopter transmission with a high helix angle of 25 deg, that, as the helix angle increases beyond this value, the band of contact decreases. This increases contact stresses, but tooth thickness increases and bending stress decreases with the square of tooth thickness. Reference 50 also states that the low helix angles recommended in the literature refer to soft gear material such as non-case-hardened industrial and marine gears, where wear is the design limitation, and lists Reference 48 in its bibliography. The shape of the tooth influences beam load capacity, and usually addendum/dedendum teeth (see Figure 102) are stronger than all-dedendum teeth (see Figure 103). Another factor affecting beam strength is tooth fatigue life, which, in Novikov gears (see Reference 48), tends to be more sensitive to center distance variation than is the case with involute teeth.

At present, considerations of required gear tooth proportions, helix angle, ratio, and reliability make the Novikov gear unattractive as a planetary gear (see Reference 50). In an open mesh without an idler, the estimated allowable bending fatigue strength could be increased 1.4 times because there is no reversal of tooth load. The beam bending stress of Novikov and involute gears for the study propeller gear mesh is given in Table XXIII, based on equations and data given in Reference 50.

Dynamic

Low helix angles, on the order of 11 deg, may result in Novikov gearing with greater noise and higher impact loads than for involute gears of similar size. Also, the lower contact ratio limit of 1.2 recommended in the Russian literature (see Reference 50), compared to usual contact ratios in involute helical gears of 2.0 or more, results in rougher transmission of power. As a guide to dynamic load (see Reference 49), if the maximum dynamic load is defined as the load required to bend the combined teeth of a gear pair by an amount equal to the pitch errors, then the typical Novikov tooth is required to take a dynamic load 50% higher than the dynamic load on the comparable involute tooth because, while the errors could be the same, the Novikov tooth has higher stiffness. Dynamic loads for Novikov and involute tooth forms are given in Table XXIII, for the study propeller gear mesh based on Buckingham's short equation for involute teeth. The Novikov dynamic load listed is 1.5 times the involute dynamic load, based on the above discussion.

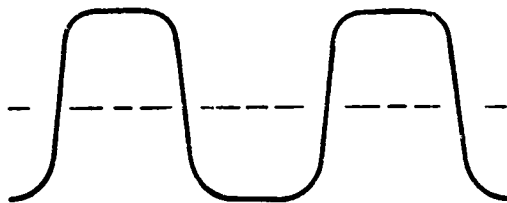


FIGURE 102. ADDENDUM-DEDENDUM GEAR TEETH

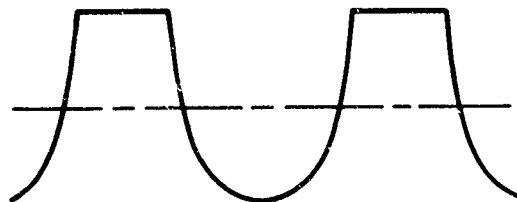


FIGURE 103. ALL-DEDENDUM GEAR TEETH

EFFICIENCY AND LUBRICATION

The Novikov tooth form (see References 47 and 49) results in 1/2% greater efficiency relative to tooth power losses. Novikov gears may realize weight reduction over involute gears when the pinion-face-to-diameter ratio is at least one. This results in a wider face width for Novikov gears than for involute gears, and consequent small-diameter envelope restriction on antifriction bearing size and capacity could possibly require the use of hydrodynamic bearings and higher power loss than involute gears on antifriction bearings.

DISCUSSION

Of all the literature surveyed in this report (see also References 51, 52, and 53), only References 50 and 51 dealt with an aircraft gear transmission. Reference 50 presented a design analysis of a helicopter gear transmission, and Reference 51 reported on experimental analysis of aircraft gears. Thus, Reference 50 was used as a guide for the calculations summarized in Table XXIII.

Table XXIII data for the Novikov gear show that as helix angle increases, contact stress increases and bending stress decreases. Based on this characteristic, Reference 50 initially recommended a high helix angle of 25 deg. However, experimental results in Reference 51 for the followup gear test program indicated that the 25 deg helix angle resulted in a design too heavily in favor of bending or beam stress over contact stress. Therefore, Reference 50 indicated that a lower helix angle might be desirable. Table XXIII data bear this out and show that a helix angle of 20 deg and face/diameter ratio of 0.75 may give a reasonable balance between contact and bending stress of the Novikov gear propeller transmission. At 20 deg helix angle and face/diameter ratio 0.75, Table XXIII shows the following for the Novikov gear, contact stress of 107,000 psi and a bending stress of $(120,000 \pm 22,800) / 2 = 71,400$ psi at a contact ratio of $1.22 \pm 2.43/2 = 1.82$; for the involute spur gear, a contact stress of 122,000 psi and a bending stress of 52,200 psi at a face/diameter ratio of 1.0 and a minimum contact ratio of 1.05.

Comparison of the involute stresses (Table XXIII) shows that the involute pinion contact and bending stresses are less than the allowable strengths, but no direct comparison can be made for the Novikov pinion since (see Reference 50) calculated gear stresses are really index numbers and, strictly, can be compared only with experimentally determined strengths for Novikov teeth. However, if involute strengths are used as a guide and it is assumed, as in Reference 50, that bending stress in Novikov teeth does not reverse because of the open mesh, then the Novikov tooth form for 20 deg helix angle and 0.75 face/diameter ratio compares favorably in contact and bending stress to the involute spur pinion with a face/diameter ratio of 1.0 and the same diameter. Without an experimental verification of the assumed Novikov strength data, any conclusion that the smaller face/diameter ratio of the Novikov gear means that a weight saving is premature.

In the referenced literature, there is a complete lack of any dynamic load analysis of Novikov gear teeth, except for the statement in Reference 49 previously mentioned. Therefore, this report (see Table XXIII) assumes that the dynamic load of Novikov gear teeth is 1.5 times the dynamic load of involute gear teeth as indicated in Reference 49. On this basis, Table XXIII shows that the Novikov gear at a face/diameter ratio of 0.75 is somewhat more heavily loaded dynamically at $(15,300 \pm 18,300) \times 2 = 16,800$ lb than the involute gear at 12,200 lb, with a face/diameter ratio of 1.0. However, this statement needs more experimental and theoretical verification.

CONCLUSIONS AND RECOMMENDATIONS

It is concluded, on the basis of the literature surveyed, that, although the Novikov gear initially appears to have a substantial advantage relative to Hertz contact stress, the advantage is substantially lost when adequate consideration is given to tooth bending and to dynamic loading. Based on steady transmitted load, the Novikov tooth form may have significant weight advantage over the involute in applications where wear or contact stress is the prime criterion. Novikov teeth are comparable to involute teeth when beam strength is the criterion. However, Novikov gears may be at a disadvantage compared to involute gears when the effects of dynamic loads are included. It is concluded that some weight advantage may be possible depending on the particular configuration and operating requirements. At best, the weight saving from the use of Novikov gears would be small for propeller gearbox requirements, and the introduction of these gears would require considerable research and development.

It is recommended that any design development of the Novikov tooth form be conducted jointly with an extensive experimental program to derive fatigue strengths and dynamic load factors, and with a theoretical program to develop a suitable dynamic analysis.

APPENDIX V
STUDY OF METHODS TO ADJUST THE DYNAMIC RESPONSE
OF INVOLUTE GEARS

INTRODUCTION

Appendix IV considered the possibility of achieving minimum weight gears for the subject propeller gearbox by using a circular arc or Novikov tooth shape to increase load capacity. However, it was concluded that the Novikov tooth probably has no real weight advantage over the involute tooth form when dynamic loads must be considered, as in aircraft gears. Consequently, this appendix considers the objective of achieving minimum weight gears by modifying the gear teeth so that they will benefit from certain dynamic effects: (1) tooth stiffness would be changed so as to properly place the gear pair resonant frequency where dynamic loads will be low, and (2) damping can be built into the teeth so that dynamic load peaks are reduced. By reducing the dynamic loads, the damage due to tooth bending fatigue, contact stress, and surface wear is reduced, so that the tooth face width can be reduced. The following describes Richardson's dynamic load analysis (see References 54 and 55) and then discusses methods for reducing dynamic loads, thus allowing lighter weight gears.

DYNAMIC LOAD ANALYSIS

For years, Buckingham's method (see Reference 56) was used as the standard for dynamic load analyses. It was recognized, however, that Buckingham's method gives an upper limit to the dynamic load and does not define the response peaks. Within the past ten years, Richardson of MIT developed a method based on a cam analysis of tooth action, including errors, which is considered to be more realistic. Richardson considers a mating gear pair with forces and moments shown in Figure 104, and he uses the dynamic models shown in Figure 105. With the assumptions that static friction is negligible during dynamic operation, that input and output gear torques T_1 and T_2 are constant and equal to their average values, and that viscous damping may be described by a force proportional to the relative velocities of the two gears along the line of action, Richardson arrives at the equation of motion

$$m\ddot{S}_r + b\dot{S}_r + \bar{W}_n + \bar{W}_{n+1} = \bar{W}_t \quad (14)$$

where

$$m = \frac{m_1 m_2}{m_1 + m_2} - \frac{1}{\frac{R_{B1}^2}{J_1} + \frac{R_{B2}^2}{J_2}} = \text{The effective mass at the line of action}$$

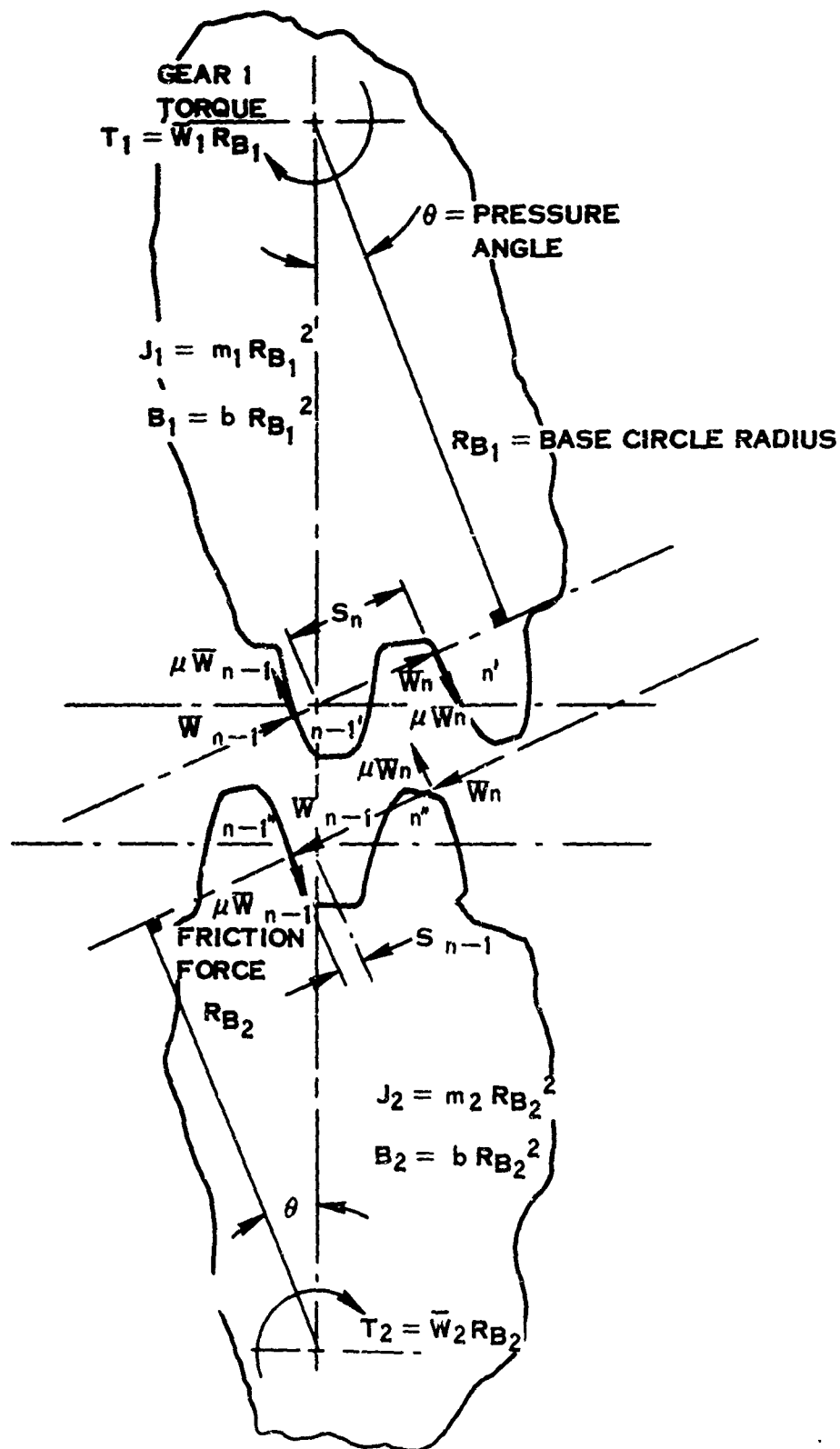
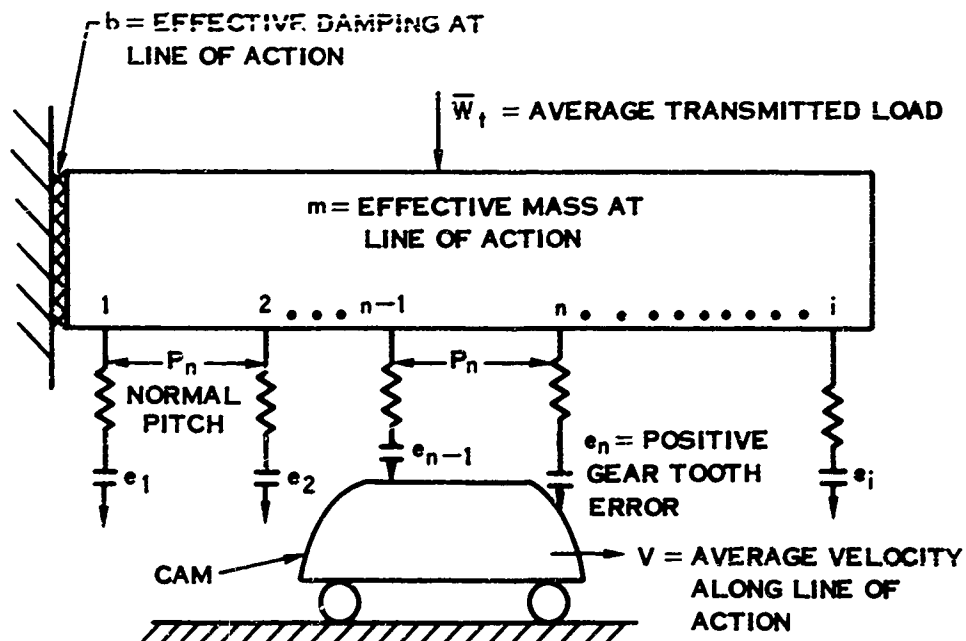
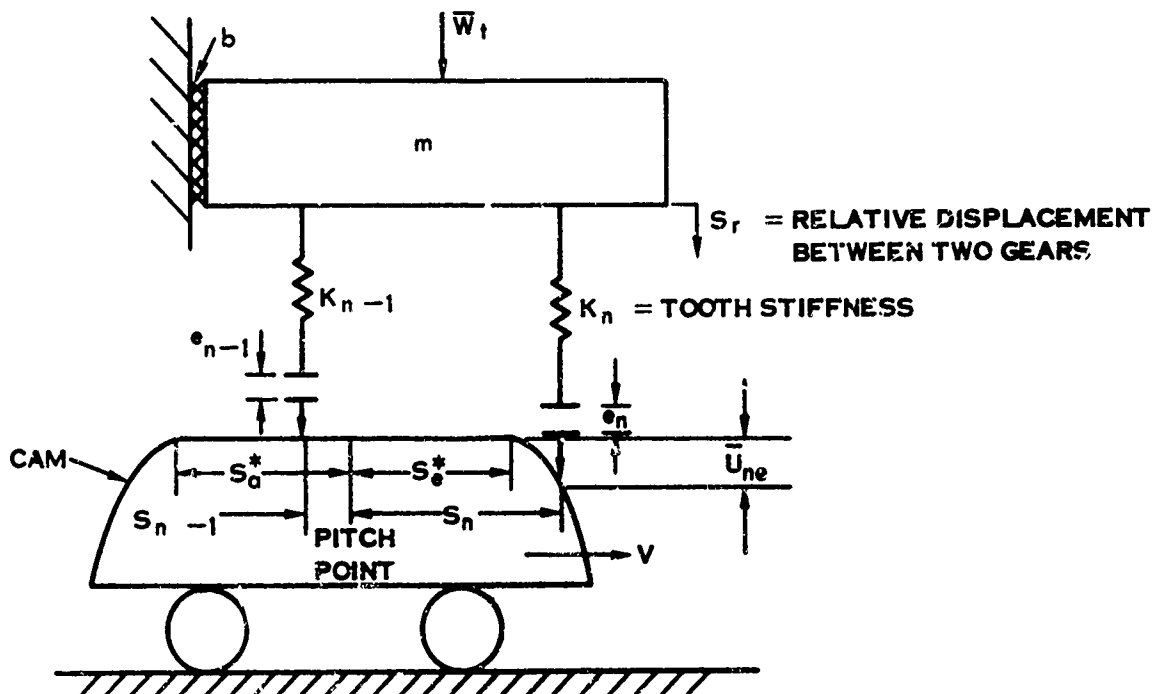


FIGURE 104. FREE-BODY DIAGRAM FOR MATING GEARS



A. RELATIVE MOTION MODEL FOR A GEAR SET WITH DIFFERENT TOOTH PAIRS



B. MODEL FOR PERIOD WHERE THE GEARS MOVE FROM THE POINT WHERE TOOTH - PAIR $n-1$ IS AT THE PITCH POINT TO WHERE TOOTH - PAIR n IS AT THE PITCH POINT

FIGURE 105. RICHARDSON'S DYNAMIC MODELS FOR A GEAR PAIR

$$b = \frac{B}{R_B^2} \quad = \text{The effective damping at the line of action}$$

$$\bar{W}_t = \frac{T}{R_B} \quad = \text{The effective load at the line of action}$$

$$\bar{W}_n = K_n S_r \quad = \text{The } n \text{ tooth pair spring load}$$

$$\bar{W}_{n-1} = K_{n-1} S_r \quad = \text{The } (n-1) \text{ tooth pair spring load}$$

$$S_r \quad = \text{Relative displacement between the two gears}$$

$$R_B \quad = \text{Radius of the base circle}$$

Equation (14) holds for one cycle during which tooth pair (n-1) is at the pitch point and either runs on the flat of the "cam" or disengages while tooth pair (n) engages and runs on the "cam" flat until it reaches the pitch point and the cycle ends; see Figure 105. The tooth engagement or disengagement deformation can be represented by the equations

$$\bar{U}_{(n-1)d} = C_d (-S_d^* - S_{n-1})^2 \quad (15)$$

$$\bar{U}_{ne} = C_2 (P_n - S_e^* + S_{n-1})^2 \quad (16)$$

where C_d and C_r are "cam" constant and S_{n-1} , S_n , S_d^* , S_e^* and \bar{U}_{ne} are defined in Figure 105b (see Reference 55). Equations (14), (15), and (16) are equivalent to a nonlinear second-order differential equation which was solved on a digital computer for the dynamic load ratio or "magnification factor" as a function of dimensionless cycle time T_c that relates the time required for the tooth to traverse one normal pitch P_n to the period of the natural Richardson frequency (see Figure 106).

Since propeller drive gears operate continuously in the high-speed range, toward the left of Figure 106, i. e., $T_c < 10$, it is apparent that a reduction in dynamic load of 2 or 3 to 1 is possible either by introducing damping of about $\xi = 0.1$ or by reducing the dimensionless parameter $T_c < 3$. The latter can be accomplished by operating at a higher speed or by making the teeth flexible so as to reduce the gear pair resonant frequency ω_n . The first and second stages of the advanced

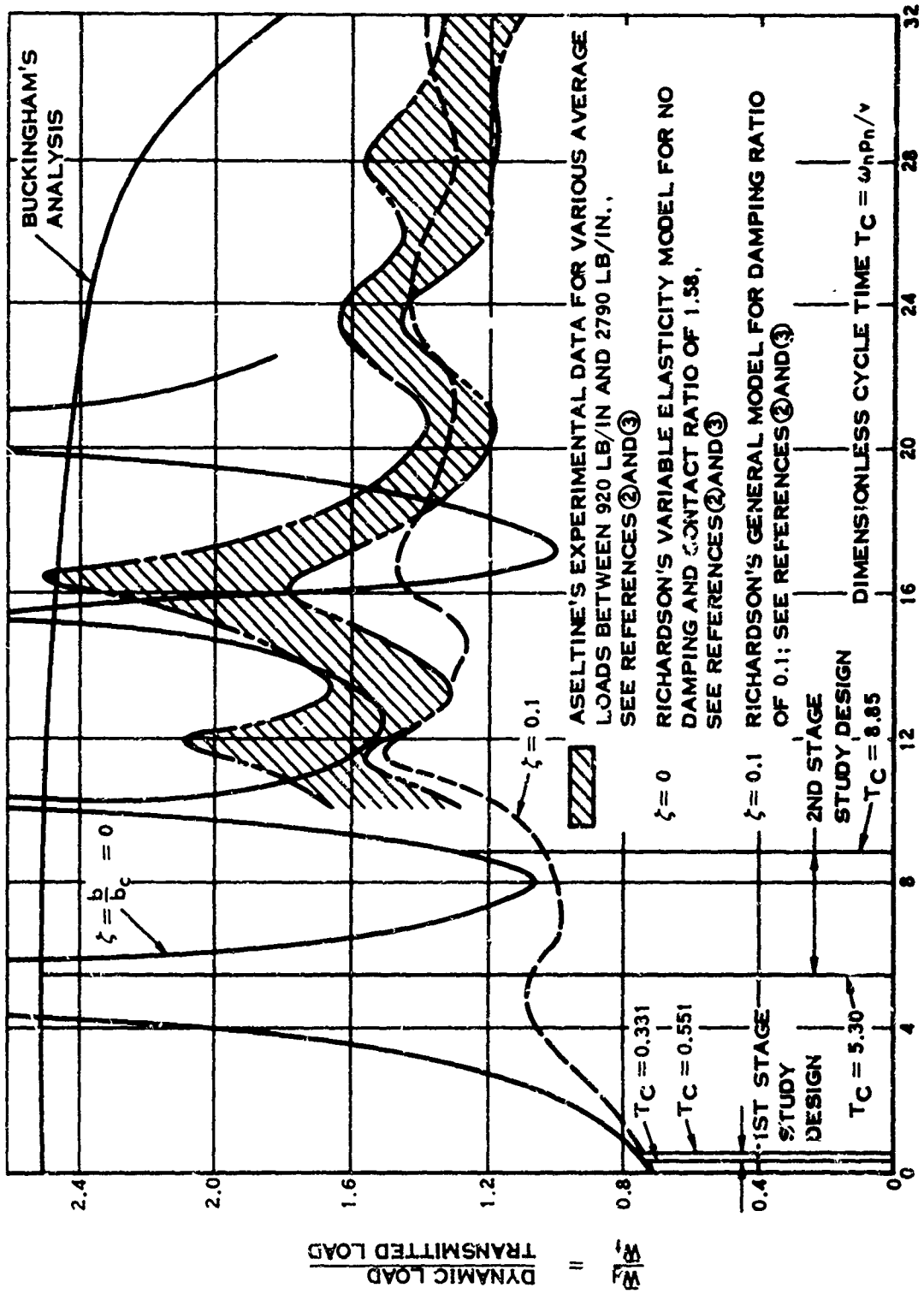


FIGURE 106. DYNAMIC LOADS ON CLEAR TEETH

propeller gearbox discussed above in the report are reviewed below in light of the above theory and thinking.

ANALYSIS OF FIRST STAGE

For the USAAVLABS propeller first-stage gearing, the maximum of 23,000 rpm results in a value

$$T_c = \frac{\omega_n P_n}{v} = \frac{(2.95 \times 10^4)(0.333)}{3,400} = 0.331$$

for which Figure 106 gives, whether damped or undamped.

$$\frac{\bar{W}_d}{\bar{W}_t} = 0.73$$

compared to 2.5 according to Buckingham or conventional analysis. In the preceding calculation for T_c ,

$$\omega_n = \sqrt{\frac{k}{m}} = \sqrt{\frac{0.281 \times 10^6}{0.60324}} = 2.95 \times 10^4 \text{ rad/sec}$$

$$k = \text{tooth pair stiffness} = \frac{1.88 \times 10^6}{\text{in. of face}} \quad 2.8 \text{ in of face} \quad \frac{E_{ri} = 16 \times 10^6}{E_{st} = 30 \times 10^6} = 2.8 \times 10^6 \frac{16}{\text{in.}}$$

$$m = \frac{1}{\frac{R_{b1}^2}{J_1} + \frac{R_{b2}^2}{J_2}} = \frac{1}{\frac{(1.4)^2}{0.60736} + \frac{(7.58)^2}{1.334}} = 0.00324$$

$$P_n = P_c \cos \theta = \frac{2\pi R_G}{N} \cos \theta = \frac{2\pi (1.4)}{21} \cos 25^\circ = 0.383$$

$$v = \frac{(23,000 \text{ rpm})(3.14)(2.82 \text{ in.})}{60 \text{ sec/min}} = 3,400 \text{ in/sec}$$

The minimum first-stage rpm of 13,800 results in a value

$$T_c = \frac{23,000}{13,800} \times 0.331 = 0.551$$

for which Figure 106 gives

$$\frac{\bar{W}_d}{\bar{W}_t} = 0.75 \text{ undamped and } \frac{\bar{W}_d}{\bar{W}_t} = 0.73 \text{ for damping ratio}$$

of $\zeta = 0.10$.

Thus, throughout the operating speed range, the peak dynamic load is only $0.75/2.5 = 30\%$ of the present^{ly} used design load, and the face width can be reduced by 70% . This results in a $(70\%) (6.8 \text{ lb} + 1.1 \text{ lb}) = 5.5 \text{ lb}$ reduction of the rim weight of the first-stage gear pair. By reducing the rim width, the gear inertia is reduced and the gear tooth stiffness is decreased, so that the net effect of T_c is small. Also, a saving is possible in the housing simply because the face width is reduced $0.70 \times (2.8 \text{ in.}) = 2.0 \text{ in.}$, resulting in a shorter envelope. The gear disk, shaft, and bearings cannot be significantly reduced, since their sizing depends primarily on the transmitted load.

ANALYSIS OF SECOND STAGE

Similarly, for the second-stage gearing, the maximum rpm gives

$$T_c = \frac{\omega_n^2 J_n}{v} = \frac{(1.51 \times 10^4)^2 (0.317)}{0.905 \times 10^3} = 5.30$$

for which Figure 106 gives $\frac{\bar{W}_d}{\bar{W}_t} = 2.5$ undamped or $\frac{\bar{W}_d}{\bar{W}_t} = 1.08$ for a damping

ratio $\zeta = 0.10$. It must be noted that the second-stage gearing is a planetary with the sun gear driving and with ring gear fixed. The pitch line velocity v used to find T_c is determined (see Reference 58, page 130) for the sun-planet mesh as maximum rpm to be

$$v_s = 0.5236 \times 4466 \times 5.000 \left(\frac{47}{47 + 43} \right) \left(\frac{133}{133 + 47} \right) = 4.520 \frac{\text{ft}}{\text{min}} = 4.520 \times \frac{12}{60} = 905 \text{ in./sec}$$

and for the planet-ring gear mesh to be

$$v_r = 0.5236 \times 4466 \times 5.000 \left(\frac{133}{133 - 43} \right) \left(\frac{47}{133 + 47} \right) = 4.520 \frac{\text{ft}}{\text{min}} = 905 \text{ in./sec}$$

Thus, for each mesh

$$v_s = v_r = v = 905 \text{ in./sec}$$

In the preceding calculation, the following quantities appear:

Center distance sun-to-planet	= 5.0 in.
Sun rpm	= 4,466
Teeth in sun	= 47
Teeth in planet	= 43
Teeth in ring gear	= 133

For the second-stage gearing and minimum rpm,

$$T_c = \frac{23,000}{13,000} \times 5.3 = 8.85$$

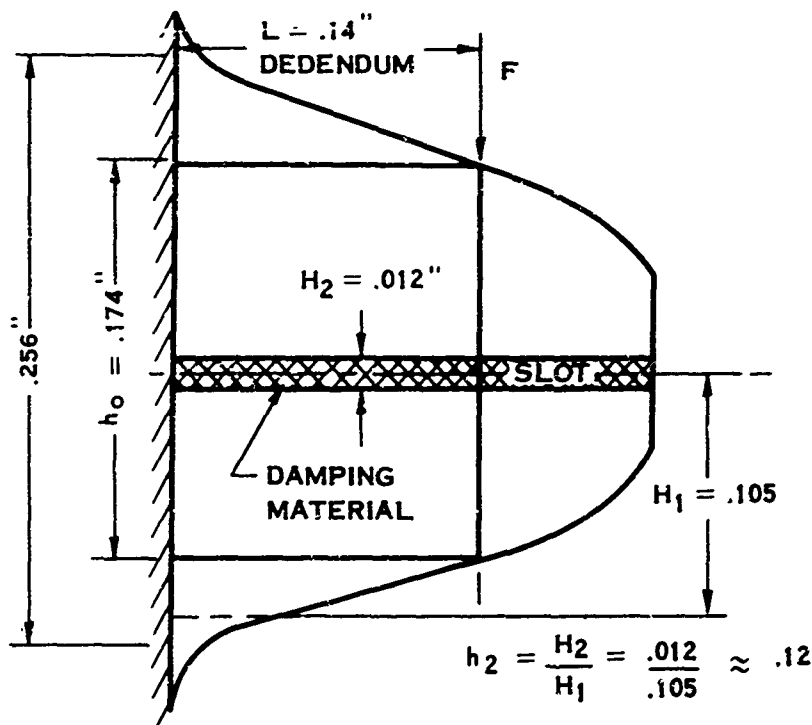
for which Figure 106 gives $\frac{\bar{W}_d}{\bar{W}_t} = 1.30$ undamped and $\frac{\bar{W}_d}{\bar{W}_t} = 1.03$ for a damping ratio of $\zeta = 0.10$.

For the second-stage gearing, the combination of mass, tooth stiffness, and speed causes peak dynamic loads which it is desirable to reduce. Usually there is little damping in gears, so that the dynamic load approaches the limit defined by Richardson's $\zeta \approx 0$ curve or by Buckingham's curve (see Figure 106). Comparison with experimental data from several tests reported in the literature and conducted by us shows that the small amount of damping present in conventional gears limits dynamic loads below the Buckingham curve. In this case, the operating speed spans the dynamic load peak, $T_c \approx 0.5$. It is unlikely that the gear geometry could be changed with assurance so as to restrict the operating range within the dynamic load valley at $T_c \approx 8$. It is also unlikely that the gear pair frequency could be reduced by a factor of 3 (i. e., tooth pair spring constant reduced by a factor of 9) so as to restrict the operating range to $T_c < 3$. However, for a damping ratio of $\zeta = 0.1$, the maximum dynamic load is $1.08/2.5 = 0.43$ percent of the undamped value, so that the face width could be reduced by 57 percent. Thus, there is a potential weight saving of about $(0.57)(1.2 \text{ lb}) = 0.7 \text{ lb}$ in the sun gear, $0.57(1.1 \text{ lb})(5 \text{ planets}) = 3.1 \text{ lb}$ in the planet, and $0.57(3.1 \text{ lb}) = 1.8 \text{ lb}$ in the ring gear, for a total saving of about 5.6 lb if the dynamic load could be reduced.

Introduction of additional damping can be accomplished by adding material to slots in the teeth, to slots between the teeth, or by Coulomb damper rings shrunk or attached to the gear rim.

Tooth Slots

The concept of using high-damping-capacity material in tooth slots is illustrated by the slotted tooth shown in Figure 107 for the approximate dimensions of the second-stage gearing teeth. The slotted tooth can be considered as a laminated



DAMPING MATERIAL : POLYSTYRENE,
 $G_2 = 14,500 \text{ PSI}, E_2 = 3G_2 = 43,500 \text{ PSI}$

DAMPING ANALYSIS

$$\frac{D_C}{D_2} = \frac{\text{DAMPING FACTOR OF TOOTH}}{\text{DAMPING FACTOR OF SLOT}} = \frac{3(1+h_2)^2 \bar{X}}{1 + [2+3(1+h_2)^2] \bar{X} + [1+3(1+h_2)^2][1+D_2^2] \bar{X}^2}$$

$$= \frac{3(1+.12)^2 1.33}{1 + [2+3(1+.12)^2] 1.33 + [1+3(1+.12)^2][1+1.6^2] (1.33)^2} = \frac{5.00}{1+7.00+(4.75)(3.56)(1.77)} = .132$$

WHERE $\bar{X} \approx \frac{17.600}{EH_2} \left(\frac{G_2}{f}\right) = 1.33$ FOR TOOTH GEOMETRY AND MATERIAL
 $f \approx 1000 \text{ CPS}, E = 16 \times 10^6 \text{ PSI}$

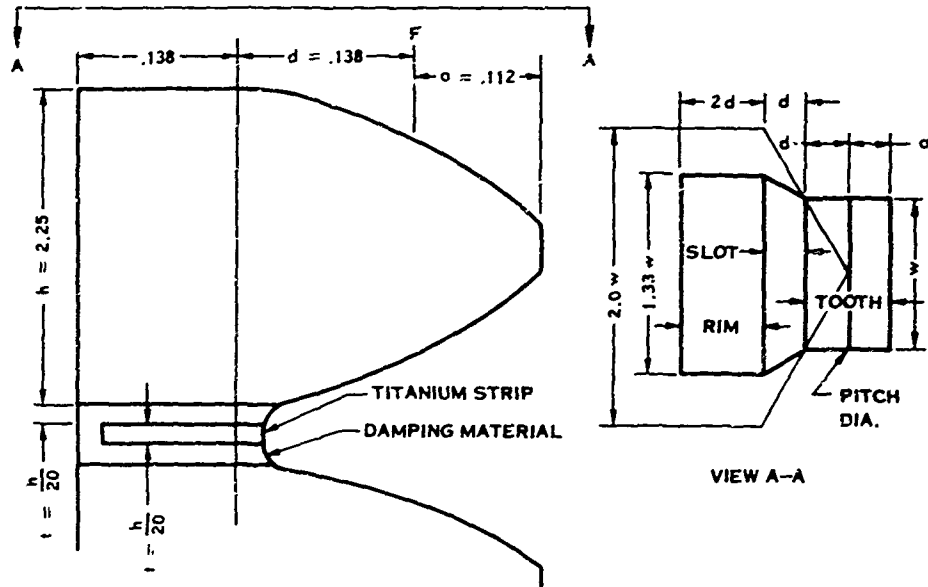
$D_C = 0.132 \quad D_2 = 0.132 \times 1.6 \approx 0.21$

$\zeta = \frac{C}{C_C} = \frac{D_C}{2} = 0.105$ CRITICAL DAMPING RATIO OF COMPOSITE TOOTH STRUCTURE

FLEXIBILITY ANALYSIS:

$\bar{X} = 1.33, \bar{Y} = 3(1+h_2)^2 = 3(1+0.12)^2 = 3.75$
 GIVES THE COMPLEX DYNAMIC FLEXURAL RIGIDITY $B_C^* \approx 4.0(B_1 + B_3)$
 WITHOUT THE SLOT DYNAMIC FLEXURAL RIGIDITY $B_{1+3} \approx 4.0(B_1 + B_3)$
 THUS SLOTTED TOOTH HAS $\frac{B_C^*}{B_{1+3}} \times \left(\frac{h_0}{f}\right)^3 \times 100 = \frac{4.0(0.198)^3}{4.0(0.210)^3} \times 100 = 84\%$
 STIFFNESS OF UNSLOTTED TOOTH

FIGURE 107. TOOTH SLOT DAMPING AND FLEXIBILITY



DAMPING MATERIAL: RUBBER

60 DUROMETER

$$\text{SHAPE FACTOR} = \frac{\text{LOAD AREA}}{\text{PERIPHERAL AREA}} = \frac{d}{t} = 11$$

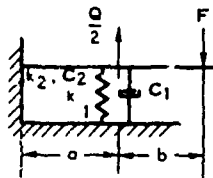
$\sigma = 4000$ PSI FOR 10% STRAIN

$$E = \frac{\sigma}{\epsilon} \times \text{DYNAMIC FACTOR} = \frac{4000}{0.10} \times 1.8 = 40,000 \times 1.8 = \underline{72,000 \text{ PSI COMP. MOD.}}$$

$$\text{CRITICAL DAMPING RATIO } \zeta = \frac{C}{C_c} = \frac{B}{2} = \frac{1.0}{2} = 0.50$$

DIAMETRAL PITCH = 9.0

COMPRESSIVE LOAD Q



$$\text{FOR } \frac{h}{a} = 2, \frac{b}{a} = \frac{5}{4}, \frac{E}{G} \approx 2.5$$

ELEMENTARY BEAM THEORY INCLUDING SHEAR CORRECTION AND FULL SUPPORT GIVES

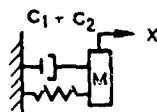
$$\frac{F}{Q} = \frac{\left[1 + \frac{3}{2} \frac{b}{a} + \frac{E}{4G} \frac{h^2}{a^2} \right]}{\left[1 + \frac{E}{4G} \frac{h^2}{a^2} + \frac{E}{G} \left(\frac{h^3}{4a^3} \right) \frac{2G}{E_f a} \right]}$$

$$\frac{F}{Q} = \frac{\left[1 + \frac{3}{2} \left(\frac{5}{4} \right) + \frac{1}{4} (2.5) (2)^2 \right]}{\left[1 + \frac{1}{4} (2.5) (2)^2 + (2.5) \left(\frac{1}{4} \right) (2)^3 \frac{2G}{E_f (2h)} \right]} = \frac{5.4}{3.5 + 5.0 \frac{G}{E_f h}}$$

$$\text{ASSUME } \frac{G}{E_f h} = 0.4 \frac{E_f}{E_f h} = 4 \text{ OR } \frac{E_f}{E_f h} = 10 \quad \text{THEN } \frac{Q}{F} = \frac{5.4}{3.5 + (5.0)(4)} = \frac{5.4}{23.5} \approx 0.23$$

$$\text{LET } \frac{1}{h} = \frac{1}{20}, \text{ THEN } E_f = \frac{E}{200} = \frac{16,000,000}{200} = \underline{80,000 \approx 72,000 \text{ PSI HARD RUBBER}}$$

DAMPING RATIO COMPOSITE BEAM



$$M\ddot{X} + (C_1 + C_2)\dot{X} + (k_1 + k_2)X = 0$$

$$Q = k_1/(k_1 + k_2) = 0.23, (F-Q) = k_2/(k_1 + k_2) = 0.77$$

$$\text{RUBBER } C_1/C_C = 0.50 \text{ AND } C_1 = 1.00 \frac{k_1}{w_n}$$

$$\text{TITANIUM } C_2/C_C = 0.005 \text{ AND } C_2 = 0.010 \frac{k_2}{w_n}$$

FIGURE 108. RIM SLOT DAMPING AND FLEXIBILITY

maintain constant stressing. Actually, Reference 60 says that the relative stressing will be only about 1.33 instead of 1.77 at the end, so that the final width is $1.33 \times 0.43 = 0.57$. Thus, the resulting rim width reduction of 43% is approximately the same as the 41% for the previous case. The actual weight reduction will be less because the added tooth height is not fully compensated for by the narrower tooth width. For the planets, the weight is reduced about 36%, or about 90% of that obtained by the tooth slots. Thus, the total weight reduction by this approach would be about 2.5 pounds.

By milling slots and putting damping material between the teeth, the stiffness of the tooth is decreased to about 25% of its original value. Although this change in flexibility alone decreased T_c about 50 percent, the J of the system also decreases, so that T_c is only slightly reduced.

It is apparent from Figure 106 that if slotting could make the teeth 10 times more flexible with no increase in J , no damping would be required, since T_c would be less than 3.

Reference 59 shows that the loss factor of polystyrene is 2.0 and that its damping ratio $\zeta = 2.0/2 = 1.0$, which is twice as much as that of hard rubber. This suggests that polystyrene in compression may be better than hard rubber and possibly better than polystyrene in shear. However, more study of the dynamic factor for polystyrene in compression is needed to verify this suggestion.

Slots between the teeth tend to isolate the dynamic action of a tooth from the adjacent teeth. It appears likely that this is beneficial. This decoupling effect could be optimized by varying the configuration of the damping and spacer material.

Coulomb Damping

The concept of introducing damping to gear teeth through rubbing rings has been used for many years, and it is shown in several variations in Figure 109. However, as Figure 109 indicates, application of dry-friction damping rings will probably require more weight than the tooth or rim slot damping previously described, because of the weight of the rings and clamps required to apply it. Hence, Coulomb damping rings appear to offer less potential weight reduction.

CONCLUSIONS AND RECOMMENDATIONS

It is concluded from this study that it is theoretically possible to reduce the maximum dynamic tooth loads up to $1/3$ of the otherwise anticipated values in two ways: (1) by assuring that the teeth are flexible enough and that the entire operating speed range is high enough that the dimensionless parameter $T_c < 3$; (2) by providing tooth damping so the damping ratio $\zeta = c/cc \approx 0.1$. Reducing the dynamic load results in a proportionate reduction in face width and therefore in rim weight, but it makes little change in the weight of the gear disc

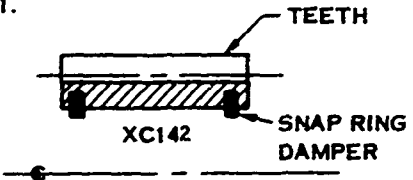
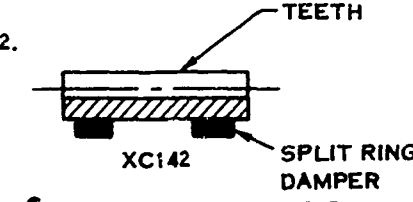
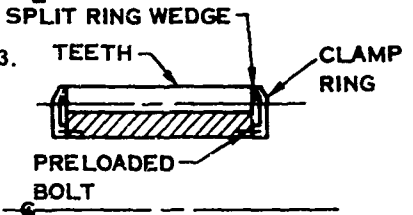
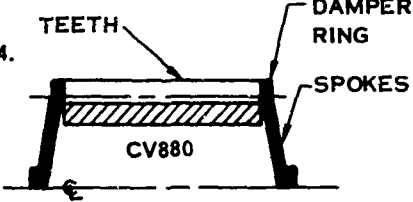
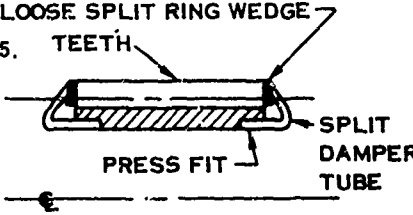
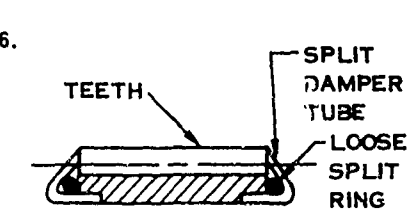
	ADVANTAGE	DISADVANTAGE
<p>1.</p>  <p>TEETH XC142 SNAP RING DAMPER</p>	<ol style="list-style-type: none"> 1. EASY TO INSTALL 2. CENTRIFUGAL ACTION COMPENSATES FOR WEAR 	<ol style="list-style-type: none"> 1. WEAR OVER LONG TIME 2. DOES NOT ACT DIRECTLY ON TEETH 3. WEIGHT OF RINGS
<p>2.</p>  <p>TEETH XC142 SPLIT RING DAMPER</p>	<ol style="list-style-type: none"> 1. EASY TO INSTALL 2. CENTRIFUGAL ACTION COMPENSATES FOR WEAR 	<ol style="list-style-type: none"> 1. WEAR OVER LONG TIME 2. DOES NOT ACT DIRECTLY ON TEETH 3. WEIGHT OF RINGS
<p>3.</p>  <p>SPLIT RING WEDGE TEETH CLAMP RING PRELOADED BOLT</p>	<ol style="list-style-type: none"> 1. ACTS ON TEETH 2. PRELOAD 3. CENTRIFUGAL ACTION WEDGES SPLIT RING AGAINST TEETH 	<ol style="list-style-type: none"> 1. WEAR OVER LONG TIME 2. WEIGHT OF CLAMP RINGS AND DAMPING RINGS
<p>4.</p>  <p>TEETH DAMPER RING SPOKES CV880</p>	<ol style="list-style-type: none"> 1. ACTS ON TEETH 2. PRELOAD 	<ol style="list-style-type: none"> 1. WEAR OVER LONG TIME 2. WEIGHT OF DAMPING RINGS AND SPOKES
<p>5.</p>  <p>LOOSE SPLIT RING WEDGE TEETH PRESS FIT SPLIT DAMPER TUBE</p>	<ol style="list-style-type: none"> 1. ACTS ON TEETH 2. CENTRIFUGAL ACTION TIGHTENS TUBE 3. LOOSE RING WEDGES AGAINST TEETH 	<ol style="list-style-type: none"> 1. WEAR OVER LONG TIME 2. WEIGHT OF DAMPER TUBE AND RING
<p>6.</p>  <p>TEETH SPLIT DAMPER TUBE LOOSE SPLIT RING</p>	<ol style="list-style-type: none"> 1. ACTS ON TEETH 2. TUBE WEDGES RING AGAINST TEETH AT RPM 3. CENTRIFUGAL ACTION TIGHTENS TUBE 	<ol style="list-style-type: none"> 1. WEAR OVER LONG TIME 2. WEIGHT OF DAMPER TUBE AND RING

FIGURE 109. EXAMPLES OF USING COULOMB DAMPING ON GEARS

or bearings. The shaft and housing weight is reduced because the narrower teeth require a smaller envelope. It is further concluded that this order of damping could possibly be accomplished by introducing damping material in slots in two different ways as shown in Figures 107 and 108. The weight reduction is compromised somewhat by the required additional material to carry the load, because the slot weakens the tooth somewhat.

This study has shown that a theoretical potential weight reduction is possible by incorporating a high damping capacity into involute gearing. Therefore, it is recommended that further study be applied to refine the theory of slotted gears to properly include shear effects present in deep beams, and that tests be conducted to verify the theory.

APPENDIX VI
PARAMETRIC STUDY OF THE PROPELLER BARREL STRUCTURE

INTRODUCTION

The study presented in this appendix was undertaken with the objective of optimizing propeller hub structures from the standpoint of weight. Present propeller barrel designs at Hamilton Standard have predominately been of the so-called "dual ring" construction. In this conventional design, the barrel is characterized by two heavy circular ring sections, located fore and aft of the blade retention, which are assumed to carry all primary blade loads (See Figure 110). Thus, in a study aimed at weight reduction, two methods of approach are open: (1) study the effect of varying the several geometric parameters involved in the conventional barrel design with the object of minimizing weight, and (2) study various new concepts and approaches to barrel design with the goal of reducing the barrel weight. In this investigation, both of these approaches have been followed, the former quantitatively and the latter only qualitatively.

It should be noted that a propeller barrel is usually thought of as consisting of three major elements: the hub structure, the blade retention, and the tailshaft. The present study is concerned only with the hub structure. (The blade retention is discussed in a separate appendix.) The loads acting on the hub structure imposed by the blades consist of steady centrifugal loading, steady bending loads both in and out of plane, and in- and out-of-plane vibratory loads which are 1P and higher orders. The vibratory loads may be grouped by their effect on the hub into: (1) whirl loads which are 1P, 2P, 4P, and 5P for a three-way and 1P, 3P, and 5P for a four-way; (2) symmetrical loads which are 2P and 6P for a three-way and 4P and 8P for a four-way propeller; and (3) reactionless loads which are 3P and 6P for a four-way (do not exist for a three-way). To analyze the first-order effects and the symmetrical vibratory loads which cause a hub deformation similar to steady bending, it is necessary, in this optimization study, to consider only vibratory loads of 1P for a three-way and both 1P and 2P for a four-way.

PARAMETER STUDY OF THE CONVENTIONAL BARREL DESIGN

For the purposes of analysis, the conventional barrel design has been represented by a collection of curved beams and rigid blocks as shown in Figure 110. The rigid blocks represent the fairly heavy blade retention, and the curved beams represent the more flexible interring portion of the barrel. In order to calculate the loads and stresses in the barrel, a simplified analysis previously developed was used. In this analysis the load paths in the barrel (i. e., front-to-rear ring load ratio, resulting from applied centrifugal blade loads, steady bending in-and out-of-plane moments, and 1P bending in-and out-of-plane moments) are postulated in advance.

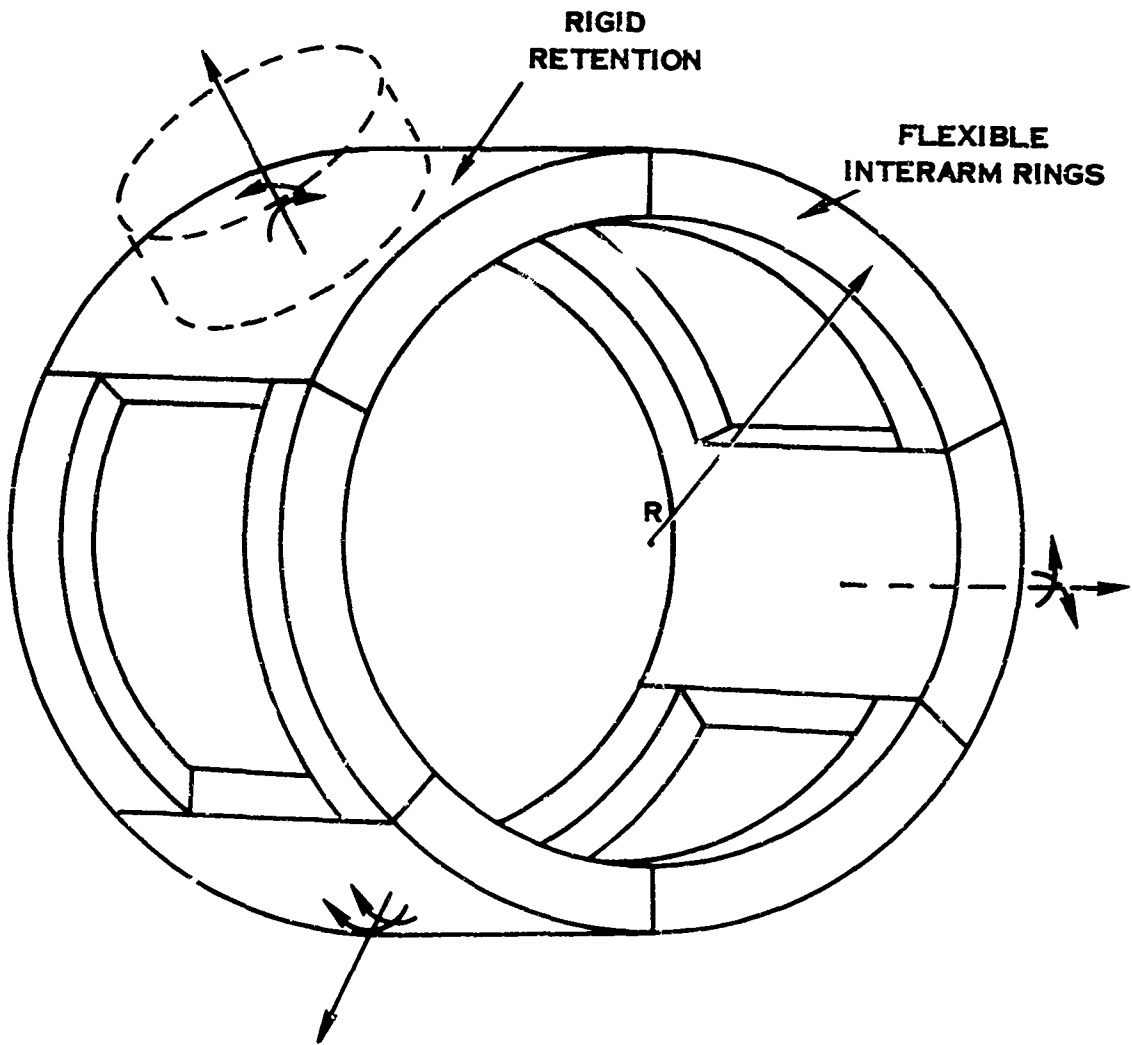


FIGURE 110. CONVENTIONAL BARREL, ANALYTICAL MODEL

In the primary portion of the barrel (neglecting blade retention and tailshaft) the following parameters were selected as having a major influence on stress and weight: gross barrel diameter, front-to-rear ring spacing, front-to-rear ring stiffness ratio, retention diameter, and ring section shape. For the sake of simplicity, a three-way barrel has been used in the analysis; however, extension of the result to a four-way barrel could easily be made and would show the same trends.

Figures 111 through 115 show the analytical results obtained from the present study for centrifugal load, steady out-of-plane moment, steady in-plane moment, 1P in-plane moment, and 1P out-of-plane moment, respectively. In these graphs $(P/W)/(\sigma_0/\rho)(1/V_0)$ or $(M/W)/(\sigma_0/\rho)(1/V_0)$ is plotted against retention radius for several values of barrel radius; (P/W) or (M/W) represents the load capacity/weight ratio, (σ_0/ρ) is the strength/density ratio for the barrel material, and $(1/V_0)$ is the reciprocal of a reference barrel volume when the barrel diameter is 12 inches and the retention diameter is 6 inches.

As can be seen from Figures 111, 112, and 113, the greatest load-carrying capacity per unit weight for the centrifugal load and for both steady bending load cases occurs when the barrel diameter is made as small as possible and the retention diameter is made as large as possible. For the 1P in-plane moment case, the greatest capacity/weight is achieved by making the barrel diameter small. However, for barrel radii less than about 7 inches, capacity/weight is optimized by making the retention radius as large as possible; and for barrel radii greater than about 7 inches, capacity/weight is optimum at one particular value of retention radius as given by Figure 114. For the 1P out-of-plane moment case, capacity/weight is optimized by making the barrel diameter small and by choosing the optimum retention radius from Figure 115. It should be noticed in Figures 114 and 115, however, that the optimum retention radius (in those cases where a single optimum exists) is very close to being the largest retention which could practically be used for the given barrel diameter. To summarize these results, therefore, it can be said in general that the greatest capacity/weight ratio is obtained by making the barrel diameter small and the retention diameter large, regardless of the loading condition.

It has been found from the present simplified theory that the gross barrel loads (ring loads) are not affected by front-to-rear ring stiffness ratio or by ring section shape. For this reason, a material may be chosen for the barrel based strictly on considerations of strength/density ratio, without regard for the material modulus of elasticity. In addition, this indicates that ring section shape may be chosen to minimize the stress for a given load, without regard for stiffness. Obviously, this stress is minimized by having a section which is thick in the plane of the ring and narrow out of plane.

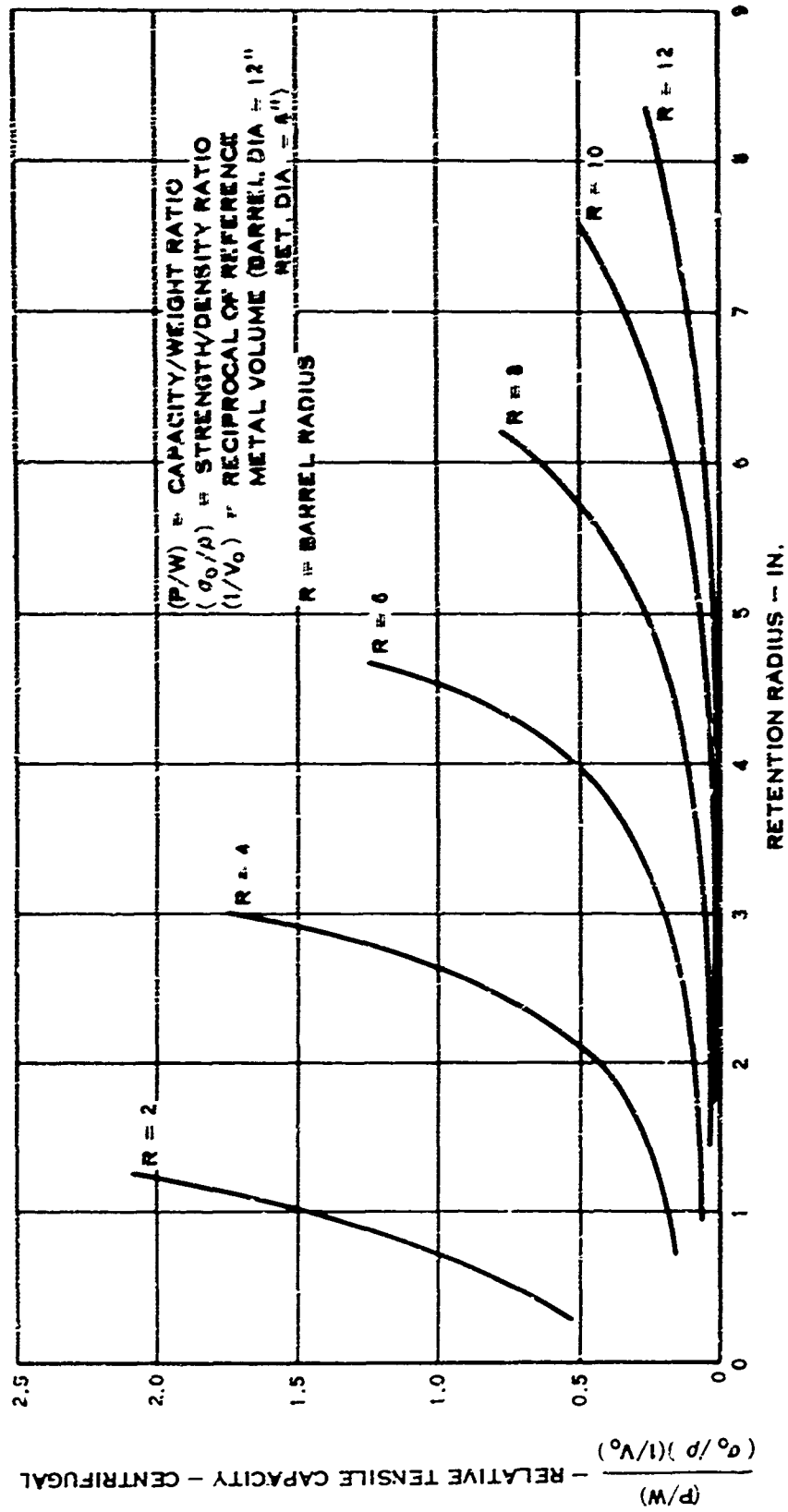


FIGURE 111. BARREL CAPACITY UNDER CENTRIFUGAL LOADING

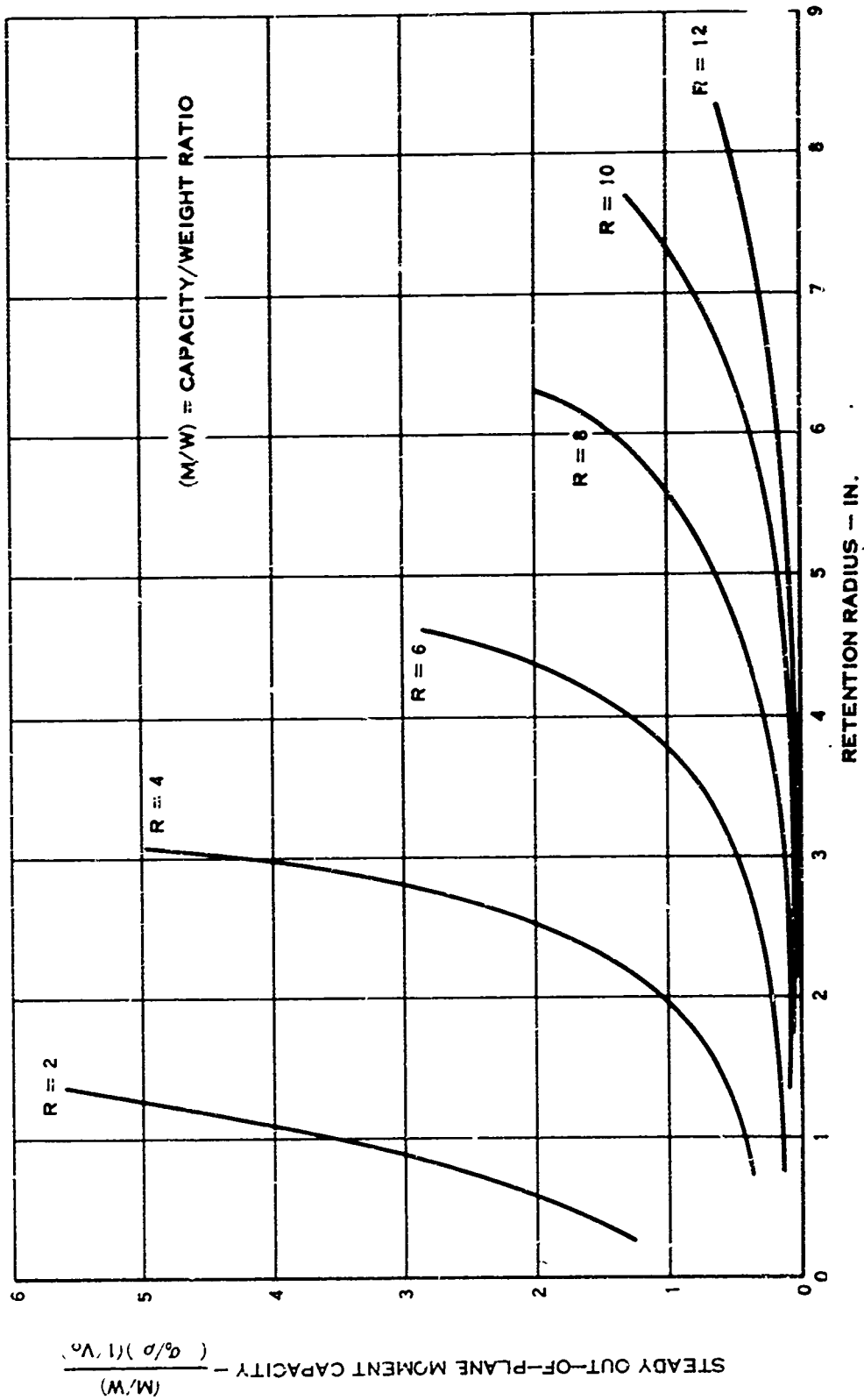


FIGURE 112. BARREL CAPACITY UNDER STEADY OUT-OF-PLANE BENDING LOADS

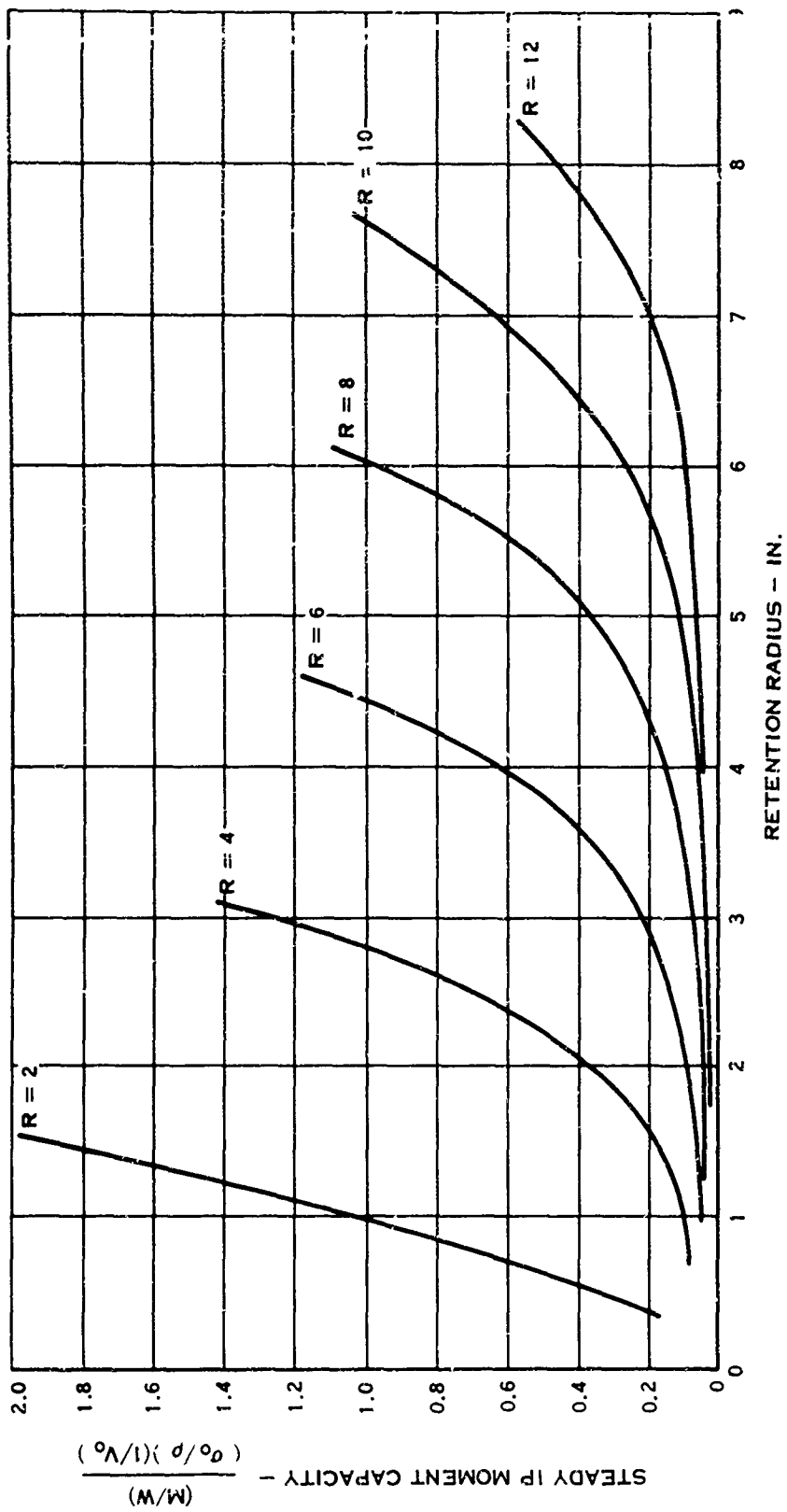


FIGURE 113. BARREL CAPACITY UNDER STEADY IN-PLANE BENDING LOADS

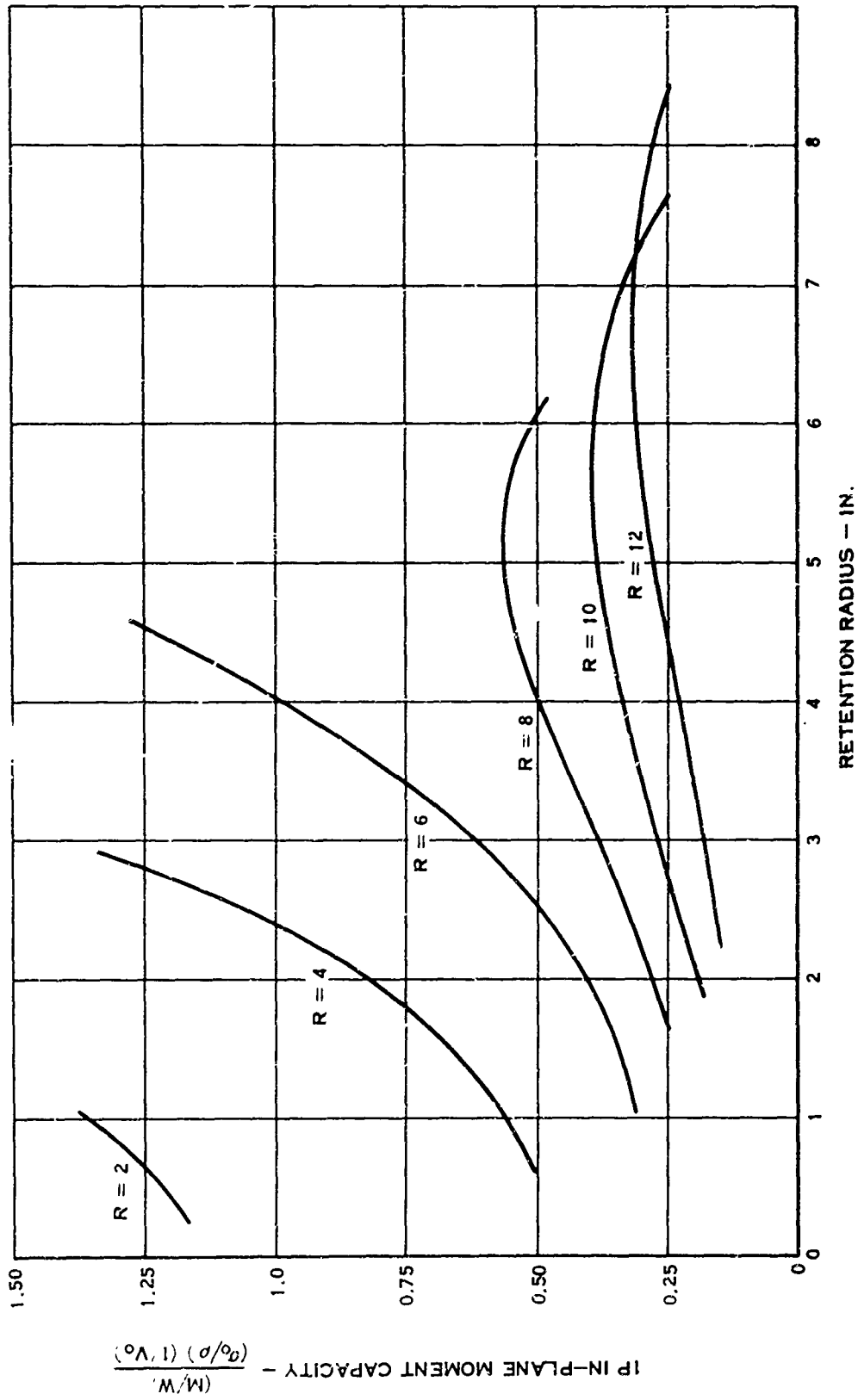


FIGURE 114. BARREL CAPACITY UNDER 1P IN-PLANE BENDING LOADS

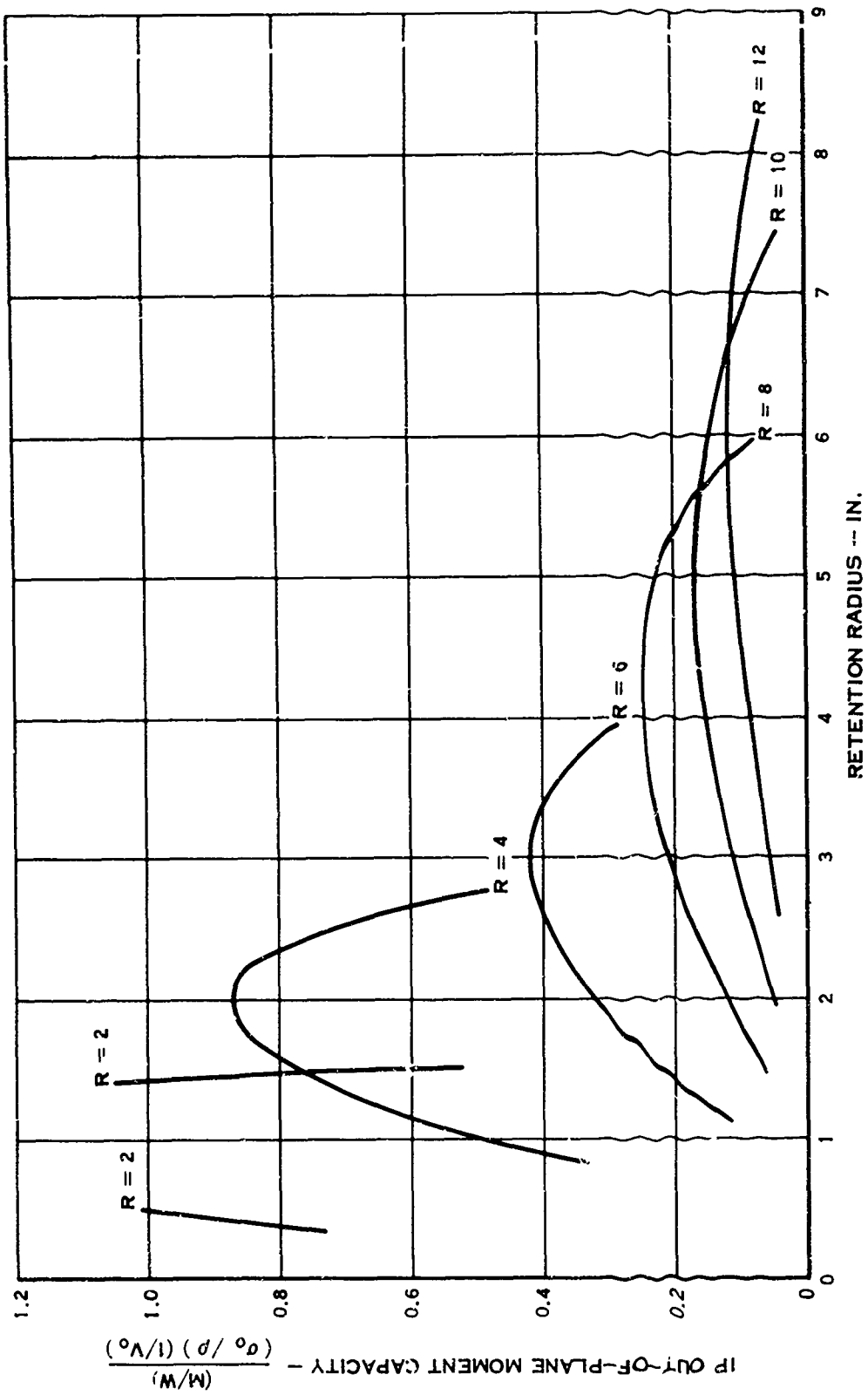


FIGURE 115. BARREL CAPACITY UNDER 1P OUT-OF-PLANE BENDING LOADS

It has been found that front-to-rear ring spacing does not affect gross barrel loads (ring loads) except in the out-of-plane moment cases, both steady and 1P. Because of this, in the centrifugal load and in-plane moment cases, capacity/weight is optimized by making the ring spacing small, since weight is saved thereby; whereas, in the out-of-plane moment cases, capacity/weight is nearly independent of spacing due to load and weight effects' offsetting one another.

In order to establish the accuracy of the simplified analysis used in this study, one set of barrel parameters was used in conjunction with a more sophisticated structures analysis recently developed. This analysis is quite complex and was considered to be excessively time-consuming for the complete study; hence, the simplified analysis was used. This method, however, ensures that compatibility is satisfied and does not require specification of load paths in advance. Results obtained from this case indicate that the simplified analysis is sufficiently accurate for the purposes of the present study. Centrifugal load and in-plane moment cases were in very good agreement, with out-of-plane moment cases showing a somewhat larger discrepancy.

For a conventional barrel design, the results of this study indicate that the barrel should be small, with a retention as large as practical consistent with barrel diameter and with ring spacing as close as practical consistent with retention diameter. Because of the relationship between stress and displacement, it is believed that such an arrangement would also be beneficial from the standpoint of hub stiffness. In current designs, the barrel is already very nearly as small, and has a close ring spacing, as is practical and consistent with actuator requirements; thus, it is believed that significant weight reductions can best be achieved through the use of new design concepts. Two such concepts will be discussed in the following paragraphs.

NEW BARREL DESIGN CONCEPTS

In contrast to the conventional barrel design, which uses circular rings as load-carrying members, two new concepts have been analyzed which make use of other structural elements. The first new concept begins with the premise that the loads in a four-way barrel can best be carried by means of an x-member as shown in Figure 116A. From this premise has evolved a design which consists essentially of two crossed cylinders, arranged in such a way that each cylinder is continuous through the other; see Figures 49 and 50. In this design, however, holes must be placed in the cylinders to accommodate the actuator mechanism and the connecting links from the actuator to the blades.

The crossed-cylinder design possesses many obvious advantages. Some of these are at least partially dissipated, however, by the actuator cutout. The load-carrying capacity for a given weight in this design should be quite good for the

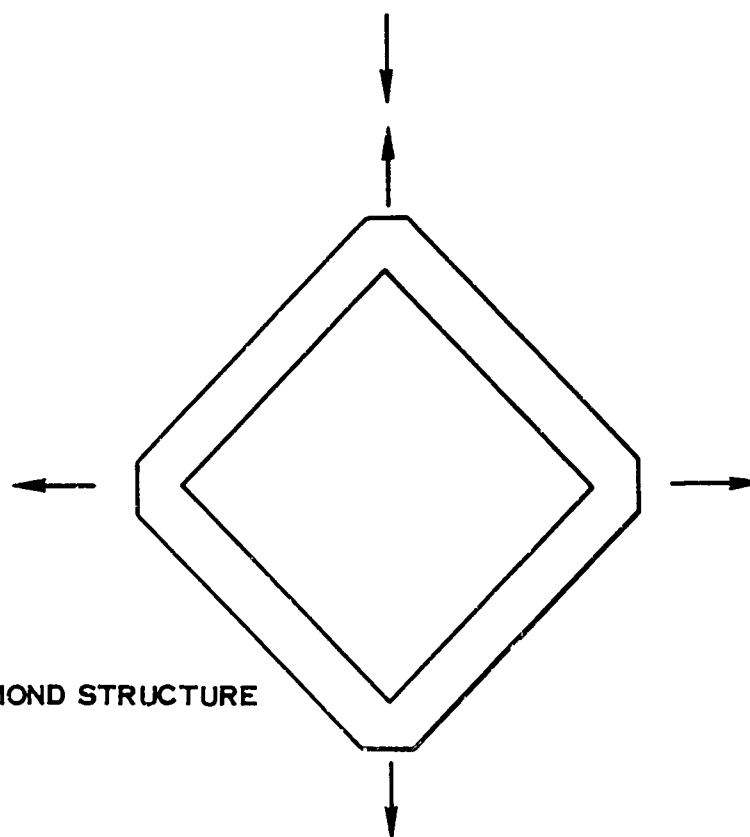
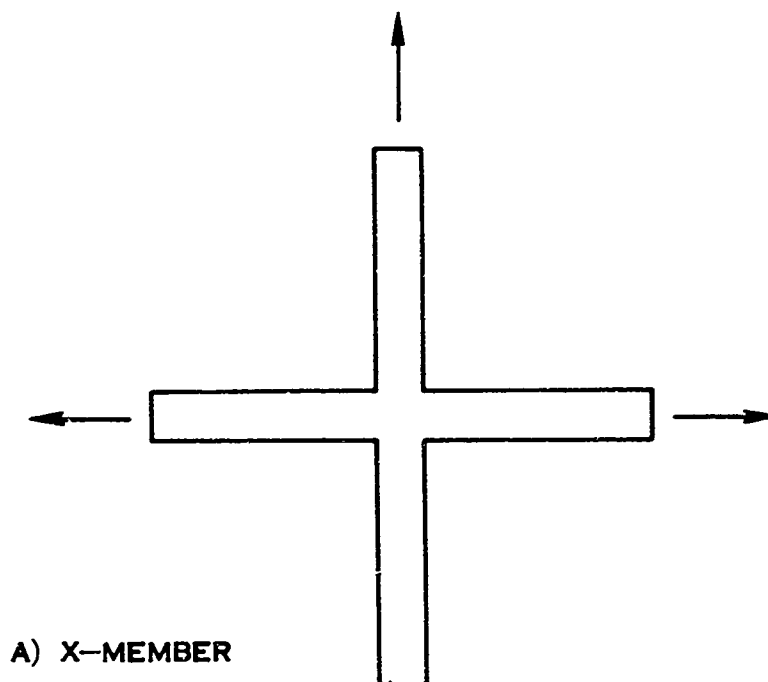


FIGURE 116. BASIC LOAD-CARRYING BARREL STRUCTURES

centrifugal load case. A tendency toward nonuniform barrel arm flexibility caused by the actuator cutout is reduced by a diamond-shaped reinforcing member around the actuator cutout, and by the support from the curvature of the other intersecting cylinder.

Although the centrifugal loads of two opposing blades are carried almost entirely by the cylinder joining these blades, some deformation of the other cylinder will probably occur. The magnitude of the resulting local bending stresses, and thus the required size of the local fillets, was not evaluated in detail in this study. This would best be determined by a model test during a detail design of the barrel.

For in-plane moment loading (steady, 1P, and 2P), the cylinder design should be quite good, although once again the stresses in the perpendicular cylinder due to deformation of the loaded cylinder must be taken into account. The out-of-plane moment case (steady, 1P, and 2P) represents the most troublesome loading situation for the design. For this type of loading, a portion of the load-carrying advantage of the cylinders themselves is lost because of the actuator cutout, and a portion of the load is supported by the diamond-shaped reinforcing member. For steady and 1P out-of-plane bending, this diamond-shaped member is fairly efficient; for 2P bending, it would be somewhat less efficient, but still better than the conventional barrel design.

The second new design concept begins with the assumption that the loads in a barrel with any number of blades can be efficiently carried by means of a diamond structure as shown in Figure 116B. From this assumption has evolved a design which represents a shell-type structure (Figures 51 and 118). In this barrel design, each point in a retention ring is connected by a straight line to a point in the adjacent ring having the same fore-and-aft dimension (see Figure 117). This results in a barrel which is a monocoque shell structure, the interarm areas being sections of an elliptic cylinder. In order to carry the actuator and tailshaft, a connection arrangement can be devised, and the open square area can be filled in as shown in Figure 117.

Such a monocoque barrel can be made quite compact, and, for the centrifugal load case, the load-carrying capacity for a given weight should be quite good because centrifugal loads do not cause bending in the interarm areas. However, to limit retention deflection and to ensure uniform retention stiffness, the thickness of the elliptic interarm areas would be tailored. This would be done by making the interarm sections thicker at the top and bottom and thinner in the middle so as to compensate for the difference in the length of the generating line.

For steady out-of-plane bending loads, the monocoque barrel should have a good capacity-to-weight ratio for the same reasons as given for the centrifugal case.

For steady in-plane bending, this barrel would be somewhat less efficient, as most

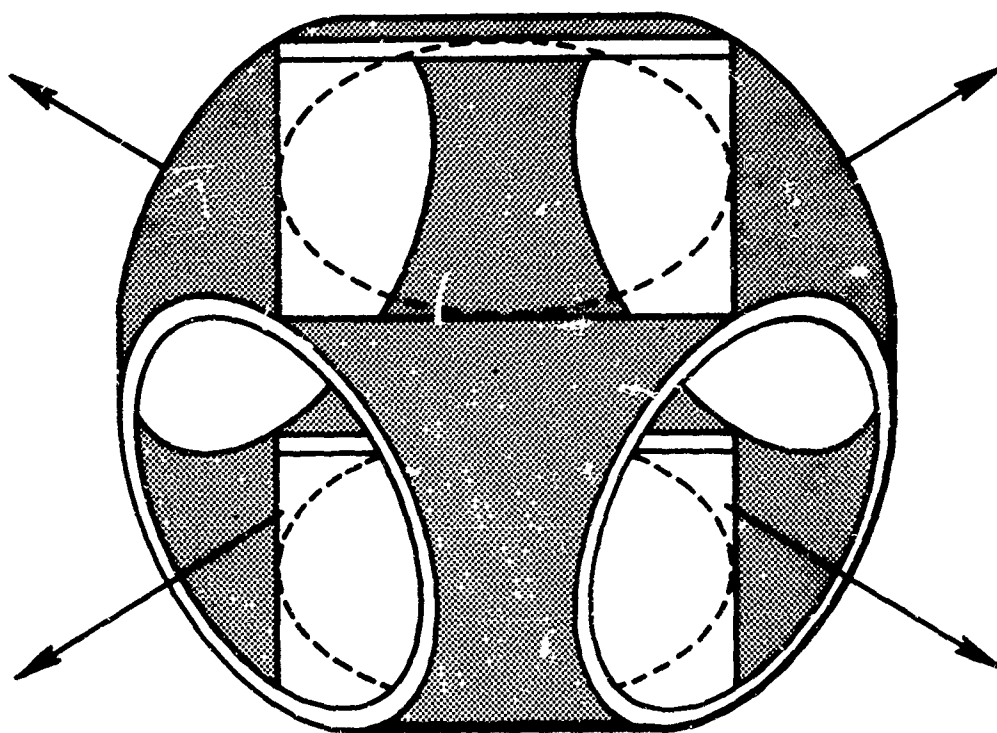


FIGURE 117. SKETCH OF MONOCOQUE SHELL BARREL CONCEPT

of the load would be carried by the center portions of the interarm areas which are of smaller thickness. Because these areas are short, however, it is believed that the efficiency should be moderately good.

In the case of 1P out-of-plane bending, the load paths in this barrel are quite complicated; hence, the relative efficiency is difficult to estimate even qualitatively. It would appear that a share of the load goes into a shearing action of the interarm areas, and here again the short length of the generating line in the center should be advantageous. It would also appear that some nonuniform deformation of the retention may occur. A more detailed analytical study of this loading case would be required to determine the optimum location and amount of additional material required to stiffen the retention.

The behavior of the barrel under 1P in-plane loading should consist predominately of tension and bending in the interarm areas, and the design should be relatively efficient for this case.

For 2P out-of-plane bending, most of the load is carried by bending of the thicker interarm areas near the top and bottom of the barrel. Because these areas are the thickest part of the shell wall, the efficiency should not be too poor, even though these areas are fairly long in span. For the 2P in-plane bending case, the monocoque design is less efficient, and it is possible that some local shell bending in the interarm areas may occur. Because of this, it may be necessary to thicken the center of the interarm areas. This could lead to a nonuniform retention flexibility.

In summary, it can be stated that both new barrel concepts possess certain advantages and disadvantages, but it has been shown that both designs are superior to the conventional design on a capacity/weight basis.

The crossed-cylinder concept tends to isolate the retention structure from the gross barrel structure, while the shell-type concept uses the retention as an integral part of the gross barrel structure. For the specific four-way propeller design point of this study, the crossed cylinder concept was favored. However, under different design conditions or in going to a three-way propeller, the comparison could change; and, since both designs are potentially lighter than conventional designs, it is suggested that both are deserving of further detailed study.

APPENDIX VII
PARAMETRIC STUDY OF THE INTEGRAL BALL-RACE BLADE RETENTIONS

A parametric study was conducted to determine the optimum ball-race blade shank retention configuration. The object was to minimize the ball-race blade retention weight for adequate retention stiffness, axial load capacity, and moment capacity by varying some specified geometry parameters. The parameters considered, which are illustrated in Figure 118, include the pitch diameter, ball diameter, race spacing, ball-race fit, and number of races. To make the results comparable, the geometry parameter of overall retention length and the stress parameters of nominal barrel arm stress, blade shank stress, and ball-race contact stress were held constant.

This study was based upon the standard ball-race retention and does not include the four-point bearing race retention discussed in the main body of the report.

ANALYSIS

The analysis used for calculating ball-race blade retention stiffness and moment and rocking capacities had been previously derived and frequently used. The retention stiffness calculation considered axial and bending stiffness by using an equivalent axial load of $L_{equiv.} = L + 4M/PD$. The moment and rocking capacities were determined from the expression $L + 4KM/PD$, where the value of $4 \cdot K/PD$ would express the moment or rocking capacity. If $L < 4 \cdot KM/PD$, then retention rocking occurs (load L is then not sufficient to support moment M on the retention diameter PD), whereas the moment capacity is reached when the sum of the quantities $L_{const.}$ and $4KM/PD$ develop the allowable Hertz stress. Therefore, for blade retentions of equal axial load potential, the value of $4K/PD$ determines either moment or rocking capacity.

In the multiple-race retention configurations, axial load capacity does not necessarily increase proportionally with number of races, as one might conclude. This occurs, in general, for geometry as shown in Figure 118 because one race of a multiple-race configuration is more highly loaded than an adjacent race. Therefore, the retention is inefficient, since the geometry parameters, ball size, pitch diameter, etc., are chosen for the highest race load instead of for the nominal load. A simplified analysis shows that a double-race retention can, by incorporating the correct uniform thickness of the barrel arms and blade shanks, have equal loads on each race due to axial load. For a triple race retention, the barrel arms and blade shank must be tapered or stepped to allow equal load distributions. At higher race numbers, designing the correct barrel arm and blade shank shapes for equal load distribution becomes more complicated and difficult. Also, the ball-race tolerancing, which directly affects the load sharing of the races, becomes more critical.

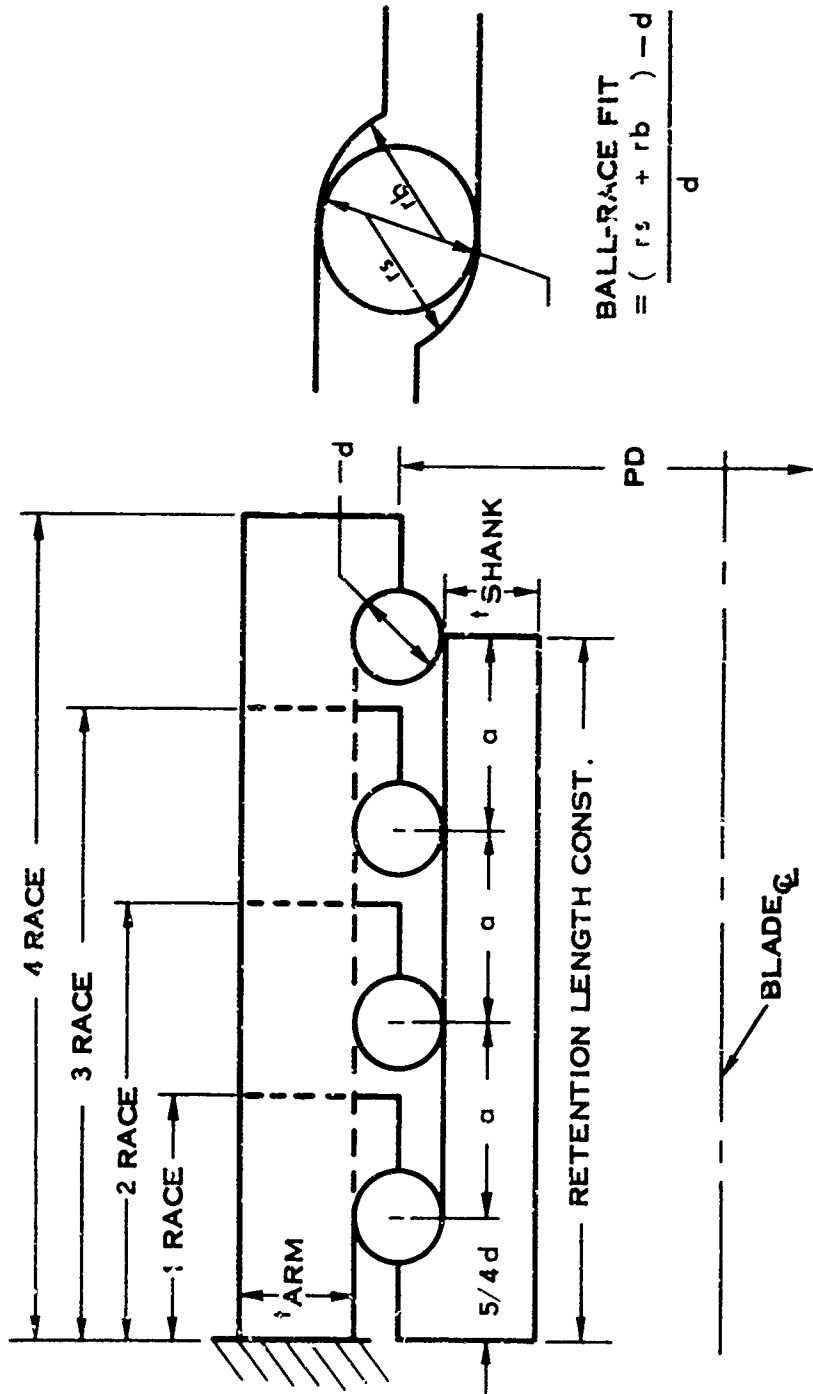


FIGURE 118. DESIGN PARAMETERS FOR THE SINGLE- AND MULTIPLE-BALL-RACE RETENTIONS

It was assumed in this analysis that equal-load sharing would exist, in all cases, on proper design of the barrel arms and blade shank thicknesses. For simplicity, constant barrel arm and blade shank thicknesses were also assumed for all retentions. These two assumptions are inconsistent, since equal load sharing requires tapered walls. This makes the three- and four-race retentions somewhat heavier; hence, this study tends to slightly discredit these retentions. It is believed that a detailed analysis in this area would show that a properly tapered three- or four-race retention is nearly the same weight as a one- or two-race retention, but practical tolerancing limits would give the advantage to one or two races.

Axial load capacities were determined by calculating and scaling nominal axial stress in the barrel arms and blade shanks, and by calculating relative maximum Hertzian contact stresses which were found to be proportional to axial load in the following way, for constant ball-race fit:

$$L \text{ axial load} = PD \cdot N \cdot d \cdot K(N)$$

where PD is the race pitch diameter, d is the ball diameter, N is the number of races, and $K(N)$ is the load-sharing factor for the N races, which, as mentioned above, is assumed to be $K(N) = 1.0$. Thus, for the same ball-race fit, axial load capacities for a given weight are determined. The weight of each retention was calculated assuming the axial length that was consistent with a four-race retention. This means that a single-race retention includes in its weight a portion of the blade spar. These calculated parameters are used to define the retention efficiencies of retention stiffness/weight and moment or rocking capacity/weight for various numbers of races and axial race spacings. Two other relationships involving the effect of ball-race fit and PD/d on retention stiffness were calculated using the above analyses. The effect of the parameter PD/d , the axial load capacity/weight, and the relationship between PD /axial capacity and number of races for various ball sizes were also calculated for the four retentions studied. Using the optimum values of PD/d and the PD /axial capacity, race number, and ball size relationships, optimum values of PD and d were determined in terms of axial load/race number.

RESULTS AND DISCUSSION

Values of retention parameters used in this study are summarized in Table XXIV. The values were used to plot moment, axial load, and stiffness efficiencies versus number of races in Figures 119, 120, and 121, respectively. Also plotted are the stiffness efficiency versus ball race fit in Figure 122 and the axial load efficiency versus PD/d in Figure 123. As shown in Figures 119 through 121, values of a d of one to four were chosen. However, a value of a d equal to 1 is not possible, and a value of about 1-1/2 is a practical lower limit.

TABLE XXIV
 USAVLABS RETENTION PARAMETRIC ANALYSIS
 (DATA ARE NORMALIZED TO A FOUR-RACE RETENTION)

NO. OF RACES	PITCH DIAMETER (PD)	$(N-1)A/R$ $R = PD/2$ $A = \text{ROW SPACING}$	BALL DIAMETER	TOTAL RETENTION WEIGHT	AXIAL LOAD CAPACITY	ROCKING AND MOMENT CAPACITY	OVERALL RETENTION STIFFNESS
4	1.0	0.812	1.0	1.0	1.0	1.0	1.0
3	1.26	0.514	1.0	.886	1.0	1.16	1.39
2	1.445	0.297	1.31	.825	1.0	1.36	1.51
2	1.445	0.175	1.31	.749	1.0	1.28	1.52
1	1.825	0	2.08	.851	1.0	1.59	1.66

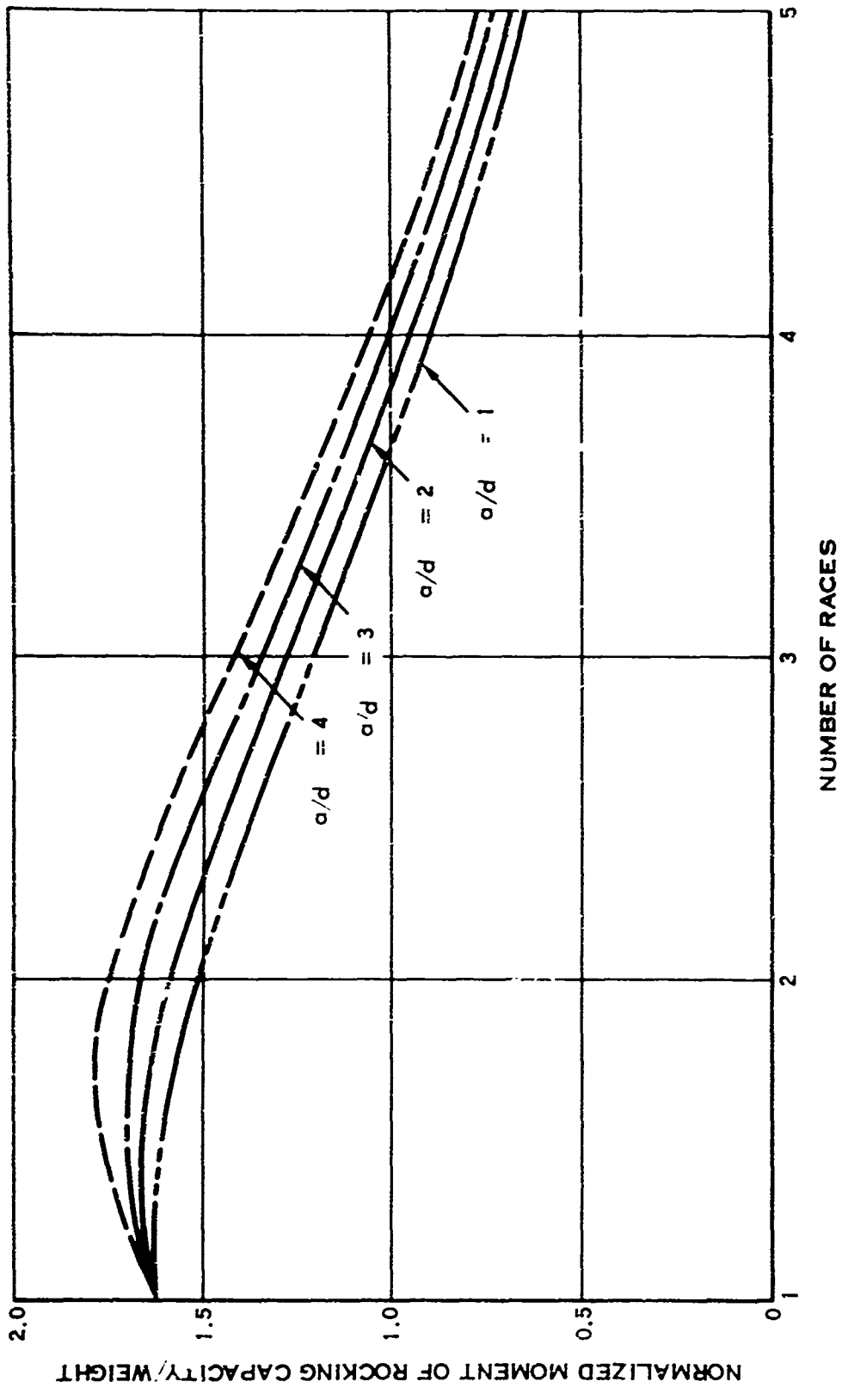


FIGURE 119. EFFECT OF NUMBER OF RACES ON MOMENT CAPACITY/WEIGHT

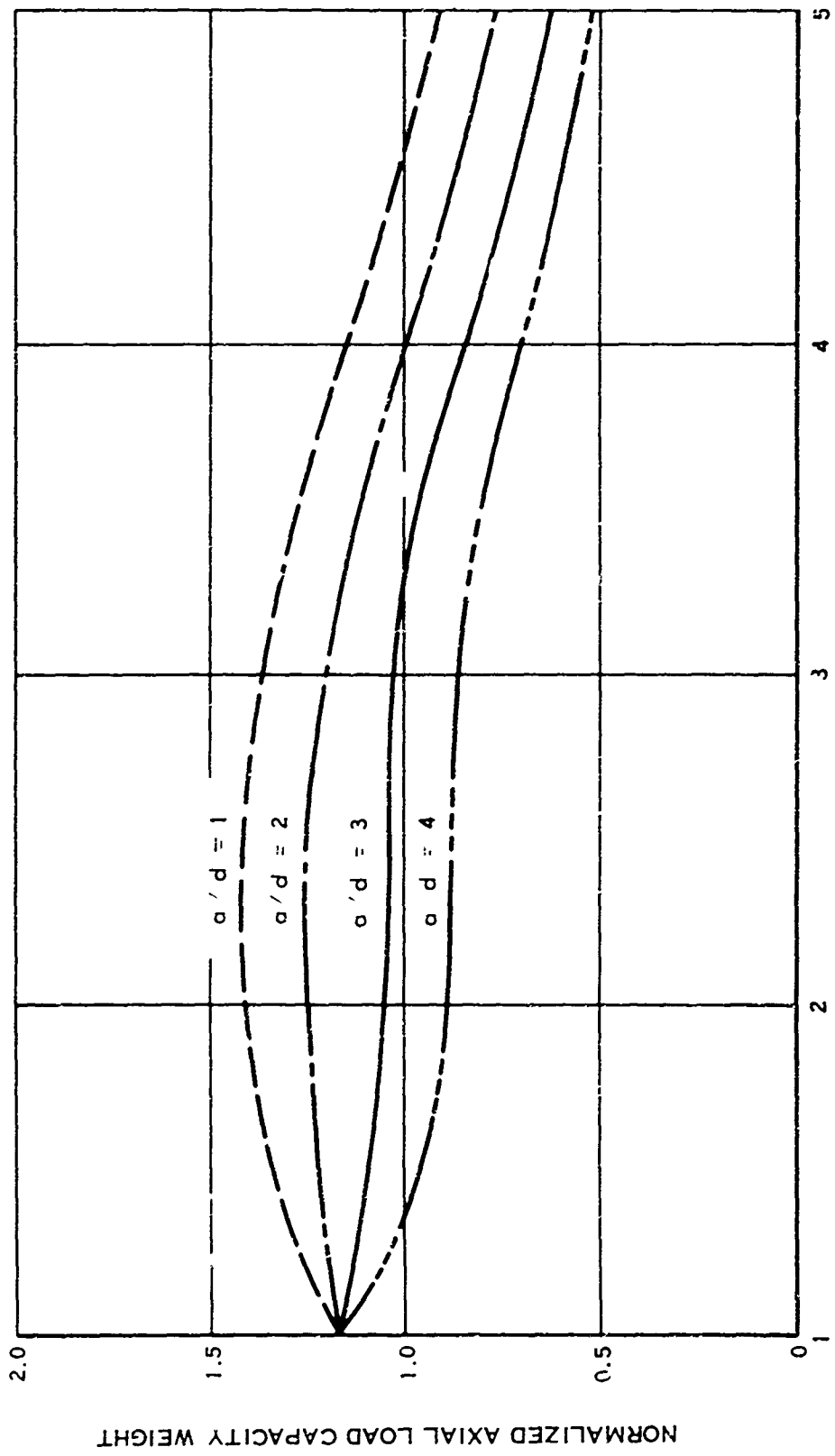


FIGURE 120. EFFECT OF NUMBER OF RACES ON AXIAL LOAD CAPACITY/WEIGHT

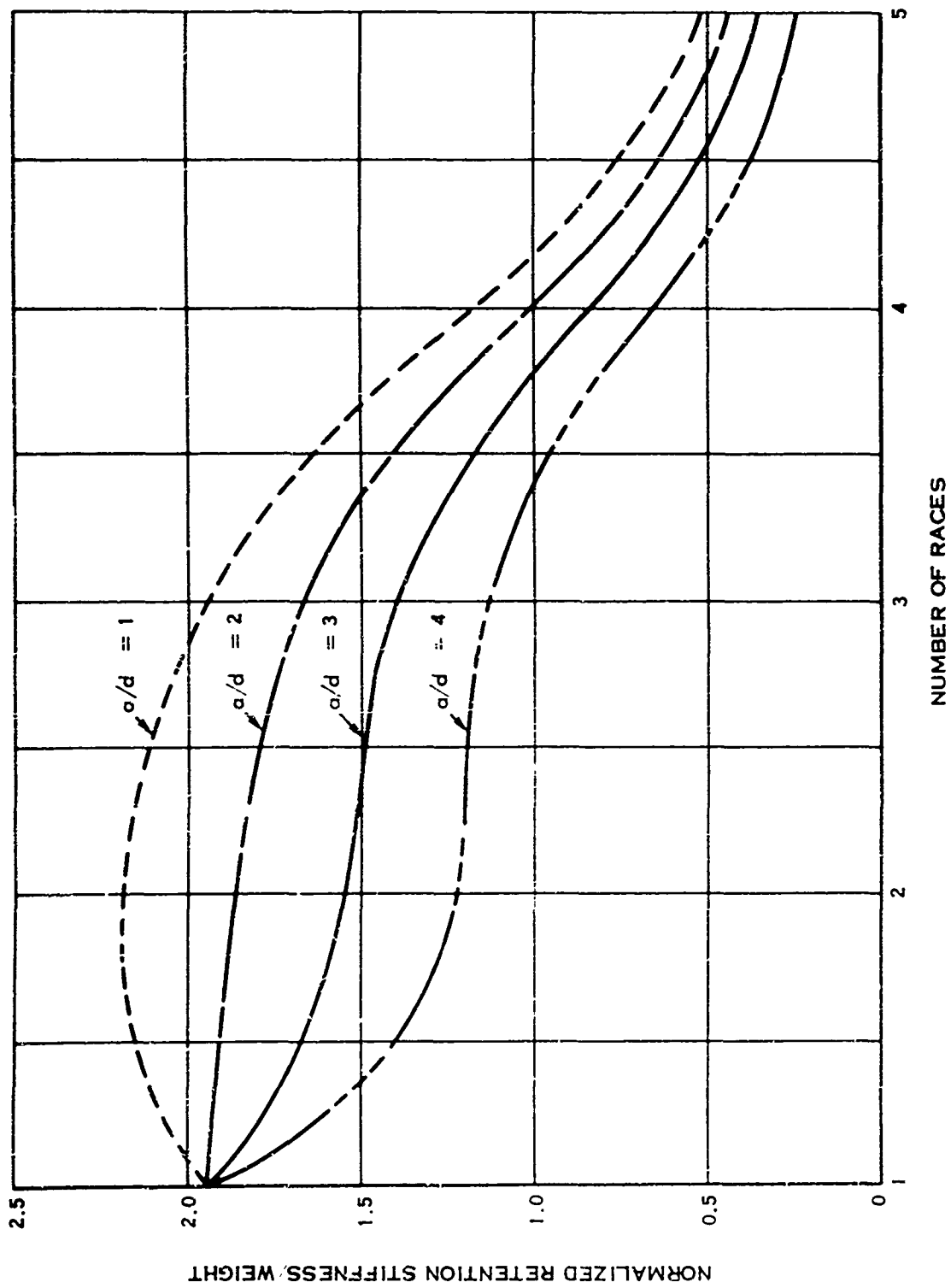
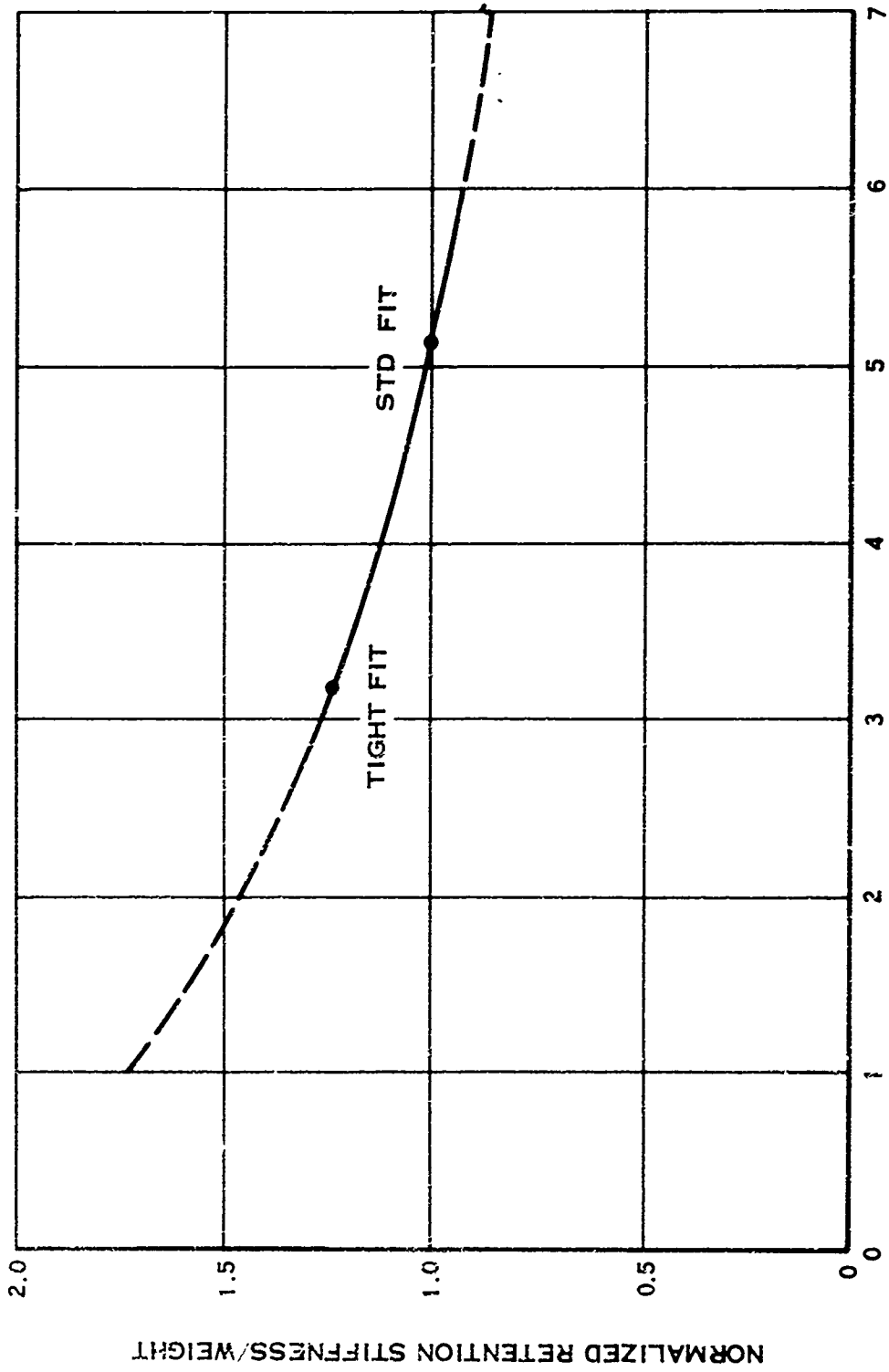


FIGURE 121. EFFECT OF NUMBER OF RACES ON RETENTION STIFFNESS/WEIGHT



BALL - RACE FIT = RSHANK + RBARREL - DBALL X100/DBALL

FIGURE 122. EFFECT OF BALL-RACE FIT ON RETENTION STIFFNESS/WEIGHT

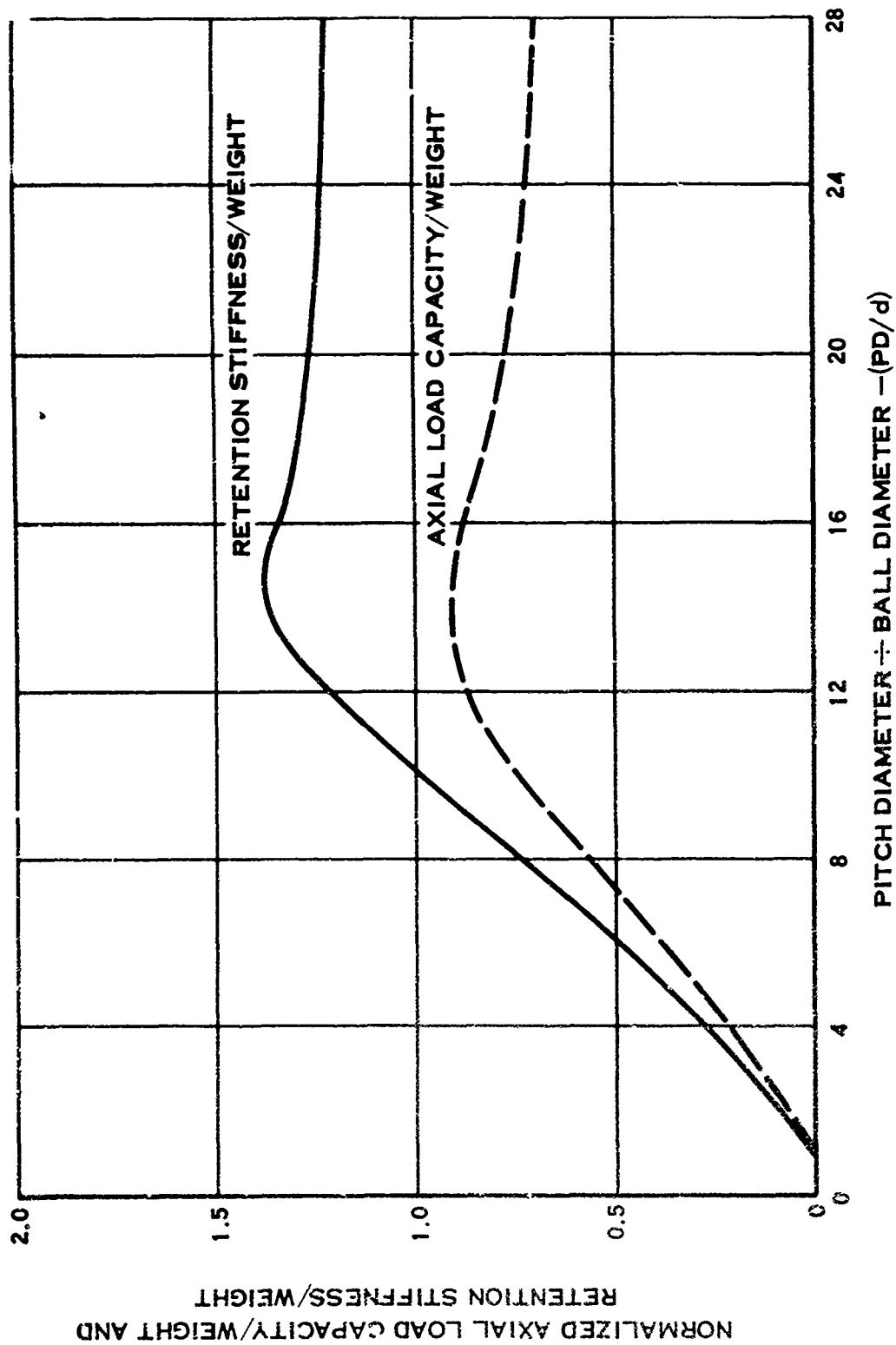


FIGURE 123. EFFECT OF RETENTION DIAMETER--TO--BALL DIAMETER RATIO

The values of moment or rocking capacity/weight as affected by race number and spacing, as shown in Figure 119, indicate that a dual-race retention is superior to the single-race retention for a /d ratios of 2-1/2 or smaller. At greater a/d ratios, the single-race retention is superior to the dual-race retention. Similarly, in Figure 120, the axial load capacity/weight effects are shown for the same design parameters. Here, for a/d of 2 or less, the dual race is again superior; whereas, for a/d greater than 2-1/2, the single race is superior. Therefore, for maximum moment or rocking/weight and maximum axial load for maximum capacity/weight, a dual race with small a/d ratios should be selected.

The effect of retention stiffness/weight for the same design parameters, as shown in Figure 121, indicates that the single race is superior to 2, 3, and 4 races for a/d ratios of 2 or greater, but two races are best for a minimum a/d of about 1-1/2. The stiffness per weight can be improved for a given retention by tightening the ball-race fit as indicated in Figure 122. Also, by tightening the ball-race fit, contact Hertz stresses are reduced on an equal load basis, allowing greater load capacity. However, since thickness of the barrel arm and blade shank must be increased to maintain their same nominal stresses, it is not obvious that a ball-race fit that is tighter than a standard fit has a weight benefit relative to axial load capacity. At best, this weight benefit, if any, would be small.

After determining the optimum number of races N and spacing a/d, which, in general, is a closely spaced dual or single race, it is necessary to determine the optimum PD/d ratio based on axial capacity/weight and retention stiffness/weight. Shown in Figure 123 are efficiency relationships calculated for one- and two-race retentions. Here, the optimum value of PD/d lies between 14 and 20. Using the above values and the relationships of Pd/axial capacity versus race number of different ball sizes presented in Figure 124, the final parameters of PD and (d) can be calculated. The following ball sizes and pitch diameters were determined as a function of N/L ratios for PD/d ratios of 14 and 20:

$$\begin{array}{rcl}
 \text{PD/d} = 14 & d = 2.36 \times 10^{-3} \sqrt{L/N} \\
 & \text{PD} = 33.0 \times 10^{-3} \sqrt{L/N} \\
 \\
 \text{PD/d} = 20 & d = 1.98 \times 10^{-3} \sqrt{L/N} \\
 & \text{PD} = 27.7 \times 10^{-3} \sqrt{L/N}
 \end{array}$$

Since a number of different combinations of N, PD, and d can be chosen and still satisfy the optimum PD/d ratio, it is necessary to mention that the smallest ball size should be chosen which still meets the axial load requirements. This is to ensure the most uniform possible load distributions within the raceways. If larger, and consequently fewer, balls are used, the possibility of local stress concentrations within the retention or throughout the barrel could be increased.

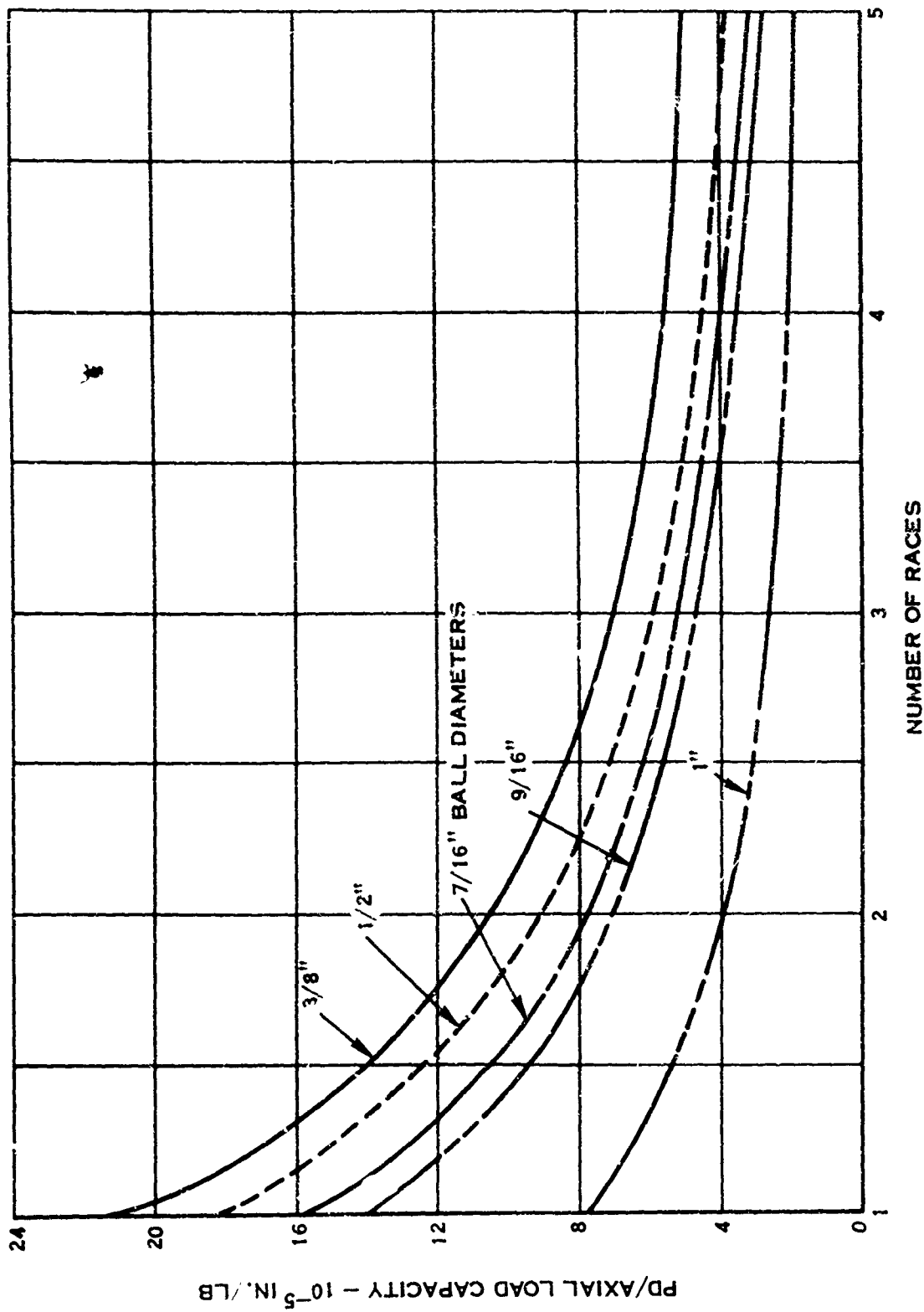


FIGURE 124. EFFECT OF NUMBER OF RACES ON AXIAL LOAD CAPACITY

Figures 119 and 121 all show that a/d should be as small as possible for minimum weight. Therefore, for $a/d = 1.5$, which is near the practical minimum limit, comparative weights are summarized in Table XXV for one-, two-, and three-race retentions derived for constant values of moment or rocking capacity, axial load capacity, and retention stiffness.

TABLE XXV. RELATIVE WEIGHTS, $a/d = 1.5$
(DATA ARE NORMALIZED TO A TWO-RACE RETENTION)

RACES	ROCKING OR MOMENT CAPACITY	AXIAL LOAD CAPACITY	RETENTION STIFFNESS
1	1.05	1.14	1.05
2	1.00	1.00	1.00
3	1.24	1.04	1.13

The two-race retention is lightest, but the weight penalty for a single race is only 5% on rocking capacity and retention stiffness and 14% on axial load capacity; whereas the weight penalty for the triple race is only 4% based on axial load capacity, but 24% based on rocking capacity. All things considered, the one- and two-race retentions appear to be the best choices.

CONCLUSIONS

By investigation of specified geometry parameters of the single- and multiple-race blade shank retentions, a theoretical minimum weight retention can be obtained for adequate moment capacity, axial load capacity, and retention stiffness.

It was found that the race spacing should be as small as possible for any number of races; a value of $a/d = 1.5$ is suggested as being near the practical minimum. With this race spacing, the two-race retention is lightest, the one-race retention next, followed by the three-race retention. However, the weight penalty could be as low as 4% or as high as 24%, depending upon the particular loading and stiffness requirements.

At any race number, a tight ball-race fit improves the retention stiffness/weight and increases Hertz stress capacity for a given load. The optimum value of PD/d is 14, but PD/d values as high as 20 increase the weight by only 13 percent.

Finally, by choosing the optimum race number (PD/d ratio between 14 and 20) and by knowing the axial load, several optimum retention configurations can be selected by using the relationships involving the effect of ball size on race number and PI/d axial load capacity. However, by choosing the smallest ball size that will permit safe loading, an optimum retention configuration can be selected.

APPENDIX VIII
STABILITY ANALYSIS OF THE CYCLIC PITCH PROPELLER
INCLUDING IXP ISOLATION METHODS

INTRODUCTION

This study was initiated to analyze the stability considerations of conceptual designs for the propeller. This study includes cyclic pitch for the elimination or reduction of 1P blade stress and/or for the generation of aircraft control moments. The specific purpose of this study is to investigate the feasibility of these concepts in terms of static divergence and dynamic stability. (List of symbols used in Appendix VIII is shown on Table XXVI.)

ANALYSIS

The first part of this analysis developed the aerodynamic forces produced by a four-bladed propeller whose hub is executing a whirling motion about the static center of the system. The system is described as a two-degree-of-freedom system in pitch and yaw, shown in Figure 125. The vector diagram, Figure 126, shows hub motion $\dot{\omega}$ s and $\dot{\xi}$ as well as the component of inflow velocity perpendicular to the disc. The angle β describes the inclination of the airstream to the propeller. The above quantities produce velocity components parallel to the resultant airfoil velocity of magnitude

$$V_p = \dot{\omega} \frac{V_o}{U} + \dot{\xi} \frac{\Omega r}{U} - V_o \sin \beta \left(\frac{\Omega r}{U} \right) \cos \Omega t \quad (17)$$

where $U^2 = V_o^2 + (\Omega r)^2$ and V_o is the airstream velocity; see Figure 126.

The components perpendicular to the velocity U produce effective blade angle changes of

$$\alpha_1 = -\dot{\omega} \frac{\Omega r}{U^2}; \quad \alpha_2 = \dot{\xi} \frac{V_o}{U^2}; \quad \alpha_3 = \frac{V_o^2}{U^2} \sin \beta \cos \Omega t \quad (18)$$

In addition to these induced angle changes, the pitch and yaw motions result in blade angle changes of

$$\alpha_4 = \psi \sin \Omega t - \theta \cos \Omega t$$

TABLE XXVI- SYMBOLS USED IN APPENDIX VIII

SYMBOL	DEFINITION
e_{θ} , e_{ψ}	PIVOT DISTANCE IN PITCH AND YAW
I_p	POLAR MOMENT OF INERTIA OF PROPELLER
I_y , I_z	MOMENTS OF INERTIA ABOUT Y AND Z AXES
l	UNIT AERODYNAMIC LOADING
L_y , L_z	RESULTANT PROPELLER AERODYNAMIC LOADS
m_y , m_z	UNIT AERODYNAMIC LOADS
M_y , M_z	RESULTANT PROPELLER AERODYNAMIC LOADS
r	RADIUS
R	PROPELLER TIP RADIUS
S_{θ} , S_{ψ}	SUSPENSION STIFFNESS
U	STEADY-STATE BLADE SECTION VELOCITY
V_0	AIRSTREAM VELOCITY
V_p	BLADE SECTION VELOCITY DUE TO PERTURBATIONS
ω , s	PROPELLER HUB MOTIONS
X, Y, Z	COORDINATE SYSTEM
α_1 , α_4	BLADE ANGLE CHANGES DUE TO PERTURBATIONS
Ω	PROPELLER SPEED
ω	WHIRL FREQUENCY
θ , ψ	PITCH AND YAW DEGREES OF FREEDOM
β	INFLOW ANGLE
$\beta_{\theta} , F_{\psi}$	DAMPING FACTOR IN PITCH AND YAW
λ	EIGENVALUE OF MATRIX

Further, if we allow for cyclic pitch based upon angular motion of the propeller (similar to the swashplate technique used on helicopters) and for the addition of cyclic pitch through the actuator mechanism, the resultant blade angle seen by the blade is given as

$$\alpha = \alpha_0 + \psi \sin \Omega t - \phi \cos \Omega t - \dot{\alpha} \frac{\Omega r}{U} + \dot{s} \frac{V_0}{U} - \frac{V_0^2}{U^2} \sin \beta \cos \Omega t + k_1 \dot{\theta} \sin \Omega t + k_2 \dot{\psi} \cos \Omega t + \theta_f \cos \Omega t + \psi_f \sin \Omega t \quad (19)$$

where k_1 and k_2 are mechanical ratios between propeller pitch or yaw and the resulting blade angle changes. The quantities θ_f and ψ_f are the forced blade angle changes caused by the actuator.

From Figure 125, it can be seen that

$$\alpha = -\dot{\psi} r \cos \Omega t - \dot{\theta} r \sin \Omega t \quad (20)$$

so that

$$\dot{\alpha} = -\dot{\psi} r \cos \Omega t - \dot{\theta} r \sin \Omega t + \Omega \dot{\psi} r \sin \Omega t - \Omega \dot{\theta} r \cos \Omega t \quad (21)$$

and

$$\dot{s} = -\dot{\psi} e_{\psi} \sin \Omega t + \dot{\theta} e_{\theta} \cos \Omega t \quad (22)$$

Using Equation (17) and the expression for U , we can see that the resultant velocity into the blade section is

$$V = \sqrt{V_0^2 + (\Omega r)^2} + \dot{\alpha} \frac{V_0}{U} + \dot{s} \frac{\Omega r}{U} - \frac{V_0 \Omega r}{U} \sin \beta \cos \Omega t \quad (23)$$

Now, the lift on an airfoil is given by the relation

$$l = \frac{1}{2} \rho c V^2 C_{l_{\alpha}} \alpha \quad (24)$$

where ρ is the air density, c is the blade chord, $C_{l\alpha}$ is the section lift curve slope, and β is the angle of attack of the blade. Substituting Equations (13) and (25) into (24), we obtain

$$\begin{aligned} (l_0 + l) = \frac{1}{2} \rho c C_{l\alpha} & \left[U + \dot{\psi} \frac{V_0}{U} + \dot{\beta} \frac{\Omega r}{U} - \frac{V_0 \Omega r}{U} \sin \beta \cos \Omega t \right]^2 \\ & \left[\alpha_0 + \psi \sin \Omega t \right. \\ & - \theta \cos \Omega t - \dot{\psi} \frac{\Omega r}{V^2} + \dot{\beta} \frac{V_0}{U^2} - \frac{V_0^2}{U^2} \sin \beta \cos \Omega t + k_1 \theta \sin \Omega t \\ & \left. + k_2 \dot{\psi} \cos \Omega t + \theta_f \cos \Omega t + \psi_f \sin \Omega t \right] \end{aligned}$$

Expanding this equation, dropping the steady-state angle of attack, α_0 , and linearizing results in

$$\begin{aligned} l = \frac{1}{2} \rho c C_{l\alpha} & \left[\left(-V_0^2 \dot{\theta} + V_0 \dot{\theta} e_{\theta} + \Omega r^2 \dot{\psi} - V_0^2 \dot{\beta} + U^2 k_2 \dot{\psi} + U^2 \psi_f \right) \cos \Omega t \right. \\ & \left. + \left(V_0^2 \dot{\psi} - V_0 \dot{\psi} e_{\psi} + \Omega r^2 \dot{\theta} + U^2 k_1 \theta + U^2 \theta_f \right) \sin \Omega t \right] \quad (25) \\ & = l_1 \cos \Omega t - l_2 \sin \Omega t \end{aligned}$$

The individual perturbation blade loads at radius r can now be added to obtain the hub resultants as

$$l_Z = \frac{V_0}{U} \left[-l_1 \cos \Omega t + l_3 \cos \Omega t + l_2 \sin \Omega t - l_4 \sin \Omega t \right]$$

where subscripts to the blade designations are as given in Figure 126. This reduces to

$$l_Z = \frac{1}{2} \rho V_0^2 S \left(\frac{4cV_0}{UR^2} \theta - \frac{4c}{UR^2} \dot{\psi} e_{\psi} - \frac{4cr^2 \Omega}{UV_0 R^2} \dot{\beta} + \frac{4cV_0 \beta}{UR^2} - \frac{4cU}{V_0 R^2} \left[k_2 \dot{\psi} + \theta_f \right] \right) \quad (26)$$

where S' is the disc area and R is the blade tip radius. Similarly,

$$l_Y = \frac{1}{2} \rho V_0^2 S' \left(\frac{icV_0}{UR^2} \dot{\psi} - \frac{ic\dot{\psi}e\psi}{U^2R^2} - \frac{icr^2\Omega}{UV_0R^2} \dot{\psi} + \frac{icU}{V_0R^2} \left[k_1\dot{\psi} + \psi_f \right] \right) \quad (27)$$

The out-of-plane forces producing moment about the four-way hub centerline are of the form

$$m_Y = \frac{\rho r^2}{U} \left[-l_1 \sin \Omega t + l_3 \sin \Omega t - l_2 \cos \Omega t + l_4 \cos \Omega t \right]$$

which reduces to

$$m_Y = -\frac{1}{2} \rho V_0^2 S'R \left(\frac{4\Omega r^2 c}{UR^3} \dot{\psi} - \frac{4\Omega r^2 c}{UV_0R^3} \dot{\psi} e\psi + \frac{4\Omega^2 r^4 c}{UV_0^2 R^3} \dot{\theta} + \frac{4\Omega r^2 c U}{V_0^2 R^3} \left[k_1\dot{\psi} + \psi_f \right] \right) \quad (28)$$

Similarly,

$$m_Z = \frac{1}{2} \rho V_0^2 S'R \left(\frac{4\Omega r^2 c}{UR^3} \dot{\theta} - \frac{4\Omega r^2 c}{UV_0R^3} \dot{\theta} e\psi - \frac{4\Omega r^4}{UV_0^2 R^3} \dot{\psi} - \frac{4\Omega r^2 c}{UR^3} \dot{\psi} - \frac{4\Omega r^2 c U}{V_0^2 R^3} \left[k_2\dot{\psi} + \theta_f \right] \right) \quad (29)$$

It should be noted that the air loads, when summed over all blades, are not dependent upon the propeller rotational azimuth angle Ωt . Equations (26) through (29) must now be integrated over the blade radius, giving the final loads as

$$L_Z = P_1\dot{\theta} - P_2 e\dot{\theta} - P_3\dot{\psi} + P_1\dot{\psi} - P_4 (k_2\dot{\psi} + \theta_f) \quad (30)$$

$$L_Y = P_1\dot{\psi} - P_2 e\dot{\psi} + P_3\dot{\theta} + P_4 (k_1\dot{\theta} + \psi_f)$$

and the final moments become

$$M_Y = -P_5 \dot{\psi} + P_6 e_{\psi} \dot{\psi} - P_7 \dot{\theta} - P_8 (k_1 \theta + \psi_f) \quad (31)$$

$$M_Z = P_5 \theta - P_6 e_{\theta} \dot{\theta} - P_7 \dot{\psi} - P_8 (k_2 \psi + \theta_f) + P_9 \beta$$

where the coefficients are given in the List of Coefficients (page 312).

Writing the equations of motion of the system gives

$$I_z \ddot{\psi} + B_{\psi} e_{\psi}^2 \dot{\psi} + S_{\psi} \dot{\psi} + I_p \Omega \dot{\theta} = L_y e_{\psi} + M_z \quad (32)$$

$$I_y \ddot{\theta} + B_{\theta} e_{\theta}^2 \dot{\theta} + S_{\theta} \dot{\theta} - I_p \Omega \dot{\psi} = L_z e_{\theta} + M_y$$

Substituting Equations (29) and (31) into (32) and eliminating time-dependent terms provides two equations for determining the steady propeller attitude; i. e.,

$$(S_{\psi} - P_1 e_{\psi} + P_8 k_2) \psi - (P_4 k_1 e_{\psi} + P_9) \theta = P_4 e_{\psi} \psi_f - P_8 \theta_f + P_5 \beta \quad (33)$$

$$(P_4 e_{\theta} k_2 + P_5) \psi + (S_{\theta} - P_1 e_{\theta} + P_8 k_1) \theta = P_1 e_{\theta} \psi_f - P_4 e_{\theta} \theta_f - P_8 \psi_f$$

These equations can be solved for θ and ψ .

Returning now to Equations (32), we write these in the following form:

$$a_1 \ddot{\psi} + b_1 \dot{\psi} + c_1 \psi + e_1 \dot{\theta} + f_1 \theta = 0 \quad (34)$$

$$b_2 \dot{\psi} + c_2 \psi + d_2 \dot{\theta} + e_2 \theta + f_2 \theta = 0$$

where the coefficients are given in the List of Coefficients. In the matrix form,

$$\begin{bmatrix} a_1 & 0 \\ 0 & b_1 \end{bmatrix} \begin{bmatrix} \ddot{q} \\ \dot{q} \end{bmatrix} + \begin{bmatrix} b_1 & e_1 \\ b_2 & e_2 \end{bmatrix} \begin{bmatrix} \dot{q} \\ q \end{bmatrix} + \begin{bmatrix} c_1 & f_1 \\ c_2 & f_2 \end{bmatrix} \begin{bmatrix} q \\ \theta \end{bmatrix} = 0 \quad (35)$$

where $q = [\psi, \theta]^T$. Simplifying the above expression, we have

$$[A] \begin{bmatrix} \dot{v} \\ v \end{bmatrix} + [E] \begin{bmatrix} v \\ q \end{bmatrix} = 0 \quad (36)$$

where $\{v\} = \{\dot{q}\}$ (27)

and the two-by-two matrices are given in the List of Coefficients.

$$\ddot{\begin{bmatrix} q \\ v \end{bmatrix}} = \begin{bmatrix} 0 & I \\ -[A]^{-1}[C] & [-A]^{-1}[B] \end{bmatrix} \begin{bmatrix} q \\ v \end{bmatrix} = \begin{bmatrix} \bar{U} \\ \bar{V} \end{bmatrix} \begin{bmatrix} q \\ v \end{bmatrix} \quad (38)$$

Since $\begin{bmatrix} \dot{q} \\ v \end{bmatrix} = \lambda_s \begin{bmatrix} q \\ v \end{bmatrix}$, Equation (38) produces the typical eigenvector problem

$$[\lambda_s [I] - [\bar{U}]] k_s = 0 \quad (39)$$

Equation (39) can now be solved for the complex eigenvalues, which show whether the system possesses either static or dynamic instabilities.

DISCUSSION

During this study, a number of cyclic pitch systems were investigated which were designed to eliminate or reduce the 1P blade stressing. These concepts may be divided into two categories, i. e., self-regulating and controlled systems. The self-regulating systems involve removing some of the restraints on the system and coupling pitch and/or yaw motion to blade pitch change. These systems will be discussed in detail in the following paragraphs. The controlled systems involve conventional mounting of the propeller system, sensing the inflow in some manner, and either changing the propeller angular orientation or introducing forced blade pitch change at a frequency of 1P. These latter systems do not affect the dynamic stability, but they do have an influence on the static divergence. However, static divergence is easily eliminated for a conventionally mounted system, so that we shall assume that the controlled systems are satisfactory. These systems can eliminate essentially all 1P stressing if they are properly calibrated.

We shall now consider the self-regulating system. The first system that we considered was one in which the propeller is gimballed in the pitch sense only, and in which a pitch displacement produces cyclic blade angle change in the vertical blades. If the pivot point of this system is behind the propeller, the resultant system is stable; however, for a gimbal at the propeller plane, the system is unstable. In both of these cases, the 1P stressing is not eliminated or reduced in magnitude, but merely rotated 90 degrees in time.

The next logical step is to gimbal the system in both pitch and yaw, retaining the cyclic blade angle changes as linear functions of the pitch and yaw angles. This

configuration was analyzed only for the case where the gimbaling was located at the propeller disc center. The analysis was applied to the fully gimbaled propeller design, using estimated system parameters. Figure 127 shows the results of the analysis and predicts that, for the cyclic pitch ratio of 2:1 shown in the cyclic pitch design, the system is unstable at about 259 knots. This plot also shows that as the cyclic pitch ratio is increased, the instability speed increases, and a ratio of about 6.5:1 proves satisfactory for a maximum speed of 350 knots; i. e., $1.2V_D = 420$ knots.

A study was also made to determine the effect of damping on the divergent speed. cursory analyses of the Coulomb cases were run for damping coefficients up to 1,000 in.-lb-sec/rad. The maximum change in the divergent speed was about 2% for damping parameters in this range, implying that damping is insufficient to have any appreciable effect.

The fully gimbaled propeller does not completely eliminate 1P blade aerodynamic loads, but it does decrease their magnitude. For each condition, the steady-state equilibrium angles were calculated, and these were then substituted into equation (25) to determine the 1P blade loads. It was found that the new 1P blade loads varied linearly from 50% of the normal values at 50 knots to 20 percent at 320 knots, from which speed they remain nearly constant at 20 percent.

The case of helicopter antitorque rotors was considered as possibly disproving the above-discussed divergence of a gimbaled propeller. A typical rotor was evaluated and was shown to have a divergent speed of 170 knots. This is far above the inflow velocity that this rotor ever experienced, and the high velocities in the plane of the propeller are not significant in terms of whirl-flutter divergence. Therefore, there appears to be no inconsistency between the foregoing analytical results and test experience.

Figure 128 shows the variation of divergent speed with polar moment of inertia of the propeller. As 1P is reduced, the blades can be made lighter, which will decrease the polar moment of inertia and consequently increase the divergent speed. Thus, a decrease of 40% in polar moment of inertia will increase the divergent speed by about 17%.

CONCLUSIONS

This study has shown that a self-regulating 1P reducing system for a propeller would be achieved by a fully gimbaled propeller; however, it presents stability problems. If the blade cyclic pitch ratio is high enough, i. e., at least 6.5:1, stability could be achieved for maximum aircraft velocities up to 350 knots for the propeller considered in this study. The amount of 1P reduction with this system varies from 50% at 50 knots to 80% at 320 kn. Reduction of the propeller polar moment of inertia increases the whirl-flutter critical speed by a modest percentage. The available damping in the gimbal joint appears to have an insignificant effect on the stability of the system.

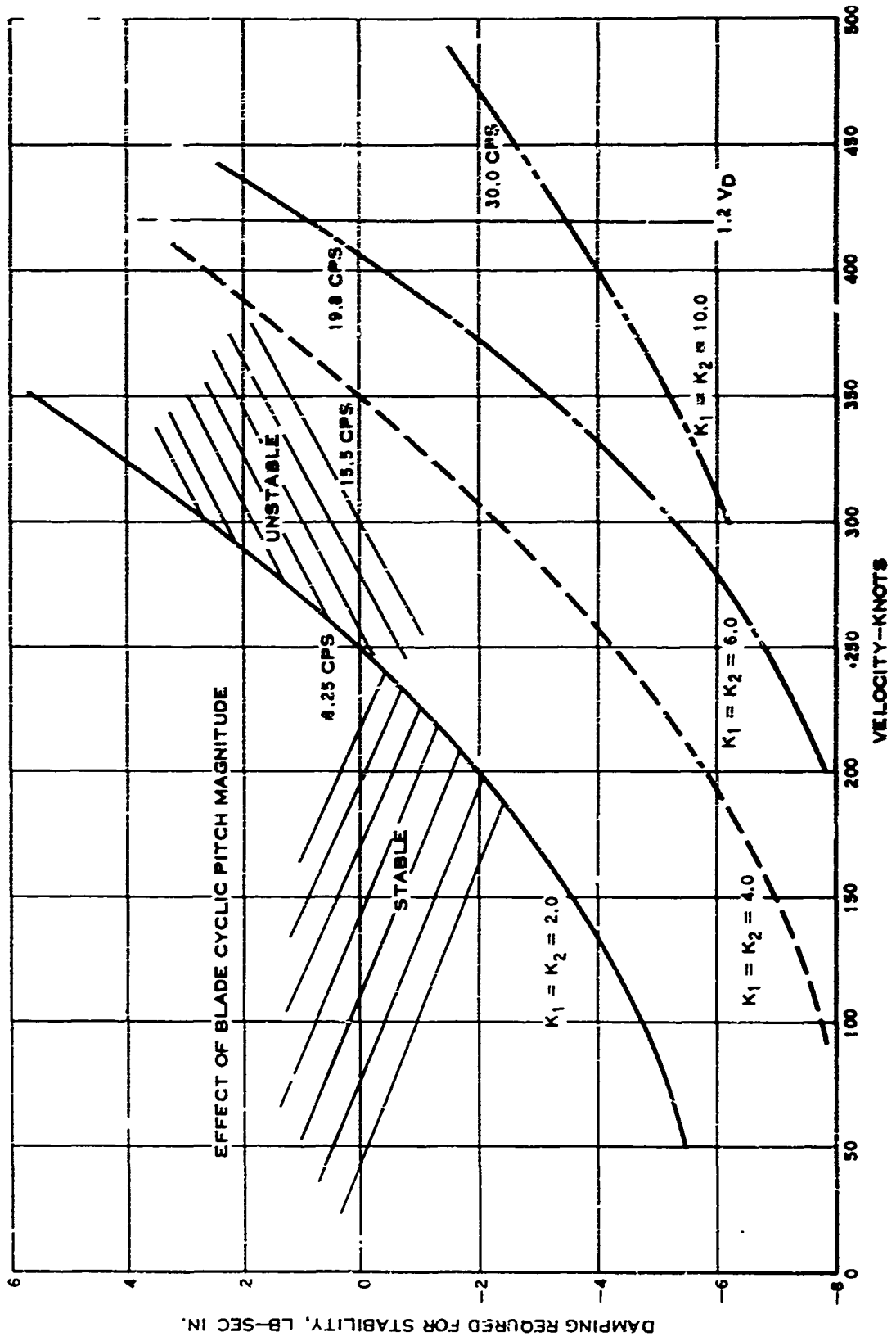


FIGURE 127. FLUTTER PLOT FOR FULLY GIMBALED PROPELLER

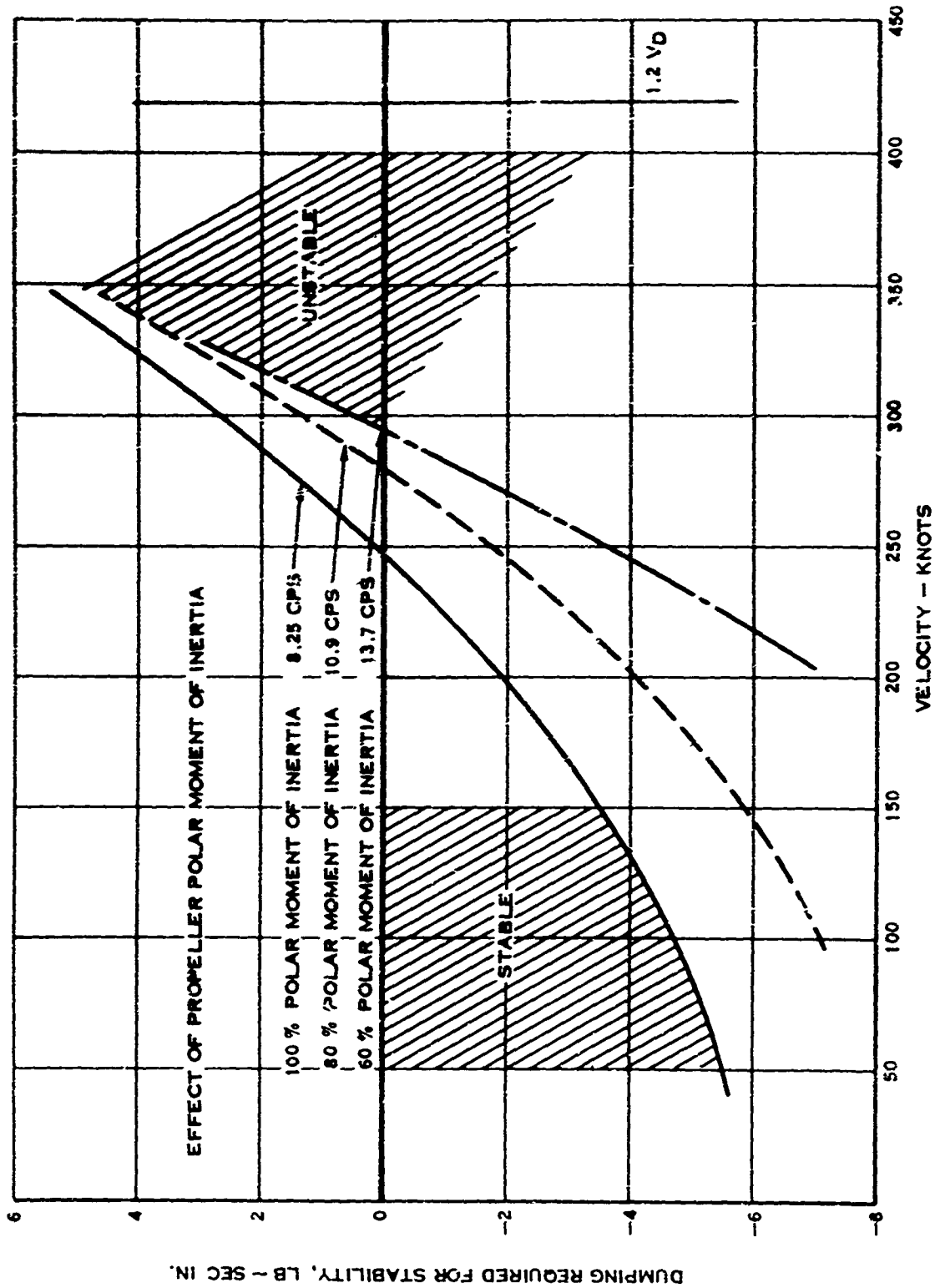


FIGURE 128. FLUTTER PLOT FOR FULLY GIMBALED PROPELLER

A controlled propeller system that senses the 1P shaft moment and forcibly cycles the blade pitch at a 1P frequency to eliminate the shaft moment will minimize the 1P blade stressing and will be a stable system.

List of Coefficients

The coefficients for equations (25) and (26) are given below:

$$P_1 = \frac{1}{2} \rho V_0^2 S' \left(\frac{4V_0 I_1}{\Omega R^2} \right)$$

$$I_1 = \int_{\eta=0}^1 \frac{K c a \eta}{\sqrt{\eta^2 + \left(\frac{J}{\pi}\right)^2}}$$

$$P_2 = P_1 \cdot V_0$$

$$P_3 = \frac{1}{2} \rho V_0^2 S' \left(\frac{4 I_2}{V_0} \right)$$

$$I_2 = \int_{\eta=0}^1 \frac{K c \eta^2 d\eta}{\sqrt{\eta^2 + \left(\frac{J}{\pi}\right)^2}}$$

$$P_4 = \frac{1}{2} \rho V_0^2 S' \left(\frac{4 \Omega I_3}{V_0} \right)$$

$$I_3 = \int_{\eta=0}^1 K c \sqrt{\eta^2 + \left(\frac{J}{\pi}\right)^2} d\eta$$

$$P_6 = P_5 / V_0$$

$$P_7 = \frac{1}{2} \rho V_0^2 S' R \left(\frac{4 \Omega R}{V_0^2} I_4 \right)$$

$$I_4 = \int_{\eta=0}^1 \frac{K c \eta^3 d\eta}{\sqrt{\eta^2 + \left(\frac{J}{\pi}\right)^2}}$$

$$P_8 = \frac{1}{2} \rho V_0^2 S' R \left(\frac{4 \Omega^2 R}{V_0^2} I_5 \right)$$

$$I_5 = \int_{\eta=0}^1 K c \eta^2 \sqrt{\eta^2 + \left(\frac{J}{\pi}\right)^2} d\eta$$

$$\eta = r/R$$

$$\frac{J}{\pi} = \frac{V_0}{\Omega R}$$

$$K = \frac{A}{2 + A \sqrt{1 - M^2} \left[1 + \left(\frac{\pi}{J}\right)^2 \eta^2 \right]}$$

where A is the blade aspect ratio, and M is the Mach number.

List of Coefficients (Continued)

$$a_1 = I_d + e \frac{2}{\Omega} m_p$$

$$b_1 = P_2 e \frac{2}{\Omega} + P_7 + \beta_{\psi} e \frac{2}{\Omega}$$

$$c_1 = S_{\psi} - P_1 e \frac{2}{\Omega} + P_8 k_2$$

$$e_1 = I_p \Omega - P_3 e \frac{2}{\Omega} + e_{\theta} P_6$$

$$f_1 = -P_4 e \psi k_1 - P_5$$

$$b_2 = -I_p \Omega - e \psi P_6 + e_{\theta} P_3$$

$$c_2 = P_4 e_{\theta} k_2 + P_5$$

$$d_2 = I_d + e \frac{2}{\theta} m_p$$

$$e_2 = P_2 e \frac{2}{\theta} + P_7 + \beta_{\theta} e \frac{2}{\theta}$$

$$f_2 = S_{\theta} - e_{\theta} P_1 + P_8 k_1$$

$$[A] = \begin{bmatrix} a_1 & 0 \\ 0 & b_1 \end{bmatrix}$$

$$[B] = \begin{bmatrix} b_1 & c_1 \\ b_2 & c_2 \end{bmatrix}$$

$$[C] = \begin{bmatrix} c_1 & f_1 \\ c_2 & f_2 \end{bmatrix}$$

APPENDIX IX
PARAMETRIC OPTIMIZATION STUDY
OF TWO-PIECE HOLLOW PROPELLER BLADES

INTRODUCTION

In support of the basic objective of the propeller study program to evaluate material and design concepts which will produce a significant reduction in propeller system weight, and since the blade weight and dynamic characteristics have the prime influence on the design and weight of the entire propeller, a parametric study of the blade is presented here. A thorough review of the potentialities of new materials and blade proportions to obtain the best general configuration for propeller blades was considered necessary. This appendix presents a theoretical analysis and results of this parametric study of blade properties and materials.

In general, the number of blades and external dimensions of the blades are defined by aerodynamic considerations. Thus, the structural design requires the selection of the shell and spar materials and configuration which satisfy the aerodynamic envelope and structural requirements and which give the minimum weight. This parametric blade study has produced some basic curves which should be useful in optimizing the design of propeller blades.

This appendix is divided into five sections. The first section covers the parametric analysis and discusses its possible limitations; the second discusses the results of the analysis from a geometric standpoint; the third discusses the results from a materials standpoint; the fourth shows the analysis and how it could be used to approximate a blade design for the study; and the fifth presents a cursory look at integrated dynamic effects on frequencies, using an energy approach.

This parametric analysis was limited to blade section optimizations for moment capacity and for stiffness. Because the dynamic characteristics of the blade involve the integrated effects of the section stiffness and weights, the true optimum design for the sections will be influenced by their interactions. In this study, this interaction was done in an iterative way with some guideline. (A list of symbols used in Appendix IX is shown in Table XXXV at the end of this appendix.)

PARAMETRIC ANALYSIS

The parametric analysis uses previously derived theoretical relationships as a basis to analyze section geometry and material changes. Figure 129 is a schematic approximation of a cross section of a two-piece blade construction used in this analysis. The section was assumed to be symmetrical about the y-axis, and the blade

thickness was assumed to be a cosine curve expressed as $h = h_0 \cos \frac{\pi x}{b}$. This

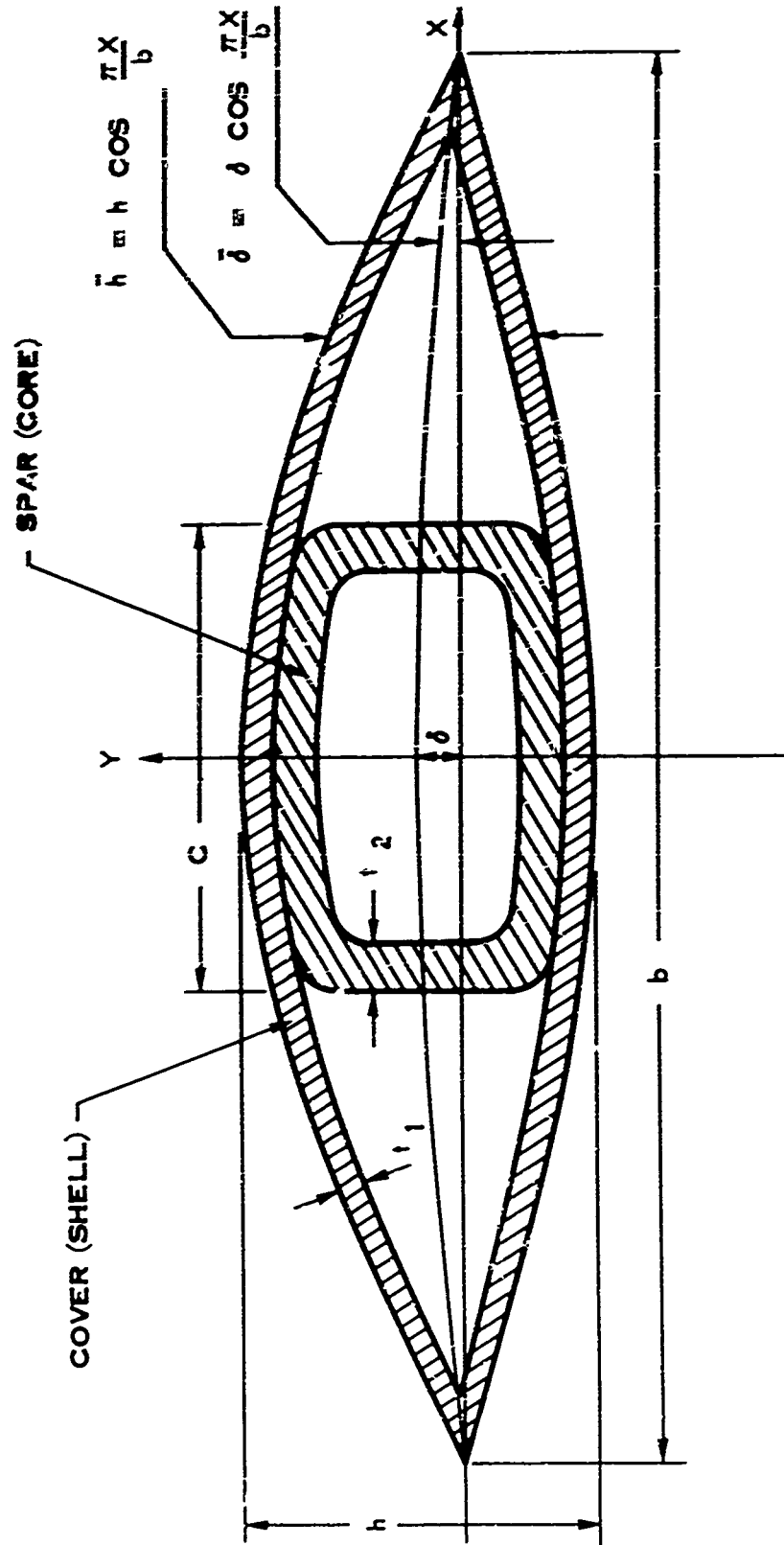


FIGURE 129. APPROXIMATION OF THE TWO-PIECE BLADE SECTION

approximation is quite good for series 16 and 65 airfoil sections; and, although series 64 sections are not symmetrical, this approximation is still considered to be reasonable. The analysis was expanded to include camber, which was also assumed to be a cosine function expressed as $\delta = \delta_0 \cos \frac{\pi x}{b}$.

The analysis uses thin-wall theory for calculating the section characteristics of the shell. The mean perimeter was taken as being equal to the outside perimeter, and distances from the x-axis to the center of the shell wall were assumed to be equal to the distances to the outside of the shell. It will be shown that the shell is usually quite thin, making these assumptions very reasonable.

Calculations for the core (spar) characteristics, on the other hand, differ in that the core thickness is less than the blade thickness by an amount equal to twice the shell wall thickness. These calculations also differ in that the above assumptions for mean perimeter and y distances are not made for the core.

Since, as stated before, the external dimensions of the blade are fixed by aerodynamics, the only design parameters are core width and shell and core wall thickness. The two main design concerns are blade dynamics or critical speeds and blade statics or load-carrying capacity and deflections. The object, then, is to vary these design parameters so that the stiffness and load capacities of the blade are of the desired magnitude, while the weight and polar moment of inertia are kept to the minimum.

The various blade section characteristics as functions of the three design parameters are calculated for the edgewise and flatwise section moduli, torsional stiffness, flatwise moment capacity, torsional moment capacity, polar mass moment of inertia, and, of course, weight. The edgewise and flatwise section moduli are needed for static deflections and, when used in conjunction with weight and polar mass moment of inertia, give an indication of blade frequencies. The moment capacities, both flatwise and torsional, are calculated for both shell and core based on their respective strengths, the lower value of which is the controlling moment capacity for the blade.

All of the blade characteristics have been calculated in the form of nondimensional parameters. However, in most cases where these parameters contain material properties, the actual value has been used. For example, the weight parameter is $W/bh\gamma_2$, where γ_2 is the density of the core material. Where the actual value for the core material density is used, the weight parameter appears as W/bh , similarly, the parameter for polar moment of inertia, $I_p/hb^3\gamma_2$ and the parameters for bending and torsional moment capacity $M/h^3\sigma_2$ and $T/hb^2\tau_2$ may appear as I_p/hb^3 , M/h^3 , and T/hb^2 , respectively.

Due to the complexity of these equations, a computer program was developed which calculated the blade section characteristics for various combinations of the three design parameters (core width and core and shell wall thickness) and the two fixed external parameters (blade thickness and camber).

The study shows that the optimum blade configuration, from a structural point of view, has no shell. Obviously, from aerodynamic considerations, there must be a shell, and its thickness is determined by factors such as impact damage, erosion, and temperature. The study points out that the thinnest shell possible is the best for an optimum weight configuration. This is discussed in the second portion of this appendix, Blade Geometry.

Based on the above discussion, the shell wall thickness can be considered fixed or, at most, limited to a very narrow range. The blade section characteristics for any one particular airfoil section can now be considered as functions of only two design parameters (core width and core wall thickness) and three fixed parameters (shell wall thickness, blade thickness, and camber). With this idea, all the information resulting from the analysis can be arranged in two convenient charts from which the optimum theoretical cross-section configuration for any load condition can be easily chosen. Figures 130 and 131 are examples of these charts, where Figure 130 presents bending characteristics and Figure 131 presents torsional characteristics. Figure 130 is a plot of flatwise moment carrying capacity as a function of core width for various values of core wall thicknesses. Similar graphs of weight as well as of flatwise and edgewise bending stiffness can be plotted, and these can then be cross-plotted on the first graph to give constant weight and stiffness contours as shown in Figure 130. Figure 131 is a similar chart for the torsional properties, with torsional moment capacity plotted versus core width and with contours of weight, torsional stiffness, and polar moment of inertia superimposed. As stated before, all of these characteristics are in the form of nondimensional parameters independent of blade size.

There are several limitations in the program and in the charts which should be noted at this time. The basic limitations of the analysis have already been discussed. These are the thin-wall assumptions and the airfoil approximations. Another limitation comes into effect when the core/blade width ratio, c/b , approaches unity. First, of course, it must be realized that, because of the presence of the shell, c/b can never actually be unity. The maximum value of c/b is expressed as

$$\left(\frac{c}{b}\right)_{\max} = \frac{2}{\pi} \cos^{-1} 2 \frac{t_1}{h}$$

which is plotted in Figure 132. Any calculations with c/b greater than this value are erroneous. Even as c/b approaches this maximum value, errors are generated in the program which place extra material in the leading and trailing edges of the blade. This causes moment capacities and stiffness to decrease with c/b ,

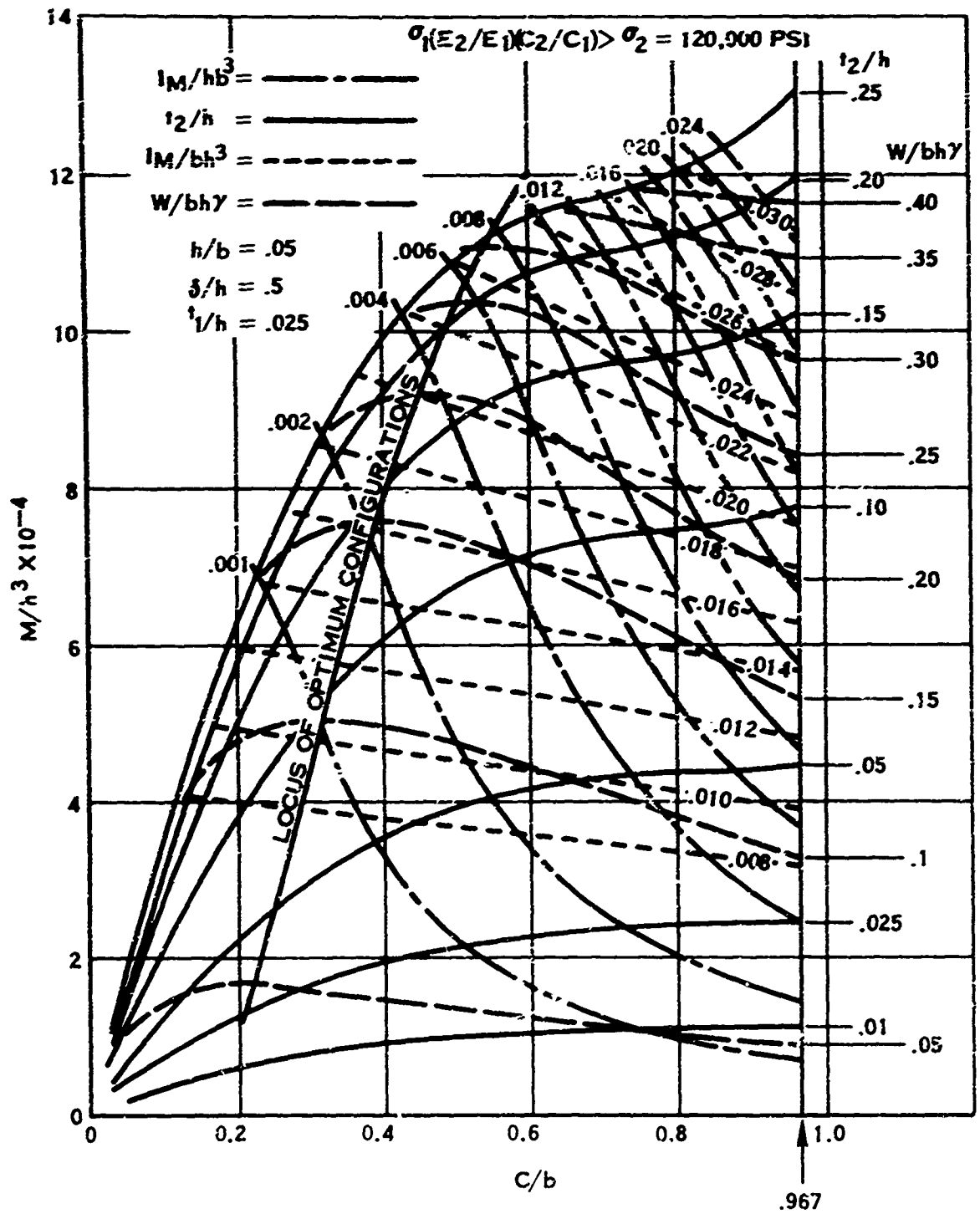


FIGURE 130. BLADE DESIGN CHART (S-GLASS COVER/BORON-ALUMINUM SPAR)

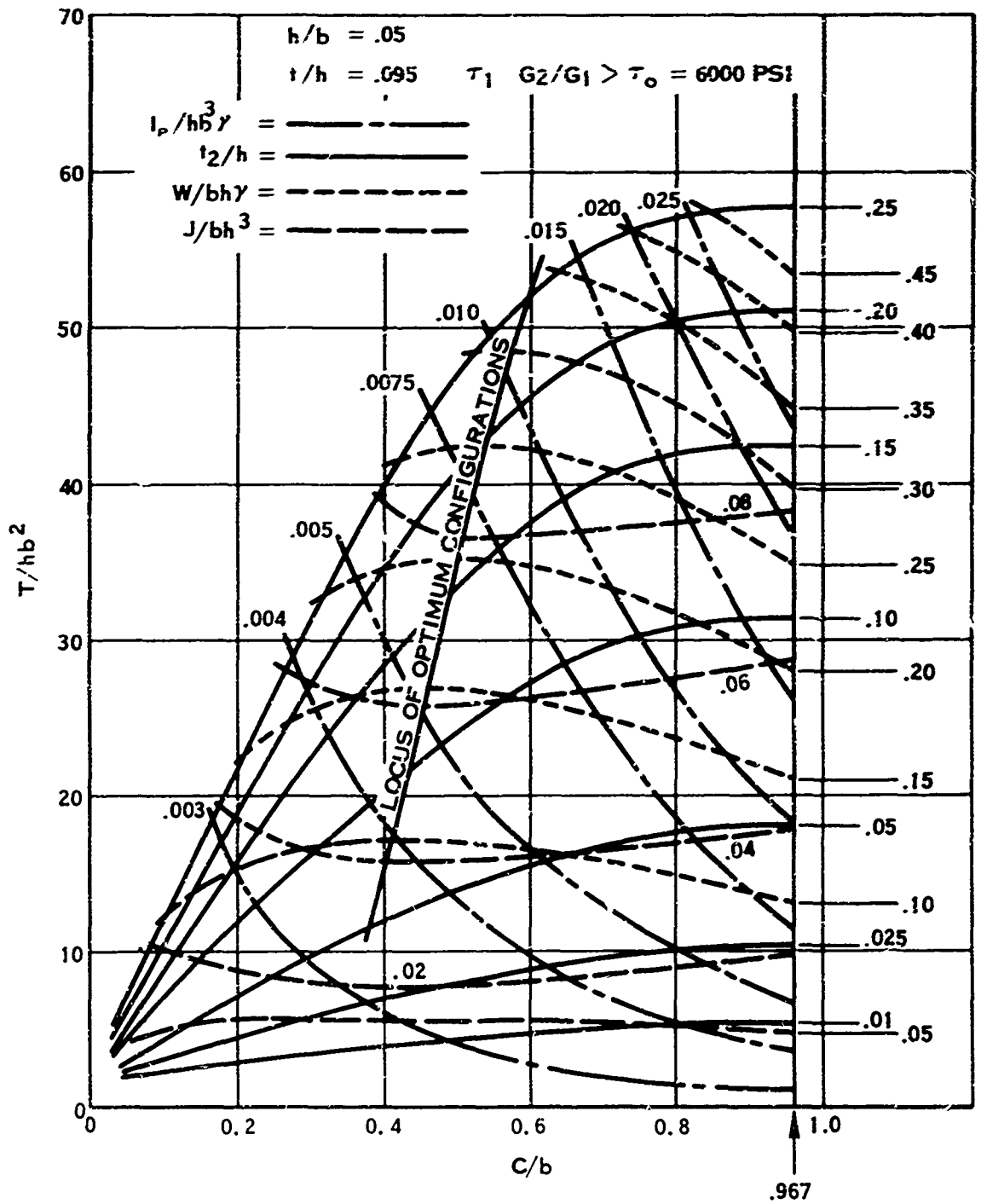


FIGURE 131. S-GLASS COVER/BORON-ALUMINUM BLADE SECTION TORSIONAL PROPERTIES

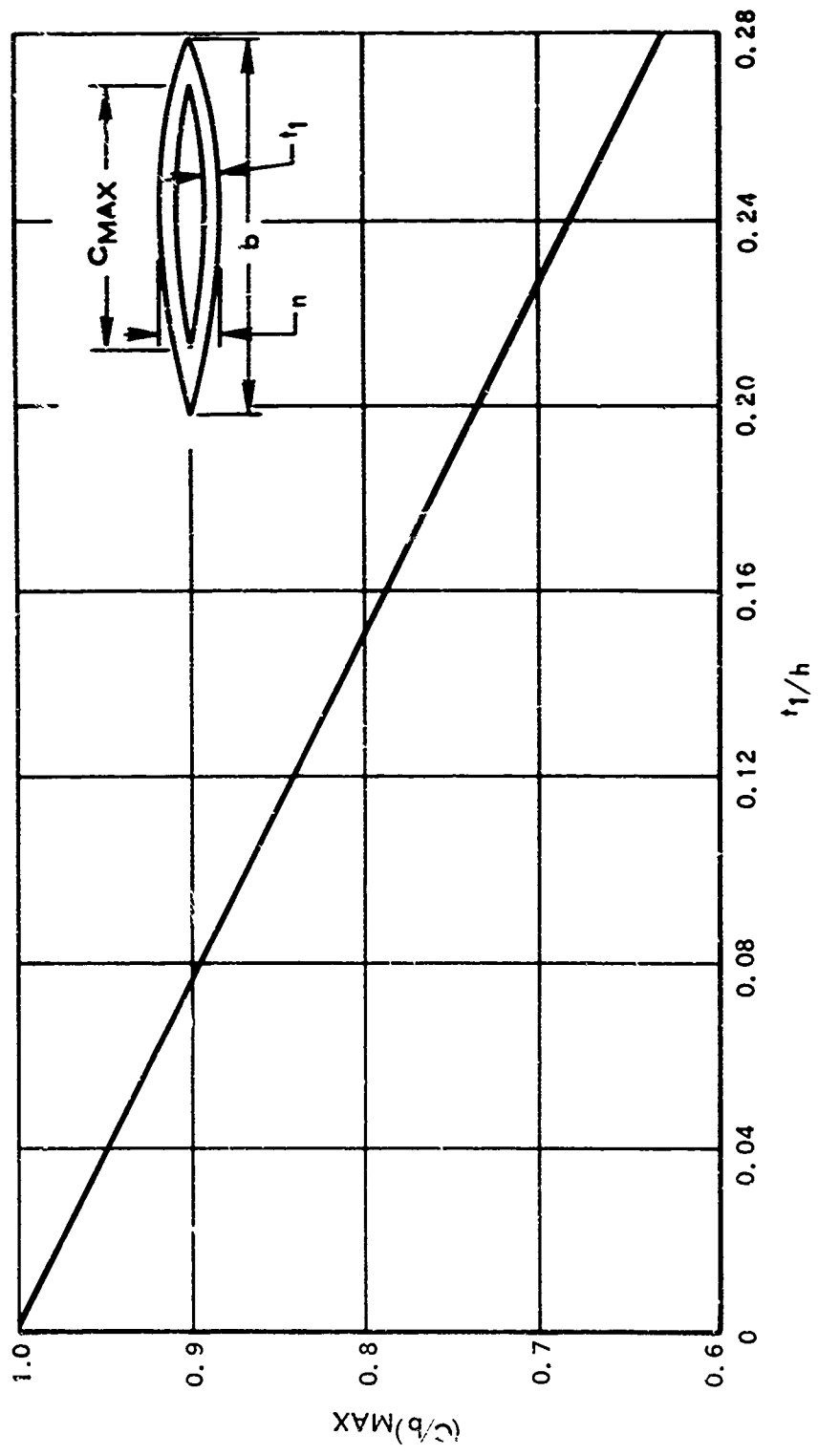


FIGURE 132. BLADE SECTION GEOMETRY LIMITS SPAR WIDTH

whereas, in actuality, they should continue to increase, although perhaps at a slower rate than for smaller values of c/b .

At the other extreme, c/b equal to zero does not necessarily preclude there being a core, since the upright portions at the end of the core still exist. Thus, although theoretically the family of curves for different core wall thicknesses should meet at a single point when $c/b = 0$, the numbers from the analysis would not necessarily show this, and the curves would then be adjusted.

Fill material, which may be required between the core and shell, and in the mono-coque construction when $c/b = (c/b)_{\max}$, has not been included in the analysis. This will cause all weight values read from the subsequent charts to be somewhat optimistic.

Moment capacities are presently based upon the stresses in the core and shell on the camber side of the airfoil; whereas, for highly cambered sections, the leading and trailing edges first tend to become stress limited and, in that case, the edge stressing becomes the controlling design factor. The neglect of this effect tends to show highly cambered sections with wide cores to better advantage than is actually the case.

Present-day propeller designs are such that the above limitations will seldom cause any problems. Core widths usually range from 20 to 80 percent of the blade width, and in this range the charts are quite accurate. Camber is usually small and the shell material quite strong, so that the leading and trailing edges are seldom the limiting regions of the two-piece blade. In the range from $c/b = 0.2$ to 0.8 , the addition of filler material does not affect the general shape of the weight contour lines, but causes only the absolute magnitude to be slightly in error. Hence, for present-day propeller designs and future designs, these design charts should prove to be useful for optimizing the blade section geometry.

BLADE GEOMETRY

Before results of this geometrical parametric study can be presented, a brief discussion on chart usage is required.

Figure 130 is basically a plot of bending moment capacity M/h^3 versus core width, c/b , for various values of core wall thickness, t_2/h . Superimposed on this are constant weight contours (dotted lines). The object in choosing an optimum configuration is to carry a given moment using the least amount of weight. This condition is met at the peaks of weight contour lines. At points other than this, the weight is greater for the same moment capacity or moment capacity is less for the same weight. Thus, a locus of optimum configurations as shown in Figure 130 exists along these peaks. Once the aerodynamic bending moment for the particular section in question is known, the optimum configuration is easily found from this op-

imum line. Also superimposed on the charts are contours of constant major and minor moments of inertia; hence, these values for the chosen configuration can also be obtained.

This same procedure is used for the torsional properties in Figure 131. Here, torsional moment capacity is plotted as a function of core width for various core wall thicknesses, and superimposed are contours of constant weight, polar moment of inertia, I_p/hb^3 , and torsional stiffness, J/bh^3 . The optimum configuration for the blade section is then that point which satisfies both load conditions.

These charts show that core width for the optimum configuration ranges from a relatively narrow 20% for lightly loaded blades to a maximum of 60% for the heavily loaded blades. Core wall thicknesses also vary between these two extremes from $t_2/h = 0.01$ to $t_2/h = 0.25$. However, because the weight contours have relatively flat peaks, there exists, in reality, a band of optimum core widths and core wall thicknesses where structural efficiency varies only slightly, thus affording a modest degree of design flexibility.

In addition to their use in optimizing the core-shell geometry, these charts also serve to highlight the inherent advantage of the two-piece blade over the monocoque design. The largest advantage is apparent at the lightly loaded region, with smaller but still significant advantages existing at the medium and highly loaded regions. In the lightly loaded regions of Figure 130, the moment capacity of a monocoque section, for a weight parameter of 0.05, drops by 48% from the optimum two-piece construction. In the medium region with a weight of 0.15, this decrease is 30%; for the highly loaded region where weight is 0.30, this figure is 12%. In reality, these losses would be even higher due to the greater amount of filler material and edge stock required in the monocoque construction, which is not accounted for in the charts. The additional edge stock is needed in monocoque construction to minimize the high local stressing at the inside leading and trailing edge fillets.

Figure 133 is a plot of maximum bending moment capacity versus shell wall thickness for cambers of $\delta/h = 0$ and $\delta/h = 0.5$ holding a constant weight of $W/bh\gamma_2 = 0.25$ and a constant blade thickness of $h/b = 0.05$. This plot confirms the results of the original study and the assumption made, in the first section of this appendix, that the optimum blade has the thinnest possible shell.

Figure 133 also indicates that camber decreases the moment capacity per weight. However, the effect is small; a camber of $\delta/h = 0.5$, which would be quite large for most present-day propeller blades, causes a decrease in moment capacity per weight of about 7%. Camber has no apparent effect on torsional properties.

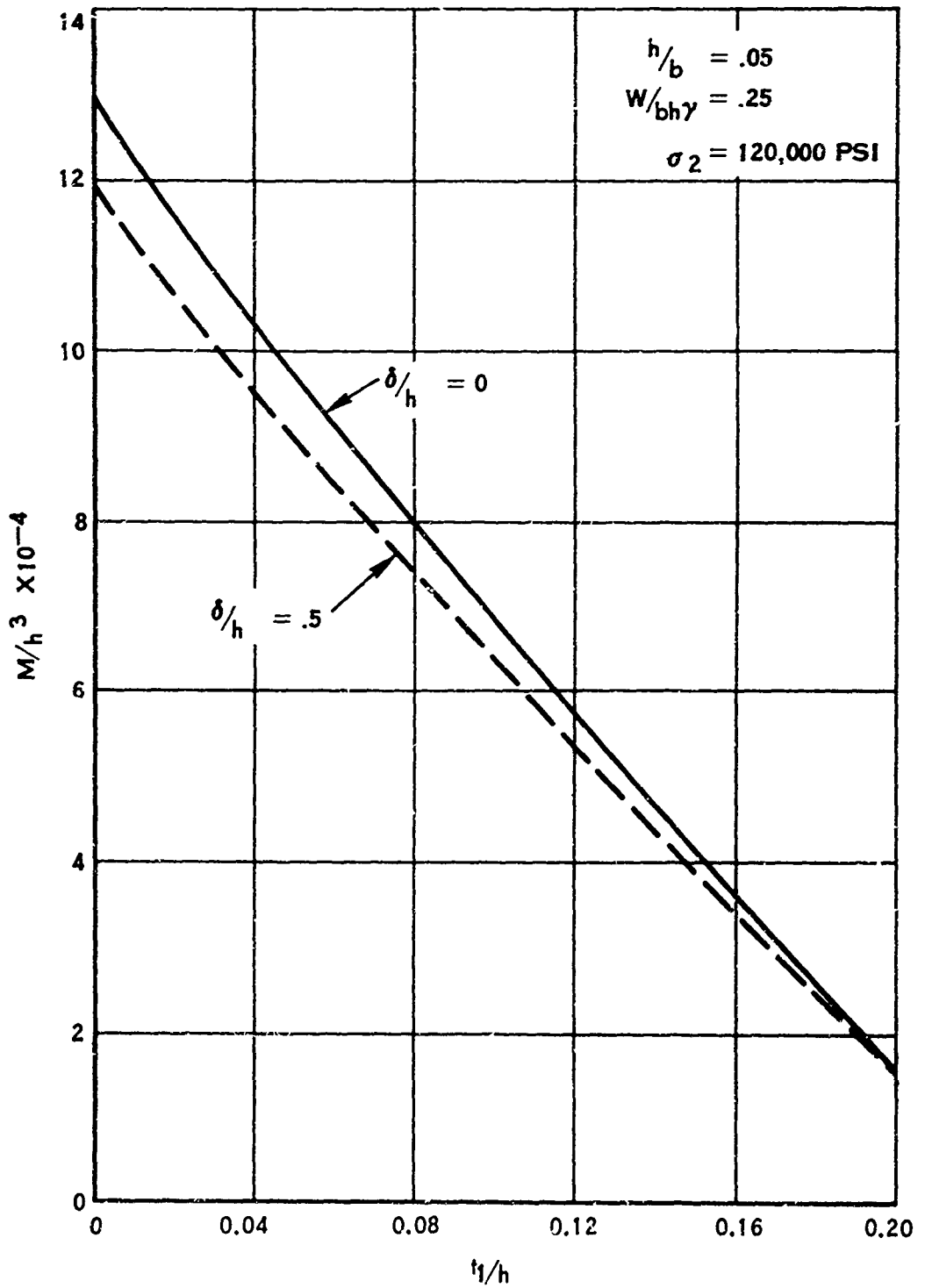


FIGURE 133. MAXIMUM MOMENT CAPACITY VS SHELL WALL THICKNESS FOR CONSTANT WEIGHT

BLADE MATERIAL

Perhaps the first major consideration in the structural design of lightweight blades is the selection of core and shell materials. As an example, the charts of Figures 130 and 131 were based on a blade incorporating a shell of woven S-glass at ± 45 degrees fiber orientation and a core of boron-aluminum fibers in an aluminum matrix with all the fibers running radially outward along the blade. Because the shell will operate in an environment where it must contend with temperature variations and exposure to surface damage (both erosion and impact), the design limits for this material are based on damaged strengths at appropriate temperature levels.

On the other hand, the protected environment of the core (being completely encased in the shell) permits the use of design limits based on the higher undamaged material strengths.

In the case of a two-piece blade where both pieces are designed to mutually act as a primary structure, the optimum design, for best material utilization, would require that both elements reach their respective material design limits simultaneously. However, from the previous analysis, it is evident that, with the shell-spar type of construction, the minimum blade weight is achieved with the shell serving primarily as an aerodynamic fairing and carrying only a relatively small percentage of the total blade load. Accordingly, it is important, in the structural design of the shell-spar blade, that the shell be designed to operate sufficiently below the design limits of its material, that it does not become a limiting factor in the structural design of the blade.

Four shell materials were analyzed in combination with the boron-aluminum core, and the results do substantiate the above conclusions. The four materials were woven S-glass, unwoven S-glass, boron/epoxy with 20% of the fibers running longitudinally and 80% at ± 45 degrees, and a combination of 80% woven S-glass and 20% boron/epoxy with the boron fibers running longitudinally. The structural properties for each of these materials, and for others mentioned later in this appendix, are presented in Tables XXVII and XXVIII.

Rather than prepare complete parametric charts for each of these cases, a comparison was made by examining moment capacities, stiffness, and weights for a chosen blade configuration of $c/b = 0.4$ and $t_2/h = 0.15$.

Results of these four designs are given in Table XXIX for $h/b = 0.05$, $\delta/h = 0.5$, and $t_1/h = 0.025$. The first three columns list the dimensionless parameters for flatwise bending moment capacity, flatwise bending moment of inertia, and weight as calculated by the computer program. The last two columns list moment capacity per weight and flatwise bending stiffness per weight. The column-capacity-per-weight parameter was highest at 130 for the woven S-glass shell, and stiffness per

TABLE XXVII. SHELL MATERIALS

MATERIAL	LB/IN ³	PSI X 10 ⁻⁶			PSI _{ults} X 10 ⁻³			DAMAGED PSI _{fat} X 10 ⁻³		
	γ	E _x	E _y	G _{xy}	σ_x	σ_{xy}	τ_{xy}	σ_x	σ_y	τ_{xy}
WOVEN S-GLASS ±45	0.068	3.4	3.4	1.75	37	37	32.5	8.1	-	-
UNWOVEN S-GLASS ±45	0.065	1.63	1.63	1.8	4.0	4.0	7.2	-	-	-
970 GLASS	0.070	4.1	4.1	2.1	45	45	40	9.7	-	-
BORON EPOXY 20% @ 0°	0.071	10.3	6.2	8.0	25	11	28	4.9	-	-
20% BORON EPOXY @ 0° 80% S-GLASS	0.0686	9.92	3.4	1.62	37.1	5.52	10.6	5.4	-	-
BORON-AL 100% @ 0°	0.095	30	12	10	160	10	6	15	-	-

TABLE XXVIII. CORE MATERIALS

MATERIAL	LB/IN ³ γ	PSI $\times 10^{-6}$			PSI $\times 10^{-3}$			UNDAMAGED PSI $\times 10^{-3}$		
		E_x	E_x	G_{xy}	σ_x	σ_y	τ_{xy}	σ_x	σ_y	τ_{xy}
BORON/AL 100% @ 0°	0.096	30	12	10	160	10	6	30	—	1.8
BORON/EPOXY 50% @ 0°	0.071	20	6.1	5.5	53	10	19	16	—	5
CARBON/EPOXY 50% @ 0°	0.0535	16.5	4.5	4.3	27.5	7	12.5	7	—	.9
D6A STEEL	0.283	30	30	11	185	185	110	35	—	21
TITANIUM	0.160	15.8	15.8	6.3	180	180	108	25	—	15
BORON/EPOXY 100% @ 0°	0.071	36	3	1	135	4.8	7.2	25	—	1
BORON/EPOXY 75% @ 0°	0.071	28	4.7	3.2	85	8	12	18.2	—	3

weight was 33.6. Because weaving has a strengthening effect for multidirectional loading, unwoven S-glass is much weaker than woven S-glass by a factor of 4, but the moment capacity/weight of the blade decreased by only 0.77% and stiffness/weight by only 1.8%, indicating that this shell does indeed carry a very small percentage of the total load.

In the case of the boron/epoxy shell with only 20% longitudinal fiber orientation, the shell did become the limiting factor due to the low strength and high modulus of this material. Consequently, total blade stiffness increased to 37 but capacity was reduced by 50%. The combination S-glass - boron/epoxy shell was again limiting, and the blade was only slightly better than the all-boron/epoxy shell. The analytical technique of tailoring blade materials in this fashion is quite effective, and further studies should be conducted to develop more exact design criteria.

To generate a similar picture of the relative standings of the several pertinent core materials, five cases were analyzed with S-glass as the shell material and boron/aluminum, boron/epoxy, carbon/epoxy, D6A steel, and titanium as core materials. Tables XXX and XXXI give the results of the bending and torsional calculations for the 78-inch radius of the blade design with a chosen design configuration of $c/b = 0.4$ and $t_2/h = 0.15$. Table XXXII gives bending results for the 24-inch blade radius with the same design configuration. For both blade sections, the bending capacity per weight, Mb/Wh^2 , was the highest with the boron/aluminum core with 100 percent fiber orientation at 0° . Titanium had about 70 percent of the capacity of boron/aluminum, and steel had 55 percent of the capacity at the 78-in. radius and 40 percent at the 24-in. radius. The boron/epoxy and carbon/epoxy cores were oriented with 50% of the fibers at 0 degrees and 50% at ± 45 degrees to obtain a desired torsional/bending stiffness ratio. Because of the relatively low bending strength associated with this configuration, these materials had only 30 to 50 percent of the capacity of the boron/aluminum core. The boron/aluminum core also exhibited the best bending stiffness-to-weight ratio, EI/Wh^2 , with boron/epoxy and carbon/epoxy about equal and slightly lower than the boron-aluminum, and with titanium and D6A steel sharing the last spot with about one-third to one-half the efficiency of boron/aluminum.

Table XXXI gives the torsional results for the 78-inch radius for these same core materials. The first three columns are the parameters for the torsional moment capacity T/hb^2 , torsional stiffness J/bh^3 , and polar mass moment of inertia I_p/hb^3 . The last two columns are torsional capacity per weight and torsional stiffness per polar moment of inertia.

Due to the low shear strengths of the composite materials, titanium and steel were superior in torsional capacity. Boron/epoxy was the best of the composite materials, with about two-thirds the capacity of the titanium and steel. Boron/aluminum and carbon/epoxy were about equal, with only 15% of this capacity. From a frequency

TABLE XXX. BENDING PROPERTIES BASED ON FATIGUE, 78-INCH RADIUS

SHELL	CORE $t_2/h = 0.15$	$\frac{M}{h^3} \times 10^{-3}$	$\frac{Im}{bh^3}$	$\frac{W}{bh}$	$\frac{Mb}{Wh^2} \times 10^{-4}$	$\frac{EI}{Wh^2} \times 10^{-6}$
S-GLASS $t_1/h = .07$	BORON-AL 100% @ 0°	19.1	0.0154	0.0216	89.0	21.39
	BORON/EPOXY 50% @ 0°	8.24	0.0167	0.0184	44.5	18.10
	THORNELL/EPO. 50% @ 0°	5.0	0.0175	0.0162	30.6	17.65
	D6A STEEL	22.3	0.0154	0.0451	49.5	10.23
	TITANIUM	17.9	0.0177	0.0296	60.7	9.45
970 GLASS	BORON-AL 100% @ 0°	19.7	0.0177	0.0219	90.2	21.87
BORON-AL 100% @ 0°	BORON/EPOXY 100% @ 0°	SHELL LIMITS 18.6	0.0314	0.0224	83.0	50.40
BORON-AL 100% @ 0° $t_1/h = .02$	BORON/EPOXY 100% @ 0°	SHELL LIMITS 14.3	0.0225	0.0128	111.0	63.0
	BORON/EPOXY 75% @ 0°	SHELL LIMITS 11.6	0.024	0.0128	92.0	52.0
	BORON/EPOXY 50% @ 0°	SHELL LIMITS 9.2	0.0267	0.0128	72.0	41.6
NOTE	$\frac{t}{b} = .05$					
	$\frac{s}{h} = .5$					
	$\frac{c}{b} = .4$					

TABLE XXXI. TORSIONAL PROPERTIES BASED ON FATIGUE, 78-INCH RADIUS

SHELL	CORE $t_2/h = 0.15$	$\frac{T}{hb^2}$	$\frac{J}{hb^3}$	$\frac{I}{hb^3} \times 10^3$	$\frac{T}{Wb}$	$\frac{GJb^2}{Iph^2} \times 10^{-6}$
S-GLASS $t_1/h = 0.07$	BORON-AL 100% @ 0°	8.35	0.057	0.974	386	584
	BORON/EPOXY 50% @ 0°	26.4	0.065	0.929	1425	383
	THORNEL/EPO. 50% @ 0°	5.1	0.070	0.897	323	334
	D6A STEEL	95.7	0.056	1.31	2120	458
	TITANIUM	76.2	0.063	1.09	2570	354
970 GLASS	BORON-AL 100% @ 0°	8.6	0.059	0.998	390	595
BORON-AL 100% @ 0°	BORON EPOXY 100% @ 0°	SHELL LIMITS				
		6.8	0.612	1.26	302	480
BORON-AL 100% @ 0° $t_1/h = 0.02$	BORON/EPCXY 100% @ 0°	SHELL LIMITS				
		2.4	0.223	0.456	186	487
		SHELL LIMITS				
	BORON/EPOXY 75% @ 0°	3.7	0.112	0.456	293	785
	BORON/EPOXY 50% @ 0°	5.2	0.091	0.456	404	1100
NOTE $h/b = 0.05$						
$s/h = 0.5$						
$c/b = 0.4$						

TABLE XXXII. BENDING PROPERTIES BASED ON ULTIMATE STRESS,
24-INCH RADIUS

SHELL	CORE $t_2/h = 0.15$	$\frac{M}{h^3} \times 10^{-3}$	$\frac{I_m}{bh^3}$	$\frac{W}{bh}$	$\frac{W_b}{Mh^2} \times 10^{-4}$	$\frac{EI}{Wh^2} \times 10^{-6}$
S-GLASS $t_1/h = 0.0075$	BORON-AL 100% @ 0°	29.0	0.0188	0.0154	193	36.5
	BORON/EPOXY 50% @ 0°	9.7	0.0190	0.0117	85	32.2
	THORNEL/EPO. 50% @ 0°	5.2	0.0190	0.0091	57	34.5
	D6A STEEL	34.6	0.0188	0.0436	79.3	12.9
	TITANIUM	34.0	0.0190	0.0251	135	12.0
970 GLASS	BORON-AL 100% @ 0°	30.0	0.0189	0.0155	193	36.5
BORON-AL 100% @ 0°	BORON/EPOXY 100% @ 0°	—	—	—	—	—
BORON-AL 100% @ 0° $t_1/h = 0.0055$	BORON/EPOXY 100% @ 0°	26.6	0.0200	0.0117	226	61.2
	BORON/EPOXY 75% @ 0°	17.0	0.0203	0.0117	144	48.5
	BORON/EPOXY 50% @ 0°	11.0	0.0209	0.0117	92.6	35.6
NOTE	$h/b = 0.2$					
	$s/h = 0.15$					
	$c/b = 0.4$					

standpoint, the torsional stiffness per polar moment of inertia is of more interest than stiffness per weight. In this respect, boron/aluminum was best, with steel having 80 percent of this efficiency, and with the boron/epoxy, titanium and carbon/epoxy about equal, with two-thirds the capacity of the boron/aluminum.

Design charts were drawn for the bending characteristics of the boron/aluminum, D6A steel, and titanium core blades (Figures 134, 135, and 136); from these, plots of maximum moment capacity versus weight based on fatigue strength were drawn (see Figure 137). This shows boron/aluminum to be the best material in this respect, as was to be expected from the above discussion. For most load conditions, titanium is better than steel; however, for very high loads, $M/h^3 > 21,400$, the steel becomes more efficient. This is due to the fact that the fatigue strength for titanium is lower than that for steel; and although the titanium is lighter than the steel, it requires more than this weight in extra material to overcome the strength problem. The greatest advantage of titanium over steel for the configuration at the 78-in. radius is at a moment parameter, M/h^3 , equal to 16,000. Here the titanium is 16% lighter than the steel. The boron/aluminum has the greatest advantage over steel at $M/h^3 = 20,000$, where the weight savings is 40%. Figure 138 presents the corresponding bending-stiffness-versus-weight plot for optimum moment capacity. Again boron/aluminum is superior to titanium or steel.

Tables XXX, XXXI, and XXXII also give the results for a boron/aluminum core with a 970 glass shell. The properties of this shell material are somewhat superior to S-glass, but since the shell is doing very little structurally, total performance did not improve greatly.

Recent tests have shown that the erosion properties of boron/aluminum are equivalent or superior to those of titanium. Based on this, a two-piece blade with a boron/epoxy core and boron/aluminum shell was analyzed using the optimization program, and the results are also shown in Tables XXX, XXXI, and XXXII. The tensile strength of boron/aluminum drops so drastically (from 160,000 to 14,000 psi UTS) when any fibers are placed at 45 degrees that all fibers must be longitudinal for the shell. Although the tensile strength of boron/epoxy also decreases as fibers are placed at 45°, the drop is much more gradual. Shear strength and shear modulus, on the other hand, increase as fibers deviate from 0 degrees, thus making it somewhat of an advantage to vary the directions of the layers of the boron/epoxy core material. Tables XXX, XXXI, and XXXII show the results for a core fiber arrangement of 100 percent at 0° and 50% at 0 degrees. Because of the extra strength of the boron/aluminum shell over S-glass, shell thickness t_1/h has been reduced from 0.07 to 0.02. Bending stiffness and bending moment capacity per weight, torsional moment capacity per weight, and torsional stiffness per polar moment of inertia have been plotted versus percent fibers at 0°; see Figure 139. With 70% of the fibers at 0 degrees, the bending moment capacity per weight is 85×10^4 and torsional moment capacity per weight is 310, making this configuration nearly equi-

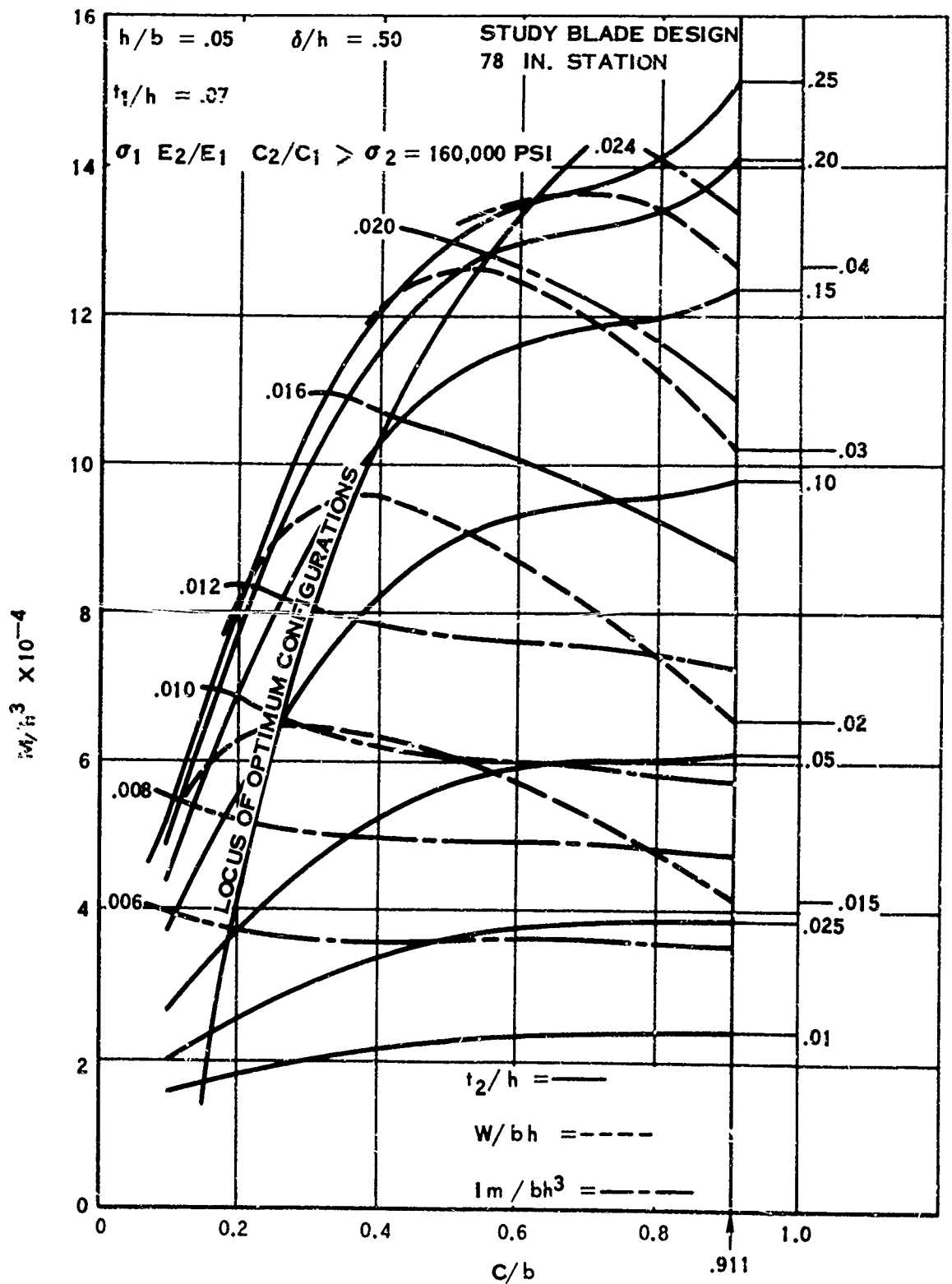


FIGURE 134. PROPERTIES OF S-GLASS/BORON-ALUMINUM BLADE SECTION

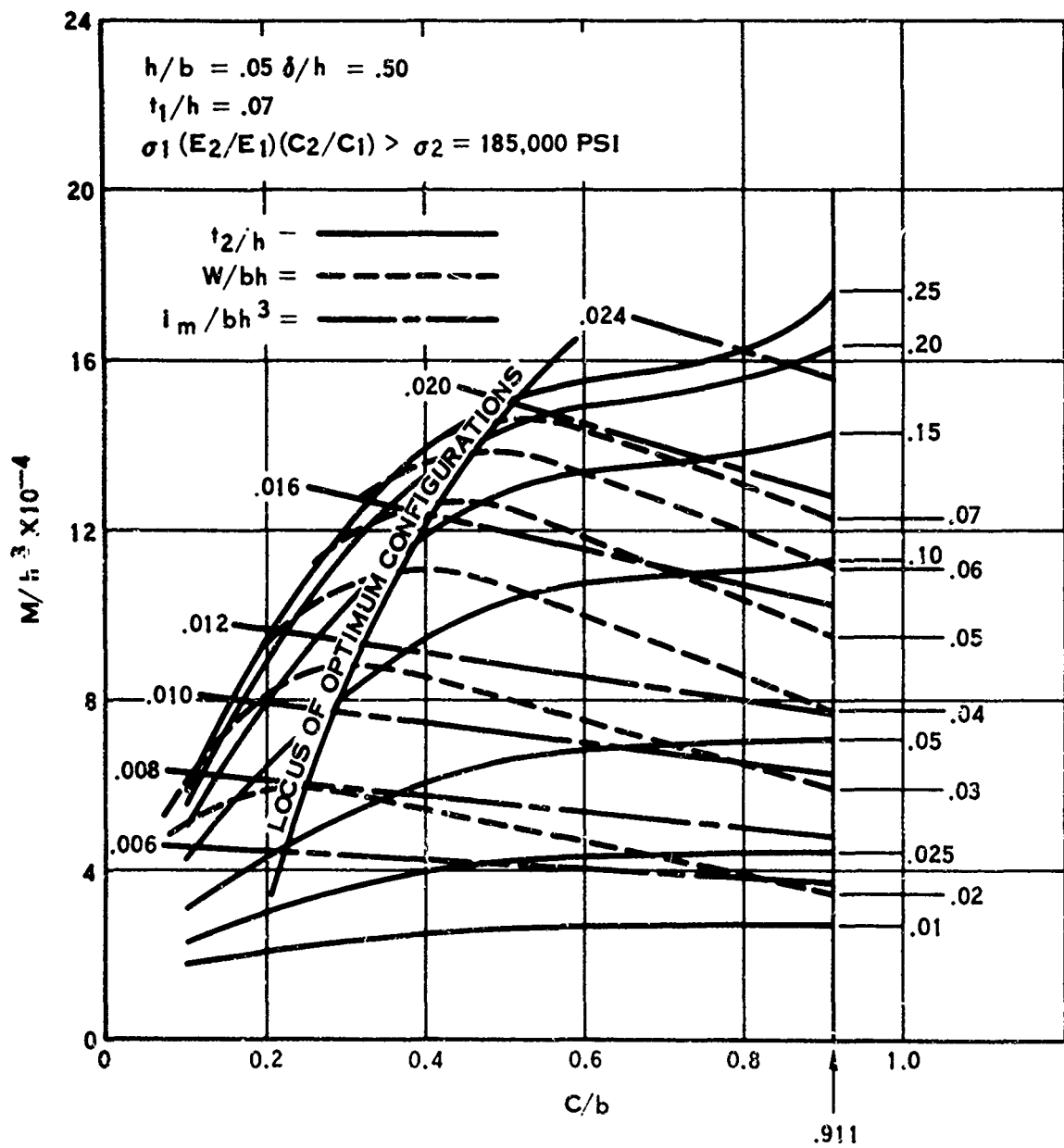


FIGURE 135. S-GLASS COVER/D6A STEEL SPAR BLADE SECTION PROPERTIES

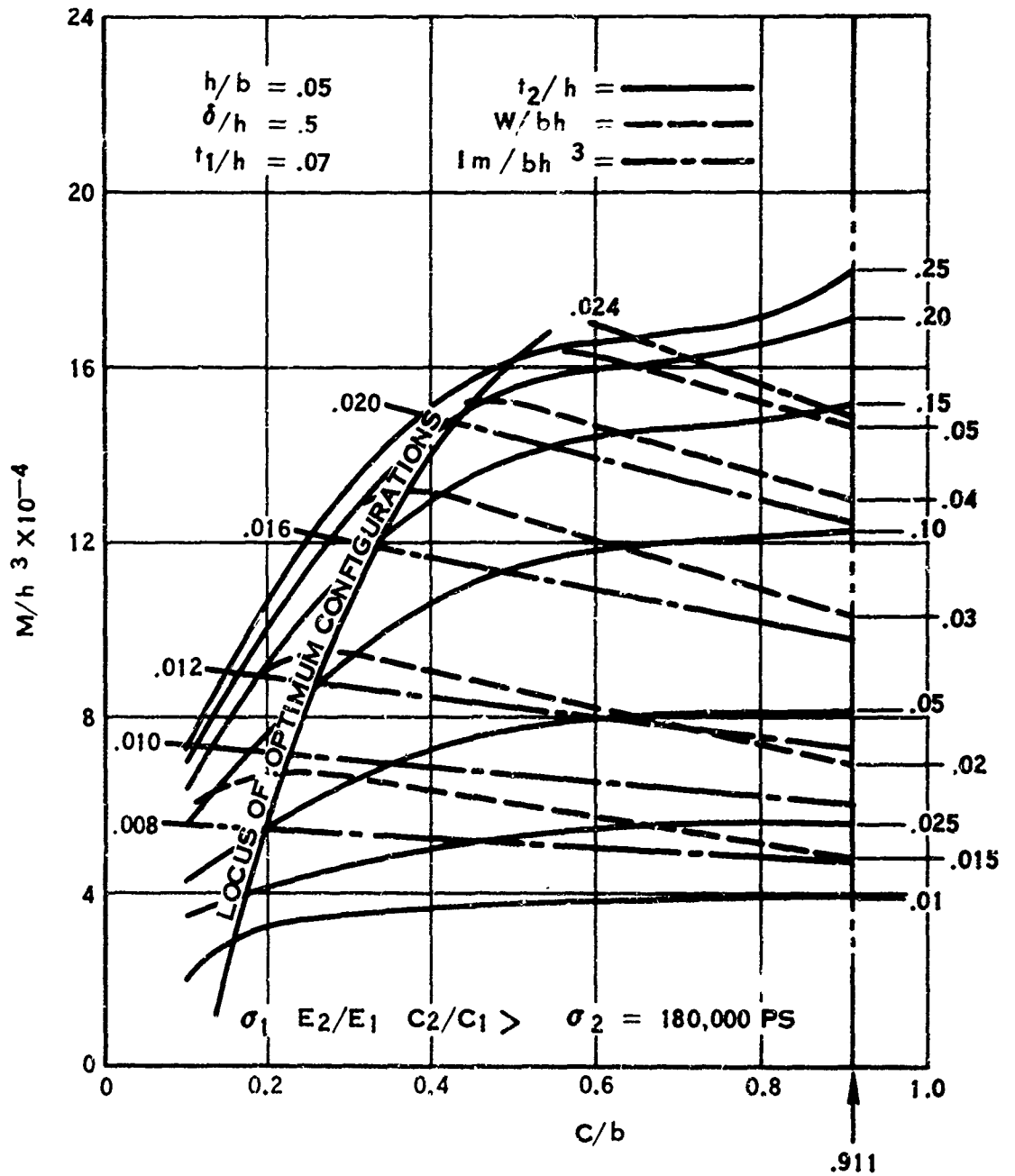


FIGURE 136. S-GLASS COVER/TITANIUM SPAR BLADE SECTION PROPERTIES

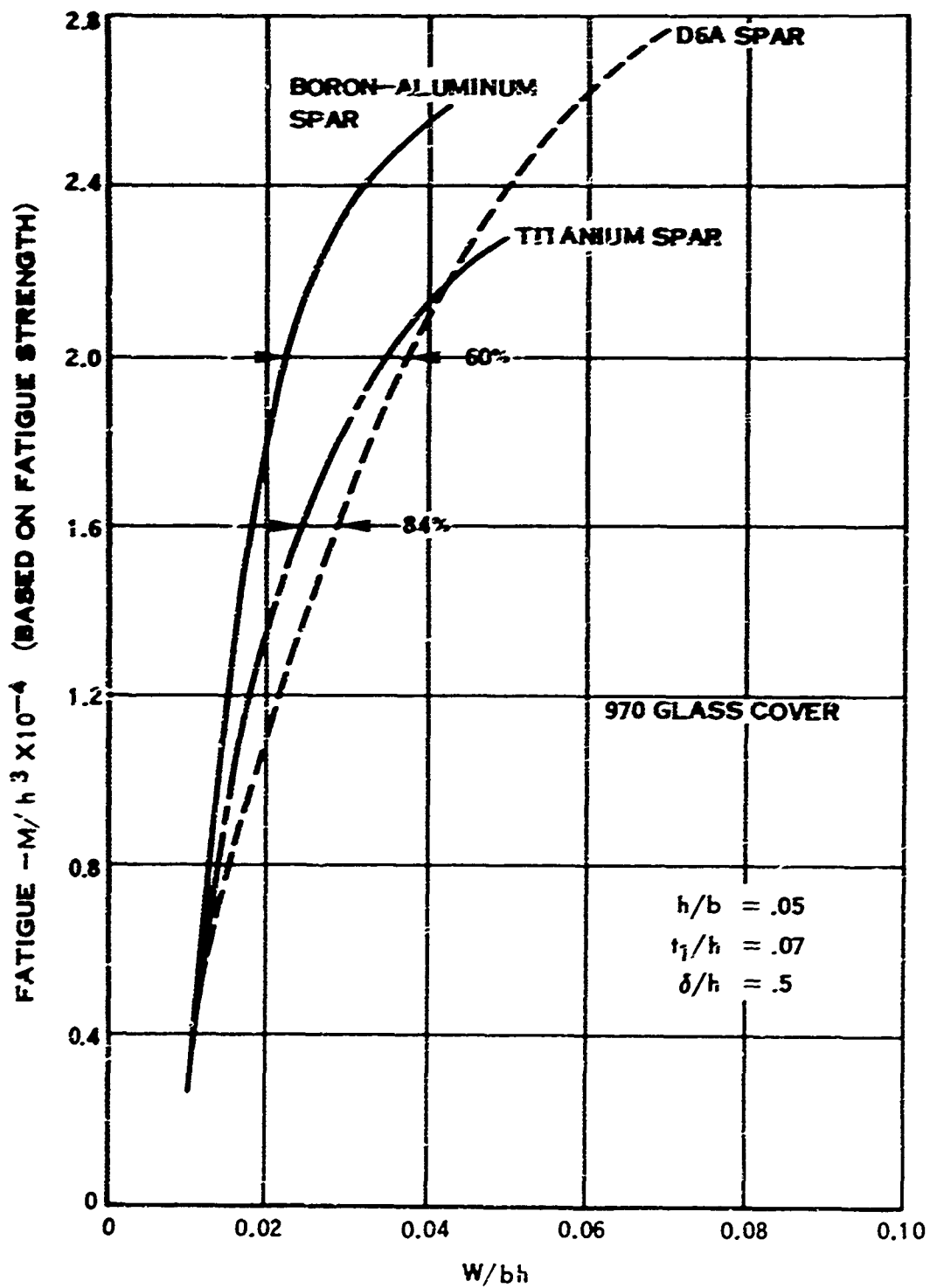


FIGURE 137. SPAR MATERIAL VS MOMENT CAPACITY

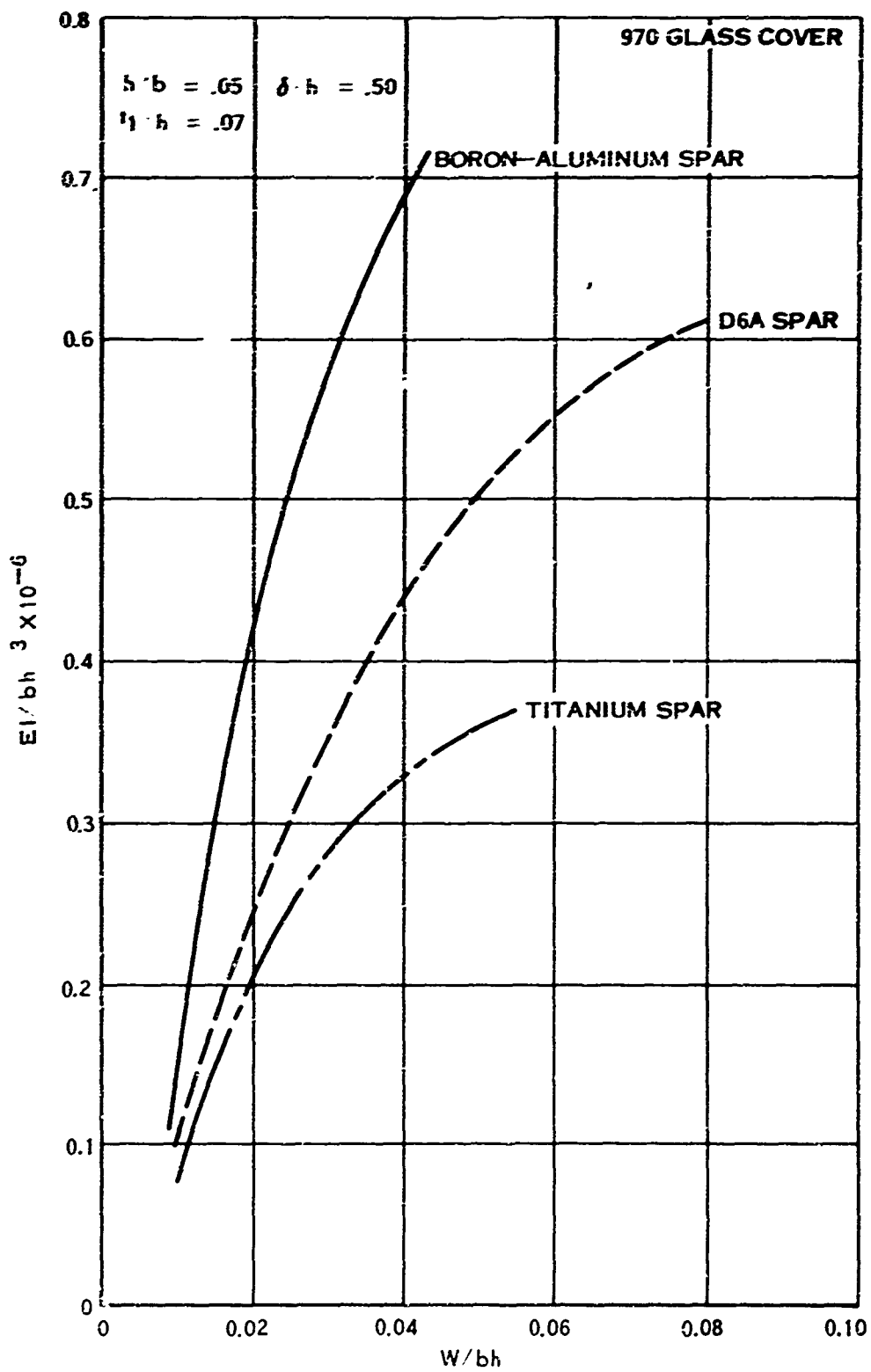


FIGURE 138. SPAR MATERIAL VS BENDING STIFFNESS

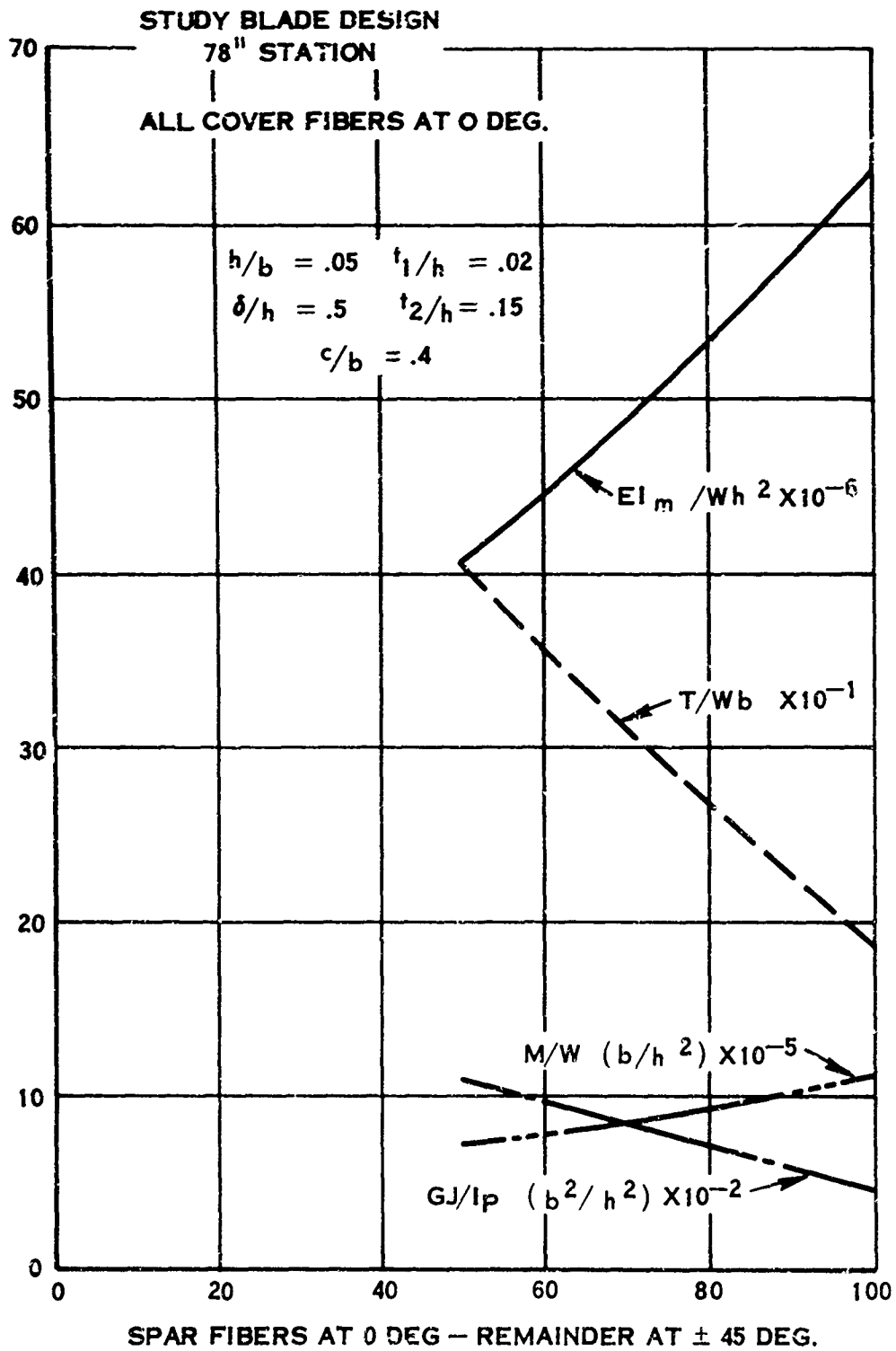


FIGURE 139. BORON-ALUMINUM COVER/BORON-EPOXY SPAR

valent to the boron-aluminum core/S-glass shell configuration (89×10^4 and 386) from a capacity standpoint. The major advantage lies in the stiffness parameters. Bending stiffness per weight is about 2-1/3 times that of the boron/aluminum core blade, and torsional stiffness per polar moment of inertia is about 1-1/2 times the value of this blade.

This design has a few drawbacks which require further investigation before the relative merit of this type of blade construction can be truly evaluated. The shell material for most blade designs carries only a small percentage of the loads, whereas the boron/aluminum shell in this case is carrying a major portion. Should it become severely damaged, the core may become overstressed and a complete blade failure might occur. If the shell should receive only minor damage, then repair and maintenance become a problem. At present, it appears that the only method of repair is a complete replacement of the shell, whereas damage in an S-glass shell can be repaired locally in the field.

Tailoring the blade properties by proper fiber orientation will be a very useful technique in future blade design. This advantage presently appears to outweigh the disadvantages of this type of construction, and studies should be continued to investigate this concept further.

EXAMPLE BLADE DESIGN

The external dimensions of the propeller blade have already been established by aerodynamics, and a two-piece boron/aluminum core/S-glass shell has been developed by blade design. This section presents the design procedure using the parametric analysis for the study blade.

The external dimensions of this blade, established by aerodynamics, are given in Table XXXIII. By 1975, it is expected that 970 glass, rather than E or S glass, will be used for the shell material. Based on its greater strength, the shell was thinned 9 mils (one layer) over the original design. See Table XXXIII. This thinning was based on chordwise stiffness requirements for maintaining the cross-sectional shape under load.

The 24-in., 54-in., and 78-in. stations were selected to be optimized using the parametric analysis. The design charts for the bending characteristics corresponding to these stations were drawn (Figures 140, 141, and 134) using an allowable design strength of 160,000 psi for the boron/aluminum core, which is the limiting factor. The aerodynamic 1P loads for these three stations are given in Table XXXIV. These loads include an estimated magnification factor due to blade dynamics. The ground rule in this blade design was to keep the 1P bending stress at or below 16,000 psi and the 1P plus higher orders below 20,000 psi. Since the charts were drawn for 160,000 psi, the moment parameter scale, M/h^3 , had to be divided by a factor

TABLE XXXIII. FIXED PARAMETERS OF THE BLADE DESIGN

R	b	h	h/b	s	s/h	t _i	t _i /h	θ
12	18.10	5.466	0.302	0.436	0.080	0.027	0.00495	58.5
15	18.10	4.923	0.272	0.457	0.093	0.027	0.00548	55.0
18	18.10	4.435	0.245	0.481	0.108	0.027	0.00610	52.0
24	18.00	3.600	0.200	0.538	0.149	0.027	0.00750	46.2
30	17.85	2.999	0.168	0.611	0.204	0.027	0.00900	41.2
36	17.60	2.534	0.144	0.673	0.266	0.036	0.0142	36.8
42	17.30	2.197	0.127	0.663	0.302	0.036	0.0164	33.0
48	16.90	1.994	0.118	0.642	0.321	0.045	0.0226	29.5
54	16.55	1.688	0.102	0.639	0.379	0.045	0.0268	26.2
60	16.10	1.562	0.097	0.613	0.393	0.054	0.0346	23.0
66	15.60	1.248	0.080	0.559	0.447	0.054	0.0433	20.5
72	15.00	1.020	0.068	0.480	0.470	0.054	0.0530	18.0
78	14.10	0.775	0.055	0.373	0.482	0.054	0.0698	15.8
84	11.10	0.466	0.042	0.190	0.408	0.054	0.1160	14.0
86	8.40	0.269	0.032	—	—	0.054	0.2010	13.5
88.5	3.20	0.096	0.030	—	—	SOLID	1.000	12.6

STUDY BLADE DESIGN
24 IN. STATION

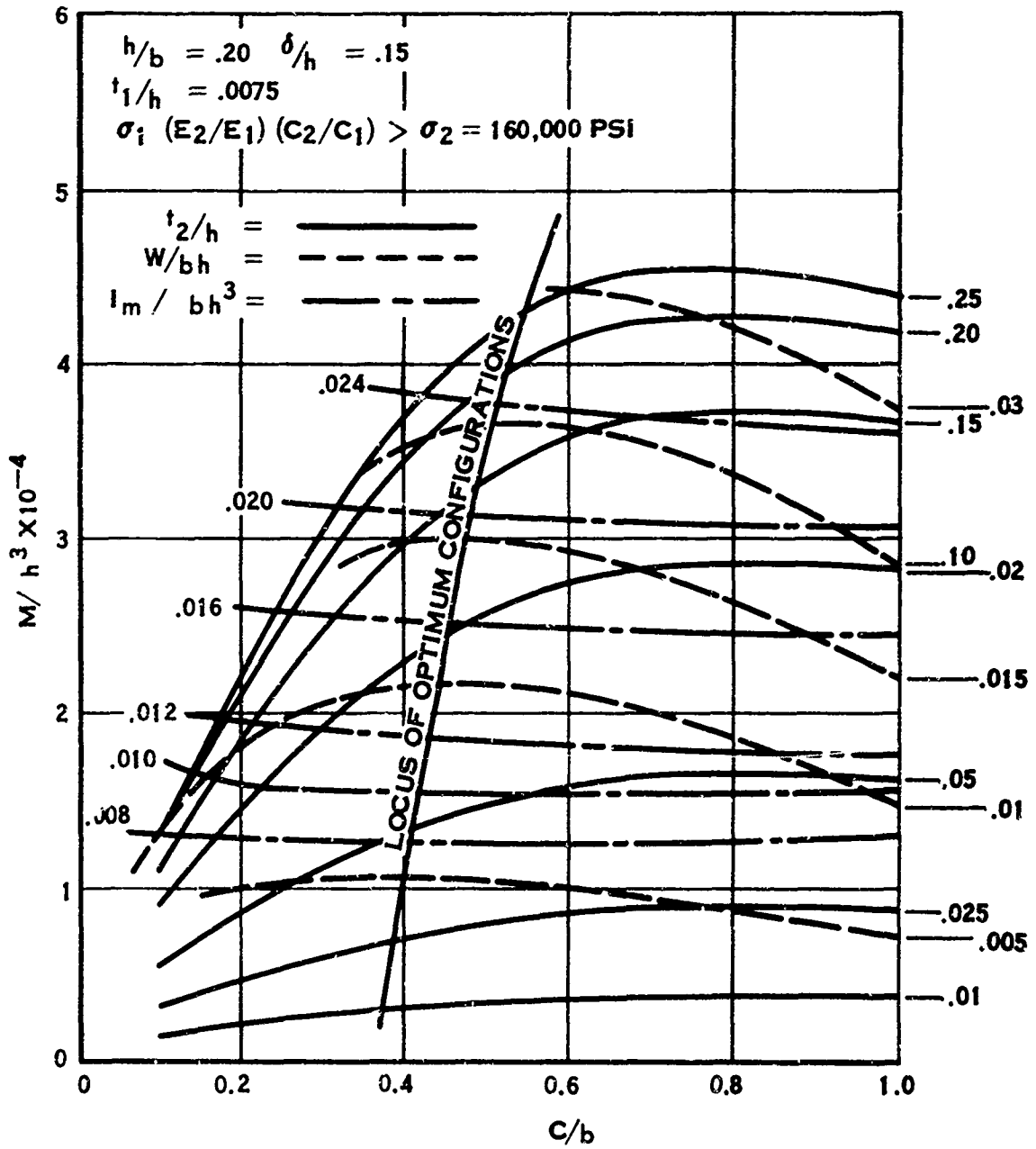


FIGURE 140. PROPERTIES OF S-GLASS SHELL/BORON-ALUMINUM BLADE SECTION

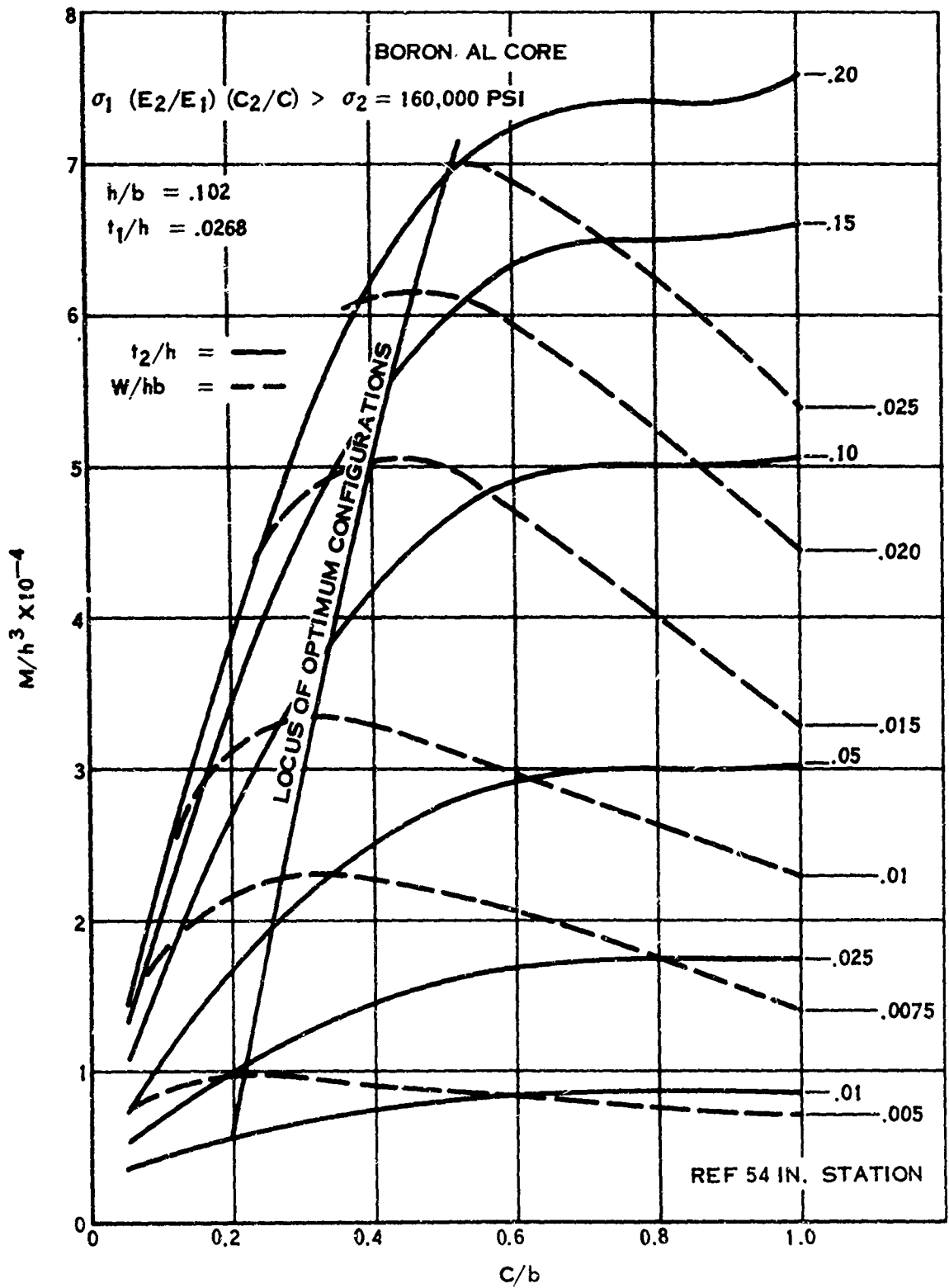


FIGURE 141. 970 GLASS COVER/BORON-ALUMINUM SPAR BLADE SECTION PROPERTIES

TABLE XXXIV. BLADE DESIGN				
R (IN)	IP MOMENT (IN·LB)	M/h^3 CORRECTED FOR CHARTS	c/b	t_2/h
24	30,000	6,400	0.5	0.025
54	7,200	15,000	0.3	0.033
78	500	9,000	0.3	0.03

of 10. Usually this factor will not be quite so simple, making the moment scale quite difficult to read. An easier method is to correct the value of M/h^3 by multiplying it by σ chart/ σ design, which was done in this example. The resulting corrected moment parameters for the three stations in question are given in Table XXXIV. From the charts, the optimum core wall thicknesses and core widths were found for the three sections and are also given in Table XXXIV. The core widths at these stations were designed to be larger than the charts indicated was necessary in order to reduce the required amount of fill between the shell and core. The core wall thickness was also increased to an arbitrarily chosen minimum of 20 mils at the 78-in. station.

Calculations have shown that the resulting core geometry is adequate to resist buckling and plate vibration problems without the aid of internal foam fill.

The core was centered at the 45% chord position rather than at the center line of the blade. Structural properties increased slightly at the inboard region, where series 64 airfoil sections are used. However, the main purpose in doing this was to reduce the aerodynamic twisting moment at the shank and thereby to reduce the actuator structural requirements.

Figure 142 is a plot of the core width, core wall thickness, and the blade thickness of the USAAVLABS blade. The calculated stress distribution for this design is shown in Figure 143. The 1P stress is relatively constant at 16,000 psi between the 30- and 60-in. stations, which was the desired distribution. The maximum steady stress, bending plus centrifugal, is 22,300 psi, which is within the stress limits of the blade material. This is based on an offset of 1 in.

A critical speed diagram for this blade is shown in Figure 144. The point of interest here is the 2P/1F critical speed, which is located at 1410 rpm. Experience has shown it desirable that this critical speed be approximately 10% above the operating speed range to avoid excessive vibratory stress magnification. The example being considered met this requirement without any changes, once it had been configured to give acceptable static and dynamic stresses.

In some cases, a blade which is designed to meet various stressing criteria will not have satisfactory critical speeds. When this happens, it will be necessary to resort to other techniques to shift the critical speeds out of the operating range. A discussion of one such method is presented in the next section.

INTEGRATED DYNAMIC EFFECTS

The parametric study presented herein defines the optimum theoretical cross-section configuration for given requirements, such as section modulus, capacity, torsional

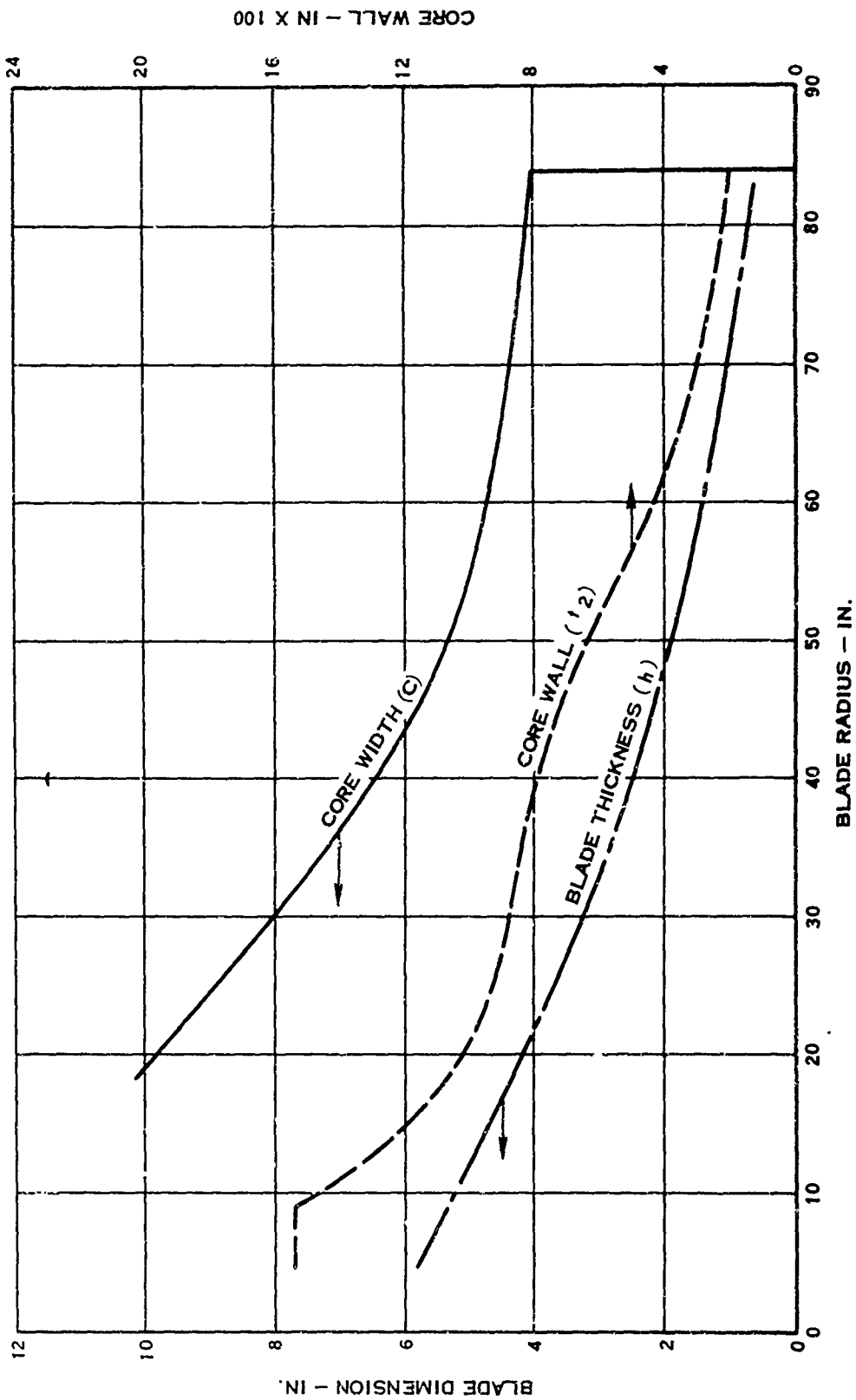


FIGURE 142. BLADE DESIGN DIMENSIONS

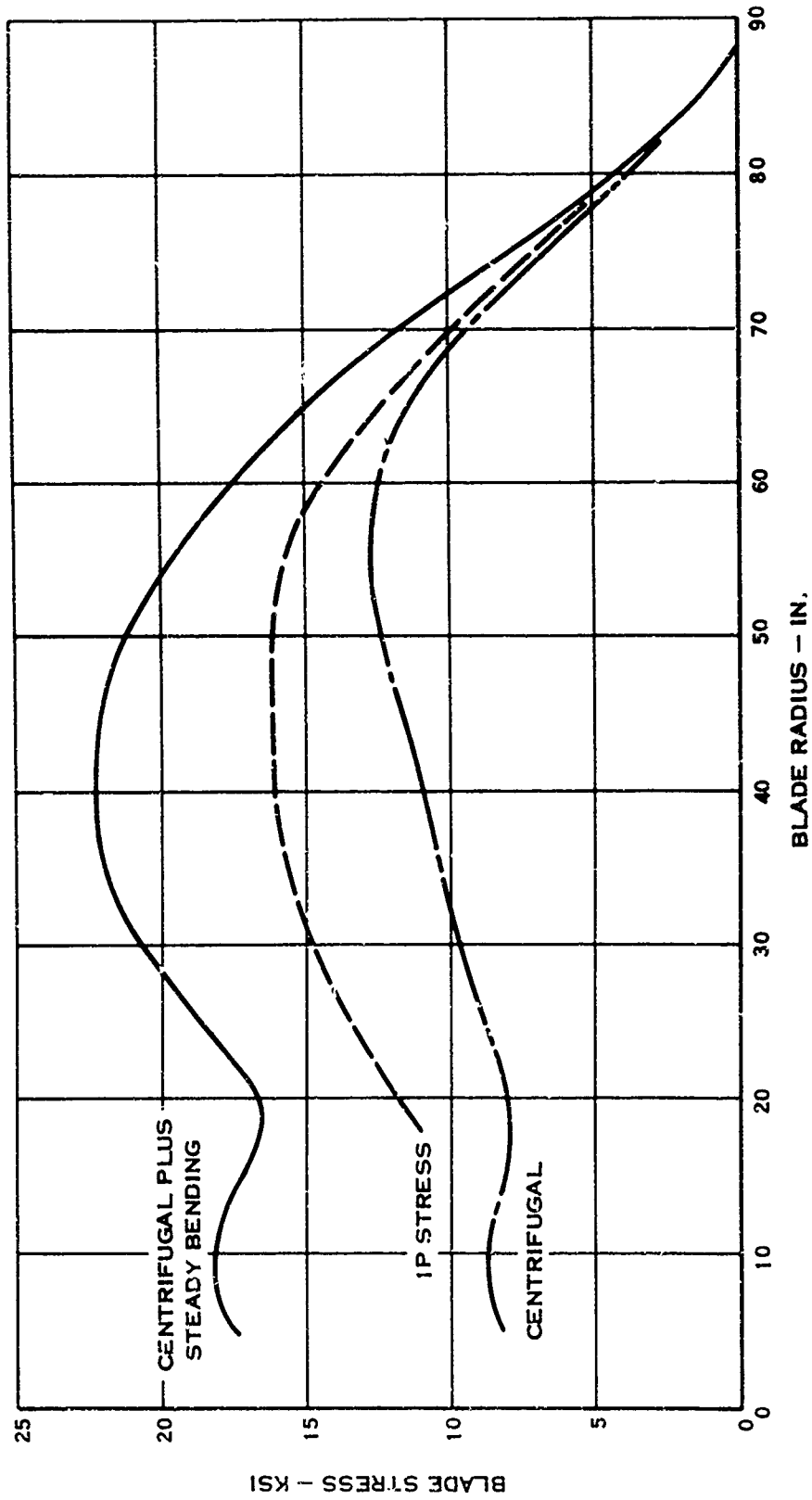


FIGURE 143. CALCULATED STRESS DISTRIBUTIONS FOR BLADE DESIGN

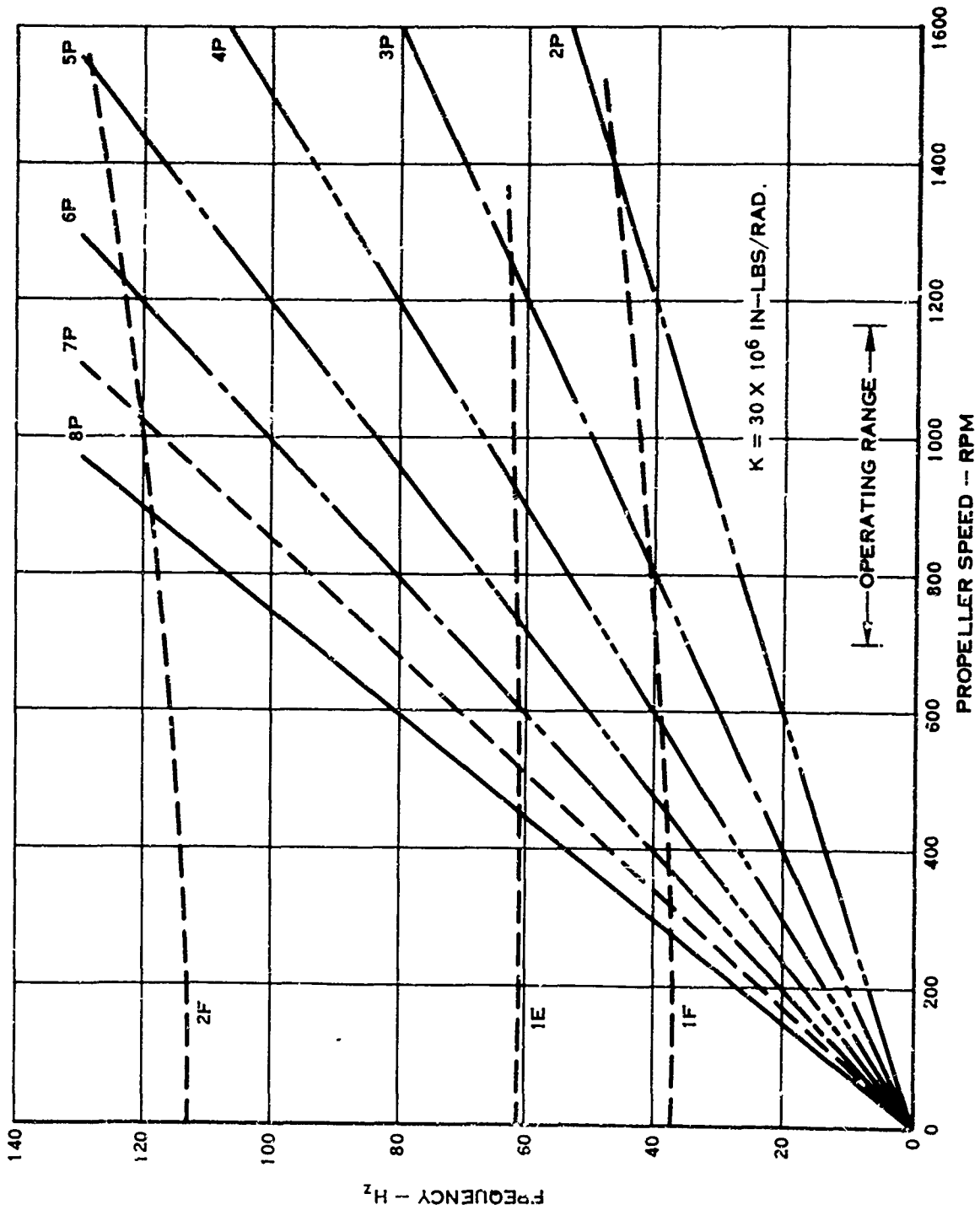


FIGURE 144, CRITICAL SPEED DIAGRAM

stiffness, etc. For load-carrying capacity, such information is sufficient, because the capacity is a function only of the load and of the properties at the given station. However, the dynamic and deformation design considerations for blades involve the integrated effects of the section properties over the length of the blade. In general, the most important of these integrated effects are the first torsional and first flatwise bending frequencies, which must be above specific defined values in order to prevent stall flutter and high bending response to vibratory loads, respectively. Thus, it is desirable to have some method by which the present parametric study results can be systematically used to modify the optimum blade design from that initially obtained, solely on the basis of load-carrying capacity and manufacturing feasibility.

In general, the fundamental, static flatwise natural frequency can be obtained approximately by equating the potential and kinetic energy of the dynamic system for this mode; i. e.,

$$PE = \frac{1}{2} \int_a^R EI_M (y_F'')^2 dx = \frac{1}{2} \frac{\omega^2}{g} \int_a^R A \gamma y_F^2 dx = KE$$

$$\text{or } \omega^2 = \frac{gE}{\gamma} \frac{\int_a^1 I_M (y_F'')^2 d(\frac{x}{R})}{\int_a^1 A (y_F)^2 d(\frac{x}{R})} = \frac{gE I_0}{\gamma R^4} \frac{\int_a^1 \left(\frac{F_{PE} R^4}{I_0} \right) dp}{\int_a^1 F_{KE} dp} \quad (40)$$

where y_F , I_M , and A are the flatwise deflection, effective flatwise section modulus, and equivalent areas of the blade, and a is the relative shank clamping radius. The torsional frequency can be treated similarly. This analysis assumes $I_M \gg I_m$ and $y_F/y_E \gg 1$, which is usually the case. F_{PE} and F_{KE} are influence coefficients and equal $I_M (y_F'')^2$ and $A y_F^2$ as functions of x/R , respectively; see Figure 145.

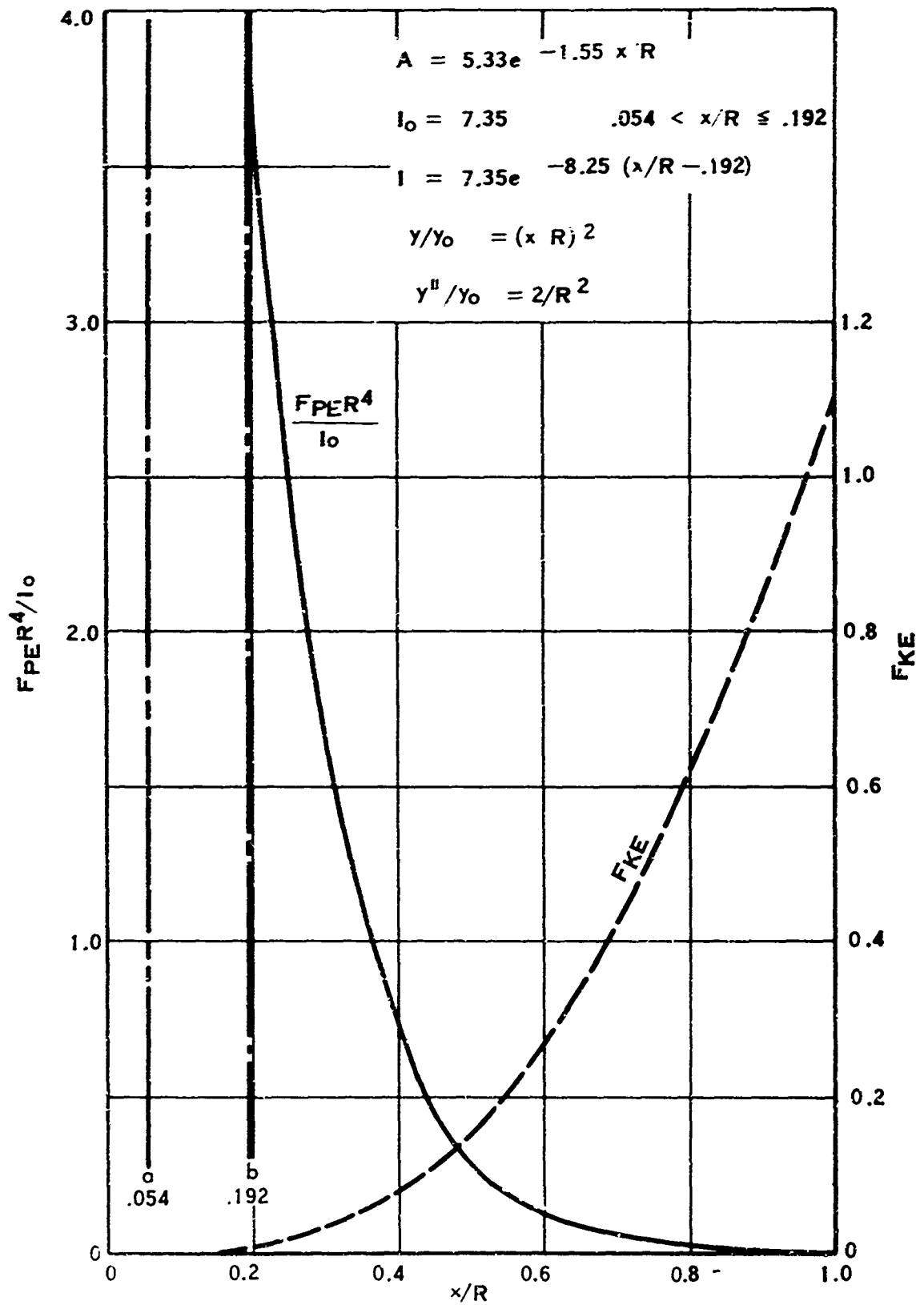


FIGURE 145. FREQUENCY INFLUENCE COEFFICIENTS

Now, assuming that the mode shape does not change, the change in frequency per change in section properties is obtained by differentiating Equation 40 as follows:

$$2 \omega d\omega = \frac{gE}{\gamma} \frac{\int_a^1 dI_m (v''')^2 dp}{\int_a^1 A(y)^2 dp} - \omega^2 \frac{\int_a^1 dA y^2 dp}{\int_0^R A y^2 dp}$$

$$\text{or } \frac{d\omega}{\omega} = \frac{1}{2} \left[\frac{\int_a^1 dI_m (v''')^2 dp}{\int_a^1 I_m (v''')^2 dp} - \frac{\int_a^1 dA y^2 dp}{\int_a^1 A y^2 dp} \right] \quad (41)$$

$$\text{or } \frac{d\omega}{\omega} = \frac{1}{2} \frac{1}{\int_a^1 F_{PE} dp} \left[\int_a^1 F_{PE} \left(\frac{dI_m}{I_m} \right) dp - \frac{\gamma \omega^2}{gE} \int_a^1 F_{KE} \left(\frac{dA}{A} \right) dp \right] \quad (42)$$

Thus, if after designing the blade to have the proper load capacity the flatwise

natural frequency is not right, the above equations may be used along with the parametric results to determine what sections are to be modified to get the desired change in frequency.

Analysis of a number of blades shows that the flatwise deflection is approximated by the equation

$$y/y_0 = \left(\frac{x}{R}\right)^n \quad (43)$$

where n usually falls between 2 and 3. Thus,

$$y''/y_0 = \frac{n(n-1)}{R^2} \left(\frac{x}{R}\right)^{n-2} \quad (44)$$

where $(n-2)$ is 0 to 1. Plots of blade section properties (see Figure 146) show that they vary approximately as follows:

$$\begin{aligned} A &\approx A_0 - \left(\frac{x}{R}\right) & a < \frac{x}{R} = 1 \\ I &= I_0 & a < \frac{x}{R} < b \\ I &= I_0 e^{-\beta\left(\frac{x}{R} - b\right)} & b < \frac{x}{R} = 1 \end{aligned} \quad (45)$$

Although the actual section values may be used in Equation (40), (41), or (42), sufficient accuracy can be obtained by using the approximate values of Equations (43), (44), and (45). If this is done, one finds that the influence coefficients for fractional changes in the section properties vary with blade radius as indicated in Figure 145. Thus, inboard of $\frac{x}{R} \approx 0.4$, changes in section properties influence primarily the potential energy; whereas outboard of $\frac{x}{R} \approx 0.6$, changes in section properties affect primarily the kinetic energy. Between $\frac{x}{R} = 0.3$ and 0.6 , both potential and kinetic energy are usually affected.

The above concepts were tried on the study blade design. It was found that $n \approx 2$, $a = 0.054$, $b = 0.192$, $A_0 = 5.33 \text{ in}^2$, $I_0 = 7.56 \text{ in}^4$, $\alpha = 1.55$, $\beta = 7.18$, $R = 88.5''$, $E = 30 \times 10^6 \text{ psi}$, and $\gamma = 0.096 \text{ lb/in}^3$. Introducing these results into Equation (40) gives

$$\omega^2 = \frac{gE}{R^4} \left(\frac{l_0}{R^4}\right) \frac{\int_0^1 \left(\frac{F_{PE} R^4}{l_0}\right) dp}{\int_0^1 F_{KE} dp} = \frac{386 \times 30 \times 10^6 \times 7.56 \times 1.083}{0.096 \times 88.5^4 \times 0.299}$$

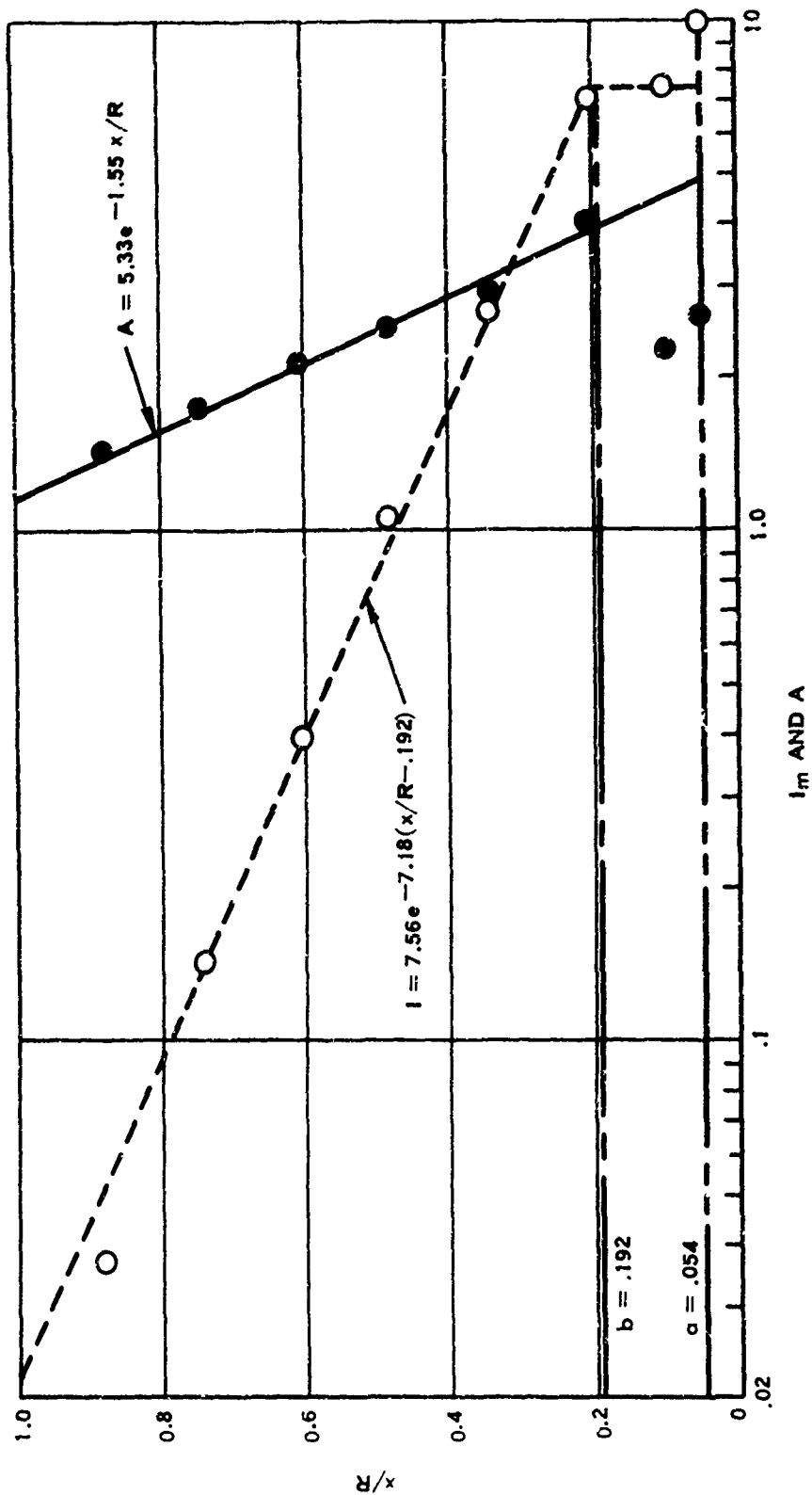


FIGURE 146. SECTION PROPERTIES OF BLADE DESIGN

$$= 54,600 \quad \text{or } \omega = 234 \text{ rps} \quad \text{or } f = 37.3 \text{ cps}$$

This result compares quite well with the static frequency of 37.5 cps obtained by the computer program. It is interesting to note that even by assuming the wrong deflection curve with $n = 3$, the resulting frequency is 33 cps. Introducing the same parameters into Equation (42) gives

$$\frac{d\omega}{\omega} = \frac{1}{2} \frac{1}{\int_0^1 \left(\frac{F_{PE} R^4}{I_0} \right) dp} \left[\int_a^1 \frac{F_{PE} R^4}{I_0} \frac{dI_m}{I_m} dp - \frac{\gamma \omega^2 R^4}{gE I_0} \int_a^1 F_{KE} \left(\frac{dA}{A} \right) dp \right]$$

$$\frac{d\omega}{\omega} = \frac{1}{2} \frac{1}{1.083} \left[\int_a^1 \left(\frac{F_{PE} R^4}{I_0} \right) \left(\frac{dI_m}{I_m} \right) dp - 3.62 \int_a^1 F_{KE} \left(\frac{dA}{A} \right) dp \right]$$

$$\frac{d\omega}{\omega} = 0.461 \int_a^1 \left(\frac{F_{PE} R^4}{I_0} \right) \left(\frac{dI_m}{I_m} \right) dp - 1.67 \int_a^1 F_{KE} \left(\frac{dA}{A} \right) dp \quad (46)$$

where the influence coefficients are as given in Figure 145. By using the parametric information along with the approximate relationship given by Equation (46), it should be possible to obtain the optimum parametric blade design for both load capacity and first flatwise frequency requirements. A similar approach could be used for the torsional frequency. However, a blade that meets the load-carrying and flatwise frequency requirements will usually have a torsional frequency sufficiently high to preclude stall flutter. The fractional change in flatwise frequency under load should be approximately the same as for the static case.

CONCLUSIONS

Since the shell generally contributes only a small percentage to the structural efficiency of the propeller blade, the selection of a shell material is not critical with respect to blade structural capacity. The major requirement is that this shell material be consistent with the core material. If the shell is the limiting factor, then the structural efficiency of the blade suffers greatly in comparison with a blade of similar core material and nonlimiting shell material. The selection of a shell material with a high strength allows the shell to be made thinner, thereby increasing the structural efficiency of the blade. The most promising materials for propeller blades of the early 1970's appear to be the boron/aluminum composite as the core material and S-glass as the shell material. Further studies are required to investigate the possibilities of a boron/epoxy core, boron/aluminum shell construction and a combination S-glass-boron/epoxy shell over a boron/aluminum core.

For an optimum blade configuration, the shell should be as thin as possible, limited only by its environmental conditions such as temperature, erosion, and impact damage. The core width and core wall thickness for optimum configuration should vary according to the loading conditions. The optimum configurations for various load conditions are shown as a line in the design charts. In reality, there exists a fairly large band of cross-section configurations where very little structural efficiency is lost.

The techniques described in this appendix have been employed to design a blade for the study point design application. Structural capacity sized the blade, with critical speeds being a secondary issue. The blade weight turned out to be 26 lb, which is approximately 40% of the weight of a present day steel core blade, 47% of a D6A core blade, and 71% of a titanium core blade.

The parametric study and the resulting computer program are the first steps toward the ultimate goal of automating and systematizing the design and optimization of propeller blades.

TABLE XXXV — SYMBOLS USED IN APPENDIX X

SYMBOL	DEFINITION
A	EQUIVALENT AREA
b	BLADE WIDTH (CHORD)
C	CORE WIDTH
C _c	DISTANCE FROM X AXIS TO CAMBER SIDE OF CORE
C _s	DISTANCE FROM X AXIS TO CAMBER SIDE OF SHELL
D	$\frac{\pi^2}{4} \left\{ \frac{s^2}{b^2} + \frac{h}{4b^2} \right\}$
E ₁	YOUNG'S MODULUS OF SHELL
E ₂	YOUNG'S MODULUS OF CORE
G ₁	SHEAR MODULUS OF SHELL
G ₂	SHEAR MODULUS OF CORE
H ₁₀	AREA ENCLOSED BY OUTSIDE PARAMETER OF SHELL
H _{1i}	AREA ENCLOSED BY INSIDE PARAMETER OF SHELL
H ₂₀	AREA ENCLOSED BY OUTSIDE PARAMETER OF CORE
H _{2i}	AREA ENCLOSED BY INSIDE PARAMETER OF CORE
H ₁	$1/2 (H_{10} + H_{1i})$
H ₂	$1/2 (H_{20} + H_{2i})$
h	BLADE THICKNESS
I _M	MOMENT OF INERTIA ABOUT Y AXIS
I _m	MOMENT OF INERTIA ABOUT X AXIS

TABLE XXXV — CONTINUED

SYMBOL	DEFINITION
I_p	POLAR MASS MOMENT OF INERTIA
J	CROSS PRODUCT OF INERTIA
M_c	BENDING MOMENT CAPACITY OF CORE
M_s	BENDING MOMENT CAPACITY OF SHELL
P_1	MEAN PERIMETER OF SHELL
P_2	MEAN PERIMETER OF CORE
T_c	TORSIONAL MOMENT CAPACITY OF CORE
T_s	TORSIONAL MOMENT CAPACITY OF SHELL
t_1	SHELL WALL THICKNESS
t_2	CORE WALL THICKNESS
t_3	$t_1 + 1/2 t_2$
t_4	$t_1 + t_2$
W	WEIGHT
δ/h	CAMBER
δ_{cg}	DISTANCE FROM X AXIS TO CENTER OF GRAVITY
δ_{ct}	DISTANCE FROM X AXIS TO CENTER OF TWIST
δ_{ho}	DISTANCE FROM X AXIS TO NEUTRAL BENDING AXIS
γ_1	DENSITY OF SHELL
γ_2	DENSITY OF CORE
δ_c	TENSILE STRENGTH OF CORE MATERIAL
δ_s	TENSILE STRENGTH OF SHELL MATERIAL

TABLE XXXV – CONTINUED

SYMBOL	DEFINITION
T	SHEAR STRENGTH OF CORE MATERIAL
T_s	SHEAR STRENGTH OF SHELL MATERIAL
a	CLAMP RADIUS
R	BLADE RADIUS
Y_f	FLATWISE BLADE DEFLECTION

REFERENCES

1. GENERALIZED METHOD OF PROPELLER PERFORMANCE ESTIMATION, Hamilton Standard Manual No. PDB 6101A, Hamilton Standard Division of United Aircraft Corporation, Windsor Locks, Connecticut.
2. GENERALIZED METHOD OF VARIABLE CAMBER PROPELLER PERFORMANCE ESTIMATION, Hamilton Standard Manual No. PDB 6408, Hamilton Standard Division of United Aircraft Corporation, Windsor Locks, Connecticut.
3. GENERALIZED METHOD OF SHROUDED PROPELLER PERFORMANCE ESTIMATION, Hamilton Standard Manual No. PDB 6220, Hamilton Standard Division of United Aircraft Corporation, Windsor Locks, Connecticut.
4. deDecker, R. W. , INVESTIGATION OF AN ISOLATED MONOCYCLIC V/STOL PROPELLER PERFORMANCE AND OSCILLATORY STRESS, Vertol Division of the Boeing Company, USAAVLABS Technical Report 65-80, U. S. Army Aviation Materiel Laboratories, Fort Eustis, Virginia, February 1966, AD 629647.
5. Weick, F. W. , and Wenzinger, C. J. , THE CHARACTERISTICS OF A CLARK Y WING MODEL EQUIPPED WITH SEVERAL FORMS OF LOW-DRAG FIXED SLOTS, NACA Report 407, 1932.
6. Weick, F. E. , and Shortal, J. A. THE EFFECT OF MULTIPLE FIXED SLOTS AND A TRAILING EDGE FLAP ON THE LIFT AND DRAG OF A CLARK Y AIR-FOIL, NACA Report 427, 1932.
7. Theodorsen, T. . and Stickle, G. W. , EFFECT OF A TRAILING EDGE EXTENSION ON THE CHARACTERISTICS OF A PROPELLER SECTION, NACA ACR L4121, 1944.
8. Bursnall, W. J. , EXPERIMENTAL INVESTIGATION OF THE EFFECTS OF VORTEX GENERATORS ON THE MAXIMUM LIFT OF A 6-PERCENT-THICK SYMMETRICAL CIRCULAR-ARC AIRFOIL SECTION, NACA RM L52624, 1952.
9. Spencer, R. H., Sternfeld, H. , Jr. , and McCormick, B. W. , TIP VORTEX CORE THICKENING FOR APPLICATION TO HELICOPTER ROTOR NOISE REDUCTION, USAAVLABS Technical Report 66-1, U. S. Army Aviation Materiel Laboratories, Fort Eustis, Virginia, September 1966, AD 644317.

10. AEROSPACE STRUCTURAL METALS HANDBOOK, ASD-TDR-63-741, Supp. 4, March 1957.
11. ALLOY DIGEST, Engineering Alloys Digest, Inc., Upper Montclair, N. J.
12. 18% NICKEL MARAGING STEELS, SUMMARY DATA, International Nickel Co., March 30, 1965.
13. VASCOMAX - 18% NICKEL ULTRA HIGH STRENGTH MARAGING STEELS, Vanadium Alloys Steel Co., 1966.
14. A NEW HIGH STRENGTH STAINLESS SUITABLE FOR CRYOGENIC USE, Cryogenic Technology, Vol. 1, No. 6, 1965.
15. ALMAR 362, A MARAGING STAINLESS STEEL, Allegheny Ludlum Steel Corp., Pittsburgh, Penna., 1966.
16. Borik, F., Jastusson, W. M., and Zackacy, V. F., FATIGUE PROPERTIES OF AN AUSFORMED STEEL, Trans. ASM, Vol. 56, Sept. 1963, pp. 326-338.
17. Simenz, R. F., and Macoritto, W. L., EVALUATION OF LARGE TITANIUM ALLOY FORGINGS, AFML-TR-65-206, July 1965.
18. Simenz, F. R., and Macoritto, W. L., EVALUATION OF LARGE TI-6Al-4V AND IMI 679 FORGINGS, AFML-TR-66-57, April 1966.
19. TITANIUM - 1966, LECTURES GIVEN AT NORAIR SYMPOSIUM, DMIC Memorandum 215, September 1, 1966.
20. Matusovich, C. J., EVALUATION OF TWO TITANIUM FORGING ALLOYS, USAAVLABS Technical Report 67-43, U. S. Army Aviation Materiel Laboratories, August 1967, AD 662700.
21. McClaren, S. W., and Cook, O. H., PROCESSING, EVALUATION, AND STANDARDIZATION OF TITANIUM ALLOY CASTINGS, Interim Reports, 15 March 1967 and 15 June 1967, Air Force Contract F-33615-67-C-1173, MMP Project NR9-169.
22. Fisher, P. A., Meredith, P. C., and Thomas, P. E., NEW HIGH STRENGTH MAGNESIUM CASTING ALLOYS FOR AEROSPACE APPLICATIONS, SAE Preprint 660656, Presented at Aeronautic & Space Engineering and Manufacturing Meeting, Los Angeles, Calif., Oct. 3-7, 1966.

23. Schotky, L. McDonald, and Johnson, Henry A. Editors. **BERYLLIUM TECHNOLOGY, VOLS. 1 & 2.** Gordon & Breach, Science Publishers, Inc., New York, 1966.
24. Gross, A. G., Jr., and Colterman, L. E., **EFFECTS OF THERMAL MECHANICAL VARIABLES ON THE ANISOTROPY OF FORGED BERYLLIUM.** AFML-TR-66-333, December 1966.
25. **METALWORKING NEWS,** July 10, 1967. p. 16.
26. Fenn, R. W., Jr., Crooks, D. D., and Underwood, E. E., **MATERIALS IN DESIGN ENGINEERING,** Sept. 1964, pp. 103-107.
27. **MECHANICAL PROPERTY DATA, 62BE-38AL ALLOY, ANNEALED SHEET,** Battelle Memorial Institute. March 1967.
28. Fenn, R. W., Jr., Crooks, D. D., Brodie, R. W., and Chinowsky, S., **COMPARISON OF LIGHTWEIGHT STRUCTURAL MATERIALS: BE, AND ALLOYS OF BE, MG, AL AND TI,** SAE Preprint 660652 presented at Aeronautic & Space Engineering & Mfg. Meeting, Los Angeles, Calif., Oct 3-7.
29. Van Hamersveld, J. A., Svendsen, Thomas S., and Hayes, W. C., **MAKING SATELLITE STRUCTURES FROM BERYLLIUM-LOCKALLOY,** Metal Progress, Feb., 1967.
30. **LOCKALLOY,** The Beryllium Corp., August 1964.
31. Schwartz, H. S., and Spain, R. G., **COMPOSITE MATERIALS,** AFML, Presented at AISS/ASME 8th Structures, Structural Dynamics & Materials Conf., Palm Springs, Calif., March 29-31, 1967.
32. Krieder, K. G., Varholak, E. M., and Schile, R., **INVESTIGATION OF PLASMA SPRAYED METAL MATRIX REINFORCED COMPOSITES,** Quarterly Report, Air Force Contract AF-33-616-67-C1655.
33. Adams, D. F., Eoner, D. R., and Thomas, R. L., **MECHANICAL BEHAVIOR OF FIBER REINFORCED COMPOSITE MATERIAL,** Technical Report AFML-TR-67-96, May 1967.
34. **FMS 2001A - ADVANCED COMPOSITE MATERIALS SPECIFICATION,** General Dynamics/Fort Worth, Feb. 10, 1967.

35. Schwartz, H. S. , MECHANICAL BEHAVIOR OF BERYLLIUM WIRE REINFORCED PLASTIC COMPOSITES, PART I - STATIC MECHANICAL PROPERTIES, AFML-TR-66-4-4, Pt, January 1967.
36. APPLICATION OF COMPOSITE MATERIALS TO RAMJET INLET STRUCTURE, VOL. I - STRUCTURAL DESIGN AND EVALUATION OF MATERIALS, Fourth Quarterly Report, Contract AF 33(615)-5320, July 1967.
37. Kreider, J. G. , and Leverant, G. R. , BORON FIBER METAL MATRIX COMPOSITES BY PLASMA SPRAYING, Technical Report AFML-TR-66-219, July 1966.
38. Kreider, K. , Varholak, E. , and Schile, R. , INVESTIGATION OF PLASMA SPRAYED METAL MATRIX FIBER REINFORCED COMPOSITES, Interim Reports, 14 June 1967 & 14 Sept. 1967, Air Force Contract F33615-67-C-1655.
39. STRUCTURAL DESIGN GUIDE FOR ADVANCED COMPOSITE APPLICATIONS, Prepared by Southwest Research Institute, Contract No. AF 33(615)-5142, Sept. 1967.
40. Buckingham, E. , MANUAL OF GEAR DESIGN, New York. Industrial Press, 1955.
41. METHOD OF EVALUATING LOAD RATINGS FOR BALL BEARINGS, Section 9, Revision #4, AFBMA Inc. , New York, Oct. 1960.
42. METHOD OF EVALUATING LOAD RATINGS FOR ROLLER BEARINGS, Section 11, AFBMA Inc. , New York, July 1960.
43. Munson, H. E. , TESTING AND EVALUATION OF 42CB (5023) AND 4270 BEARING STEEL, Marlin Rockwell Co. , Final Report M-R-C Research Proposal No. 1486, June 24, 1965.
44. Given, P. S. , TECHNICAL EVALUATION OF A MODIFIED AISI 52100 STEEL FOR AERO/SPACE BEARINGS, SKF Industries, King of Prussia, Pa. , Report 435-65-1, July 30, 1965.
45. Jones, A. B. , Consulting Engineer, COMPUTER PROGRAM, Newington, Conn. , Nov. 17, 1967.
46. Stodola, A. . STEAM AND GAS TURBINES, VOL. II, McGraw-Hill Book Co. . inc. . 1927, pp. 796-797.

47. Allan, T. . SOME ASPECTS OF THE DESIGN AND PERFORMANCE OF WILDHABER-NOVIKOV GEARING, Proc. of the Inst. of Mech. Eng. , 1964-1965, pp. 931-54.
48. Chironis, N. , DESIGN OF NOVIKOV GEARS, Product Engineering, Sept. 17, 1962, pp. 91-102.
49. Walker, H. , A CRITICAL LOOK AT THE NOVIKOV GEAR, The Engineer, April 1960, pp. 725-729.
50. INVESTIGATION OF THE CONFORMAL GEAR FOR HELICOPTER POWER TRANSMISSION, The Boeing Co. , Vertol Division, TRECOT Technical Report 64-28, June 1964.
51. Mack, J. C. , Alberti, J. P. , and Lemanski, A. J. , AN EXPERIMENTAL EVALUATION OF THE CONFORMAL GEAR, USAAVLABS Technical Report 66-8, February 1966, AD 630925.
52. Austin, R. G. , ADVENT OF THE ECONOMIC HELICOPTER, Flight International, July 20, 1967, pp. 110-111.
53. A PROGRESS REPORT ON WILDHABER - NOVIKOV GEARING, Product Engineering, June 25, 1962, pp. 88-89.
54. Richardson, H. H. , STATIC AND DYNAMIC LOAD, STRESS, AND DEFLECTION CYCLES IN SPUR-GEAR SYSTEM, D.A.C.L. Research Memorandum, R. R. 7454-1, June 30, 1958.
55. Howland, J. S. , AN INVESTIGATION OF THE DYNAMIC LOADS IN SPUR-GEAR TEETH, S. M. Thesis at M.I.T. , February 1962.
56. Buckingham, E. , ANALYTICAL MECHANICS OF GEARS, McGraw Hill Book Co. , Inc. , 1949.
57. Buckingham, E. , MANUAL OF GEARING DESIGN SECTION TWO, Machinery, New York, 1935.
58. Yin, T. P. , Kelly, T. J. , and Barry, J. E. , A QUANTITATIVE EVALUATION OF CONSTRAINED - LAYER DAMPING, ASME Paper No. 67-Vibr. -26, March 1967.
59. Ungar, E. E. , and Hatch, D. K. , HIGH DAMPING MATERIALS, Product Engineering, April 17, 1961.

60. Heywood, R. E. , DESIGNING BY PHOTOELASTICITY, Chapman & Hall Ltd. , 1952, p 210.
- 61. Westervelt, W. W. , THEORETICAL ANALYSIS OF CAM ROLLER STRESSES, Hamilton Standard Internal Memorandum VI#90, January 10, 1958.
- 62. Roark, Raymond J. , FORMULAS FOR STRESS AND STRAIN, McGraw-Hill Book Co. , 1954.

DOCUMENT CONTROL DATA - R & D

(Security classification of title, body of abstract and indexing annotation must be entered when the overall report is classified)

1. ORIGINATING ACTIVITY (Corporate author) Hamilton Standard Division of United Aircraft Corporation Windsor Locks, Connecticut		2a. REPORT SECURITY CLASSIFICATION Unclassified	
		2b. GROUP	
3. REPORT TITLE FEASIBILITY STUDY OF ADVANCED V/STOL PROPELLER TECHNOLOGY			
4. DESCRIPTIVE NOTES (Type of report and inclusive dates) Final Report			
5. AUTHOR(S) (First name, middle initial, last name) William M. Adamson			
6. REPORT DATE June 1968	7a. TOTAL NO. OF PAGES 384	7b. NO. OF REFS 62	
8a. CONTRACT OR GRANT NO. DAAJ02-67-C-0073	8a. ORIGINATOR'S REPORT NUMBER(S) USAAVLABS Technical Report 68-33		
b. PROJECT NO. Task IG121401D14415	8b. OTHER REPORT NO(S) (Any other numbers that may be assigned this report)		
c.			
d.			
10. DISTRIBUTION STATEMENT This document has been approved for public release and sale; its distribution is unlimited.			
11. SUPPLEMENTARY NOTES		12. SPONSORING MILITARY ACTIVITY U. S. Army Aviation Materiel Laboratories Fort Eustis, Virginia	
13. ABSTRACT A feasibility study of advanced V/STOL propeller systems for the 1970-1975 time period was conducted. The primary objective of the study was to investigate the application of new materials and new design concepts to define the maximum reductions in specific weight of the complete propeller system (including reduction gearbox) attainable in this time period. Preliminary designs of future propeller systems presented in the report are over 50 percent lighter than comparable present-day V/STOL systems. Three integral gearbox propeller systems, with and without cyclic pitch and with and without a cross-shaft drive pad, were defined in this report using the advanced technology indicated as feasible by the study. Each major component of the IGB propeller system was optimized and then merged into complete system designs. A summary weight tabulation is presented showing the relative contributions of each major component of the propeller system to the total indicated weight reductions. A significant portion of the weight reductions is shown to be achievable by 1970, since the technology required is presently under development or is a natural extension of existing technology. Other significant weight reductions, such as those resulting from the use of boron blade spars and titanium gearing, are at an early phase of their technology development and are, at this time, not considered attainable much before 1975.			

Unclassified

Security Classification

14. KEY WORDS	LINK A		LINK B		LINK C	
	ROLE	WT	ROLE	WT	ROLE	WT
Propeller Gearbox V/STOL Propulsion						

Unclassified

Security Classification